Contributions
to Current Research
in Geophysics (CCRG)
4

Monsoon Dynamics

Editor: T.N. Krishnamurti

Springer Basel AG

Contributions
to Current Research
in Geophysics (CCRG)
4

Monsoon Dynamics

Editor: T.N. Krishnamurti
Florida State University

Reprinted from PAGEOPH

1978 Springer Basel AG

Reprinted from Pure and Applied Geophysics (PAGEOPH), Volume 115 (1977), No. 5-6

CIP-Kurztitelaufnahme der Deutschen Bibliothek

Monsoon dynamics: reprinted from PAGEOPH/ed.:
T. N. Krishnamurti. - 1. Aufl.
(Contributions to current research in geophysics;
4)
ISBN 978-3-0348-5760-4 ISBN 978-3-0348-5759-8 (eBook)
DOI 10.1007/978-3-0348-5759-8

NE: Krishnamurti, Tiruvalam N. [Hrsg.]

Ursprünglich erschienen bei Birkhäuser Verlag, Basel, 1978
Softcover reprint of the hardcover 1st edition 1978

ISBN 978-3-0348-5760-4

CONTENTS

Editor's Note

In recent years there has been a major revival of interest on the problems of the monsoons. Within the First GARP (Global Atmospheric Research Program) Global Experiment (FGGE), the major importance of the monsoons is recognized and a major monsoon observational subprogram has been proposed to be conducted in 1978 to 1979. The major objectives of these experiments would be to provide a better understanding of the monsoons on planetary and regional scales. The monsoon problem is a complex interaction of the land-ocean and the atmosphere. The heating of the earth's surface by radiative processes and of the earth's atmosphere by sensible and latent heat fluxes from the lower boundary, by dry and deep moist convective processes and by radiative processes provides a complex broad scale field of the so-called 'differential heating' that drives the large scale monsoons. The broad scale monsoon system is being recognized as an unsteady feature which grows and decays exhibiting local instabilities on different space and time scales. Scale interactions are inherent to the monsoon dynamics problems. The present special volume was initiated at the request of the editors, around July 1976, and in the role of a Special Editor, I was asked to solicit from a number of recent workers in the field their research and review contributions. This issue by no means defines the state of the art, however it is intended to cover many of the more important and recent areas of emphasis. I feel that it provides a useful scientific background for those wishing to participate in the planetary and the regional aspects of the forthcoming GARP Monsoon Experiment and to those who wish to pursue research on the many unsolved problems.

T. N. KRISHNAMURTI

Pageoph, Vol. 115 (1977), Birkhäuser Verlag, Basel

Some Theoretical Problems of the Planetary-Scale Monsoons

By CHIH-PEI CHANG[1])

Summary—Some important theoretical problems of the planetary-scale monsoons which have arisen from recent advances of observational studies are reviewed. These include: (1) the requirement of a strong damping mechanism in the planetary scale vorticity budget of summer monsoon and a similar but weaker requirement for the winter monsoon; (2) the localized barotropic instability of the summer monsoon which is a result of the strong zonal asymmetry of the planetary-scale flow and causes significant nonlinear energy conversions; and (3) the oscillations of the planetary-scale monsoons. It is pointed out that these problems are inter-related and their understanding is also important for the proper simulation of other scales of motion of the monsoon circulation.

Key words: Monsoon: Oscillation, vorticity budget; Barotropic instability.

1. Introduction

The monsoon circulation of both the northern summer and the northern winter (hereafter the word 'northern' will be neglected) are characterized by large planetary scale quasi-stationary waves in the subtropics and tropics. As have been shown by KRISHNAMURTI (1971a), KRISHNAMURTI, KANAMITSU, KOSS and LEE (1973b) and others, these waves are a result of the thermally direct overturnings induced by the differential heating associated with the land-sea distribution. The major component of the heating is the convective latent heat release which is most intense over the Tibetan and Mexican highlands during summer and the maritime continent of the Malaysia-Indonesia region during winter. Mainly due to the availability of the commercial aircraft data, the principal features of these zonal asymmetries have been best depicted by the wind analyses near 200 mb by KRISHNAMURTI and ROGERS (1970), KRISHNAMURTI *et al.* (1973b) and SADLER (1975). During summer these features include a strong anticyclone centered over the Tibetan plateau, a weaker anticyclone over Mexico and elongated troughs oriented northeast–southwest in the mid-Pacific and mid-Atlantic. These are all well presented in Fig. 1 which shows the time-mean streamfunction at 200 mb for June–August 1967 as determined by KRISHNAMURTI (1971a). During winter a large streamfunction high over the equatorial South China

[1]) Department of Meteorology, Naval Postgraduate School, Monterey, California 93940, USA.

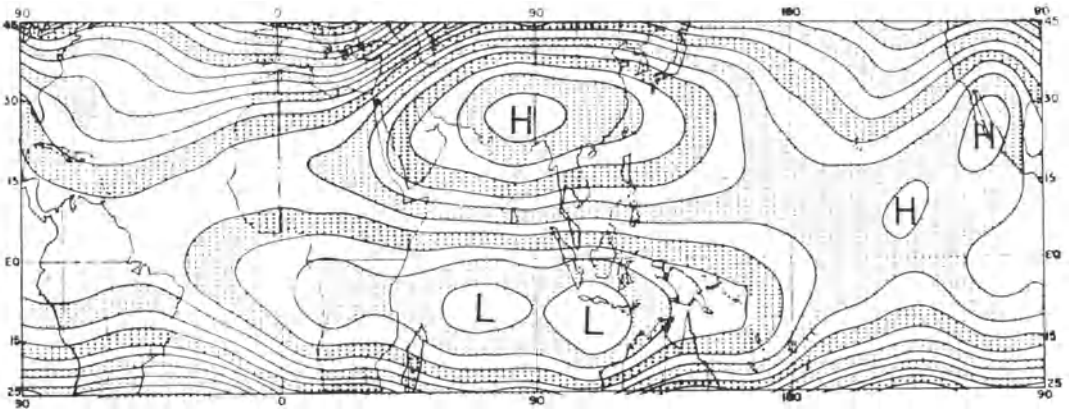

Figure 1
Summer mean (June–August 1967) 200-mb streamfunction, contour interval is 50 × 10^5 m^2 sec^{-1}. (From KRISHNAMURTI, 1971a.)

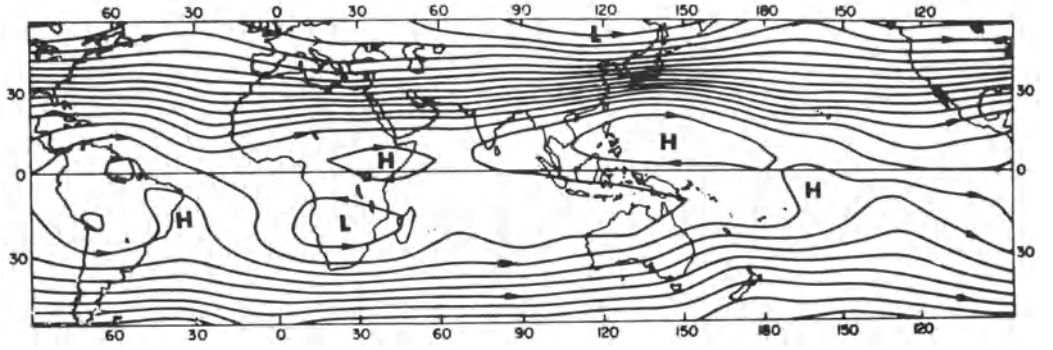

Figure 2
Winter mean (December–February 1971) 200-mb streamfunction, contour interval is 50 × 10^5 m^2 sec^{-1}. (From KRISHNAMURTI *et al.* 1973b.)

Sea and western Pacific replaces the Tibetan high to become the most pronounced planetary scale feature, with two weaker highs appearing over the equatorial eastern Africa and the northeastern South America and three oceanic troughs extending from the equator to the southern subtropics. These features are shown in Fig. 2 which is the 200 mb time-mean streamfunction for the winter of 1971 determined by KRISHNAMURTI *et al.* (1973b).

A number of interesting theoretical problems have arisen from the observed monsoon circulations. In this paper we will review some of the problems that are related to the planetary-scale monsoon. They include:

(1) The requirement of a strong damping mechanism in the planetary scale vorticity budget,

(2) The localized barotropic instability associated with the planetary-scale summer monsoon, and
(3) Oscillations of the planetary-scale monsoons.

2. *The requirement of a strong planetary scale damping mechanism*

In a linear, one-level numerical model, HOLTON and COLTON (1972) used the barotropic vorticity equation to diagnose the budget of the seasonal-mean planetary scale vorticity at 200 mb during summer. They used the 200 mb mean divergence observed by KRISHNAMURTI (1971a, b) as the steady forcing function with a mean zonal flow also specified by the observed values. Figure 3 shows the velocity potential

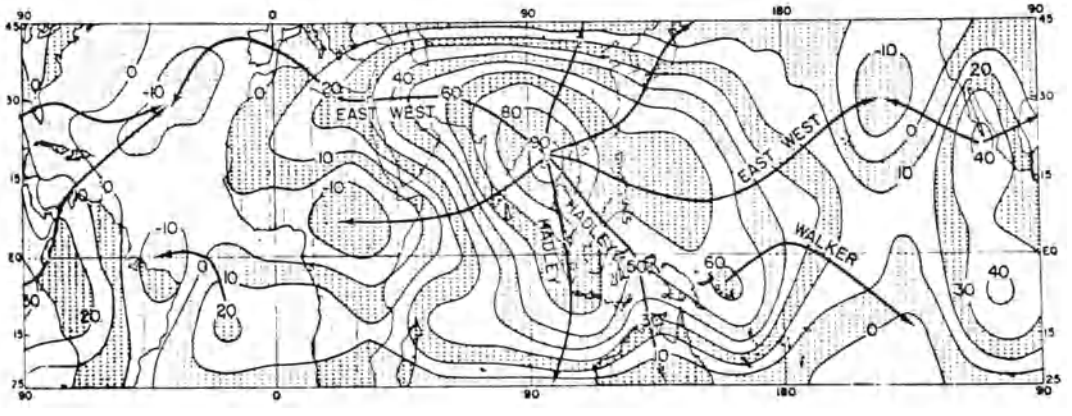

Figure 3
Summer mean (June–August 1967) 200-mb velocity potential, contour interval is 10×10^5 m^2 sec^{-1}. The few streamlines sketched indicate the direction of the mean divergence motions. (From KRISHNAMURTI, 1971a.)

computed by KRISHNAMURTI (1971a) which expresses the observed mean divergence field. Comparing this figure with Fig. 1, it is evident that the time-mean vorticity and divergence fields are approximately half-cycle out of phase. However, the resultant steady-state planetary scale vorticity field calculated by HOLTON and COLTON is about one-quarter cycle out of phase from the divergence field, unless a very strong damping term is added to the mean vorticity equation. This difficulty arises because, in the absence of strong damping, the main balance in the vorticity equation is between the generation by horizontal divergence and the advection by mean flow. This near-balance requires that the vorticity be one-quarter cycle out of phase from the divergence. The very efficient generation by the strong divergence also causes the amplitudes of the long waves to be significantly larger than those observed. Figure 4 (from HOLTON and COLTON, 1972) compares the diagnosed and observed amplitudes

and phases of the streamfunction for zonal wavenumber one as a function of latitude. When the linear damping coefficient is increased from a modestly strong value of 5×10^{-6} sec^{-1} to a very strong value of 1.5×10^{-5} sec^{-1}, the discrepancy disappears and the phase and amplitude of the long waves become in close agreement with observations.

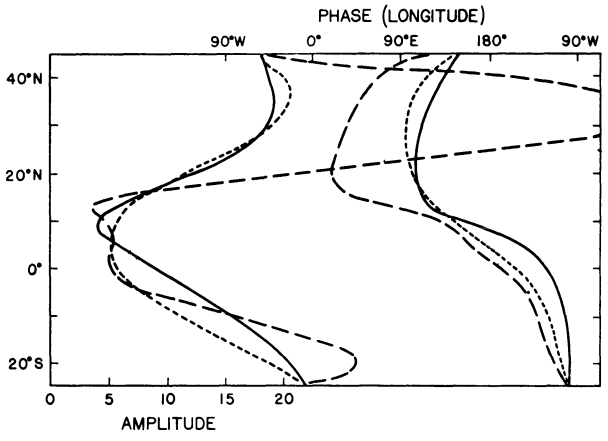

Figure 4

Amplitude in units of 10^6 m^2 sec^{-1} (left-hand curves) and phase (right-hand curves) of the streamfunction for zonal wavenumber 1 as a function of latitude. Solid curve is observed streamfunction; short and long dashes are the solutions computed by HOLTON and COLTON (1972) for damping rate of 1.5×10^{-5} sec^{-1} and 5×10^{-6} sec^{-1}, respectively. (From HOLTON and COLTON, 1972.)

HOLTON and COLTON's (1972) findings suggest that a very strong sink with a damping time scale faster than 1 day is required to balance the linear vorticity budget of the seasonal-mean 200 mb planetary-scale flow during summer. This damping is much stronger than the normal dissipation process in the upper troposphere whose damping time is on the order of weeks. In looking for an explanation of this excessive damping requirement, they suggested that two possible mechanisms not included in their model may be responsible for the strong damping. The first is the vertical mixing of vorticity by cumulonimbus convection which is very strong over the Asian continent and Mexican highland during the northern summer. This mechanism has been suggested by RIEHL and PEARCE (1968), REED and RECKER (1971), WALLACE (1971), WILLIAMS and GRAY (1973) and others to balance the vorticity budget of the synoptic-scale easterly waves in the tropical troposphere. However, HOLTON and COLTON (1972) felt that it alone is still insufficient to account for the required fast damping. They then proposed the second mechanism which is related to the day-to-day fluctuations of the monsoon vorticity and divergence fields observed by KRISHNAMURTI (1971b). Considering deviations from the time mean, the complete divergence term in the time-mean vorticity equation is $\langle(\zeta + f)\delta\rangle = (\langle\zeta\rangle + f)\langle\delta\rangle + \langle\delta'\zeta'\rangle$ where ζ and f are the relative and planetary vorticities, respectively; δ is divergence and the primes are deviation from the time mean $\langle\ \rangle$. The last term, which was excluded in

HOLTON and COLTON's linear calculations, tends to be negative according to the observed out-of-phase correlation of the fluctuating vorticity and divergence fields. This term therefore may counteract the vorticity generation by the time-mean divergence. HOLTON and COLTON then speculated that the combination of this fluctuation correlation and the cumulus mixing mechanisms could be responsible for the less than one day damping time.

The requirement of a strong vorticity sink has also been confirmed by other numerical investigations that do not include the strong damping. As a follow up of the work of HOLTON and COLTON (1972), COLTON (1973) used a semi-spectral representation of the one-level nonlinear barotropic vorticity equation to study the scale interactions of the 200 mb summer monsoon flow forced by the observed mean divergence. As a consequence of the inclusion of only modest damping (time scale 5 days), the resultant planetary-scale waves have amplitudes considerably larger than the seasonal mean values. Westward phase shifts of 50° for the Tibetan high and 30° for the mid-Pacific trough, in comparison with the observed positions, are also produced by the model (Fig. 5). ABBOTT (1973) developed a 3-level nonlinear quasi-geostrophic hemispheric model to simulate the time-mean climatology of the summer

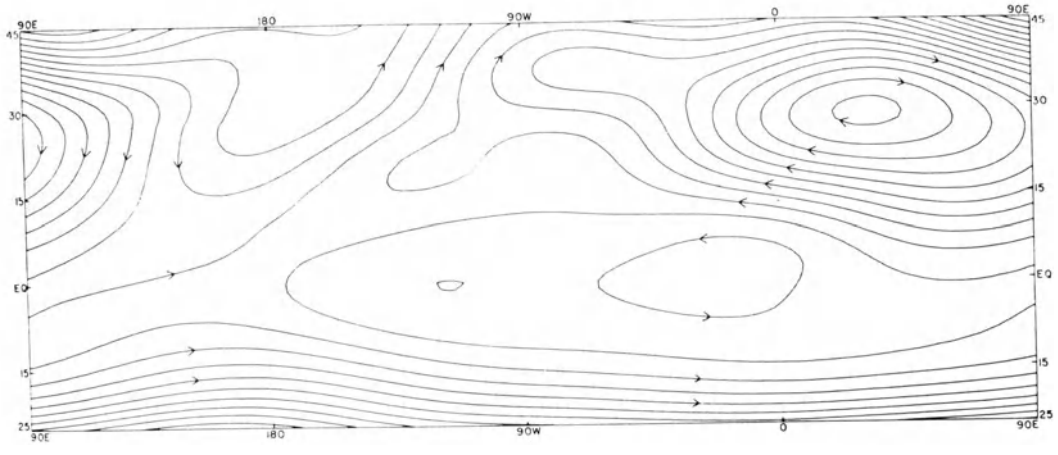

Figure 5
Streamfunction of the forced motion averaged over days 15 through 40 of the numerical integration by COLTON (1973). Contour interval is 50×10^5 m^2 sec^{-1}.

monsoon. To drive the monsoon circulation, he specified a steady heating distribution which was found by inverting the governing equations with the vorticity field giving by the observed time-mean values. This heating distribution (Fig. 6) in turn successfully simulates the principal features of the planetary-scale flow as well as the nonlinear energy exchanges. However, it is about a quarter cycle out of phase from that implied by the observed mean divergence field and the satellite cloud data. This apparently is also due to the absence of a strong damping mechanism in the model which forces a

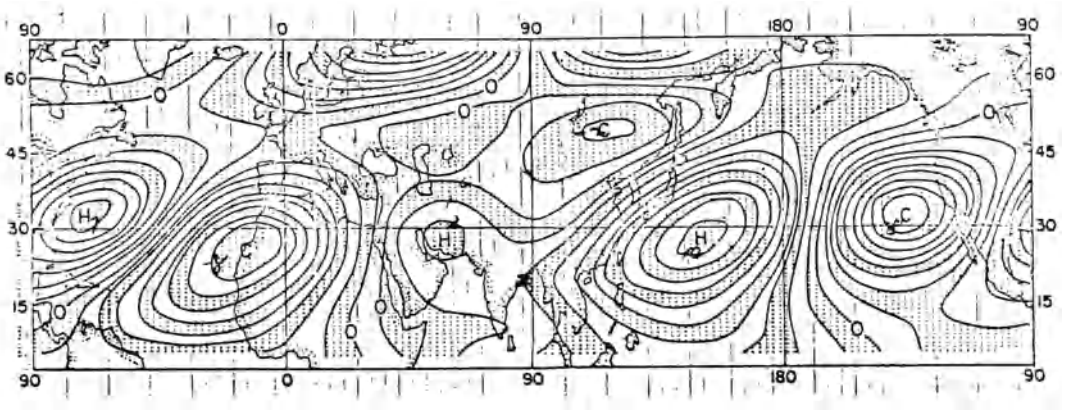

Figure 6
Time-independent horizontal distribution of the diabatic heating rate at 350 mb as computed by ABBOT (1973). Isopleths are at 5×10^{-3} m^2 sec^{-1}.

balance between the advection and generation of vorticity. In a 3-component semi-spectral primitive equation model, MURAKAMI (1974) also used a specified heating function to study the planetary scale monsoon flow during summer. Without the inclusion of the strong damping and allowing the specified heating to fluctuate with time, he was able to obtain the proper amplitude and phase of the long waves. However, the resultant divergence field in his model is somewhat different from that observed by KRISHNAMURTI (1971a). The greatest discrepancy occurs at 200 mb, where KRISHNAMURTI (1971a) found very strong divergence in the Tibetan high area during the 1967 summer, while in MURAKAMI's (1974) model this level is almost non-divergent. The model also produces a different horizontal distribution of long wave divergence compared to the observed 1967 distribution, with the Tibetan divergence center shifted slightly to the east and the mid-Atlantic convergence center shifted to the longitude of central Africa. Thus the magnitude of divergence forcing is much reduced and a phase shift between divergence and anticyclonic vorticity also results[2]). In addition, the advective effect is not properly treated because the zonal mean flow is not allowed to interact with the three interacting long waves. Hence it is unclear what is the main mechanism that produces the correct amplitude and phase of the vorticity field.

Looking for alternative sources for the strong damping, BARCILON and COOPER (1974) hypothesized that a thermal boundary layer effect could operate in the atmosphere during summer monsoon. In their simple analytical model a sinusoidal temperature variation is applied at the lower boundary which provides the planetary scale differential heating. A number of solutions were found for a balance between

[2]) However, MURAKAMI (personal communication) found that this horizontal distribution of divergence is in good agreement with the 1970 summer data.

the horizontal advection and vertical diffusion of heat in the thermodynamic energy equation, and one of them allows a half-cycle out of phase shift between the upper level vorticity and divergence. However, since the monsoonal differential heating in the real atmosphere is mainly due to the latent heat release of cumulus convection which is maximum in the middle-upper troposphere, it is uncertain whether BARCILON and COOPER's (1974) theory is completely applicable to the real atmosphere.

Another explanation for the observed vorticity-divergence phase relationship was offered by PAEGLE and PAEGLE (1976). They speculated that a high pressure region with strong pressure gradients may cause the geostrophic vorticity to become less than one-half of the negative planetary vorticity. This implies that the balance equation becomes non-elliptic and, under certain rather strong assumptions, leads to a rapid vorticity adjustment with strong horizontal divergence occurring in the negative relative vorticity region. However, the resultant steady-state absolute vorticity vanishes and this efficiently eliminates the generation of vorticity by divergence. Such large negative values of relative vorticity are not observed in the large-scale monsoon flow. In fact the minimum seasonal mean relative vorticity at 200 mb during the 1967 summer as observed by KRISHNAMURTI is $\sim -3 \times 10^{-5}$ sec^{-1}, which occurs in the vicinity of the Tibetan and Mexican highs near 30°N. This magnitude is considerably smaller than that of the Coriolis parameter. Thus it appears unlikely that this super-gradient effect is relevant to the planetary-scale monsoon problem.

To test the hypotheses proposed by HOLTON and COLTON (1972), CHANG and PENTIMONTI (1977) used a 3-level primitive equation model with a 4° finite-difference resolution in both the zonal and meridional directions. The zonal mean flow is included using a Newtonian term which maintains the proper north-south temperature gradient by continuously adjusting each temperature toward a thermal equilibrium determined by the zonally symmetric climatology. The zonally asymmetric motions are generated by a specified perturbation heating function whose horizontal distribution follows that of the 200 mb seasonal mean divergence observed by KRISHNAMURTI (1971b). It turns out that this heating distribution almost reproduces the observed mean divergence in the upper troposphere, which suggests that the choice of the forcing function is proper. Two experiments were carried out by integrating the model in time until 25 days after it reached the respective steady states. Both experiments include only weak damping (time scale >7 days) in the free atmosphere but the heating function was held steady only in the first experiment and allowed to fluctuate in time with an amplitude equal to one-half of the time-mean heating in the second experiment. The fluctuation period was set to 10 days. Comparing the results of the two experiments, CHANG and PENTIMONTI found essentially no difference between the time-mean planetary scale fields except a slightly reduced amplitude for the fluctuating case. Figure 7 is their time-mean wind field at 250 mb (near the upper level of the model) for the fluctuating heating case. It can be seen that the simulated Tibetan and Mexican anticyclones are shifted about 30° and 25°, respectively, from the observed positions. These phase shifts are almost identical to those produced by

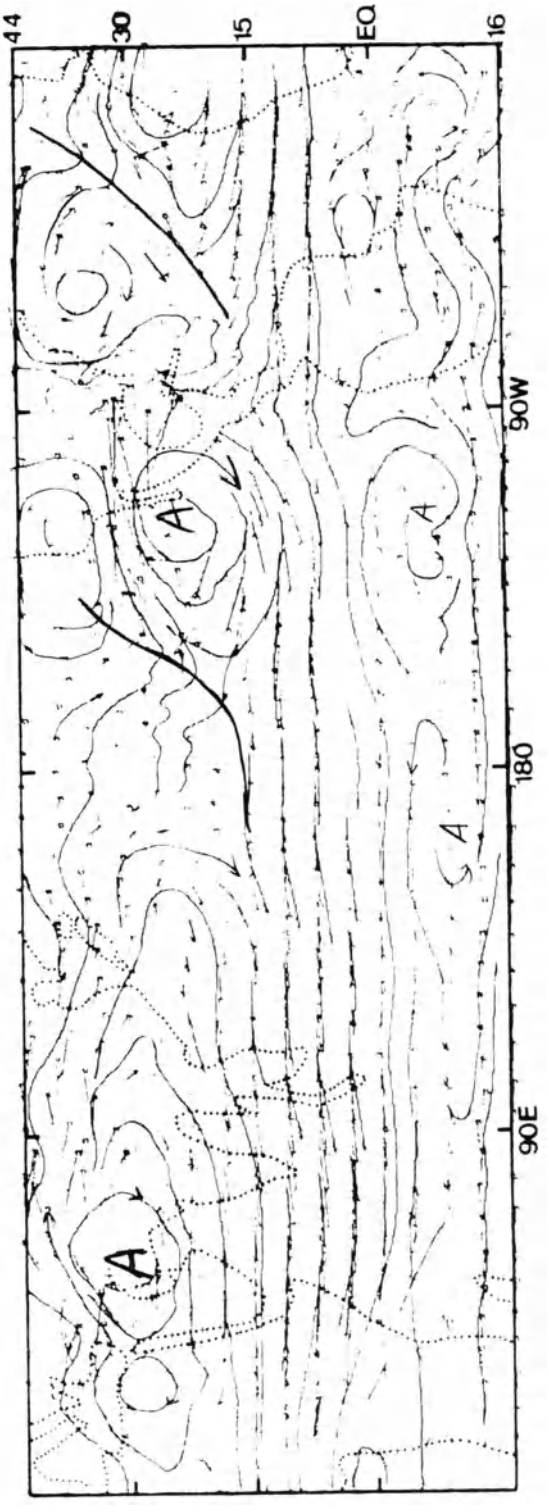

Figure 7
Time-mean wind field at 250 mb forced by a fluctuating heating function as computed by CHANG and PENTIMONTI (1977).

their steady-heating case. Thus the fluctuating component as specified in the model is almost inconsequential in providing the damping needed for the phase shift problem. On the other hand, in both experiments the amplitudes of the long waves are not excessively large compared to observations. This result is similar to that of ABBOTT (1973) and seems to suggest that nonlinear processes could be responsible for part of the planetary-scale vorticity sink deduced by HOLTON and COLTON's linear calculations. The fluctuation of the planetary-scale flow apparently enhances these nonlinear conversions resulting in the further reduction of its time-mean amplitude.

A noteworthy feature in CHANG and PENTIMONTI's (1977) time-mean fields is that the positions of the upper tropospheric mid-oceanic troughs do not have significant phase errors as those of the anticyclones. As pointed out by KRISHNAMURTI, DAGGUPATY, FEIN, KANAMITSU and LEE (1973a), the damping due to cumulus transports should not operate over the relatively cloud-free oceanic areas. With the inclusion of nonlinear processes (and also large-scale vertical advections), the damping requirement implied by the phase errors of CHANG and PENTIMONTI's time-mean upper level anticyclones is weaker than that found by HOLTON and COLTON (1972). Perhaps a damping time longer than 1 day, which seems more reasonable than HOLTON and COLTON's value if interpreted as due to the cumulus transports, may be sufficient. In this case a numerical experiment similar to CHANG and PENTIMONTI's, but incorporating a moderately strong damping term with time scale order of a few days in the continental convective area only, may provide some insight as to whether cumulus transport processes are responsible for the missing vorticity sink.

The studies mentioned above all concern the summer monsoon only. During winter KRISHNAMURTI *et al.* (1973b) observed that the rotational component of the seasonal-mean flow of the active monsoon region is almost one order smaller than that of the summer monsoon, while the divergent component has a comparable magnitude. The reason for this appears to be the proximity of the winter monsoon convections to the equator, which reduces the efficiency of vorticity generation by horizontal divergence. However, the importance of a dissipation mechanism in the winter monsoon was also brought out in a few theoretical studies recently. In a linear study of the stationary forcing in the tropical atmosphere, WEBSTER (1972, 1973) found that the primary response in the equatorial region corresponds to the atmospheric Kelvin waves (HOLTON and LINDZEN, 1968). A theoretical calculation shows that the zonal wavelength of this Kelvin wave response is very long while its vertical wavelength is very short [O(1 km)]. The former agrees quite well with observed equatorial stationary circulations such as the winter monsoon, but the latter is one order of magnitude shorter than the observed vertical wavelengths. This discrepancy arises because the equatorial Kelvin waves behave like internal gravity waves in the zonal-vertical plane and their phase speed, c, is related to an equivalent depth scale h by the relationship $c = (gh)^{1/2}$. These stationary waves are imbedded in a mean easterly zonal current so that they have a Doppler-shifted phase speed of a few meters per second, which implies a very short vertical wavelength. To get around this problem

in simulating the observed stationary motions, WEBSTER (1972, 1973) adopted a two level numerical model with friction which is quite successful in reproducing many of the observed features.

Very recently CHANG (1977) re-examined this problem by incorporating linear damping terms in the thermally forced Kelvin wave equations. The dispersive relationship of the Kelvin waves may be written as $c\lambda = S^{1/2}$, where λ is the vertical wavenumber and S is a static stability parameter. The linear damping introduces an imaginary part to c which causes λ to become complex also. Consequently the dispersive relationship becomes quadratic and has two types of solutions. The first type arises when the inertial time scale is faster than the damping time scale. This solution resembles the regular internal gravity waves whose vertical wavelength decreases as the Doppler-shifted phase speed decreases. The second type, called the viscous mode by CHANG (1977), arises when the damping time scale dominates over the inertial time scale and its vertical wavelength increases as the Doppler phase speed decreases (Fig. 8). This solution is also much more trapped in the vertical so that it has appreciable amplitude only in the region of thermal forcing (troposphere). In the inviscid limit this solution reduces to a trivial solution with vanishing amplitude. For a reasonable range of physical parameters, CHANG (1977) calculated a vertical wavelength of >17 kms for the stationary response, which is a significant improvement over the inviscid theory. The horizontal structure of this solution is also in good

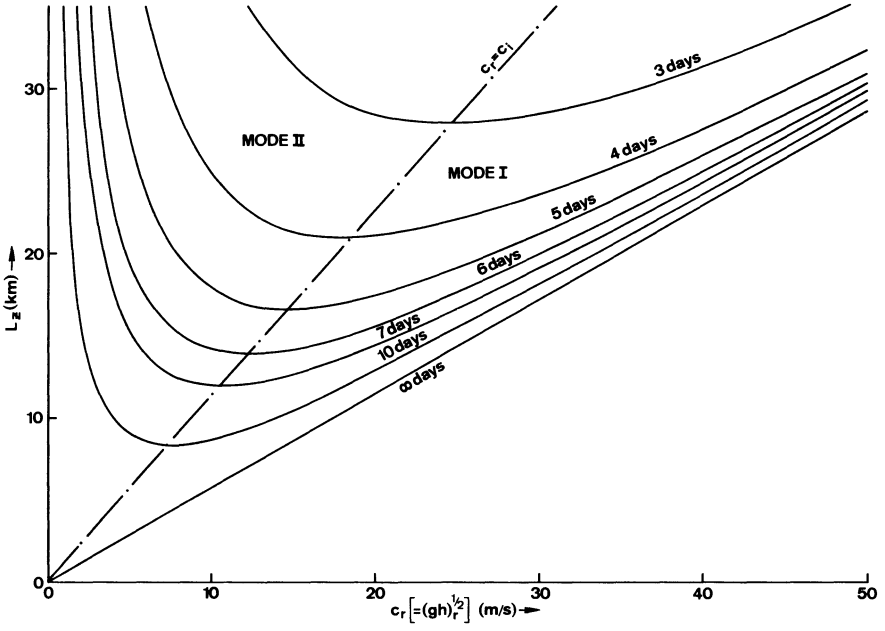

Figure 8
Real Doppler-shifted phase speed, c_r, as a function of vertical wavelength, L_z, and damping time for the Kelvin waves. (From CHANG, 1977.)

agreement with observations and WEBSTER's (1972, 1973) numerical model. This requirement of a damping mechanism with time scale on the order of 5 days is much weaker than that found by HOLTON and COLTON (1972) for the summer monsoon and could well be explained by cumulus transports. Detailed observational studies of the winter monsoon are needed to improve the theoretical understanding of this problem.

3. Localized barotropic instability of the planetary scale summer monsoon

As mentioned previously, the amplitude of stationary long waves during summer is better simulated by the nonlinear models than by the linear models when excessively large damping is excluded. This apparently is due to the barotropic energy conversions from planetary to both zonal and synoptic scales which are allowed in the nonlinear models only. Observational evidence of this type of energy conversion has been presented by KANAMITSU, KRISHNAMURTI and DEPRADINE (1972), who computed the wave-zonal flow and wave–wave energy exchanges for the tropical belt from 15°S to 15°N using the 1967 summer 200 mb wind data analyzed by KRISHNAMURTI and ROGERS (1970). In particular, they showed that the synoptic scale waves receive kinetic energy at a fairly significant rate (order of 10^{-5} m^2 sec^{-3}) from both the zonal flow and the planetary-scale waves. A similar result for the equator to 30°N belt was also obtained by KRISHNAMURTI *et al.* (1973b).

Transient synoptic-scale wave disturbances have been observed in the tropical upper troposphere in all seasons. During summer, the most active season, the disturbances are found to occur primarily in two types of regions. One type is in the vicinity of the mid-oceanic troughs (RICK, 1959; SADLER, 1967; MILLER and CARLSON, 1970; FRANK, 1970) where the disturbances may assume the form of open waves or closed vortices. Occasionally these disturbances may develop in the vertical or be coupled with low level waves, and intensification leading to tropical cyclone development sometimes may also follow. Another region of transient wave activity is along the upper tropospheric easterly jet over the Indian ocean, where KRISHNAMURTI and ROGERS (1970) have reported fairly regular occurrences of synoptic-scale disturbances. Apparently these regions are where most of the barotropic energy conversion from zonal and planetary scales to the synoptic scale takes place. Thus it appears that the nonlinear energy transfers of the summer monsoon have a persistently localized nature. Another evidence of this is related to the linear barotropic instability criterion, which has been shown by MERILEES (1968) to be usually satisfied if nonlinear energy exchanges are very prominent. The upper tropospheric zonal mean flow of the summer monsoon does not satisfy this criterion, but regions of large negative gradients of relative vorticity (Fig. 9) where this instability criterion is satisfied locally can be found in the seasonal mean 200 mb analysis (KRISHNAMURTI, 1971b). These negative vorticity gradients occur mainly in the vicinity of the easterly jet and

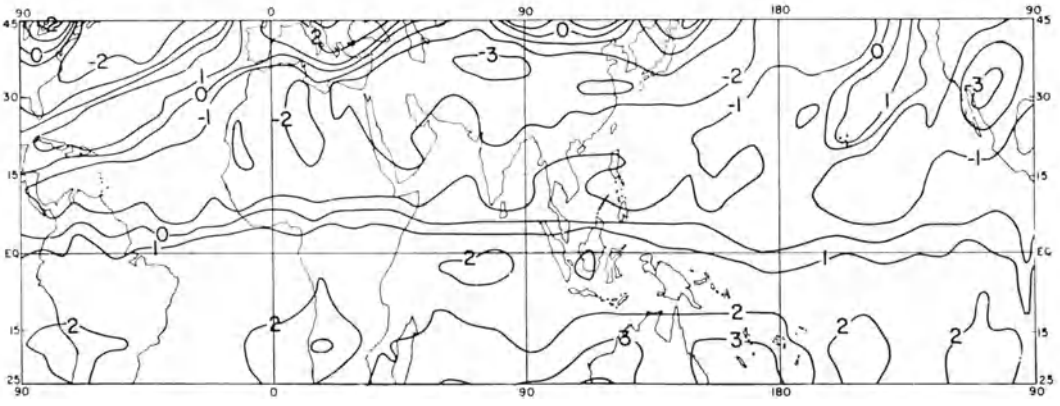

Figure 9
Summer mean (June–August 1967) relative vorticity at 200 mb, contour interval is 10^{-5} sec^{-1}. (From KRISHNAMURTI, 1971b.)

the mid-oceanic troughs, and on some individual days their magnitude may even greatly exceed the seasonal mean values. Therefore it is plausible that at least some of the transient synoptic wave activities in these regions is generated by the localized (and sometimes short term) barotropic instability, which is clearly a result of the zonal asymmetry of the planetary-scale summer monsoon.

The kinetic energy conversions from the planetary scale and the zonal flow to the synoptic scale in the upper troposphere have been simulated numerically by ABBOTT (1973) and KRISHNAMURTI *et al.* (1973a). The conversions produced by ABBOTT's (1973) model are roughly of the same order of magnitude as those computed by KANAMITSU *et al.* (1972). However, the conversions obtained by KRISHNAMURTI *et al.* (1973a) are about one order smaller. This appears to be related to their treatment of the Tibetan high as a fixed barrier which prevents vorticity transport across the boundary of the barrier. As a consequence, barotropic instability cannot be realized in the immediate vicinity of the Tibetan high and the total amount of energy extracted from the larger scales by the synoptic scale within a fixed period of time must be greatly reduced. Nevertheless, KRISHNAMURTI *et al.* (1973a) were able to simulate the gross features of the planetary scale waves in the upper troposphere, such as the mid-oceanic troughs and the Mexican high. Apparently once the strength, shape and position of the Tibetan high are fixed in the experiment, the interaction of the zonal mean flow and this blocking high is sufficient to produce mechanically many other features of the circulation.

In the numerical model by COLTON (1973), attention is focused on the development of the synoptic-scale disturbances in the easterly jet and in the mid-Pacific trough regions where the barotropic instability criterion is locally satisfied. Near the easterly jet the model produces disturbances that propagate westward at a phase speed slightly less than the local speed of the jet and continue to grow until they are well past the

longitude of the jet maximum. After reaching the maximum amplitude they begin to decay fairly rapidly. Many features of these disturbances resemble those analyzed by KRISHNAMURTI and ROGERS (1970) in the Indian Ocean and African region. In the mid-Pacific trough the model also produces waves and vortices whose movement and behavior are quite similar to those observed in daily synoptic charts. In both regions the growing disturbances exhibit a latitudinal tilt in opposition to the lateral shear of the quasi-steady basic flow, which is characteristic of the barotropically unstable waves.

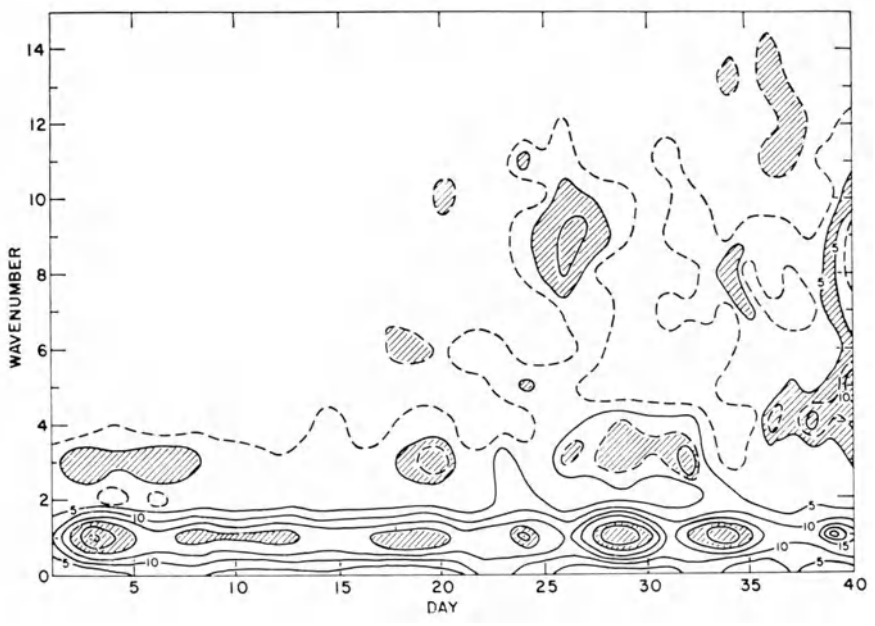

Figure 10
Zonal average kinetic energy at 20N as a function of time and wavenumber as computed by COLTON (1973). Contour interval is 5 m^2 sec^{-2}. Hatched areas are regions of energy maximum.

In studying the barotropic energy exchanges, COLTON (1973) also examined the time evolution of the computed kinetic energy spectrum. An example of this is given in Fig. 10 which shows the zonally averaged energy at 20°N as a function of time and wavenumber. A noteworthy feature is that when the energy of wavenumber 1 is at a maximum, the energy at the short waves is usually at a minimum, and vice versa. This suggests that energy exchanges take place continuously between the forced long waves and the transient disturbances. The disturbances remove energy from the planetary scale during the growing stage and feed energy back into the planetary scale during the decaying stage. As a consequence the amplitude of the time mean planetary-scale waves is smaller than that produced by a linear model. Since no dissipation is provided for the transient waves all energy extracted from the forced motion must either remain in the transient waves or be transferred back to the forced motion. COLTON

(1973) speculated that the actual damping of the planetary scale by the local barotropic instability may be more effective if some dissipation mechanism for the transient synoptic waves is included.

Although COLTON's (1973) model lacks a sufficient damping mechanism and therefore produces a basic flow that is somewhat too intense and has a phase shift problem, it nevertheless illustrates the interesting phenomenon of waves developing and decaying in a spatially varying basic flow which contains locally unstable and stable regimes. To gain further physical insight into this phenomenon, especially with respect to the easterly jet of the summer monsoon, TUPAZ, WILLIAMS and CHANG (1977) formulated a 1-level numerical model using the barotropic vorticity equation to study this problem from a linear instability point of view. In their model the basic zonal wind is approximated by a steady easterly Bickley (hyperbolic-secant-squared) jet which increases slowly from the inflow (eastern) boundary to a longitude in the middle of a rectangular domain, then decreases slowly downstream towards the outflow (western) boundary. The basic meridional wind is derived in such a way that the total basic flow is non-divergent. Periodic forcing is introduced on the inflow boundary and a radiation condition, whereby a wave is allowed to propagate its energy out of the domain, is applied at the outflow boundary. The model is integrated from zero interior perturbation streamfunction until the perturbation fields vary periodically in time at each grid point. At this quasi-steady state the waves move through the region and grow or decay in space only, in reaction to the local stability properties of the basic flow.

To compare the numerical results with the 'local growth rate' concept of the parallel flow theory, TUPAZ *et al.* (1977) developed a simple analytical model to calculate the effects of the local instabilities. This is done by considering an equation that allows for propagation and growth or decay, $\psi'_t + c(x)\psi'_x = n(x)\psi'$, where t is time, x the zonal coordinate, and ψ' the perturbation streamfunction. The local phase speed c and local growth rate n can be obtained from the parallel flow theory. When a periodic solution with a frequency ω and an amplitude $F(x)$ is introduced, the downstream variation of F with respect to a reference point x_0 may be written as

$$F(x) = F(x_0) \exp\left[-i \int_{x_0}^{x} \omega \, dx/c(x)\right] \exp\left[\int_{x_0}^{x} n(x) \, dx/c(x)\right].$$

In this equation the local wavelength is ω/c and the local spatial growth rate is n/c. Figure 11 compares the steady state envelope for ψ' of the numerical solution and the corresponding $F(x)$ for a case in which the central speed of the easterly jet is increased from 15 m sec^{-1} at $x = -10\,000$ km to 30 m sec^{-1} at $x = 0$ and then reduced to 15 m sec^{-1} at $x = 10\,000$ km. The curve for $F(x)$ can be shifted up or down in the diagram by changing x_0, but its shape does not change. Two $F(x)$ curves are included in Fig. 11, one for $x_0 = 280$ km and the other for $x_0 = 4200$ km, both based on the local wavelength distribution measured from the numerical solution. It is evident from this figure that both the numerical solution and the local growth rate of the

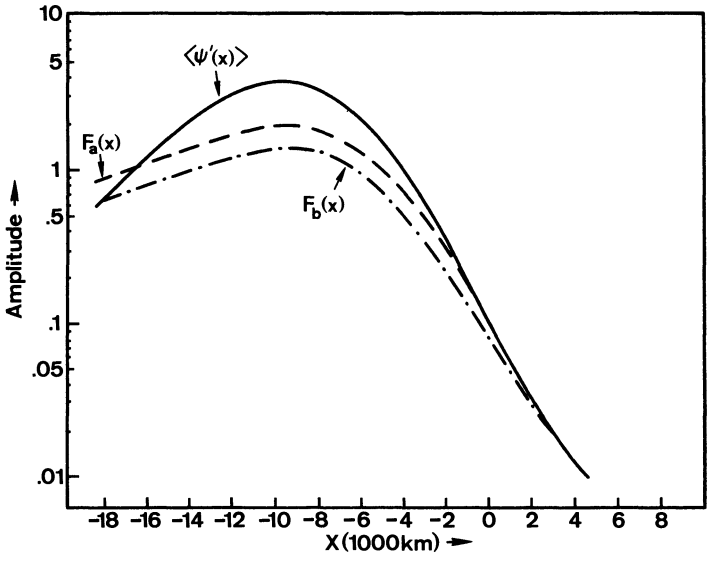

Figure 11
Comparison of wave packet envelopes in a locally unstable mean flow: $\langle\psi'\rangle$, computed from a numerical model; $F_a(x_0 = 280$ km) and $F_b(x_0 = 4200$ km), computed from an analytical model based on the parallel flow theory. (From TUPAZ *et al.* 1977.)

parallel flow theory put the maximum amplitude of the perturbations at $x = -9800$ km, well past the jet maximum. This is in good agreement with the results obtained by COLTON (1973) and CHANG and PENTIMONTI (1977), and is qualitatively consistent with KRISHNAMURTI and ROGERS' (1970) observation that the most active disturbance area extends downstream from the jet maximum near the southern tip of India to central Africa (see Fig. 10.2, top panel, of KRISHNAMURTI, 1971b). This longitude of maximum amplitude corresponds to the neutral point of the basic flow, and is immediately understandable from the local growth rate concept: a wave coming in from the inflow boundary will grow as it moves downstream in the locally unstable region, until it reaches the neutral point where it begins to decay. However, the numerical solution has a larger maximum amplitude than that predicted by the local growth rate of the parallel flow theory. The waves actually grow faster in the unstable region and decay faster in the stable region. TUPAZ *et al.* (1977) evaluated the energy equation for the numerical model and found that the most important term for perturbation energy production is the Reynold stress term proportional to the meridional shear of the basic zonal wind. This term is also the only source term for a parallel flow model, and it depends on the phase structure of the perturbation field. Figure 12 compares the local phase tilt of the wave from the numerical model with that from the parallel flow theory at two longitudes: $x = 0$ km (jet maximum) and $x = -2800$ km (slightly downstream from jet maximum). At both places the phase tilt from the numerical model is significantly larger than that of the parallel flow theory.

Thus apparently the downstream variation of the basic flow augments the phase tilt of the waves which gives a larger growth rate in the unstable region. A similar situation is found in the stable region where the dynamic damping due to the continuous spectrum effect is enhanced by a stronger tilt in the same direction of the basic shear of the easterly jet. These results indicate that the barotropic energy exchanges associated with a zonally varying easterly jet which is locally unstable can actually be more prominent than those predicted by the local growth rate from the parallel flow theory. Hence the presence of the planetary-scale asymmetries during the summer monsoon strengthens the nonlinear energy conversions resulting in significant activity of synoptic-scale disturbances.

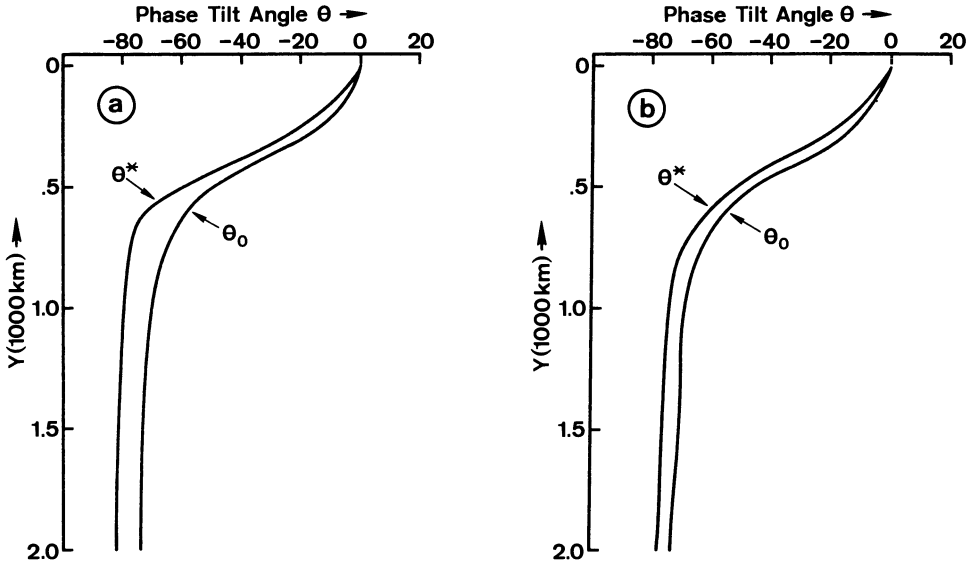

Figure 12
Comparison of the phase tilts of waves in a locally unstable mean flow computed by a numerical model (θ^*) and the parallel flow theory (θ_0) at two longitudes: (a) $x = 0$ where $\bar{u}(x, 0) = -30$ m sec^{-1} and (b) $x = 2800$ km where $\bar{u}(x, 0) = -27.3$ m sec^{-1}. (From TUPAZ *et al.* 1977.)

Although TUPAZ *et al.* (1977) employed linear equations only, their results may also shed some light on the effects of the transient waves on the basic flow. The waves remove kinetic energy from the basic flow (both zonal and planetary scale) and most of this energy is removed on the downwind side of the jet maximum. Therefore it may be expected that in a nonlinear extension of their model the planetary scale will experience maximum damping west of the easterly jet maximum, which undoubtedly will affect the amplitude and phase of the forced planetary-scale waves.

4. *Oscillations of the planetary-scale monsoons*

The summer monsoon circulation is known to exhibit many fluctuations in a variety of time scales within each season. The most notable fluctuation is the alternating active and break periods of the monsoon. During the break periods most of the circulation characteristics may diminish or even reverse over the broad monsoon region. Less dramatic variations occur more frequently than the active-break cycles, although sometimes they are limited to local regions. Figure 13 shows the power spectrum of the 1967 summer 200 mb streamfunction over a region of the Tibetan high, analyzed by KRISHNAMURTI *et al.* (1973a). A pronounced oscillation periodicity is noted around 10–13 days and a secondary spectral peak occurs near 3 days. A similar spectral distribution for the tropospheric wind field of the 1962 summer was found by M. MURAKAMI (1976), where the main peaks occur at 10–15 days and 4–5 days. Both of these investigators felt that the shorter period oscillation may be a manifestation of the synoptic-scale westward propagating monsoon depressions. The longer period oscillation, on the other hand, appears to be related to the break monsoon and other broad-scale variations of the monsoon circulation. The 10–15 day periodicity of this oscillation has also been noted during many other years. For example, it is reflected in the daily rainfall data of 1963, 1971 (MURAKAMI, 1972), and 1972, 1973 (KRISHNAMURTI and BHALME, 1976).

After detecting a spectral peak near the 13-day periodicity in many parameters of the planetary-scale monsoon system of the 1967 summer, KRISHNAMURTI and BHALME (1976) calculated the phase relationship between the oscillation of these parameters. Their result suggests that in a 13-day cycle the sequential strengthening of the mon-

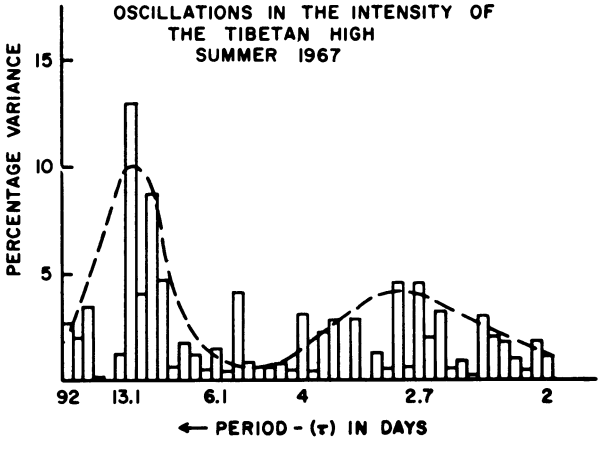

Figure 13
Percent variance spectrum of the intensity of the Tibetan High during June–August 1971. The dashed line is a smoothed envelope. (From KRISHNAMURTI *et al.*, 1973a.)

soon system including the monsoon trough, the cloud brightness, the surface Mascarene high, the upper Tibetan high and easterly jet, and the central Indian rainfall occur after the dry and moist destabilization of the lower troposphere. This will then be followed by a weakening of the system in the same sequence after dry and moist stabilization. On the other hand, M. MURAKAMI (1976) used a composite technique to study the 1962 summer monsoon, noting that it is difficult to verify the statistical significance of the cross-spectral quantities of this period range derived from a 3-month time series of daily data. He found that the intensification and weakening of convection and other low- and upper-level winds are closely in phase for the 15-day cycle during this season. In any case, there is strong evidence that many components of the planetary-scale monsoon are involved in this oscillation.

The observed 10–15 day oscillation raises an interesting question concerning its physical mechanism. KRISHNAMURTI and BHALME (1976) proposed that it may be a result of a cloud-radiative feedback mechanism in which the enhanced convection causes increased cloud cover which in turn reduces the incoming short-wave radiation and stabilizes the lower troposphere. This is then followed by decreased convection and cloudiness, and therefore increased short-wave radiative heating at the surface which renews the active convection. Another possible oscillation mechanism is revealed by a simple, domain-averaged, atmosphere-ocean interacting model by WEBSTER and LAU (1977). In their model the large heat capacity of the ocean causes it to respond slowly to the solar heating while the atmosphere temperature reaches a maximum due to heating at the land surface. After a period of time the ocean temperature peaks and this feeds back to the atmosphere through convection resulting in another temperature maximum. Although this process alone is unlikely to produce subsequent maxima without the participation of other mechanisms, it may still be relevant to some of the active-break cycles because RAMAMURTHY's (1969) survey (quoted in KRISHNAMURTI and BHALME, 1976) indicates that there are only one or two major breaks during most of the summer monsoon seasons. Other possible mechanisms for the planetary-scale oscillation may include interactions between hemispheres and between stationary and propagating long waves as mentioned by KRISHNAMURTI and BHALME (1976), and nonlinear vacillations between different scales. The latter mechanism produces a 5-day oscillation of the planetary scale in COLTON's (1973) barotropic model, which is purely dynamical and does not provide dissipation processes for the synoptic scale. If thermodynamics and synoptic damping are included, the interaction would become more complex and the oscillation period could be modified.

The planetary-scale circulation during the winter monsoon also exhibits significant variations, largely due to the influence of the cold air outbreaks from the Asian continent. These outbreaks often interfere with the main winter convective region in the maritime continent and cause widespread weather changes in the South China Sea and Malaysia–Indonesia region, including the development of strong synoptic-scale disturbance activity. Since this convective region provides the major energy

source for the thermally direct, planetary-scale east-west overturning and Hadley cells (KRISHNAMURTI *et al.* 1973b), its variations directly influence the circulations in the entire tropics and southern mid-latitudes during winter. These planetary-scale zonal and lateral teleconnections are reflected in the analyses by MURAKAMI and UNNINAYAR (1977) and KRISHNAMURTI *et al.* (1973b) despite their limited data base. The initiation and progress of theoretical studies in this area would depend heavily on the expansion of our present observational knowledge of this problem.

5. *Concluding remarks*

The three problems reviewed here are inter-related to each other. For example, the localized barotropic instability is a reflection of the strong nonlinear energy transfer which appears to be quite relevant to the damping of the planetary-scale flow during the summer monsoon. Also CHANG and PENTIMONTI's (1977) experiment indicates that these energy conversions are more pronounced when the planetary scale contains an appreciable oscillation. The enhanced upper tropospheric instability in summer due to both time and spatial variations of the planetary scale also has important ramifications for the synoptic-scale disturbances. At least in the mid-oceanic trough regions, the upper-level disturbances may develop in the vertical and could be related to some of the weather-producing easterly waves and tropical cyclones. A different type of problem arises for the winter monsoon during which the upper tropospheric synoptic-scale waves and zonal flow feed energy to the planetary scale (KRISHNAMURTI *et al.* 1973b). This on the one hand removes the nonlinear processes as a possible damping mechanism, and on the other hand requires an explanation for the energy source of the synoptic scale. Clearly much more effort is needed to answer these questions, whose importance lies in the fact that a thorough understanding of the planetary scale is crucial for the proper simulation of the entire multiple-scale monsoon circulation.

Acknowledgements

I wish to thank Professors R. T. Williams, J. R. Holton, P. J. Webster, T. Murakami, T. N. Krishnamurti and G. J. Haltiner for helpful discussion. This work was supported by the Atmospheric Science Section, National Science Foundation, under Grant DES75-10719, and by the Naval Environmental Prediction Research Facility.

REFERENCES

ABBOTT, D. A. (1973), *Scale interactions of forced quasi-stationary waves at low latitudes*, Rept. 73–2, Dept. of Meteorology, Florida State Univ., Tallahassee, 190 p.

BARCILON, A., and COOPER, A. L. (1974), *A simple model for the east–west circulations found at 200 mb*

during the summer of the northern hemisphere, Presented at Fall Annual Meeting, Amer. Geophys. Union, Abstract published in Transactions *56*, 1123.

CHANG, C.-P. (1977), *Viscous internal gravity waves and low-frequency oscillations in the tropics*, J. Atmos. Sci. *34*, 901–910.

CHANG, C.-P., and PENTIMONTI, R. J. (1977), *A numerical study of time-mean northern summer monsoon with steady and fluctuating heating*, Proc. Internatl. Sym. on Monsoons, New Delhi, India.

COLTON, D. E. (1973), *Barotropic scale interactions in the tropical upper troposphere during the northern summer*, J. Atmos. Sci. *30*, 1287–1302.

FRANK, N. L. (1970), *On the nature of upper tropospheric cold core cyclones over the tropical Atlantic*, Ph.D. thesis, Florida State Univ., Tallahassee.

HOLTON, J. R., and COLTON, D. E. (1972), *A diagnostic study of the vorticity balance of 200 mb in the tropics during the northern summer*, J. Atmos. Sci. *29*, 1124–1128.

HOLTON, J. R., and LINDZEN, R. S. (1968), *A note on "Kelvin" waves in the atmosphere*, Mon. Wea. Rev. *96*, 385–386.

KANAMITSU, M., KRISHNAMURTI, T. N., and DEPRADINE, C. (1972), *On scale interactions in the tropics during northern summer*, J. Atmos. Sci. *29*, 698–706.

KRISHNAMURTI, T. N. (1971a), *Tropical east-west circulations during the northern summer*, J. Atmos. Sci. *28*, 1342–1347.

KRISHNAMURTI, T. N. (1971b), *Observational study of the tropical upper troposphere motion field during the northern hemisphere summer*, J. Appl. Meteor. *10*, 1066–1096.

KRISHNAMURTI, T. N., and BHALME, H. N. (1976), *Oscillations of a monsoon system. Part I. Observational aspects*, J. Atmos. Sci. *33*, 1937–1954.

KRISHNAMURTI, T. N., DAGGUPATY, S. M., FEIN, J., KANAMITSU, M., and LEE, J. D. (1973a), *Tibetan high and upper tropospheric tropical circulations during northern summer*, Bull. Amer. Meteor. Soc. *54*, 1234–1249.

KRISHNAMURTI, T. N., KANAMITSU, N., KOSS, W. J., and LEE, J. D. (1973b), *Tropical east-west circulations during the northern winter*, J. Atmos. Sci. *30*, 780–787.

KRISHNAMURTI, T. N., and ROGERS, B. (1970), *200 millibar wind field June, July and August 1967*, Rept. 70-2, Dept. of Meteorology, Florida State Univ., Tallahassee.

MERILEES, P. E. (1968), *An interpretation of barotropic instability in terms of the frequency of momentum convergence*, Mon. Wea. Rev. *96*, 32–38.

MILLER, B. I., and CARLSON, T. N. (1970), *Vertical motions and the kinetic energy balance of a cold low*, Mon. Wea. Rev. *98*, 363–374.

MURAKAMI, M. (1976), *Analysis of summer monsoon fluctuations over India*, J. Meteor. Soc. Japan *54*, 15–31.

MURAKAMI, T. (1972), *Equatorial stratospheric waves induced by diabatic heat sources*, J. Atmos. Sci. *29*, 1129–1137.

MURAKAMI, T. (1974), *Steady and transient waves excited by diabetic heat sources during summer monsoon*, J. Atmos. Sci. *31*, 340–357.

MURAKAMI, T., and UNNINAYAR, M. S. (1977), *Changes in atmospheric circulations during the northern hemisphere winter*, Submitted to Mon. Wea. Rev.

PAEGLE, J., and PAEGLE, J. (1976), *On the realizability of strongly divergent supergradient flows*, J. Atmos. Sci. *33*, 2300–2307.

RAMAMURTHY, K. (1969), *Some aspects of the break in the Indian Southwest monsoon during July and August*. Forecasting Manual No. IV-18.3, India Meteor. Dept., Poona, 1–57.

REED, R. J., and RECKER, E. E. (1971), *Structure and properties of synoptic-scale wave disturbances in the equatorial western Pacific*, J. Atmos. Sci. *28*, 1117–1133.

RICKS, E. (1959), *On the structure and maintenance of high-tropospheric cold-core cyclones of the tropics*, M. S. thesis, Univ. of Chicago.

RIEHL, H. and PEARCE, R. P. (1968), *Studies on the interaction between synoptic and meso-scale weather elements in the tropics*, Rept. 126, Dept. of Atmospheric Science, Colorado State Univ., Ft. Collins.

SADLER, J. C. (1967), *The tropical upper tropospheric trough as a secondary source of typhoons and a primary source of tradewind disturbances*, Final Rept., Contract AF19(628)-3860, Air Force Cambridge Research Labs., 44 p.

SADLER, J. C. (1975), *The upper tropospheric circulation over the global tropics*, Rept. UHMET75-05, Dept. of Meteorology, Univ. of Hawaii, Honolulu, 35 p.

TUPAZ, J. B., WILLIAMS, R. T., and CHANG, C.-P. (1977), *A numerical study of the locally unstable barotropic easterly jet*, Proc. Internl. Symp. on Monsoons, New Delhi, India.

WALLACE, J. M. (1971), *Spectral studies of tropospheric wave disturbances in the tropical western Pacific*, Rev. Geophys. Space Phys. *9*, 557–612.

WEBSTER, P. J. (1972), *Response of the tropical atmosphere to local steady forcing*, Mon. Wea. Rev. *100*, 518–541.

WEBSTER, P. J. (1973), *Temporal variation of low-latitude zonal circulations*, Mon. Wea. Rev. *101*, 803–816.

WEBSTER, P. J., and LAU, K. M. W. (1977), *Simulation of the global monsoon sequence by a simple ocean-atmosphere interacting model*, Proc. Internl. Sym. on Monsoons, New Delhi, India.

WILLIAMS, K. T., and GRAY, W. M. (1973), *Statistical analysis of satellite-observed trade wind cloud clusters in the western North Pacific*, Tellus *25*, 313–336.

(Received 15th June 1977)

Pageoph, Vol. 115 (1977), Birkhäuser Verlag, Basel

Hemispheric Simulation of the Asian Summer Monsoon

By DOUGLAS A. ABBOTT[1])

Abstract – A three-level, β-plane, filtered model is used to simulate the Northern Hemisphere summer monsoon. A time-averaged initial state, devoid of sub-planetary scale waves, is integrated through 30 days on a 5° latitude-longitude grid. Day 25 through day 30 integrations are then repeated on a 2.5° grid. The planetary-scale waves are forced by time-independent, spatially varying diabatic heating. Energy is extracted via internal and surface frictional processes. Orography is excluded to simplify synoptic-scale energy sources.

During integration the model energy first increases, but stabilizes near day 10. Subsequent flow patterns closely resemble the hemisphere summer monsoon. Climatological features remain quasi-stationary. At 200 mb high pressure dominates the land area, large-scale troughs are found over the Atlantic and Pacific Oceans, the easterly jet forms south of Asia, and subtropical jets develop in the westerlies. At 800 mb subtropical highs dominate the oceans and the monsoon trough develops over the Asian land mass. The planetary scales at all levels develop a realistic cellular structure from the passage of transient synoptic-scale features, e.g., a baroclinic cyclone track develops near 55°N and westward propagating waves form in the easterlies.

Barotropic redistribution of kinetic energy is examined over a low-latitude zonal strip using a Fourier wave-space. In contrast to higher latitudes where the zonal flow and both longer and shorter waves are fed by barotropic energy redistribution from the baroclinically unstable wavelengths, the low-latitude waves have a planetary-scale kinetic energy source. Wave numbers 1 and 2 maintain both the zonal flow and all shorter scales via barotropic transfers. Transient and standing wave processes are examined individually and in combination.

Wave energy accumulates at wave numbers 7 and 8 at 200 mb and at wave number 11 in the lower troposphere. The 800-mb waves are thermally indirect and in the mean they give energy to the zonal flow. These characteristics agree with atmospheric observation. The energy source for these waves is the three wave barotropic transfer. The implications of examining barotropic processes in a Fourier wave-space, vice the more common approach of separating the flow into a mean plus a deviation, are discussed.

Key words: Monsoon: 3 level model; Hemispheric circulation.

1. Introduction

In the tropics and subtropics during the Northern Hemisphere summer months, the motion field of the upper troposphere is dominated by large amplitude, quasi-stationary, planetary waves. These waves are so persistent in the daily data that they appear almost unaltered in monthly averaged data. They are very prominent in the analyses of KRISHNAMURTI and RODGERS (1970) which consist of 200-mb streamlines and isotachs for a zonal strip (27.5°S to 47.5°N latitude) during the summer of 1967.

[1]) Headquarters Air Weather Service, Scott AFB, IL 62225, USA.

The analyzed data have been examined in detail by KRISHNAMURTI (1971a, b). He found that the wind field is highly rotational even at low latitudes and on any given day zonal harmonics one and two account for nearly 80 percent of the variance of the rotational wind. These harmonics exhibit a pronounced northeast to southwest tilt in the Northern Hemisphere. Thus, they transport westerly momentum out of the tropics toward the mid-latitude westerly jets. Wave number 1 is an upper tropospheric manifestation of the outflow of the Asian monsoon whereas wave number 2 contains the 200-mb mid-oceanic troughs created by land-ocean distribution.

The characteristics of the monsoon are discussed by FLOHN (1968) whereas the oceanic troughs are described by RAMAGE (1959) and ASPLIDEN *et al.* (1966) respectively for the Pacific and Atlantic Oceans. These planetary-scale features contain a series of smaller scale eddies on any given day. While the zonal average Hadley cell is rather weak, local Hadley cells are prominent, particularly over and south of the Asian continent. East–west overturnings of equivalent strength emanate from the Asian monsoon outflow and sink into the oceanic troughs. These have been discussed by KRISHNAMURTI (1971a). The equatorial Walker circulation (BJERKNES *et al.*, 1969) is a weak secondary feature compared to the higher latitude east–west vertical-plane circulations. The southward branch of the local Hadley cell produces an easterly jet south of Asia extending into Africa (KOTESWARUM, 1958). This jet lies between 10°N and 15°N with maximum speeds in excess of 75 m/sec near 150 mb. The jet can become barotropically unstable as synoptic-scale disturbances form and propagate through it. Krishnamurti found a peak in variances of the meridional wind around wave number 8 at 200 mb. This is somewhat longer than the synoptic waves characteristic of the lower troposphere. Indeed the two regimes seem to be uncoupled in the absence of vigorous organized convection.

The lower tropospheric flow regimes are comprehensively discussed by RIEHL (1954). The subtropical oceans are dominated by migratory anticyclones in the summer. These anticyclones statistically produce a zone of light wind and high pressure classically referred to as the horse latitudes. A strong low-level temperature inversion is found over the eastern Atlantic and Pacific Oceans. The air is relatively dry above the inversion and conditionally unstable up to mid-tropospheric levels over the entire summer tropics and subtropics. The planetary scale divergence patterns associated with continent, ocean differential heating, topography, and radiative cooling help form this inversion (LAHIFF, 1971). The inversion weakens downstream (to the west) as successive cumulus penetrations add heat and moisture to the low levels. Numerical general circulation studies such as MANABE (1969) suggest that sea surface temperatures strongly regulate cumulus activity thus controlling downstream modifications of the inversion in the strong low-level easterlies which lie south of the horse latitudes. These easterlies converge into the ITCZ, a confluent wind regime which represents a meeting of the flows from the two hemispheres formed by the 'heat equator'. During the northern summer, the ITCZ exhibits large zonal asymmetries and lies between 10°N and 25°N. Persistent quasi-stationary heat lows are found over

the subtropical continents. STRUNNING and FLOHN (1969) report that African tropical rain forests with their high evaporation rate and general cloudiness have a heat budget resembling a tropical ocean more than a continent. The arid regions to the north exhibit the highest surface temperatures and help maintain the heat lows through large earth to air sensible heat transfers. The African heat lows are generally cloud-free due to lack of moisture. Intense low-level dry convection exists in a regime of upper level, planetary scale descent. Over the Sahara desert, the surface temperature changes by 10K within 10° of latitude. The atmosphere's response to this strong baroclinic zone is an easterly jet near the 700-mb level south of the ITCZ. BURPEE (1972) found that synoptic scale easterly waves form in this region deriving their perturbation energy from barotropic and baroclinic sources. They then propagate westward through the low-level easterlies. This type of wave motion was first documented by RIEHL (1945, 1948). PALMER (1951, 1952) found similar waves over the Pacific. WALLACE (1970) used time, longitude sections of satellite cloud photos to show that waves propagating off the coast of Africa may travel all the way to the west Pacific.

Even from cursory examination of daily streamline-isotach analyses, it is evident that both the upper and lower tropospheric regimes contain considerable energy in the quasi-stationary planetary scale waves (10 000 km $\leq$ wave length). These must be forced waves as free waves of this length would retrograde westward at a rapid rate. The nature of the forcing is well known. CHARNEY and ELIASSEN (1949) showed that zonal asymmetries in orography and surface friction could produce such waves. SMAGORINSKY (1953) demonstrated that diabatic heating produced similar results. Later SALTZMAN and RAO (1964) showed that the best results require inclusion of all three forms of forcing.

It is shown in this work that the upper tropospheric manifestations of the summer monsoon can be reproduced in a quasi-barotropic numerical simulation. The simplicity of the model permits the isolation of barotropic energy processes.

2. *Experiment design*

Complete numerical simulation of the tropical general circulation is a complex problem. However, much can be learned from simple models. Scale analysis is a useful tool for isolating the physics of the dominant motions. The goal is to gain insight into barotropic energetics for the tropics.

There is no clear way to isolate the tropics from mid-latitudes. Furthermore, MAK (1969) demonstrated that events at high latitudes can exert an important influence on low latitude motions. Table 1 summarizes the scale arguments of CHARNEY (1948, 1963) and BURGER (1958). It is useful to note that all vorticity equation terms form a subset of terms contained in the quasi-geostrophic vorticity equation while all divergence equation terms form a subset of the nonlinear balance equation

terms. This suggests that these two equations are valid in both regimes for predicting first order effects of the evolution of the synoptic scale in the presence of quasi-stationary planetary scale motions. An alternate viewpoint is that insipient synoptic scale development is quasi-geostrophic in mid-latitudes and quasi-barotropic at low latitudes. The β-plane assumption can be used since the quasi-stationary nature of the planetary scale is of primary interest.

Table 1

First order terms of the vorticity and divergence equations shown by scale of motion and region of applicability. The subscripts in VI (nonlinear balance) denote partial differentiation.

Vorticity equations	Divergence equations
I. Quasi-geostrophic	IV. Geostrophic balance
$\frac{\partial}{\partial t}\nabla^2\psi = -J(\psi, \nabla^2\psi + f) + f\frac{\partial \omega}{\partial p}$	$f_0\nabla^2\psi = \nabla^2 gZ$
II. Barotropic	V. Linear Balance
$\frac{\partial}{\partial t}\nabla^2\psi = -J(\psi, \nabla^2\psi + f)$	$\nabla\cdot f\nabla\psi = \nabla^2 gZ$
III. 'Burger balance'	VI. Nonlinear balance
$J(\psi, f) = f\frac{\partial \omega}{\partial p}$	$\nabla\cdot f\nabla\psi = \nabla^2 gZ + 2J(\psi_x, \psi_y)$

Region	Scale	Vorticity	Divergence
Tropics	Synoptic	II	VI
	Planetary	III	V
Mid-latitudes	Synoptic	I	IV
	Planetary	III	V

a. Model equations

The forecast equations are the vorticity equation and the omega equation.

$$\frac{\partial}{\partial t}\nabla^2\psi = -J(\psi, \nabla^2\psi + f) + f_0\frac{\partial \omega}{\partial p} + \nu\nabla^4\psi \tag{1}$$

$$\sigma\nabla^2\omega + f_0^2\frac{\partial^2\omega}{\partial p^2} = f_0\left\{\frac{\partial}{\partial p}J(\psi, \nabla^2\psi + f) - \nabla^2 J\left(\psi, \frac{\partial\psi}{\partial p}\right)\right\} - \frac{R}{pc_p}\nabla^2 H. \tag{2}$$

The variables are defined in Table 2. If H and σ are defined and boundary conditions are specified for ψ and ω, then (1) and (2) comprise a closed system.

Table 2
Definition of independent variables, dependent variables, mathematical operators, and other parameters of the model.

Independent Variables		Mathematical Operators	
x	east-west coordinate	$J(A, B)$	Jacobian operator, operating on scalars A and B
y	north-south coordinate	∇	two-dimensional vector gradient operator
p	pressure		
t	time		

Parameters		Dependent Variables	
c_p	specific heat at constant pressure	Z	geopotential height of a pressure surface
C_d	surface frictional drag coefficient	T	temperature
f	Coriolis parameter	u	eastward velocity component
f_0	Coriolis parameter at 22°N	v	northward velocity component
g	acceleration of gravity	ψ	streamfunction of the horizontal motion field
H	diabatic heating rate	χ	horizontal velocity potential
R	gas constant for dry air	$\mathbf{V}_d$	divergent component of the horizontal wind vector
V_0	representative vector magnitude of the lower boundary rotational velocity	ω	vertical component of velocity in pressure coordinates
φ_0	representative air density at lower boundary	ω_f	frictionally induced component of omega at lower boundary
σ	static stability parameter	ω_h	time-independent component of omega at lower boundary
ν	coefficient of eddy viscosity		

b. Initialization

On any given day both stationary and transient planetary-scale waves exist. To obtain a realistic estimate of the stationary components, the wind field of time-averaged July 1967 data is analyzed at three levels (850 mb, 500 mb, and 200 mb) from the equator to 75°N. A velocity stream-function is then computed from the wind data using the indentity in (3).

$$\nabla^2\psi = \frac{\partial v}{\partial x} - \frac{\partial u}{\partial y}. \tag{3}$$

The 850-mb stream-function is linearly interpolated to 800 mb for convenience in vertical differencing, and a Fourier filter is used to remove all sub-planetary zonal harmonics so that the initial state consists of waves; $N = 0, 1, 2,$ and 3; on each pressure surface. The cosine weighted area average of the stream-function is adjusted at each level to provide vertical consistency commensurate with the assumed hydrostatic balance inherent in (2).

$$T = -f_0 p R^{-1} \frac{\partial \psi}{\partial p}. \tag{4}$$

c. Boundary conditions

The numerical model includes three levels in the vertical, each bounded laterally by the equator and 70°N. A free-slip wall is imposed at 70°N. On the equator the planetary waves of the initial state are assumed to be stationary for all time. Two boundary rows are needed to compute the nonlinear terms in (1). ω is assumed to be zero at 50 mb, while at the lower boundary ω is calculated as the sum of a frictionally induced component, ω_f, and a planetary-scale, time-independent component, ω_h. Since ψ is not defined at 950 mb, the values at 800 mb are used in (5). Note that orographic forcing is omitted. Its

$$\omega_f = -g\varphi_0 f_0^{-1} C_d V_0 \nabla^2 \psi \tag{5}$$

inclusion would have introduced a sub-planetary scale wave source thereby contaminating the experiment.

d. Steady, planetary scale forcing

If it is assumed that the data represent a reasonable approximation to the summer atmosphere's standing planetary scale waves, one can then define the distribution of divergence needed to maintain these stationary waves. The vorticity time tendency and the dissipation terms are set equal to zero in (1), and residual divergence is then calculated at each grid point. Given the point value of divergence and the upper boundary condition, downward integration yields point values of ω. ω_h can now be calculated as a residual of ω and ω_f. Next, the forcing which produces internal values of ω can be specified. Implicit in (2) is the following form of the first law of thermodynamics.

$$\frac{\partial T}{\partial t} = -J(\psi, T) + p\sigma R^{-1}\omega + c_p^{-1} H + \nu \nabla^2 T. \tag{6}$$

Stationary waves must have an associated stationary thermal structure. The diabatic heating rate, H, is calculated from (6) as all other terms are known. The cosine weighted area average of H is subtracted from each level to prevent systematic warming or cooling.

e. The integration

The initial state is integrated through 30 days on a 5° by 5° latitude–longitude grid. Day 25 is then linearly interpolated to a 2.5° by 2.5° grid and the last five days are reintegrated. A second-order, predictor-corrector time derivative is used (MATSUNO, 1966). Centered, second-order differences are used to approximate the linear spatial derivatives, and the nonlinear terms use the formulation suggested by ARAKAWA (1966).

3. *Experiment results*

During the numerical integration, the kinetic energy first increases, but then stabilizes at about day 10. The weak, time-averaged features of the initial state become obscured by transient motions on all scales and the resultant simulation closely resembles the general circulation of the Northern Hemisphere summer. Of course, the fine structure of the ITCZ is absent. Both the physics and the spatial resolution are inadequate for its representation. The 200 mb circulation patterns are particularly striking. It is of interest to compare the details of the simulated flow to those typically observed. Another interesting feature is the barotropic redistribution of kinetic energy. A comparable examination of potential energy is not undertaken since the results are predetermined to a large extent by the assumed diabatic heating. During the last few days of the experiment, mid-tropospheric synoptic scale waves develop over Africa and propagate westward. These waves are examined in some detail. A more thorough investigation of these and other features is available in ABBOTT (1973).

a. Circulation features at 200 mb

Streamline-isotach analysis of time-averaged July 1967 data is shown in Fig. 1. The large-scale features resemble the daily analyses of KRISHNAMURTI and RODGERS (1970), and the prominent climatological features discussed earlier are easily detected. While the analysis is rather subjective in data sparse regions, the data are surely adequate to resolve zonal harmonics, $N = 1$, 2, and 3. Removal of the subplanetary scale motions leaves wave patterns clearly depicting wave two with anticyclonic flow over land and cyclonic flow over the oceans. Wave 1 is evident in the dominance of the Asian high pressure zone over the Mexican zone. Wave 3 is much smaller in amplitude, but contributes to the northeast to southwest tilt of the circulations (see Fig. 2).

Day 30 of the numerical coarse-mesh integration is presented in Fig. 3. It is clear that shorter scale waves, $N = 4, 5, \ldots$, are again present. One could easily find a real data analogue to this numerical simulation. Wind speeds in the easterly and subtropical westerly jet streams range from 24 to 40 m sec^{-1} in good agreement with observation. Worthy of mention is the fact that on any random day of the integration the mid-oceanic troughs and continental high pressure zones are found near their climatological positions. The same is true at the other levels which are not shown.

The horizontal distribution of time-independent diabatic heating at 350 mb is presented in Fig. 4. The general areas of heating and cooling are in reasonable agreement with results obtained from atmospheric data by BROWN (1964); however, Brown's results contain sub-planetary scale extrema. There is close correspondence between the heating pattern and the initial vertical motion field as seen in Fig. 5. The planetary scales in the model are thermally direct in agreement with KRISHNAMURTI (1971a).

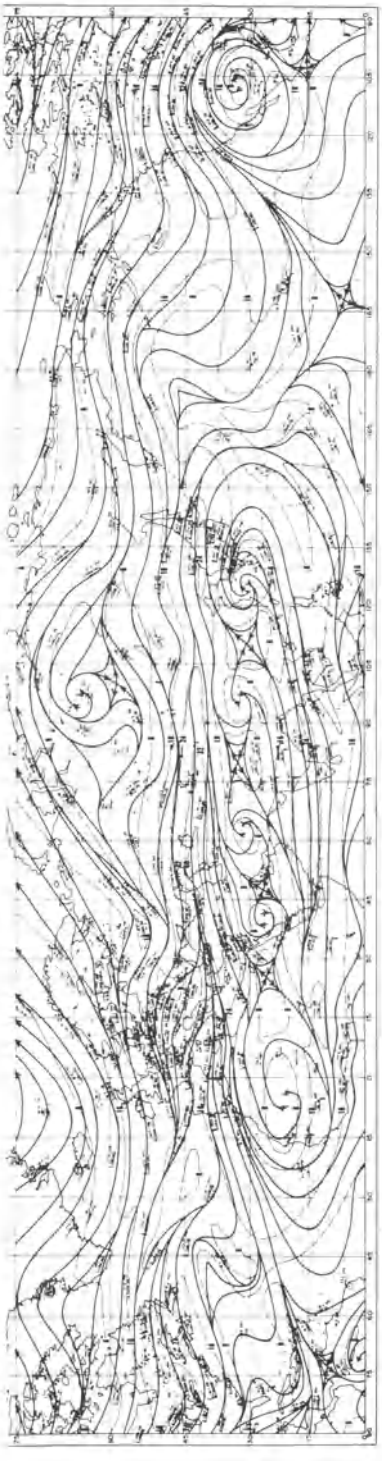

Figure 1
Streamline, isotach analysis of time-averaged, July 1967, 200-mb data. The analysis is on a mercator projection which covers the Northern Hemisphere between the equator and 75°N. The isotachs are drawn at 8 m sec^{-1} intervals.

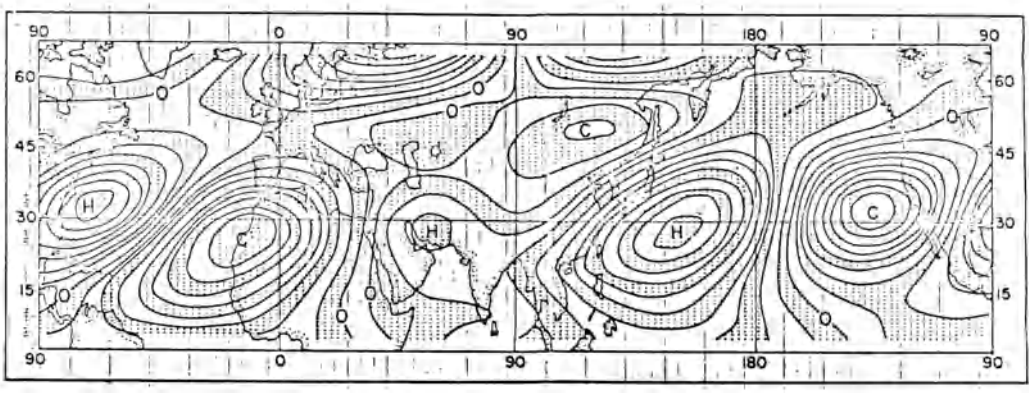

Figure 2
Initial state 200-mb streamfunction prior to removal of sub-planetary scale wave numbers, $N > 3$. Removal of these waves smooths the pattern, but changes to the large-scale features are negligible.

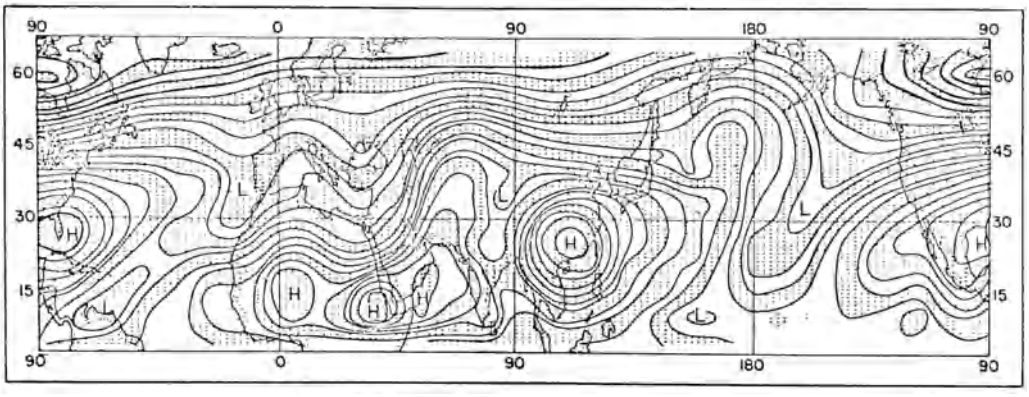

Figure 3
Streamfunction at 200 mb on day 30 of the coarse-mesh simulation.

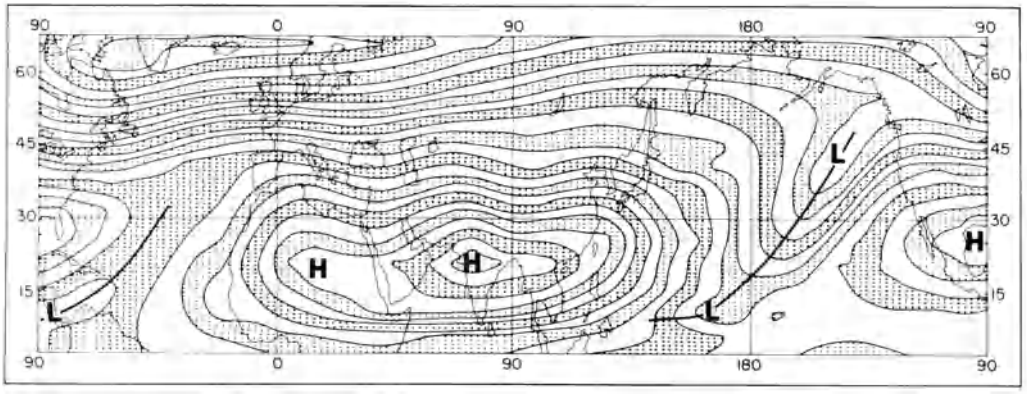

Figure 4
The horizontal distribution of time-independent, diabatic heating rate at 350 mb. Isopleths are at $5{\cdot}10^{-3}$ $m^2\ sec^{-3}$ intervals.

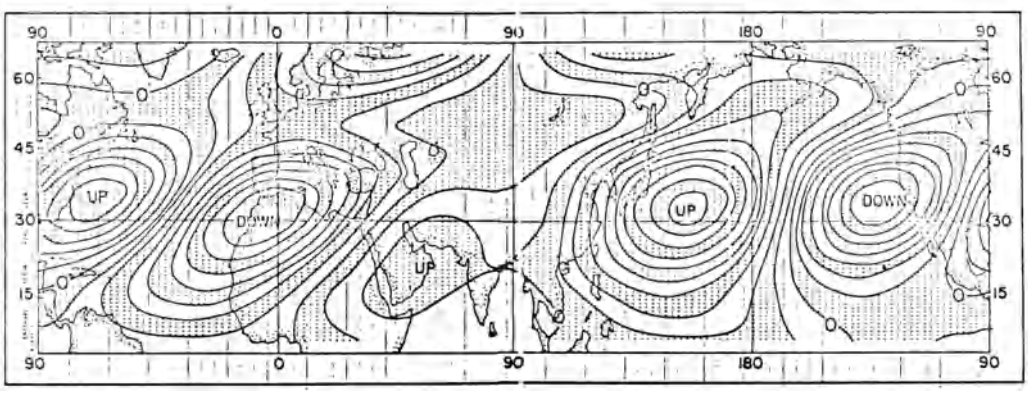

Figure 5
Initial distribution of omega at 350 mb. The isopleth interval is 10^{-4} mb sec^{-1}.

The origin and termination of the horizontal portion of the planetary-scale, east–west overturning can be computed from continuity considerations.

$$\nabla^2 \chi = \frac{\partial \omega}{\partial p} \tag{7}$$

$$\mathbf{V}_d = -\nabla \chi. \tag{8}$$

These divergent flows emanate from positions a few degrees westward of the maximum upward motions and converge into regions a few degrees southward of the maximum sinking motions. The fields of χ, ω, and H are consistent with one another in the model, but the extrema are shifted eastward of the ψ extrema. In the atmosphere the extrema of ψ and χ are nearly coincident (KRISHNAMURTI, 1971b), while the distributions of ω and H are not well known.

Using linear theory, HOLTON and COLTON (1972) examine the energetic consequences of the superposition of these extrema. Because of the large production of anticyclonic vorticity in the vicinity of the anticyclonic maxima, they find an extremely high value of dissipation is required. Obviously, the nonlinear wave-to-wave energy transfers must produce the bulk of the required dissipation. COLTON (1973) verifies this. Another possibility also exists. KRISHNAMURTI and HAWKINS (1968) suggest that mass flux in cumulus elements statistically distributed over large-scale waves can dominate (in a thermodynamic sense) the vertical motions associated with the waves. Neglect of production and destruction of vorticity by meso- and cumulus-scale motions may well account for the phase difference between waves in the ψ and χ fields. The simplicity of the model used here precludes investigation of this possibility; however, the barotropic processes are examined in some detail.

b. Barotropic energy conversions

A rather complete picture of mid-latitude energetics has evolved during the past two decades. Excellent survey articles are available in OORT (1964) and SALTZMAN (1970). These studies show that North of 20°N in summer, waves $N = 1, 2, \ldots, 15$ are all barotropically stable (wave-zonal interactions increase the energy of the zonal flow) and waves $N = 2$ and $N = 6, 7, \ldots, 10$ supply energy to both longer and shorter waves via barotropic wave-to-wave energy transfers. The energy sources are presumably thermal forcing related to land-sea distribution for wave number 2 and baroclinic instability for wave numbers 6 through 10.

The behavior of the kinetic energy spectrum is quite different at lower latitudes. KANAMITSU *et al.* (1972) considered a 15°S to 15°N strip of the 200-mb subjective analyses of KRISHNAMURTI and RODGERS (1970) and computed the summer average barotropic exchanges. KANAMITSU *et al.* (1972) isolate the time rate of change of kinetic energy associated with a zonal harmonic $N < 16$ produced by nonlinear interactions with wave numbers M and P. Vertical advection terms are not included. Figure 6 compares these results to those obtained from identical calculations averaged over the last 20 days of a 7.5°N to 20°N strip of the coarse-mesh simulation under

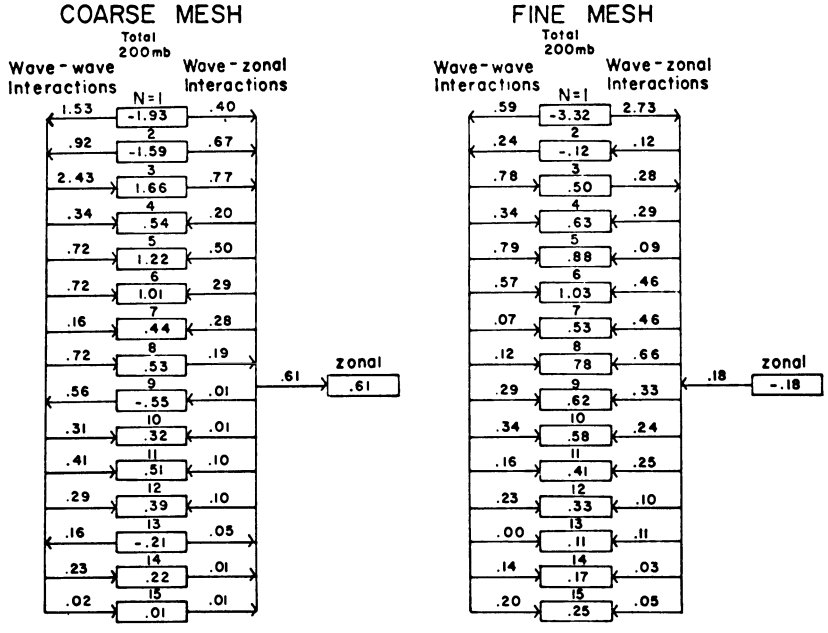

Figure 6

Total wave-space kinetic energy barotropic redistribution at 200 mb from the coarse-mesh twenty day average is shown with the corresponding fine-mesh atmospheric data energy redistribution from KANAMITSU *et al.* (1972). Only the three wave–wave interactions are included. The regions are 7.5°N to 20°N for the coarse-mesh and 15°S to 15°N for the fine-mesh. Units are 10^{-5} m^2 sec^{-3}.

consideration here. (See Appendix I, KANAMITSU *et al.* (1972) for the explicit mathematical form of the energy equation.) The overall agreement of the simulation and the atmospheric data indicates the importance of large scale barotropic processes at low latitudes. The primary differences are the direction of the wave number 2, zonal flow exchange and the direction of transfer of the cumulative wave, zonal flow exchange. Since the north–south slope of wave number 2 reverses in the 15°S to 15°N region (KRISHNAMURTI, 1971a), but not in the 7.5°N to 20°N region it is possible that the former difference results from the different regions considered. The results of KIDSON *et al.* (1969) indicate this is the case for the latter difference as both studies agree in their respective areas of applicability.

The total average exchange has been further broken into a steady and a transient part for each wave number. These results are summarized in Fig. 7. The exchanges are grouped into planetary and sub-planetary scales based on the observed direction of three-wave energy exchanges. In spite of the different zonal strips and time averages, the results are in excellent agreement. In contrast to mid-latitude dynamics, wave numbers $N > 2$ tend to receive energy from the zonal flow. The energy of the zonal flow is in turn maintained by the planetary waves. The bulk of the synoptic scale wave energy does not come from classical barotropic instability, but rather from three-wave energy transfers involving the planetary scale waves. The planetary

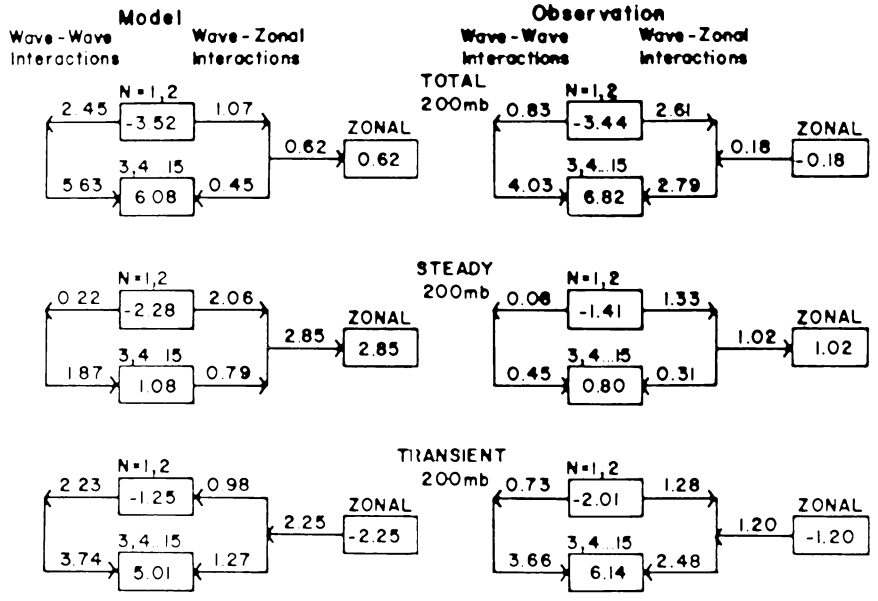

Figure 7

Composite information from Figure 6. *Model* is from the coarse-mesh 20 day experiment and *observation* is from KANAMITSU *et al.* (1972). The total exchanges are further separated into steady and transient parts with all three categories (total, steady, and transient) summed over the indicated wave groups. The region is 7.5°N to 20°N and units are 10^{-5} m^2 sec^{-3}.

scale waves are in turn maintained by the thermally direct monsoonal, vertical-plane circulations. Clearly, studies using a 'local' mean wind to investigate classical barotropic instability are capturing the planetary-scale contribution via aliasing. What appears to be zonal flow to wave transfer is likely to be dominated by the aliased three-wave transfers. Of course, the results of such studies will be dependent on the distance over which the local average is computed.

c. Fine-mesh, coarse-mesh comparison

The effects of horizontal resolution in finite difference models have been addressed by MANABE *et al.* (1970), WELLCK *et al.* (1971), and others. All findings are in general agreement, a primary result being that eddy transport processes are more efficient in high resolution models and the intensity of the resultant general circulation is stronger. These effects are due to better resolution of gradients and the shift of eddy dissipation to sub-synoptic scale motions.

Additional interesting insights are gained from inspection of nonlinear barotropic energy transfers in wave space with parallel coarse and fine grid experiments. Since the parallel experiment involves only a five-day period, the results will not necessarily be identical to longer averages. Furthermore, in the present experiment there is no 'truth' to which the results can be compared. However, the fine-mesh model presumably more closely approximates the barotropic nature of the tropical atmosphere. With this in mind, consider the five-day averages in Fig. 8 and the longer term results presented earlier in Fig. 6. The dominant features are the energy sources at wave numbers 1 and 2, energy accumulation at wave number 3, and a secondary accumulation at wave number 8. Wave numbers $N > 3$ tend to receive energy from the zonal flow given a sufficiently long time average. Yet, a given wave number fluctuates between barotropic stability and instability in cycles of a few days.

The instantaneous exchanges were computed for day 26, 27, and 28 of the coarse and fine mesh experiments. Only day 28 is shown here; see Fig. 9 (additional results are available in ABBOTT, 1973). Since the initial states were identical at day 25, this provides a view of the spatial truncation problem via wave-space energetics. Day 26 marks the end of the first 24 hours of the parallel forecast. The direction and magnitude of both wave-to-wave and wave-to-zonal energy exchanges are in general agreement for $N \leq 10$. Discrepancies become more common at day 27 and by day 28 the relationship between the two is nearly random. Two interesting features stand out. First, the daily planetary-scale exchanges have the same direction as their time averages, but sub-planetary scale daily exchanges change direction from day to day. This suggests that planetary-scale energy transfers are more systematic. Secondly, waves 7 and 8 tend to accumulate energy from day to day as well as in the time average. KRISHNAMURTI (1971b) found a wave number 8 spectral peak in the daily-average summer v wind-component spectra, and KANAMITSU *et al.* (1972) found a corresponding peak in the wave-space energy transfers. The systematic accumulation of

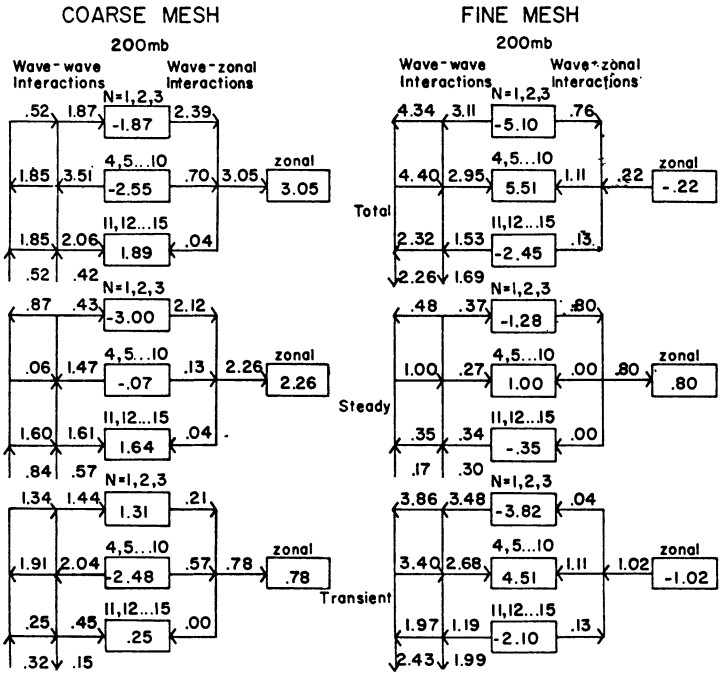

Figure 8

Flow diagram for the kinetic energy exchanges at 200 mb from five day average fine-mesh and parallel coarse-mesh experiments. The wave–wave interactions are separated into a sum of three-wave and two-wave (left), three-wave (right), and interactions with waves $N > 15$ (below). The region is 7.5°N to 20°N and units are 10^{-5} m^2 sec^{-3}.

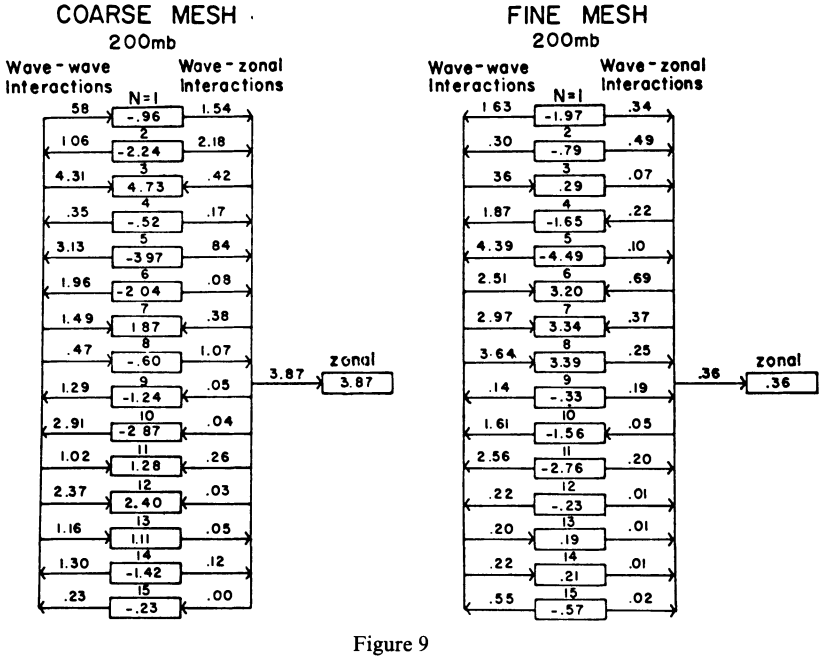

Figure 9

Wave space kinetic energy transfers at 200 mb on day 28 of the coarse- and fine-mesh experiments. Only the three wave–wave interactions are included. The region is 7.5°N to 20°N and units are 10^{-5} m^2 sec^{-3}.

energy at this wave number suggests that it is a poorly tuned resonant mode of the regime characteristic of the 200-mb tropical summer circulation.

d. Easterly waves

Late in the experiment, easterly waves develop over the African continent at 500 mb. Since the model is dry these waves do not amplify significantly as they propagate westward. Figure 10 displays a three-dimensional cross-section of the atmosphere on day 3 of the fine mesh experiment. The geographical region covers the

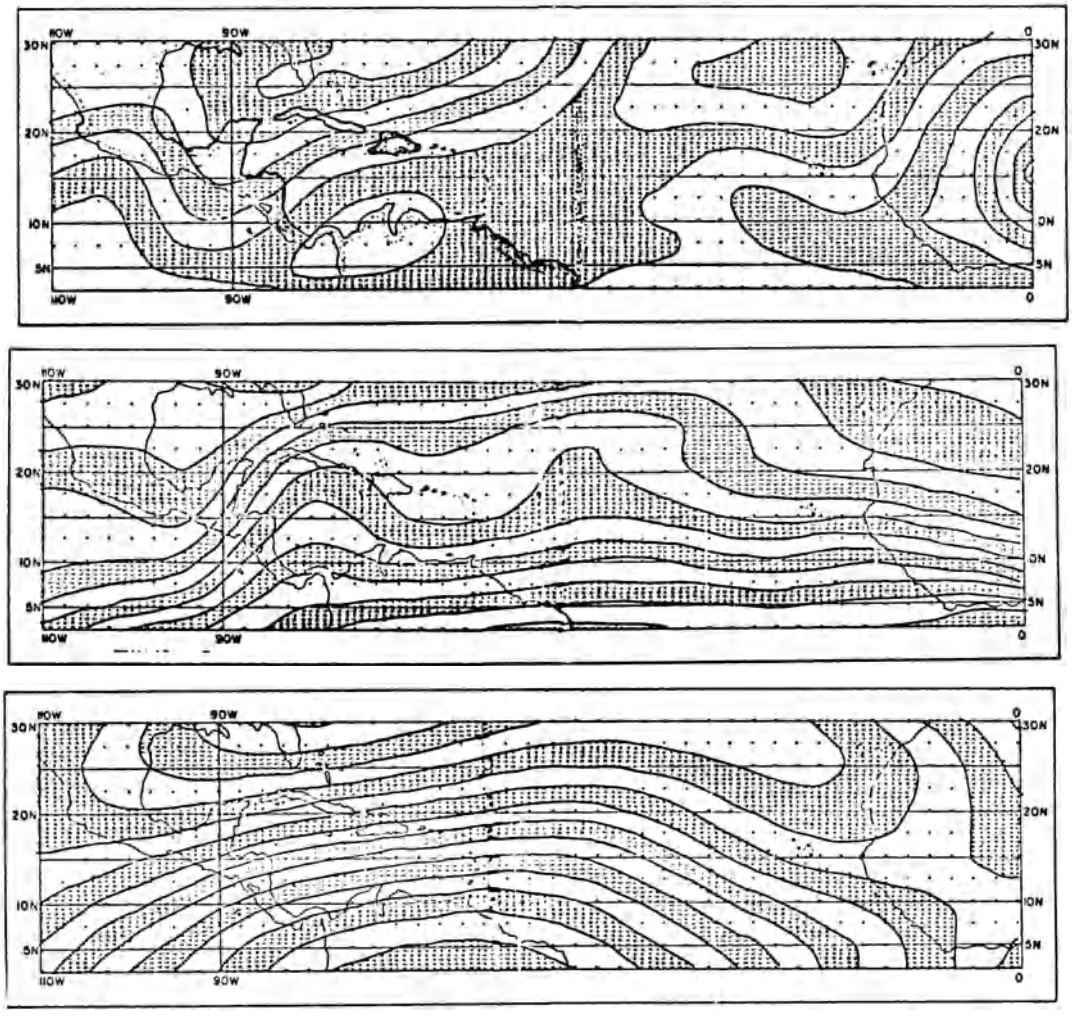

Figure 10
Streamfunction at three levels over the South Atlantic Ocean on day 28 (day three of the fine-mesh experiment). From bottom to top are the 800-mb, 500-mb, and 200-mb fields from the fine-mesh experiment.

South Atlantic from 0° to 110°W longitude and 2.5°N to 30°N latitude. At 800 mb the waves are not discernible, but the subtropical high lies along the northern boundary with the climatological col near the eastern extremity of the region. Strong easterly trade winds (blowing parallel to the stream-function isopleths) are evident. At 500 mb there are two distinct waves near the center of the region. At 200 mb the western extremity of the Asian, African anticyclone complex is at the extreme right. The mid-oceanic trough extends through the center of the region from upper right to lower left of center. A portion of the Mexican anticyclone is at the upper left and an easterly wave which has passed through the region is at the extreme left. While this atmosphere has developed from a highly artificial initial state, it is characteristic of a typical summer day.

The 500-mb waves are predominantly wave number 11. Systematic wave-to-wave energy transfers increase the energy of this wave number throughout the latter five days of both experiments. A smaller amount of energy is transferred from wave number 11 to the zonal flow. Thus, even though the wave is barotropically stable in the classical sense, it receives substantial amounts of energy via barotropic processes. Figure 11 shows that while the larger scale motions are thermally direct, wave number 11 is dissipating kinetic energy by converting it to potential energy. The 650-mb vertical motion patterns are representative of small scales at 500 mb since the short waves do not have significant amplitude at 800 mb.

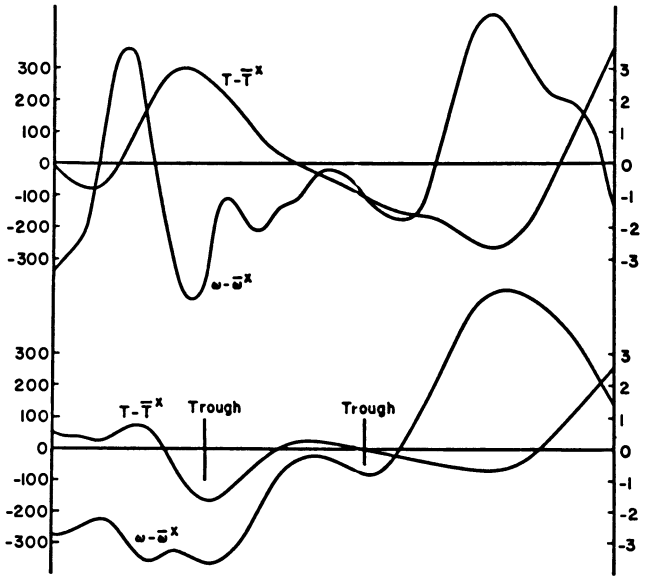

Figure 11

Vertical x-p cross section on day 28 at 17.5°N. The upper diagram pertains to 350 mb and the lower diagram pertains to 650 mb. Units are in degrees Kelvin (right) and 10^{-6} mb sec^{-1} (left). The easterly wave troughs are indicated for the 500-mb wave number 11.

If due account is taken of the lack of vertical resolution it is readily seen that the behavior and structure of these waves are in good agreement with observation (RIEHL, 1954). The waves have a cold core with subsidence west of the trough axis and rising motion to the east. They are barotropically stable and they are converting kinetic energy into potential energy. An examination of the horizontal boundary flux of energy in wave-space (not shown here) reveals that wave number 11 energy is being exported from the 7.5°N to 20°N zonal strip. Thus there is no question of the local barotropic energy source.

4. Summary and conclusions

The large-scale climatology of the upper tropospheric tropical summer is shown to form via the inclusion of east–west heating in a hemispheric general circulation experiment. On the synoptic scale, the model is quasi-geostrophic at high latitudes and quasi-barotropic in the tropics. Time-independent, zonally asymmetric heating is the only important external forcing. Throughout the integration the large scale monsoonal features maintain their climatological positions (e.g., 200-mb anticyclonic ridges remain over land areas and mid-oceanic troughs remain over the oceans, etc. The initial state contains only planetary scales; however, after the first 10 days, the planetary scales become more cellular, the cells being composed of shorter transient scales. This cellular structure is in essential agreement with the structure of the upper tropical troposphere. An easterly jet forms over the Indian Ocean at about 10°N and periodically extends into Africa. This is also in agreement with observation. Subtropical jet streams form on the east sides of the oceanic troughs and baroclinic cyclone tracks are seen in the westerlies near 55°N. At 500 mb, a low-level easterly jet develops over Africa and easterly waves begin to propagate westward from the vicinity of Africa. Given the lack of vertical resolution in the present model, this feature also agrees with observation.

The vertical-plane, solenoidal circulation can be inferred from the vertical velocity patterns. Locally strong Hadley cells and intense east–west circulations exist. The east–west circulations are in general agreement with KRISHNAMURTI (1971a), but the maxima are shifted somewhat eastward. The diabatic heating rate which drives the vertical circulations is in reasonable agreement with observation (BROWN, 1964).

The kinetic energy budget is examined in detail using a Fourier wave-space representation of the energy equations. Only the region from 7.5°N to 20°N is considered. Calculations (not presented) indicate the energetics of higher latitudes agree with SALTZMAN (1970). A 20-day average from the model atmosphere is compared to the summer average results of KANAMITSU *et al.* (1972). Potential energy budgets are not examined since they are predetermined by the experiment design. The energy calculations produce a number of interesting results.

Parallel coarse and fine mesh integrations indicate the role of barotropic energetics

in the known relationship between horizontal resolution and model accuracy. Whereas in the early portion of the parallel experiments the direction and magnitude of the nonlinear energy transfers are in general agreement for wave numbers $N < 10$. This agreement has deteriorated markedly 48 hours later. Agreement is poor from the beginning for shorter waves even though these waves are well resolved in both models. It appears that one of the major problems in short term predictability is the inability of relatively coarse grids to accurately predict nonlinear barotropic processes. When the wave-to-wave accumulation of energy on a given wave number proceeds in the wrong direction for a sufficiently long time to rival the initial wave-energy predictability is lost.

The planetary-scale asymmetries of diabatic heating have a dominant role in creating and maintaining the observed tropical and subtropical climatological motion field. Available potential energy is created on the planetary scale. Most of this energy is baroclinically converted to kinetic energy thus maintaining the energy of the atmosphere's very long waves. This planetary-scale energy is subsequently transferred barotropically to both the zonal flow and to higher wave numbers. These transfers are the primary energy source for the observed zonal flow and for synoptic-scale eddy motions.

The barotropic kinetic energy transfers from planetary-scale motions to smaller scales provide an alternate view of the nature of barotropic processes. KUO (1949) shows that a necessary condition for waves to barotropically amplify at the expense of the energy of the zonal flow is the existence of a critical point in the north–south absolute vorticity distribution. This study has shown that waves can amplify barotropically in the absence of zonal instability. The wave-to-wave interactions are an important energy source for preferred wavelengths. The preferred wavelengths (wave numbers 7 and 8 at 200 mb and 11 at 500 mb) correspond to observed spectral peaks in the energy transfers and in the atmospheric wave energy. This mechanism appears to be the energy source for the thermally indirect, barotropically stable waves in the low-level easterlies. The source is not apparent when all waves are summed as the wave-to-wave exchange becomes identically zero. The bulk of the energy comes from the planetary scale. The planetary scale is in turn maintained by the thermally forced monsoonal circulations. Investigation of heat sources and their distribution is a goal of MONEX. Perhaps an understanding of the redistribution of potential energy in wave-space will be forthcoming.

Acknowledgements

The author is indebted to Prof. T. N. Krishnamurti for his advice and guidance and to Dr. M. Kanamitsu for the computer program which calculates wave-to-wave energy transfers. Financial support for this work was received at Florida State University by the Atmospheric Science Section of the National Science Foundation,

Grant GA 17822; the Department of Defense THEMIS Contract No. DAAB-07-69-C-0062; the U.S. Naval Oceanographic Office Contract No. N62306-70-C-0451; and the Air Force Institute of Technology. Computer support was provided by the National Center for Atmospheric Research (sponsored by National Science Foundation).

REFERENCES

ABBOTT, D. A. (1973), *Scale interactions of forced quasi-stationary planetary waves at low latitudes*, PhD Dissertation, Dept. of Meteorology, Florida State University, 155 pp.

ARAKAWA, A. (1966), *Computational design for long term numerical integration of fluid motion*, Computational Physics, *1*, 119–145.

ASPLIDEN, C. I., DEAN, A. G. and LANDERS, H. (1966), *Satellite study, tropical North Atlantic, 1968*, Report No. 66-4, Florida State University.

BJERKNES, J. (1969), *Atmospheric teleconnections from the equatorial Pacific*, Mon. Wea. Rev. *97*, 163–172.

BROWN, J. A. (1964), *A diagnostic study of tropospheric diabatic heating and the generation of available potential energy*, Tellus *16*, 371–388.

BURGER, A. P. (1958), *Scale considerations of planetary motions of the atmosphere*, Tellus *10*, 195–205.

BURPEE, R. W. (1972), *The origin and structure of easterly waves in the lower troposphere of North Africa*, J. Atmos. Sci. *29*, 77–90.

CHARNEY, J. G. (1948), *On the scale of atmospheric motions*, Geophys. Publ. *17*, 17 pp.

CHARNEY, J. G. (1963), *A note on large-scale motions in the tropics*, J. Atmos. Sci. *20*, 607–609.

CHARNEY, J. G. and ELIASSEN, A. (1949), *A numerical method for predicting the perturbations of the middle latitude westerlies*, Tellus *1*, 38–54.

COLTON, D. E. (1973), *Barotropic scale interactions in the tropical upper troposphere during the northern summer*, J. Atmos. Sci. *30*, 1287–1302.

FLOHN, H. (1968), *Contributions to a meteorology of the Tibetan highlands*, Atmos. Sci. Paper No. 130, Colorado State Univ., Fort Collins.

HOLTON, J. R. and COLTON, D. E. (1972), *A diagnostic study of the vorticity balance at 200 mb in the tropics during the northern summer*, J. Atmos. Sci. *29*, 1124–1128.

KANAMITSU, M., KRISHNAMURTI, T. N. and DEPRADINE, C. (1972), *On scale interaction in the tropics during northern summer*, J. Atmos. Sci. *29*, 698–706.

KIDSON, J. W., VINCENT, D. G. and NEWELL, R. E. (1969), *Observational studies of general circulation of the tropics: Long term mean values*, Quart. J. Roy. Meteor. Soc. *95*, 258–287.

KOTESWARUM, P. (1958), *The easterly jet stream in the tropics*, Tellus *10*, 43–57.

KRISHNAMURTI, T. N. (1971a), *Tropical east–west circulations during the northern summer*, J. Atmos. Sci. *28*, 1342–1347.

KRISHNAMURTI, T. N. (1971b), *Observational studies of the tropical upper tropospheric motion field during the Northern Hemisphere summer*, J. Appl. Meteor. *10*, 1066–1096.

KRISHNAMURTI, T. N. and HAWKINS, R. S. (1970), *Mid-tropospheric cyclones of the southwest monsoon*, J. Appl. Meteor. *9*, 440–458.

KRISHNAMURTI, T. N. and RODGERS, E. B. (1970), *200-mb wind field June, July, and August, 1967*, Report No. 70-2, Dept. of Meteorology, Florida State University, 114 pp.

KUO, H. L. (1949), *Dynamic instability of two-dimensional non-divergent flow in a barotropic atmosphere*, J. Meteor. *6*, 105–122.

LAHIFF, L. N. (1971), *A numerical study of a subtropical marine stable layer*, PhD Dissertation, Dept. of Meteorology, Florida State University.

LORENZ, E. N. (1955), *Available potential energy and the maintenance of the general circulation*, Tellus *7*, 157–167.

LORENZ, E. N. (1972), *Barotropic instability of Rossby wave motions*, J. Atmos. Sci. *29*, 258–264.

MAK, M. K. (1969), *Laterally driven stochastic motions in the tropics*, J. Atmos. Sci. *29*, 41–63.

MANABE, S. (1969), *The atmospheric circulation and the hydrology of the earth's surface*, Mon. Wea. Rev. *97*, 739–774.

MANABE, S., SMAGORINSKY, J., LEITH, J. L. Jr., and STONE, H. M. (1970), *Simulated climatology of a general circulation model with a hydrologic cycle: III. Effects of increased horizontal computational resolution*, Mon. Wea. Rev. *98*, 175–212.

MATSUNO, T. (1966), *Numerical integrations of the primitive equations by a simulated backward difference method*, J. Meteor. Soc. Japan *44*, 76–84.

OORT, A. H. (1964), *On estimates of the atmospheric energy cycle*, Mon. Wea. Rev. *92*, 483–493.

PADRO, J. (1973), *A spectral model for CISK-barotropic energy sources for tropical waves*, Quart. J. Roy. Meteor. Soc. *99*, 468–479.

PALMER, C. E., *Tropical meteorology*, in *Compendium of Meteorology* (Am. Met. Soc. 1951), pp. 859–880.

PALMER, C. E. (1952), *Tropical meteorology*, Quart. J. Roy. Meteor. Soc. *82*, 123–164.

RAMAGE, C. S. (1959), *Hurricane development*, J. Meteor. *16*, 227–237.

RIEHL, H. (1945), *Waves in the easterlies and the polar front in the tropics*, Dept. of Meteorology, Univ. of Chicago Misc. Rept. 17, 79 pp.

RIEHL, H. (1948), *On the formation of typhoons*, J. Meteor. *5*, 247–264.

RIEHL, H., *Tropical Meteorology*, McGraw-Hill (New York, 1954), 392 pp.

SALTZMAN, B. (1957), *Equations governing the energetics of the large scales of atmospheric turbulence in the domain of wave number*, J. Meteor. *14*, 513–523.

SALTZMAN, B. (1970), *Large-scale atmospheric energetics in the wave-number domain*, Rev. Geophys. Space Phys. *8*, 289–302.

SALTZMAN, B. and SANKAR RAO, M. (1964), Final Report. General Circulation Research, U.S.W.B. Contract No. CWB-10763.

SMAGORINSKY, J. (1953), *The dynamical influence of large scale heat sources and sinks on the quasi-stationary mean motions of the atmosphere*, Quart. J. Roy. Meteor. Soc. *79*, 342–366.

STRUNING, J. O. and FLOHN, H. (1969), *Investigations on the atmosphere circulation about Africa*, Meteorologisches Institut der Universitat Bonn, 55 pp. (Heft 10).

WALLACE, J. M. (1970), *Time-longitudinal sections of tropical cloudiness* (Dec. 1966–Nov. 1967). Dept. of Atmos. Sci., Univ. of Washington, ESSA, National Satellite Center, ESSA Technical Report NESC 56.

WELLCK, R. E., KASAHARA, A., WASHINGTON, W. M. and DESANTO, G. (1971), *Effect of horizontal resolution in a finite-difference model of the general circulation*, Mon. Wea. Rev. *99*, 673–683.

YANG, C. H. (1967), *Nonlinear aspects of the large-scale motion in the atmosphere*, Sci. Report No. 08759-1, Dept. of Meteorology and Oceanography, Univ. of Michigan, Ann Arbor.

(Received 15th June 1977)

Pageoph, Vol. 115 (1977), Birkhäuser Verlag, Basel

Diagnosis of the Satellite-Observed Radiative Heating in Relation to the Summer Monsoon

By JAY S. WINSTON[1]) and ARTHUR F. KRUEGER[1])

Abstract – Seasonal and monthly global patterns of outgoing longwave radiation, albedo, absorbed solar radiation, and net radiation have been derived from scanning radiometer observations aboard the NOAA polar orbiting satellites since June 1974. These patterns, along with patterns of interannual differences in seasonal and monthly heating, are examined for the three summers of 1974–76 over the Eastern Hemisphere in relation to the variations in the summer monsoon and the major circulation features. During portions of the summer of 1975 the monsoon was more active than in 1974 and 1976, as evidenced by increased albedo and decreased longwave radiation over large sections of India, the Indian Ocean, Southeast Asia, and the Western Pacific. The roles of clouds, snow cover, and other surface characteristics in modulating the radiation balance and circulation are discussed. The pre-monsoon radiative heating in spring is examined with respect to monsoon onset and intensity in the three years.

Key words: Monsoon: role of radiative heating.

1. Introduction

Values of the components of the earth-atmosphere radiation budget over the globe have been derived from scanning radiometer measurements aboard the NOAA polar orbiting satellites since June 1974. These components consist of the outgoing longwave radiation, the albedo and the absorbed solar radiation, and the net radiation. Maps of these quantities are routinely prepared for months and seasons. Important details of the procedures for obtaining these radiation values are described elsewhere (GRUBER, 1977), but it should be noted that the observations are taken near 9 a.m. and 9 p.m. local standard time so that the albedo is derived solely from a morning observation, while the outgoing longwave radiation is the mean of the two observation times.

In this paper the radiation budget components are examined with respect to the Asian summer monsoon for the years 1974–76. The main purpose of this examination is to gain some initial insights into the basic climatology of the radiative energy budget of the monsoon, and also, for the three years of radiation data, some of the year-to-year variations in the energy budget and the monsoon. Since the summer Asian monsoon is such a large-scale phenomenon, the analysis of the radiation budget patterns

[1]) National Oceanic and Atmospheric Administration, National Environmental Satellite Service, Washington, D.C. 20233, USA.

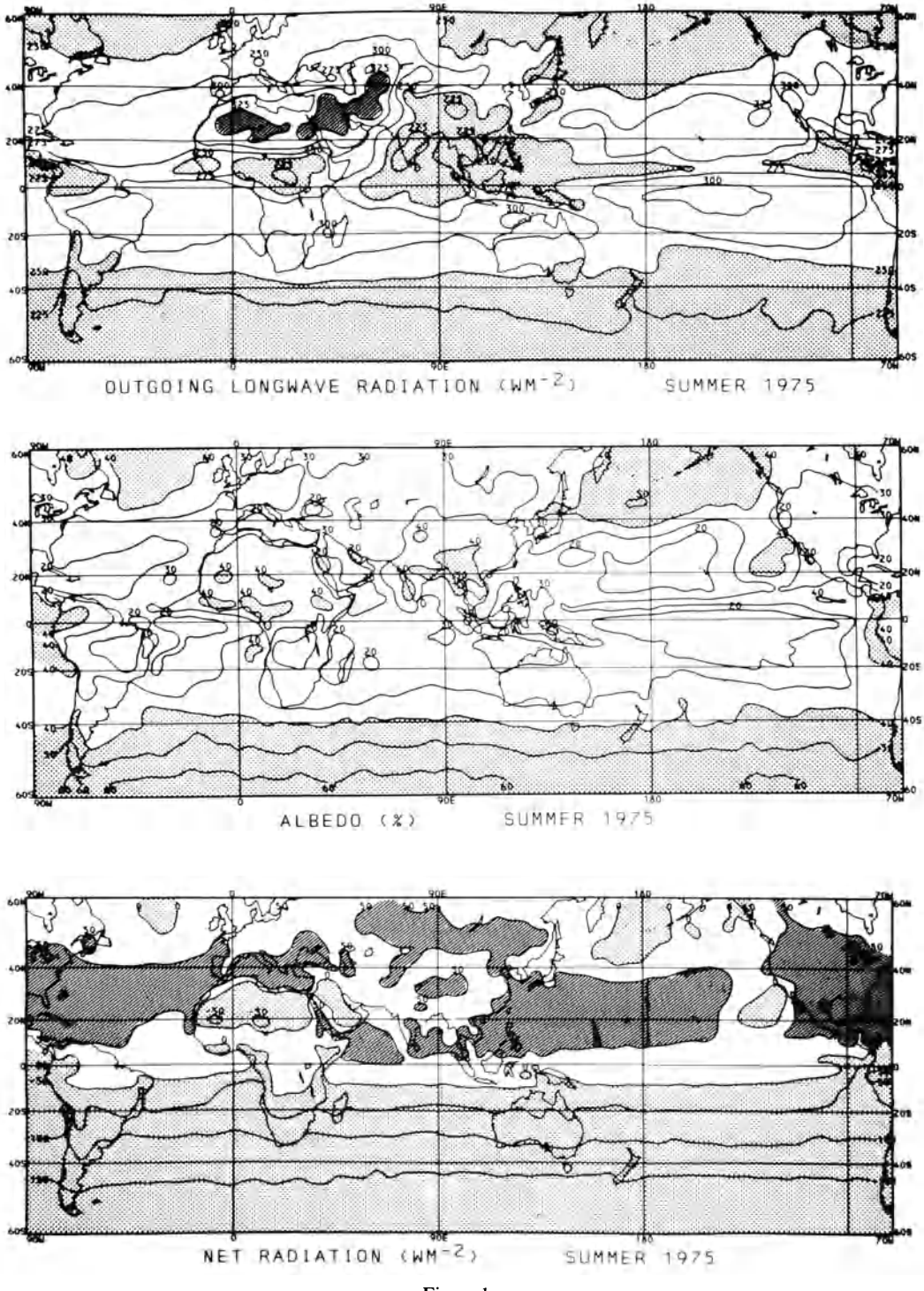

Figure 1
Outgoing longwave radiation (upper), albedo (middle) and net radiation (lower) for summer 1975.

in this report generally extends over a substantial portion of the Eastern Hemisphere and also into other seasons of the year as well as the summer season.

2. *Summer radiation balance*

The essential features of the summer radiation climatology are illustrated in Fig. 1. It is useful to examine this globally since the Southeast Asian monsoon is such a dominant circulation; and fluctuations in the monsoon appear in turn to have global ramifications, as occurred, for example, during 1972 (KRUEGER and WINSTON, 1975).

The impact of the monsoon circulation on the cloudiness (much of it convective), and of course on the outgoing longwave radiation is apparent in the upper part of Fig. 1. Note the huge area covered by values less than 250 Wm^{-2}, which can be considered to represent, in tropical latitudes, the area covered by major cloudiness (i.e., large amounts of cloudiness reaching to high tropospheric levels). Other, smaller areas that are less than 250 Wm^{-2} occur over Africa and Central America. The major desert areas extending from North Africa into Soviet Central Asia with high surface temperatures and mostly clear skies are generally indicated by values in excess of 325 Wm^{-2}. Relatively large values occur over the oceans associated with the tradewind flow, where both the amounts and heights of the clouds are generally low. Note in particular the extent of the equatorial Pacific dry zone. The western boundary, as indicated approximately by the 275 Wm^{-2} contour, appears to have been west of 'normal' during this period, but was farther east during 1976.

The albedo (middle figure) to a large extent tends to vary inversely with the longwave cooling. The principal exceptions to this are found over the deserts and where substantial low cloudiness (with few higher clouds) occurs. Note how the major monsoon features are also indicated.

The net radiation for the earth-atmosphere system is shown at the bottom of Fig. 1. While a strong meridional gradient is present over mostly all longitudes of the Southern (winter) Hemisphere, this is not the case for the Northern (summer) Hemisphere. Instead there are noteworthy west–east fluctuations in the radiative heating. Between 20° and 40°N major areas of cooling occur over the Sahara and Arabian deserts as well as the Eastern Pacific. Major areas of heating occur over the oceans – note for example the large area greater than 50 Wm^{-2} over the Western Pacific. Much of this energy is probably stored in the oceans and released to the atmosphere at some later time and place. In contrast, north of 40°N more radiation is received over the Eurasian land mass than over the oceans where cooling occurs – note the North Pacific for example. Again a west–east perturbation in the radiative heating exists – in this case out of phase with that at lower latitudes. Since the summer monsoon has been likened to a giant thermal circulation between the continent and the surrounding oceans, the degree of this differential radiative heating of Eurasia and the surrounding oceans is relevant.

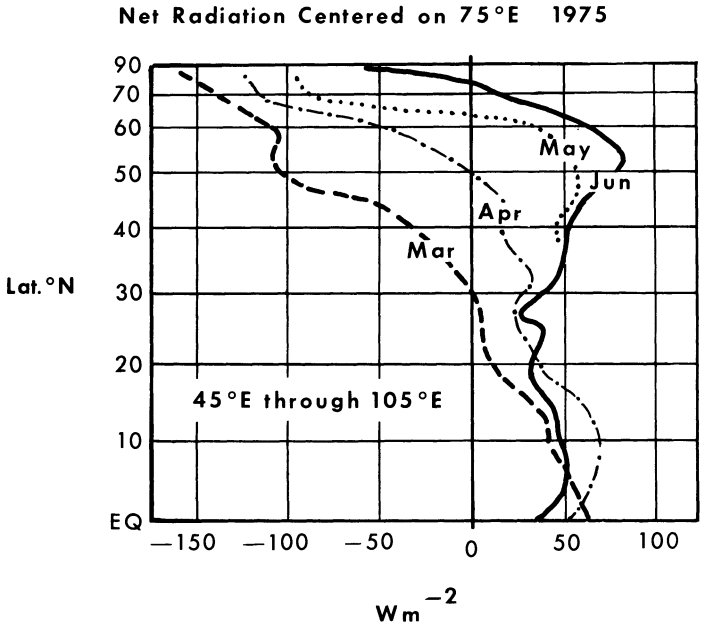

Figure 2
Net radiation (earth-atmosphere) centred at 75°E for March, April, May and June 1975.

The evolution of this heating during spring over the Eurasian continent is presented in Fig. 2 which shows the distribution of the net radiation zonally averaged over a 60° longitude sector centered at 75°E. A maximum appears near 50°N in May and by June the radiative heating here is around 75–100 Wm^{-2}. Since storage of energy must be relatively small in the land itself, much of this energy should appear in the atmosphere in the form of storage or an export of heat from the Asian Continent, some of it probably transported to the radiative sink over the North Pacific. It is interesting that this increase in net radiation during spring is accompanied by a decrease in albedo of about 30 percent, largely as a result of the disappearance of the Asian snowcover. As the snow melts, of course, some of the radiative heating is utilized to change the snow to water and vapor.

The degree to which this continental heating during late spring and early summer drives the monsoon circulation over Southern Asia is unclear. Undoubtedly differential continent-ocean heating plays a major role in the development of the southwest monsoon. However, it is recognized that monsoon theories which depend solely upon ocean-continent contrasts to drive them are inadequate (PISHAROTY and ASNANI, 1958). For one thing, since they neglect condensation heating, they do not account properly for the high level circulation above the monsoon. In addition, they neglect the interaction of the monsoon with the rest of the general circulation. What the radiation data suggests is that there is a continent-ocean exchange process during late spring and early summer that probably plays an important role in modulating the

global heat transfer process. This process would depend upon snow cover and cloudiness and their effect in turn upon the surface and atmospheric heat balances. Since the southwest monsoon is such a significant feature of the Northern Hemisphere's summertime circulation it is likely that it has a strong interaction with energy sources and sinks over distant areas.

A heating influence over the Asian land mass that is considered to have an important effect upon the monsoon is that over the Tibetan plateau (FLOHN, 1958). It is therefore appropriate to examine this region's radiation balance also. Figure 3 shows the variation of the net radiation for a point near Lhasa in Tibet as contrasted with that over Pakistan for the period from June 1974 to August 1976. The heating over Tibet is greater than over Pakistan in all months. It becomes positive in February, a month before that over Pakistan, and it rapidly increases during spring to 75–95 Wm^{-2}. With an atmospheric storage no larger than perhaps 15 Wm^{-2} (OORT and VANDER HAAR 1976; TUCKER, 1965), this surplus would then largely be balanced by

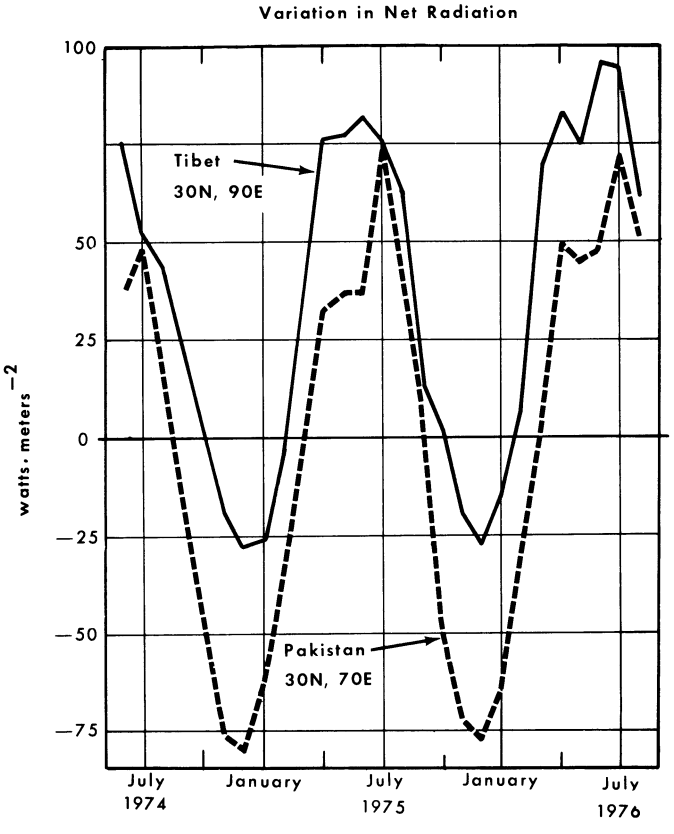

Figure 3
Variation in net radiation for Tibetan Plateau (30°N, 90°E) as contrasted with that over Pakistan (30°N, 70°E).

a heat flux divergence from the plateau. Interestingly the difference between the two regions is generally greater in the spring than in summer. In fact, in July 1974 and 1975, the differences were negligible. The role of the Tibetan plateau is very likely one of initiating updrafts early in the season and starting the flow towards the mountains. Later in the season, after the low level water vapor has increased and the air becomes convectively unstable, condensation heating very likely becomes the dominant heat source.

3. Evolution of the summer monsoon over the Indian subcontinent and some year-to-year differences

For this discussion we will use the outgoing longwave radiation to monitor the onset of the monsoon. This parameter is shown for the two springs of 1975 and 1976 in Fig. 4 and for the three summers 1974, 1975 and 1976 in Fig. 5. Further discussion of radiation changes during these three years can be found in WINSTON (1976). The most striking feature of spring over the Indian subcontinent is the west–east ridge of high values of outgoing radiation extending across India at 20°N latitude during March and near 30°N by May. These very high values, especially those in excess of 325 Wm^{-2}, are associated with the well-known premonsoon season heat wave. On the other hand the cooler Tibetan plateau is clearly indicated by the very low values just to the northeast. Already at this time of the year cumulus convection becomes active over the Himalayas and also contributes to this low outgoing radiation. Evidence of the monsoon cloudiness appears during early spring over Sumatra and Malaysia where radiation values of 250 Wm^{-2} occur. As the season advances, this cloudiness spreads westward and also northwestward across Southeast Asia and the Bay of Bengal. During June it spreads over Southern India. However the ridge of high outgoing radiation near 30°N keeps this monsoon cloudiness and rainfall over the south separated from that over the Himalayas until July when it gives way. By this time a northeast–southwest axis of high values of outgoing radiation becomes fully established from Saudi Arabia to Soviet Central Asia. Concomitantly the monsoon spreads northwestward over the rest of India. Since substantial parts of India, especially the central and northwest, receive more than 80 percent of their annual rainfall from the summer monsoon, this evolution from June to July shown in Fig. 5 is an important event. Sometimes it is delayed.

Such a delay is dramatically shown in the longwave radiation distribution over India during June 1976 (Fig. 5). Notice how the radiation values less than 250 Wm^{-2} are located over Eastern India, Bangladesh and the Bay of Bengal. Except for a small area over the southwestern coast, the radiation over the rest of Southern India is greater than 250 Wm^{-2}, in contrast to June 1974 and 1975. During June 1975 radiation values even less than 225 Wm^{-2} occurred over Southern India. July 1976, however, was considerably improved over June 1976, as monsoon cloudiness and

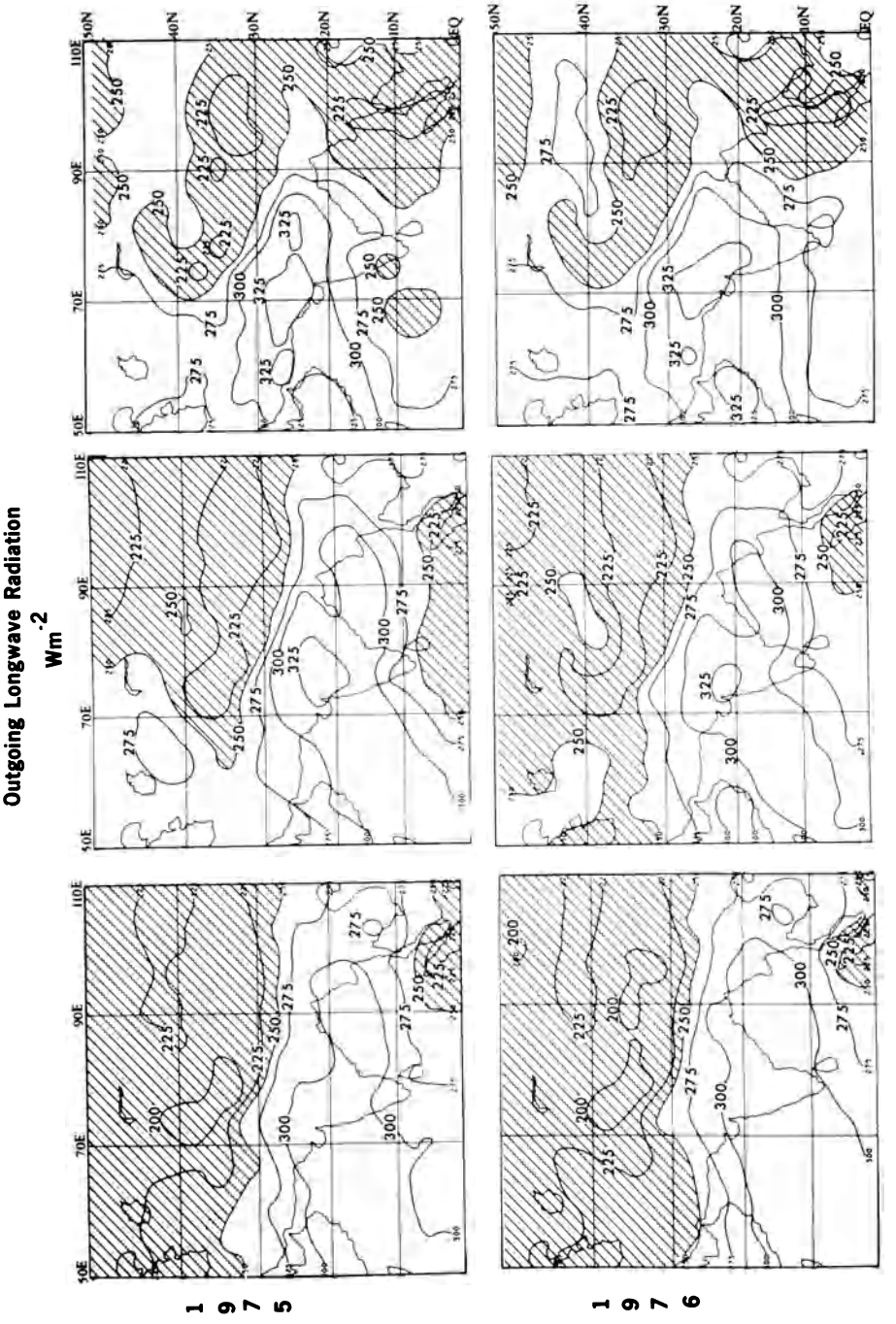

Figure 4
Outgoing longwave radiation for spring months of 1975 and 1976. Radiation less than 250 Wm^{-2} shaded.

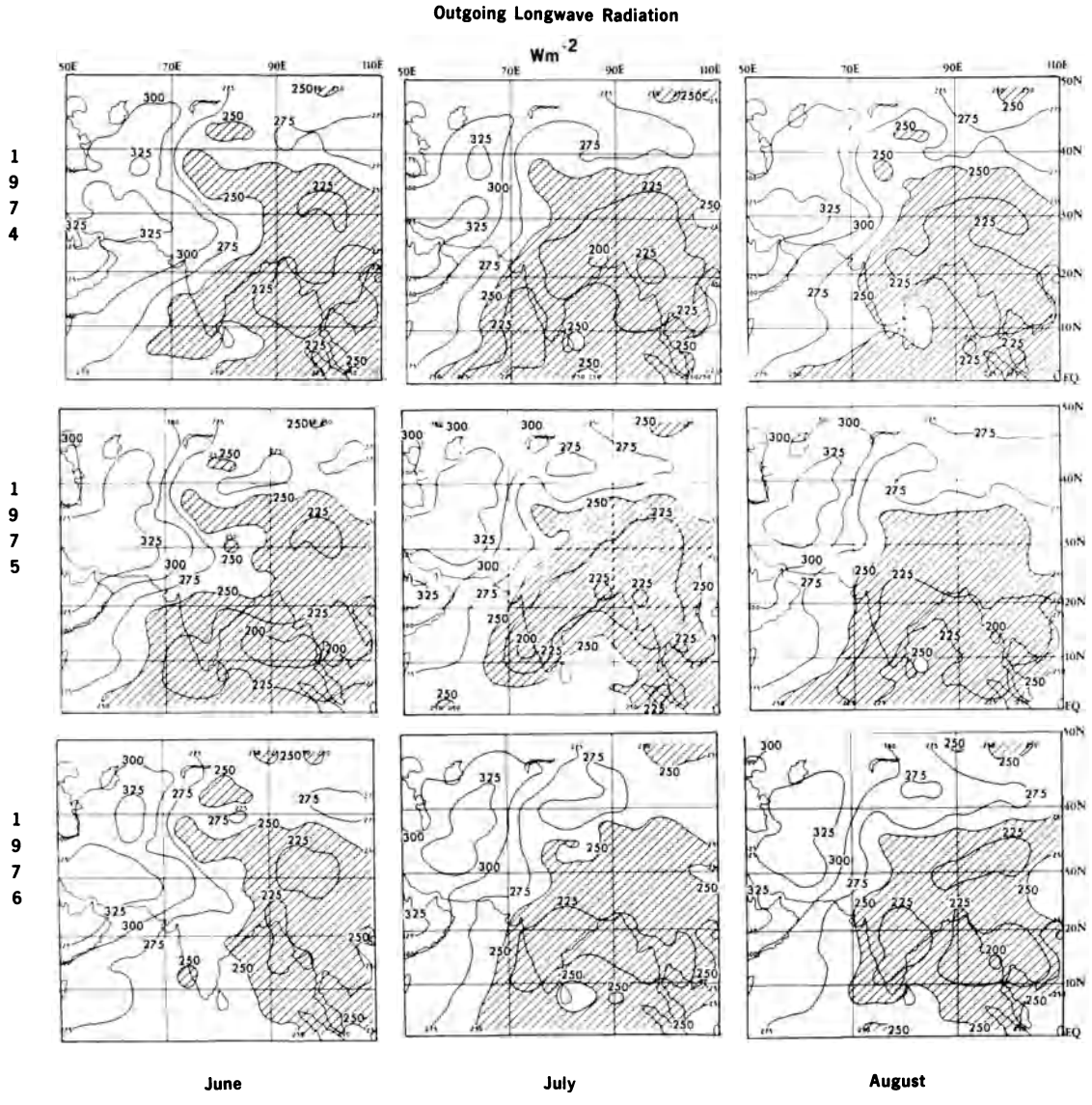

Figure 5
Outgoing longwave radiation for summer months of 1974, 1975 and 1976. Radiation less than 250 Wm^{-2} shaded.

rains spread over India, although the outgoing radiation was not as low as during July 1975. Of the three years presented in Fig. 5 the 1975 monsoon season appears to be the best developed, especially over the south and east. Low radiation values appeared over the southern tip of India already in May and during June spread rapidly northward to about 20°N latitude. The 1974 season, in contrast to both 1975

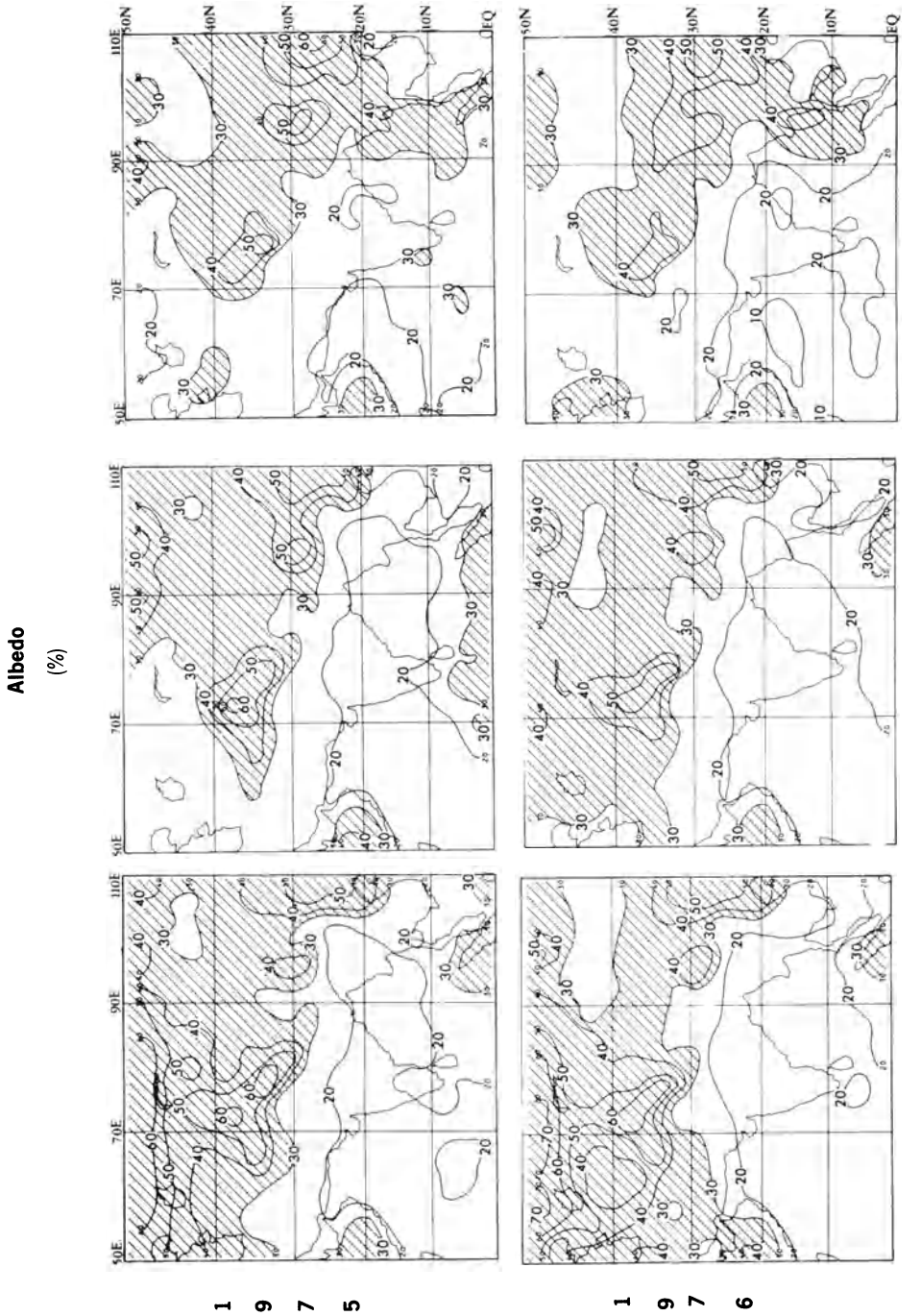

Figure 6
Albedo for spring months of 1975 and 1976. Values greater than 30 percent shaded.

and 1976, had the lowest outgoing radiation over Northeast India, Nepal and the Himalayas; while over Southern India higher values were observed.

In an attempt to see what differences preceded the summer monsoons of 1975 and 1976 we will look at the albedo patterns during the preceding springs (Fig. 6). Particularly interesting are the high albedos in early spring over Soviet Central Asia and the northwest Himalayan mountain complex. Note especially that during April 1976 these albedos were greater and to a large extent this was probably due to greater snow cover during the 1975–76 winter than the previous one. This is shown in Fig. 7 which is prepared from snow cover data presented by MATSON (1977). The impact of this higher albedo on the absorbed solar radiation during the 1976 spring season is shown in Fig. 8. This figure is the difference between the spring seasons of 1975 and 1976 and, as it indicates, the solar radiation was reduced over a large area of the South Central Soviet Union (approximately 35°–55°N, 40°–80°E). The maximum reduction of more than 25 Wm^{-2} occurred over Northern Kazakhstan.

This raises a rather fundamental question about the role of Eurasian snow cover on the Indian monsoon. Referring back to Fig. 7 it can be seen that the Eurasian snow cover preceding the devastating 1972 monsoon was the greatest of the decade (also see WMO, 1973). Snow cover was one parameter monsoon forecasters attempted

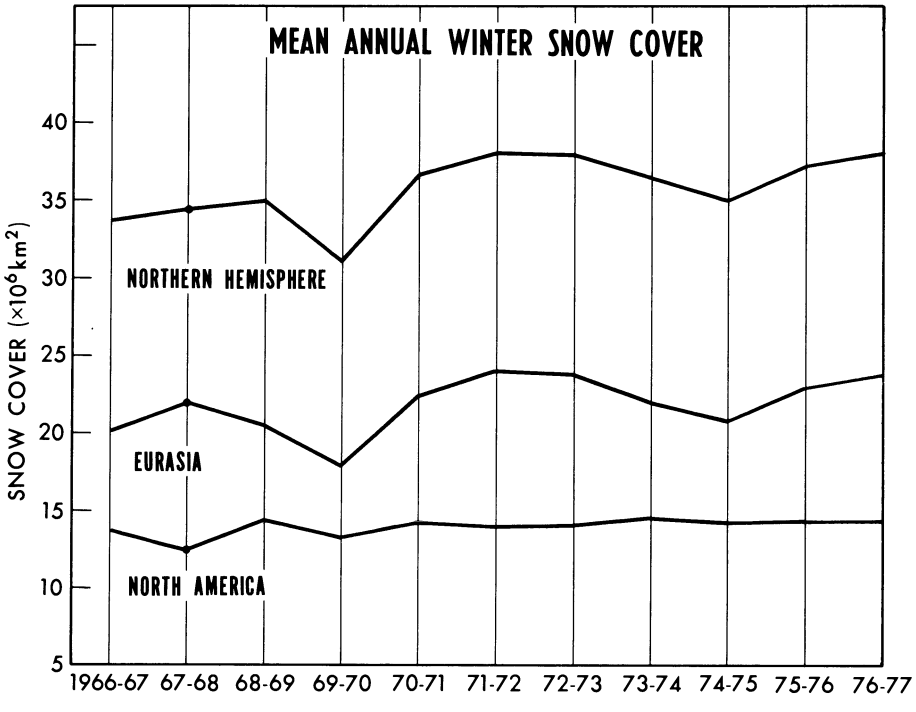

Figure 7
Variation in mean annual winter snow cover (Matson 1977). Note in particular the variation over Eurasia.

to use with rather limited success a century ago (BLANFORD, 1884), but a recent study by HAHN and SHUKLA (1976) again suggests that it may be relevant.

Other factors, of course, have been found to be related to the monsoon. The significance of many of these is discussed in the paper of RAO and RAMAMOORTHY (1958). Perhaps the most interesting relations are with distant events – events that occur perhaps halfway around the world. Earlier we referred to the fact that the monsoon influences such a large area that it is nearly a global phenomenon. This is implied in its relation to the 'Southern Oscillation' of Sir Gilbert Walker which essentially measures the pressure difference between the Southeastern Pacific and Indonesia. As such it is a measure of the South Pacific tradewinds. They in turn are related to sea surface temperatures in the eastern equatorial Pacific. It has been noted that the major failure in the southwest monsoon during 1972 was associated with weak Pacific trades, a low value of the Southern Oscillation Index, and above normal temperatures over much of the equatorial Pacific (KRUEGER and WINSTON, 1975; QUINN, 1976).

Similar changes although not as extreme, occurred during 1976 (KRUEGER, 1976; QUINN, 1976). In this year the monsoon began rather late, was rather active during July and August, and receded somewhat earlier than usual during September, the net result being a somewhat weaker monsoon. Since the changes in the Pacific trades were also accompanied by changes in cloudiness and probably rainfall, there were accordingly major changes in the earth-atmosphere radiation balance and its components. An example of this is shown in Fig. 9 which shows the outgoing longwave

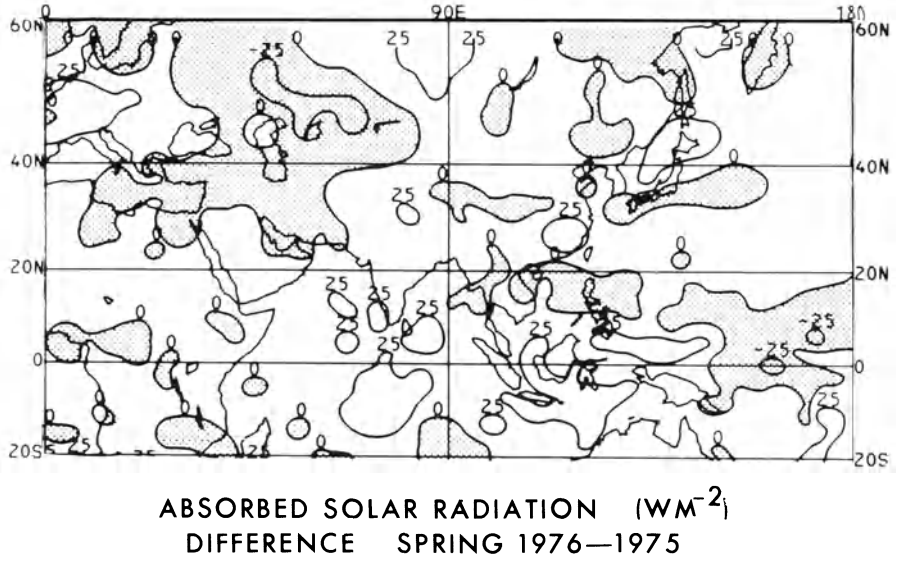

Figure 8
Differences in absorbed solar radiation over Eurasia between spring 1975 and 1976. Note how much lower the absorbed solar radiation was during spring 1976 near the Caspian Sea.

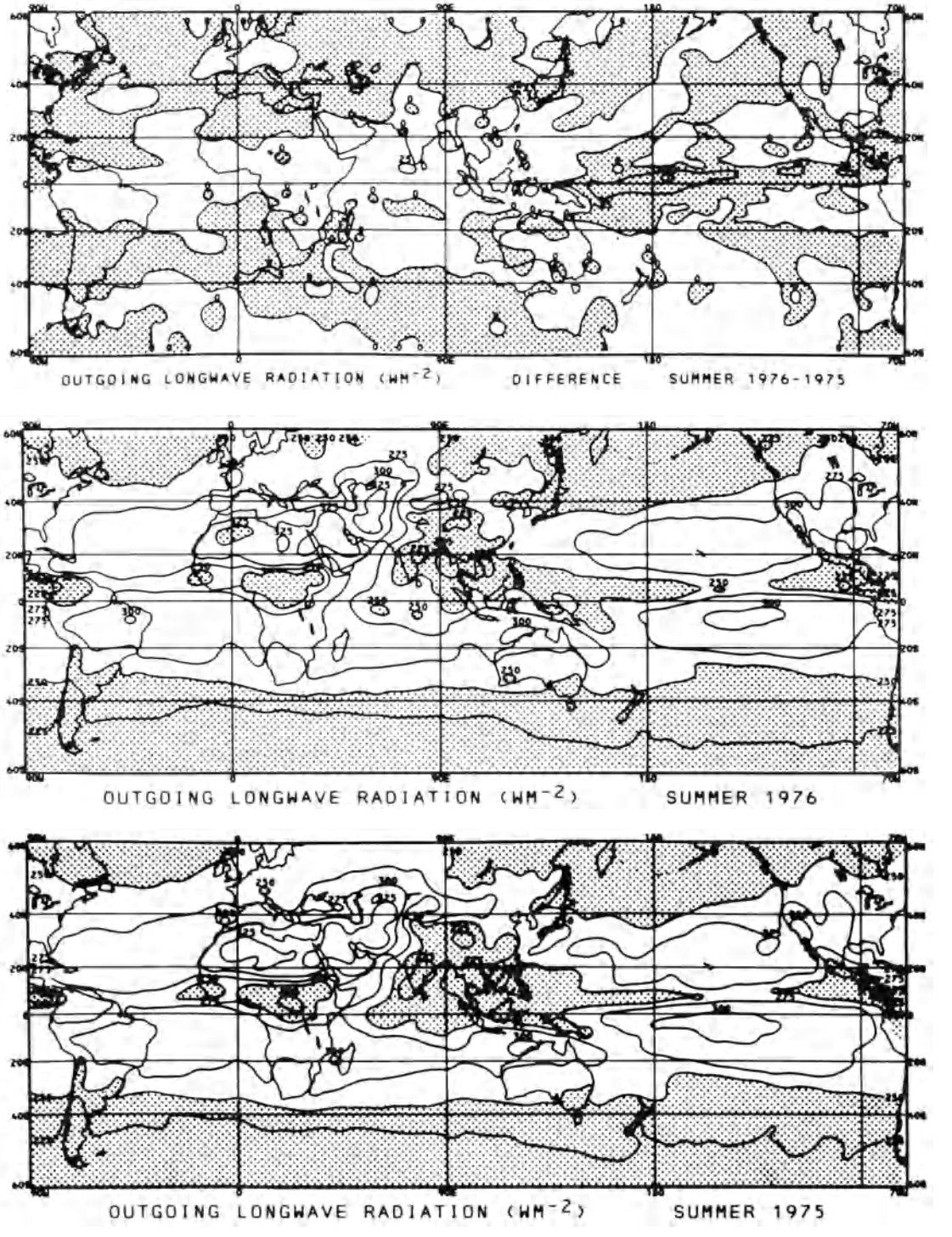

Figure 9
Outgoing longwave radiation for the summers of 1975 and 1976 and differences between them (lower figure).

radiation for the two summers of 1975 and 1976 with the changes between the two shown at the bottom. The somewhat weaker monsoon during 1976 (as compared with 1975) is indicated by the positive radiation changes over the Indian subcontinent. But these positive changes are seen to be part of an extensive area of increased longwave radiation at low latitudes extending from South America eastwards to New Guinea – more than half way around the earth. By contrast, the equatorial Pacific eastward from New Guinea was characterized by decreases in longwave radiation, indicating more cloudiness and convection during the 1976 summer season. Thus major changes in the regions of condensation heating over the tropics accompanied the weaker Asian monsoon in the summer of 1976.

4. *Conclusion*

We have examined the large-scale features of the summer radiation budget and have noted the radiation surplus occurring over Eurasia and the deficit downstream over the Pacific. Preliminary consideration of the energy storage in the land and atmosphere then suggests an energy flux divergence from the Asian land mass. Clearly this should be pursued further. It would be particularly useful to calculate this energy flux between the continent and ocean directly from wind and geopotential data. In addition it is now possible with the greater number of observations available to update TUCKER'S (1965) early estimates of atmospheric energy storage.

The continental heating should largely be modulated by cloud cover and surface features such as snow cover. Snow cover over Soviet Central Asia and the Himalayas resulting from winter and spring storminess may, in fact, have contributed to delaying the 1976 summer monsoon. Concurrently, however, distant changes were taking place, especially over the Pacific, and they also seem to be related.

It is apparent that we have looked at only the radiation balance and its components here and have largely neglected the circulation, and particularly, the condensation heating. Yet fluctuations in the radiation balance largely arise in response to fluctuations in the circulation and condensation heating. We hope that further comparative studies utilizing satellite and other improved measurements in future years can furnish new insights into the behavior of the monsoon circulation and its energy transformations.

REFERENCES

BLANFORD, H. F. (1884), *On the connexion of the Himalaya snowfall with dry winds and seasons of drought in India,* Proc. Roy. Soc. London *37*, 3–22.

FLOHN, H. (1958), *Recent investigations on the mechanism of the 'Summer Monsoon' of Southern and Eastern Asia,* Symposium on the mechanism of the 'Summer Monsoon' of Southern and Eastern Asia. Symposium on Monsoons of the World, New Delhi, Feb. 19–21, 1958.

GRUBER, A. (1977), *Earth-atmosphere radiation budget*. To be published as a NOAA/NESS Technical Report.

HAHN, D. G. and SHUKLA, J. (1976), *An apparent relationship between Eurasian snow cover and Indian monsoon rainfall*, J. Atmos. Sci. *33*(12), 2461–62.

KRUEGER, A. F. and WINSTON, J. S. (1975), *Large-scale circulation anomalies over the tropics during 1971–72*. Mo. Wea. Rev. *103*(6), 465–473.

KRUEGER, A. F. (1976), *Circulation over the tropics and ocean warming in the Eastern Pacific during 1976*, Proceedings of the NOAA Climate Diagnostics Workshop, Nov. 4–5, 1976, Washington, D.C., U.S. Dept. of Commerce, NOAA.

MATSON, M. (1977), Winter Snow-cover maps of North America, 1966–76, NOAA Tech. Memo NESS 84, Washington, D.C.

OORT, A. H. and VANDER HAAR, T. H. (1976), *On the observed annual cycle in the ocean-atmosphere heat balance over the Northern Hemisphere*, J. Phy. Oceanogr. *6*(6), 781–800.

PISHAROTY, P. R. and ASNANI, G. C. (1958), *Dynamical theories of the Monsoons—a survey*, Symposium on Monsoons of the World, New Delhi, Feb. 19–21, 1958.

QUINN, W. H. (1976), *An improved approach for following and predicting Equatorial Pacific changes and El Nino*, Proceedings of the NOAA Climate Diagnostics Workshop, Nov. 4–5, 1976, Washington, D.C., U.S. Dept. of Commerce, NOAA.

RAMASWAMY, C. (1976), *Synoptic aspects of droughts in the Asiatic monsoon area*, Proc. Ind. Nat. Sci. Acad. *42A*(2/3), 109–132.

RAO, K. N. and RAMAMOORTHY, K. S. (1958), *Seasonal (monsoon) rainfall forecasting in India*, Symposium on Monsoons of the World, New Delhi, Feb. 19–21, 1958.

TUCKER, G. B. (1965), *The distribution and annual cycle of local heating rate throughout the troposphere in the Northern Hemisphere*, Met. Mag. *94*(1116), 205–214.

WINSTON, J. S. (1976), *Radiation budget variations (1975–76 compared with 1974–75)*, Proceedings of the NOAA Climate Diagnostics Workshop, Nov. 4–5, 1976, Washington, D.C., U.S. Dept. of Commerce, NOAA.

WORLD METEOROLOGICAL ORGANIZATION (1973), *Significant weather in 1972*, WMO Bull. *22*, 99–107.

(Received 15th June 1977)

Pageoph, Vol. 115 (1977), Birkhäuser Verlag, Basel

Spectrum Analysis Relevant to Indian Monsoon

By MASATO MURAKAMI[1])

Abstract – Recent investigations on Indian monsoon by the method of spectrum analysis are reviewed from the viewpoint of various aspects of its application. The assessment is also made on their results and discussions. Through these processes, it emerged that there exist at least two kinds of quasi-periodic variations in the summer monsoonal fluctuation over India and adjacent regions. One appears as a spectral peak around the 5-day period and another is around the 15-day period.

The former one is conspicuous along the monsoon trough region in northern India. The results of cross-spectrum analysis show that it reflects the passage of westward-moving, synoptic-scale disturbances called monsoon lows. The latter seems to be related to the large-scale variation of monsoon activity itself, though it is also likely to have some associations with the cyclogenesis of monsoon depressions. The recent application of spectral method to this large-scale interrelation is also discussed along with the results of some non-spectral studies and the remaining problems are pointed out.

Key words: Monsoon: spectrum analysis, fluctuations.

1. Introduction

In the past decade, the application of the spectrum analysis to the tropical disturbances has achieved a substantial success over the tropical Pacific area (see the reviews of YANAI, 1971 and WALLACE, 1971). Through these investigations, it turned out that this method is quite helpful in seeing the characteristic features of quasi-periodic disturbances in the data sparse region, like a tropical Pacific. Besides, we can examine the dynamical quantities, such as momentum and heat flux, associated with each kind of disturbance by using the method of cross-spectrum analysis. Even when we can get a sufficiently dense observation network, these methods are useful in investigating the situation in which the disturbances with different periodicities simultaneously exist.

Therefore, it is a matter of course that attempts have been made to apply this spectral technique to the other regions as well. As for the monsoon disturbances over India, these attempts started at early 70's though the spectral analysis, from the viewpoint of climatic changes, have been performed earlier. As we already know from the accumulated experiences of synoptic analyses (RAMAGE, 1971; RAO, 1976), the major cyclogenesis of synoptic-scale disturbances takes place over the north Bay of Bengal, northern India and the eastern Arabian Sea during the summer monsoon

[1]) Department of Meteorology, The Florida State University, Tallahassee, Florida 32306, USA.

season. Some of them show the quasi-periodic behavior. For example, it is known that the weak disturbances called 'monsoon lows' are formed at intervals of roughly 5 days and monsoon depressions are formed with the frequency of about 1.8 per month. We also know that there exists a variation of monsoon activity itself with a periodicity somewhat longer than 10 days. This knowledge constitutes a valuable background for the application of spectrum analysis to this region.

In this article, an attempt will be made to review the results obtained by the above-mentioned spectral method. The topics are mainly concerned with the variations in the troposphere during the northern summer with the periodicity ranging from about 4 days up to 20 days, following the same concern appearing in the past investigations. The variation longer than the seasonal march will be discussed in other articles and so is beyond the scope of this review.

In Section 2, the remarkable periodicities picked up in the spectrum of individual variable are discussed. The horizontal extent of these periodicities and the horizontal propagation of the disturbances associated with each periodicity are discussed in Section 3. Section 4 deals with their mean vertical structure revealed by the cross-spectrum analysis applied to the data of various altitudes. In Section 5, we also review the results of a recent study which tried to reveal the situation associated with the large-scale fluctuation of monsoon activity itself. However, as one can see in the following sections, the results of spectral analysis in this field have not been accumulated yet. The spectrum analysis on the monsoon disturbances is still in the initial stage of investigation. Therefore, one should keep it in mind that some of the results and interpretations ought to be examined and verified in the course of further investigations.

2. *Prominent periodicity*

It has long been recognized that the monsoon rainfall over India shows a substantial fluctuation with the time scale somewhat longer than 10 days. Figure 1 exhibits the example of this fluctuation shown by MURAKAMI (1972). In his theoretical investigation of the equatorial Kelvin wave, it is referred to as the oscillation with a period of about 16 days. The oscillation of this time scale can be also seen in FINDLATER's (1969) earlier work in which the relationship between the monsoon rainfall over the western coast of India and the intensity of so-called Somali jet over the eastern coast of Africa was examined. Matters concerned with this particular topic will be discussed in Section 5.

The first attempt to apply the spectral method to the investigation of monsoon disturbances was made by ANANTHAKRISHNAN and KESHAVAMURTY (1970). They examined the time series of the wind, rainfall and surface pressure at selected stations all over India for the years 1965 and 1967. Part of their results are shown in Fig. 2. In the power spectra of pressure departures, they picked up the peaks around 6 to 8 days

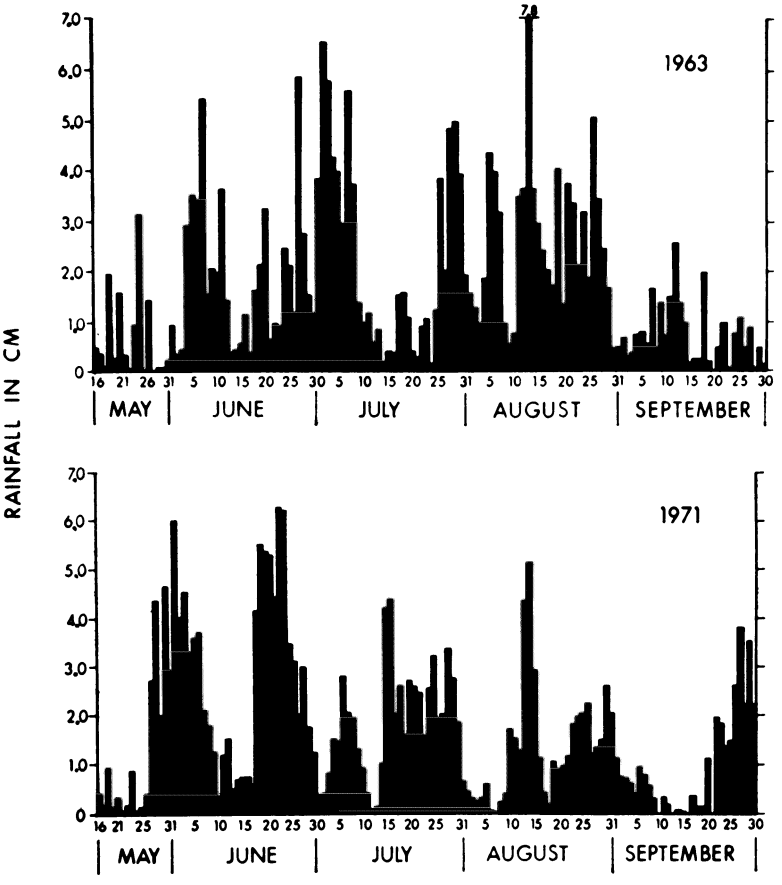

Figure 1
Daily rainfall (cm/day) along the western coast (Konkan, Coastal Mysore, and Kerala) of India during the summers of 1963 and 1971. (MURAKAMI, 1972.)

and 4 to 5 days as remarkable ones during the summer monsoon season and peaks around 2 weeks and 4 to 5 days during the winter season. However, as seen in these figures, their spectra show an intense red noise tendency, probably because the linear trend and the long-term variation such as seasonal march are not fully removed in advance. In the sense of statistical evaluation, this makes it difficult to specify each peak as the one with physical substance.

BHALME and PARASNI (1975) analyzed the time-series of the meridional gradient of sea level pressure over India during the summer season. They tried to remove the trends and long-term fluctuations by applying the orthogonal polynomial to the daily raw data and further verified the obtained spectra statistically following the procedure prescribed by MITCHELL (1966). The spectra obtained for the years 1961 through 1970 are shown in Fig. 3 together with the line of a 95 percent confidence limit. Though

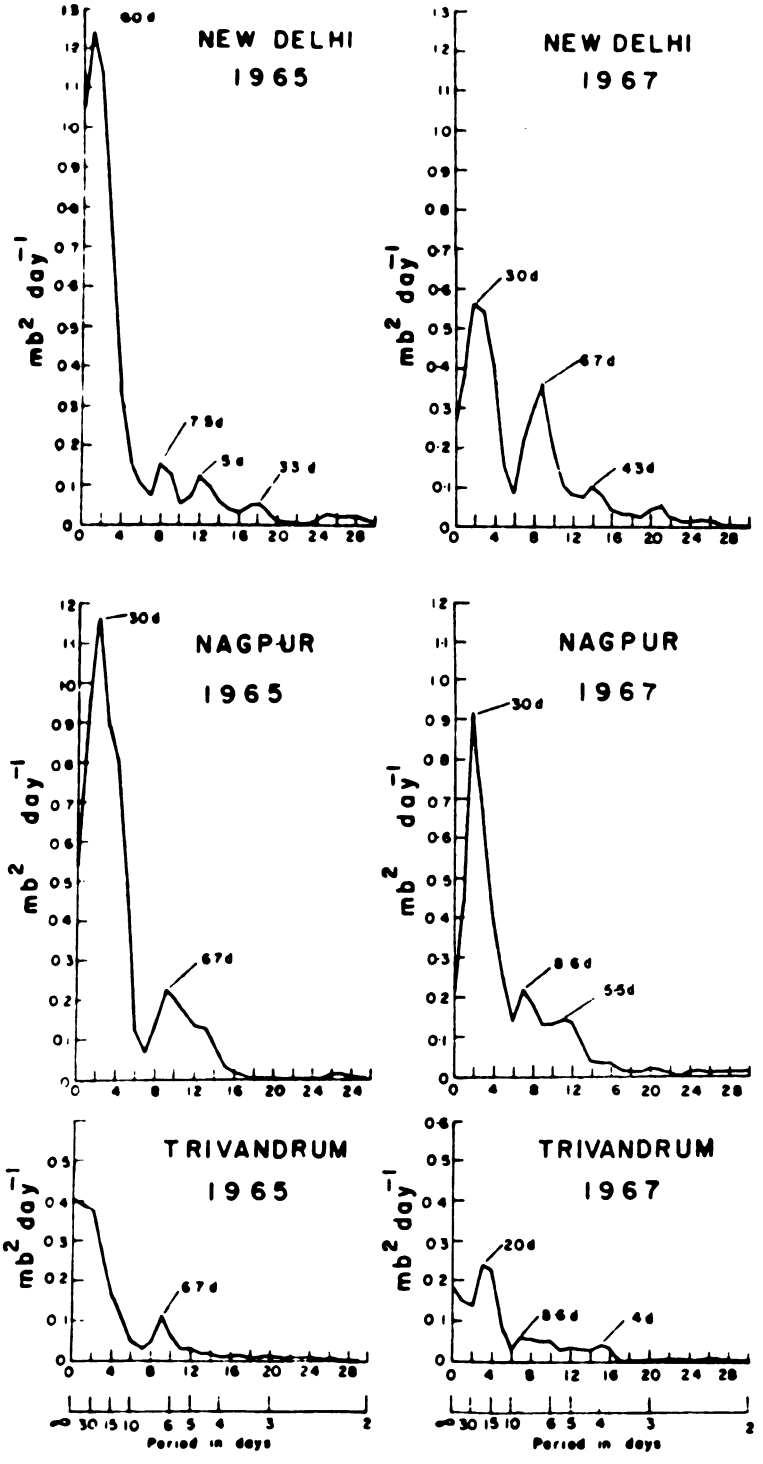
NEW DELHI
1965
60 d
7.5 d
5 d
3.3 d
NEW DELHI
1967
30 d
6.7 d
4.3 d
NAGPUR
1965
30 d
6.7 d
NAGPUR
1967
30 d
8.6 d
5.5 d
TRIVANDRUM
1965
6.7 d
TRIVANDRUM
1967
20 d
8.6 d
4 d
mb² day⁻¹
Period in days

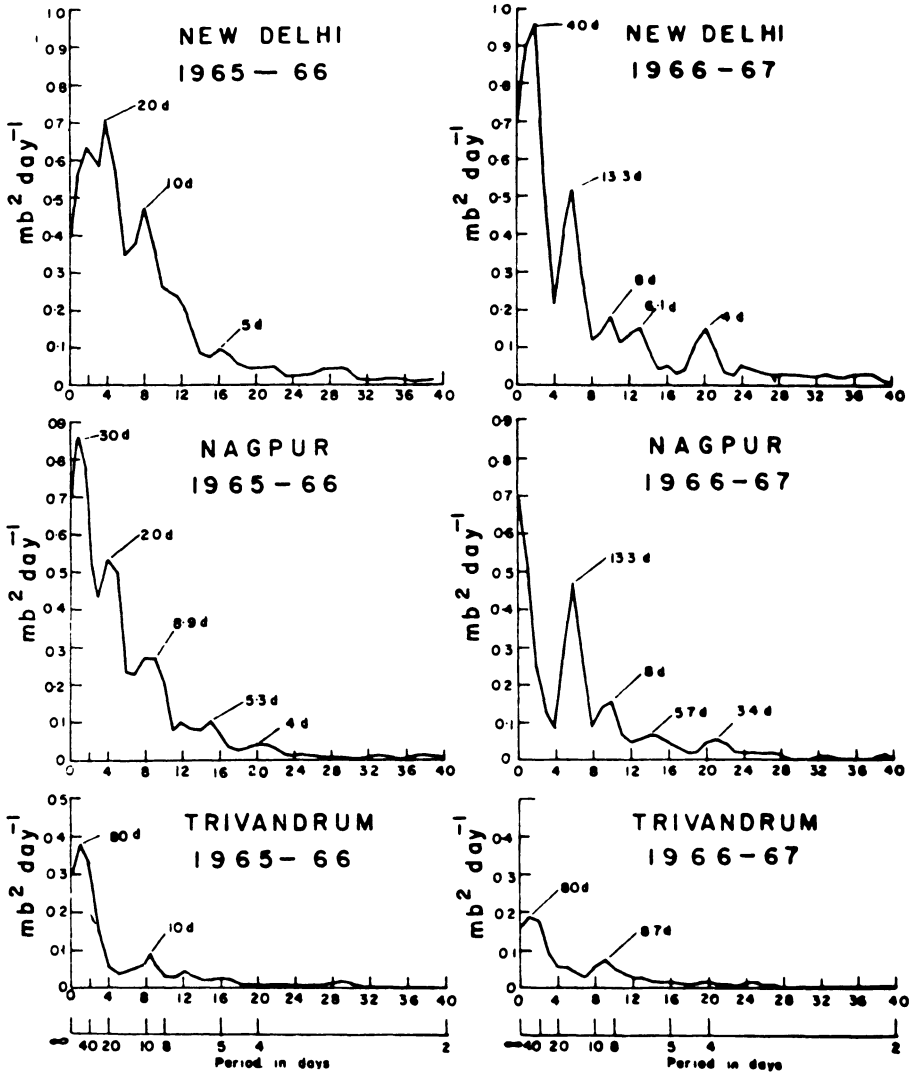

Figure 2
Power spectra of daily pressure departure during (a) summer, and (b) winter season. (ANANTHAKRISHNAN and KESHAVAMURTY, 1970.)

the spectra still show the red noise type distribution, we can see that the peaks around 4 to 6 days and 12 to 15 days repeatedly appear as the statistically significant ones. They also pointed out that the 5 to 6 day periodicity can be noticed more conspicuously over northern India though the figure is not shown in this paper.

The periodicities around 5 days and 12 days are also reported in the extensive study made by KRISHNAMURTI and BHALME (1976). Figure 4 shows their result on the variation of sea-level pressure over the monsoon trough region in northern India.

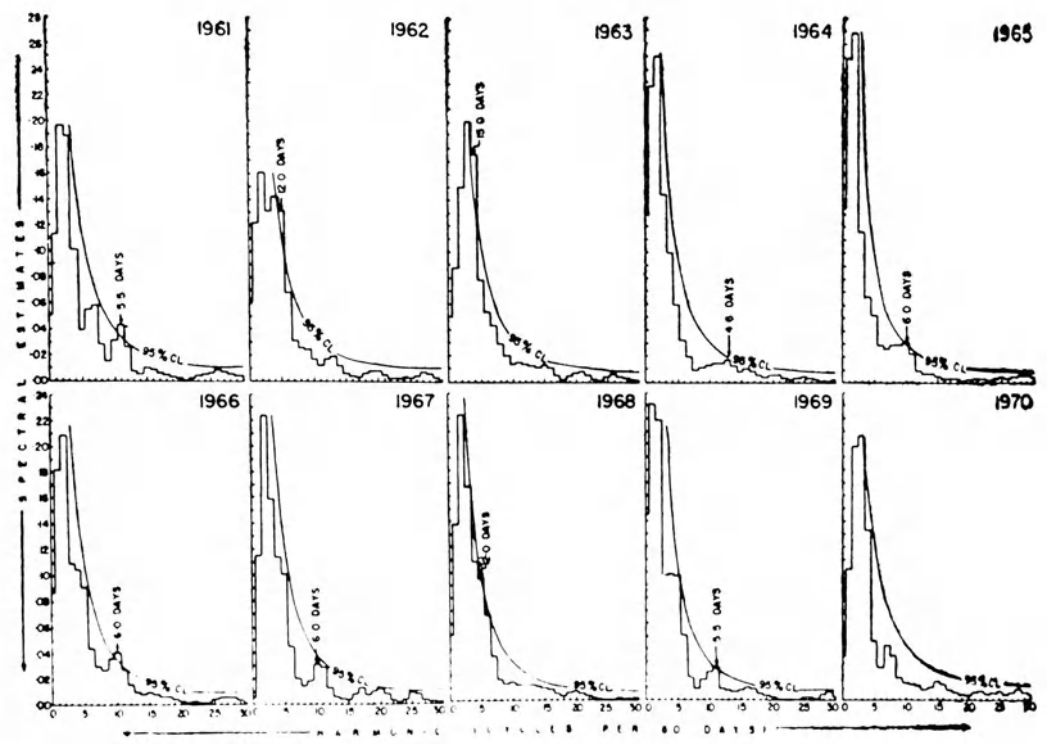

Figure 3
Power spectra of pressure gradient across peninsular India (BHALME and PARASNIS, 1975.)

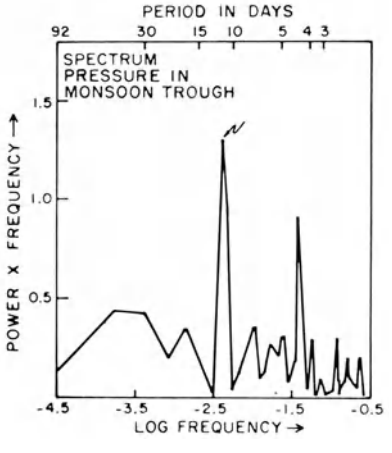

Figure 4
Power spectra of the sea level pressure over the monsoon trough region during the summer of 1967. (KRISHNAMURTI and BHALME, 1976.)

The peaks appear very distinctly at the period of 11.5 days and 4.5 days. This analysis was performed in the summer monsoon season (July through September) and the least square linear trend was removed from the raw data prior to the application of spectral method. They also adopted an alternative representation of the power spectra used by ZANGVIL (1975) instead of the conventional one. In this representation, the product of the power spectral density times frequency is plotted against the natural log of frequency. It is proved that this representation is suitable when the variation with a certain time scale is localized in the time series. It can represent a proper spectral peak instead of red noise spectra which will appear in this case when the conventional representation is used.

The analysis of the temporal fluctuation of the summer monsoon over India was also carried out by M. MURAKAMI (1976). Figure 5 shows the vertical distribution of power spectral density of zonal and meridional wind component at Calcutta (23°N, 88°E). This station is located close to the north Bay of Bengal where the major cyclogenesis of monsoon disturbances takes place. What is notable in this figure is the

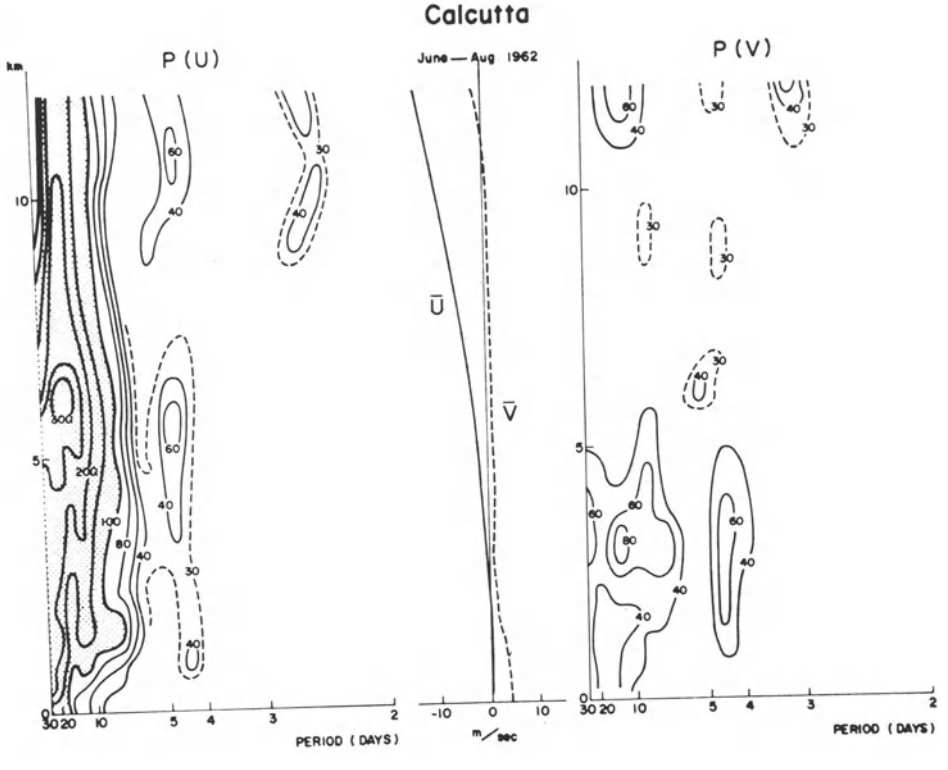

Figure 5

Vertical distributions of the power spectral densities of zonal (left) and meridional (right) wind components and their mean values. Units of the densities are $(m/sec)^2$ day and the values more than 100 are shaded. (MURAKAMI, 1976.)

intense spectral peak around the 15-day period appearing exclusively in the variation of zonal wind throughout the upper and lower levels. It also shows another remarkable peak around the 5-day period which appears in both zonal and meridional winds as well. They are somewhat confined in the lower troposphere below the 6 km level or so in contrast with the peak around the 15-day period.

Spectrum analysis of the variation in the upper atmosphere cannot be well performed, even in recent years, due to the poor upper air observation over the monsoonal area. By using the result of the elaborate work done by KRISHNAMURTI and RODGERS (1970), KRISHNAMURTI *et al.* (1973) showed that the intensity of the upper tropospheric Tibetan high also oscillates with a period around 13 to 15 days and 3 days. HIROTA (1975) applied the spectrum analysis to the time series of rocket data and found that the periodicity of about 15 days is also dominant in the summer stratosphere and mesosphere above 30 km. As for the mechanism of its excitation, he refers to the possibility that it is instigated by the vertical propagation of wave energy originated by the monsoonal fluctuation in the summer troposphere. However, the verification and further analysis on these subjects still remain to be done under future investigation.

Through the above-mentioned efforts to specify the characteristic time-scale of the variations, it emerges that the quasi-periodic oscillations around the 15-day and 5-day period exist in the temporal fluctuation associated with monsoons, especially with the summer monsoon over the Indian subcontinent and adjacent regions. Though the periodicity around 3 days reported by KRISHNAMURTI *et al.* (1973) and the one around 7 days discussed by KESHAVAMURTY (1972, 1973) are also likely to exist, it seems that a larger accumulation of observational knowledge is still needed to establish their physical substantiality. Anyway, in the following sections we shall discuss the investigations and try to reveal the characteristic features of the disturbance which cause each periodicity.

3. Horizontal cross spectra

Once we manage to pick up the certain periodicity, the next step is almost inevitably directed at finding the nature of the disturbances which cause this periodicity. This step requires the knowledge of their horizontal scale, longitudinal and/or latitudinal propagation and their vertical structure, including both kinematic and thermal variables. This knowledge is also useful when we try to discuss the dynamical aspect of the disturbance, such as the flux of physical property and the energy budget, and so on. Spectral method can be a helpful tool in this kind of investigation when we use a technique of cross-spectrum. Cross-spectrum between the different time series consists of two quantities, namely co-spectrum and quadrature-spectrum. By knowing these quantities, we can derive the phase difference and the coherence between the two time series provided that a certain frequency is specified (MARUYAMA, 1968). In

the present section we will discuss the results of this technique applied to the data of different stations distributed in the horizontal domain.

The application of the horizontal cross spectrum analysis to summer monsoon disturbances was intensively performed by KESHAVAMURTY (1973). By using the data during the summer of 1967, he picked up three major periodicities in the variation of the meridional wind, namely the ones around 15–20 days, 5–6 days and 7–9 days. He tried to identify these periodicities with the known monsoon disturbances by examining the longitudinal phase differences of the oscillations and thus deriving the longitudinal wavelength and phase velocity of the disturbances associated with them. (The actual procedure will be shown immediately in the context of M. MURAKAMI's (1976) analysis.) After examining the vertical distribution of the power spectral density as well, he concluded that the periodicities around 15–20 days, 5–6 days and 7–9 days correspond to the passage of monsoon depressions, weaker but frequent monsoon lows and the waves in the middle and upper troposphere, respectively.

However, there are some questions about his way of spectral application. One is that he did not try to remove the linear trend nor long-term variation and his spectra sometimes show the magnificent spectral density in the lower-most frequency range as being similar to those of ANANTHAKRISHNAN and KESHAVAMURTY (1970), previously exhibited in Fig. 2. Since the distortion from the genuine sinusoidal wave, such as skewness etc., in the actual variation and the discrete version appearing in the actual procedure of estimation are likely to cause the distortion in the spectral estimates through the coupling between the frequencies, the extreme red noise and/or the very extreme power in the low frequency are unfavorable to get a reliable estimate in the moderate or high frequency range. The matters related to the discrete version of the spectral calculation were recently discussed by RIKIISHI (1976).

Another point is that his longitudinal cross-spectrum analysis involves the stations distributed in the somewhat wide range of latitude. That is, from Lucknow (27°N, 81°E) in the north to Port Blair (12°N, 93°E) in the south. This may be misleading in the longitudinal cross-spectrum analysis unless the disturbance has a sufficiently large latitudinal extent, compared with the above range, and has no significant horizontal tilt of the wave axis.

From the above point of view, M. MURAKAMI (1976) re-examined the temporal variation of the meteorological variables by using the data during the summer of 1962. He picked up two major periodicities as previously discussed in the context of Fig. 5, and examined the horizontal distribution of their appearance. Figure 6 exhibits the horizontal distribution of the power at a 3-km level contributed by two period ranges which contain major spectral peaks. The power around the 10 to 15-day period is shown in terms of the zonal wind, because this periodicity is mainly dominant in the zonal wind variation as discussed before. Note that this aspect already implies the different situation from monsoon depressions which accompany both zonal and meridional wind variations.

The distributions in Fig. 6 indicate that the amplitude of the disturbance associated

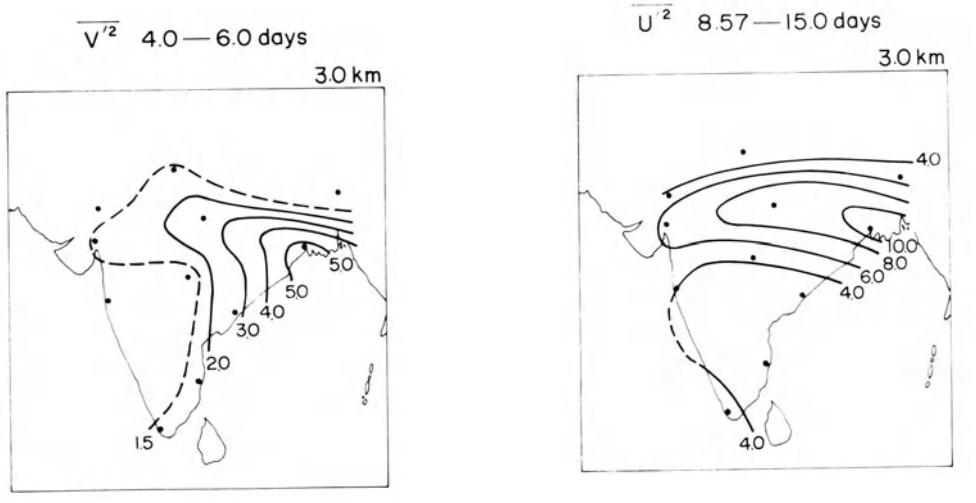

Figure 6
Horizontal distribution of the variances at 3-km level produced by (a) the meridional wind in the period range 4.0 through 6.0 days, and (b) the zonal wind in the period range 8.57 through 15.0 days. Units are m^2/sec^2. (MURAKAMI, 1976.)

with each periodicity is somewhat confined to the northern part of India, especially to the one associated with a 10 to 15-day periodicity. This region corresponds to the mean location of the so-called monsoon trough during the summer monsoon season. The figure also suggests that it is more appropriate to use the stations located within this large amplitude when we examine the longitudinal propagation of the disturbance.

The result of the thus-performed longitudinal cross spectrum analysis as to the periodicity around 5 days is shown in Fig. 7. This diagram represents the relationship between the phase difference ($\Delta\theta$) of the oscillation and the longitudinal difference ($\Delta\lambda$) of the stations. The same representation was adopted in KESHAVAMURTY's (1973) analysis, discussed above. Values in the diagram are estimated from the data of the meridional wind component and averaged in the lower troposphere 0.3 through the 5.4 km level. The regression line is drawn subjectively after that.

One can easily see in the figure that the phase difference increases systematically with increasing longitudinal difference. It is well approximated by the line drawn in the diagram. Since the positive $\Delta\lambda$ means the eastward direction, the positive inclination of the regression line indicates that the disturbance in this period range propagates westward through this region. One can estimate the longitudinal wavelength of the disturbance from the value of inclination of the line. In this case, it shows the wavelength of about 25° to 30° longitude. One can also estimate its phase speed from the wavelength, because we already know the periodicity of the disturbance. It is about 5° to 6°/day when we adopt 5 days as the mean periodicity.

Above results on the wavelength and the direction of propagation agree well with

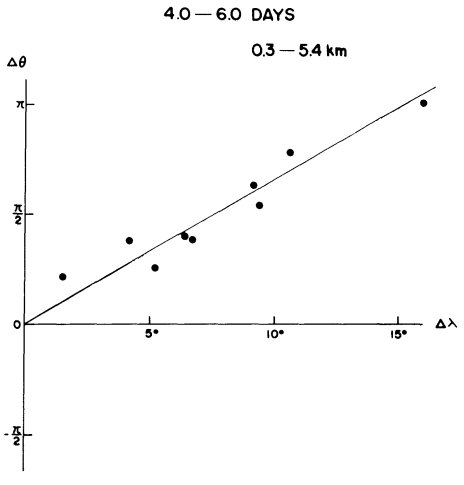

Figure 7
Relationship between the phase difference of the meridional wind variation ($\Delta\theta$) and the longitudinal difference ($\Delta\lambda$) of the stations in the period range 4.0 through 6.0 days. (MURAKAMI, 1976.)

the discussion of KESHAVAMURTY (1973) on the disturbance with the same periodicity. This agreement also supports the statement that the above periodicity, appearing over the monsoon trough region in northern India, reflects the passage of monsoon lows through this region as originally claimed in KESHAVAMURTY'S work. However, as for the oscillation around the 10 to 15-day period, the horizontal cross spectra of zonal wind in MURAKAMI'S (1976) work did not show any tendency of propagation. The values of phase differences are small and they occasionally take positive or negative signs, though the figure is not shown in this paper. This means that the disturbance associated with this periodicity may have a very large horizontal scale and/or it oscillates as a standing wave. The behavior of this disturbance will be discussed further in the following sections.

4. Vertical structure

The technique of cross spectrum is also applicable to the data of the different altitudes at one station. KESHAVAMURTY (1972) examined the vertical phase difference of the meridional wind variation associated with three major periodicities, namely 15–20 days, 5–6 days and 7–8 days, picked up by his former work using the same data set. After examining the data of Nagpur (21°N, 79°E) and Calcutta (23°N, 88°E), he reported that the axes of the disturbances associated with the above periodicities are either nearly vertical or tilt slightly westward with height. As he further pointed out, a westward tilt of the axis means the northward heat transport when we take into account the geostrophic and hydrostatic balance. Considering this with the

existence of the intense northward gradient of the mean temperature over India during the summer monsoon season, it implies the conversion from the eddy available potential energy to the zonal available potential energy, being opposite to that accompanied by baroclinic instability.

By using the spectral method, M. MURAKAMI (1976) also examined the vertical structure of monsoon lows which are picked up as the ones associated with the periodicity around 5 days. Figure 8 shows the vertical distribution of variances, coherences and phase differences relative to the 3-km level based on the data of the meridional wind variation at Calcutta (23°N, 88°E). It is shown that the variance of the meridional wind reaches its maximum at about the 3-km level and decreases with height above. The coherence relative to the 3-km level also becomes small in the upper levels. On the other hand, the profile of phase differences in time shows the systematic phase increase with height, though the inclination is rather slight except for the uppermost layers. Considering this phase distribution with the fact that the disturbance in this period range propagates westward, as previously shown in Fig. 7, it can be concluded that the axis of monsoon lows tilts slightly westward with height.

The same technique was also applied to the temporal variation of thermal variables. Figure 9 shows the vertical distribution of variances of the temperature and the specific humidity together with their phase differences relative to the 7.2 and 3-km levels, respectively. It is remarkable that the temperature variation shows the large variance in the upper levels in contrast with the meridional wind. Variances of the specific humidity are nearly constant below the 3-km level, but the phase distribution indicates that its axis tilts eastward with height in the lower troposphere.

Up to this point we have discussed the vertical structure of each variable separately. However, in order to get the total structure of the disturbance, we should get further information on the mutual phase relationship between the oscillations of different variables. This purpose can be achieved by the inter-variable cross-spectrum analysis. Figure 10 represents the synthesized mean vertical structure of monsoon laws which bring the periodicity of about 5 days, as discussed above. In this process the amplitude was estimated from the power of each variable and the relative phase relationship was obtained from the results of inter-variable cross-spectrum analysis. It should be noted that the original phase difference in time has been transformed into the longitudinal difference in this figure by considering the result that the monsoon lows propagate westward and their longitudinal wavelength is about 30°. The vertical trough line was determined as the one where the meridional wind changes from northerly to southerly.

The structure of the meridional wind in Fig. 10 shows that the cyclonic circulation of the monsoon law is prominent below the 500-mb level or so. The trough line tilts slightly westward, as previously discussed in the context of Fig. 8. On the other hand, the associated anomaly of the temperature is large in the upper levels and the area of warm anomaly nearly coincides with the trough in these levels. It indicates that the monsoon low has a warm core in its upper part. This upper warm core is also consistent with the fact that the intensity of the cyclonic circulation decreases with height in the

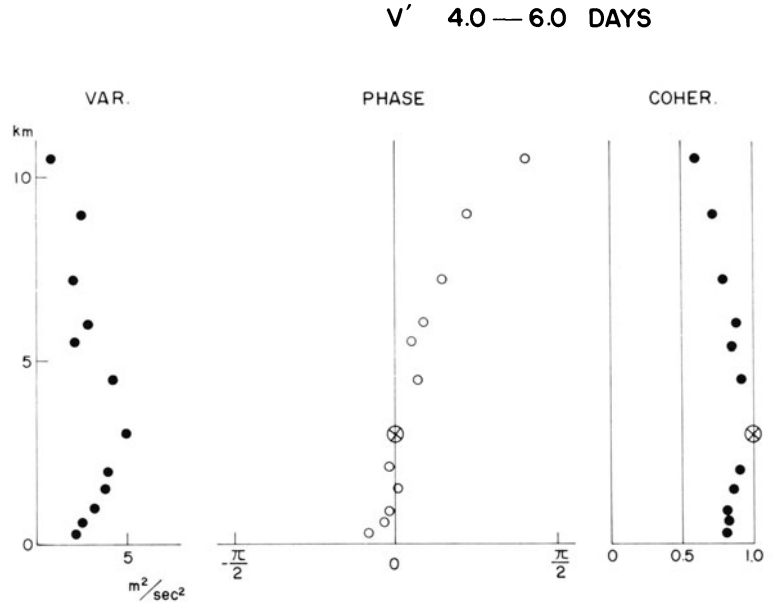

Figure 8
Vertical distributions of the variance (left), the phase differences (middle) and the coherences (right) of the meridional wind at Calcutta in the period range 4.0 through 6.0 days. (MURAKAMI, 1976.)

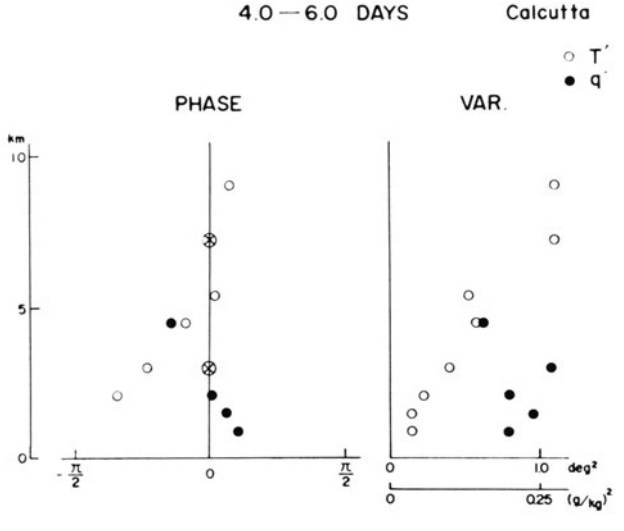

Figure 9
Same as Fig. 8 except for the phase (left) and the variance (right) of temperature (T') and the specific humidity (q').

upper levels. As for the configuration of specific humidity, the area of moist anomaly appears east of the trough in the lower troposphere. We can see that this area coincides well with the southerly wind. Relatively dry anomaly takes place in the west of the trough with the northerly wind.

As mentioned above, this structure is based on the data at Calcutta which is located on the coast of the north Bay of Bengal. In other words, Fig. 10 shows the structure of monsoon lows at the time when they cross the coast of the Bay. Recently, MURAKAMI (1977) examined the structure of these monsoon lows by using the station located in the inland area of northern India. It is found that a drastic change takes place in the configuration of specific humidity when the lows proceed into the inland area, while the structure of the meridional wind and the temperature remain relatively unchanged.

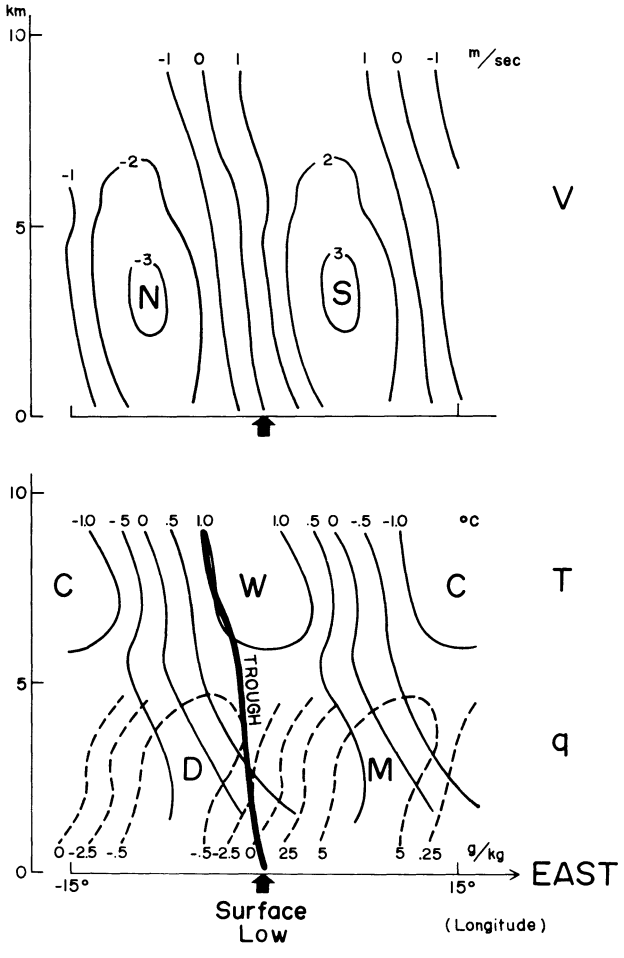

Figure 10
Mean vertical structure of monsoon lows at Calcutta. (MURAKAMI, 1976.)

When monsoon lows pass through the inland area, a moist anomaly occurs in the west of the trough in contrast with the configuration shown in Fig. 10. This configuration of the moist anomaly over the inland area, however, is rather consistent with our synoptic experience. That is, the major rainfall occurs ahead of the trough when the lows travel westward through the inland part of the monsoon trough region in northern India. As is already known, there exists, longitudinally, very different situations along the axis of monsoon trough between the north Bay of Bengal and the inland of the subcontinent, including the large-scale geographic contrast. It is speculated that this difference is likely to cause the change in the configuration of enhanced convective activity associated with the lows and this change, in turn, can bring the difference in the configuration of thermal anomalies such as specific humidity.

As for the variation with a period of 10 to 15 days, M. MURAKAMI (1976) depicted a different picture from KESHAVAMURTY (1972, 1973), who regarded it as the mode of monsoon depressions. As discussed in the previous section, the oscillation of this period range is prominent mainly in the zonal wind component in the monsoon trough region. Besides, it was found that this zonal wind oscillation is closely related to the variation of monsoonal rainfall in the western coast of India. By using the time-composite technique, he further showed that this quasi-periodic variation has a nature of the standing oscillation. This standing nature and the horizontal extent imply the existence of the large-scale circulation cell and its overturning. It is suggested that the north–south circulation between the Bay of Bengal and the Tibetan plateau and the east–west one between the Indian subcontinent and the Indo-China region can play an important role in this oscillation.

5. Application to the large-scale aspects

As already well recognized through the past observations, the monsoon is not a local phenomenon but is actually a part of large-scale circulation system which extends over both the winter and the summer hemispheres. It consequently implies that the variation of monsoonal activity ought to be studied in the context of the variation of this large-scale circulation system. It also suggests that there is a close interrelationship between the sequences occurring in the different places within the regime of this circulation.

FINDLATER (1969) found that kind of linkage between the monsoonal rainfall in the western coast of India and the low-level, cross-equatorial jet (so-called Somali jet) over the eastern coast of Africa. Figure 11 shows the result of his analysis. It is clearly shown that there is a good association between the intensities of the two parameters. In addition, we can also clearly see that the temporal variations show the quasi-periodicity, which can be specified somewhat in the range from 10 to 20 days.

T. MURAKAMI (1976) applied a space-time correlation technique to the daily

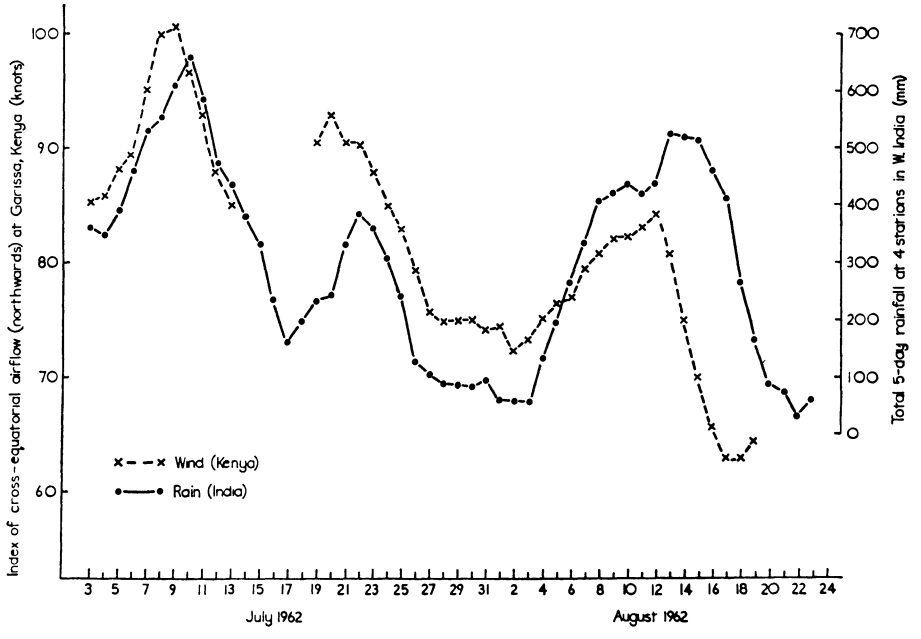

Figure 11
Cross equatorial airflow at Garissa, Kenya in relation to rainfall at four stations in western India. (FINDLATER, 1969.)

satellite cloudiness data. It is noted that the cloudiness fluctuations over India during the summer monsoon period has a remarkable positive correlation with those over Indo-China, Indonesia and the central South Pacific. Negative correlation was obtained with the variations over the north Pacific, the central Indian Ocean and the African region. It is also briefly mentioned that the power spectra of the cloudiness are apt to exhibit a pronounced peak in the period range from 15 to 25 days over the monsoon region. This tendency was also discussed by ZANGVIL (1975) who performed a spectrum analysis on the satellite cloud brightness data in the summer of 1967. He pointed out that the variance of a long period (10 to 15 days) shows its maximum over the Indian Ocean and southeast Asia, while the variance of the short period (3.53 to 5.45 days) tends to concentrate in the zonal strips corresponding to the mean location of ITCZ.

KRISHNAMURTI and BHALME (1976) recently made a comprehensive spectral study on the 'quasi-biweekly' oscillation of the monsoon. Using the data in the summer of 1967, they applied the method of power spectrum analysis to the time series of nine parameters illustrated in Fig. 12. The spectral peak around the 15-day period has been picked up as a conspicuous feature, together with the peak around the 5-day period. One example of their power spectra has been previously shown in Fig. 4. Paying attention to the peak around the 15-day period, they further examined the phase differences between the oscillations of those parameters by the method of cross-

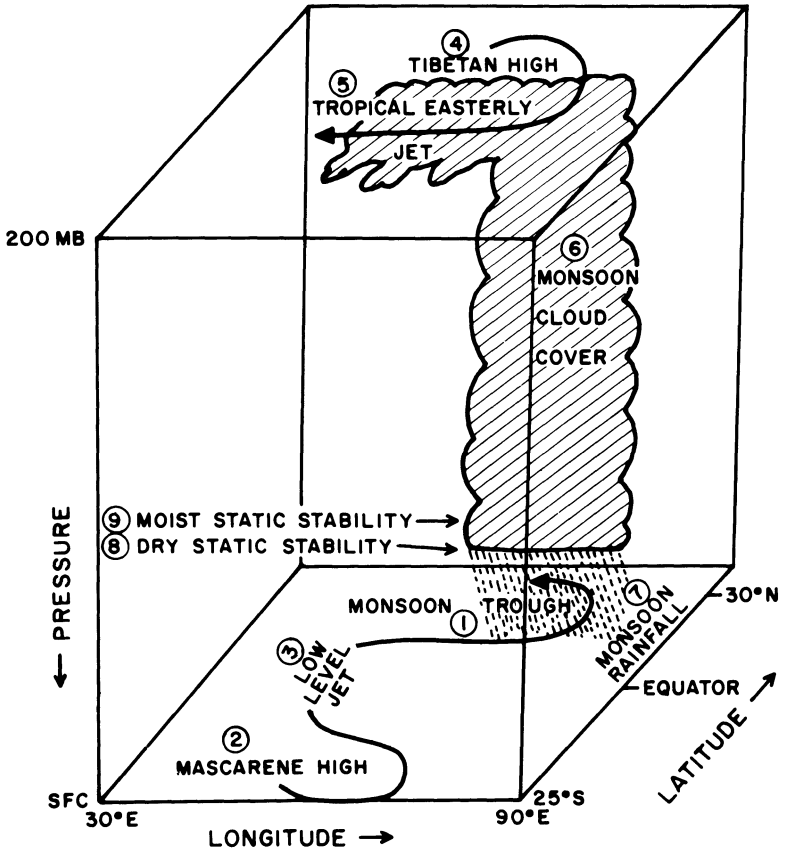

Figure 12
A schematic outline of the nine elements of the monsoon system considered by KRISHNAMURTI and BHALME (1976).

spectrum analysis. Figure 13a,b represent thus obtained phase diagrams for the stabilizing and destabilizing periods, respectively. Though these two diagrams show the same result, except for the phase difference of 1/2 cycle, they are exhibited separately for the purpose of getting a clear insight of the sequence. The stars denote the phase which is specified as the occurrence of four major monsoon depressions during the period of analysis.

Starting with the maximum dry static instability in Fig. 13a, it is followed by the maximum moist static instability. Then the monsoon trough reaches its minimum pressure and the satellite brightness shows the maximum after that. The Mascarene high of the southern hemisphere becomes most intense about 1.5 days after the maximum intensity of monsoon trough. The Tibetan high in the upper troposphere reaches its peak value after that and is followed by an intensification of the tropical easterly jet. It is then that the maximum rainfall occurs over central India. Its phase-delay from

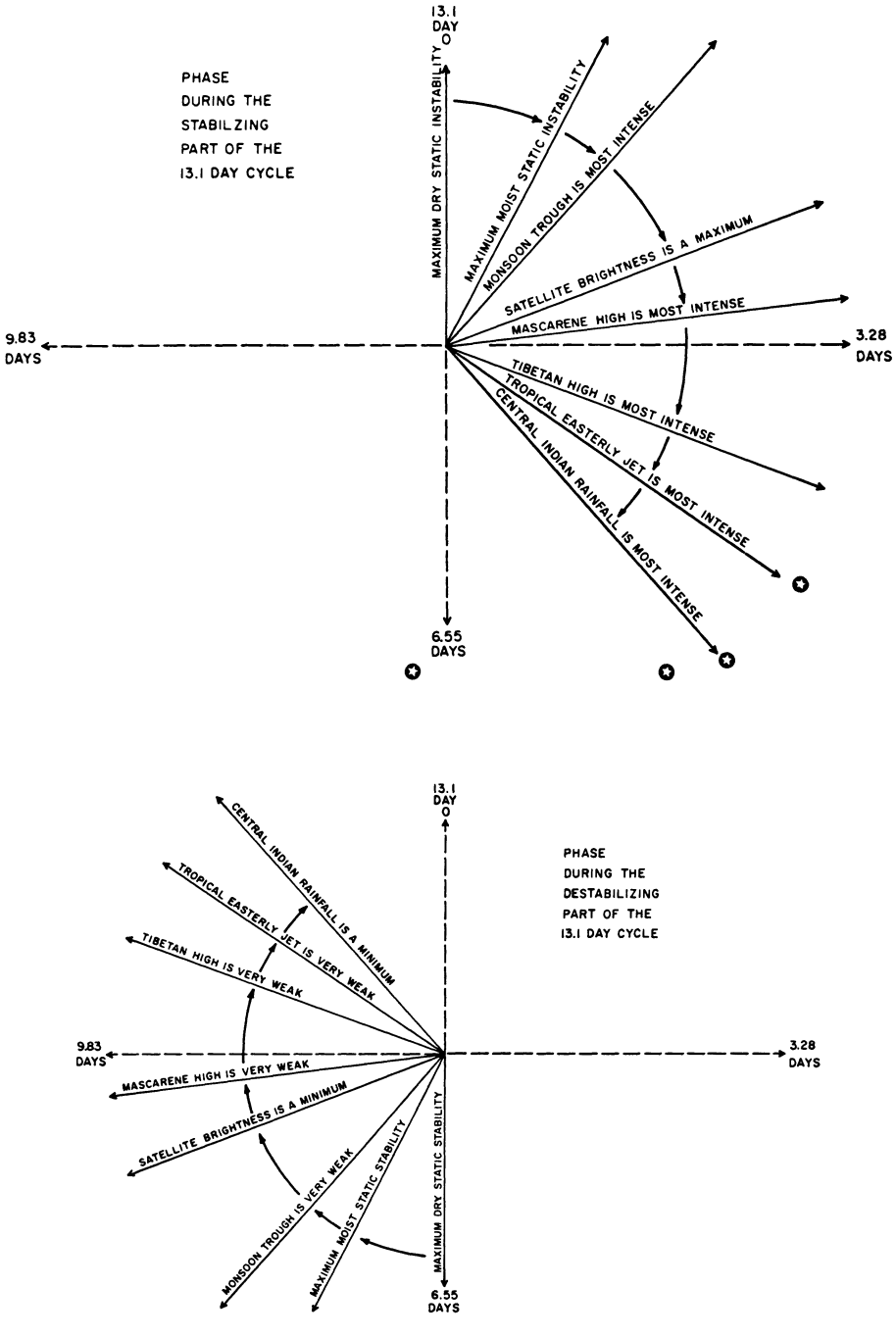

Figure 13
Phase diagram for the elements of the monsoon system during (a) the stabilizing part, and (b) the destabilizing part of the 13.1 day cycle. (KRISHNAMURTI and BHALME, 1976.)

the occurrence of the maximum dry instability is about 5.2 days. During the destabilizing period, shown in Fig. 13b, we can see that the same sequence takes place in the reversed sense.

The above-mentioned sequence draws our interest to a further interpretation of the phenomena, though it is certainly not an easy task to get a convincing story from the limited examples exhibited. KRISHNAMURTI and BHALME (1976) gave one interpretation by taking into account the effect of solar insolation and the variation of the Hadley cell. Their story is as follows:

During the period of strong solar insolation and lack of large cloud cover, the dry static instability over central India increases. This period is likely to be characterized by the large-scale subsidence and shallow convection, both of which play a significant role in restoring the conditional instability over the tropics. Thus it brings the maximum moist instability. Meanwhile, the surface heat low is extending into central India, leading to the maximum intensity of the monsoon trough. Then, the situation of enhanced cloud brightness takes place and this brings the intensification of the Hadley type overturning. The rising branch is supposedly located over northeastern India and the sinking branch is presumed to intensify the Mascarene high over the subtropical region in the southern hemisphere.

It is then explained that the 'build up' of the Hadley type overturning intensifies the Tibetan high and the tropical easterly jet. This situation is presumed to comprise the favorable conditions for the formation of monsoon depressions and the quasi-biweekly mode of the rainfall in central India is attributed to these depressions. This is also the stage in which the enhanced convective activity and the reduced insolation due to the large cloud amount, cause the stabilization of the lower atmosphere. The destabilizing cycle shown in Fig. 13b starts hereafter.

The interpretation mentioned above deserves careful consideration and, to the best of the author's knowledge, it is the first attempt to give a consistent and closed explanation of the monsoonal fluctuation from the viewpoint of inter-hemispheric system. However, as one could have easily noticed, the above story still has some physical ambiguities to be further examined and revealed. For example, the mechanism which is directly responsible to the cyclogenesis of monsoon depressions should be investigated further. The above story does not have quantitative bases, either such as heat or as a momentum budget associated with the monsoonal fluctuation. Besides, the story might be different when we consider the interaction with other regions such as southeast Asia and western Pacific. Anyway this analysis has raised a challenging problem which should be investigated thoroughly by using more complete data set.

6. Concluding remarks

In this paper, the spectral investigations performed on the subject relevant to the Indian monsoon have been discussed and an assessment made of their results. It

emerged that the various independent analyses showed the spectral peaks of around 15 days and 5 days in common. This fact indicated that the physical substantiality of these periodicities was very likely. It should also be noted that there are some results which show other spectral peaks, but their appearance is somewhat occasional and not very convincing at present. We should accumulate more results and carry out closer examination, including the statistical evaluation, in order to establish the existence of these periodicities.

The investigation on the structure of the disturbance associated with the specified periodicity can be accomplished by the technique of cross-spectrum analysis. It turned out that the disturbances which cause the oscillation around the 5-day period in the summer monsoon show their main amplitude in northern India along the range from the north Bay of Bengal through the monsoon trough region. Horizontal cross-spectrum analysis revealed the fact that they are propagating westward and have a wavelength of about 25 to 30 degrees in longitude. It is concluded that they correspond to the synoptic disturbances called 'monsoon lows' which are formed and travel westward in the region mentioned above. Their vertical structure was also obtained by the method of cross-spectrum analysis which was performed vertically. It has been exhibited that the cyclonic circulation associated with monsoon lows was prominent mainly in the lower troposphere and its axis tilts slightly westward with height. They also bear the warm-cored structure in their upper part. This vertical structure along with the periodicity and wavelength provides us with main elements to be considered when we do the theoretical study on their cyclogenesis.

As for the oscillation around the 15-day period, recent analyses show that it is related to the large-scale fluctuation of the monsoon circulation itself. Though the fluctuation is also likely to have some connections with the formation of monsoon depressions over the north Bay of Bengal, it seems inappropriate to link the depressions directly with the 15-day period oscillation. The monsoon depression itself belongs to the group of westward-moving, synoptic-scale disturbances and its structure is rather similar to that of monsoon lows. It seems that the 15-day mode is not the one moving one-directionally, but is essentially a large-scale standing oscillation.

Quite recently, KRISHNAMURTI *et al.* (1977) examined the situation which leads to the formation of monsoon depressions. In their analysis of the surface pressure along the latitude of 20°N, it is shown that two different kinds of disturbances exist. One is the planetary-scale standing oscillation (longitudinal wavenumber = 1) with a period of about 15 days, which seems to reflect the variation of the monsoon trough over northern India. Another is the smaller scale (wavenumber 3 to 12) westward-moving waves coming from western Pacific across Indo-China. They claim that the interaction between these two modes over the north Bay of Bengal is responsible for the formation of monsoon depressions. In addition, they showed that the impact of the typhoon which reaches the coast of Southeast Asia can often be a trigger of this interaction.

As for the large-scale aspect of the monsoonal fluctuation around the 15-day

period, spectrum analysis shows that this periodicity can be seen in the various parameters which are supposedly associated with the monsoon circulation. By examining the phase difference between the oscillations of different parameters, we can get the sequence of events which occur during the cycle of fluctuation. Though the detailed discussion is not repeated here, it is likely that the variation of monsoon activity is closely related to the variation of the insolation due to the change of cloudiness and the variation of the Hadley-type overturning which affects both the summer and winter hemispheres.

However, we should concede that the total explanation of the mechanism of the monsoonal fluctuation has not been achieved yet. For example, the existence of the east–west circulation and the scale interaction with the disturbances embedded in the large-scale circulation seem to be important factors, which should be taken into account by the further investigation. Besides, we should be careful when we interpret the results of cross-spectra, because the sequential occurrence of events does not necessarily mean the existence of the causal relationship between them. Anyway, the above subject will be one of the best-fitted problems in the forth-coming FGGE/MONEX.

Acknowledgments

The author wishes to express his thanks to Prof. T. N. Krishnamurti for his valuable encouragement throughout the work. The author is also indebted to Mr. Gary Van Dan for photographic work.

This work was supported by the Atmospheric Sciences Section of the National Science Foundation under Grant ATM 75-18945.

References

ANANTHAKRISHNAN, R. and KESHAVAMURTY, R. N. (1970), *On some aspects of the fluctuations in the pressure and wind fields over India during the summer and winter monsoon seasons*, Proc. Symp. Tropical Meteorology, Honolulu, Hawaii.

BHALME, H. N. and PARASNIS, S. S. (1975), *5–6 days oscillations in the pressure gradients over India during SW monsoon*, Indian J. Met. Geophys. *26*, 77–80.

FINDLATER, J. (1969), *A major low-level air current near the Indian Ocean during the northern summer*, Quart. J. Roy. Meteor. Soc. *95*, 362–380.

HIROTA, I. (1975), *Spectral analysis of planetary waves in the summer stratosphere and mesosphere*, J. Meteor. Soc. Japan *53*, 33–44.

KESHAVAMURTY, R. N. (1972), *On the vertical tilt of monsoon disturbances*, J. Atmos. Sci. *29*, 993–995.

KESHAVAMURTY, R. N. (1973), *Power spectra of large-scale disturbances of the Indian southwest monsoon*, Indian J. Met. Geophys. *24*, 117–124.

KRISHNAMURTI, T. N. and RODGERS, E. B. (1970), *200 mb wind field June, July, August 1967*, Tech. Report No. 70–2, Florida State University.

KRISHNAMURTI, T. N., DAGGUPATY, S. M., FEIN, J., KANAMITSU, M. and LEE, J. D. (1973), *Tibetan high and upper tropospheric tropical circulations during northern summer*, Bull. Amer. Meteor. Soc. *54*, 1234–1249.

KRISHNAMURTI, T. S. and BHALME, H. N. (1976), *Oscillations of a monsoon system, Part I: Observational aspects*, J. Atmos. Sci. *33*, 1937–1954.

KRISHNAMURTI, T. S., MOLINARI, J., PAN, H. L. and WONG, V. (1977), *Downstream amplification and formation of monsoon disturbances*, Submitted for publication to Mon. Wea. Rev.

MARUYAMA, T. (1968), *Time sequence of power spectra of disturbances in the equatorial lower stratosphere in relation to the quasi-biennial oscillation*, J. Meteor. Soc. Japan *46*, 327–342.

MITCHELL, J. M., Jr. (1966), *Climatic change*, WMO Tech. Note *79*, 33–75.

MURAKAMI, M. (1976), *Analysis of summer monsoon fluctuations over India*, J. Meteor. Soc. Japan *54*, 15–31.

MURAKAMI, M. (1977), *On the structure of monsoon lows over the inland area of northern India*, Submitted for publication to J. Meter. Soc. Japan.

MURAKAMI, T. (1972), *Equatorial stratospheric waves induced by diabatic heat sources*, J. Atmos. Sci. *29*, 1129–1137.

MURAKAMI, T. (1976), *Cloudiness fluctuations during the summer monsoon*, J. Meteor Soc. Japan *54*, 175–181.

RAMAGE, C., *Monsoon Meteorology* (Academic Press, New York 1971) 296 pp.

RAO, Y. P. (1976), *Southwest monsoon*, Meteorological Monograph, Indian Meteorological Department.

RIKIISHI, K. (1976), *Method of computing the power spectrum for equally spaced time series of finite length*, J. Appl. Meteor. *15*, 1102–1110.

WALLACE, J. M. (1971), *Spectral studies of tropospheric wave disturbances in the tropical western Pacific*, Rev. Geophys. Space Phys. *9*, 557–612.

YANAL, M., *A review of recent studies of tropical meteorology relevant to the planning of GATE* in Experiment Design Proposal for the GARP Atlantic Tropical Experiment, Vol. 2, Annex 1 (ICSU/WMO 1971).

ZANGVIL, A. (1975), *Temporal and spatial behavior of large-scale disturbances in tropical cloudiness deduced from satellite brightness data*, Mon. Wea. Rev. *103*, 904–920.

(Received 15th June 1977)

Pageoph, Vol. 115 (1977), Birkhäuser Verlag, Basel

On the Role of the Asian Monsoon in the Angular Momentum and Kinetic Energy Balances of the Tropics[1])

By ABRAHAM H. OORT and PAUL H. CHAN[2])

Abstract – The balance conditions of relative angular momentum and time-mean kinetic energy and their annual variations are studied for the Northern Hemisphere tropical belt. The belt is divided into two roughly equal size parts, the monsoon and the extramonsoon regions. The data used consist of all available daily rawinsonde reports from the world aerological network for the two 5-year periods 1958–63 and 1968–73.

In winter, the trade winds in the monsoon and extramonsoon regions are both sources of westerly relative angular momentum for the middle latitude circulation. However, it is found that the angular momentum gained in the extramonsoon region of the Tropics is mostly destroyed by a net southward flow of mass in that region, and becomes regenerated in the monsoon region by a net northward flow of mass there. This excess of angular momentum together with the angular momentum picked up locally in the monsoon region is almost all exported across its northern boundary. It is further found that in winter the Tropics are also an important source of mean kinetic energy for middle latitudes. Again almost all export of kinetic energy was found to take place across the northern boundary of the monsoon sector. Most of this energy must be generated through the pressure gradient term inside the monsoon region itself, the transformation from transient eddy kinetic energy being very small. The proper evaluation of the pressure gradient appears to be the main stumbling block in the present study, preventing us from estimating the generation and thereby, as a residual, the frictional dissipation in the two regions.

In summer, the extramonsoon region remains a source of angular momentum, but the monsoon region with its surface westerlies acts as a sink, leading to a sharp reduction (and even a midsummer reversal) of the export into middle latitudes. Also the export of mean kinetic energy almost vanishes in summer, except for a small southward transfer across the equator. The calculations for two 5-year periods give very similar estimates and thereby show the reliability of the results.

Key words: Monsoon: Effect on angular momentum, effect on kinetic energy; Tropical general circulation.

1. Introduction

The purpose of this study has been to consider the role of the Asian monsoon system in the atmospheric general circulation. Usually in general circulation studies the zonal anomalies are lumped together as transient and/or standing eddies. However, the Asian monsoon 'eddy' is of such a large scale that it seems justified to study it by itself as one of the most important quasi-stationary eddies in the atmosphere.

[1]) Parts of this paper were presented at the International Symposium on Monsoons, March 7–12, 1977 in New Delhi, India.

[2]) Geophysical Fluid Dynamics Laboratory/NOAA, and Geophysical Fluid Dynamics Program, Princeton University, Princeton, New Jersey 08540, USA.

From this global perspective, we have studied the balances of angular momentum and time-mean kinetic energy for the Northern Hemisphere (NH) Tropics. One of our primary objectives has been to compare the monsoon region with the remainder of the NH Tropics as possible sources or sinks for angular momentum and kinetic energy, both in summer and winter.

Previous relevant studies are those by KESHAVAMURTY (1968, 1971) on the summer monsoon balance, and by NEWTON (1971b) and NEWELL *et al.* (1972, Chapter 4) on the annually varying balance.

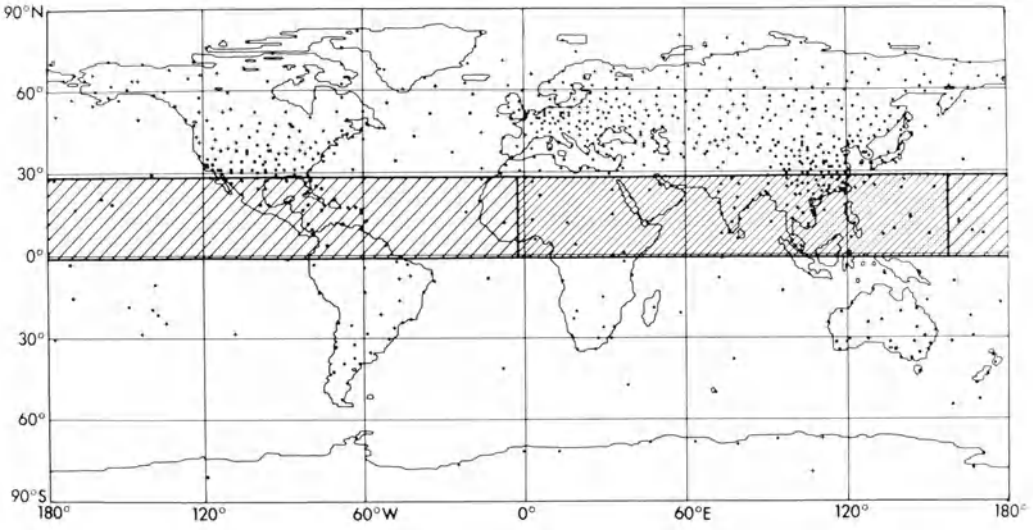

Figure 1
Map of the location of rawinsonde stations used in the present analyses (for the 1958–63 period only stations north of 10°S were available). The monsoon and extramonsoon regions are indicated by heavy and light shading, respectively.

As a data base we have used all daily rawinsonde reports from the global network shown in Fig. 1 for the two 5-year periods May 1958 through April 1963 (only stations north of 10°S), and May 1968 through April 1973. Rather arbitrarily the tropical belt between 1.25°S and 28.75°N was divided into a monsoon region (heavy shading) ranging from the 2.5°W meridian eastward to 157.5°E, and an extramonsoon region (light shading) as the remainder of the belt. Areawise, the monsoon region covers 44 percent of the zonal belt. Figure 1 shows clearly that the station distribution is fairly poor because we have only 106 stations in the monsoon and 55 in the extra-monsoon region. Nevertheless, our choice of a large monsoon region did enable us to estimate with reasonable accuracy at least the gross properties of the monsoon system.

The choice of the monsoon region was made largely on the basis of the areal extent of the upper level easterly jet during summer as given, e.g., on SADLER's (1975)

maps. For easy reference, his maps of the long-term mean streamflow at 200 mb for the months of January and July are reproduced in Fig. 2. One could argue that boundaries near 30°W and 150°E might have been better because more of the African monsoon would have been included in the monsoon region. However, some preliminary calculations with different boundaries (not presented here) show that our conclusions do not depend much on the precise location and dimensions of the region chosen.

To set the background for what follows, a short description of the mean 200 mb flow as depicted in Fig. 2 will be given for the NH tropical belt. In January the

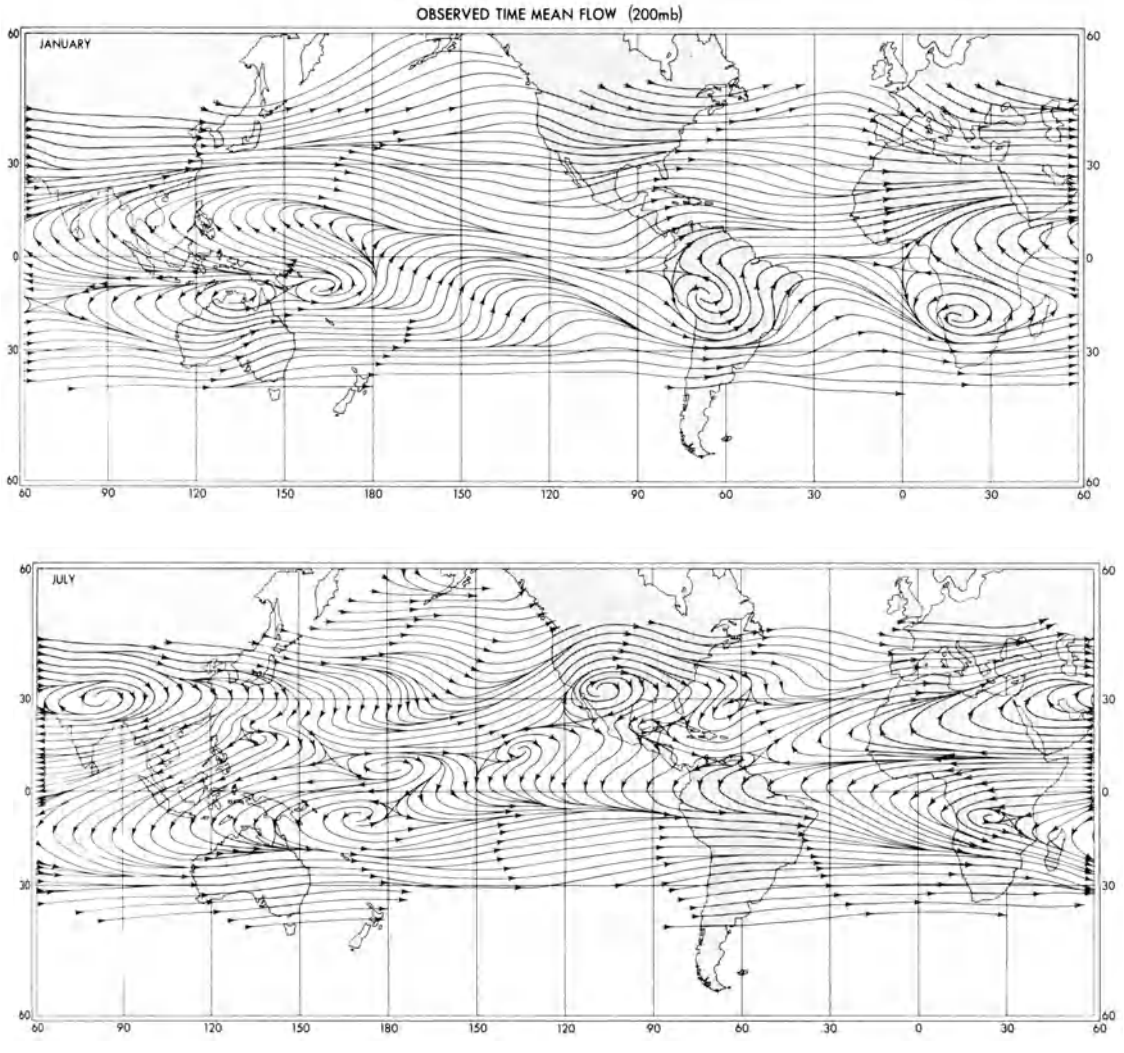

Figure 2
Observed long-term mean streamlines at 200 mb for the months of January (top) and July (bottom) after SADLER (1975).

northern half of the belt is dominated at all latitudes by a strong westerly flow with a noticeable southerly component over southeast Asia and over the Gulf of Mexico. In the southern half of the belt strong south-easterly winds are found in the eastern hemisphere and generally westerlies in the western hemisphere. In July the NH Tropics between about 30°W and 150°E are dominated by the summer easterly jet, while the flow over the rest of the region seems to be more broken up with predominantly westerly winds in the northern and easterly winds in the southern half.

For further reference, we also show the vertical distribution of the zonal and

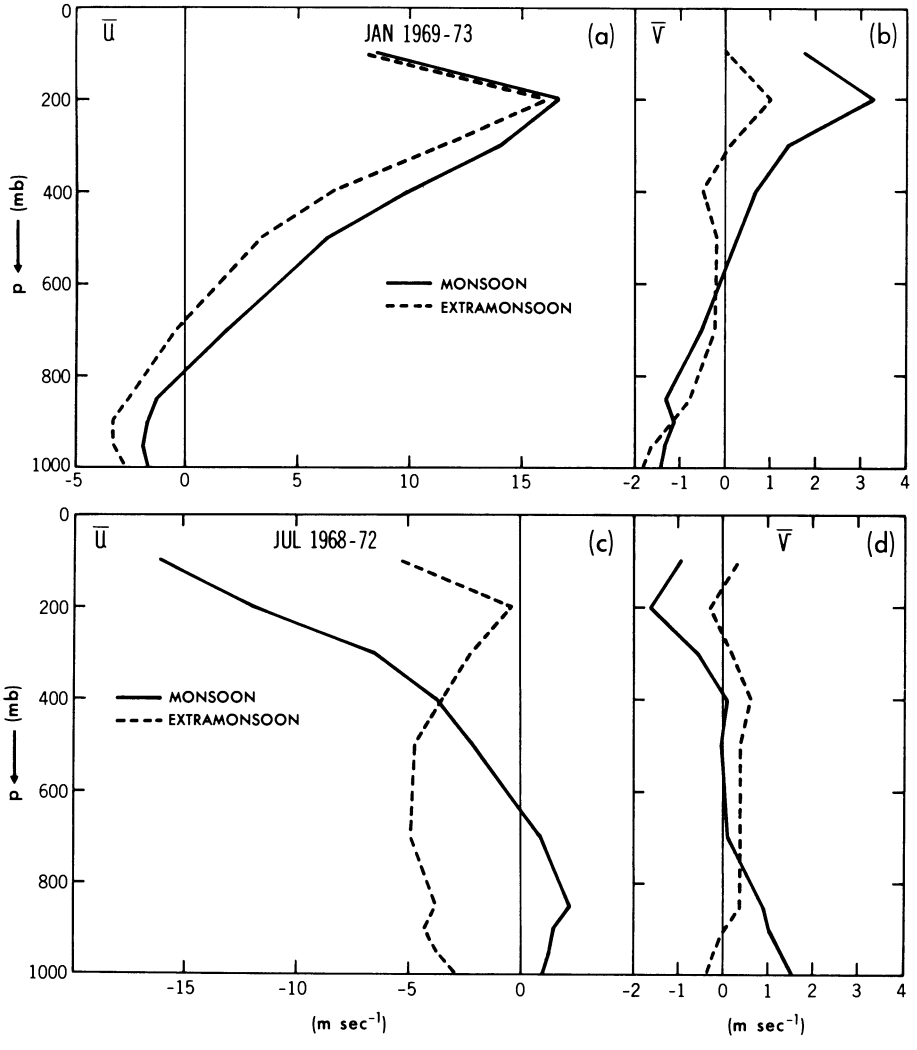

Figure 3
Vertical distribution of the mean zonal and meridional wind components averaged over the monsoon and extramonsoon regions for January (top) and July (bottom). Units are in m sec^{-1}.

meridional wind components averaged over the entire monsoon (solid lines) and extramonsoon (dashed lines) regions in Fig. 3. This figure is based entirely on our data set. Figure 3b for January shows clearly the NH winter Hadley-type circulation over both regions, but much more intense in the monsoon region. For July, Fig. 3d exhibits the penetration of the Southern Hemisphere winter Hadley circulation over the land-dominated monsoon region, while the extramonsoon region (representative for the tropical oceans) still shows the remainder of the Northern Hemisphere winter cell especially at low levels. This interesting point was brought out before by SCHULMAN (1973). The corresponding distributions of the mean zonal wind component in Fig. 3a show in winter slightly stronger westerlies over the monsoon than over the extramonsoon region. In summer, Fig. 3c shows the most dramatic differences between the two regions with, in the monsoon region, westerlies at low levels and the easterly jet at high levels. These results again tend to illustrate the large quasi-permanent zonal anomalies which are characteristic of the tropical circulation.

2. *Angular momentum balance*

In the presently accepted scheme of the general circulation, the tradewinds pick up westerly angular momentum through friction at the surface so that the Tropics may be considered as the principal source region of relative angular momentum. At high levels in the troposphere this angular momentum is then transported to the sink regions in middle and high latitudes where the surface westerlies return the angular momentum to the earth. The question arises what the relative roles of the monsoon and the extramonsoon regions are as tropical source regions.

The vertically integrated balance equation of relative angular momentum (A) for a limited region may be written in the following symbolic form

$$\frac{DA}{Dt} = B(A) + G_{FV}(A) + G_{PG}(A) + F(A) \tag{1}$$

where DA/Dt = rate of change of A with time,
$B(A)$ = rate of influx of A at the boundaries,
$G_{FV}(A)$ = rate of generation of A due to the Coriolis effect ('fv-term'),
$G_{PG}(A)$ = rate of generation of A due to east–west pressure differences at the meridional boundaries of the region,
$F(A)$ = rate of increase of A due to friction at the earth's surface and due to the mountain torque.

The actual expressions for these terms are given in KESHAVAMURTY (1968) and are repeated in Appendix A1.

For the tropical zone as a whole $G_{FV}(A)$, involving the net flow of mass across a latitude circle, is very small (see NEWTON, 1971b), and $G_{PG}(A)$ reduces to zero. For

convenience, the so-called mountain torque was incorporated in $F(A)$. Thus equation (1) may be simplified to the form

$$DA/Dt = B(A) + F(A). \tag{2}$$

The computed seasonal variation in zonal mean relative angular momentum and in its balance are illustrated in Fig. 4. All terms in the angular momentum balance will be expressed in Hadley units as proposed by NEWTON (1971a), where 1 Hadley unit = 10^{25} g cm^2 sec^{-2}. The shift from mean westerlies in winter to mean easterlies in summer is quite pronounced. However, in the actual balance the time rate of

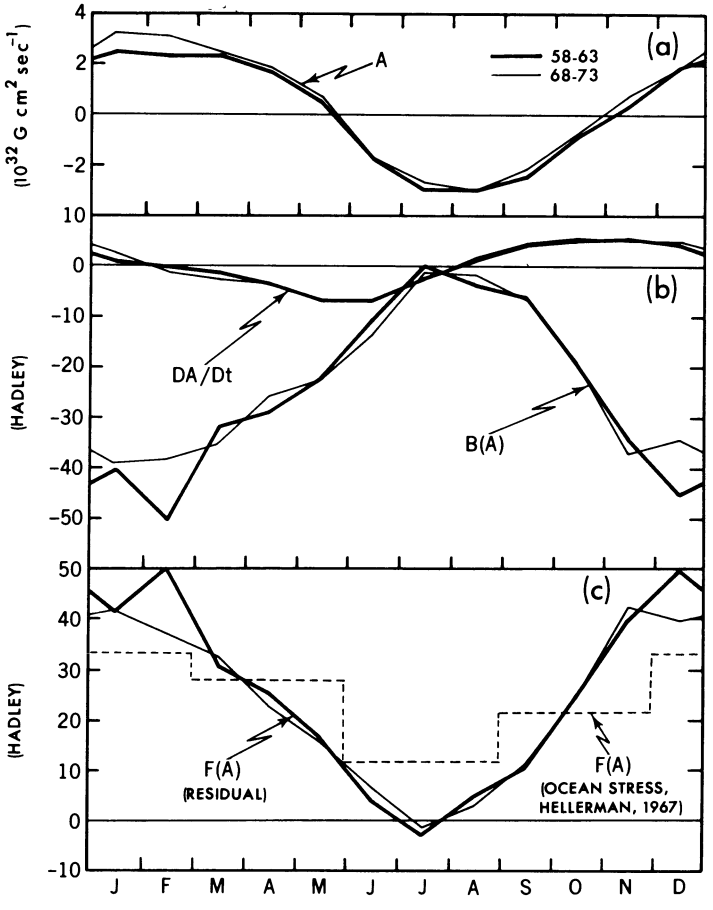

Figure 4

Annual variation of the angular momentum balance for the northern tropical belt (between 1.25°S and 28.75°N) for the two 5-year periods 1958–63 and 1968–73. Shown are (a) the vertically integrated relative angular momentum, (b) the time rate of change of A and the boundary influx, and (c) the friction torque computed both as a residual from our data and independently from HELLERMAN's (1967) ocean stress values. 1 Hadley unit = 10^{25} g cm^2 sec^{-2}.

change, DA/Dt, is relatively small compared with the boundary outflow from the Tropics, $B(A)$, and the pick-up of angular momentum by surface friction in the trade winds, $F(A)$. Only in summer are the three terms of comparable magnitude. The frictional gain, $F(A)$, was computed as a residual in equation (2). The residual method is probably the most reliable method presently available to estimate the frictional gain, at least on a zonal mean basis. For comparison HELLERMAN's (1967) stress values based on actual wind data over the oceans, but extrapolated over land are also shown. Because of the sensitivity of the result to the unknown land values, these last estimates are quite tentative. Nevertheless the seasonal trend in HELLERMAN's

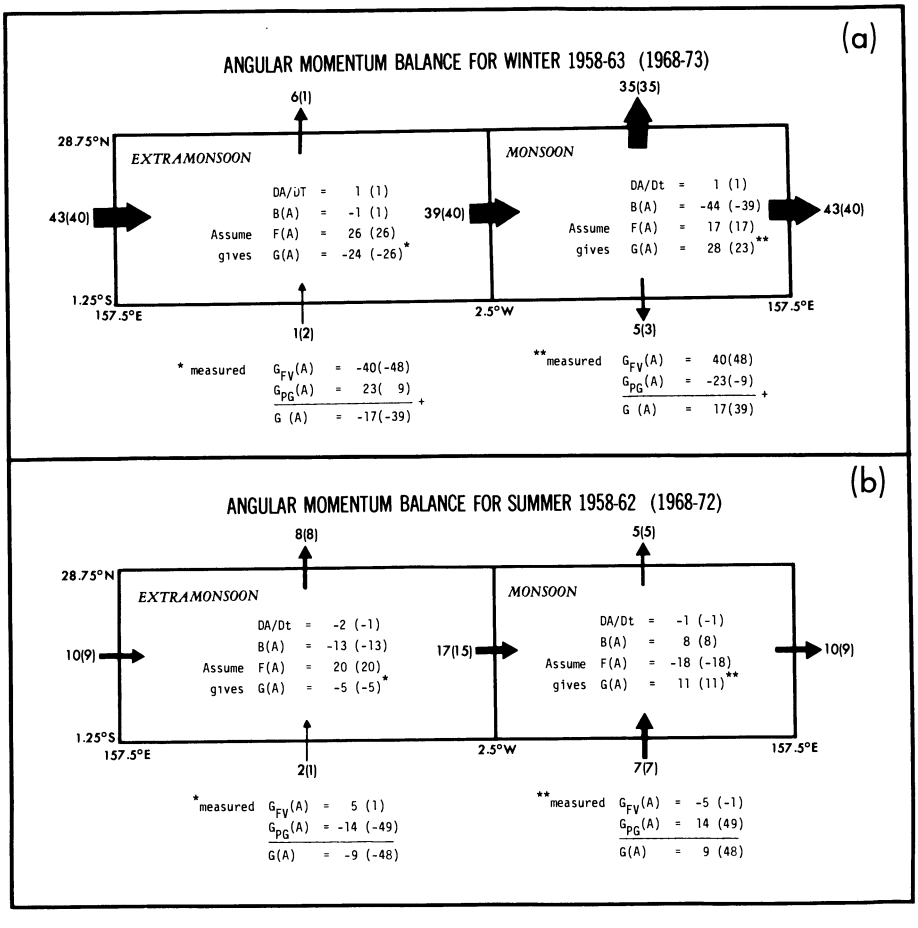

Figure 5

Schematic diagrams of the angular momentum balance for the northern tropical belt for winter (a) and summer (b). Values are given for the 1958–63 period and in parentheses for the 1968–73 period. Inside each box a residual estimate of the total generation rate $G(A)$ is given using HELLERMAN's (1967) adjusted ocean torque values $F(A)$. Below each box actually measured generation rates are shown; they are probably less reliable, especially $G_{PG}(A)$. Units are in Hadley.

results is similar to ours. The curves for the two 5-year periods follow the same pattern and show the stability of the present results.

If one separates the tropical belt into a monsoon and an extramonsoon part, striking differences become apparent. This is shown schematically in Figs. 5a and 5b for the winter (December, January and February) and summer (June, July and August) seasons, respectively.

Before discussing the actual results, the method of evaluation of the various terms will be mentioned. The rate of change with time, DA/Dt, and the boundary fluxes, $B(A)$, are computed directly from our rawinsonde analyses. On the other hand, the friction term, $F(A)$, cannot be computed directly. It was estimated using HELLERMAN's (1967) stress values adjusted to fit our zonal mean values shown before in Fig. 4c. Next equation (1) enabled us to compute as a residual the total generation rate, $G(A) = G_{FV}(A) + G_{PG}(A)$, associated with the net ageostrophic meridional flow of mass in each region. For comparison, directly computed generation rates are also shown at the bottom of each diagram. An examination of the results for the two 5-year periods suggests that the $G_{FV}(A)$ term can be measured fairly reliably, but that the analysis of the east–west pressure gradient in $G_{PG}(A)$ is unreliable. (This unfortunately excluded the possibility of estimating the frictional gain in each sector in a residual manner as was done for the zonal mean case.) Nevertheless, the picture that emerges is clear.

In winter, practically all export of angular momentum, $B(A)$, from the Tropics takes place in the monsoon sector across its northern boundary. However, about 60 percent of the total surface gain, $F(A)$, occurs in the extramonsoon and only 40 percent in the monsoon region. Since there is no net lateral flow of angular momentum from the extramonsoon into the monsoon region, the only solution to this apparent contradiction lies in the contribution of the ageostrophic north–south flow of mass.

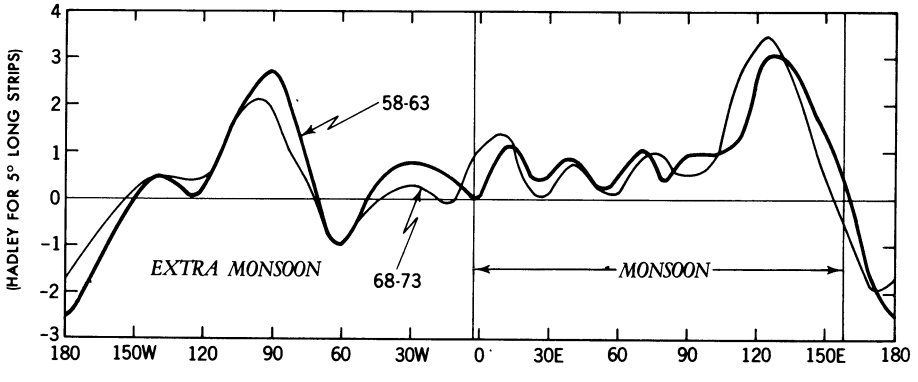

Figure 6
Northward flux of relative angular momentum across the northern boundary (27.5°N) of the tropical belt during winter as a function of longitude.

Thus almost all relative angular momentum picked up at the surface in the extramonsoon trade winds must be destroyed by a southward ageostrophic flow of mass $(\bar{v} - \bar{v}_g)$, and recreated in the monsoon region by a compensating, equal in magnitude, northward ageostrophic flow of mass. (The mass weighted average northward flow in the monsoon region is computed to be on the order of 30 cm sec^{-1}, of which almost half is geostrophically balanced.) To close the cycle this excess of relative angular momentum together with the angular momentum picked up at the surface in the monsoon region itself is all exported at the northern boundary toward middle latitudes. The actual distribution with longitude of this export is shown in Fig. 6. Major peaks of export occur near 90°W and 130°E, associated with the mean northward flow over the Gulf of Mexico and just east of the Asian continent. In the extra-

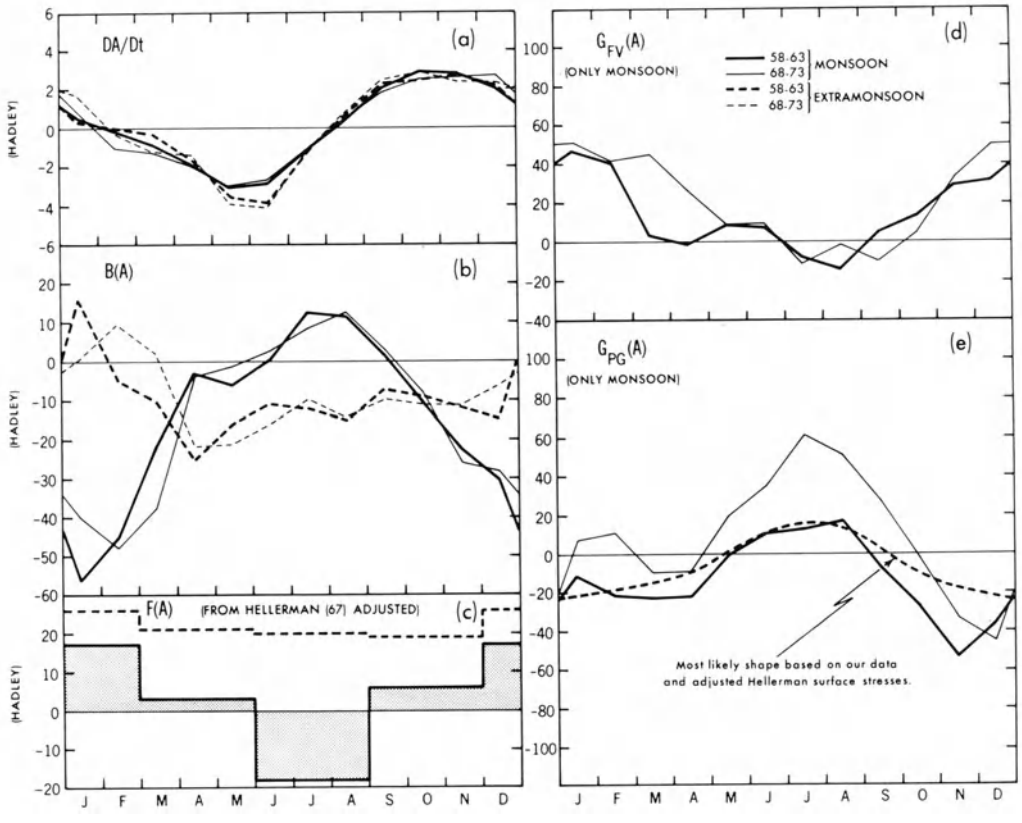

Figure 7

Annual variation of the angular momentum balance for the monsoon (solid) and extramonsoon (dashed) regions for the two 5-year periods. Shown are (a) the time rate of change of A, (b) the boundary influx, (c) the friction plus mountain torque estimates for each season from HELLERMAN (1967) and OORT and BOWMAN (1974), adjusted to fit our zonal mean estimates, (d) measured generation rates associated with the Coriolis effect, and (e) measured generation rates (very unreliable) associated with the pressure gradient effect and our best estimate of this effect (dashed). Units are in Hadley.

monsoon region there is strong compensating southward transport, while in the monsoon region the transport is generally poleward.

The most striking differences between winter and summer in Fig. 5 are found for the monsoon region in the terms $B(A)$ and $F(A)$. These large differences are presumably associated with the Asian land mass north of this region. In the extramonsoon region, which is covered mostly by oceans, the seasonal changes in $B(A)$ and $F(A)$ are considerably smaller, as one would expect. In the monsoon region we calculate a complete reversal from a frictional gain of 17 Hadley units in winter to a frictional loss of 18 Hadley units in summer. This loss is associated with the summer monsoon westerlies over the Indian Ocean. It appears to be partly balanced by an influx of angular momentum across the lateral and southern boundaries (see Fig. 5b), and partly by a (poorly measured) west-to-east pressure gradient. The summer generation due to a net meridional flow of mass seems small in both regions.

More detailed information on the annual cycle in the different components of the angular momentum balance is contained in the graphs in Fig. 7. Shown are curves for each component for the monsoon and extramonsoon regions, (in Figs. 7d and 7e for the generation terms, only the graphs for the monsoon are shown because the extramonsoon curves would equal the mirror image of the monsoon curves with respect to the x-axis) and for the two 5-year periods. The graphs seem to be self explanatory. Let us only mention that in the friction curves for the monsoon a mountain torque contribution of $+3.9$, $+0.5$, -4.6 and $+1.4$ Hadley has been included for winter, spring, summer and fall, respectively, as computed from OORT and BOWMAN's (1974) results.

As a final item of possible interest we have separated the monsoon region into two layers in the vertical. The lower layer between 1012.5 mb (or the ground) and 600 mb contains the summer westerly winds and the upper layer between 600 and 75 mb contains the summer easterly jet. For these two layers the annual variation of angular momentum and the generation due to the fv-term are depicted in Fig. 8. As was shown by KESHAVAMURTY (1968), but only for the summer case, the clear positive correlation between these two quantities suggests the importance of mean meridional overturnings in maintaining the observed vertical distribution of angular momentum of the monsoon throughout the year.

3. *Mean kinetic energy balance*

The maintenance of the time-mean flow in the atmosphere can also be investigated through a study of its kinetic energy balance. As in the case of angular momentum, the role of the Tropics split into a monsoon and an extramonsoon region will be shown.

The vertically integrated balance equation of the kinetic energy of the time-mean flow (K_M) for a limited region may be written in the following symbolic form

$$DK_M/Dt = B(K_M) + C(K_{TE}, K_M) + G(K_M) + D(K_M) \quad (3)$$

where DK_M/Dt = rate of change of K_M with time,

$B(K_M)$ = rate of influx of K_M across the boundaries through (a) a flux of existing mean kinetic energy and (b) the work by eddy stresses,

$C(K_{TE}, K_M)$ = rate of conversion from transient eddy to time-mean kinetic energy,

$G(K_M)$ = rate of generation of K_M due to flow down the mean pressure gradient,

$D(K_M)$ = rate of frictional (and small-scale) dissipation of K_M.

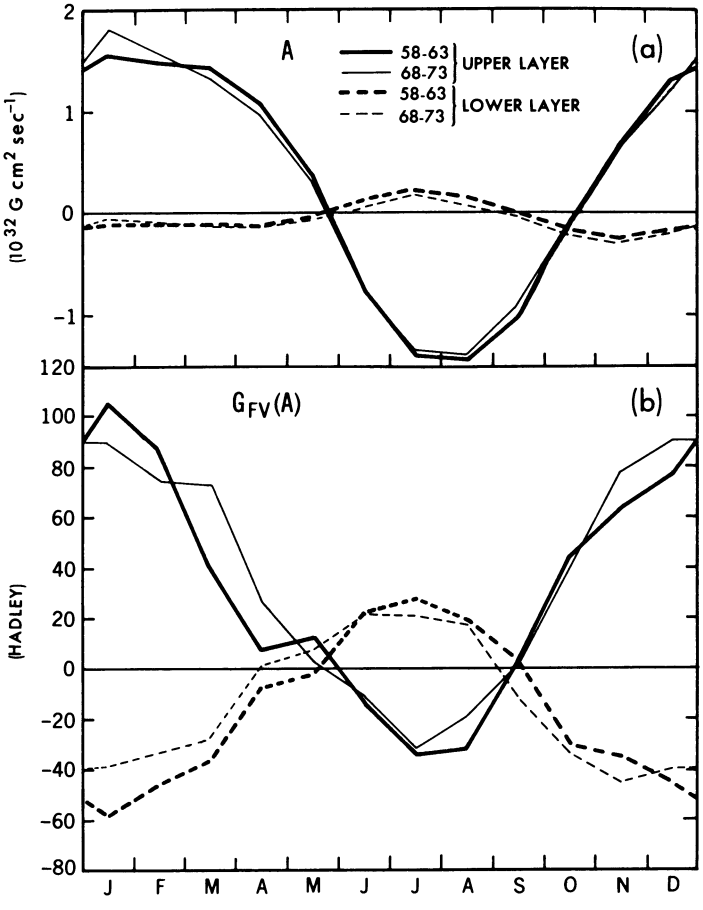

Figure 8

Annual variation of (a) the angular momentum in the monsoon region for the upper (600–75 mb) and lower layers (1012.5–600 mb), and (b) the generation rate of A associated with the Coriolis effect for the same 2 layers.

The actual expressions for these terms are shown in Appendix A2. All results will be presented as average values per unit area in units of W m^{-2}. To convert these average values for the zonal belts, monsoon region and extramonsoon region to total contributions one should multiply them by the area, namely 1.28, 0.57 and 0.71 $\times$ 10^{14} m^2, respectively.

The magnitude of the time-mean (K_M) and transient eddy (K_{TE}) forms of kinetic energy can be considered as a measure of the general level of activity in a certain region. Figure 9a shows annual plots of these two forms of energy for the tropical belt. In winter, the mean motions seem to dominate over the transient ones by a factor of about 1.5, while in summer they are equally strong. In spite of the obvious importance of transient phenomena with time-scales less than one month, the present paper only deals with the quasi-stationary monthly mean flow field.

The contributions by the various terms in the balance of K_M are presented in Figs. 9b through 9e. The rate of change of K_M with time is found to be a small term (please note differences in vertical scales in Fig. 9). Its annual curve shows a major maximum in early winter and a minor maximum in early summer. A similar double maximum can, of course, be seen in the curve for K_M. The conversion rate from transient eddy to stationary kinetic energy is somewhat larger (on the order of 0.3 W m^{-2}) than the rate of change and consistently from eddy to mean flow. (Only the horizontal component of $C(K_{TE}, K_M)$ could be evaluated here.) However, the most important terms in the balance are undoubtedly $B(K_M)$, $G(K_M)$ and $D(K_M)$. Of these terms the boundary flux $B(K_M)$ can be measured quite accurately. The present results show a strong outflow equivalent with about 1.3 W m^{-2} in winter diminishing to an outflow equivalent with about 0.2 W m^{-2} in summer. Since this outflux occurs at the northern boundary, it shows that the Tropics constitute an important source region of mean kinetic energy for the winter hemisphere circulation. The generation term $G(K_M)$ can be split into a zonal part $-\bar{u}g(\partial\bar{z}/\partial x)$ and a meridional part $-\bar{v}g(\partial\bar{z}/\partial y)$. As will be discussed further in the next section, the meridional component appears to give the major positive contribution in the total generation. The present authors suspect that the computed dissipation rates for the mean flow in the Tropics are somewhat on the high side. However, at present no reliable estimates are available of local dissipation rates in the Tropics (KUNG, 1975, OORT and PEIXÓTO, 1974).

The breakdown into monsoon and extramonsoon contributions is shown schematically in Figs. 10a and 10b for winter and summer, respectively. As in the case of angular momentum, almost all boundary outflow of K_M in winter occurs across the northern boundary of the monsoon region. Since there is no net lateral inflow from the extramonsoon region, K_M has to be generated inside the monsoon region itself. The computed generation rate $G(K_M)$ of more than 6 W m^{-2} is actually too large positive. These large values for $G(K_M)$ would lead to unrealistically large residuals for the frictional dissipation rates $D(K_M)$ in the monsoon region. Moreover, in the extramonsoon region a negative generation rate is calculated. This would in

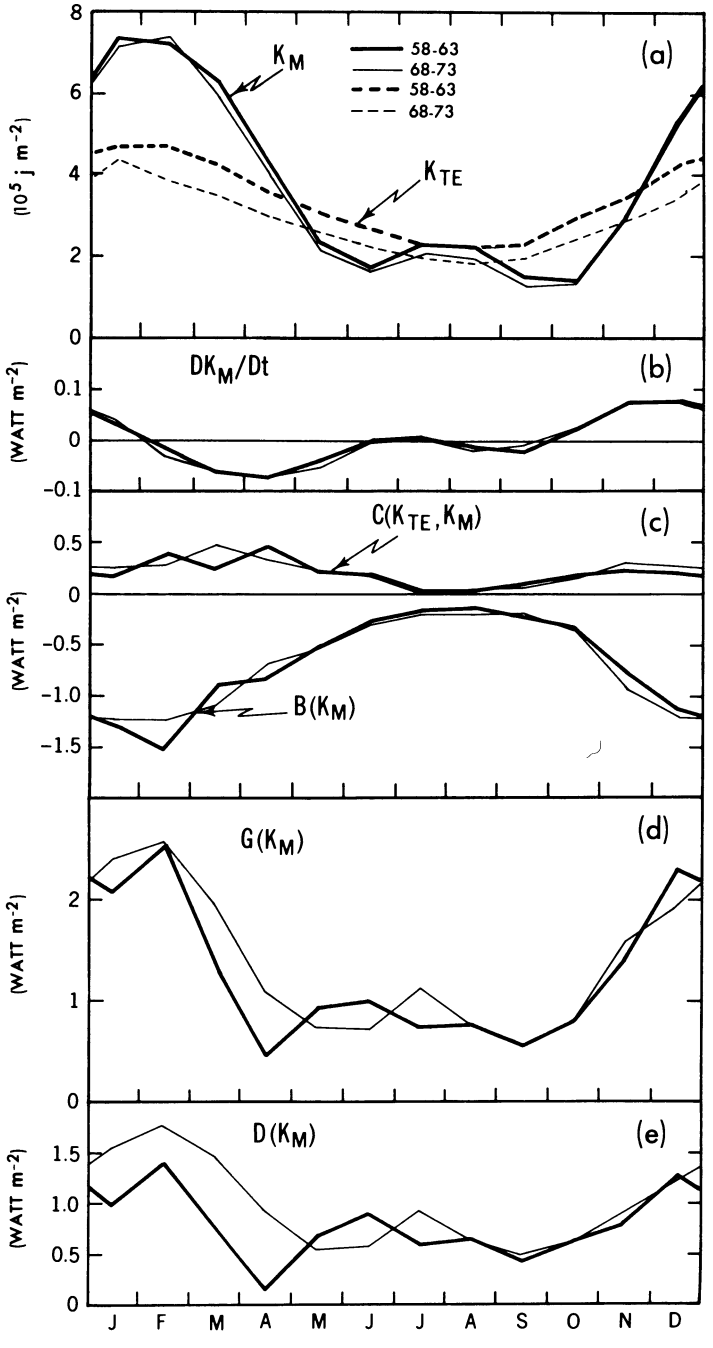

Figure 9

Annual variation in the balance of time-mean kinetic energy for the northern tropical belt for two 5-year periods. Shown are (a) the transient eddy and mean kinetic energy, (b) the time rate of change, (c) the conversion rate from transient to mean kinetic energy, and the boundary influx, (d) the generation rate and (e) the dissipation rate computed as a residual. (The transient eddy kinetic energy curve for the 1958–63 period is consistently higher than for the 1968–73 period because in the first period interannual variations are included in the variance computation.) Units are in W m^{-2}.

turn lead to computed negative dissipation rates. It is likely that these problems are partly due to the great difficulties involved in estimating the zonal pressure gradient $g(\partial\bar{z}/\partial x)$.

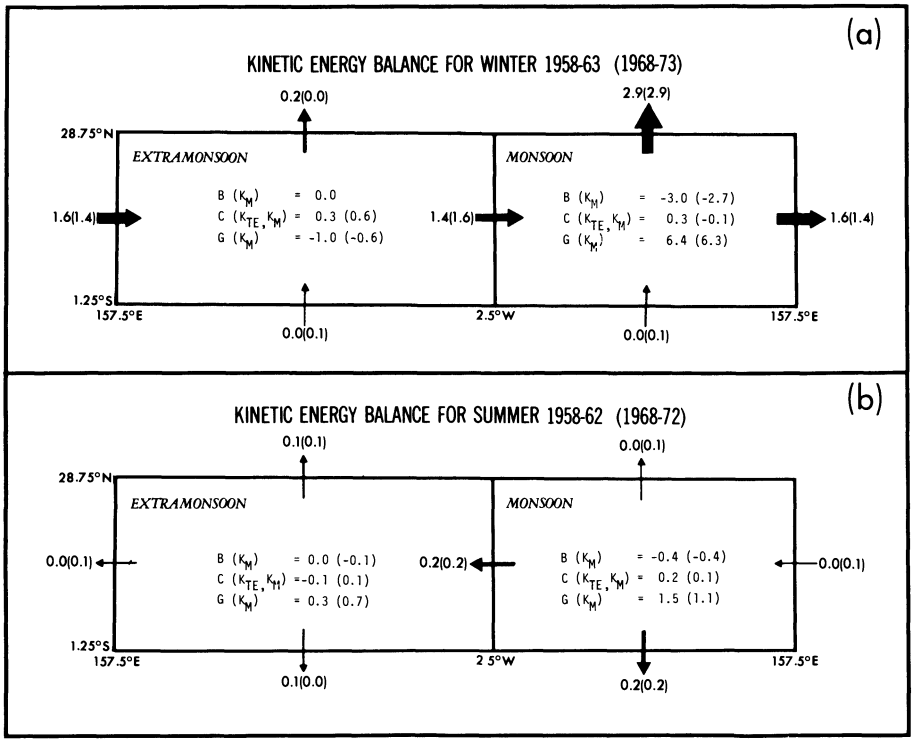

Figure 10
Schematic diagrams of the mean kinetic energy balance for the northern tropical belt for winter (a) and summer (b). Values are given for the 1958–63 period and in parentheses for the 1968–73 period. Because the generation rates are not reliable, no residual estimates of frictional dissipation are given. Units are in W m^{-2}.

In summer, the outflow is very small and mostly across the equator into the Southern Hemisphere. The monsoon region seems again to be the source region for K_M. The generation rate estimates show a similar bias as in winter, namely, that they seem to be too large positive in the monsoon region and too small positive in the extramonsoon region. Nevertheless, it seems reasonable to accept that in summer both the generation and dissipation rates of the mean flow are larger in the monsoon region (on the order of 1 W m^{-2}) with its very strong monsoon currents than in the extramonsoon region. Thus, qualitatively the computed generation rates may give the correct picture.

The annual variation in DK_M/Dt, $B(K_M)$ and $C(K_{TE}, K_M)$ for the monsoon and extramonsoon regions is shown in more detail in Fig. 11. There is, in general, good

agreement between the 1958–63 and 1968–73 estimates for these terms. The estimates for $C(K_{TE}, K_M)$ are almost always positive, but small. They fluctuate between -0.2 and 0.8 W m^{-2}.

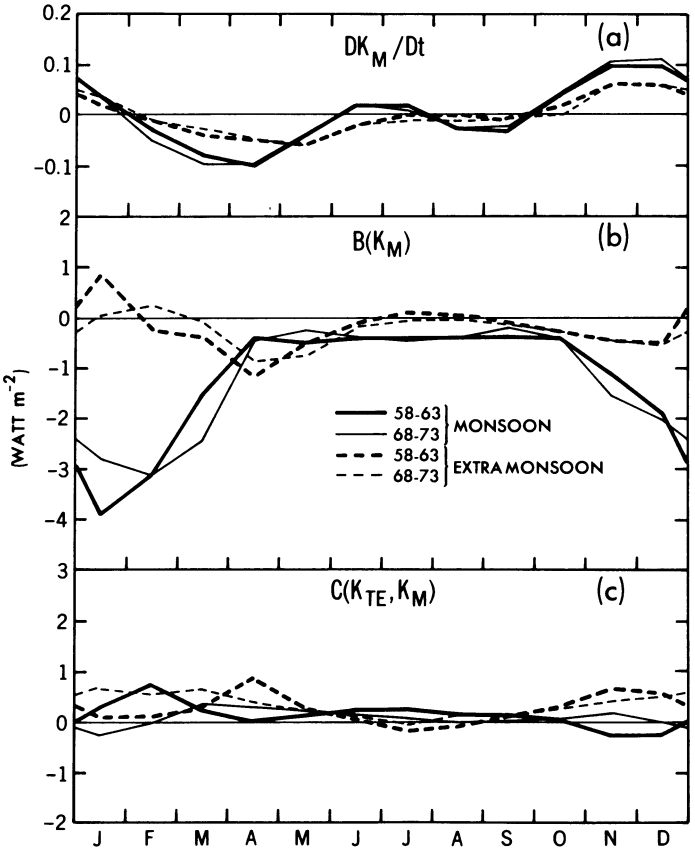

Figure 11
Annual variation of various terms in the mean kinetic energy balance for the monsoon (solid) and extra-monsoon (dashed) regions for the two 5-year periods. Shown are (a) the time rate of change, (b) the boundary influx and (c) the conversion rate from transient eddy to mean kinetic energy. Units are in W m^{-2}.

4. *Some final remarks*

Let us come back to the discussion of the generation term $G(K_M)$. This term can be split into a zonal and a meridional component:

$$G(K_M) = -g \int \bar{u} \frac{\partial \bar{z}}{\partial x} dm - g \int \bar{v} \frac{\partial \bar{z}}{\partial y} dm \tag{4}$$

or

$$G(K_M) = -\int f\bar{u}\,\bar{v}_g\,dm + \int f\bar{v}\bar{u}_g\,dm, \tag{4a}$$

where $\bar{u}_g$ and $\bar{v}_g$ indicate the geostrophic parts of $\bar{u}$ and $\bar{v}$. Equation (4a) shows that in case the mean motions are geostrophic, no mean kinetic energy can be generated and the two components would exactly cancel each other.

To illustrate to what extent the measured velocities are in geostrophic balance, the zonal and meridional components are plotted separately for the tropical belt in Figs. 12a and 12b and for the monsoon region in Figs. 12c and 12d, respectively. Also shown are curves of $\int f\bar{u}\bar{v}\,dm$. From the bottom graphs it is clear that the zonal flow component $\bar{u}$ is in fairly close geostrophic balance, the ageostrophic component contributing to a small, positive generation rate. On the other hand, the top graphs seem to show that the meridional flow component $\bar{v}$ is not in geostrophic balance. Because the pressure gradient term $-\bar{u}g(\partial\bar{z}/\partial x)$ is found to be quite small, the principal balance in the mean zonal kinetic energy equation must be between the $f\bar{u}\bar{v}$ term, the export of mean zonal kinetic energy at the boundaries, and the frictional dissipation.

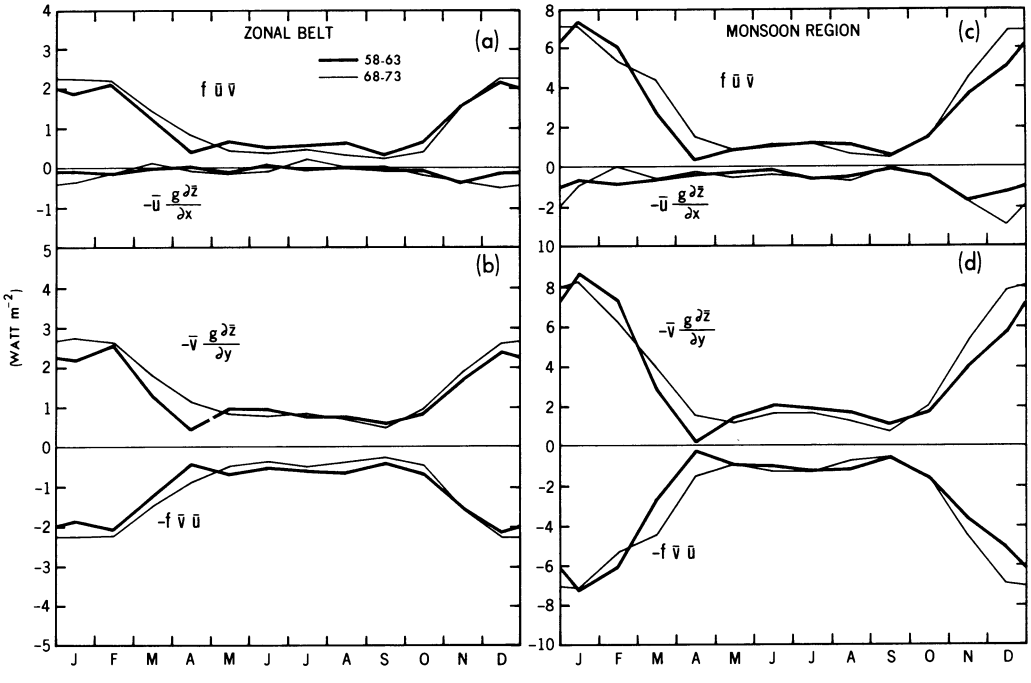

Figure 12

Annual variation of the pressure gradient and Coriolis terms in the zonal (top graphs) and meridional (bottom graphs) components of the mean kinetic energy equation for the zonal belt as a whole (left) and for the monsoon region (right). Units are in W m^{-2}.

The total generation of kinetic energy as given by the flow down the pressure gradient has also been discussed by many other authors, notably by HOLOPAINEN (1964) for a network of aerological stations over the British Isles and by KUNG (1970, 1971) for North America and recently also for the Marshall Islands area in the Tropics (KUNG, 1975). As was found in the present study, reasonable values for the generation rates and inferred dissipation rates can only be obtained after very careful analysis of large quantities of data. The tropical data analyzed by KUNG (1975) showed small but reasonable values for the eddy kinetic energy balance components in summer (on the order of 0.1 W m^{-2} or less). However, for the total kinetic energy KUNG found too large values (on the order of 5 W m^{-2}) for the generation and dissipation rates probably due to the smallness of the sample. Further research on the global distribution of generation and dissipation rates in the atmosphere is clearly needed. Very little is still known quantitatively about the role of continents and oceans, or the role of Tropics and extratropics, as sources or sinks of kinetic energy.

Acknowledgements

The authors would like to thank Mr. S. Hellerman for the use of his wind stress data, Drs. J. Shukla and S. Manabe for their valuable suggestions and comments, and Mr. D. Hahn and Dr. Y. Kurihara for critically reading the manuscript.

Appendix A1

The balance equation of relative angular momentum for a region bounded by meridians λ_1 and λ_2 and latitude circles ϕ_1 and ϕ_2 may be written as follows (see KESHAVAMURTY, 1968)

$$\underset{(1)}{\frac{\partial}{\partial t}\int \bar{u}a\cos\phi\, dm} = \underset{(2)}{-g^{-1}\iint \overline{u^2}\, a^2\cos\phi\, d\phi\, dp\Big|_{\lambda_1}^{\lambda_2}} \underset{(3)}{- g^{-1}\iint \overline{uv}\, a^2\cos^2\phi\, d\lambda\, dp\Big|_{\phi_1}^{\phi_2}}$$

$$\underset{(4)}{+\int (f\bar{v} + \overline{vu}a^{-1}\tan\phi)\, a\cos\phi\, dm}$$

$$\underset{(5)}{-\iint \bar{z}a^2\cos\phi\, d\phi\, dp\Big|_{\lambda_1}^{\lambda_2}} \underset{(6)}{+\iint \bar{\tau}_{0x}a^3\cos^2\phi\, d\lambda\, d\phi}$$

where term (1) = rate of change of angular momentum with time = 'DA/Dt' in the text,

(2) = influx of angular momentum through boundaries at longitudes λ_1 and λ_2,

(3) = influx of angular momentum through boundaries at latitudes ϕ_1 and ϕ_2,

(2) + (3) = '$B(A)$' in the text,

(4) = creation of angular momentum due to Coriolis and curvature effects = '$G_{FV}(A)$' in the text,

(5) = generation of angular momentum due to east–west pressure differences = '$G_{PG}(A)$' in the text,

and (6) = source of angular momentum due to surface friction (for simplicity the mountain torque term is thought to be included here) = '$F(A)$' in the text.

Further a = average radius of the earth,

dm = mass element,

f = Coriolis parameter,

g = acceleration resulting from gravity,

p = pressure,

t = time,

u, v = eastward, northward wind components,

z = 'geopotential' height,

λ = geographic longitude,

$\bar{\tau}_{0x}$ = x-component of surface frictional stress and the mountain torque,

ϕ = geographic latitude,

$\bar{(\ )}$ = time average of ( ),

$(\ )' = (\ ) - \bar{(\ )}$ = departure from time average.

Appendix A2

The balance equation of the kinetic energy in the time-mean flow for a region bounded by meridians λ_1 and λ_2 and latitude circles ϕ_1 and ϕ_2 may be written as follows

$$\frac{\partial}{\partial t}\int \tfrac{1}{2}(\bar{u}^2 + \bar{v}^2)\, dm = \underset{(1)}{} -g^{-1}\int\int (\bar{u}\tfrac{1}{2}(\bar{u}^2 + \bar{v}^2) + \bar{\mathbb{V}}\cdot\overline{\mathbb{V}'u'})a\, d\phi\, dp\Big|_{\lambda_1}^{\lambda_2}$$
(2)

$$-g^{-1}\int\int (\bar{v}\tfrac{1}{2}(\bar{u}^2 + \bar{v}^2) + \bar{\mathbb{V}}\cdot\overline{\mathbb{V}'v'})a\cos\phi\, d\lambda\, dp\Big|_{\phi_1}^{\phi_2}$$
(3)

$$+\int (\overline{u'\mathbb{V}'}\cdot\nabla\bar{u} + \overline{v'\mathbb{V}'}\cdot\nabla\bar{v} + \overline{\omega'\mathbb{V}'}\cdot\frac{\partial}{\partial p}\bar{\mathbb{V}}$$
(4)

$$+ a^{-1}(\overline{uu'v'} - \overline{vu'^2}) \tan \phi)\, dm - g \int \bar{\mathbb{V}} \cdot \nabla \bar{z}\, dm \tag{5}$$

$$+ \int \bar{\mathbb{V}} \cdot \bar{\mathbb{F}}\, dm \tag{6}$$

where term (1) = rate of change of mean kinetic energy with time = 'DK_M/Dt' in the text,

(2) = influx of mean kinetic energy through boundaries at longitudes λ_1 and λ_2,

(3) = influx of mean kinetic energy through boundaries at latitudes ϕ_1 and ϕ_2,

(2) + (3) = '$B(K_M)$' in the text,

(4) = rate of conversion from transient eddy to time-mean kinetic energy = '$C(K_{TE}, K_M)$' in the text,

(5) = rate of generation of mean kinetic energy due to flow down the pressure gradient = '$G(K_M)$' in the text,

(6) = rate of frictional dissipation of K_M = '$D(K_M)$' in the text.

New symbols not defined before are:

$\mathbb{F}$ = frictional force vector,

$\mathbb{V}$ = horizontal vector wind = (u, v),

∇ = horizontal del-operator = $(\partial/a \cos \phi\, \partial\lambda, \partial/a\, \partial\phi)$,

ω = vertical pressure velocity.

References

HELLERMAN, S. (1967), *An updated estimate of the wind stress on the world ocean*, Monthly Weather Review *95*, 607–626, (see also corrections in Monthly Weather Review *96*, 63–74 (1968)).

HOLOPAINEN, E. O. (1964), *Investigation of friction and diabatic processes in the atmosphere*, Societas Scientiarum Fennica, Commentationes Physico-Mathematicae XXIX:9, 47 pp.

KESHAVAMURTY, R. N. (1968), *On the maintenance of the mean zonal motion in the Indian summer monsoon*, Monthly Weather Review *96*, 23–31.

KESHAVAMURTY, R. N. (1971), *On the maintenance of the mean Indian southwest monsoon circulation and the structure and energetics of monsoon disturbances*, Ph.D. thesis, University of Mysore, India, 294 pp.

KUNG, E. C. (1970). *On the meridional distribution of source and sink terms of the kinetic energy balance*, Monthly Weather Review *98*, 911–916.

KUNG, E. C. (1971), *A diagnosis of adiabatic production and destruction of kinetic energy by the meridional and zonal motions of the atmosphere*, Quart. J. Roy. Meteor. Soc. *97*, 61–74.

KUNG, E. C. (1975), *Balance of kinetic energy in the tropical circulation over the Western Pacific*, Quart. J. R. Met. Soc. *101*, 293–312.

NEWELL, R. E., KIDSON, J. W., VINCENT, D. G. and BOER, G. J., *The General Circulation of the Tropical Atmosphere and Interactions with Extratropical Latitudes*, Vol. 1, (M.I.T. Press, Cambridge, Mass. 1972), 258 pp. (see Chapter 4, pp. 131–164).

NEWTON, C. W. (1971a), *Mountain torques in the global angular momentum balance*, J. Atmos. Sci. *28*, 623–628.

NEWTON, C. W. (1971b) *Global angular momentum balance: earth torques and atmospheric fluxes*, J. Atmos. Sci. *28*, 1329–1341.

OORT, A. H. and BOWMAN, H. D., II (1974), *A study of the mountain torque and its interannual variations in the Northern Hemisphere*, J. Atmos. Sci. *31*, 1974–1982.

OORT, A. H. and PEIXÓTO, J. P. (1974), *The annual cycle of energetics of the atmosphere on a planetary scale*, J. Geophys. Res. *79*, 2705–2719.

SADLER, J. C. (1975), *The upper tropospheric circulation over the global Tropics*, UHMET 75–05, University of Hawaii, Honolulu, Hawaii.

SCHULMAN, L. L. (1973), *On the summer hemisphere Hadley cell*, Quart, J. R. Met. Soc. *99*, 197–201.

(Received 15th June 1977)

Pageoph, Vol. 115 (1977), Birkhäuser Verlag, Basel

Monsoonal Quasi-Stationary Ultralong Waves of the Tropical Troposphere Predicted by a Real Data Prediction Over a Global Tropical Belt

by M. KANAMITSU[1])

Abstract – The mechanisms of the maintenance of the tropical upper tropospheric quasi-stationary ultralong waves during the northern hemisphere summer season are briefly reviewed and discussed. Diagnostic and prognostic studies indicate that the waves are maintained by the land–ocean contrast heating. These scales of motion as a whole (sum of the zonal wavenumbers 1, 2 and 3) are considered to supply kinetic energy to all other scales of motion.

The ultralong waves predicted in the real data numerical prediction experiment over the global tropics using a multi-level primitive equation model are examined and compared with the observed climatological waves. The predicted waves are found to have several similarities with the observations. Further investigations of the baroclinic nature of the waves indicate that their thermal structure is essential for understanding their dynamics.

The vorticity budget computations are performed for the predicted ultralong waves at 200 mb and also compared with the climatological observations. It is found that the advection term is one of the leading terms in the vorticity equation.

This study indicates that the tropical quasi-stationary ultralong waves are fully nonlinear, non-geostrophic, three-dimensional waves forced mainly by the convective heating over the monsoon Indian subcontinent.

Key words: Monsoon, Tropical ultralong waves.

1. Introduction

Although the tropical troposphere has long been considered as a primary source region for the general circulation of the atmosphere, studies on the detailed four-dimensional global tropical circulations have not been performed until recently. This was mainly due to the poor observational coverage over the tropics. Research on tropical circulations started from several regional synoptic climatological studies over the area of rich upper air observations (e.g., RIEHL, 1954; KOTESWARAM, 1958; FLOHN, 1964). These studies indicated the existence of several typical quasi-stationary upper tropospheric flow patterns. However, these findings had not been combined to give overall global tropical circulations until the recent analyses by KRISHNAMURTI and ROGERS (1970) became available. They collected commercial aircraft reports

[1]) Meteorological College/Japan Meteorological Agency, Asahi-cho, Kashiwa-shi, Chiba, 277, Japan.

from the major airports in the various tropical countries, and combining them with standard observations, analyzed 92 days of wind fields at 200 mb during June, July and August of 1967.

Based on these massive analyses, KRISHNAMURTI (1971a,b) made several quantitative and qualitative studies of the tropical upper tropospheric circulations during the northern hemisphere summer season. He showed that the flow fields were characterized by a number of very large scale quasi-stationary cyclonic and anti-cyclonic circulations which were expressed mostly by the zonal wavenumbers 1 and 2. He also pointed out that these ultralong waves (zonal wavenumber 1 and 2) had strong southwest to northeast tilt which effectively transported westerly momentum toward the north pole. KRISHNAMURTI (1971a) and KANAMITSU *et al.* (1972) computed the barotropic energetics using the 92 days of analyses and found that the ultralong waves acted as a kinetic energy source for smaller scales of motion and also for the zonal motion.

The most comprehensive energetics of the tropical upper troposphere during the northern summer, which were able to be evaluated or be estimated from up-to-date observations, were compiled by KRISHNAMURTI *et al.* (1973a). Figure 1 shows the estimated direction of the energy exchange/conversion processes. They may be interpreted as follows. The available potential energy (APE) of the ultralong waves, P_L, is generated by the land-ocean contrast heating, H_L. The kinetic energy (KE) of

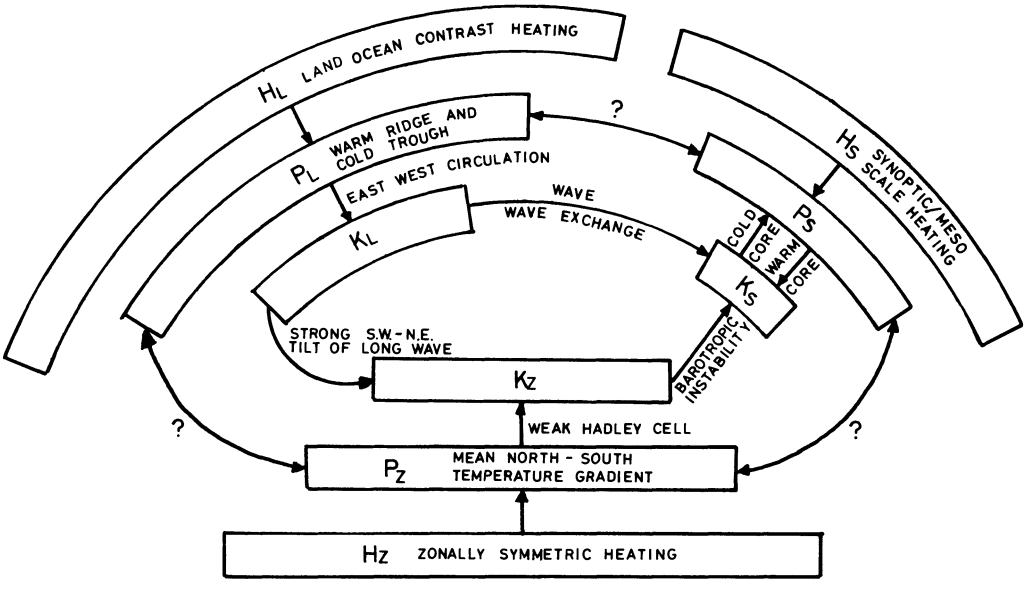

Figure 1

Energy diagram of the tropical upper troposphere estimated from observations during northern hemisphere summer. *L* stands for ultralong waves, *S* for other shorter waves and *Z* for zonal flows. *H*, *P* and *K* express heating, available potential energy and kinetic energy, respectively. A question mark denotes that the process is unknown. (After KRISHNAMURTI *et al.*, 1973a.)

the ultralong waves, K_L, is maintained by the conversion from P_L through the east-west direct overturnings. The zonal motion receives KE from the ultralong waves and also from the zonal APE by the Hadley circulation. The short waves receive KE from the ultralong waves and from the zonal motion through barotropic energy exchange processes. Thus, it is clear that the upper tropospheric tropical circulation during the northern hemisphere summer is maintained by the land-ocean contrast heating of the scale of zonal wavenumbers 1 and 2.

Although additional analyses became available in recent years (e.g., NEWELL *et al.*, 1972, 1974; KRISHNAMURTI *et al.*, 1975a), they were not complete enough to proceed further with studies on the energetics of the tropical troposphere. For example, observations at the middle troposphere are extremely poor due to the lack of aircraft reports. Furthermore, observations of the mass fields (temperature or height) are more sparse than that of the winds. Thus, further observational studies of the energetics of the tropical troposphere are seriously hindered by the data problems. This lack of observations will hopefully be resolved by the First GARP Global Experiment (FGGE) and by the Monsoon Experiment (MONEX).

It will be helpful to summarize some of the important unsolved problems on the energetics of the northern hemisphere summer tropical circulations:

(a) Types of heating responsible for the generation of the ultralong wave scale APE.
(b) Directions of the APE exchanges between the different scales.
(c) Types of heating associated with the short waves.
(d) Conversion between APE and KE in the short wave scales.
(e) Complete energetics at various levels.

There are other approaches to attack the above problems without waiting for better observational systems. They are simulation type experiments, which may be classified into three different types.

The first type is the pure numerical simulation experiment using so-called global circulation models. Two simulation experiments, one by MANABE *et al.* (1974) and the other by WASHINGTON and DAGGUPATY (1975) are the only successful studies so far reported. The former study provided energetics of the simulated circulations over the tropics and pointed out that the eddy APE conversion to eddy KE is significant over the northern hemisphere summer tropics. It also showed that the pressure work term is fairly large, and noted the middle latitude influence on the tropics. Nonlinear interaction terms were shown to be not too important.

In the related paper, HAHN and MANABE (1975) discussed the role of the Tibetan plateau for the maintenance of the monsoon (Tibetan high at the upper troposphere). They concluded that convective heating is responsible for the generation of the typical monsoon flow patterns. Thus, these studies partly answered some of the questions listed earlier. However, no attempt has been made to separate the scales

of motion to address the problems on the maintenance of the quasi-stationary ultralong waves in the tropical atmosphere.

The second type of simulation experiment may be called the idealized model experiment. This type of experiment greatly simplifies the physics of the model to isolate the major causes of the phenomena in question, but it frequently sacrifices the accuracy of the simulation. Several experiments of this type have been performed (WEBSTER, 1972, 1973; ABBOTT, 1973; COLTON, 1973; KRISHNAMURTI *et al.*, 1973a) and are critically reviewed by KRISHNAMURTI *et al.* (1973a). These experiments successfully demonstrated that the tropical upper tropospheric circulations are maintained by the land-ocean contrast heating. However, the simulated results were not accurate enough to answer the unsolved problems listed above. It should be noted that the second type of simulation experiments raised new questions on the vorticity budget of the ultralong waves. In order to avoid unnecessary confusion, this subject will be reviewed and discussed in a later part of this paper (Section 6).

The third type of simulation experiment is the real data numerical prediction experiment. This approach seems to be similar to the first type but model dependence may be less critical since the initial field is taken from the observations. The only documented experiment performed in this category is the real data global prediction by MIYAKODA *et al.* (1974). Unfortunately, since their initial fields are not taken from the summer season, their results are not relevant to the objectives of this paper.

The author recently performed a prediction experiment over a global tropical belt for the purpose of investigating skill in the medium range prediction over the low latitudes. The experiment indicated that the most important features in the tropics, the quasi-stationary ultralong waves, are reasonably well treated by the model.

It is the purpose of this paper to discuss the structures, energetics and vorticity budget of the predicted ultralong waves and to compare them with the observed climatological waves discussed in this section. We also address the problems listed above and attempt to relate the results of this experiment to them.

2. *Brief description of the prediction model*

The prediction model used in the experiment originated from the Florida State University's Tropical Prediction Model (KRISHNAMURTI *et al.*, 1973). But the model is extensively modified and improved for the purpose of applying it to prediction over the global tropics. Since it is not the purpose of this paper to discuss the prediction model, a brief description may be sufficient here. A complete description can be found in the technical report by KANAMITSU (1975).

The model is a multilevel primitive equation model using pressure as a vertical coordinate. The momentum equations include surface drag and eddy diffusion terms which are formulated, respectively, by the simple aerodynamic formula and by the

Laplacian type diffusion with linear coefficients. The thermodynamic equation includes radiation, latent heat release by condensation of water vapor, heat exchange with lower boundaries (ground and ocean surfaces) and eddy diffusion. Longwave radiative cooling is formulated as a function of water vapor content and temperature of the air. Shortwave radiation includes diurnal variation. Unlike longwave radiation, the role of shortwave radiation is not to heat directly the atmosphere but to heat the ground first and then to heat the atmosphere through the boundary layer processes. These heat exchange processes are especially important over very dry areas. It is noted that the effect of cloud cover has not been included in the computations of the radiative processes. Latent heating is divided into two types, large-scale condensation and convection, which are classified by the static stability of the atmosphere. It is believed that the convective heating normally dominates the large-scale condensation in the tropics. The experiment confirmed this fact and furthermore indicated that the convective heating is an order of magnitude larger than other diabatic heating. The atmosphere exchanges heat and moisture with ground/ocean surfaces in the model. The fluxes of heat and moisture from the lower boundaries are assumed to be proportional to the difference of temperature and moisture between the air and the ground surfaces, respectively. Moreover, the temperature and the moisture of the ground surfaces are predicted from the heat balance equation of the ground, which is determined by the radiative processes and the ground surface conditions. Ocean temperatures are taken from the climatology and are fixed in time. Water vapor is treated as a dependent variable. It is supplied from ground/ocean surfaces and consumed by the condensation and the diffusion processes. The effects of topography are included in the model in a way such that the parcel of air at the lowest pressure level (1000 mb) senses the slope of the terrain and reacts with a vertical motion without physically being blocked or deflected by the topography.

The domain of the prediction covers a latitudinal belt of the width 25S to 45N. The model has four layers in the vertical with the 100 mb surface as a top level at which vertical p-velocities are assumed to vanish. Horizontal grid size is 2.5° latitude/longitude. At the north and the south boundaries, the north–south component of the wind is assumed to be zero. This eliminates middle latitude forcing on the tropics.

The finite difference schemes used in the model are the semi-Lagrangian advective scheme with the Matsuno scheme for the time integration, the upstream differencing scheme for the vertical advection terms and the modified Heun scheme (HALTINER, 1971) for the pressure gradient terms.

3. *Initial data, initialization and prediction*

Tropical real data predictions frequently suffer from a severe sparseness of observations. To overcome this difficulty, extensive efforts have been made in this study. Several analyzed maps were collected from various countries in the tropics.

Commercial aircraft data were collected following KRISHNAMURTI (1971a). We also utilized cloud motion vectors derived from the geostationary satellites (both SMS I and II were operating during the period of this study). These derived winds were especially useful for the analyses at the low levels over the ocean areas. Other additional materials (e.g., satellite pictures, climatological maps, etc.) were also used for the analyses. Data coverage is especially large at the surface and at the 200–300 mb levels due to the ship and the commercial aircraft observations.

Winds (streamlines and isotachs) and temperatures at the standard pressure levels (surface, 850, 700, 500, 300 and 200 mb levels), surface pressure and relative humidity fields were hand analyzed. These analyses were manually digitized on the 2.5° latitude/longitude grids.

Initialization is another important but unsolved problem of the real data prediction over the tropics particularly when the equator lies in the middle of the domain. We used an iterative initialization procedure (WINNINGHOFF, 1973), which successfully eliminated the external gravity waves excited by the initial imbalance between the mass and the velocity fields.

6 August 1972, 00GMT is the initial map time. The quality of the prediction has been found to differ greatly from place to place depending on the quality (accuracy and density) of the observations. Some transient disturbances are very well predicted up to a few days. Studies on the detailed verification of the prediction will be published elsewhere in the near future.

4. Structure of the predicted ultralong waves

We shall first show the initial and the 6-day prediction of the 200 mb streamline (Fig. 2). Both fields show all of the characteristic features during the northern hemisphere summer season, i.e., the Tibetan high, the Mexican high and the two mid-oceanic troughs (KRISHNAMURTI, 1971a), which maintained their quasi-stationary nature during the 6-day prediction. We should note that the small scale features in the initial field are filtered out by the adjustment processes (mentioned later) during the first 36 hours of prediction. Time variations of the phases and the amplitudes of the ultralong waves (obtained by the zonal Fourier analysis) during the 6-day prediction (not shown) indicates that wavenumbers 1 and 2 have quasi-stationary character, while wavenumber 3 has a transient nature with large temporal variability.

For the purpose of comparing the predicted waves with the climatological observations, we emphasize the horizontal structure of the wave at the 300 and 200 mb levels. We defined the latitudinal band of 15N to 30N as a reference domain; here the Tibetan high and the two mid-oceanic troughs have their maximum intensities. We have eliminated the first 36 hours of the prediction from the diagnostic calculations. This was necessary because of the internal adjustment that takes place in the model and is caused by the poorly observed thermal fields. All the calculations in the

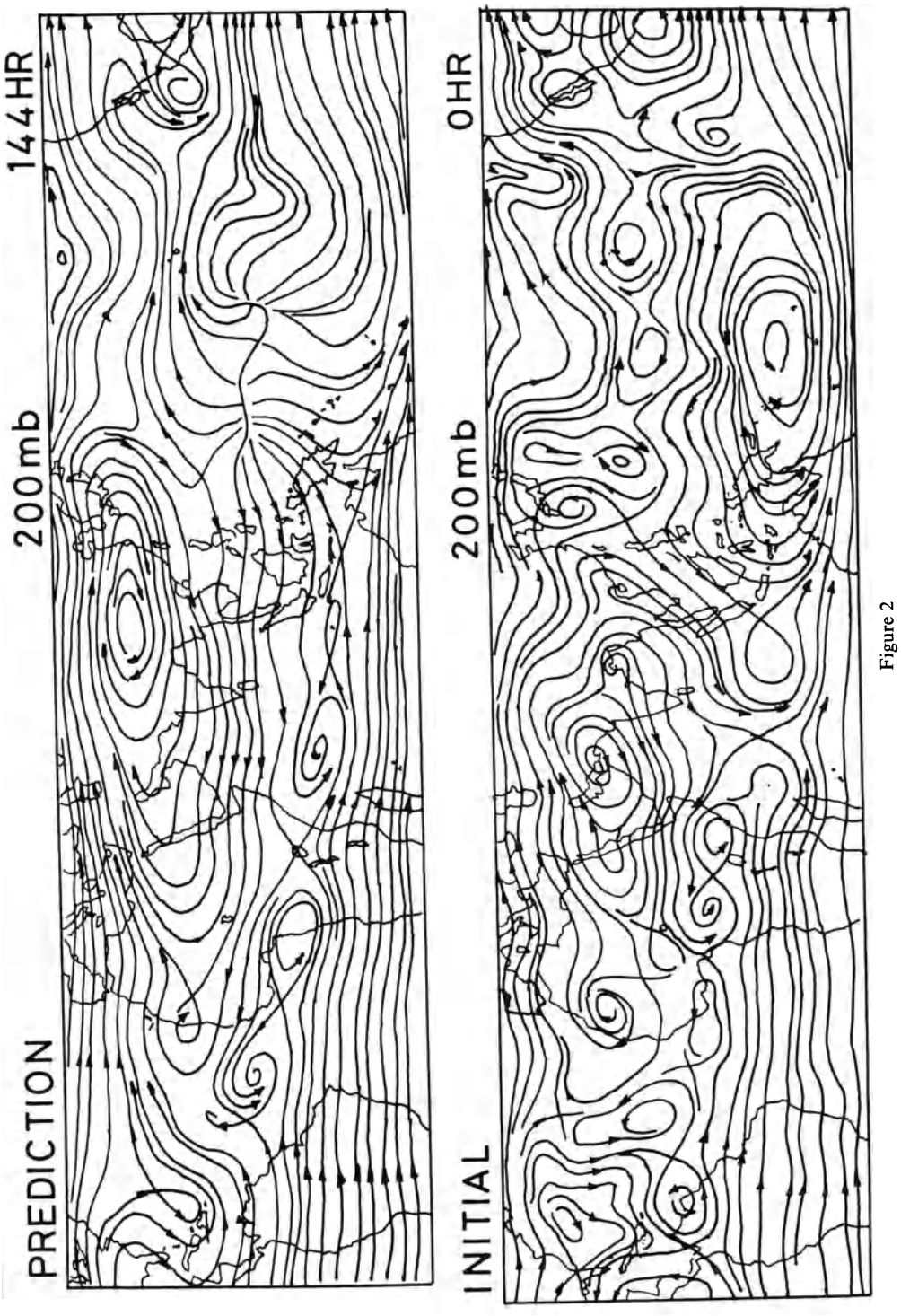

Figure 2
Initial (top) and 6-day predicted (bottom) streamline fields at 200 mb. Streamlines are drawn by computer from u and v component of the winds at the grid points.

following sections are the time means of the computations made for the predictions available at every 2 hours from hour 38 to hour 144 (total 54 maps).

Before discussing the structure of the ultralong waves, we shall briefly present the time mean zonally averaged fields. The results are shown in Fig. 3. Compared to the climatology (e.g., NEWELL *et al.*, 1972), the equatorial easterlies are somewhat weaker and narrower but the geometry is not too different. The distribution of the zonally averaged north–south component of the wind resembles that of the climatology very well. Strong southwesterly flow south of 10N corresponds to the strong upper level return current of the Hadley circulation.

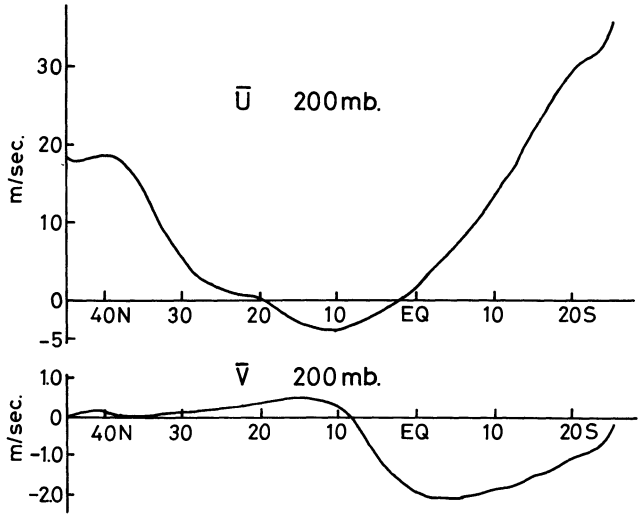

Figure 3
Latitudinal variation of the zonally averaged u (top) and v (bottom).

Next, we present structures of the ultralong waves. Considering the synoptic characteristic feature of the tropical atmosphere, i.e., two highs over the continents and two troughs over the oceans, we shall concentrate our interest on zonal wavenumber 2. Figure 4 shows that to the north of 15N, troughs and the ridges have distinct southwest to northeast tilt. The phase relation between u and v shows that westerly momentum is transported away towards the north pole from the latitude where the zonal westerly is minimum (easterly maximum). This implies that the easterly jet is maintained by the barotropic energy exchange processes. These characteristics are in very good agreement with the long-time mean observed ultralong waves studied by KRISHNAMURTI (1971a). Sensible heat transport by the wave is shown to be small because the phase difference between T and v is about a quarter of a wavelength. This indicates that the exchange between the zonal available potential energy (ZAPE) and the eddy available potential energy (EAPE) cannot be too large. To the south of 15N, the phase of u shifts nearly 90° (one half of a wavelength).

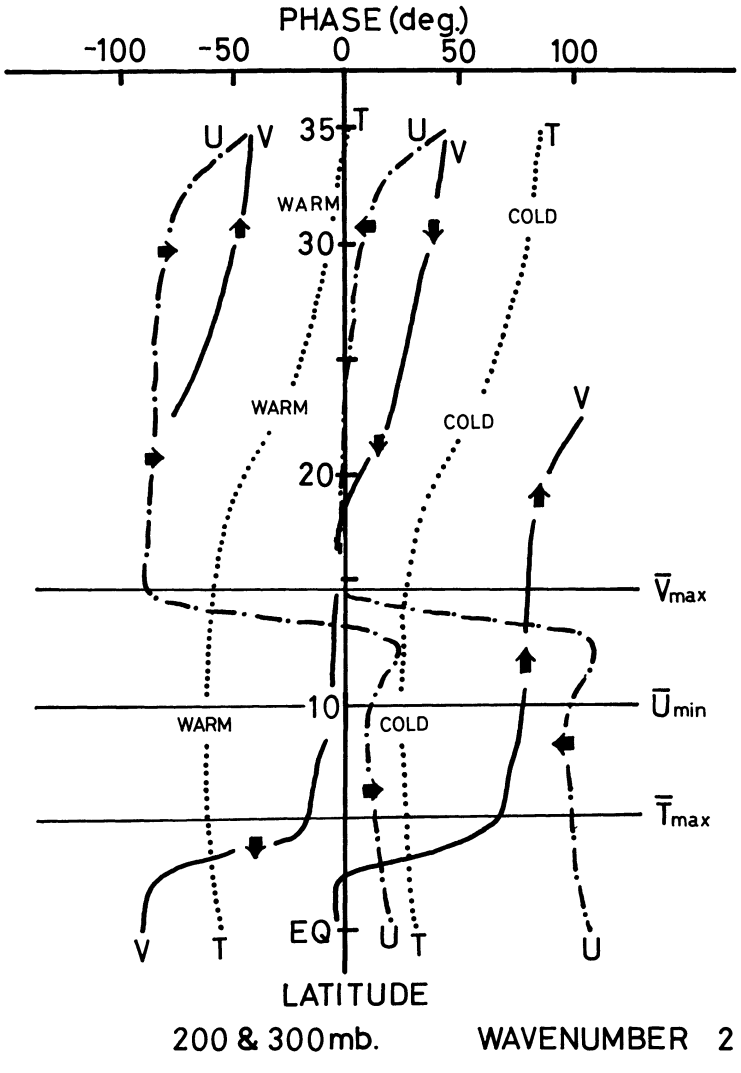

Figure 4

Horizontal structure of the wavenumber 2 at 200 mb (for u and v) and 300 mb (for temperature) levels. Solid, dash-dot and dot lines indicate the phase angle of the maximums and the minimums of v, u and temperature (T) respectively. Maximums and minimums are indicated by the proper arrows and lables on the line (for example, upward arrow indicates maximum northward winds). Latitudes of maximum $\bar{v}$, minimum $\bar{u}$ and maximum $\bar{T}$ are also shown by the thin horizontal lines.

This indicates that the circulation center of the zonal wavenumber 2 lies at around this latitude. We see that the wave transports the westerly momentum away from this latitude towards the equator.

We shall next show the vertical structure of the ultralong waves (wavenumber 1 and 2). We selected 30N where the center of the Tibetan high is located as a reference

latitude. One of the characteristic features of the vertical structure of the wave is that the potential temperature fields (θ) have nearly the same phase angles at all levels (Fig. 5). This indicates that the entire troposphere is warm over the continents and cold over the oceans. Vertical p-velocity fields (ω) show that the warm air is rising and the cold air is sinking, implying that the EAPE of the ultralong waves is converted to the kinetic energy of the same scale. These longitudinal circulations correspond to the east-west circulations first pointed out by KRISHNAMURTI (1971b). It is also noted from Fig. 5 that the diabatic heating (H) has nearly the same phase angle as the temperature, which indicates that EAPE is generated by diabatic heating whose major contribution comes from the convective heating (H_c) on the same scale.

The fields of θ, ω and H are not exactly in phase. The phase differences between θ and H are about 10–20°, maximum H being east of the temperature maximum. The phase relations between the H and ω are reversed for wavenumbers one and two; maximum H being east of the ω maximum for wavenumber two and west for wavenumber one (except above 400 mb). Their differences are 20–40°. Although no quantitative studies were made, it seems reasonable to conclude from these phase relationships that the diabatic heating is not merely balanced by the adiabatic cooling term in the thermodynamic equation. It is widely believed that these two terms tend to balance each other in the tropics (HOLTON, 1972), but present study seems to suggest that the horizontal advection terms are equally important.

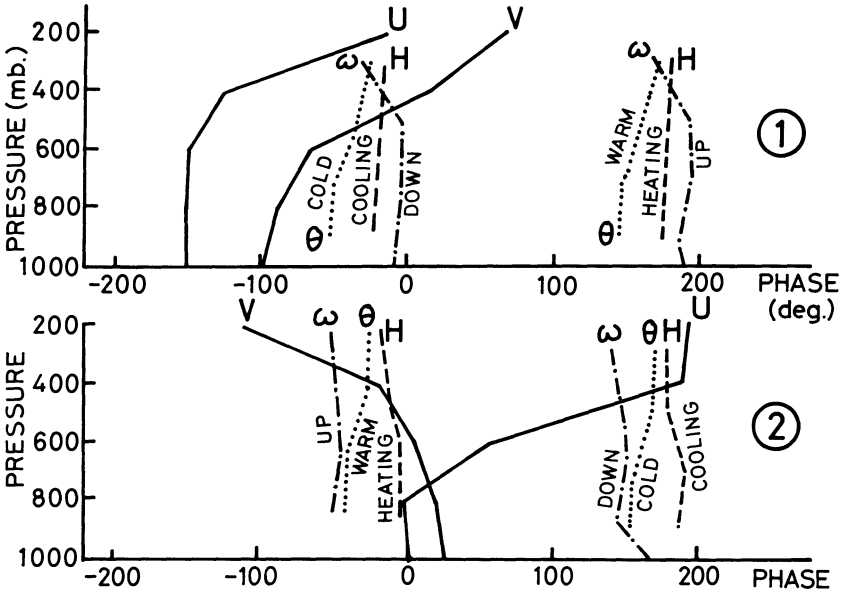

Figure 5

Vertical structures of wavenumbers 1 (top) and 2 (bottom) at 30N. Each line shows vertical variation of the phase angle of the variables: temperature (dot lines), heating (dash lines) and vertical p-velocity (dash-dot lines). Solid lines indicate phase angles of maximum u and v as labeled at the top of each line. Phase angle of wavenumber 2 is doubled. For the wavenumber 1, phase angle of 0° corresponds to 90W longitude.

The north–south component of the wind has very distinct vertical tilt. The wavenumber 1 has eastward tilt with height, while the wavenumber 2 has westward tilt; both are small at the low levels and very large at the upper levels. The waves at the surface and the 200 mb level are approximately out of phase, which is consistent in the geostrophic sense with the temperature structure of the troposphere. The amplitudes of the waves are found to have a minimum at the middle levels.

It may be possible to conclude from these simple Fourier analyses, that the ultralong waves in the tropics are forced by the convective heating that dominates over the continent and is probably caused by the monsoonal rainfall. This will be further examined quantitatively in the following sections.

5. *Energetics of the predicted waves*

The energy equations in the wavenumber domain are symbolically expressed as follows.

$$\begin{aligned}
\frac{\partial K(0)}{\partial t} &= \sum_{n=1}^{\infty} M(n) + C(0) - D(0) \\
\frac{\partial K(n)}{\partial t} &= -M(n) + L(n) + C(n) - D(n) \\
\frac{\partial P(0)}{\partial t} &= \sum_{n=1}^{\infty} R(n) - C(0) + G(0) \\
\frac{\partial P(n)}{\partial t} &= -R(n) + S(n) - C(n) + G(n).
\end{aligned} \tag{1}$$

Here, $K(n)$ is the kinetic energy, KE, of the wavenumber n, $n = 0$ being the zonal flow, $P(n)$ is the available potential energy, APE, of the wave and t is time. On the right side of the equations, $M(n)$ is the exchange of wave KE with the zonal flow, $C(n)$ is the conversion from APE to KE, $D(n)$ is the dissipation, $L(n)$ is the KE exchange between the waves, $R(n)$ is the energy exchange between the ZAPE and EAPE, $G(n)$ is the generation and $S(n)$ is the APE exchanges between the waves. Complete forms of the terms will be found in SALTZMAN (1970). It should be noted that the energy equations (1) must include additional boundary flux and pressure work terms when applied to the open system. Numerical procedures for the evaluation of the terms involve zonal Fourier transforms and finite differences in the north-south direction and in the vertical. In order to save computer time, we have truncated the maximum wavenumber at 15. The computations are made for the latitudinal zone of 15N to 30N. Although this is an open system, we did not make efforts to compute the boundary terms. Thus, the energy diagrams in this study are not complete in any sense.

Figure 6 gives computed energetics at 300 mb, the level where comparison with climatological observations are available. Let's first look at the magnitudes of the energies of the different wavenumbers shown in the boxes of Fig. 6. A very interesting

result is that the APE and KE of the ultralong waves (namely wavenumbers 1 and 2) are much larger than those of the zonally averaged fields. This fact and the strong energy exchanges with other scales of motion (which will be mentioned later) makes it difficult to perform linear analyses of the ultralong waves in the tropics. Large amplitudes of wavenumbers 1 and 2 are also pointed out by KRISHNAMURTI (1971a) in his observational study. One apparent difference from the climatological observations is the exceptionally small amount of energy in the wavenumber 3. As noted before, the wavenumber 3 has a strong transient nature in this experiment.

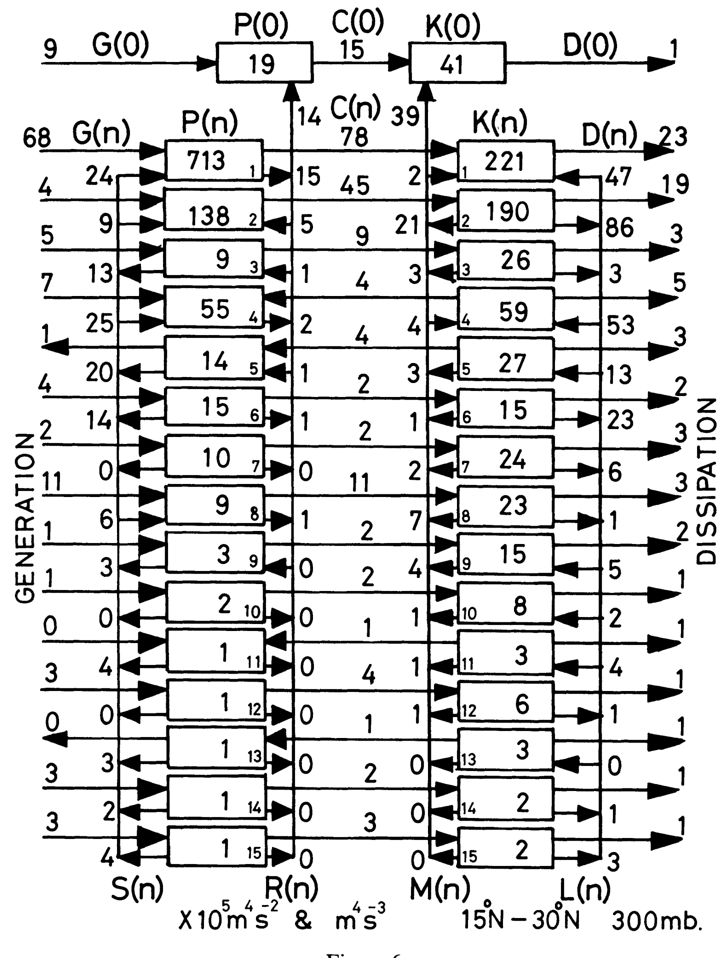

Figure 6

Barotropic and baroclinic energetics in the wavenumber domain computed at 300 mb over the domain between 15N to 30N from the prediction experiment. Each conversion is labeled at the top and the bottom of the figure. *G* stands for generation, *D* for dissipation, *S* for wave-wave exchange of APE, *E* for wave-zonal exchange of APE, *M* for wave-zonal exchange of KE, *L* for wave-wave exchange of KE and *C* for the conversion between APE and KE. *P* and *K* denote APE and KE respectively. Small numbers in the boxes are wavenumbers. Boxes at the top are the zonally averaged field. (Units: $\times 10^5$ m^4 sec^{-2} for *P* and K; m^4 sec^{-3} for conversions).

We shall next examine the energy generation/conversion processes. The largest generation of the APE is observed in the scale of wavenumber 1. This is expected from the maximum convective activity predicted over the Indian monsoon area, and also from the large amplitude and high correlation of the temperature field. Another interesting feature of Fig. 6 is the second largest generation of APE on the scale of wavenumber 8. This scale of motion is shown to describe the transient tropical disturbances by KRISHNAMURTI (1971a). He computed the variance of the stream-function from the observed winds and found a secondary peak at the wavenumber 8. The heating associated with this scale is convective heating which seems to be released at the upper tropospheric warm core of these disturbances.

The wavenumber 1 seems to generate zonal APE through the up-the-gradient transport of temperature, but the magnitude is not too large compared to the generation/conversion processes. The exchange of APE among the waves show that the ultralong waves (including wavenumber 4 but excluding wavenumber 3 which has very small APE) receive APE from smaller scales. This additional mechanism for the generation of APE of the quasi-stationary ultralong waves is particularly interesting in this experiment. Conversions from APE to KE are common characteristics at all scales except the wavenumbers 4, 5 and 11 whose conversion rates are relatively small. We note again that the rate of the energy conversion also has a secondary peak at the wavenumber 8.

Barotropic energy exchanges are shown on the right half of Fig. 6. The largest exchange between the zonal motion and the waves is observed for wavenumber 2. This is consistent with the horizontal tilt of the wave mentioned earlier. Most of the other waves also supply kinetic energy to the zonal flow. Wave to wave energy exchanges are complex, but the wavenumber 2 is the distinct kinetic energy source for other scales of motion. The wavenumber 1 receives fairly large amounts of kinetic energy from other scales of motion (and also from the zonal motion). However, the observation (KANAMITSU *et al.*, 1972) shows that the wavenumber 1 is the largest energy source for other scales of motion and also for the zonal motion. This difference can be mainly explained by the difference of the latitudinal zone selected for the two studies (15S to 15N for the observation and 15N to 30N for the present case). Since various incompatibilities between the observational study and the prediction study (domain, level, period, etc.) make detailed comparison of each individual wave somewhat unreliable, we shall not further discuss the differences. There are secondary barotropic energy sources for other waves and for the zonal motion in the scales of wavenumbers 6, 7 and 8, which are maintained by the conversion from the available potential energy of the same scale. These barotropic energy exchange processes of the shortwaves indicate that the waves are barotropically stable for the zonal motion and also for the larger scales of motion. This, however, does not agree with the observational energetics (KANAMITSU *et al.*, 1972). Although this may be explained by several other reasons, we would like to take the view that this is merely a consequence of the transient character of the shortwaves. It is reasonable to conclude that the climato-

logical long-time mean character of the transient disturbances cannot be studied from the short period prediction experiment. It should, however, be noted that the climatological characters of the ultralong waves can still be studied from relatively short periods of data if the waves have large variances and quasi-stationality, and if the transient (shorter) waves do not have significant effects on the ultralong waves. Fig. 6 seems to show that these conditions are approximately satisfied in the present case. However, it is still possible that some of the differences between the observation and the prediction are due to this short period of data.

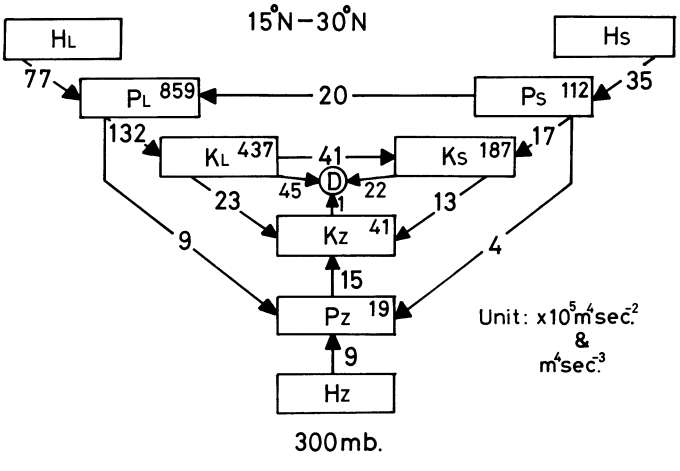

Figure 7

Energy diagram computed from the prediction experiment at 300 mb. Notations are the same as Fig. 1. D stands for dissipation. (Units: same as Fig. 6).

In order to summarize the comparison between the predicted and the observed energetics, Fig. 7 is constructed from Fig. 6 by re-classifying the 15 wavenumbers to two scales as was done in making Fig. 1. Here, $1 \leq n < 4$ are the 'long' (L) scales and $4 \leq n \leq 15$ are the 'short' (S) scales. It is noted that this re-classification of the scales lowers the accuracy of the energetics by reducing the space resolution and makes the comparison with the observation more meaningful. Fig. 1, which is used as an observation, includes several estimated energy conversion processes. For example, all the baroclinic energetics are qualitatively estimated from the seasonal mean temperature, wind, precipitation and cloudiness fields. The processes (H_S, P_S) and (P_S, K_S) are estimated from the averaged nature of the tropical transient disturbances. Thus, the comparisons between the numerical study and the observations must be viewed in this context. Comparison of Figs. 1 and 7 reveals astonishingly similar energy conversion/generation processes between the two. This similarity is considered to be due to the largest variances of the quasi-stationary ultralong waves observed in the daily weather maps as well as in the long-time mean maps. This fact provides a strong basis for the use of real data prediction experiments for the study of the quasi-stationary ultralong waves.

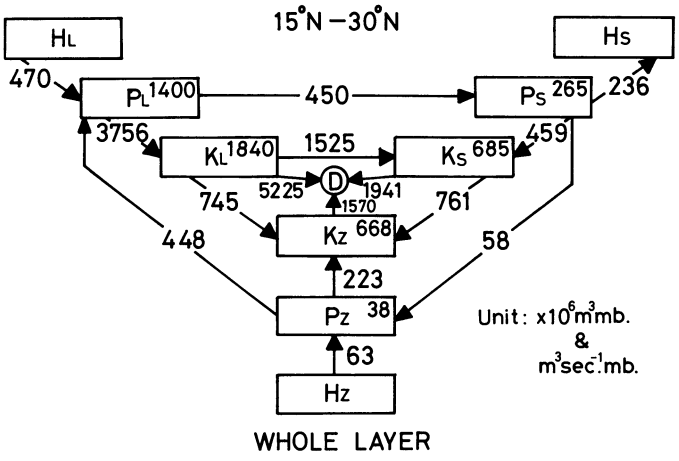

Figure 8
Same as Fig. 7 except for whole troposphere (1000–200 mb integrated). (Unit: $\times 10^6$ m^3 mb for P and K; m^3 sec^{-1} mb for conversions.)

Although we cannot make a quantitative comparison with the observations, this experiment provides the energetics of the entire troposphere. Figure 8 shows the whole-layer integrated energetics, in the manner similar to Fig. 7. Complete reversals of the direction of the exchange/generation processes with 300 mb energetics are noted for (P_L, P_Z), (P_L, P_S) and (H_S, P_S). This indicates that the thermal structures of the waves have large variation in the vertical with respect to the wind fields. This is consistent with the vertical structures of the waves shown in Fig. 5. One of the most interesting results is that the short wave APE is destroyed by the diabatic heating (convective heating). This seems to correspond to the observational fact that most of the tropical tropospheric transient disturbances are cold core at low levels (BAUMHEFNER, 1968; REED and RECKER, 1971; PEDGLEY and KRISHNAMURTI, 1976; KRISHNAMURTI *et al.*, 1976), where maximum convective heating is expected. As shown before, since APE of this scale is generated at the 300 mb level, there is a competition of the generation/destruction of APE among the levels. This result, together with the APE exchange from long waves to short waves, indicates that for the entire tropical troposphere, APE is generated at the ultralong wave scale and is transferred to the smaller scales by the nonlinear processes. It is then destroyed by the diabatic heating. This process is very similar to the kinetic energy exchange processes between the different scales of motion noted earlier.

6. *Vorticity budget of the ultralong waves*

The first study of the vorticity budget of the tropical upper troposphere (200 mb) was performed by HOLTON and COLTON (1972). Using a linearized vorticity equation

they pointed out that the balance of the terms in the equation could not be established unless an unrealistically large dissipation term is included. This had been expected from the configurations of the streamfunction and the velocity potential fields computed by KRISHNAMURTI (1971b), which indicated that the location of the maximum anticyclonic vorticity (Tibetan high) approximately coincided with the location of the maximum (positive) divergence. The large dissipation term mentioned above has been explained by Holton and Colton as a consequence of vorticity transport by cumulus convection. However this has been questioned by COLTON (1973) and KRISHNAMURTI *et al.* (1973a) primarily because the equation that Holton and Colton used was not general enough to take into account the effects of nonlinearity in space as well as in time.

Two other studies (ABBOTT, 1973; COLTON, 1973) attempted to simulate the tropical circulation by simply forcing the atmosphere with the observed long-time mean divergence or the implied heating. They both encountered difficulties in matching the locations of the maximum anticyclonic vorticity and the maximum divergence. ABBOTT (1973) computed the field of divergence which was required to make the location of the observed climatological ultralong waves stationary, and found that unlike the observations, the center of the divergence must lie about 90° longitude east of the Tibetan high. COLTON (1973), on the other hand, forced the atmosphere by the observed divergence (with the maximum located roughly over the Tibetan plateau) and found that the anticyclonic circulation center appeared 90° longitude west of the divergence center. These experiments indicate that there must be a phase difference of 90° between the fields of vorticity and divergence, implying that there must be a balance between the divergence term and the beta term in the vorticity equation.

Many years before these studies, the vorticity budget of the very large-scale motions was studied theoretically by BURGER (1958). He did so from the point of view of the scale analysis, which compares the magnitudes of the terms in the vorticity equation. He concluded that the ultralong waves (whose wavelengths are comparable with the earth's radius) have a quasi-stationary nature as a result of an approximate balance between the divergence and the beta terms. This is consistent with the numerical experiments mentioned above. The inconsistency between the observations and the theoretical/numerical work still remains an unsolved problem of the forced tropical ultralong waves.

It is therefore desirable to present the results of the vorticity budget computed for the ultralong waves predicted in the real data prediction experiment. We first propose a different approach to the calculation of the budget of the vorticity. This formulation can be regarded as forming the phase and the amplitude equations, which are derived fairly easily as shown below. First, by applying the Fourier transform to the vorticity equation (in pressure coordinates), we obtain the vorticity equation in the wavenumber domain, i.e.,

$$Z_t(n) = -\sum_{m=-\infty}^{\infty}[Z_x(m)U(n-m) + Z_y(m)V(n-m) + Z_p(m)W(n-m)] - \sum_{m=-\infty}^{\infty}\Delta(m)Z(n-m) - f\Delta(n) - \beta V(n) + \sum_{m=-\infty}^{\infty}[V_p(m)W_x(n-m) - U_p(m)W_y(n-m)] + Y_x(n) - X_y(n) \tag{2}$$

where n is the wavenumber, t is time, x is the east–west coordinate, y is the north–south coordinate and p is pressure which is used as a vertical coordinate. The subscripts show derivatives with respect to each variable. f is the Coriolis parameter and $\beta = df/dy$. U, V, W, Z, Δ, X and Y are the Fourier transforms of the x-component of the wind, y-component of the wind, vertical p-velocity, vorticity, divergence, x-component of the frictional force and y-component of the frictional force, respectively. The first term on the right is the advection term, the second and third terms are the divergence terms, fourth term is the beta term, fifth term is the tilting term and the last two terms are the frictional terms. Next, by differentiating the phase of each wavenumber, $\lambda(n)$, with respect to time, we obtain,

$$\lambda_t(n) = \frac{i}{2n|Z(n)|^2}[Z(-n)Z_t(n) - Z(n)Z_t(-n)]. \tag{3}$$

Substituting (2) into $Z_t(n)$ and $Z_t(-n)$ above, we can obtain phase velocity equation for the wavenumber n. Moreover, since it is still possible to identify the physical meaning of the terms on the right hand side of (2), we can calculate the contribution of each term to the phase velocity of the wave. Similar procedures can be applied to the amplitudes of the waves, $A(n)$, whose time derivatives can be expressed as,

$$A_t(n) = \frac{1}{|Z(n)|}[Z(-n)Z_t(n) + Z(n)Z_t(-n)]. \tag{4}$$

Before applying the above equations, it is desirable to present the horizontal structure of the predicted ultralong waves (wavenumber 2 is selected in this case). Figure 9 clearly shows that between the latitudinal belt of 25N to 40N, the divergence and the vorticity are approximately out of phase, which is in good agreement with the climatological observations.

Each term of (3) and (4) is evaluated using the history tapes of the prediction. Since the prediction equations and the budget equations have completely different forms, the computed phase velocities and the time change of the amplitudes from (3) and (4) do not agree with the predicted ones. In order to match these values, each term was corrected in proportion to the magnitude of the term. As in the case of energetics, the wavenumber is truncated at 15. Table 1 shows phase velocities caused by the terms in the vorticity equation at different latitudes for the wavenumber 2 (although not shown here, wavenumber 1 has similar results). To the north of 25N, it is very clear that the advection is the largest in magnitude and is quasi-balanced by the sum of the

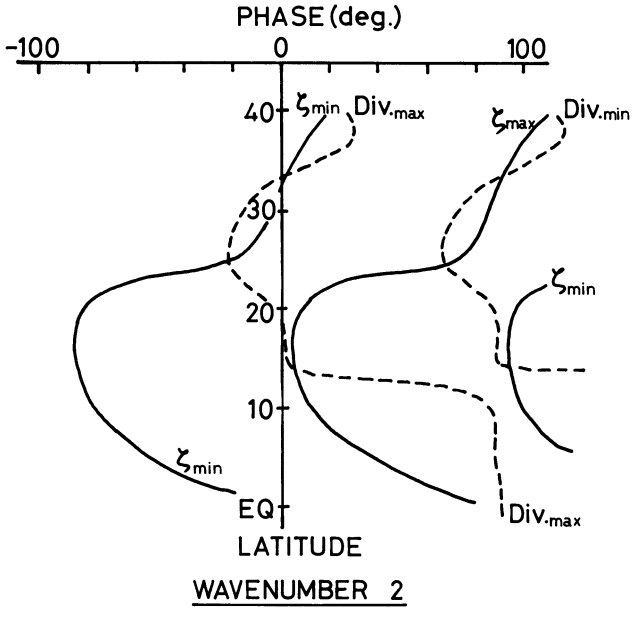

Figure 9
Latitudinal variation of the phase angle of vorticity (solid lines) and divergence (dashed lines) for the wavenumber 2.

Table 1

Phase velocities induced by the various terms of the vorticity equation, computed from 200 mb wavenumber 2 at different latitudes. (*Unit: degree longitude day*$^{-1}$)

Latitude	Advection	$-D\zeta$	$-fD$	$-\beta v$	Tilting	Friction	$\partial/\partial t$
30N	25.1	2.5	−6.8	−18.1	0.2	−0.3	2.6
25N	54.5	−1.5	−13.8	−31.8	0.7	−1.4	6.7
20N	0.8	−0.5	2.0	−1.4	0.2	0.6	1.7
15N	5.6	−0.1	0.0	−5.3	−0.1	−0.1	0.0

Table 2

Changes of amplitudes caused by the various terms of the vorticity equation, computed from 200 mb wavenumber 2 at different latitudes. (*Unit:* $\times 10^{-11}$ sec^{-2})

Latitude	Advection	$-D\zeta$	$-fD$	$-\beta v$	Tilting	Friction	$\partial/\partial t$
30N	−2.1	−2.6	6.4	−1.3	−0.0	−0.1	0.3
25N	−4.6	−0.7	4.4	0.8	0.0	−0.4	−0.5
20N	−1.5	0.5	−3.7	7.0	−0.6	−1.4	0.3
15N	−1.7	0.0	−4.2	6.6	0.9	−1.6	0.0

divergence terms and the beta term. To the south of 25N, the magnitude of the terms are much smaller and there is no apparent balance of terms in these lower latitudes.

As shown in Table 2, to the north of 25N, vorticity is generated by the divergence term $(-fD)$ and consumed by other terms. The advection term is again very important for the balance of terms. To the south of 25N, the vorticity is generated by the beta term and consumed by other terms. Considering the vorticity budget and the horizontal structure of the waves (Figs. 4 and 9), it seems that the wavenumber 2 has characteristics that are very different north and south of about 20–25N.

The results of this section may be summarized as follows. The large-scale balance appears to hold for the ultralong waves north of approximately 20N. The leading terms are the advection term, divergence terms and the beta term. It should be emphasized here that the advection term cannot be neglected as has been done by BURGER (1953). The importance of the advection term agrees with the results of the scale analysis made by DELAND (1965) who has taken into account the latitudinal scales of the ultralong waves. DICKINSON (1968) also discussed the importance of the latitudinal scale. It is noted that the predicted ultralong wave has relatively small north–south width as has been shown by the abrupt change of the structure of the wavenumber 2 at about 20N.

There still remains a serious question on the vorticity budget as indicated by the simulations by ABBOTT (1973) and COLTON (1973), who included the advection term but could not solve the quarter wave shift problem. We have no answer to this problem at this stage, but it seems important to consider the differences of the dynamics of the various models used. One possibility, we feel, is the effect of the advection of the vorticity by the divergent part of the wind, which was not taken into account in the simulations mentioned above, but is considered to be large near the strong heat sources.

7. *Concluding remarks*

The time averaged ultralong waves predicted in the real data global tropical prediction experiment with the multilevel primitive equation model are found to have fairly close similarities with the long-time averaged climatological quasi-stationary ultralong waves. The computed energetics shows that both in the experiment and in the real atmosphere, the available potential energy of the ultralong waves are generated by the land-ocean contrast heating. This available potential energy is converted to the kinetic energy of the waves of the same scale through the direct circulation, which is the manifestation of the east–west circulations. There are some differences in the barotropic energy exchanges of the individual ultralong waves between the cases. But the ultralong wave scale motion defined as the sum of the wavenumbers 1, 2 and 3 indicates that the zonal motion receives kinetic energy from the ultralong wave scale motion in the prediction as well as in the observation.

This prediction experiment thus shows that the tropical quasi-stationary ultralong waves can be studied from relatively short term (6 days) real data prediction, if the transient (short) waves do not have significant influence on the ultralong waves (this condition seems to hold most of the time in northern hemisphere summer tropics because the smaller scales of motion, as a climatological average, tend to receive energy from the ultralong waves). Accordingly, this experiment has enabled us to provide information on the structure, energetics and the vorticity budget not yet known for the real atmosphere due mainly to the lack of sufficient observations.

The predicted waves have very simple thermal structures, i.e., warm over the continent and cold over the oceans. However, the wind field has very large vertical tilt, almost discontinuous between the middle and the upper troposphere. The amplitudes of the waves seem to have a minimum at the intermediate levels.

The energetics at the 300 mb level shows that the eddy APE of the ultralong waves is generated not only by the adiabatic heating but is also supplied by the nonlinear interactions with the smaller scales. The energetics integrated over the whole troposphere is similar to that at 300 mb for the barotropic energetics but is quite different for the baroclinic energetics. This indicates the importance of the baroclinicity of the ultralong waves in the tropical/subtropical troposphere. Over the entire troposphere the small scale APE is destroyed by the convective heating but supplied by the nonlinear exchange with larger scales. It is exactly opposite at 300 mb. It should be emphasized that the major conclusion made from the observations, i.e., the tropical longitudinally asymmetric quasi-stationary circulations are maintained by the land–ocean contrast heating mainly due to the convective heating over the monsoon India, is strongly supported in this experiment.

Predicted ultralong waves show that the vorticity field is almost exactly out of phase with the divergence field, in agreement with the observations. The budget of the wavenumber 2 indicates that the advection term is one of the leading terms in the vorticity equation, which partly explains the relative locations of the divergence and the vorticity fields. It is further noted that the advections of vorticity by the divergent part of the wind seem to be important to explain the balance between these terms.

We can conclude from this experiment that the tropical quasi-stationary ultralong waves are described as fully nonlinear, non-geostrophic, forced planetary waves embedded in a zonal current with horizontal and vertical shear. They seem to have fairly clear vertical as well as horizontal scales.

Finally, we would like to comment that in order to complete this study, the results derived from the prediction experiment have to be verified from observations. However, we still don't have enough observational data to perform such verifications. Furthermore, some of the physical processes, such as the effects of cumulus convections, are not understood fully enough to evaluate their contributions to the transient and the quasi-stationary waves. We hope that FGGE, MONEX and other international programs will give us sufficient information to verify the experiment and to further improve our understanding of the tropical general circulation.

Acknowledgements

The author would like to acknowledge the continuous encouragement of Dr. T. N. Krishnamurti throughout this work. Most of the work was performed while the author was a post-doctoral fellow at the Advanced Study Program, National Center for Atmospheric Research, which is sponsored by the National Science Foundation. Computation time was also provided by the same institute.

References

ABBOTT, D. A. (1973), *Scale interactions of forced quasi-stationary planetary waves at low latitudes.* Dept. Meteor. Florida State Univ. Report, 73–2.

BAUMHEFNER, D. P. (1968), *Application of a diagnostic numerical model to the tropical atmosphere*, Mon. Wea. Rev. *96*, 218–228.

BURGER, A. (1958), *Scale considerations of planetary motions of the atmosphere*, Tellus *10*, 195–205.

COLTON, D. E. (1973), *Barotropic scale interactions in the tropical upper troposphere during the northern summer*, J. Atmos. Sci. *30*, 1287–1302.

DELAND, J. R. (1965), *On the scale analysis of traveling planetary waves*, Tellus *17*, 527–528.

DICKINSON, E. R. (1968), *A note on geostrophic scale analysis of planetary waves*, Tellus *20*, 548–550.

FLOHN, H. (1964), *Investigations on the tropical easterly jet*, Tech. Rept., Meteorological Institute, Univ. of Bonn.

HAHN, D. G. and MANABE, S. (1975), *The role of mountains in the south Asian monsoon circulation*, J. Atmos. Sci. *32*, 1515–1541.

HALTINER, G. J., *Numerical Weather Prediction*, (John Wiley and Sons, New York, 1971), 317 pp.

HOLTON, J. R., *An Introduction to Dynamic Meteorology* (AP, 1972), 319 pp.

HOLTON, J. R. and COLTON, D. E. (1972), *A diagnostic study of the vorticity balance at 200 mb in the tropics during the northern summer*, J. Atmos. Sci. *29*, 1124–1128.

KANAMITSU, M. (1975), *On numerical prediction over a global tropical belt*, Dept. Meteor. Florida State Univ. Report, 75–1.

KANAMITSU, M., KRISHNAMURTI, T. N. and DEPRADINE, C. (1972), *On scale interaction in the tropics during northern summer*, J. Atmos. Sci. *29*, 698–706.

KOTESWARAM, P. (1958), *The easterly jet stream in the tropics*, Tellus *10*, 43–57.

KRISHNAMURTI, T. N. (1971a), *Observational study of the tropical upper tropospheric motion field during the northern hemisphere summer*, J. Appl. Meteor. *10*, 1066–1096.

KRISHNAMURTI, T. N. (1971b), *Tropical east–west circulations during the northern summer*, J. Atmos. Sci. *28*, 1342–1347.

KRISHNAMURTI, T. N. and ROGERS, E. B. (1970), *200 mb wind field June, July and August, 1967*, Dept. Meteor. Florida State Univ. Report, 70–2.

KRISHNAMURTI, T. N., DAGGUPATY, S. M., FEIN, J., KANAMITSU, M. and LEE, J. D. (1973a), *Tibetan high and upper tropospheric tropical circulations during northern summer*, Bull. Amer. Meteor. Soc. *54*, 1234–1249.

KRISHNAMURTI, T. N., KANAMITSU, M., CESELSKI, B. and MATHUR, M. B. (1973b), *Florida State University's tropical prediction model*, Tellus *25*, 523–535.

KRISHNAMURTI, T. N., ASTLING, E. G. and KANAMITSU, M. (1975), *200 mb wind field June, July and August, 1972*, Dept. Meteor. Florida State Univ. Report, 75–2.

KRISHNAMURTI, T. N., KANAMITSU, M., GODBOLE, R., CHANG, C. B., CARR, F. and CHOW, J. C. (1976), *Study of a monsoon depression (II), Dynamical structure*, J. Meteor. Soc. Japan, *54*, 208–225.

MANABE, S., HAHN, D. G. and HOLLOWAY, J. L. JR. (1974), *The seasonal variation of the tropical circulations as simulated by a global model of the atmosphere*, J. Atmos. Sci. *31*, 43–48.

MIYAKODA, K., SADLER, J. C. and HEMBEE, G. D. (1974), *An experimental prediction of the tropical atmosphere for the case of March 1965*, Mon. Wea. Rev. *102*, 571–591.

NEWELL, R. E., KIDSON, J. W., VINCENT, D. G. and BOER, G. J., *The General Circulation of the Tropical Atmosphere and Interactions with Extratropical Latitudes.* Vol. 1, (MIT Press, Cambridge, Mass. and London 1972), 258 pp.

NEWELL, R. E., KIDSON, J. W., VINCENT, D. G. and BOER, G. J., *The General Circulation of the Tropical Atmosphere and Interactions with Extratropical Latitudes.* Vol. 2, (MIT Press, Cambridge, Mass. and London 1974), 371 pp.

PEDGLEY, D. E. and KRISHNAMURTI, T. N. (1976), *Structure and behavior of a monsoon cyclone over west Africa,* Mon. Wea. Rev. *104*, 149–167.

REED, R. J. and RECKER, E. E. (1971), *Structure and properties of synoptic-scale wave disturbances in the equatorial western Pacific*, J. Atmos. Sci. *28*, 1117–1133.

RIEHL, H., *Tropical Meteorology* (McGraw-Hill, New York, 1954), 392 pp.

SALTZMAN, B. (1970), *Large-scale atmospheric energetics in the wavenumber domain,* Rev. Geophys. *8*, 289–302.

WASHINGTON, W. M. and DAGGUPATY, S. M. (1975), *Numerical simulation with the NCAR global circulation model of the mean conditions during the Asian-African summer monsoon,* Mon. Wea. Rev. *103*, 105–114.

WEBSTER, P. J. (1972), *Response of the tropical atmosphere to local steady forcing,* Mon. Wea. Rev. *100*, 518–541.

WEBSTER, P. J. (1973), *Remote forcing of time independent tropical atmosphere*, Mon. Wea. Rev. *101*, 58–68.

WINNINGHOFF, F. J. (1973), *Note on a simple restorative-iterative procedure for initialization of a global forecast model,* Mon. Wea. Rev. *101*, 79–84.

(Received 15th June 1977)

Pageoph, Vol. 115 (1977), Birkhäuser Verlag, Basel

Some Aspects of the Monsoon Circulation and Monsoon Rainfall

By R. ANANTHAKRISHNAN[1])

Summary – The south Asian summer monsoon from June to September accounts for the greater part of the annual rainfall over most of India and southeast Asia. The evolution of the summer and winter monsoon circulations over India is examined on the basis of the surface and upper air data of stations across India. The salient features of the seasonal reversals of temperature and pressure gradients and winds and the seasonal and synoptic fluctuations of atmospheric humidity are discussed. The space-time variations of rainfall are considered with the help of climatic pentad rainfall charts and diagrams. The rainfall of several north and central Indian stations shows a minimum around mid-August and a maximum around mid-February which seem to be connected with the extreme summer and winter positions of the ITCZ and the associated north–south shifts in the seasonal circulation patterns. Attention is drawn to the characteristic features of the monsoon rainfall that emerge from a study of daily and hourly rainfall of selected stations. Diurnal variations of temperature, pressure, wind and rainfall over the monsoon belt are briefly treated.

Key words: Monsoon circulation: Evolution; monsoon rainfall: space-time variation.

1. Introduction

1.1. The summer and winter monsoons of south Asia constitute the most spectacular manifestations of regional anomalies in the general circulation of the atmosphere resulting from land-sea contrasts and orographical features. The land masses of north Africa and Eurasia cover about 60 per cent of the northeast quadrant of the globe whereas nearly 80 percent of the area is covered by water in the other three quadrants. Unlike the Atlantic and Pacific Oceans which are open towards the north and the south, the Indian Ocean is land-locked to the north by the Asian continent. These geographical features give rise to extreme thermal contrast between the land and the sea in summer and in winter which is the crucial factor in the development of the most pronounced monsoon circulations over this part of the globe. The role of the mountain systems, in particular the Himalayas and the Tibetan plateau, for the generation and maintenance of the south Asian summer monsoon has been demonstrated by recent numerical simulation studies (HAHN and MANABE [13]).

1.2. The summer monsoon circulation gets established towards the end of May and continues till the end of September. The winter circulation prevails for the six months from November to April. May and October are the transitional months.

[1]) Indian Institute of Tropical Meteorology, Poona 411005, India.

The transitions, which are fairly abrupt, are brought about by the response of the ocean-earth-atmosphere system to the annual cycle of solar radiation. While the large-scale features of the monsoon are repetitive from year to year, the anomalies from one year to another and the associated variations of rainfall in space and time can be appreciable, leading to floods and droughts over large areas.

1.3. The planetary monsoon circulation extends almost from the mid-Atlantic to the mid-Pacific across the tropics and sub-tropics of north Africa and Asia. The very small heat capacity of the land and the very large heat capacity of the adjacent oceans give rise to pronounced temperature contrasts between the land and the water masses in summer and in winter and this provides the source of available potential energy for driving the large-scale planetary monsoon circulation. Interaction with the mid-latitude westerlies and interhemispheric exchanges are also important aspects of the monsoon problem.

1.4. Regional peculiarities assume a dominant role with respect to the monsoonal features over India and neighbourhood. The Himalayas and the Tibetan plateau to the north, the Western and Eastern Ghats running more or less parallel to the west and east coasts of peninsular India, the Arakan Yoma and the Garo–Khasi–Jainthia hill ranges to the east, the Kirthar and Sulaiman mountain chains to the west and the Vindhya and Satpura ranges running nearly east–west across the centre of the country are important orographic features that influence the monsoon circulation and monsoon rainfall. The thermal structure of the adjoining sea areas – the Arabian Sea, the Bay of Bengal and the south Indian Ocean – and its temporal variations appear to have a modulating influence on the monsoon activity. The cold oceanic upwelling along and off the coast of Somalia during the summer months as well as the orographic features of east Africa influence the low level circulation of the Arabian Sea branch of the Indian summer monsoon.

1.5. The summer or southwest monsoon accounts for over 75 per cent of the annual rainfall for most of India. The south-eastern part of the peninsula has its main rainy season during the retreating phase of the southwest monsoon or what is commonly known as the northeast monsoon, from October to December. The extreme northern part of India which is shut off from the southwest monsoon current by orographic barriers receives precipitation in the form of rain or snow during the winter months from eastward moving extra-tropical systems known as western disturbances. These disturbances also cause precipitation over the plains and adjoining mountain ranges of north India. The period from March to May, known as hot weather season, is associated with increasing convective activity which is a prelude to the onset of the southwest monsoon. During these months there is increasing thunderstorm activity over northeast India and Bangladesh as well as in the southern parts of the peninsula. Over northwest India, including the deserts of Rajasthan, duststorms and dust-raising winds are a common feature of the hot weather months and as the season advances the atmosphere gets highly charged with dust which is carried aloft to upper tropospheric levels by convection currents. The seasonal

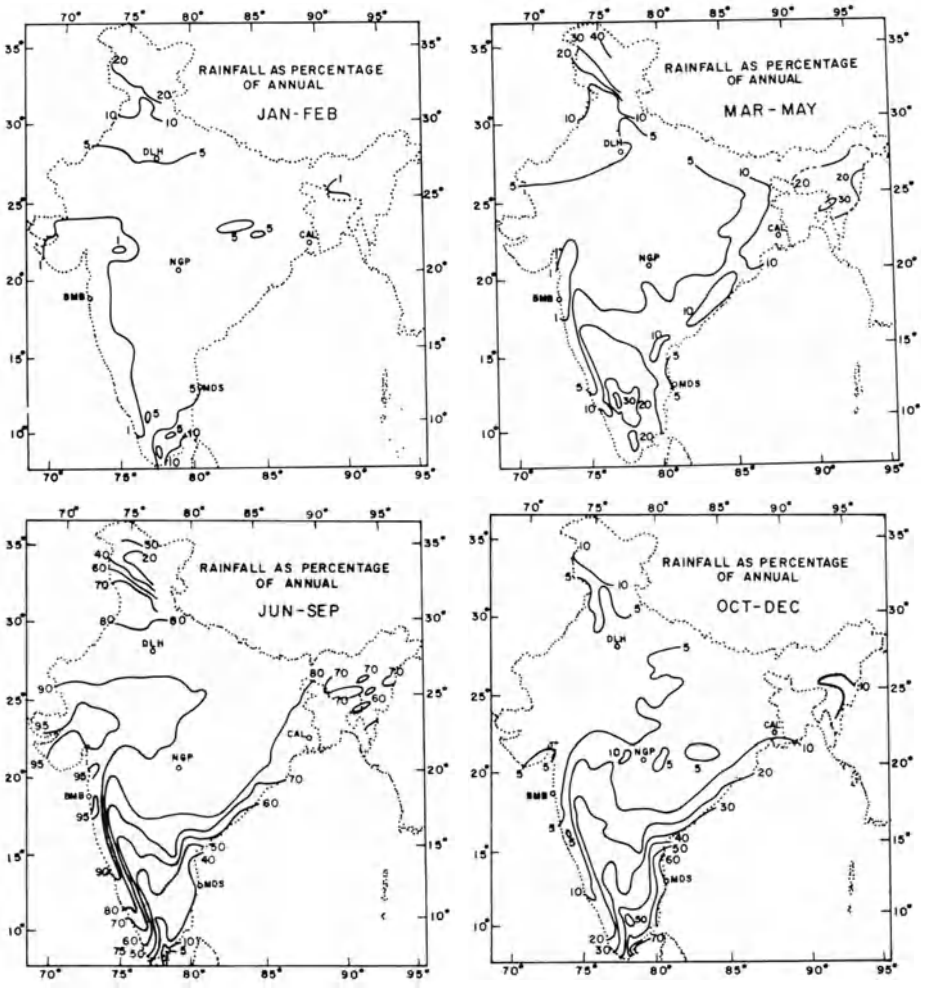

Figure 1
Seasonal rainfall as percentage of annual.

rainfall expressed as a percentage of the annual rainfall for the four Indian seasons (IMD [16]) is shown in Fig. 1.

1.6. In the following sections some aspects of the evolution of the monsoon circulation over India are discussed by focussing attention on the surface and upper air data of stations which lie close to the central meridian across India. This is followed by an examination of some of the observed features of Indian rainfall. Diurnal variations in some of the meteorological parameters are also briefly considered. The mean monthly upper air data utilised in the present study is mostly up to 1970 and covers a period of 15 to 20 years. The surface and rainfall data generally cover a period of 50 years.

2. *Seasonal variations in the thermal field*

2.1. Much insight into the evolution of the monsoon circulation over India is furnished by examination of the surface and upper air data of the three stations, Trivandrum (08° 29′N, 76° 57′E), Nagpur (21° 06′N, 79° 03′E) and New Delhi (28° 35′N, 79° 12′E), which lie approximately along the central meridian across India. The locations of these stations as well as of some others that would be referred to in the course of the paper are shown in Fig. 2(a).

2.2. Referring to Fig. 2(b) we see that the seasonal variation of mean surface temperature is small at the low latitude coastal station of Trivandrum but is considerable at Nagpur and Delhi which are inland stations. The reversal of the meridional surface temperature gradient across India from winter to summer progresses from south to north. Beginning from March in the south it is completed by the end of May throughout the country. The reverse transition is more abrupt and takes place in October.

2.3. The seasonal progression of mean monthly upper air temperatures at the three stations is shown in Fig. 3. The winter-summer reveral of the temperature gradient across India can be noticed up to the 300 mb level. At 200 mb there is hardly any temperature gradient across the country in the winter months, but a strong gradient in the same sense as at the lower levels exists in the summer months. At 150 mb the winter temperature gradient has reversed and there is a progressive increase of temperature from Trivandrum to Delhi throughout the year. The 100 mb level presents a picture exactly the reverse of the 200 mb level. The temperature gradient across India at this level is feeble during the summer monsoon months but a strong gradient prevails in the winter months. In the lower stratosphere Delhi continues to be warmer than Nagpur and Trivandrum throughout the year.

2.4. The progressive decrease of temperature from Trivandrum to Delhi up to the 200 mb level during November to April corresponds to a westerly thermal wind. Hence westerlies increase in strength with elevation up to 200 mb which is the level of the subtropical westerly jet stream over north India in these months. Above 200 mb the reversal of the thermal gradient results in weakening of the westerlies. In the summer monsoon months June to September, temperature increases from Trivandrum to Delhi throughout the troposphere and the thermal wind is easterly. Hence the low level monsoon westerlies change over to easterlies in the upper troposphere. The easterlies progressively strengthen to become the tropical easterly jet stream near the 100 mb level. It may be noted that at 100 mb Trivandrum is slightly warmer than Nagpur during the summer monsoon months. Hence the easterly jet stream attains its maximum strength a little below the 100 mb level over the south peninsula. At Nagpur the easterlies attain maximum speed at 100 mb level above which there is a decrease in speed up to about 50 mb followed by a further increase aloft up to 30 mb. Between Nagpur and Delhi temperature continues to increase

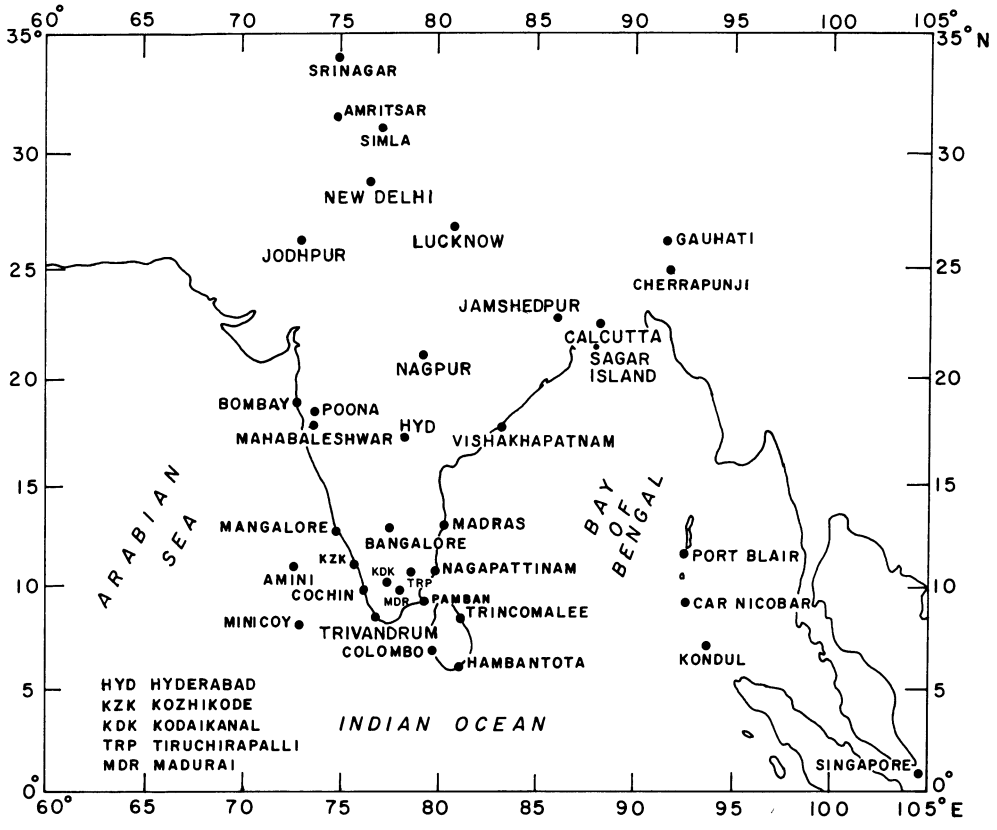

Figure 2(a)
Location of stations.

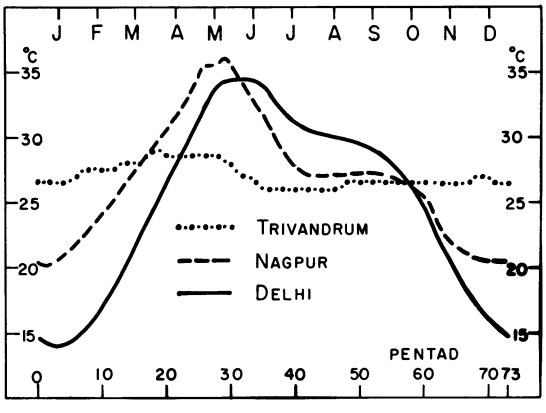

Figure 2(b)
Seasonal variation of mean surface temperature from south to north across India.

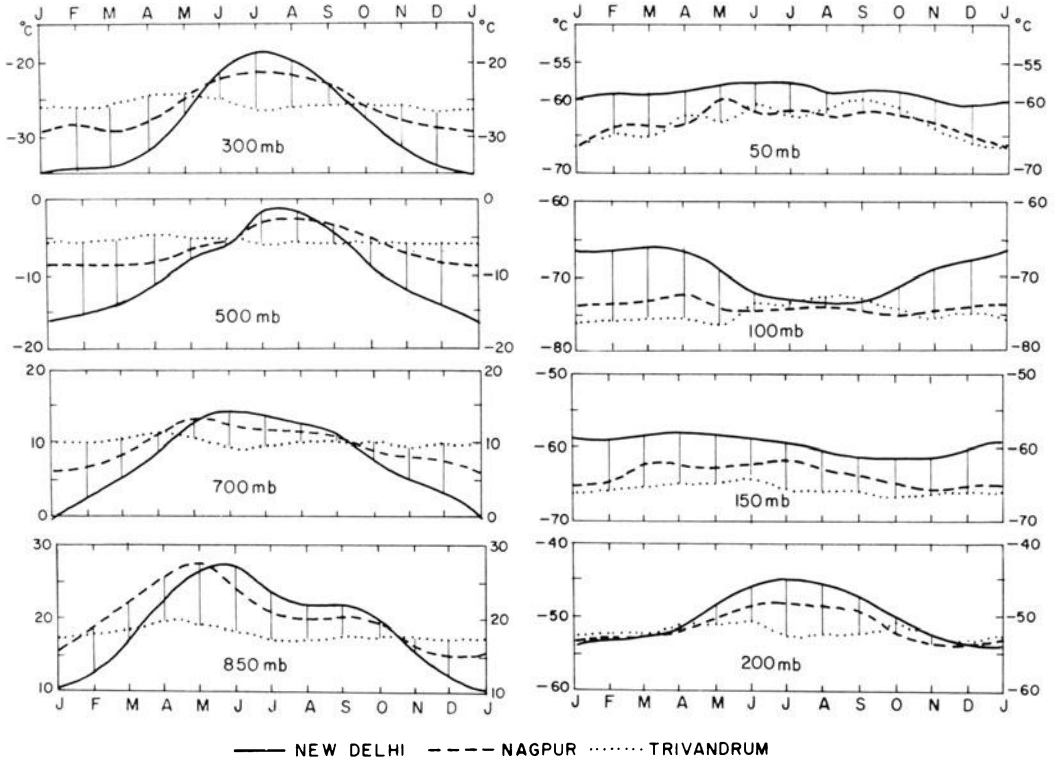

Figure 3
Seasonal variation of upper air temperature from south to north across India.

towards the north in the lower stratosphere and hence the easterlies continue to strengthen. At Delhi there is progressive increase in the speed of the easterlies up to 30 mb level without any maximum as noticed at the southern stations (Vide Fig. 8a, b,c).

3. Seasonal variations in the pressure field

3.1. The seasonal variations in the mean sea level pressure and surface winds at Trivandrum, Nagpur and New Delhi (ANANTHAKRISHNAN [4]) are shown in Fig. 4. From November to February the sea level pressure increases from south to north across India; the reverse conditions prevail from April to September. The winter–summer transition occurs about the end of March and the reverse transition by the middle of October. At Trivandrum the lowest surface pressure is reached towards the end of May and at Nagpur and New Delhi a month later.

3.2. The monthly variation of mean sea level pressure at 26 stations across India from Trivandrum in the south to Amritsar in the north (covering the latitude interval

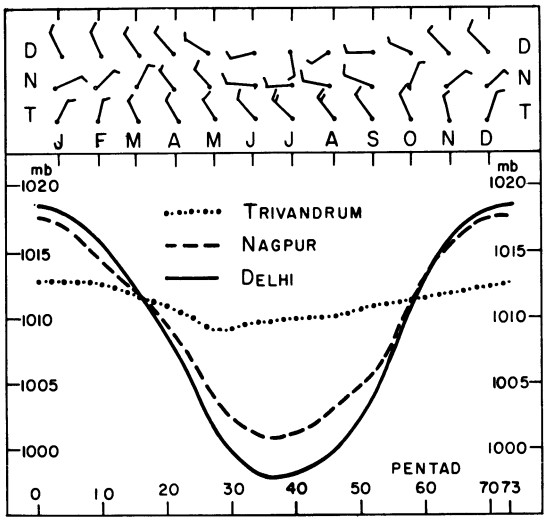

Figure 4
Seasonal variation of mean sea level pressure from south to north across India.

8° to 32°N) is shown in Fig. 5. For each month three curves are shown corresponding to the 1st, 11th and 21st of the month. Mean sea level pressure decreases from winter to summer by about 3 mb in the south and 20 mb in the north. The north–south decrease of pressure is about 6 mb in winter; the corresponding increase of pressure is about 12 mb in summer. North of 26°N the pressure gradient is flat both in summer and in winter. The time rate of change of pressure over north and central India is minimum in the second half of December and June (near the solstices). The maximum rate of fall of pressure occurs from mid-April to mid-May and the maximum rate of rise from mid-September to mid-October.

3.3. The monsoon reversal of pressure gradients and winds aloft (ANANTHAKRISHNAN and KRISHNAN [2]) is illustrated by the upper air data of Trivandrum, Nagpur and New Delhi in Fig. 6. The monthly march of contour heights of standard isobaric levels at the three stations as well as the mean monthly upper winds at the isobaric levels are shown in the diagram. In the *winter* months the pressure gradients across the country are weak at 850 mb. The positive gradient of pressure at the surface between Nagpur and Delhi is confined to a shallow layer and the gradient is already reserved at 850 mb. At 850 mb and 700 mb levels the centre of high pressure is near Nagpur with anticyclonic circulation around it giving rise to the northeast monsoon flow over the southern parts of peninsular India. The axis of the high pressure ridge shifts equatorward with elevation. At upper tropospheric levels the anticyclone ridge is close to the latitude of Trivandrum as can be seen from the light winds at this station. In February–March the ridge axis is occasionally displaced to the south of Trivandrum when westerlies pervade the entire country in the upper troposphere.

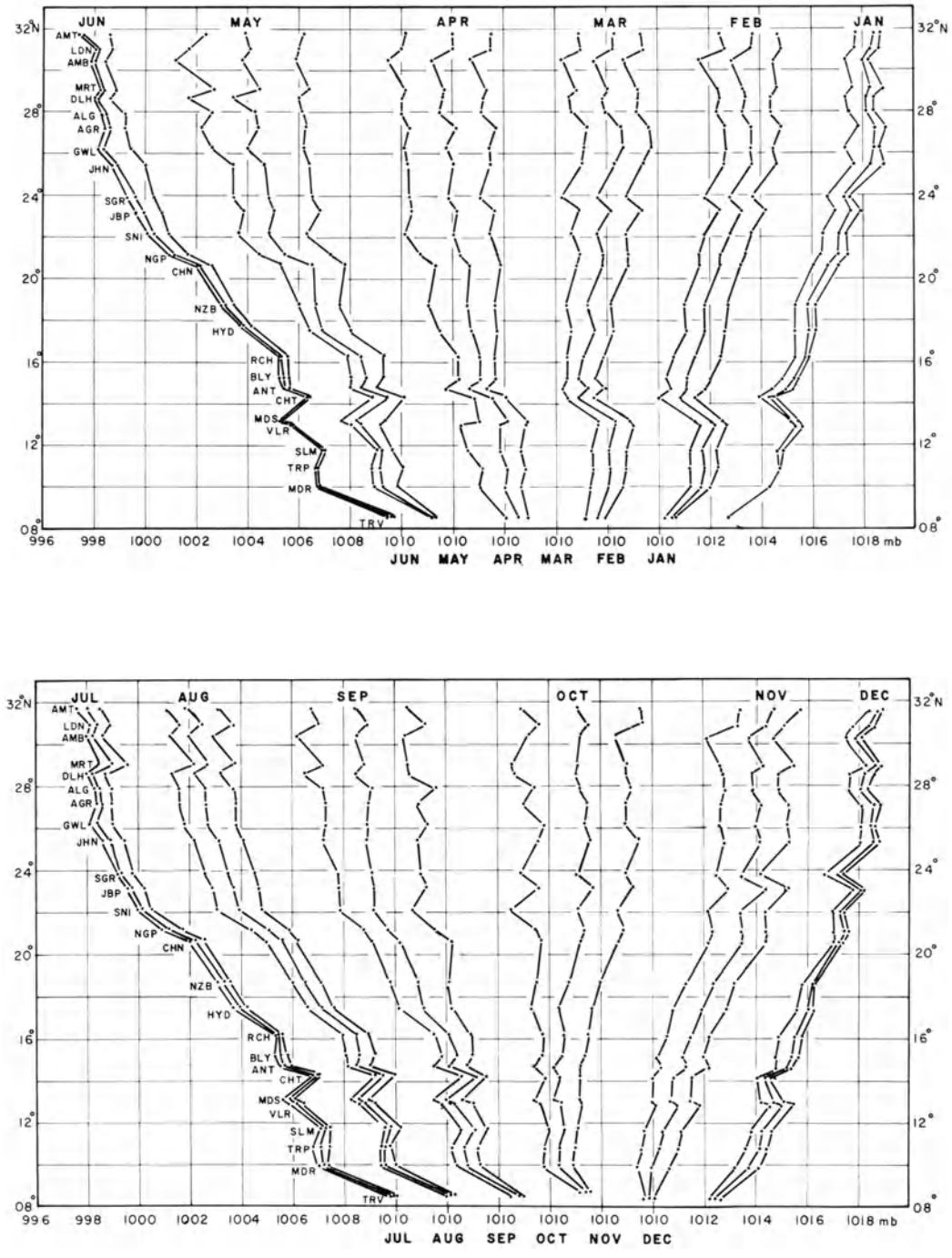

Figure 5
Monthly variation of mean sea level pressure at 26 stations across India.

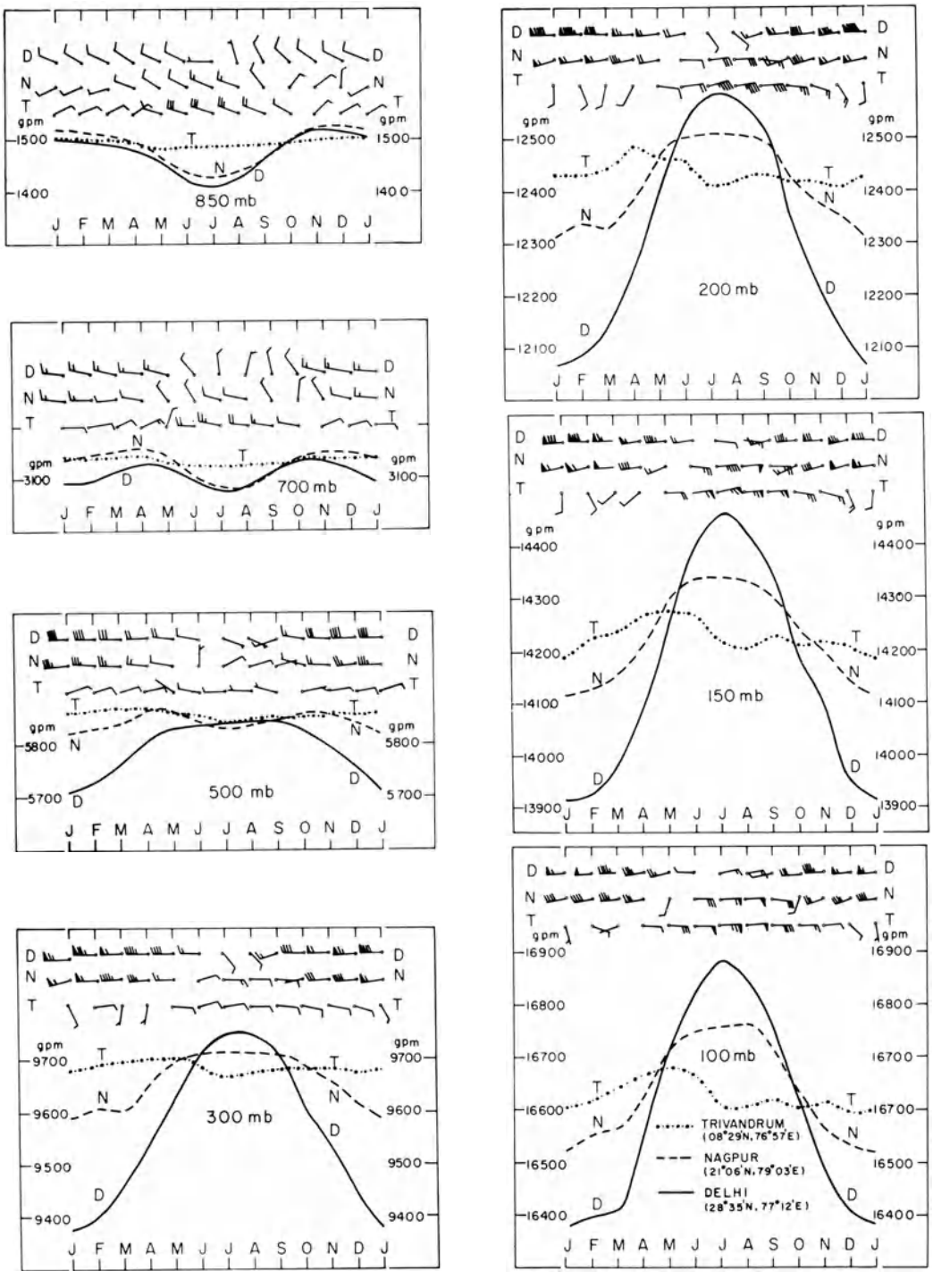

Figure 6
Seasonal variation of contour heights and winds at standard isobaric levels from south to north across India.

On such occasions the axis of the subtropical westerly jet stream is displaced appreciably southward of its mean position.

3.4. The transition to the *summer* type of pressure gradient between Trivandrum and Nagpur occurs at the surface towards the end of March. At 850 mb this transition occurs about the middle of April and at 700 mb towards the last week of May. At 500 mb level, pressure gradients across the country are very weak from June to September. Aloft there is a complete reversal of the pressure gradients and winds in the upper troposphere between summer and winter. It may be noted that from May to July while there is a steep increase in the height of the upper tropospheric pressure surfaces over Delhi indicating a progressive rise in temperature, there is a decrease at Trivandrum indicating progressive lowering of temperature in the troposphere. At Nagpur the upper tropospheric pressure surfaces have nearly constant height during the summer monsoon months. The amplitude of the annual oscillation of the 200, 150 and 100 mb pressure surface is about 500 gpm at Delhi, 200 gpm at Nagpur and 75 gpm at Trivandrum.

3.5. The abscissae corresponding to the points of intersection of the curves in Fig. 6 give the epochs at which the monsoonal reversal of pressure gradients and winds occurs at the different levels. It is found that there is a systematic time sequence of the reversals in the upper and lower troposphere. This is illustrated by Fig. 7 in

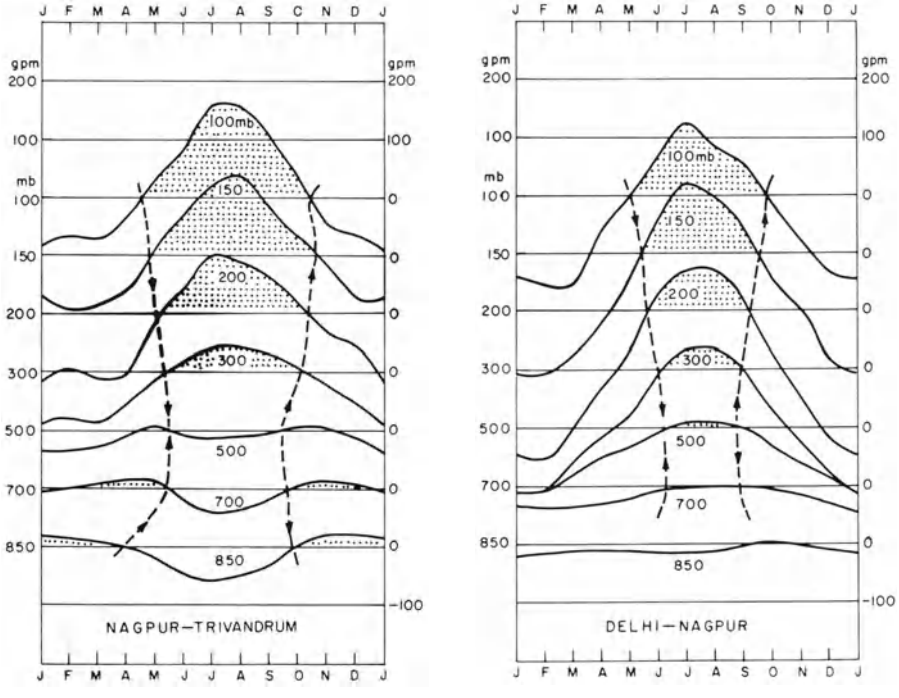

Figure 7
Vertical progression of seasonal reversal of pressure gradients across India.

which the algebraic differences in the contour heights of the standard isobaric levels are depicted against time for the pairs of stations (Nagpur–Trivandrum) and (New Delhi–Nagpur). The dotted areas in the diagram correspond to increase of pressure from south to north or easterly zonal wind.

3.6. It may be seen that the transition from the winter type of meridional pressure gradient and zonal wind circulation to the summer type sets in first in the lower layers close to the ground and in the upper troposphere close to the 100 mb level. The transition progresses upwards in the lower troposphere and downwards in the upper troposphere towards the 500 mb level. The reverse transition from summer to winter sets in first near 500 mb level from where it progresses upwards and downwards. Thus the mid-troposphere is the first to respond at the time of withdrawal of the summer monsoon and the last to respond at the time of its onset.

3.7. Between Nagpur and Trivandrum over peninsular India, the pressure gradient at 100 mb level changes sign from negative to positive by the beginning of May. The epoch of reversal progressively descends to the mid-tropospheric level by the end of the month. The corresponding change between New Delhi and Nagpur occurs at the 100 mb level by the third week of May and descends to the 500 mb level by the last week of June.

3.8. In the lower troposphere the winter–summer transition at the ground level occurs by about the end of March. Between Nagpur and Trivandrum the transition at 850 mb level occurs by mid-April and at 700 mb level towards the last week of May. Between New Delhi and Nagpur the pressure gradient is negative at 850 mb and 700 mb levels practically throughout the year. Hence no winter–summer transitions of the type between Nagpur and Trivandrum is noticed.

3.9. The summer–winter transition sets in at the mid-troposphere by the beginning of September between Nagpur and New Delhi and about a month later between Nagpur and Trivandrum. In both sectors the transitions propagate upwards in the upper troposphere and downwards in the lower troposphere. We thus see that the onset/withdrawal of the summer monsoon is associated with progressive changes in the upper and lower troposphere moving towards/away from the mid-troposphere (ANANTHAKRISHNAN [5]).

4. Seasonal variations in zonal and meridional winds

4.1. Isopleths of the mean monthly zonal and meridional winds at Trivandrum, Nagpur and New Delhi and the island station of Port Blair are shown in Figs. 8(a), (b), (c), (d). The low level summer monsoon westerly circulation extends to over 6 km at Trivandrum with the strongest westerlies near the 2 km level. Easterly circulation dominates aloft with maximum speeds exceeding 30 m/sec near the 150 mb level. This is the level of the tropical easterly jet-stream over the extreme south of peninsular India. At Nagpur easterlies prevail below 850 mb during October to March; other-

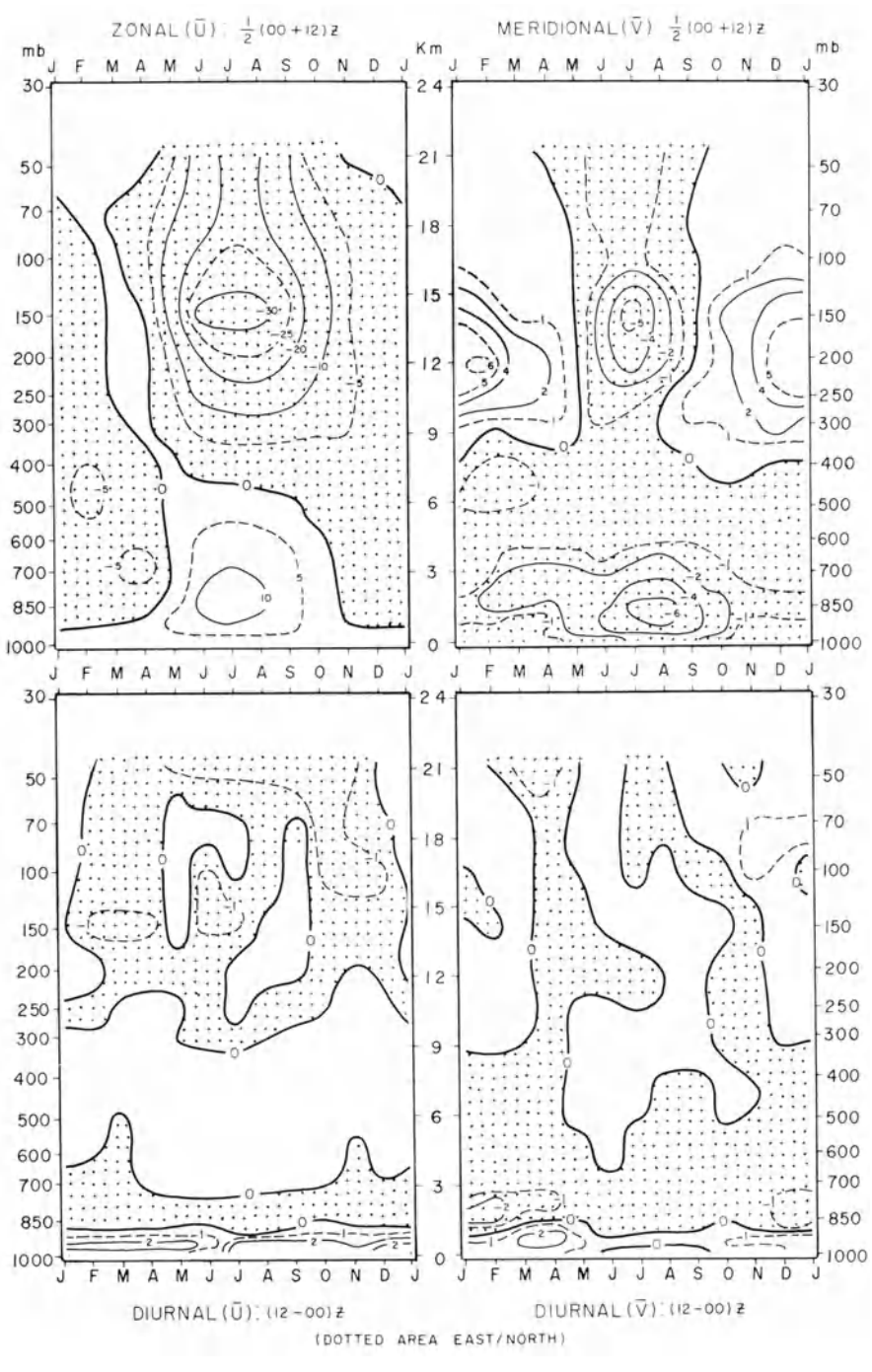

Figure 8(a)
Monthly mean zonal and meridional winds (mps) and their diurnal variation.

NAGPUR

(21° 06' N , 79° 03' E , 310 m)

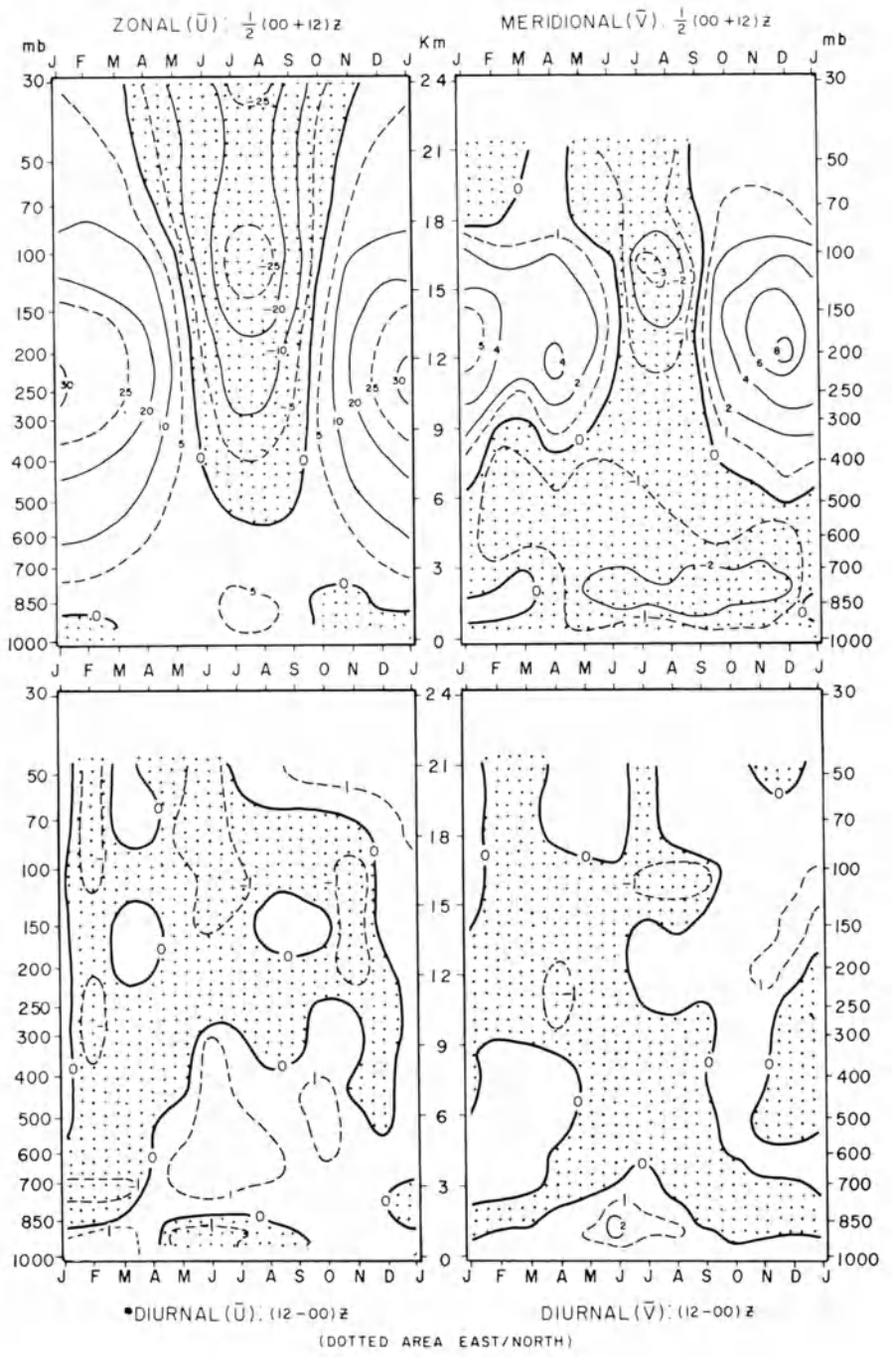

Figure 8(b)

Monthly mean zonal and meridional winds (mps) and their diurnal variation.

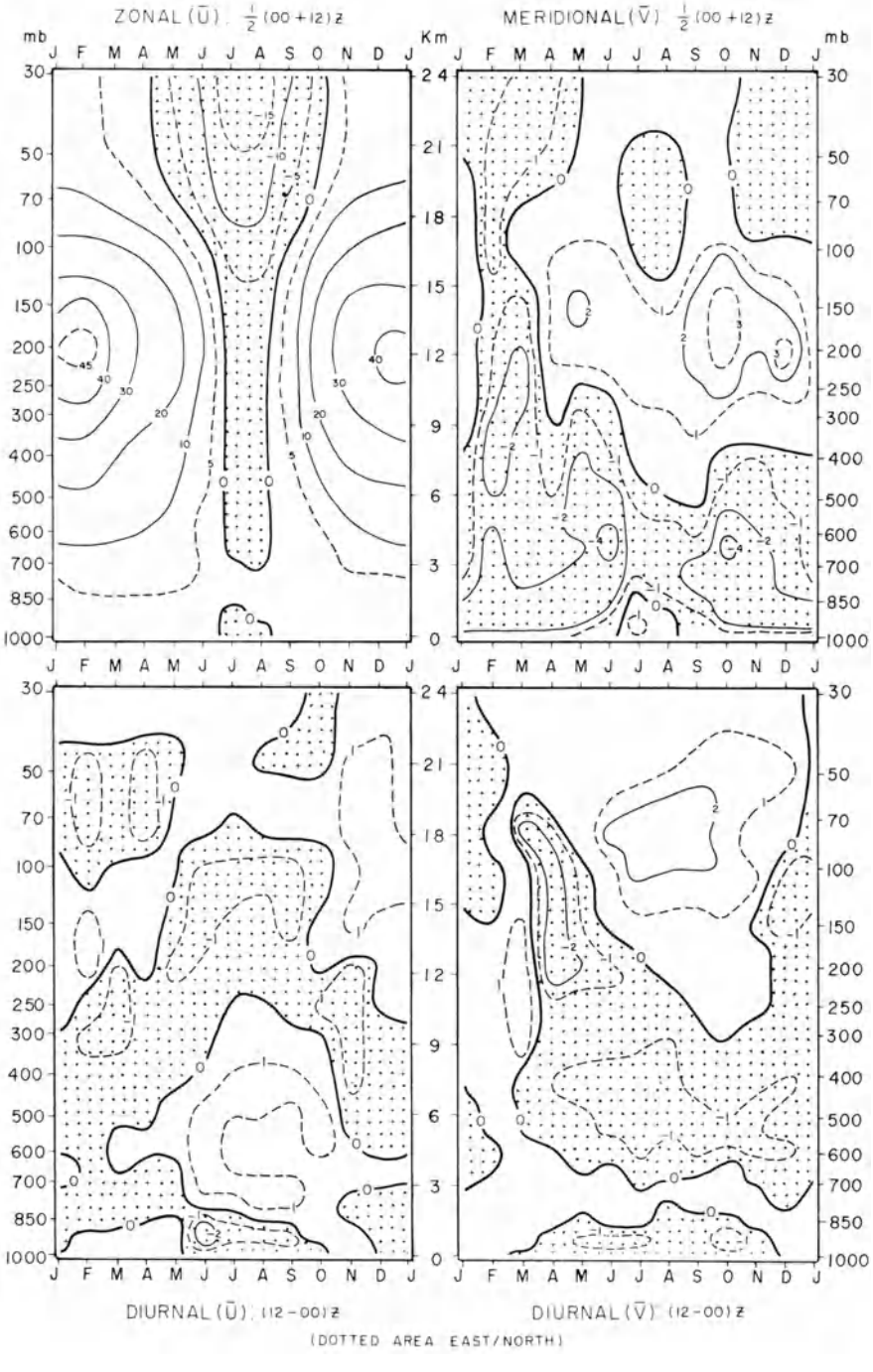

Figure 8(c)
Monthly mean zonal and meridional winds (mps) and their diurnal variation.

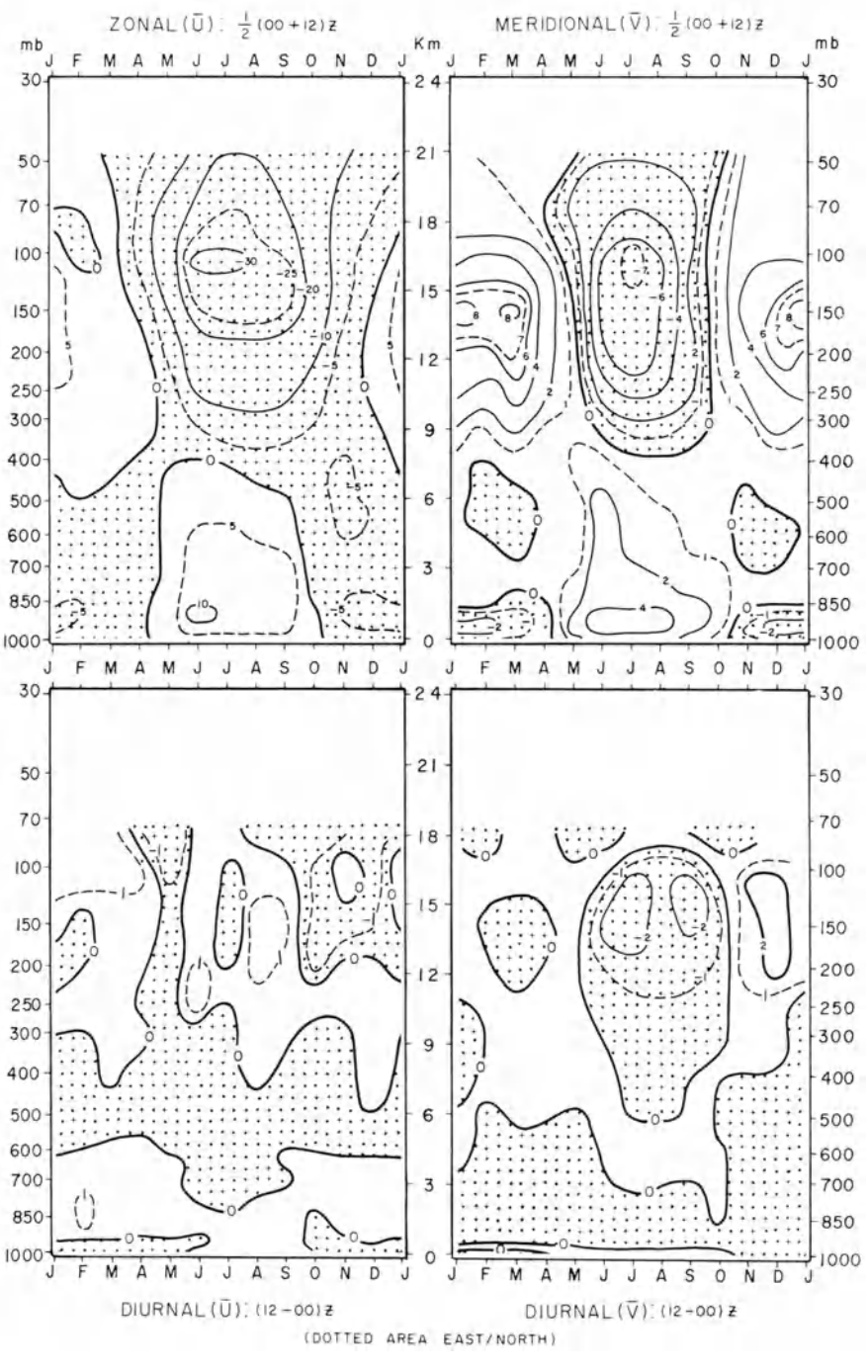

Figure 8(d)
Monthly mean zonal and meridional winds (mps) and their diurnal variation.

wise the lower tropospheric circulation is westerly throughout the year. The monsoon westerlies are weaker than at Trivandrum. The upper tropospheric summer easterlies attain maximum strength near 100 mb level above which they weaken followed by a further increase in speed near 30 mb level. At Delhi the tropospheric summer easterlies are weak and are of shorter duration than at Nagpur. They increase in speed and in duration in the lower stratosphere.

4.2. The meridional winds form part of the tropical Hadley circulation (NEWELL *et al.* [18]). During *winter* the ascending limb of the Hadley cell is south of the equator and the descending limb near 30°N with northerly flow in the lower troposphere and southerly flow in the upper troposphere. At Trivandrum the meridional winds are northerly below 400 mb with southerlies aloft. The southerlies attain maximum strength near 200 mb which is the level of the sub-tropical westerly jet stream in the winter months. More or less similar features are also noticed at Nagpur. At New Delhi the picture is somewhat similar but more complicated. During February–March northerlies are noticed at all levels.

4.3. In the *summer* monsoon months the thermal equator and the ITCZ are displaced to about 27°N over the Indian area. The ascending limb of the northern Hadley cell is near this latitude with its descending limb close to the equator. The corresponding meridional circulation should be northerly flow in the upper troposphere and southerly flow in the lower troposphere. The meridional winds at Trivandrum and Nagpur are, however, northerly throughout the troposphere. This anomaly of northerlies in the lower troposphere results from the influence of the Western Ghats on the westerly zonal flow across this mountain barrier and is readily understood on the basis of the conservation of potential vorticity of air parcels. The vertical shrinking of an air column while crossing the mountain is associated with a decrease in relative vorticity which leads to anti-cyclonic southward turning of the air current. After crossing the barrier conservation of potential vorticity leads to a cyclonic turning of the air current (HOLTON [14]). This is in conformity with the observed behaviour of the lower tropospheric westerly flow across peninsular India.

4.4. The northerly flow in the upper troposphere is strongest near 150 mb at Trivandrum and near 100 mb at Nagpur – close to the level of the maximum zonal easterlies in both cases. At new Delhi there is a shallow surface layer of southerlies of about 1 km depth in the summer monsoon months above which northerlies prevail up to the middle troposphere. In the upper troposphere the meridional flow is southerly.

4.5. At Port Blair in the Bay of Bengal the lower tropospheric meridional flow is southerly with a pronounced northerly flow in the upper troposphere. This is consistent with a Hadley cell with its ascending limb over north India and descending limb near the equator. The meridional winds at Calcutta and Gauhati are also similar to those at Port Blair. At Minicoy and Colombo, the lower tropospheric mean meridional flow shows alternate layers of northerlies and southerlies in the summer monsoon months. A similar feature is also noticed at the equatorial station

of Gan while at Singapore the meridional flow is southerly. At all the stations the upper tropospheric flow is northerly with maximum speed near 150 mb level. It is now well known (FINDLATER [11], [12]), that during the summer monsoon months strong southerly cross-equatorial flow occurs off the coast of Somalia in the lower levels. Fluctuations in the meridional flow are closely linked with the activity of the monsoon.

5. *Seasonal variation in atmospheric humidity*

5.1. Since the general air flow in the lower levels is from sea to land in the summer monsoon months and from land to sea in the winter monsoon months there is a considerable seasonal variation in the moisture content of the atmosphere. The seasonal variation in the mean monthly precipitable water vapour content of the atmosphere over the Indian area (ANANTHAKRISHNAN *et al.* [3]) is shown in Fig. 9. The maximum value of about 7 gms cm^{-2} occurs over northeast India in the peak monsoon months of July and August. As is well known, precipitable water vapour alone is not an index of rainfall activity. Synoptic and meso-scale disturbances leading to low level convergence and vertical motion of humid air are required for precipitation to occur. Thus over the south-eastern parts of the Peninsula while the precipitable water vapour is maximum in July-August, the rainfall is maximum in October-November.

5.2. Although the monthly mean precipitable water vapour is maximum during the summer monsoon months, large fluctuations in moisture content occur in association with synoptic situations. Monsoon rainfall is essentially convective in nature and ascending motions within areas of rainfall have compensating descending motions outside such areas. Aerological ascents show considerable day-to-day variations in relative humidity as is illustrated by Fig. 10 for two stations – Nagpur and Lucknow. The precipitable water vapour at Nagpur decreased from 8.15 grams cm^{-2} at 00 Z on 12 July 1970 to 5.19 grams cm^{-2} at 12 Z on 13 July 1970. At Lucknow the values of precipitable water vapour corresponding to the two tephigrams are 8.43 grams cm^{-2} on 11 July 1970 and 5.93 grams cm^{-2} on 13 July 1970.

5.3. In a recent study by the author (to be published), the daily aerological soundings at the island station of Port Blair in the Bay of Bengal for the summer monsoon months (June to September) of 1972 were objectively sorted out by a computer programme into three types depending upon the vertical profile of dew point depression. The three types represent cases in which (i) the atmosphere is highly humid (relative humidity in excess of 75 per cent) up to upper tropospheric levels; (ii) those in which the relative humidity is low (less than 50 per cent) and the atmosphere is comparatively dry above the surface friction layer; and (iii) the intermedicate type. The mean tephigrams for types (i) and (ii) which may be called the wet and dry types are shown in Fig. 11. The wet type generally corresponds to rainy situations and the

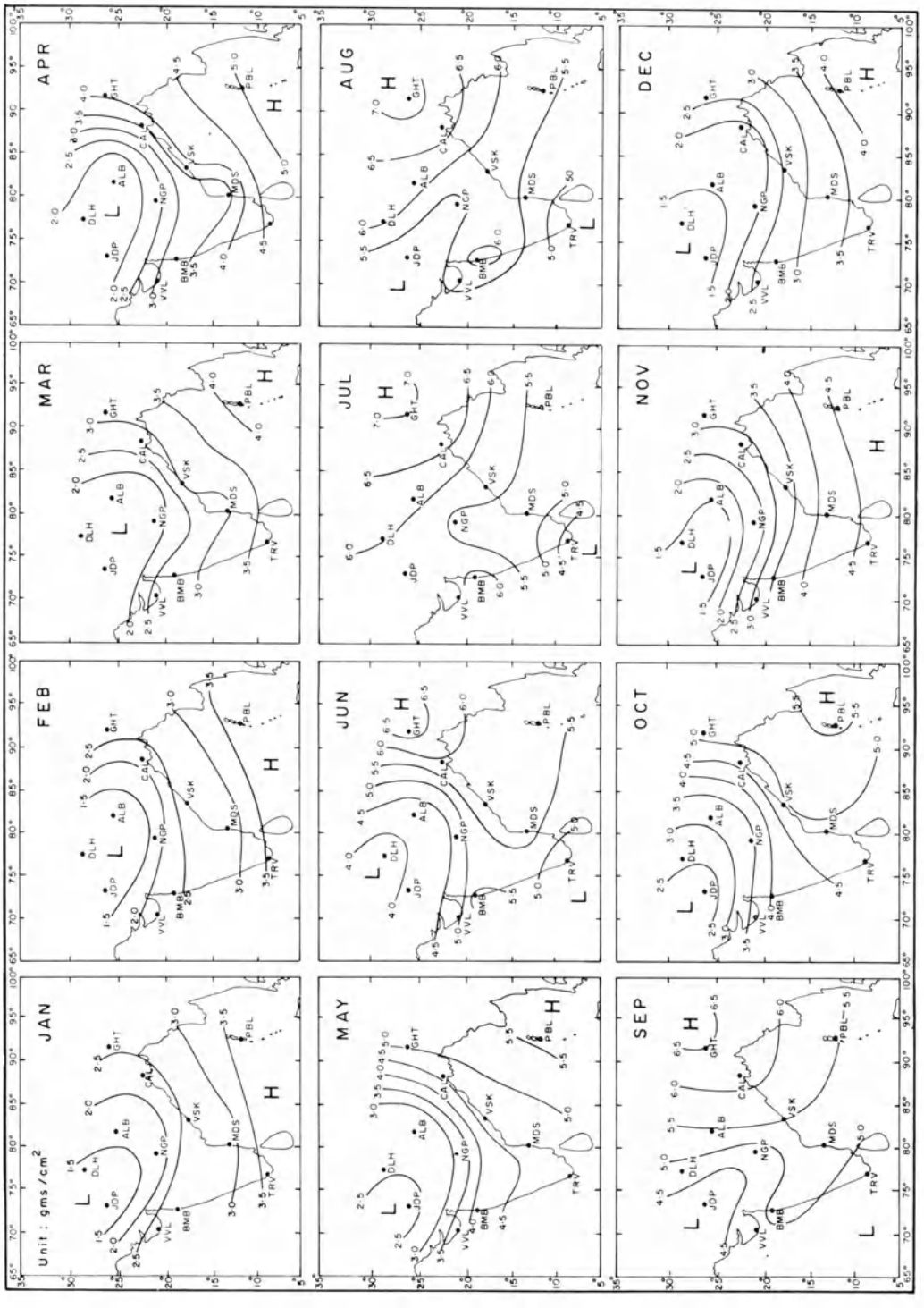

Figure 9
Seasonal variation of precipitable water vapour over India.

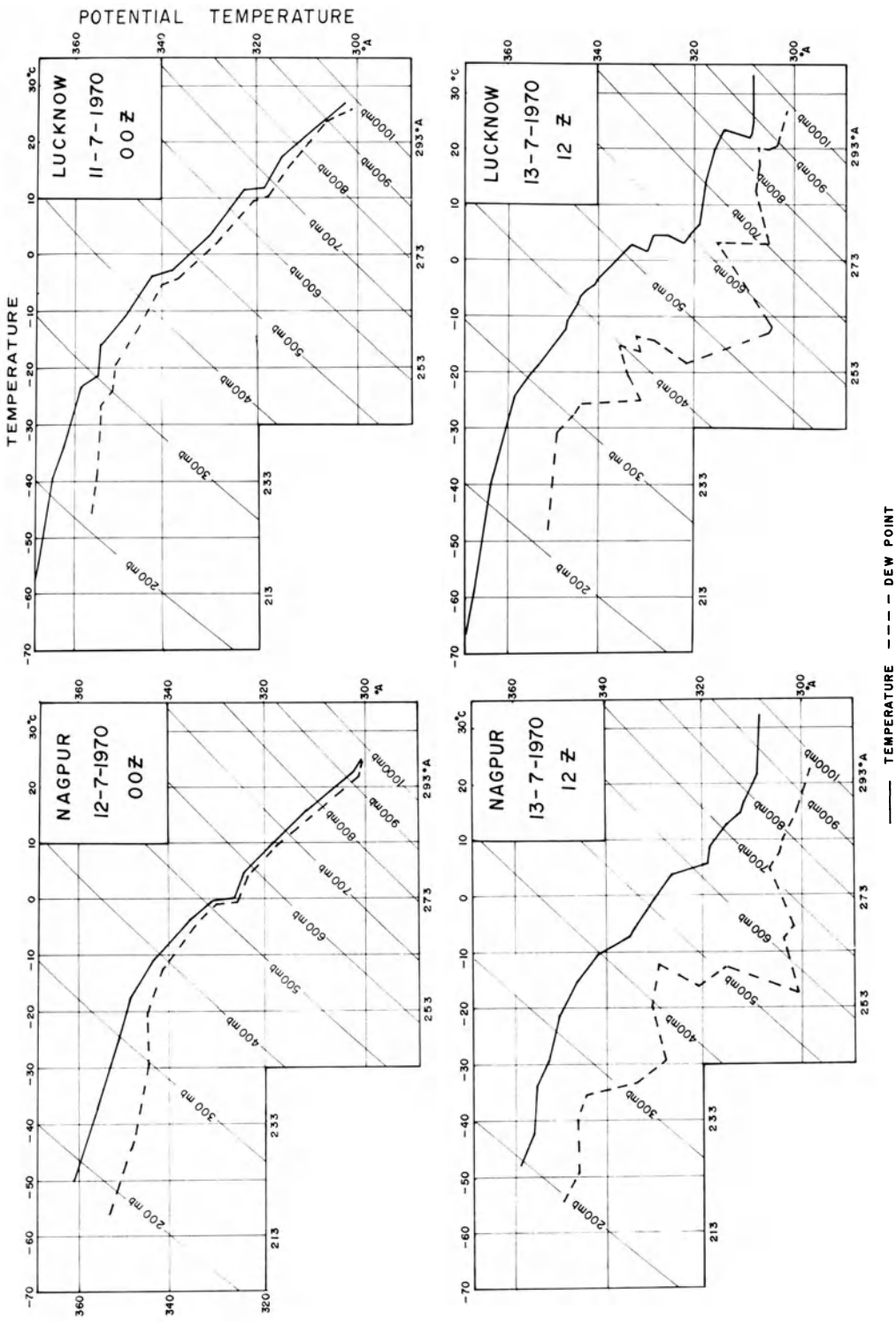

Figure 10
Tephigrams showing synoptic fluctuations of humidity during the southwest monsoon at two inland stations.

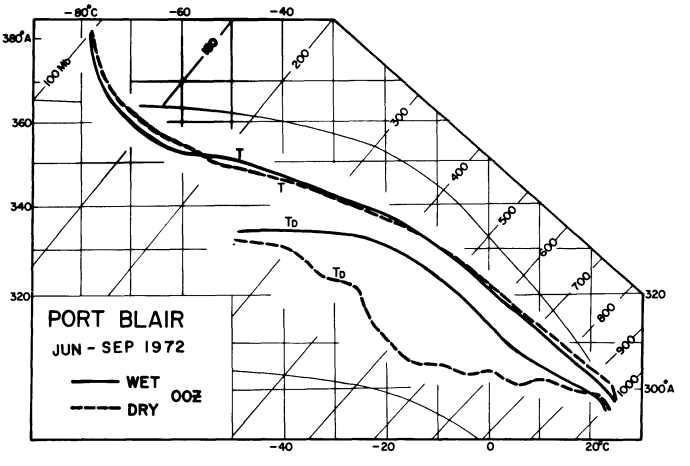

Figure 11
Mean tephigrams of Port Blair for 'wet' and 'dry' situations during the southwest monsoon months.

dry type to rainless situations at Port Blair during the summer monsoon season. It is important to emphasise that rainfall of the summer monsoon season occurs in spells associated with synoptic scale and meso-scale disturbances within the general monsoon field. While the vertical profile of the dry bulb temperature does not show large day-to-day changes; the vertical profile of dew point temperature shows considerable variations in the monsoon field.

6. Monsoon rainfall and its space-time variations

6.1. The most important aspect of the summer monsoon is the rainfall associated with it. It is this feature of the monsoon that forms the primary criterion for fixing the dates of onset and withdrawal of the monsoon over different parts of the country. At the extreme southwest coast of peninsular India as well as over Bangladesh and Assam the monsoon rains normally set in by the end of May. The monsoon rapidly advances northward along the west coast of India and more gradually in a northwesterly direction across central and northern India. By about the middle of July the monsoon is fully established over the entire country. The withdrawal starts from northwest India by the beginning of September and roughly proceeds in a direction opposite to that of the advance. In Fig. 12 are shown isolines of onset and withdrawal of the monsoon over different parts of India (IMD [15]).

6.2. It may be of interest to comment on the manner in which the lines in Fig. 12 have been arrived at. On the basis of long-term rainfall data, pentad rainfall values are worked out for individual stations and these are depicted graphically as a function of time. The pentad which shows a characteristic sharp rise of rainfall is located and the middle date of this pentad is taken as the mean date of onset for the station.

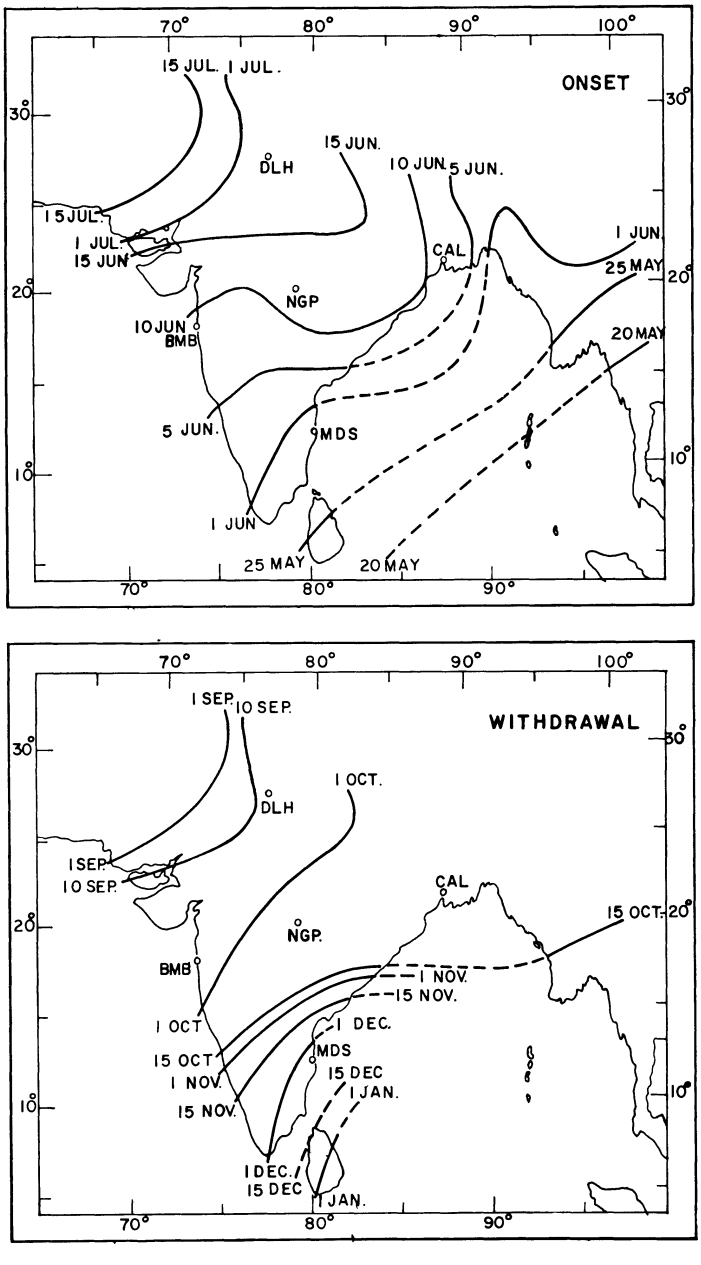

Figure 12
Progression of the onset and withdrawal of the southwest monsoon.

Similarly the pentad which shows a characteristic decrease of rainfall towards the end of the monsoon season is located and its middle date is taken as the date of withdrawal. Smooth isolines are drawn after depicting such dates on charts.

6.3. Although the procedure looks simple there are practical difficulties of a serious nature. For instance, over the extreme south of the peninsula as well as over northeast India and Bangladesh pre-monsoon thunderstorm activity gives rise to steadily increasing rainfall from the middle of April and it is not easy to decide uniquely from the rainfall curves the pentad at which the characteristic monsoon rise in rainfall sets in. There are also other difficulties. For example, when the monsoon rainfall begins to increase on the west coast, there is a decrease of rainfall to the east of the Western Ghats over the southern part of the peninsula. There are similar difficulties in fixing the date of withdrawal also. There is no objective method for fixing the dates of onset and withdrawal of the monsoon. Synoptic experience and critical assessment of changes in the upper air circulation features have to supplement the rainfall data for deciding the onset and withdrawal dates. Despite this, Fig. 12 furnishes a good working guide which high-lights the major features.

6.4. The rainfall of India and its space-time variations have been extensively studied since the classic work of BLANFORD [10] on this subject. Large space-time variations of rainfall occur during a monsoon season and from one monsoon season to another. The prediction of these variations which give rise to floods and droughts over parts of the country is an important problem of monsoon weather forecasting. We shall be concerned here with features of the long-term climatic mean rainfall (based mostly on the 50-year period 1901–50) and its spatial and temporal variations. The climatological atlases of the INDIA METEOROLOGICAL DEPARTMENT [16], [17] contain maps depicting features of monthly and annual spatial distributions. These do not bring out certain aspects of rainfall that are high-lighted when the climatic rainfall data are considered pentad-wise. Such a study was undertaken sometime back (ANANTHAKRISHNAN and PATHAN [6], [7]), and has since been extended to cover several extra-Indian stations also. A set of 73 normal pentad rainfall maps for India and the adjacent sea areas has been prepared along with normal pentad rainfall diagrams for a large number of stations. Mean pentad rainfall diagrams have also been prepared for five-degree squares covering the entire country. Some salient points are mentioned below.

6.5. Normal pentad rainfall charts for a few typical pentads are shown in Fig. 13 (a), (b). P-1 and P-10 illustrate winter rainfall in early January and mid-February. The extreme north of the country and the plains of India get winter precipitation from western disturbances. The extreme southeastern tip of India and the eastern parts of Sri Lanka also receive rain from westward moving weather systems of low latitudes. P-23 for the fifth pentad of April shows increasing rainfall over northeast India and the southern parts of the peninsula from thunderstorms of the hot weather months.

6.6. P-32 is the rainfall chart for the second pentad of June soon after the onset

of the southwest monsoon. The striking features are the high rainfall on the west coast of the peninsula and the extreme aridity of the southeastern parts of the peninsula and the northern parts of Sri Lanka which are drier than the deserts of Rajasthan during the summer monsoon months. East of longitude 90°E the rainfall again increases rapidly towards the coasts of Burma and Malaya. The dry area juxtaposed between the two rainy areas should be a region of dynamically induced descending motion. During 'break monsoon' situations the stations in this dry belt may get rainfall from westward moving low pressure systems in the south Bay of Bengal.

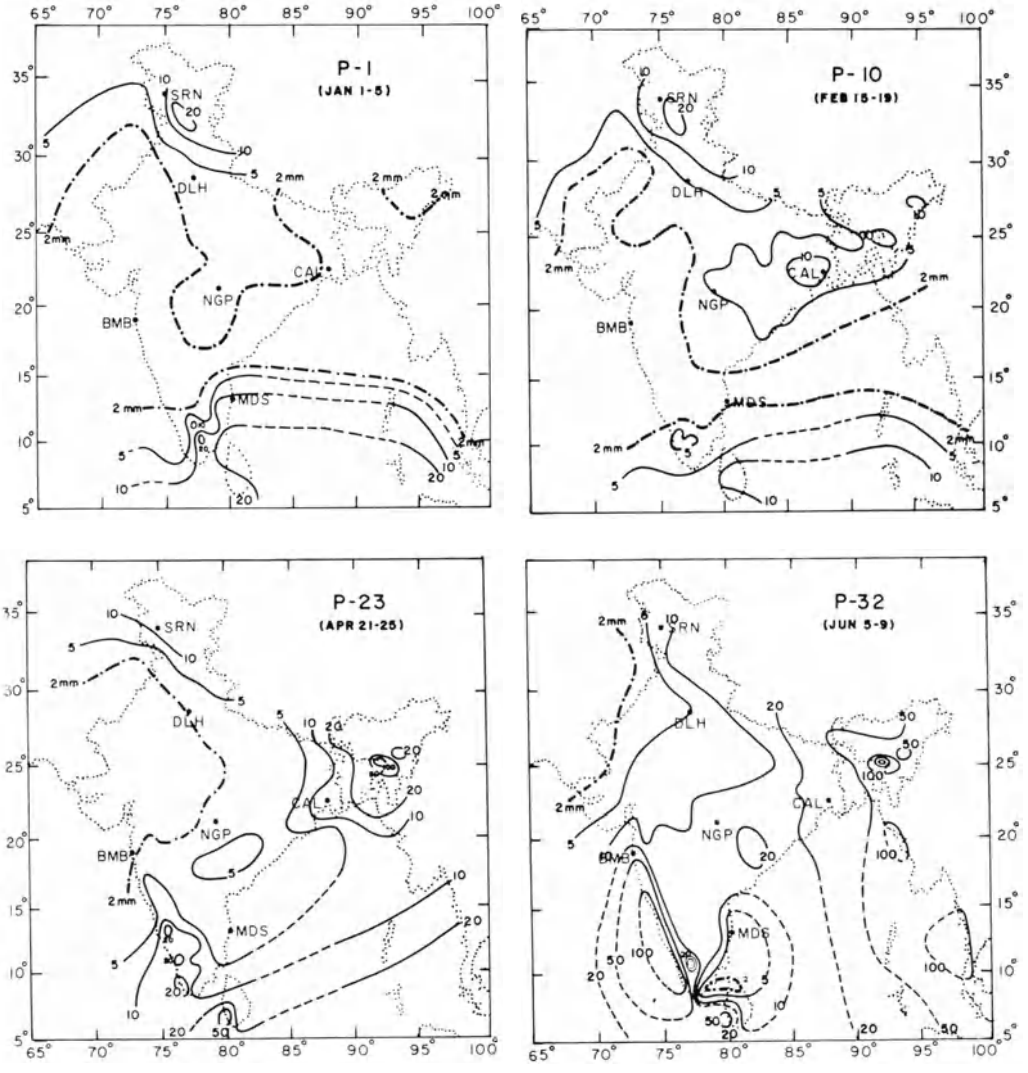

Figure 13(a)
Normal pentad rainfall charts for typical pentads.

6.7. P-41 for the fifth pentad of July illustrates the rainfall situation when the monsoon is fully established over the country. The area of smallest rainfall is the central part of the peninsula to the east of the western ghats, the aridity increasing towards the southeastern end. P-50 shows rainfall at the beginning of September when the monsoon rains have begun to decrease and the retreat of the monsoon from northwest India is commencing. P-63 for early November shows that the southwest monsoon has withdrawn from north India and the central parts of the country and the northeast monsoon rains have been established over southeast of the

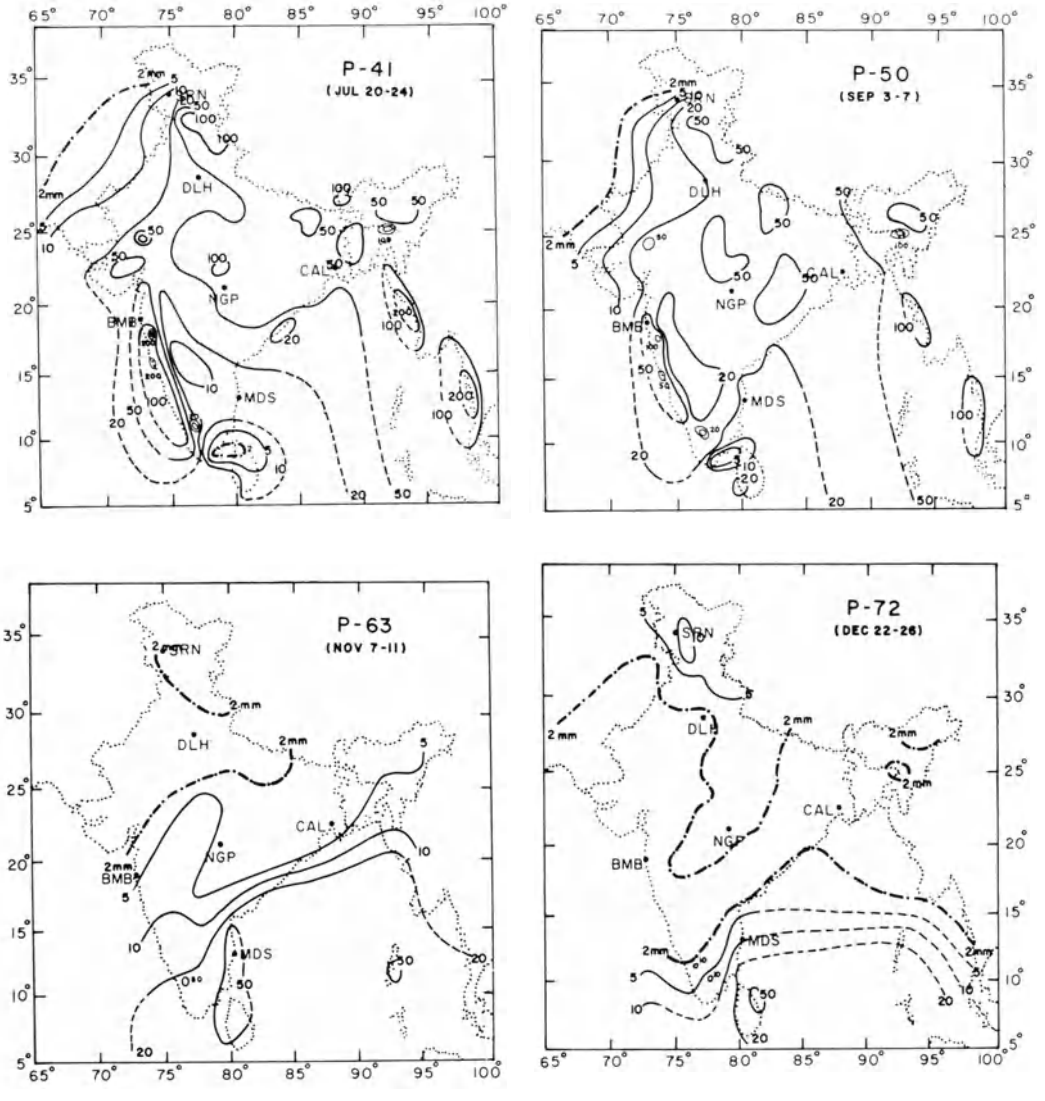

Figure 13(b)
Normal pentad rainfall charts for typical pentads.

peninsula and Sri Lanka. P-72 for the latter part of December shows that the northeast monsoon rains have decreased and winter rains have commenced over the extreme north.

6.8. Pentad rainfall diagrams for the individual stations show a large variety of patterns. Fig. 14 (a), (b) show the rainfall patterns of a number of stations south of latitude 15°N in the Arabian sea, the Bay of Bengal, on the west and east coasts of the south Indian peninsula and Sri Lanka and also in the interior of the peninsula. To facilitate interpretation of these diagrams in terms of calendar dates, the middle date corresponding to each of the 73 pentads is given in Table 1.

Table 1

Pentad	1	2	3	4	5	6	7	8	9	10
Middle date	Jan 3	8	13	18	23	28	Feb 2	7	12	17
	11	12	13	14	15	16	17	18	19	20
	Feb 22	27	Mar 4	9	14	19	24	29	Apr 3	8
	21	22	23	24	25	26	27	28	29	30
	Apr 13	18	23	28	May 3	8	13	18	23	28
	31	32	33	34	35	36	37	38	39	40
	Jun 2	7	12	17	22	27	Jul 2	7	12	17
	41	42	43	44	45	46	47	48	49	50
	Jul 22	27	Aug 1	6	11	16	21	26	31	Sep 5
	51	52	53	54	55	56	57	58	59	60
	Sep 10	15	20	25	30	Oct 5	10	15	20	25
	61	62	63	64	65	66	67	68	69	70
	Oct 30	Nov 4	9	14	19	24	29	Dec 4	9	14
	71	72	73							
	Dec 19	24	29							

6.9. It may be noted that by pentad 25 (May 1–5) a rapid rise of rainfall sets in at the island stations in the Arabian Sea as well as at the west coast stations. A similar rise is also noticed at Port Blair in the Bay of Bengal where it starts somewhat earlier. At Car Nicobar and Kondul to the south of Port Blair as well as at Colombo, the rise of rainfall commences even by end of March (Pentad 18). Examination of these rainfall diagrams shows the difficulty of fixing uniquely the dates of onset of the monsoon. The so-called 'burst' of the southwest monsoon on the west coast of India is illustrated by the diagrams for Cochin, Kozhikode and Mangalore which show a steep increase in rainfall towards the end of May. It may be noted that at Tiruchirapalli, Madurai and Bangalore in the interior of the peninsula, the onset of the monsoon on the west coast leads to a decrease of rainfall. The minimum rainfall during the summer monsoon at all these stations is reached by the end of June after which there is a slow increase as the rainfall on the west coast begins to decrease, for example between pentads 40 to 50.

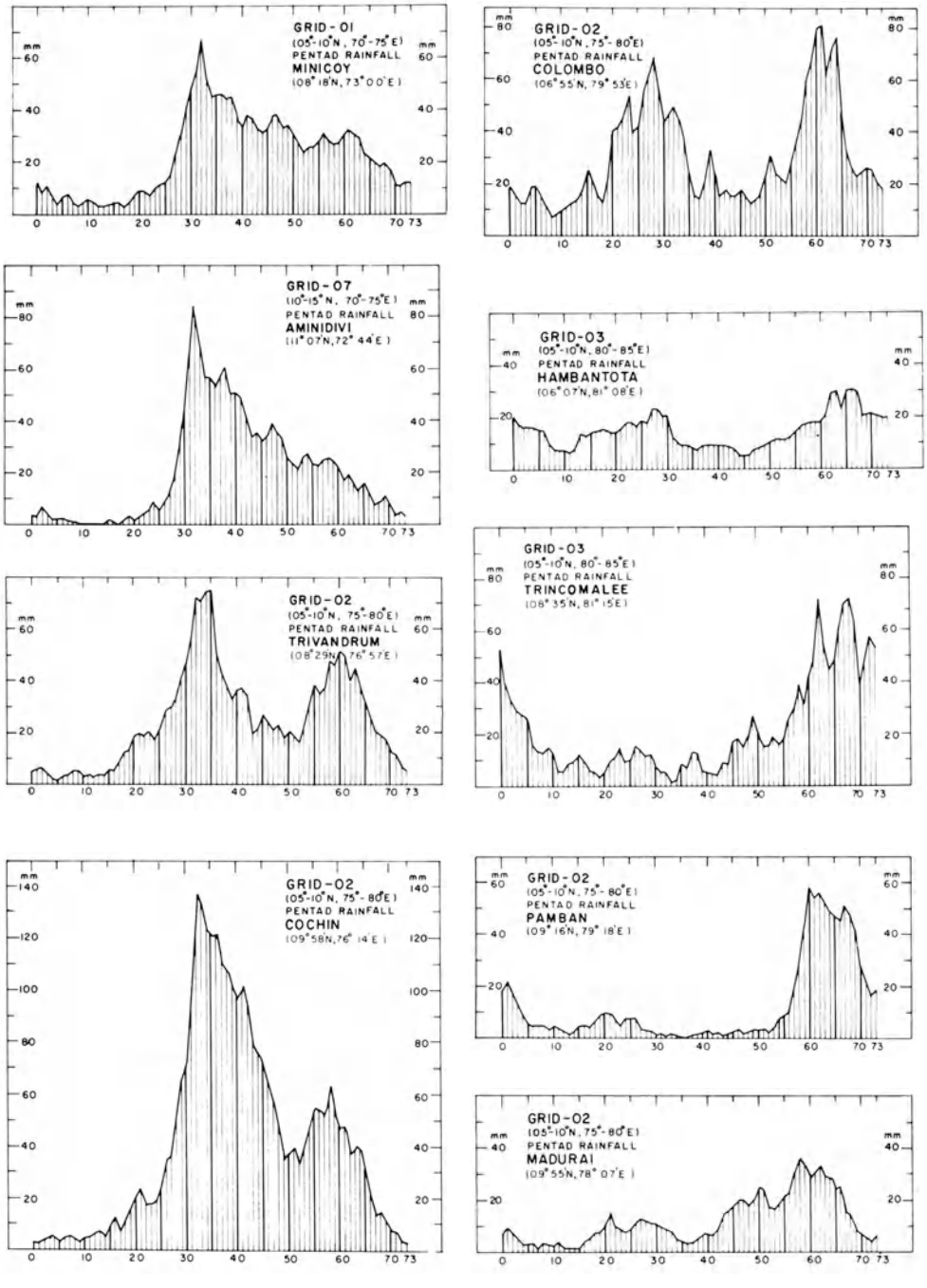

Figure 14(a)
Pentad rainfall patterns for stations south of 15°N.

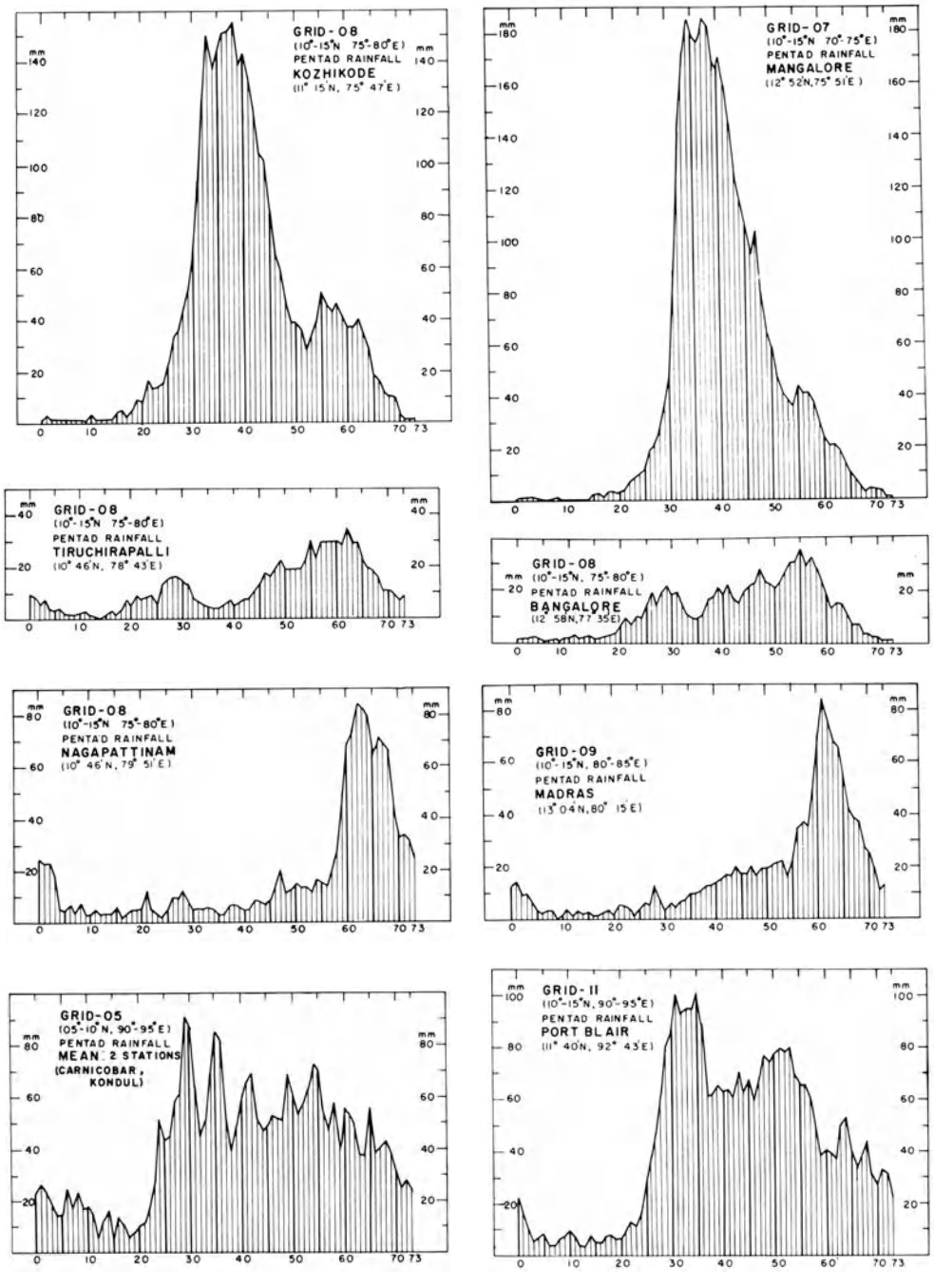

Figure 14(b)
Pentad rainfall patterns for stations south of 15°N.

6.10. Colombo, Trivandrum, Cochin and Kozhikode show two rainfall peaks. There is indication of this at Mangalore also. The relative rainfall minimum at the west coast stations occurs at pentad 52 (mid-September). The second rainfall maximum is at pentad 55 (end of September) at Mangalore and Kozhikode, at pentad 58 (mid-October) at Cochin and at pentad 60 (late October) at Trivandrum. The three stations Mangalore, Bangalore and Madras lie practically on latitude 13°N. The secondary rainfall peak at Mangalore and the primary peak at Bangalore occur at the end of September. At Madras the main rainfall peak occurs by the end of October or in early November. At Port Blair the second rainfall peak is found in mid-September. Stations on the west coast of Malaya peninsula have only a single rainfall peak unlike the stations on the west coast of India at the same latitude.

6.11. An interesting result brought out by the pentad rainfall study is the finding that a relative *rainfall minimum* around pentad 46 (mid-August) exists at several stations over north and central India (ANANTHAKRISHNAN and PATHAN [6], [7]). This feature is masked when rainfall is considered on a monthly basis and hence its existence had not been recognised by earlier studies on Indian rainfall. The mid-August rainfall minimum is conspicuous and it stands out clearly even when the pentad rainfall data of several stations are averaged. The mean pentad rainfall patterns for some five-degree squares showing the mid-August rainfall minimum are shown in Fig. 15. Pentad rainfall study also shows that there is a winter relative *rainfall maximum* over north India around pentad 10 (mid-February). This can also be seen from Fig. 15. The mid-August minimum and the mid-February maximum in the rainfall are climatological features presumably linked with the extreme northward and southward displacement of the ITCZ and the associated summer and winter circulation systems.

6.12. In seeking an explanation for the double rainfall maxima during the monsoon season shown by several stations, one has to consider the major factors that control the rainfall in the tropics. It is well known that tropical rainfall is closely associated with the inter-tropical convergence zone (ITCZ) and its seasonal oscillations. Tropical disturbances such as easterly waves, travelling low pressure systems, depressions and cyclonic storms have their origin in or close to the ITCZ. The annual north–south oscillation of the ITCZ has its maximum amplitude over the south Asian summer monsoon longitudes. Along the central Indian meridian the winter position of the ITCZ is at about 10°S; in the summer monsoon season the ITCZ may be identified with the axis of the monsoon trough over north India near 27°N. The movement of the ITCZ lags behind the sun by about 2 months; its extreme winter and summer positions are reached in February and August (RIEHL [22]).

6.13. If the centre of rainfall activity moves with the ITCZ, then stations lying between the extreme latitudes reached by the ITCZ in summer and in winter should experience two rainfall maxima as they are crossed twice by the ITCZ. The epoch of minimum rainfall during the summer monsoon should coincide with the extreme northern location of the ITCZ in August. Although the mid-August minimum of

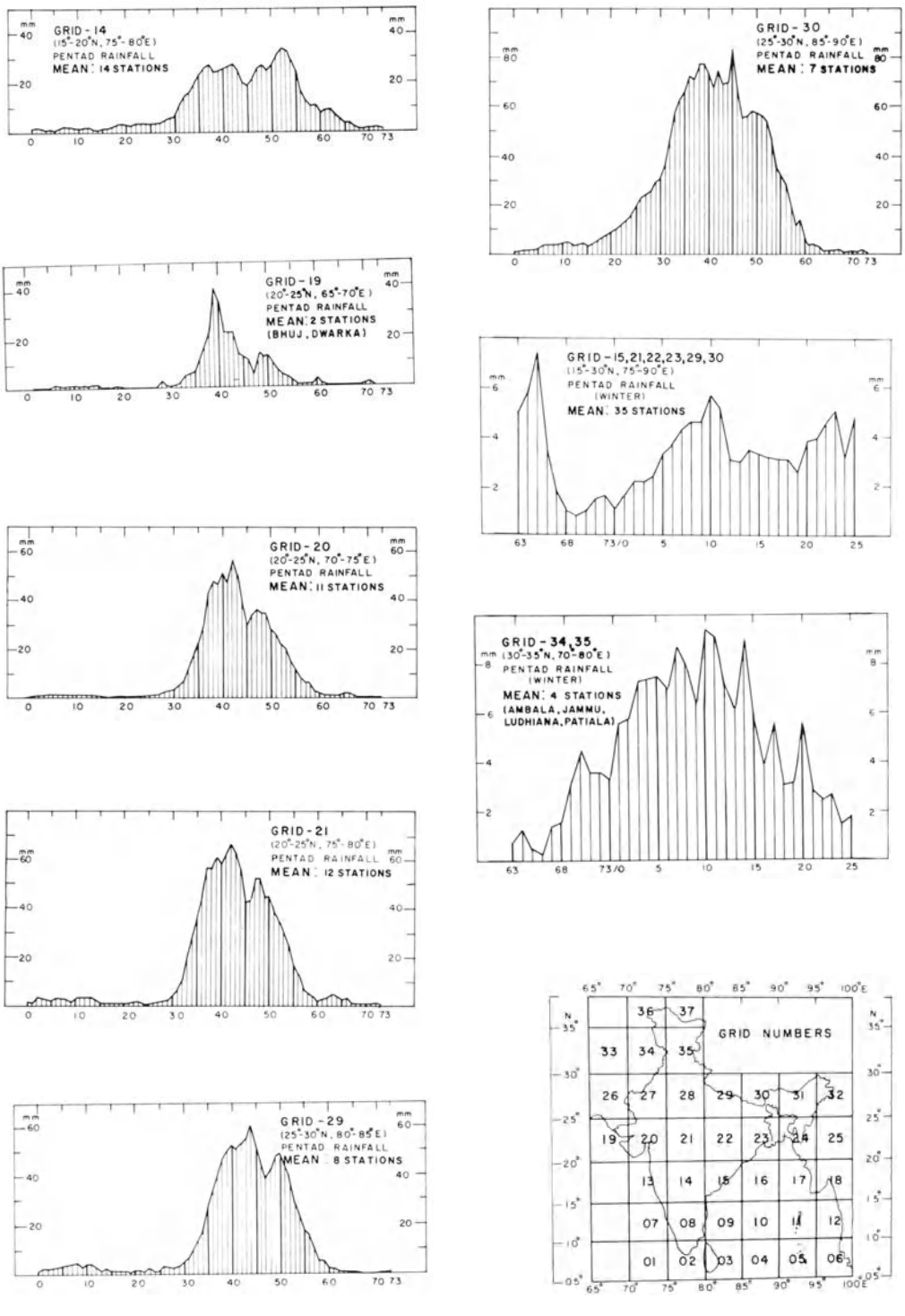

Figure 15
Mean pentad rainfall patterns illustrating mid-August minimum and mid-February maximum of rainfall.

rainfall is shown by several stations in north and central India, its existence is doubtful at some of the stations. Stations on the west coast of the southern part of the peninsula show relative rainfall minimum in mid-September, while stations on the east coast at the same latitudes (e.g., Pamban, Nagapattinam and Madras in Fig. 14) show only a single rainfall maximum in October-November. Apart from the thermal causes associated with the movement of the ITCZ, rainfall is also strongly controlled by dynamical causes resulting from orographical features, influence of low pressure systems, cyclonic disturbances, etc. It may be mentioned that a simple explanation of the observed rainfall patterns over the monsoon field on the basis of the annual migration of the ITCZ is not possible although the rainfall distribution in space and in time is very much controlled by it. This matter will be considered in greater detail in a report on the rainfall of India and adjacent areas under preparation. This study based on the rainfall data for a 50-year period will include normal pentad rainfall patterns of 280 stations over India and neighbourhood and 73 normal pentad rainfall charts for India and the adjacent areas. The diagrams reproduced in Figs. 13, 14 and 15 are some samples.

6.14. As already stated, the bulk of the annual rainfall for most parts of India is received during the summer monsoon months June to September (122 days). The manner in which the seasonal rainfall is made up by daily and hourly falls of different intensities gives insight into its composition and the physical mechanisms that produce the rain. Such a study has been made for the four stations Bombay, Calcutta, New Delhi and Madras for the 10-year period 1961–70 (ANANTHAKRISHNAN [9]). The study for Madras also covers the northeast monsoon period October–December (92 days) when this station gets the greater part of its annual rainfall. The results of the daily rainfall analysis are shown in Fig. 16.

6.15. The two sets of curves for Bombay, Calcutta and New Delhi refer to the airport (top) and city (bottom) stations respectively, for the southwest monsoon months. The curves for Madras are for the airport observatory for the northeast monsoon (top) and southwest monsoon (bottom) months. Each diagram shows three curves represented by: (i) a continuous line; (ii) set of solid dots; and (iii) set of open circles. These curves have the following meaning:

(i) For the curves represented by the continuous line, the abscissa represents cumulative percentage rainfall amount and the ordinate represents cumulative percentage number of rainy days, both scales running from 0 to 100 percent. Examination of these curves shows that 50 percent of the rainy days at the low intensity end of the spectrum account for less than 10 percent of the total rainfall, while 10 to 15 percent of the rainy days at the high intensity end of the spectrum account for 50 percent of the total rainfall. It is of interest to note that this is generally true for all the four stations despite the fact that the average daily rainfall varies from over 20 mm/day at Bombay to less than 10 mm/day at Madras during the summer monsoon season and the number of rainy days from nearly 100 at Bombay to less than half this number at Madras and New Delhi.

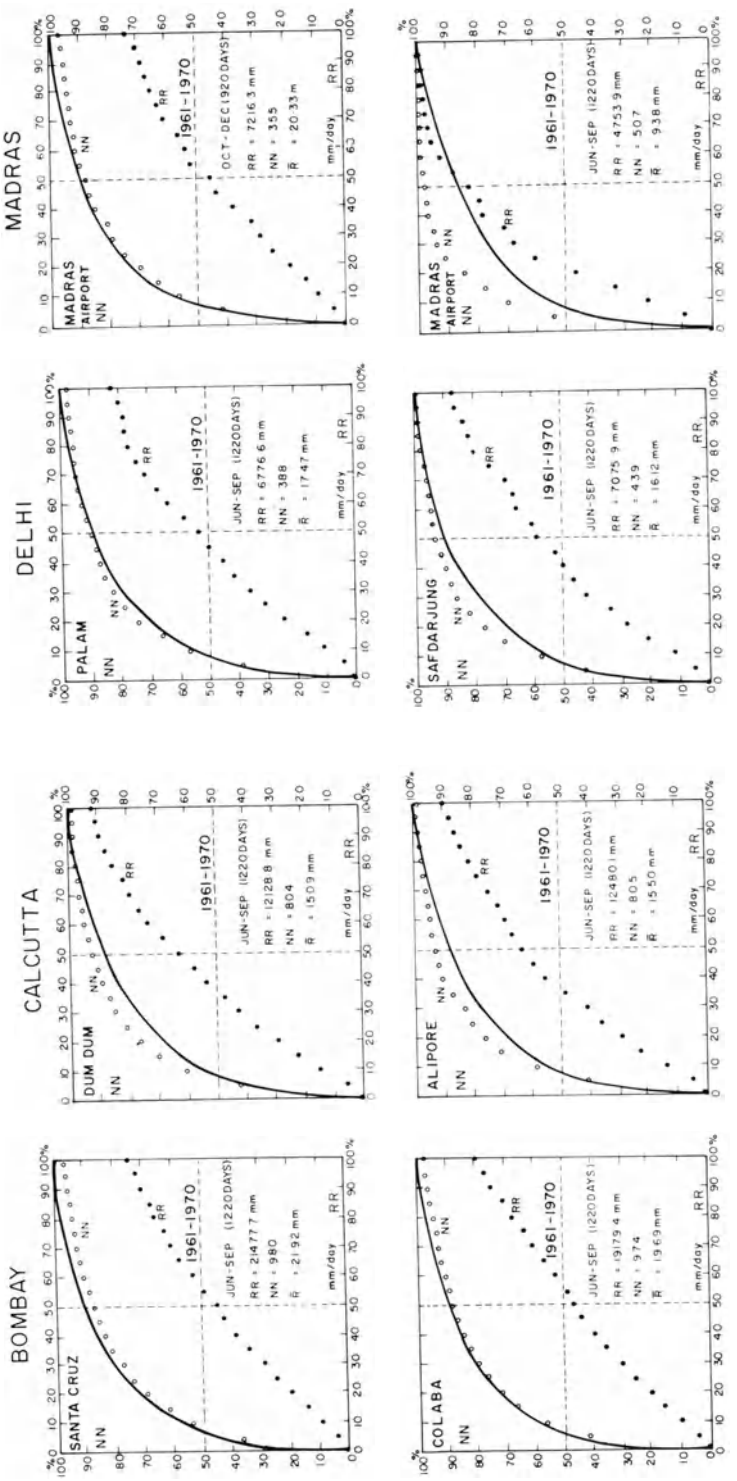

Figure 16
Percentage cumulative rainfall and cumulative number of rainy days for four stations.

(ii) For the curves represented by the solid dots, the abscissa represents rainfall intensity from 00 to 100 mm/day. The ordinate represents cumulative percentage rainfall amount from 0 to 100 per cent. From these curves one can read off the percentage of total rain contributed by falls not exceeding the daily rainfall limits shown on the abscissa scale. For example, falls of intensity not exceeding 50 mm/day contribute about 45 per cent of the total summer monsoon rainfall at Bombay and about 65 per cent at Calcutta. At Madras such falls contribute 45 per cent of the northeast monsoon rainfall and about 80 per cent of the summer monsoon rainfall. It may be noted that falls exceeding 100 mm/day contribute 20 to 25 per cent of the summer monsoon rainfall of Bombay, 10 per cent at Calcutta and a little over 25 per cent of the northeast monsoon rainfall at Madras. Such falls are absent at Madras during the summer monsoon months.

(iii) For the curves represented by the open circles, the abscissa again represents rainfall intensity from 00 to 100 mm/day. The ordinate represents cumulative percentage number of rainy days from 0 to 100 per cent. From these curves one can read off the cumulative percentage number of rainy days corresponding to daily rainfall amounts not exceeding the abscissa values. Thus the figure shows that on 55 to 60 per cent of the rainy days at Bombay, Calcutta, Delhi and Madras (NE monsoon) the rainfall does not exceed 10 mm/day; this percentage is about 70 for the summer monsoon season at Madras. On 85 to 90 per cent of the rainy days the rainfall intensity does not exceed 50 mm/day. The percentage number of days with rainfall exceeding 100 mm/day is 2 to 3 per cent at Bombay where the average number of rainy days during the southwest monsoon season is 98. The curves of solid dots and open circles considered together show that some 2 to 3 days of rainfall exceeding 100 mm/day account for 20 to 25 per cent of the summer monsoon rainfall of Bombay. The average number of rainy days for Calcutta is 80 for the months June to September. Avout 1 per cent of the rainy days (less than 1 day in the season) with falls exceeding 100 mm/day accounts for 10 per cent of the seasonal rainfall. The number of rainy days for New Delhi is about 40 and it can be seen that here again 1 day with a fall exceeding 100 mm/day accounts for about 15 per cent of the seasonal total. The number of rainy days during the northeast monsoon season at Madras is about 35

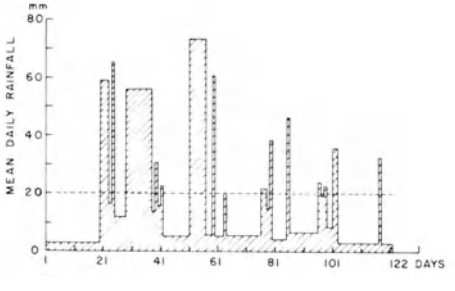

Figure 17
Pattern of monsoon rainfall at Bombay (Colaba) for June–September 1961

and one day of heavy rainfall exceeding 100 mm/day can account for 25 per cent of the rainfall of the season. Falls of such intensity do not occur at Madras during the southwest monsoon season.

6.16. The two sets of curves for Madras clearly show that the composition of the southwest monsoon rainfall is different from that of the northeast monsoon season. The rainfall is low during the summer monsoon season (mean daily rainfall = 9.4 mm) and falls of high intensity do not occur. The mean daily rainfall is a little over 20 mm during the northeast monsoon months. While falls up to 50 mm/day account for only 45 per cent of the total northeast monsoon rainfall, these account for about 85 per cent of the summer monsoon rainfall. The northeast monsoon period is the season of cyclonic disturbances in the south Bay of Bengal some of which move towards the Madras coast and give heavy rainfall over the coastal belt.

6.17. Study of the *hourly rainfall* of Bombay for the southwest monsoon season shows that the *total duration* of rainfall of all intensities is the equivalent of about 10 days which is about 10 per cent of the number of rainy days during the season. (This is on the assumption that an hour during the whole or part of which rain has fallen is considered as a full rainfall hour; this overestimates the actual duration of rainfall.) It is found that 50 per cent of the rain is contributed by falls exceeding 10 mm/hr intensity. The duration of such falls is 6 to 12 hours per month. From this it is seen that 50 per cent of the monsoon rainfall of Bombay is received in a total time interval of 24 to 48 hours distributed through some 10 days during the season. The behaviour of monsoon rainfall is generally similar at other stations. It follows that the bulk of the monsoon rainfall at a station is received in a time interval which is a small fraction of the duration of the monsoon season and is contributed by shortlived disturbances in the monsoon field. It is obvious that the supply of latent heat to the atmosphere over the monsoon region follows the same pattern as the rainfall. These findings are in agreement with the results of similar studies made elsewhere in the tropics (OLASCOAGA [19]; RIEHL [22]; RIEHL *et al.* [23]).

6.18. Fig. 17 illustrates the pattern of rainfall at Bombay (Colaba) for the monsoon season of 1961. The 122 days of the season were chronologically sorted out into spells with rainfall less than and not less than 20 mm/day. The mean daily rainfall was computed for the individual spells and these are plotted in the figure against time. It may be readily seen that most of the monsoon rainfall is made up by a few spells of heavy rain associated with active monsoon conditions. This is a typical feature of monsoon rainfall.

7. *Diurnal variations*

7.1. Just as the annual cycle of solar radiation gives rise to the seasonal changes in circulation and weather, the diurnal cycle of solar radiation gives rise to corresponding variations in meteorological parameters such as temperature, pressure,

humidity, winds, clouds and rainfall. Diurnal variations at a place depend, among other factors, on latitude, location (coastal or continental), elevation, topography and nature of the surrounding terrain. In these respects the monsoon region presents a wide variety.

7.2. The diurnial variation of *temperature* is well known. Apart from the factors mentioned above, the diurnal range of air temperature near the ground depends also on cloudiness, humidity of the air, lapse-rate in the lower atmosphere and wind. In general the diurnal range in the monsoon belt is least during the summer monsoon months June to September because of cloudy skies and strong wind. It is maximum during the months November to May when the cloudiness is small. During July–August the diurnal range of surface temperature over large parts of India varies from 4 to 8°C. The maximum range at inland stations outside the summer monsoon months can be as high as 20°C. The maximum diurnal range of 17°C occurs at Srinagar in October and at New Delhi in November when skies are clear after the withdrawal of the monsoon from north India and the activity of winter disturbances is feeble. The minimum range of about 8°C is experienced in January at Srinagar and in July–August at New Delhi. At the hill stations of Kodaikanal in the south and Simla in the north, the minimum daily range of 5° to 6°C is found in July–August; the maximum of about 9°C occurs at Kodaikanal in February and at Simla in May.

7.3. Aerological data of Indian radiosonde stations for 00 Z (morning) and 12 Z (evening) show that the temperatures in the lower troposphere undergo significant diurnal variations, the amplitude of the variations decreasing with height above the surface. In the winter months the evening temperatures are higher than the morning temperatures up to about 850 mb level. In the hot weather months of April and May, diurnal variations in the free atmosphere occur at inland stations such as Nagpur and New Delhi almost up to mid-tropospheric levels. Even in the peak summer monsoon month of July, diurnal variation of temperature in the lower troposphere is appreciable at stations such as New Delhi and Jodhpur in north India. These conclusions are based on a preliminary examination of the mean monthly 00 and 12 Z upper air temperature data of several stations for individual years. The results of this study will be published separately.

7.4. As is well known, the diurnal oscillation of surface *pressure* with maxima around 1000 and 2200 hours and minima around 0400 and 1600 hours (local time) is one of the most conspicuous features in the tropics. Harmonic analysis of the pressure oscillations reveals two prominant components S_1 and S_2 with periods of 24 and 12 hours respectively. The amplitudes of the higher harmonics and their contribution to the total variance are small.

7.5. Harmonic analysis of the monthly mean hourly pressure values of Indian stations (ALVI and JAGANNATHAN [1]) shows that the S_1 component has its maximum generally between 06 and 08 hours and the S_2 component near 10 and 22 hours (local time). The amplitudes of the S_1 and S_2 components undergo large seasonal variations which depend upon the latitude and location of the stations. In general both com-

ponents show the maximum amplitude during the hot weather period prior to the onset of the summer monsoon when the amplitude of the S_1 component exceeds that of S_2 at inland stations. The amplitudes of the oscillations tend to be minimum at most stations during the summer monsoon months. This emphasises the strong thermal control of the pressure oscillation.

7.6. Diurnal variation of *winds* such as the land and sea breezes at coastal stations is a well known feature in the tropics. The sea breeze brings relief from the oppressive summer heat. When fully developed the sea breeze penetrates deep into the interior. For example, the sea breeze from Bombay reaches up to and even beyond Poona (RAMANATHAN [21]). With growing insolation as the summer advances, a low pressure area forms inland in the afternoons accompanied by strong pressure gradient from sea to land, especially in the coastal belt, leading to vigorous influx of moisture into the country and increasing frequency of thunderstorms in the afternoon/evening.

7.7. During the southwest monsoon months the direction of the prevailing wind along the west coast of India is the same as that of the sea breeze which is now much less conspicuous because of reduced thermal contrast between sea and land due to cloudy skies and rainfall. However, at a station like Madras on the east coast of India where there is little clouding and rainfall, sea breeze is very pronounced during the summer monsoon months. This feature can be noticed from the (12–00) Z vectorial wind differences at the low levels (below 1.5 km) for Bombay and Madras in Fig. 18 (b).

7.8. Diurnal variation of surface winds due to vertical exchanges in the boundary layer arising from thermal convection is a well known phenomenon. The effect of surface friction on the air flow decreases with height and hence wind speed increases with height in the atmospheric boundary layer. Vertical exchange of momentum due to turbulent convection from ground heating leads to increase of wind speed near the ground and decrease of speed at the top of the boundary layer. Such variations are present throughout the year and are very conspicuous in the summer months. The hourly variations of wind speed for all the 12 months of the year 1963 in respect of four Indian stations are shown in Fig. 18 (a). The stations chosen are: (i) Port Blair (island station in the Bay of Bengal); (ii) Madras (coastal station on the east coast of the peninsula); (iii) Kodaikanal (hill station in south India at an elevation of 2343 metres where the Indian Solar Physics Observatory is located); and (iv) New Delhi (inland station over the Gangetic plain). Only some salient features shown by the wind diagrams will be referred to here. It may be noted that surface wind at Port Blair reaches the maximum strength in all the months between 1000 and 1400 hours IST (GMT + 05^h30^m). The lowest speeds occur between 2000 and 0600 hours. Similar features may be noted at Madras and New Delhi also. At these two stations the surface winds are strongest between 1000 and 1200 hours in the summer monsoon months and between 1200 and 1600 hours in the remaining months. At the high level station of Kodaikanal the wind behaviour is just the opposite of that noticed at the low level stations. Here the weakest surface winds occur in the afternoon hours and

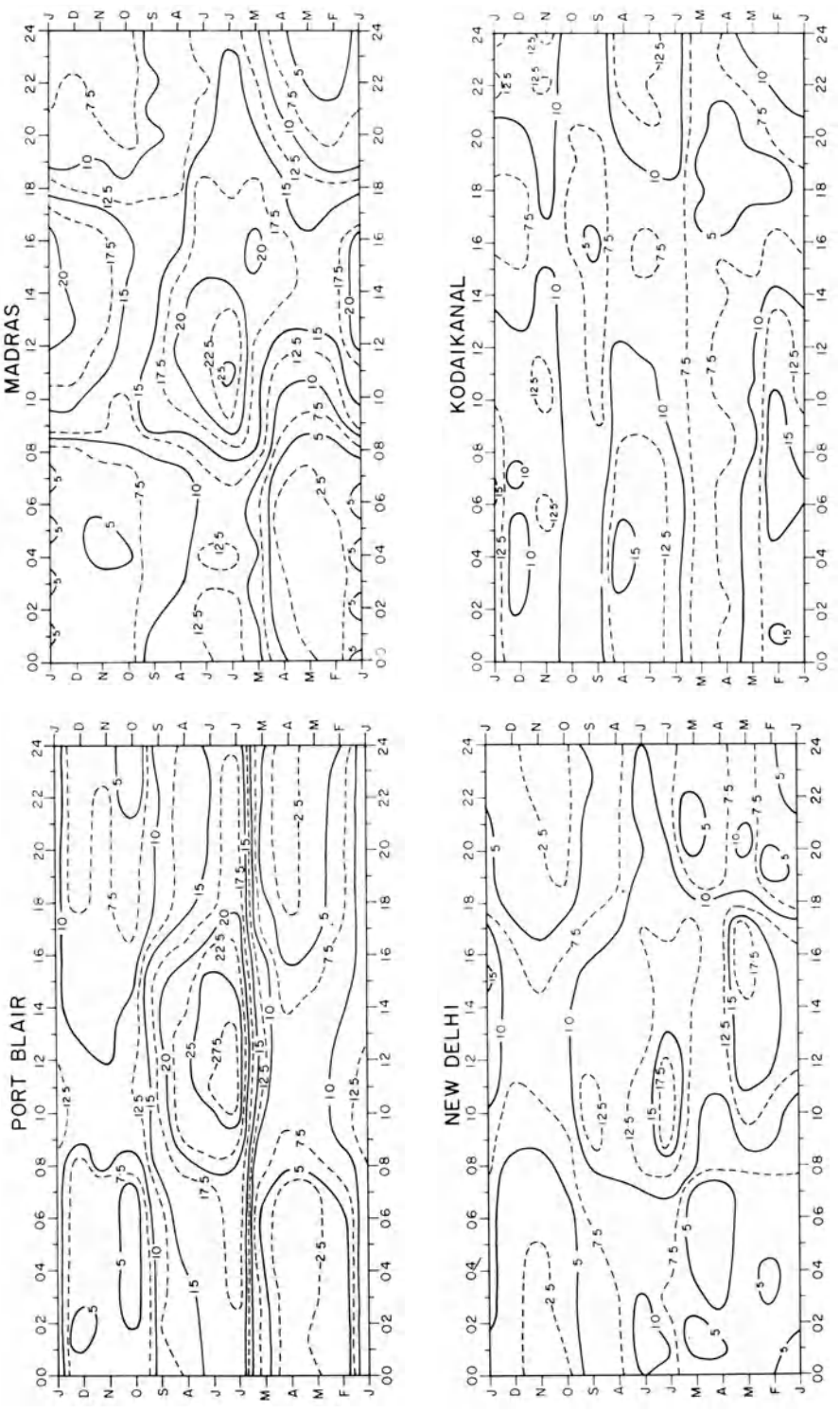

Figure 18(a)
Hourly variation of surface wind speeds (km/hr) at Port Blair, Madras, New Delhi and Kodaikanal.

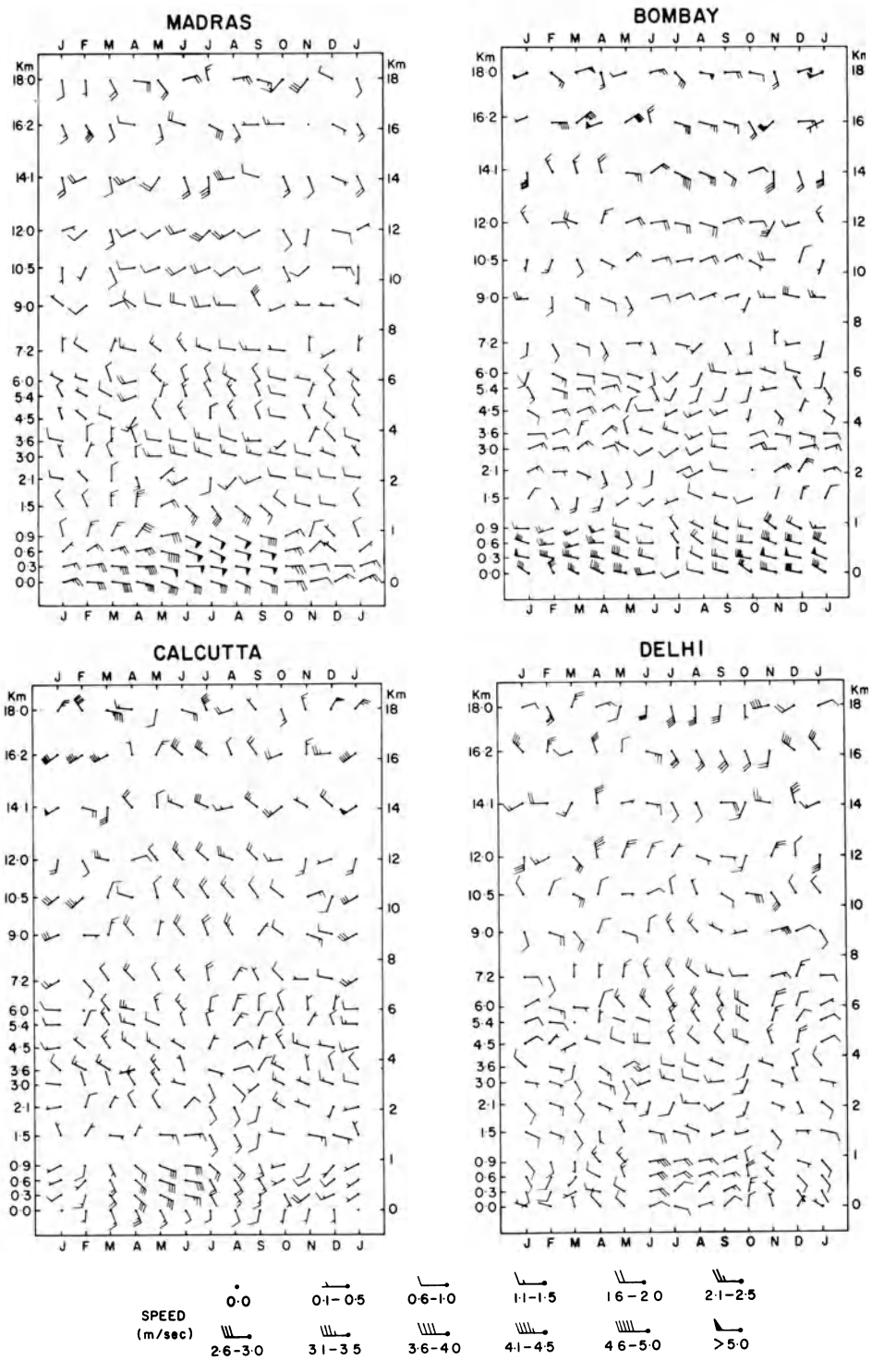

Figure 18(b)
Diurnal variation of upper winds (12 – 00) Z at Madras, Bombay, Calcutta and New Delhi.

the strongest winds in the early morning hours throughout the year. The winds at Koadaikanal may be taken to be roughly representative of conditions at the top of the surface friction layer over the plains.

7.9. Comparison of the mean monthly upper winds for 00 Z (morning) and 12 Z (afternoon) shows that systematic diurnal wind variations exist throughout the troposphere and lower stratosphere at all Indian rawin stations (ANANTHAKRISHNAN *et al.* [8]). The bottom diagrams in Fig. 8 (a), (b), (c), (d) show diurnal variations, (12 − 00)Z, in the zonal and meridional winds at the four stations Trivandrum, Nagpur, New Delhi and Port Blair. In Fig. 18 (b) are shown the vectorial wind differences (12 − 00) Z at the three coastal stations Bombay, Calcutta and Madras and at the inland station of New Delhi. The pronounced sea breeze effect may be noticed at the lowest levels for the coastal stations. In the middle and upper troposphere the diurnal variation of the wind shows organised seasonal patterns. It is of interest to note that during the summer monsoon months, the upper tropospheric easterlies are stronger at Bombay in the evening while at Madras the reverse behaviour is noticed. This would imply that the upper tropospheric pressure changes resulting from diurnal heating of the ground and the lower atmosphere result in a strengthening of the meridional pressure gradient near Bombay and its weakening near Madras from morning to evening.

7.10. A significant aspect of the diurnal wind variation concerns the meridional wind component which is generally much smaller than the zonal component. Diurnal changes in the meridional wind (12 − 00) Z are found to be of the same order as the mean meridional winds, 1/2(00 + 12) Z. It is obvious that the diurnal wind variations should be associated with corresponding changes in the fields of divergence, vorticity and vertical motion which control rainfall. The diurnal wind variations may have to be appropriately incorporated into numerical weather prediction models to yield realistic forecasts of rainfall in the tropics.

7.11. Diurnal variation of *rainfall* at a number of Indian stations has been studied by PRASAD [20] utilising the hourly rainfall data for a period of about 15 years. The nature of the variation depends on the location of the station and to some extent also on the season. The percentages of seasonal rainfall received in 3-hourly intervals (IST) at eight typical stations are listed in Table 2. The stations considered fall into four categories: (a) hill stations (Cherrapunji and Mahabaleswar); (b) coastal stations (Bombay and Madras); (c) island stations (Sagar Island); and (d) inland stations (New Delhi Jamshedpur and Hyderabad). The seasons considered are:

(I) pre-monsoon thunderstorm season (April and May);
(II) southwest monsoon season (June to September);
(III) post-monsoon season (October to December).

7.12. At the very high rainfall station of Cherrapunji on the southern slope of the Khasi–Jainthia hills in Assam, the rainfall activity is least during the afternoon hours and maximum towards mid-night and early morning. The reason for this is

Table 2
Diurnal variation of rainfall

Station	Ht asl (m)	Season	Percentage of seasonal rainfall								Seasonal rainfall (mm)
			00–03 hrs IST	03–06	06–09	09–12	12–15	15–18	18–21	21–24	
1. Cherrapunji	1313	I	18.2	17.5	12.4	7.8	5.1	6.4	11.8	20.9	2360
		II	17.4	18.4	14.5	12.8	7.4	5.7	8.6	15.3	8481
		III	18.2	15.3	11.7	9.7	12.1	9.8	9.2	14.1	413
2. Mahabaleshwar	1382	I	7.7	6.4	2.5	1.2	12.1	40.0	18.0	12.1	104
		II	11.9	11.9	11.0	11.0	14.4	16.0	12.6	11.3	5521
		III	8.6	8.7	7.5	7.4	15.4	23.5	17.6	11.1	205
3. Bombay	11	I	58.4	16.8	9.3	3.4	0.0	2.1	3.1	6.9	29
		II	13.6	14.7	15.3	13.4	11.3	9.3	9.8	12.5	2116
		III	13.7	34.1	12.6	7.4	5.2	8.6	11.6	6.7	85
4. Madras	16	I	10.4	16.6	13.3	17.2	12.7	8.8	9.5	11.6	75
		II	19.0	12.8	3.3	2.4	3.9	14.2	22.1	22.3	421
		III	17.8	16.8	11.6	11.6	10.0	9.8	8.5	13.8	605
5. Sagar Island	3	I	11.0	6.6	10.6	8.6	5.4	11.3	24.4	22.1	127
		II	15.2	19.0	14.2	14.8	11.2	7.6	8.0	10.0	1208
		III	13.0	15.5	13.6	16.9	15.1	11.4	5.2	9.3	221
6. New Delhi	216	I	11.3	6.1	7.8	4.3	7.8	37.4	11.3	13.9	12
		II	8.5	15.2	14.7	15.1	16.1	16.9	7.4	6.1	539
		III	23.8	8.9	12.3	15.4	14.2	6.7	7.9	10.8	42
7. Jamshedpur	129	I	2.3	0.4	3.8	0.6	8.2	51.1	24.5	9.0	78
		II	8.9	9.2	7.9	9.6	17.8	23.3	14.1	9.2	1085
		III	12.4	14.1	9.4	7.6	16.0	18.4	11.6	10.4	89
8. Hyderabad	545	I	21.2	8.7	3.5	0.0	5.9	20.5	26.8	13.5	54
		II	14.5	10.6	5.0	4.9	9.7	18.4	18.1	18.7	605
		III	17.3	8.9	4.4	6.5	13.6	15.6	20.8	12.8	106

I: Apr + May; II: Jun + Jul + Aug + Sep; III: Oct + Nov + Dec.

not well understood, but it is surmised that katabatic effects probably produce local convergence at night enhancing rainfall activity. Increased rainfall activity at night is a characteristic feature of several stations in the Assam valley also. At Mahabaleswar on the Western Ghats, rainfall activity is maximum in the afternoon/evening during the pre- and post-monsoon months with minimum after midnight and in the forenoon. A feeble afternoon maximum can also be noticed during the southwest monsoon months. Afternoon rainfall maximum is generally attributed to increased convective activity resulting from heating of the ground and the adjoining layers of the atmosphere.

7.13. At Bombay, Madras and Sagar Island, rainfall activity is more during the night and early morning hours. At Madras during the southwest monsoon months the period from 0600 to 1500 hours has least rainfall. Land and sea breeze effects

play a dominant role in increasing or decreasing low level convergence at coastal stations. The increased rainfall activity at night and early morning hours is attributed to greater low level convergence resulting from the interaction of land breeze with the prevailing wind when they are from opposite directions. To some extent the rainfall characteristics at Bombay and Madras can be explained on this basis.

7.14. At inland stations convective activity tends to be maximum towards afternoon/evening and least in the forenoon hours. This is borne out by the diurnal variation of rainfall at the three inland stations during April and May. The southwest monsoon rainfall at Jamshedpur and Hyderabad also shows similar behaviour. At New Delhi, however, the rainfall during the southwest monsoon months is more or less uniform from 0300 to 1800 hours with lesser rainfall during the remaining period. Diurnal variation of rainfall results from the complex interaction of several factors and a completely satisfactory explanation of all the observed features is not easy.

Acknowledgements

The author's thanks are due to Shri J. M. Pathan for help in processing a large volume of rainfall data and preparation of rainfall diagrams. Thanks are also due to Shri A. S. Gade for inking the diagrams, to Shri R. P. Mali for preparation of photo copies of diagrams and to Shri K. V. S. Madhavan for typing the manuscript. The author wishes to express his gratitude to the Director and the Governing Council of the Indian Institute of Tropical Meteorology for affording facilities for his work at the Institute. He is also grateful to the Indian National Science Academy for a research grant.

References

[1] Alvi, S. M. A. and Jagannathan, P. (1972), *Diurnal variation of pressure in India*, Mem. Ind. Met. Dept. *3*, 1–28.

[2] Ananthakrishnan, R. and Krishnan, A. (1962), *Upper air changes over India and neighbourhood associated with the southwest monsoon*, Curr. Sci. *31*, 133–136.

[3] Ananthakrishnan, R., Selvam, M. M. and Chellappa, R. (1965), *Seasonal variation of precipitable water vapour in the atmosphere*, Ind. J. Met. Geophys. *16*, 371–385.

[4] Ananthakrishnan, R. (1970), *The seasonal march of surface pressure gradients and the southwest monsoon*, Curr. Sci. *39*, 248–251.

[5] Ananthakrishnan, R. (1970), *Reversal of pressure gradients and wind circulation across India and the southwest monsoon*, Quart. J. Roy. Met. Soc. *96*, 539–542.

[6] Ananthakrishnan, R. and Pathan, J. M. (1970), *North–south oscillation of the equatorial trough and seasonal variation of rainfall in the tropics*, Preprints Sym. Trop. Met., Hawaii, Amer. Met. Soc./ W.M.O., FV-1–6.

[7] Ananthakrishnan, R. and Pathan, J. M. (1971), *Rainfall patterns over India and the adjacent seas*, Ind. Met. Dept. Sci. Rep. No. 144.

[8] Ananthakrishnan, R., Suryanarayana, R. and Sikka, D. R. (1974), *On the diurnal variation of zonal and meridional circulation in the troposphere and lower stratosphere over India*, Preprints of the papers presented at the Int. Trop. Met. Meeting, Nairobi, Kenya, Amer. Met. Soc., Boston, 105–108.

[9] ANANTHAKRISHNAN, R. (1976), *Some aspects of the variability of daily, monthly and annual rainfall at neighbouring pairs of stations and the nature of the monsoon rainfall at individual stations*, Proc. Symp. Monsoon, Indian Inst. Trop. Met. Poona, 354–364.

[10] BLANFORD, H. F. (1888), *The rainfall of India*, Ind. Met. Mem. *3*, 658, pp.

[11] FINDLATER, J. (1969a), *A major low level air current near the Indian ocean during the northern summer*, Quart, J. Roy. Met. Soc. *95*, 362–380.

[12] FINDLATER, J. (1969b), *Interhemispheric transport of air in the lower troposphere over the western Indian ocean*, Quart. J. Roy. Met. Soc. *95*, 400–403.

[13] HAHN, D. G. and MANABE, S. (1975), *The role of mountains in the south Asian monsoon circulation*, J. Atmos. Sci. *32*, 1515–1541.

[14] HOLTON, J. R., *An Introduction to Dynamic Meteorology* (Academic Press, New York, 1972), pp. 70–72.

[15] INDIA METEOROLOGICAL DEPARTMENT, *Climatological Atlas for Airmen* (Ind. Met. Dept., New Delhi, 1943).

[16] INDIA METEOROLOGICAL DEPARTMENT, *Rainfall Atlas of India* (Ind. Met. Dept., New Delhi, 1971a), 67 pp.

[17] INDIA METEOROLOGICAL DEPARTMENT, *Climatological Atlas of India* (Ind. Met. Dept., New Delhi, 1971b), 31–46.

[18] NEWELL, R. E., VINCENT, D. G., DOPPLICK, T. G., FERRUZA, D. and KINDSON, J. W. (1969), *The energy balance of the global atmosphere* in *The General Circulation of the Atmosphere* (ed. G. A. Corby) (Roy. Met. Soc., London, 1969), pp. 42–90.

[19] OLASCOAGA, M. J. (1950), *Some aspects of Argentine rainfall*, Tellus *2*, 312–318.

[20] PRASAD, B. (1970), *Diurnal variation of rainfall in India*, Ind. J. Met. Geophys. *21*, 443–450.

[21] RAMANATHAN, K. R. (1931), *The structure of the sea breeze at Poona*, Ind. Met. Dept. Sci. Rep. No. 30, Vol. 3, 131–134.

[22] RIEHL, H., *Tropical Meteorology* (McGraw-Hill, New York, 1954), pp. 12–13, 72–97.

[23] RIEHL, H., CRUZ, L., MATA, M. and MUSTUR, C. (1973), *Precipitation characteristics during the Venezuela rainy season*, Quart. J. Roy. Met. Soc. *99*, 746–757.

(Received 15th June 1977)

Pageoph, Vol. 115, 1977), Birkhäuser Verlag, Basel

Observational Aspects of the Low-level Cross-equatorial Jet Stream of the Western Indian Ocean

By J. FINDLATER[1])

Summary – Studies of all available upper wind data up to 3 km over eastern Africa and the western Indian Ocean reveal a major low-level air current circulating at about 1.5 km in the western periphery of the monsoon regime. The current originates in the southern hemisphere and penetrates progressively further north in spring until it reaches its maximum development in July. The major current is composed of systems of low-level jet streams which can be located on a daily basis, always in the same geographical areas, with speeds reaching 25–50 ms^{-1} at heights of only 1–1.5 km. Because the current is topographically-locked over eastern Africa the massive flow of air from one hemisphere to the other can be monitored and some relationships with the rainfall of parts of western India can be deduced.

This paper is only a brief review of the observational and analytical studies which have been carried out and reference should be made to original papers for details of the structure and development of the current.

Key words: Jet stream: Cross equatorial.

1. Introduction

During the months of the northern summer a zone of strong southwesterly surface winds extends from the northern part of the east coast of Somalia towards India. These strong surface winds, sometimes known as the Somali Jet, have been known for centuries. The Somali Jet, however, is only one manifestation of a much larger scale phenomenon – a major current which lies in the lowest 3 km of the atmosphere and extends from the small islands east of Madagascar across the flat arid lands of eastern Kenya, Ethiopia and Somalia, over the Arabian Sea and thence across India

2. The major current

Upper wind observations by pilot balloon methods from ships at the Kenya coast and over the western Arabian Sea in the years 1925–36 revealed winds at

[1]) East African Meteorological Department, Nairobi, Kenya, at present on secondment from the United Kingdom Meteorological Office, Bracknell.

1–2 km of about 20–25 ms^{-1} from the south and southwest respectively on occasions during the months of the northern summer (METEOROLOGICAL OFFICE, 1940), and Catalina aircraft patrolling the sea area south and east of Socotra in the years 1942–44 measured southwesterly winds of up to 35 ms^{-1} at 500 m above the sea surface. Also, records from the pilot balloon station at Ras Asir (formerly Cape Guardafui) for the summer months revealed the existence of wind speeds up to 50 ms^{-1} in the years 1930–33 (ROME, 1932–35).

In 1964 winds of 25 ms^{-1} near Socotra were reported by BUNKER (1965) and low-level jet streams were identified over peninsular India by JOSEPH and RAMAN (1966), whilst at about the same time southerly winds of 25–50 ms^{-1} blowing across equatorial Kenya were being studied by FINDLATER (1966, 1967). This study was extended by using all available pilot balloon, radar and aircraft wind data to demonstrate that all these strong wind reports during the northern summer were due to the existence of a major low-level air current which covered much of the western Indian Ocean and parts of eastern Africa, linking major synoptic systems of the two hemispheres. The major current reaches its maximum development in July and its general form and some detailed features have been described by FINDLATER (1969a).

It has been calculated that this current, circulating in the western periphery of the monsoon regime, could account for about half of the total cross-equatorial transport of air in the lower troposphere in July, (FINDLATER, 1969b).

Monthly-averaged sets of wind data from many past and present upper wind stations over eastern Africa and the western Indian Ocean have allowed analyses of the mean monthly airflow at several levels to be made, in order to gain some insight into the areal and vertical extent of the phenomenon and its development from month to month.

Although the current is a feeble feature of the southern hemisphere during the northern winter it expands and strengthens progressively to develop into the dominant feature of the low-level flow of the western Indian Ocean by July. The form of the current at 1 km in July is shown in Fig. 1 and this diagram also represents quite accurately the mean flow in June and August. Many features of interest are apparent, notably the generally light flow over the oceanic equator and the core of strong flow over the north and south Indian Ocean and over eastern Africa. The core leaves the African continent near 9°N on the Somali coast over the area of marked upwelling of cool water.

For other details of the flow in each month and at different levels reference should be made to the original analyses of FINDLATER (1971a). These analyses have been based on the densest possible network of upper wind stations and are more detailed than other representations of low-level flow in the area. For example, the atlas of RAMAGE and RAMAN (1972) uses data from only a small proportion of the upper wind stations over eastern Africa and thus does not accurately depict the flow over and near eastern Africa.

During the months of May to October the core of the current is locked to the

topography of eastern Africa. Fig. 2 shows a vertical cross-section along the equator with the core of the current standing-off some 200 km from the edge of the high ground at the same level. It is along this core and within the heavily-shaded area of Fig. 1 that maximum speeds of 25–50 ms^{-1} can be located on some days. ANDERSON

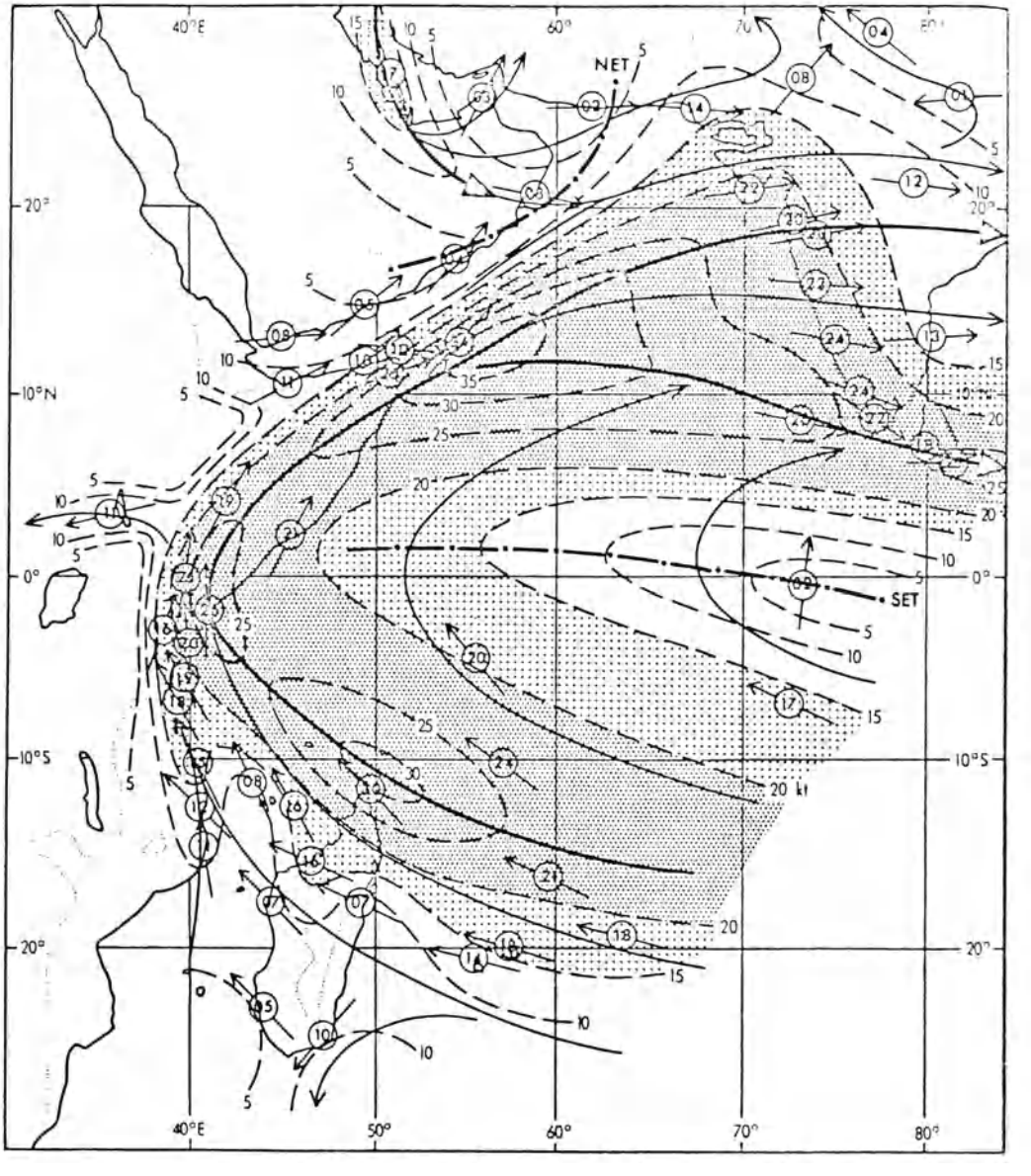

Figure 1
Mean monthly airflow at 3000 ft (1 km) in July. 1 kt = 0.5148 ms^{-1}.

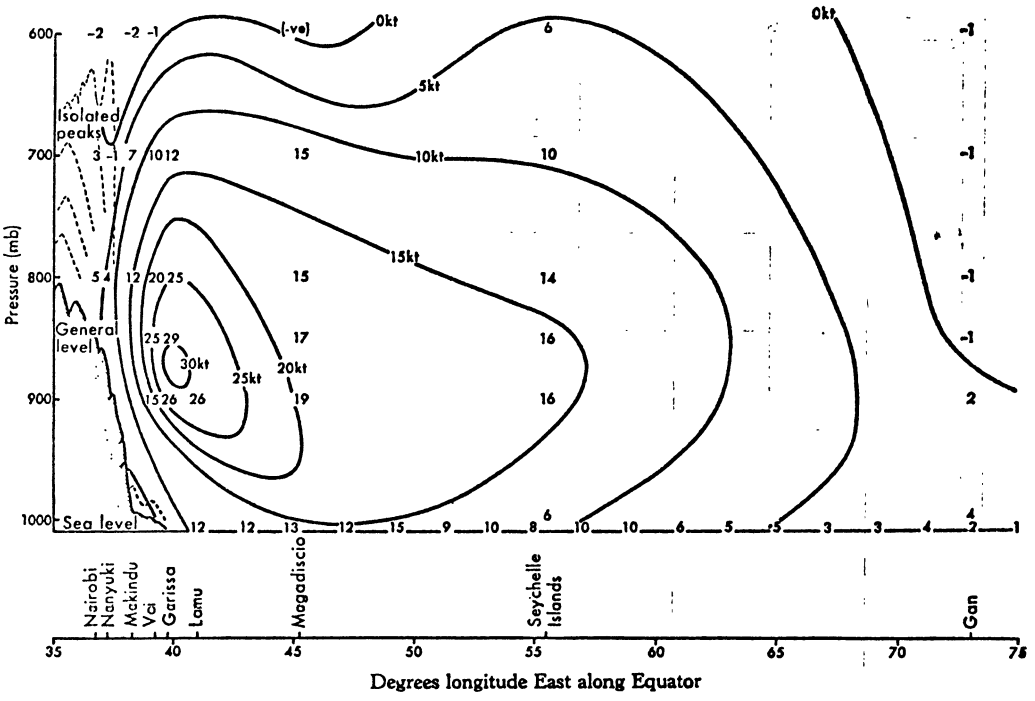

Figure 2
Mean meridional airflow at the equator in July. 1 kt = 0.5148 ms^{-1}.

(1976) has demonstrated the similarity of this phenomenon to a western boundary current controlled by the highlands of eastern Africa.

The core of the current where it passes over the flat lowlands of eastern Kenya, as shown in Fig. 2, has been explored by a meteorologically-instrumented aircraft and several important characteristics deduced (FINDLATER, 1972), one of which is that the air in the core is rising slowly whilst on each side descent takes place. Hence, at least over Kenya, the core is generally more cloudy than the flanks. On some days the current may be multi-cored.

3. The low-level jet streams

The monthly-averaged analyses of flow at low levels (FINDLATER, 1971a) reveal a well-defined axis of maximum flow and this is a reflection of the area of occurrence of the low-level jet streams which are noticeable on daily charts. These jet streams are orientated parallel to the axis of maximum flow and move along it. The low-level jet streams can be located as high-speed elements about 500–1000 km in length (along the flow), 200–400 km wide and about 1 km in depth (FINDLATER 1966, 1969a) with pronounced vertical and lateral shears. Similar dimensions were found by DESAI

et al (1976) over the central Arabian Sea and over India using ISMEX-73 data. Despite the general paucity of data in the area it is sometimes possible to track individual high-speed elements from place to place.

The highest speeds recorded in the low-level jet streams are usually close to the highlands of eastern Africa. Figure 3 shows the areas prone to high speeds and other areas, notably over inland Africa and over the oceanic equator where high speeds have not been recorded.

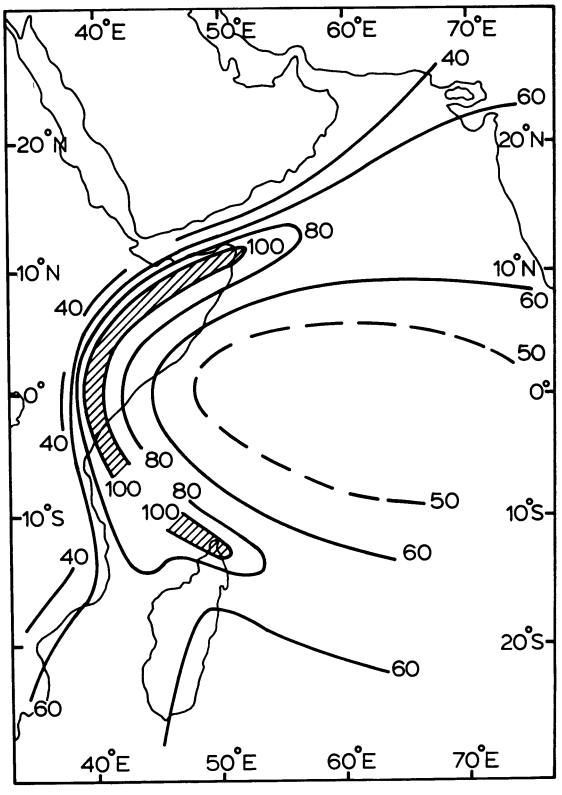

Figure 3
Smoothed isopleths of maximum wind speed (in knots) for the layer 2000–8000 ft (600–2400 m) above MSL during the period of the northern summer monsoon. 1 kt = 0.5148 ms^{-1}.

When the core of the major current retracts from eastern Africa in October the low-level jet streams can still be traced in the southern hemisphere, especially near north Madagascar. One outstanding example occurred there in October 1972 when winds at 1 km, measured by pilot balloon and radio methods, exceeded 40 ms^{-1} on five consecutive soundings over a 30-hour period, with a peak speed of 65 ms^{-1} (at 1 km) being recorded, (FINDLATER, 1974). These strong winds persisted without change of direction and were associated with very heavy rainfall downstream on the coast of eastern Africa. No cyclonic disturbance was detectable.

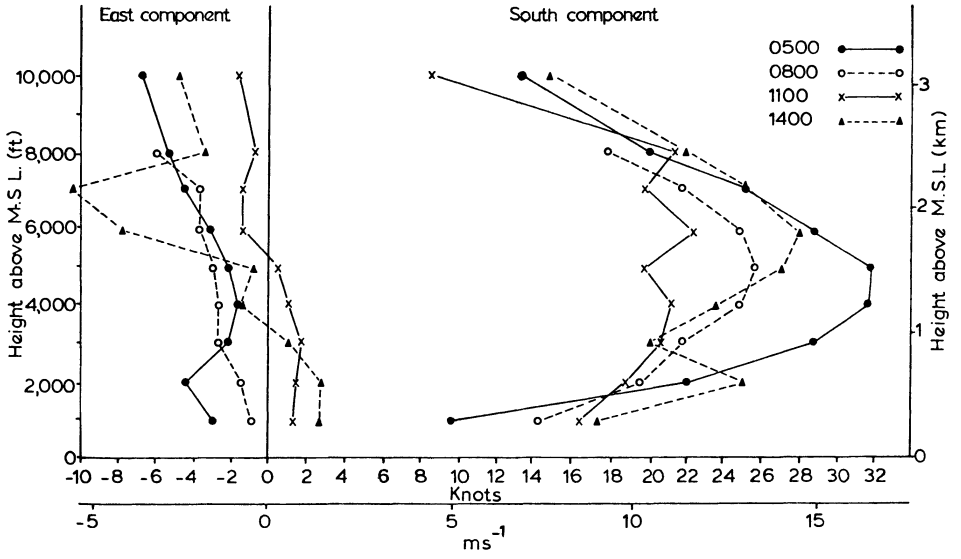

Figure 4
Mean monthly with components for July at Garissa, Kenya, in the years 1962–71, for four times of day, GMT.

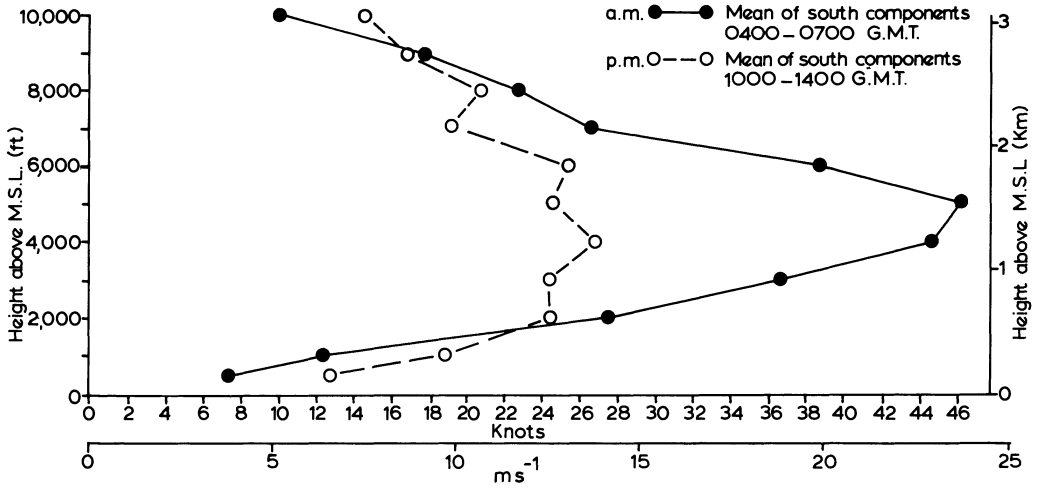

Figure 5
Mean diurnal change in the low-level jet stream system at Garissa, Kenya, during a two-month period of stronger than normal cross-equatorial flow. June and July 1973.

There is some evidence to suggest that the occurrence of low-level jet streams is associated in some way with outbreaks of cool air intruding into the southeast trade wind system of the southern Indian Ocean, or moving northwards through the Mozambique Channel. Such outbreaks are accompanied by a surge in surface pressure and often followed by a strengthening of the cross-equatorial flow over Kenya. CADET (1977) has found an association between increases in the cross-equatorial flow over Kenya and oceanic disturbances propagating eastwards across the Arabian Sea north of the equator.

Over eastern Africa the low-level jet streams are centered at about 1–1.5 km and lie in the middle of the daytime convective layer, with the monsoon inversion overlying the area at about 3 km. Over the Arabian Sea, however, the inversion and the jet streams are lower and there is some evidence that the jet lies close to, or in, the stable layer, (JAMBUNATHAN *et al.*, 1974: DESAI *et al.*, 1976).

4. *Diurnal variations*

Sufficient data have now been accumulated to make a preliminary study of the diurnal variation of the low-level jet over Kenya. At Garissa (00° 29′S 39° 38′E, 128 m) where pilot balloon soundings are made twice daily, not necessarily at the same hours each day, the diurnal variation is marked at all levels below 2 km.

Figure 4 illustrates the average diurnal variations of the south and east components of the winds up to 3 km, for four times of day at Garissa in July. It is evident that the low-level jet attains its maximum speed by the early morning, at 0500 GMT. Local time in the area is three hours in advance of GMT. Minimum speeds are recorded during the afternoon, about 1100 GMT, when surface heating is nearing its maximum. Nevertheless, it should be noted that very high speeds (up to 45 ms^{-1}) have been recorded during the afternoon on a few occasions. On average the speed of the core of the jet during the afternoon is about two-thirds of the early morning value.

During periods of stronger than average flow the ratio of afternoon to morning speed falls to about half and Fig. 5 illustrates the striking jet-like profile of the southerly wind in the early morning during a period of two months of very strong cross-equatorial flow, and the modification of the profile during the afternoon.

The surface wind under the core of the jet also exhibits a marked diurnal influence, falling to a minimum of 1–2 ms^{-1} during the night at Garissa, when no upper wind soundings are made, to an average value of 6 ms^{-1} during the afternoon. On some days the afternoon wind reaches 12 ms^{-1} but higher values are unusual.

A point of interest is that in the general area of Garissa there is a secondary surface wind maximum a few hours after dusk; this may be in association with the re-establishment of the night-time jet as the air stabilizes. Some evidence of this can be seen in Fig. 4 where a secondary wind maximum appears below 1 km at 1400 GMT, i.e., in the late afternoon.

For Mombasa (Ras Serani, 04° 04′S 39° 42′E, 20 m) on the Kenya coast, a detailed examination of the diurnal variation of the surface wind has been made by RAMSEY (1971) and this too indicates a secondary peak in the surface wind speed after dusk in July. Further downstream, over the Gulf of Aden and the Arabian Sea, diurnal variations of the surface wind have been recorded far from land. In the middle of the Gulf of Aden diurnal variations can be pronounced, and in the strong wind area over the open ocean east of Socotra the variation has been calculated to be $2\ ms^{-1}$ during July and August, (BROOKS and DURST, 1935; METEOROLOGICAL OFFICE, 1944).

5. Monitoring the cross-equatorial flow

The fact that the low-level cross-equatorial current of the northern summer is locked by the topography of eastern Africa has allowed attempts to be made to relate the vigour of the flow across the equator to events downstream, e.g., the rainfall of parts of western India. The first such analysis (FINDLATER, 1969a) indicated a strong relationship between the two parameters, with fluctuations in rainfall over western India lagging a few days behind the fluctuations of the cross-equatorial flow over Kenya. Further analyses of this type for many years, using Garissa or Mombasa (Airport, 04° 02′S 39° 37′E, 57 m) as upper wind monitor stations, have confirmed the relationship and four examples are shown in Fig. 6. The strength of the cross-equatorial flow over Kenya is not, of course, the only influence on the rainfall of western India but these analyses indicate that it can be a very important one for lengthy periods during the southwest monsoon.

The study of this relationship has been extended by examining the mean July cross-equatorial flow and the mean July rainfall of ten stations in western Maharashtra Province of India. Figure 7 shows a close relationship between wind and rainfall especially when two-year mean values (indicated by dots) are used. However, the striking feature of this analysis is the one-year lag between peaks and troughs and changes in slope of the two-year mean rainfall curve behind similar features of the two-year mean wind index curve. The correlation coefficient between the change in the two-year mean wind index and the change in the two-year mean rainfall of the group of 10 stations one year later is 0.82. An experimental forecasting technique for predicting the July rainfall of western Maharashtra Province of India for one year ahead has been derived from these data, (FINDLATER, 1977).

The comparative values of the July wind index for the 24-year period given in Fig. 7 may allow meaningful comparisons to be made of changes in the vigour of the monsoon circulation from year to year, and might also be useful in examining changes in other parameters, e.g., the degree of upwelling off the Somali coast, the strength of the largely wind-driven Somali Current, and sea surface temperature anomalies of the Arabian Sea. Indeed, the intriguing one-year lag shown in Fig. 7 might be indicative of some ocean-atmosphere feed-back mechanism.

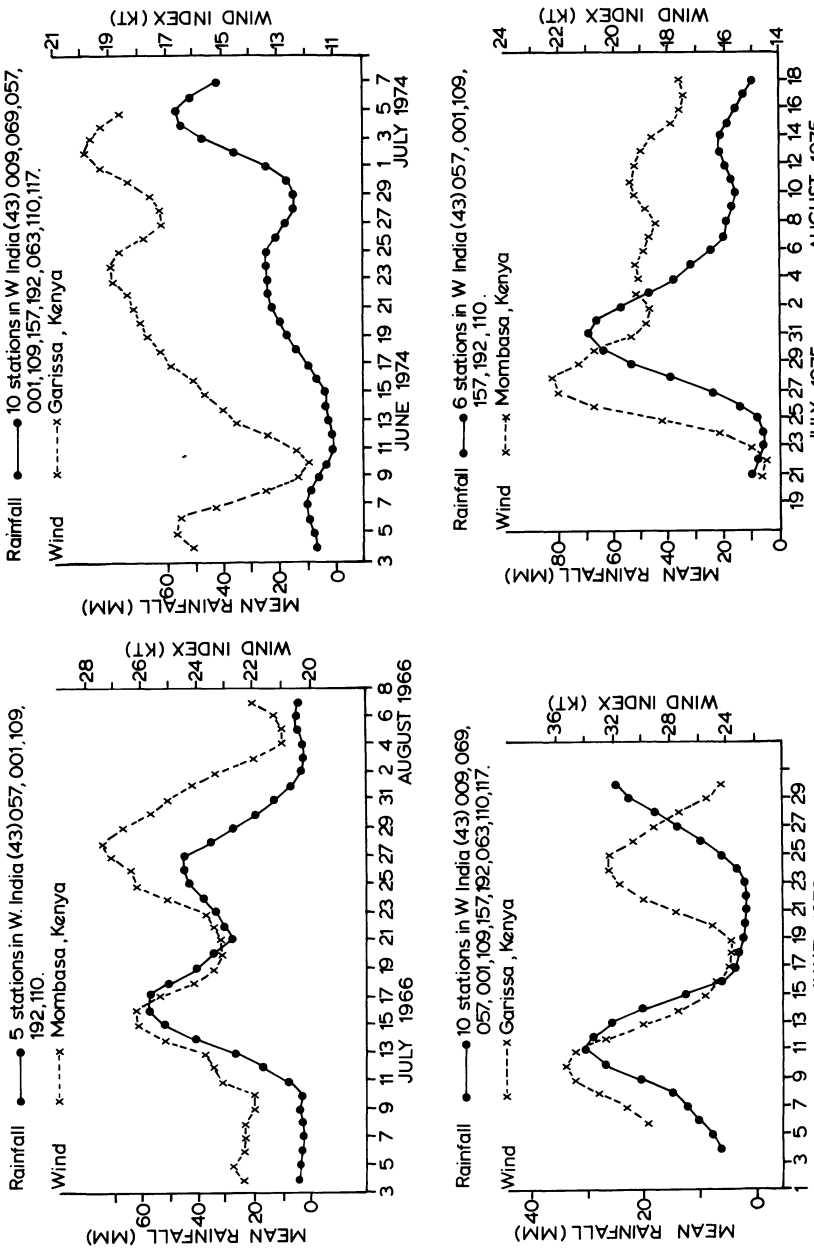

Figure 6

Four examples of the relationship between cross-equatorial flow over Kenya at Mombasa or Garissa, and the mean rainfall at groups of stations in western Maharashtra Province of India. The Indian stations are indicated by station numbers. Values of the wind index and rainfall are five-day overlapping means. The wind index is calculated from the mean of the south components of the wind at 1000, 2000, 3000, 4000 and 5000 ft above MSL. (1 kt = 0.5148 ms^{-1}. 1000 ft = 304.8 m).

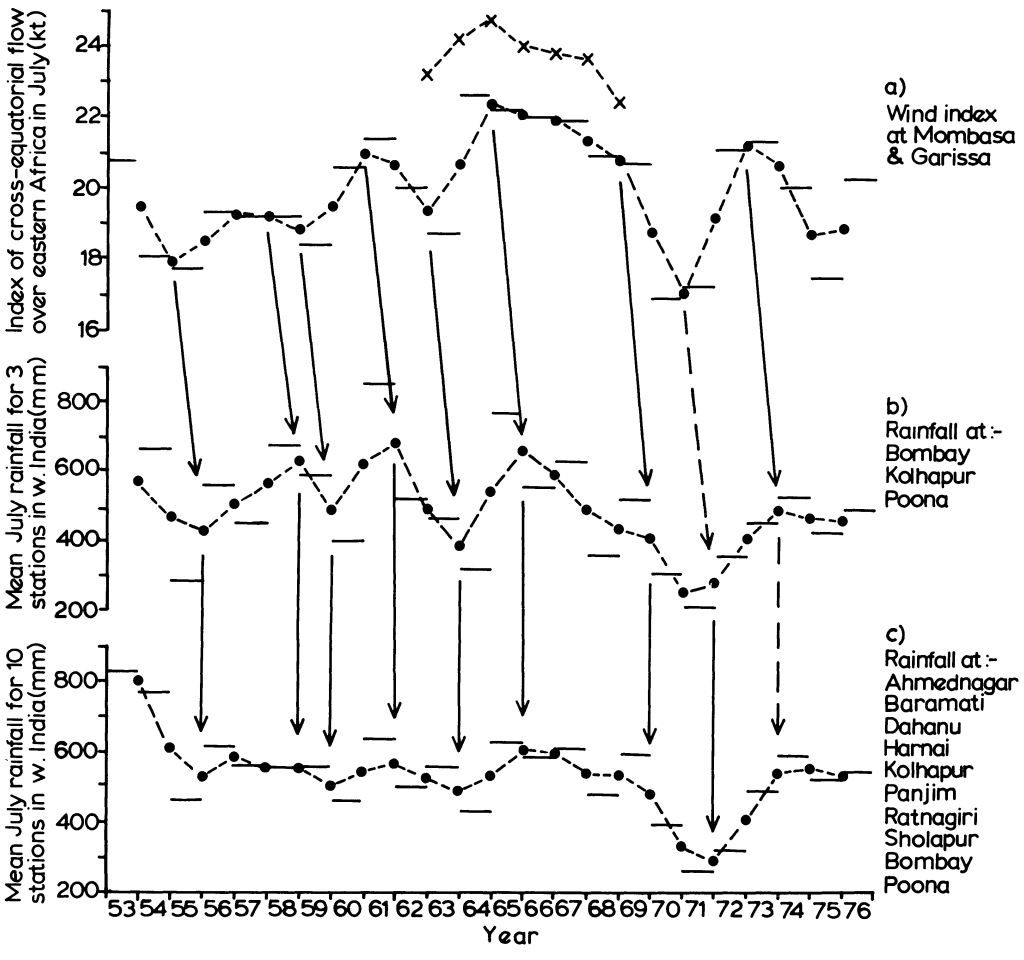

Figure 7

Comparison of the mean July index of cross-equatorial flow over Kenya (a); the mean July rainfall at three stations in western India (b); and the mean July rainfall at ten stations in western India (c). The dots represent the mean July value for two consecutive years. The crosses in Fig. 4a represent the two-year mean values at Garissa, for comparison with those of Mombasa.

6. *Conclusions*

The major current, or low-level jet stream system, whose observed characteristics have been briefly summarized in the foregoing is an important component of the circulation of the Afro-Asian monsoon of the northern summer. Although the dynamics of the system are not well understood the phenomenon exhibits some similarity to western boundary currents.

The possibility of monitoring the interhemispheric flow at the core of the current

where it is topographically-locked overland, in relation to another monsoon element – rainfall downstream – has been demonstrated, but the full implications of such monitoring have yet to be explored.

Acknowledgement

This paper is published with the permission of the Director-General of the East African Meteorological Department.

References

ANDERSON, D. L. T. (1976), *The low level jet as a western boundary current*, Monthly Weather Rev. *104*, 907–921.

BROOKS, C. E. P. and DURST, C. S. (1935), *The circulation of air by day and night during the SW monsoon near Berbera, Somaliland*, Quart. J. Roy. Met. Soc. Lond. *61*, 167.

BUNKER, A. F. (1965), *Interaction of the summer monsoon air with the Arabian Sea*, Proceedings of the Symposium on Meteorological Results of I.I.O.E., Bombay, 22–26 July 1965. Poona, India Meteorological Department, pp. 3–16.

CADET, D. (1977), *Tropical disturbances as a relationship between the cross-equatorial flow over Kenya and rainfall over the western Indian coast* (Paper submitted to the Quart. J. Roy. Met. Soc. Lond.).

DESAI, B. N., RANGACHARI, N. and SUBRAMANIAN, S. K. (1976), *Structure of the low level jet stream over the Arabian Sea and the Peninsula as revealed by observations in June and July during the monsoon experiment (MONEX) 1973 and its probable origin*, Ind. J. Met., Hydrol. Geophys. *27*, 263–274.

FINDLATER, J. (1966), *Cross-equatorial jet streams at low level over Kenya*, Meteorol. Mag., Lond. *95*, 353–364.

FINDLATER, J. (1967), *Some further evidence of cross-equatorial jet streams at low level over Kenya*, Meteorol. Mag. Lond. *96*, 216–219.

FINDLATER, J. (1969a), *A major low level air current near the Indian Ocean during the northern summer*, Quart. J. Roy. Met. Soc. Lond. *95*, 362–380.

FINDLATER, J. (1969b), *Interhemispheric transport of air in the lower troposphere over the western Indian Ocean*, Quart. J. Roy. Met. Soc. London. *95*, 400–403.

FINDLATER, J. (1971a), *Mean monthly airflow at low levels over the western Indian Ocean*, Geophysical Memoirs, Vol. XVI, No. 115 (HMSO, London).

FINDLATER, J. (1971b), *The strange winds of Ras Asir*, Meteorol. Mag., Lond. *100*, 46–54.

FINDLATER, J. (1972), *Aerial explorations of the low-level cross-equatorial current over eastern Africa*, Quart. J. Roy. Met. Soc. Lond. *98*, 274–289.

FINDLATER, J. (1974), *An extreme wind speed in the low-level jet stream system of the western Indian Ocian*, Meteorol. Mag. Lond. *103*, 201–205.

FINDLATER, J. (1977), *A numerical index to monitor the Afro-Asian monsoon during the northern summers*, Meteorol. Mag. Lond. *106*, 170–180.

JAMBUNATHAN, R. and RAMAMURTHY, K. (1974), *Wind field in the lower and middle troposphere over the Arabian Sea during the southwest monsoon of 1973*, Ind. J. Met. Geophys. *25*, 400–410.

JOSEPH, P. V. and RAMAN, P. L. (1966), *Existence of low level westerly jet streams over peninsular India during July*, Ind. J. Met. Geophys. *17*, 407–410.

METEOROLOGICAL OFFICE, *Pilot balloon observations made from H.M. Ships, 1925–36*, Met. O. 431 (HMSO, London 1940).

METEOROLOGICAL OFFICE, *Weather in the Indian Ocean*, Vol. 2, Part 2, Met. O. 451b(2) (HMSO, London 1944).

RAMAGE, C. S. and RAMAN, C. R.V., *Meteorological Atlas of the IIOE*, Part 2 (*Upper Air*) (University of Hawaii, Honolulu; National Science Foundation, Washington, D.C., 1972).

RAMSEY, B. (1971), *Surface winds at Mombasa, Kenya*, Meteorol. Mag. Lond. *100*, 293–301.

ROME (1932–35). *Ministero dell'Aeronautica, Annali dell' Ufficio Presagi.* Vols. 4, 5, & 6.

(Received 15th June 1977)

Pageoph, Vol. 115 (1977), Birkhäuser Verlag, Basel

On the Theory of the East African Low Level Jet Stream

By JOHN E. HART[1])

Abstract – Several theoretical models for the East African Low Level Jet Stream are described. They all share the notion that the northward advection of planetary vorticity across the equator, coupled with the presence of a north–south mountain barrier, leads to the formation of a low-level western boundary current (akin to the Gulf-Stream) along the equatorial east coast of Africa. They differ in the manner in which the planetary vorticity advection is balanced to obtain a quasi-steady state. A purely inertial model predicts the correct cross-stream scale of the jet, but does not reproduce the observed inner shear layer which reduces the jet velocity to zero inland near the highlands. The lateral friction model can produce a realistic jet profile if the horizontal eddy viscosity (appearing as a free parameter) is chosen appropriately. However this solution shows a recirculation, i.e., northerly flow, off the coast that has not yet been observed. Finally, a model that includes bottom friction over variable topography also can give realistic jet profiles. If one accepts that the mountains, the Beta effect, and some form of inertial or frictional acceleration act together to produce the cross-equatorial low level jet stream, then one can formulate the types of observations needed to distinguish between the various theories.

Key words: Jet Stream: Low level over E. Africa.

I. Introduction

The East African Low Level Jet (EAJ)[2]) was discovered only recently through the pioneering observational work of FINDLATER (1969, 1971, 1972, 1974). As a result, discussions of formal theoretical models attempting to describe this interesting and important phenomenon have appeared in the literature only in the last year or two. Models of the EAJ fall into two classes. One class attempts to treat only the flow along the East African coast, and through the introduction of certain simplifying assumptions the problem is reduced to an analytically tractable one which hopefully contains enough of the essential physics to indicate what may be occurring in the real atmosphere. The second class encompasses large-scale numerical models which treat the flow over a substantial part of the Indian Ocean Basin, and include many competing physical processes. A single numerical solution is examined for key balances within a subset of these processes, or several solutions are carried out omitting various effects. This review shall concentrate on the simple analytical models, although some discussion of the numerical simulations will be given.

[1]) Department of Astro-Geophysics, University of Colorado, Boulder, Colorado 80309, USA.

[2]) This is sometimes referred to as the 'Somali Jet', but since the jet is well developed quite a bit south of Somalia, the name used here seems more appropriate.

To some degree, present models of the EAJ represent extensions or alterations of theories developed to describe other related geophysical flows, namely the southerly low level jets observed above the plains east of the Rocky Mountains in the United States (HOEKER, 1963; BONNER, 1968), and oceanographic western boundary currents (see STOMMEL, 1972, for a comprehensive account of one such current, the Gulf Stream). The low level jets of the western great plains show nocturnal wind maxima at altitudes slightly less than 1 km above ground. Current theoretical descriptions of these low-level jets tend to emphasize the inertial overshoot in the diurnal planetary boundary layer which occurs when turbulence is suppressed at night due to radiative stabilization. The studies of WIPPERMANN (1973) and YAMADA and MELLOR (1975) are typical of such treatments, which essentially all contain some form of time dependent vertical eddy viscosity. For a time, early versions of the eddy viscosity model (like that of BAUJITTA and BLACKADAR, 1957) competed with an alternate view expressed by WEXLER (1961). He suggested that the strong southerly low level flow east of the Rockies was a result of the interaction of the easterly flow originating from the Bermuda high pressure zone with the north–south mountain barrier. Such an interaction in an inviscid fluid can produce an inertial boundary current, whose width scale is $\sqrt{-U_0/\beta}$. Here, β is the northward gradient of the Coriolis parameter, and U_0 is the velocity scale of the flow approaching the mountains. It happens that a northward flowing steady boundary current is only possible if $U_0 < 0$, i.e., if the flow approaches the barrier from the east.

The inertial boundary current problem is equivalent to that for the Gulf Stream (CHARNEY, 1955), and Wexler modified Charney's solutions to obtain a reasonable velocity field for the Great Plains low level jet. However, because it does not predict the strong diurnal behavior observed in these jets, recent modeling has concentrated on vertical friction effects, although some effort has been made to incorporate vertical friction and horizontal inhomogeneity together (PAEGLE and RASCH, 1973).

Observations of the EAJ (FINDLATER, 1969) indicate that at least during June and July when the jet is well developed, diurnal effects are weak.[3]) Undoubtedly this conclusion is somewhat biased by the fact that most of the data (Pibals) were obtained during the day. Nonetheless there is some evidence for considering the EAJ to be a quasi-steady structure which is influenced more by horizontal advection in a spatially inhomogeneous field than by the detailed time dependent boundary layer processes. Indeed HIDE (1970) suggested that the EAJ be interpreted as an inertial western boundary current in a manner similar to the way Wexler envisioned the Great Plains low level jets. Until recently (ANDERSON, 1976; HART, 1976) no formal theoretical analyses of the EAJ from this point of view had been presented. In Sections II and III of this paper the successes and failures of such an approach will be explored by studying several simple analytical models which suggest certain key observational tests. In Section IV, results of numerical simulations will be reviewed.

[3]) At most, diurnal effects modulate the persistent southerly cross-equatorial flow. These modulations are important, but are not treated in this paper.

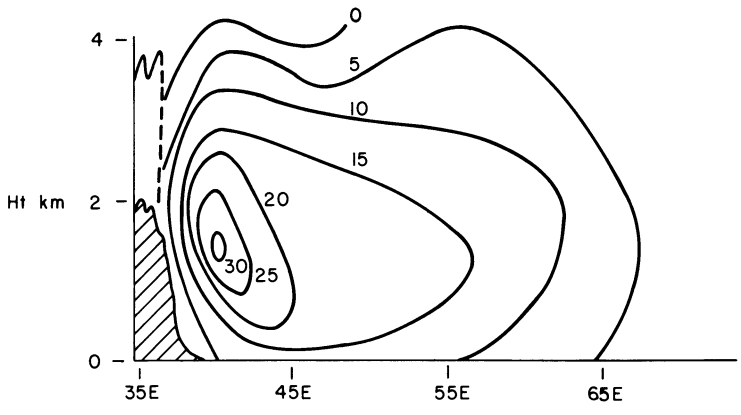

Figure 1
Contours of southerly velocity near 2°S for the mean wind in July. This is redrawn from FINDLATER (1974). Values are in knots.

Perhaps the major goal of any theory of the EAJ would be to explain the mean velocity structure of the core at various cross-sections along the coast. It is particularly attractive to model the flow in the vicinity of the equator where there is already some detailed data (FINDLATER, 1972, 1974). Figure 1 shows a typical cross-section of the observed meridional wind for July. One immediately gains the impression that the incident zonal winds are forced to flow northward in response to the mountain barrier, forming a jet near the coast. It would be nice to have an analytical theory which could explain both the vertical and horizontal structure around the core, but trying to model both simultaneously rapidly drives one to use a big computer model. Instead this paper will focus on explaining the observed horizontal structure; the strong shear on the landward side of the jet and the somewhat broader tail out over the ocean. There are several other qualitative effects, such as the reported wind speed maxima just north of the Malagasy Republic and just off the horn of Africa (FINDLATER, 1974), along with a splitting of the jet over the Arabian Sea (FINDLATER, 1971), that invite explanation. However, these effects should be viewed as somewhat tentative until further observations are made. At this point in time, the core-sections, as in Fig. 1, offer the best detailed test of theory, although even here the construction of constant velocity contours over the ocean suffers from a lack of good data.

II. A one layer model

The minimum amount of physics needed to account for the EAJ is compactly contained in a one layer model. The stratification of the actual atmosphere is represented by a free surface under the influence of a reduced gravity. This is a simple representation of the inversion usually found above the core of the jet. FINDLATER's (1972) data suggest that the gravitational acceleration g be reduced by a factor $\Delta\theta/\theta_0 \approx$

0.02, where $\Delta\theta$ is the potential temperature drop across the inversion (6°K) and θ_0 a typical average value (300°K). The fluid below the free surface at height h is then considered to be of uniform density. This is a very crude picture of the actual situation, but does represent the idea that it is the inversion which forces the incident flow to go around rather than over the highland barrier.

The motion is split up into a depth-averaged part and a deviation therefrom. Thus, the velocity $\mathbf{u}$ is written

$$\mathbf{u} = \frac{1}{D}\int_{hB}^{h} \mathbf{u}\, dz + u'(x, y, z, t),$$

where the fluid moves over topography of height $h_B(x, y)$ as in Fig. 2. Equations for the evolution of the depth averaged velocity

$$\bar{\mathbf{u}} \equiv \frac{1}{D}\int_{hB}^{h} \mathbf{u}\, dz$$

are obtained by integrating the momentum equations, neglecting interactions of primed quantities in the non-linear terms. The magnitude of the non-linear terms are probably underestimated by doing this, but their general effect is still retained in a qualitative manner. On the equatorial β-plane, where $y = 0$ is the equator, the resulting equations are:

$$\frac{\partial \bar{u}}{\partial t} + \bar{u}\frac{\partial \bar{u}}{\partial x} + \bar{v}\frac{\partial \bar{u}}{\partial y} - \beta y\bar{v} = -g'\frac{\partial h}{\partial x} + \frac{1}{\rho_0 D}\mathscr{T}_{\hat{x}}(h_B) + A\nabla^2\bar{u} \tag{1}$$

$$\frac{\partial \bar{v}}{\partial t} + \bar{u}\frac{\partial \bar{v}}{\partial x} + \bar{v}\frac{\partial \bar{v}}{\partial y} + \beta y\bar{u} = -g'\frac{\partial h}{\partial y} + \frac{1}{\rho_0 D}\mathscr{T}_{\hat{y}}(h_B) + A\nabla^2\bar{v} \tag{2}$$

$$\frac{\partial}{\partial x}\bar{u}D + \frac{\partial}{\partial y}\bar{v}D + \frac{\partial h}{\partial t} = Q. \tag{3}$$

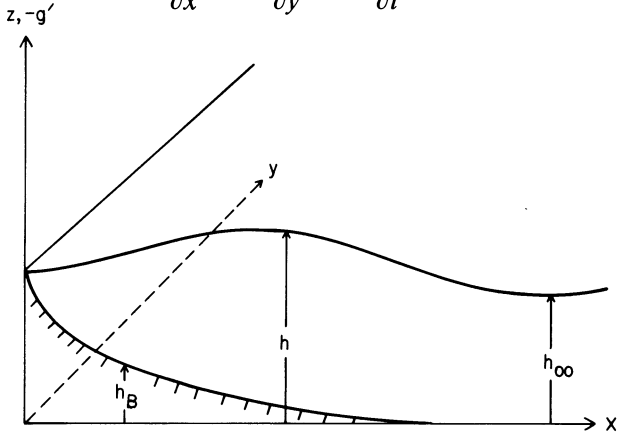

Figure 2

Geometry of the l-layer model. The fluid depth $D = h - h_B$. The local vertical component of the rotation vector is $\frac{1}{2}\beta y$, where y is the northward coordinate, zero at equator. A reduced gravity g' acts to restore the free surface to its equilibrium depth h_{00}.

The notation follows Fig. 2 where u is the eastward (x) velocity and v is the northward (y) velocity. D is the fluid depth, ρ_0 the background density, $\mathscr{T}$ the frictional bottom stress on the fluid as it moves over the surface (interfacial stress is neglected), and A is a horizontal eddy viscosity coefficient. The bottom topography h_B rises to the west and intersects the free surface at $x = 0$. In this type pf model it is convenient to represent the large scale subsidence which drives the motion as a source term in the divergence equation (3). We suppose there is a slow sinking in the high pressure belt south of the equator, and this supplies the mass which is eventually transported northwards in the EAJ. Thus Q is a specified function of y. In the absence of any mountains, a zonally symmetric solution forced by Q is possible. We assume such a solution exists far from the highlands, which are at $x = 0$. The intent then is to find out how the presence of the north–south barrier modifies the flow.

It is instructive to look at the vorticity equation formed from (1)–(3). Let ω denote the vertical vorticity of the fluid, $\partial\bar{v}/\partial x - \partial\bar{u}/\partial y$. Then

$$\underset{(1)}{\frac{\partial\omega}{\partial t}} + \underset{(2)}{(\mathbf{u}\cdot\nabla)(\omega + \beta y)} = \underset{(3)}{(\omega + \beta y)}\underset{(4)}{\left(\frac{d\ln D}{dt} - \frac{Q}{D}\right)} + \underset{(5)}{\frac{\hat{z}}{\rho_0}\cdot\nabla\times\mathscr{T}(h_B)/D} + \underset{(6)}{A\nabla^2\omega}. \tag{4}$$

Terms (2) and (3) represent relative and planetary vorticity advection respectively, while (4) describes vortex stretching. Terms (5) and (6) describe the influence of bottom and side friction. The few published fine resolution models that have attempted to describe the EAJ are based on approximations to equation (4). KRISHNAMURTI, MOLINARI and PAN (1976) find numerical solutions of the inviscid problem involving terms (1)–(4). ANDERSON (1976) solves the time dependent linear problem (terms (1), (3), and the linearized form of (4)) and the steady linear-frictional problem (terms (3) and (6)) analytically. The results of these studies, and others using different balances will be discussed in Sections III and IV.

Using the data obtained by FINDLATER (1972) during several instrumented aircraft flights across the jet core at 2°S, it is possible to estimate the magnitude of some of the terms in equation (4). These estimates are shown in Table 1. During the months of June and July when mean flow is well established term (1) is negligible with respect to planetary and relative vorticity advection.[4]) The vortex stretching term is generally small because absolute vorticity is not as large as it is in mid-latitudes where this term is usually more important. It can become important in regions where the fluid depth becomes small. The same can be said of the bottom stress term. For a linear drag law $\mathscr{T} = -\rho_0 R\bar{\mathbf{u}}$, the spindown time $\mathscr{T}_{sd} \equiv D/R$

[4]) The intent is to describe the average flow for several days, thus diurnal effects are neglected.

decreases with depth (i.e., near the intersection of the free surface with the ground) and so this term will become important near the highlands, but may probably be neglected elsewhere. The side-friction term (6) is more difficult to estimate because the horizontal eddy viscosity coefficient is unknown. Nonetheless, it is fairly obvious that whatever dissipative mechanism is included in a model for the EAJ, it cannot be larger than terms (2) and (3), and although linear models are instructive, inevitably one has to take into account the observational evidence that non-linear advection of vorticity is an important effect.

Table 1

Vorticity balance

Term	Estimator	Value
(1)	$\partial\omega/\partial t$	2×10^{-5} sec^{-1}/month $= 10^{-11}$ sec^2
(2)	$\bar{u}\dfrac{\partial^2\bar{v}}{\partial x^2}$	1 m/sec $\times$ 10 m/sec/$(2 \times 10^5)^2 \doteq 2.5 \times 10^{-10}$
(3)	$\bar{v}\beta$	10 m/sec $\times$ $2.36 \times 10^{-11} \doteq 2 \times 10^{-10}$
(4)	$\dfrac{\omega\bar{u}}{D}\dfrac{\partial h_B}{\partial x}$	$\dfrac{2 \times 10^{-5}\ \text{sec}^{-1} \times 1\ \text{m/sec} \times 0.005}{2200\ \text{m}} \doteq 5 \times 10^{-11}$
(5)	ω/τ_{sd} [a])	$\lesssim 10^{-10}$
(6)	$A\dfrac{\partial^3\bar{v}}{\partial x^3}$	?

[a]) $\tau_{sd} \equiv$ spindown time $= D/R \sim 4$ days.

III. Solutions to the one layer model

Oceanographers have long been interested in the boundary layer solutions of equation (4), because of their relevance to theories of western boundary currents like the Gulf Stream and Kuroshio. Many of the solutions presented below are arrived at simply by modifying techniques used in papers on the theoretical oceanography of such currents.

IIIa. Inviscid inertial flow

The scale analysis of Section II suggests that to a first approximation one should consider inviscid steady dynamics,

$$\bar{\mathbf{u}} \cdot \nabla\left(\frac{\omega + \beta y}{D}\right) = 0.^{5}) \tag{5}$$

Following the analysis of CHARNEY (1955) we suppose the EAJ is a boundary layer with $\partial\bar{v}/\partial x \gg \partial\bar{u}/\partial y$. This is supported by FINDLATER's (1972) observations. Intro-

[5]) We have neglected the source term here, because in the boundary layer it is much smaller than term (2) of equation (4).

duce a transport streamfunction such that

$$D\bar{v} = \frac{\partial \psi}{\partial x}, \tag{6}$$

$$D\bar{u} = -\frac{\partial \psi}{\partial y}. \tag{7}$$

Thus (5) states that potential vorticity is constant along a streamline;

$$\frac{1}{D}\left(\frac{\partial \bar{v}}{\partial x} + \beta y\right) = F(\psi). \tag{8}$$

The Bernoulli function is also conserved;

$$\frac{\bar{v}^2}{2} + g'h = G(\psi). \tag{9}$$

We assume that a zonal transport $h_0\bar{u}_0$ coming towards the highlands is prescribed as $x \to \infty, 0 \geq y \geq y_s$. A general profile which is representative of actual conditions is

$$h_0\bar{u}_0 = U_0 h_{00} \operatorname{sech}^2 \alpha(y - y_0) \tag{10}$$

or

$$\psi_0 = -\frac{U_0 h_{00}}{\alpha}[\tanh \alpha(y - y_0)] \tag{11}$$

where h_0 is the upstream fluid depth (at $x \to \infty$, $h_B = 0$) and is a function of y only. The fluid depth at the peak of the inflow is h_{00}. Figure 3 shows such a profile. The parameter y_0 locates the peak velocity, α describes the width of the incoming zonal flow. Let y_s be the most southerly latitude of the domain.

When there is no friction and no mountains (10) and (11) would be exact solutions. From the $\hat{y}$ momentum equation we find that $\bar{u}_0 = -g'/\beta y\, \partial h_0/\partial y$, or

$$h_0^2 - h_{00}^2 = -\frac{2\beta U_0 h_{00}}{g'\alpha}[y \tanh \alpha(y - y_0) - \alpha^{-1} \log \cosh \alpha(y - y_0)]. \tag{12}$$

Now in the upstream region as $x \to \infty$, $\bar{v} = 0$, so (10), (11), and (12) determine $G(\psi)$. It is

$$G(\psi) = g'\left\{h_{00} - \frac{2\beta U_0 h_{00}}{g'\alpha}\left[\frac{-\psi}{U_0 h_{00}}\left(\tanh^{-1}\left(\frac{-\alpha\psi}{U_0 h_{00}}\right) + y_0\right)\right.\right.$$
$$\left.\left. - \alpha^{-1} \log \cosh \tanh^{-1}\left(\frac{-\alpha\psi}{U_0 h_{00}}\right)\right]\right\}^{1/2}. \tag{13}$$

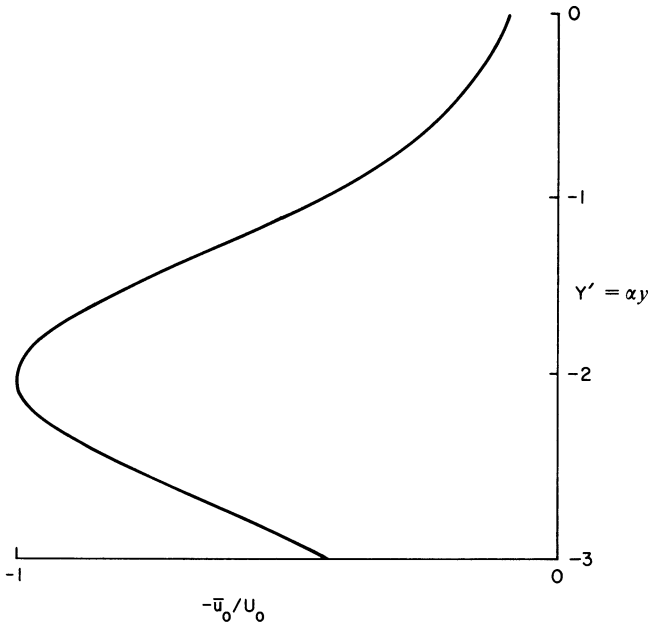

Figure 3
A typical inflow profile $h_0u_0 = U_0h_{00}\,\mathrm{sech}^2\,\alpha(y - y_0)$. By adjusting α and y_0, the location of the peak and the width of the inflow can be adjusted. The southern boundary of the domain, where we set $v = 0$, is at $y_s \leq y_0$.

In order to use equation (9) to find $\bar{v}$ everywhere in the domain, we need to determine $h(\psi)$. This can be obtained easily from equation (8) in the case of a flat bottom. Thus we consider the case of a vertical barrier at $x = 0$, and $h_B(x, y) = 0$. Then using the fact that the Bernoulli function G and the potential vorticity function F are related by $dG/d\psi = F(\psi)$, h can be calculated following CHARNEY (1955);

$$h = \left\{h_0^2(y) - \frac{2\beta y}{g'\alpha}(\psi - \psi_0(y))\right\}^{1/2}. \tag{14}$$

Combining (9), (12), (13), and (14) with the definition $\bar{v}h = \partial\psi/\partial x$ allows ψ to be determined by a simple quadrature.

There is one dimensionless parameter in this model

$$\gamma = \frac{-2\beta U_0}{g'\alpha^2 h_{00}}.$$

For presentation of results we non-dimensionalize y by α^{-1}, x by $\gamma^{1/2}\sqrt{-U_0/\beta}$ and $\bar{v}$ by $\sqrt{g'h_{00}}$. Non-dimensional quantities will be primed. Taking $h_{00} = 2.2$ km, $U_0 = -5$ m/sec, and $\alpha = 7.5 \times 10^5$ m we find that γ is about 0.25, the velocity scale is 21 m/sec, and the east–west length scale is 165 km. Figure 4 shows transport streamlines and fluid height contours over the domain. The flow comes in from the

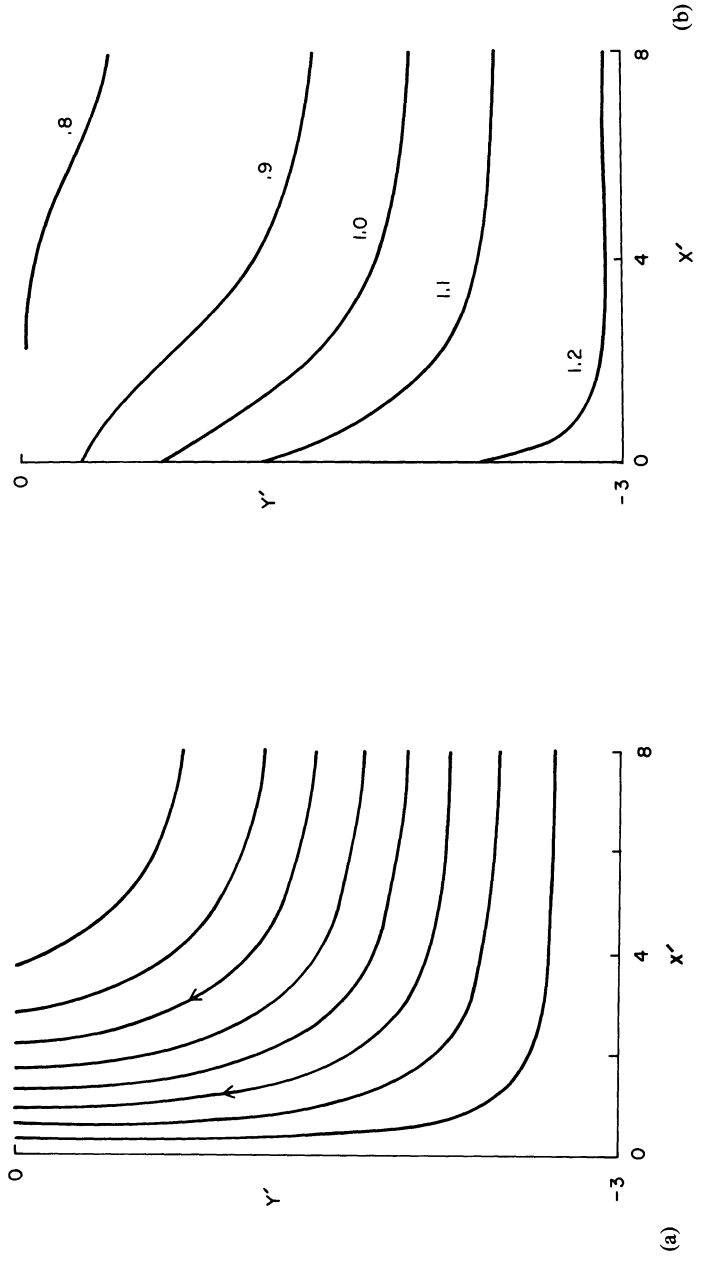

Figure 4
Solutions for the inertial boundary current. In all these contour plots $y_0' = -2$, $y_s' = -3$. In 4a and 4b, γ is 0.25, while in 4c and 4d, $\gamma = 0.65$. Figures a and c show non-dimensional transport streamlines with contour interval 0.2 and 0.3 respectively. Figures b and d show the free surface height normalized by h_{00}.

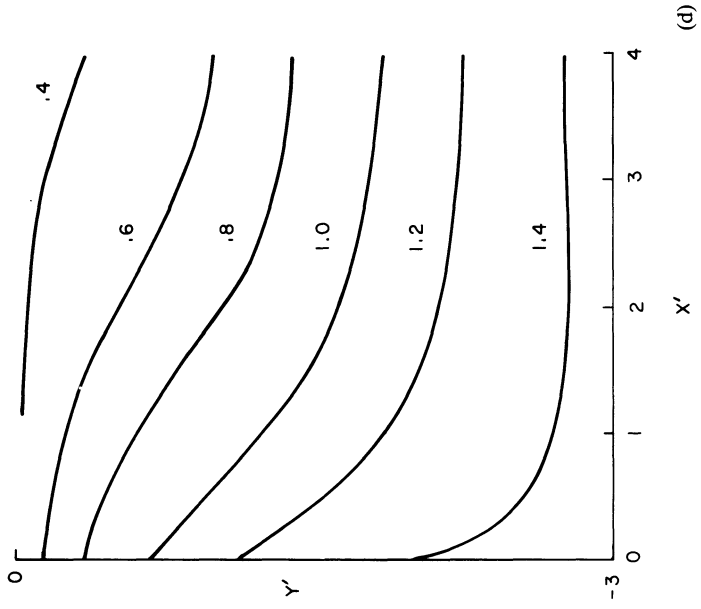

(d)

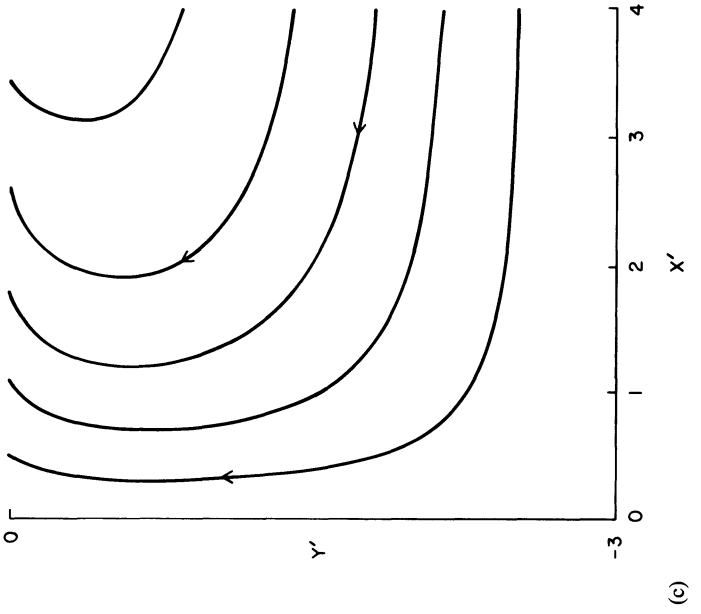

(c)

east and concentrates in a northward flowing boundary current which decreases in width as one moves northwards. As γ becomes larger (0.65) the free surface deflection increases and the transport turns away from the coast just south of the equator. This effect is found in the $\gamma = 0.25$ solution too, but it occurs north of the equator ($y = 0$). This is evidence of complete separation which occurs when the boundary layer velocity becomes high enough that h is reduced to zero. At the barrier this happens for $y_0 = y_s$ when

$$y_{sep} - y_0 = \alpha^{-1} \log [e^{1/\gamma} + \sqrt{e^{2/\gamma} - 1}].$$

Values for separation are given in Table II.

Table 2

Separation at $x = 0$ for various γ

γ	$\alpha(y_{sep} - y_0)$
0.01	100.00
0.05	20.00
0.7	10.69
0.25	4.68
0.5	2.68
1.0	1.66
5.0	0.65

For example, if the peak inflow is at 15°S, and $\gamma = 0.35$, then separation will occur at 10°N. This is roughly the location where the EAJ leaves the horn of Africa to begin its journey across the Arabian Sea to India. Note too from Fig. 4b, that although $h \to 0$ at 20°N, the free surface is almost flat south of the equator, for $\gamma = 0.25$.

Figure 5 shows velocity profiles at $y = 0$. The doubling width for the dimensional parameters used above is 300 km, while the peak velocity is 15.3 m/sec. These numbers correspond quite well with the data (e.g., Fig. 1) except for one fact. Since there is no friction in this model the peak velocity occurs right at the barrier, while the data shows a high shear zone there which reduces $\bar{v}$ to zero.

IIIb. Lateral friction

ANDERSON (1976) proposed that a lowest order description of the EAJ could be obtained by balancing planetary vorticity advection and lateral friction. For a steady state this represents a balance between terms (3) and (6) of equation (4). This means one must choose A large enough that side friction be the same order as term (3), and that non-linear advection be neglected. This is not really consistent with the data (see Table I), but the linear solution gives some idea of the effects of lateral friction.

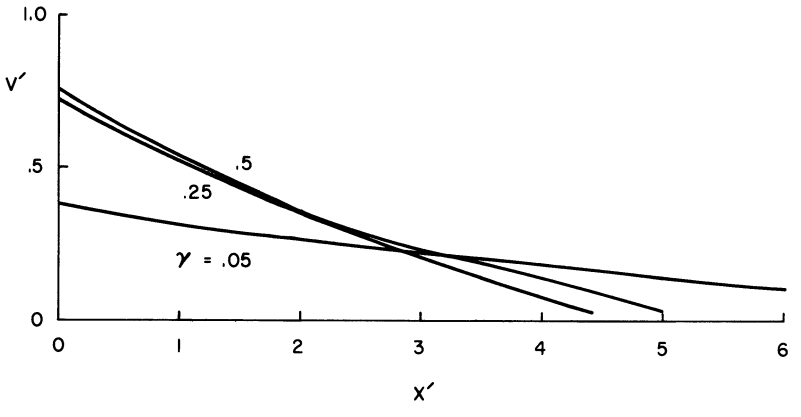

Figure 5
Northward velocity profile at the equator for various values of γ. For all curves, $y'_0 = -2$, $y'_s = -3$.

With the boundary layer approximation, the vorticity balance is

$$\beta\bar{v} = A\frac{\partial^3\bar{v}}{\partial x^3}. \tag{15}$$

This is recognized as the same equation as proposed by MUNK (1950) in his study of western boundary currents in the wind driven ocean circulation. With $h_B = 0$ and a vertical barrier at $x = 0$, the solution which has $\bar{v}(x = 0) = \psi(x = 0) = \bar{v}(x = \infty) = 0$, and an upstream inflow described by equation (10),[6]) can be written

$$\bar{v} = B \exp\left(-\sqrt[3]{\beta/A}\, x/2\right) \sin\left(0.866\sqrt[3]{\beta/A}\, x\right), \tag{16}$$

where

$$B = \sqrt[3]{\beta/A}\,(-1.15\, U_0)\{\tanh\alpha(y - y_0) + \tanh\alpha(y_0 - y_s)\}/\alpha.$$

This solution is shown in Fig. 6. It has a high shear inner structure absent from the purely inertial solution. The outer half width of the current is consistent with the data if we choose $\sqrt[3]{A/\beta} \doteq 3 \times 10^5$ m, or $A \doteq 6 \times 10^4$ m^2/sec. Whether such a value represents an accurate description of horizontal mixing in the jet is unclear. Clearly once A is chosen to give a reasonable width, then the use of a realistic inflow profile will insure that the peak speed is about right. In addition, if the primary vorticity balance *is* expressed by (15) as a result of choosing a large value of A, then the non-linear terms will make only quantitative modifications to the profile (16).

Anderson shows several interesting numerical solutions which include non-linearity as well as the effects represented in equation (15). Some of the spatial streamline structure is altered. In particular, the maximum winds shift asymmetrically north of the equator (recall the inertial solution had this property, the highest velocity was reached just before separation), where in the linear model local maxima

[6]) With a free constant added to eqn. (11) to make ψ zero at $x = 0$.

occur at the equator and at about $\pm 17°$.[7]) However, the non-linearity fails to remove the recirculation apparent in Fig. 6. There is still a region of reversed (northerly) flow associated with a region of negative $\bar{v}$ for $x\sqrt[3]{\beta/A} \gtrsim 3.6$. This is not consistent with the picture presented in Fig. 1 and a crucial test of the lateral friction theory would be to verify the existence of such a reversal in an expanded data set.

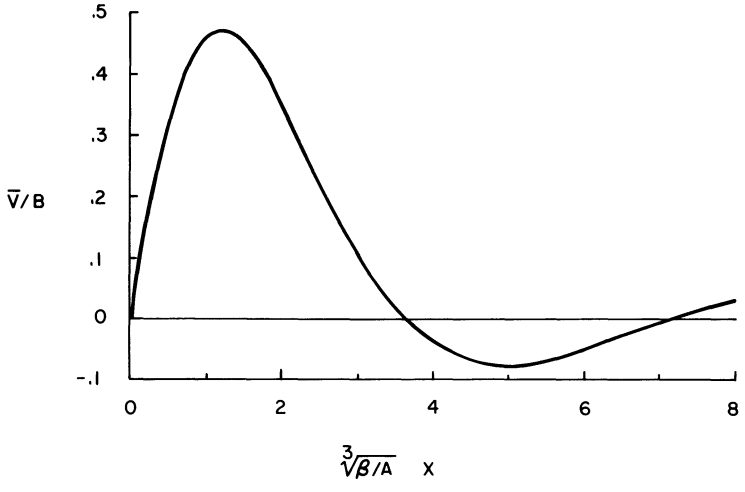

Figure 6
Dimensionless velocity $\bar{v}/B$ for the lateral friction model.

IIIc. A bottom friction model with variable topography

The large vertical shear near the ground apparent in FINDLATER's (1972) observations suggests that bottom friction may be important in the vorticity balance. In the usual STOMMEL (1948) solution for the Gulf Stream, such bottom friction solutions of the vorticity equations have maximum $\bar{v}$ velocities at the barrier at $x = 0$. We show below that solutions over variable topography do not have this property; in fact a realistic profile can be obtained.

In terms of the transport stream function ψ, the steady vorticity equation, neglecting lateral friction, becomes

$$J(\psi, \nabla^2\psi - \psi_x D_x/D) + D\beta\psi_x = -R(\nabla^2\psi - 2\psi_x D_x/D) - (\nabla^2\psi - \psi_x D_x/D + D\beta y)[\psi_y D_x/D - Q], \quad (17)$$

where we have used a linearized bottom drag law

$$\mathscr{T} = -\rho_0 R\bar{\mathbf{u}}.$$

[7]) These effects are seen most clearly by comparing Figs. 6c and 14 of Anderson's paper. Note that the symmetry in his linear solution depends on $Q(y)$, which is not the same as we have used. Nonetheless his $\bar{v}(x)$ profiles closely resemble those described by equation (16).

R is a parameter of this model. The associated viscous spindown time is again $\tau_{sd} = D/R$.

Now the inertial solution of Section 3a showed that for $\gamma \doteq 0.25$, the domain south of the equator is only slightly influenced by free surface deflections; e.g., the free surface is within 20 percent of its upstream value. However, the bottom topography is strong in the sense that it intersects the 'inversion'. Thus in equation (17) we have used the approximation that $h = h_{00}$ and $D = h_{00} - h_B(x)$. Consider model topography of the form

$$D = ax^k, \qquad 0 \leqslant x < x_0$$

$$D = D_0 = ax_0^k, \quad x \geqslant x_0.$$

The parameter settings $a = 6.7\ \mathrm{m}^{0.55}$, $k = 0.45$ gives a qualitatively accurate topography between the highlands and the coast ($x_0 = 400$ km).

Again the flow in the turning region $x > 0, y > y_s$ is driven by an upstream inflow described by (10). Since $D \to D_0 = h_{00}$ far upstream, the zonal solution (10) will be exact if

$$Q(y) = \frac{R\dfrac{\partial \bar{u}_0}{\partial y}}{\partial \bar{u}_0/\partial y - \beta y} \lesssim 0(10^{-2}\ \mathrm{m/sec}).$$

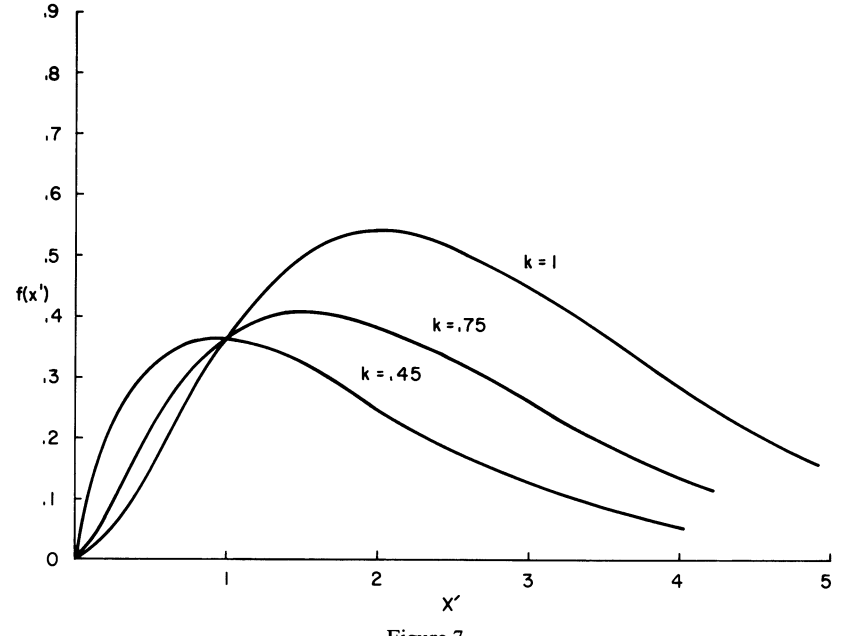

Figure 7

Northward velocity profile function $f(x')$, for the bottom friction variable topography model. The topography has the form $h_B \propto x^k$, for values of k shown. The length scale is $[R(1 + k)/\beta a]^{1/1+k}$.

In order to simply demonstrate how a variable topography coupled with vertical friction can give a northward jet we consider briefly a linear boundary layer model. Among the linear terms it can be shown that in the boundary layer the term involving Q is negligible, and that involving $\beta y\psi_x D_x$ is everywhere much smaller than $R\psi_x D_x/D$ provided $f|_{5°S} \cdot \tau_{sd} \lesssim 0(1)$. Since we anticipate a spindown time of not more than a few days, this ordering should hold. Using the boundary layer approximation, equation (17) reduces to

$$\psi_{xx} - \frac{2\psi_x D_x}{D} + \frac{D\beta\psi_x}{R} = 0 \tag{18}$$

which effectively balances the bottom friction torques generated on the sloping surface with planetary vorticity advection. It is seen that on the inside of the jet where D becomes small the β-effect is unimportant. The solution for $\bar{v}$, obtained by solving (18) for ψ_x and dividing by D, is most easily written by introducing a horizontal length scale

$$L_{\hat{x}} = \left(\frac{R(1+k)}{\beta a}\right)^{1/1+k}$$

in the x direction. In terms of the non-dimensional variable x',

$$\bar{v} = -U_0\{\tanh \alpha(y - y_0) + \tanh \alpha(y - y_s)\} \frac{\beta D_0 x'^k \, e^{-x'^{1+k}}}{\alpha R \Gamma\left(\frac{1+2k}{1+k}\right)}$$

in the region $x < x_0$.

Figure 7 shows the profile function $f(x') = x'^k e^{-x'^{k+1}}$ for several k. This model possesses the advantageous feature that a high-shear zone is created over the steeper slopes near the highlands as observed, and a broader tail for large x' which does not cross zero, indicating a lack of any flow reversal. The shear on the inner flank is about 3 times that on the outer for $k = 0.45$ and this is in the same sense as FINDLATER's observations (1972, Fig. 10). From the same figure we see that the inner shear region of the jet is about $1\frac{1}{2}°$ or 150 km wide. We can use this to estimate a consistent value of R since the inner layer dynamics will not be substantially changed

Table 3

Scale factors for the linear solution with $k = 0.45$.

τ_{sd} days	$L_{\hat{x}}m$	M
1	5.8×10^5	1.75
2	3.6×10^5	3.45
4	2.2×10^5	7.20
8	1.38×10^5	13.8
16	0.85×10^5	27.6

by the addition of the non-linear terms. Table III shows length scales $L_{\hat{x}}$ and the velocity amplification factor (the multiplication factor M for $f(x')$ to give $\bar{v}$ at $y = 0$, e.g., $v|_{y=0} = -U_0 Mf(x')$) as functions of τ_{sd}. The scales are computed using $D_0 = 2.2$ km and $\alpha = 1.33 \times 10^{-6}$ m^{-1}.

A spindown time of about 8 days would seem to be consistent with the data. This leads to a peak velocity of about $5U_0$ or 25 m/sec for an inflow velocity of 5 m/sec.

The linear solution shows how an inner shear layer can be produced over sloping terrain, but for realistic friction parameters R, the jet is too narrow and has too high a peak speed to be consistent with the mean wind data of Fig. 1. Of course we do not expect the linear boundary layer balance to apply very far away from the highlands, since non-linear effects rapidly become important as D increases. Equation (17) can be solved numerically by a fairly simple algorithm. We start with the linear boundary layer solution as an initial state, and integrate (17) over a domain $0 \leq x \leq 700$ km, $0 \geq y \geq -2000$ km on a 41 by 33 grid. The transport streamfunction ψ is zero on $x = 0$ and $y = -y_s$, and is given by equation (11) on $x = 700$ km. At $y = 0$, we set $\partial\psi/\partial y = 0$. The false transient solution evolves to a final steady state in about 20S of CDC 7600 time.

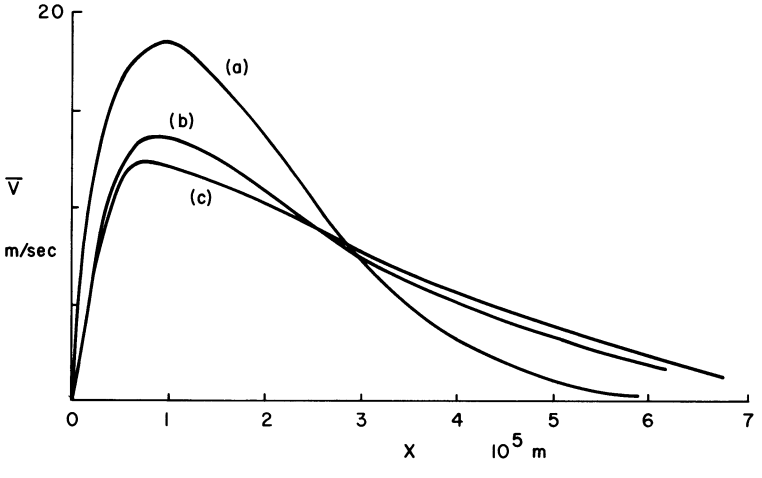

Figure 8
Velocity profile $\bar{v}(x)$ for linear (a) and nonlinear bottom friction models over variable terrain. In all cases, $\alpha = 1.25 \times 10^{-6}$ m^{-1}, $y_0 = y_s = -2 \times 10^6$ m, and $U_0 = -5$ m/sec. Curves (a) and (b) have $\tau = 4$ days, while for (c), $\tau_{sd} = 10$ days.

Figure 8 shows two $\bar{v}(x)$ profiles obtained by numerical integration, along with the analytical solution to the linear problem obtained from equation (18). It is clear that inertial effects become more important than bottom friction on the outer flank of the jet, and a much wider core emerges from the numerical solution. However, the width of the inner region is not much affected by the inertial terms, and also does

not appear to be particularly sensitive to τ_{sd}. The predicted outer e-folding distance is about 350 km, which is close to the value of $\sqrt{-U_0/\beta} = 460$ km. The mean wind data of FINDLATER (e.g., Fig. 1) shows this sort of structure, but according to this theory the mean jet should extend well off the East African Coast, and little data is currently available to verify whether or not this is really true.

IIId. Summary

Each of the western boundary current solutions to the one-layer potential vorticity equation described above has some redeeming features. The inertial solution indicates separation at approximately the right latitude, although the actual phenomena may be strongly influenced by meteorological processes to the north which tend to lead to horizontal confluence in the separation area. The addition of lateral or vertical friction creates a realistic jet profile for appropriate eddy coefficients. Since observations with even the most sophisticated instrumentation cannot evaluate the detailed vorticity balance, we must assess these models in terms of the success in predicting the jet cross-section. The theories themselves suggest one should try to obtain better data for $\bar{v}(x)$ east of the peak velocity, and especially to see if recirculation in the monthly mean occurs. In addition it would be desirable to determine the relative influence of lateral and vertical friction, and especially how the latter varies with distance from the highlands. There is considerable time-dependent and smaller scale structure within the mean core. How this is related to vertical mixing processes, or how it may be interpreted as a horizontal diffusion process should be investigated. The frictional exchange coefficients $K_z \doteq 10$ m^2/sec and $A \doteq 10^5$ m^2/sec may not be unreasonable but more detailed data on small scale eddy interactions with the jet are needed. Of course the simple models outlined above were intended primarily to suggest the basic physical processes which shape the mean core of the jet, and to provide a framework for more complicated theoretical modeling. For example, models resolving many layers in the vertical with the intent of predicting the vertical structure in the mean core should take into account the variable topography as well.

IV. Large-domain models

The previous sections have emphasized the flow of the EAJ near the coasts of Tanzania, Kenya, and Somalia. Several numerical modelers have attempted to predict the behavior of the jet in a larger domain including both the inflow and outflow regions. These models by and large lend support to the idea that the EAJ represents a western boundary current, and have the advantage of delineating certain special influences on the jet itself, like the effect of the presence of the mountainous Malagasy Republic in the upstream inflow region.

One numerical simulation which is closely related to the one layer model discussed above is that of KRISHNAMURTI *et al.* (1976). They integrated the l-layer inviscid equations for 6 days over a domain from 25°S to 25°N and 25°E to 75°E. The model included the β effect, a smoothed regional topography, and a theoretical inflow/outflow velocity prescribed along 75°E in accord with the zonal monsoon model of MURAKAMI *et al.* (1970). The other boundaries were impermeable. Although the boundary conditions are not well posed in the sense that the outflow is specified independently of what occurs inside the domain, the solutions over this wider region exhibit several interesting features beyond the demonstration that the β-effect, the upstream inflow, and the topography lead to a western boundary current. There are maxima in the wind speed just west of the north tip of Malagasy and just south of the horn of Africa. These maxima closely correspond to those observed by FINDLATER (1971) although a smoothing of the terrain probably leads to less topographic influence than is actually present; e.g., the Malagasy maximum appears to occur on the north-east side of the island. One suspects there is more topographic constraint on the actual flow field than is shown in these simulations. It is interesting that the maximum wind speed which occurs as the jet leaves the Somali coast appears to be associated with horizontal confluence of the EAJ and air flowing in a strong cyclonic gyre over the south Arabian peninsula. ANDERSON (1976) finds a similar behavior in his one-layer numerical model which includes an upward flux of mass ($Q < O$ in equation (3)) in this region. The extent to which this confluence causes the observed low level wind maximum, and the extent to which it may be caused by inertial confinement and separation needs to be distinguished. Observations indicate a fairly strong leakage west out of the EAJ through the valley between the Ethiopian and Kenyan highlands, at about 2°N, 37°E. This apparently is related to the relative minimum of the jet velocity at this latitude. However, the numerical solution of KRISHNAMURTI *et al.* (1976) predicts a very large *eastward* velocity through this valley. It is suggested that much can be learned from limited area numerical models in this region, but that the influence of boundary conditions and representations of local forcing need to be carefully assessed.

Several global circulation models have indicated the combined roles of the β-effect and the mountains in shaping the cross-equatorial flow over the western Indian Ocean. Their resolution is generally insufficient to predict the flow in any detail, but certain tendencies are still evident. HAHN and MANABE (1975) demonstrate that the cross-equatorial flow is much weaker and more diffuse when the mountains are artificially removed from the model. With the highlands included a southerly jet with approximately the observed scale is found. WASHINGTON and DAGGUPATY (1975) show solutions with similar behavior. A weaker northerly jet is observed during the north-east monsoon, and this has been simulated in a numerical model by WASHINGTON (1975). On theoretical grounds one would expect a western boundary current with northerly flow. But again, whether such a flow is inertially controlled, or dominated by lateral or bottom friction is not clear. It is unlikely that numerical

models by themselves, even with $\frac{1}{2}°$ resolution, will be able to address these questions without further observational input.

IV. Conclusions

The East African Low Level Jet Stream is probably a result of the conservation of potential vorticity of fluid moving across the equator in response to the influence of the East African Highlands on the easterly zonal flow over the southern Indian Ocean. Although the western boundary current hypothesis offers a useful conceptual framework there is obviously much room for further observational and theoretical work. So far theoreticians have concentrated on the mean horizontal spatial structure. But how does one explain the multiple cores imbedded in the mean jet (FINDLATER, 1969). Do they propagate in from upstream? Evidence for open ocean jets is meagre, and satellite photographs show only rare penetrations of frontal disturbances as far north as 20°S. If such disturbances conserve potential vorticity as they move northwards, the fine structure will be filtered out. It is tempting to suggest that finite amplitude longitudinal instability of the mean jet in the presence of convection may lead to coring. Indeed the whole question of the vertical as well as the small scale horizontal structure needs investigation. Models which have good vertical as well as good horizontal resolution will be needed and the parameterization of subgrid scale turbulence processes will demand careful attention. Closely coupled observational and theoretical study of the EAJ offers an exciting opportunity to gain considerable understanding of the physics of large scale airflow around mountains, and of the interaction of a persistent highly sheared low level current with small scale turbulent convection and transverse slope circulations.

Acknowledgement

This work was sponsored by the National Science Foundation, grant ATM76-17028.

REFERENCES

ANDERSON, D. L. T. (1976), *The low-level jet as a western boundary current*, Mon. Wea. Rev. *104*, 907–921.

BAUJITTA, K. and BLACKADAR, A. K. (1957), *Theoretical studies of diurnal wind-structure variations in the planetary boundary layer*, Quart. J. Roy. Meteor. Soc. *83*, 486–500.

BONNER, W. D. (1968), *Climatology of the low-level jet*, Mon. Wea. Rev. *96*, 833–850.

CHARNEY, J. G. (1955), *The Gulf Stream as an inertial boundary layer*, Proc. Nat. Acad. Sci. *41*, 73–740.

FINDLATER, J. (1969), *A major low level aircurrent near the Indian Ocean during the northern summer*, Quart. J. Roy. Meteor. Soc. *95*, 362–380.

FINDLATER, J., *Mean monthly air flow at low levels over the western Indian Ocean*, Geophys. Mem. No. 115, (HMSO, London, 1971), 115 pp.

FINDLATER, J. (1972), *Aerial explorations of the low-level cross-equatorial current over eastern Africa*, Quart. J. Roy. Meteor. Soc. *98*, 274–289.

FINDLATER, J. (1974), *The low-level cross-equatorial air current of the western Indian Ocean during the northern summer*, Weather *29*, 411–416.

HAHN, D. G. and MANABE, S. (1975), *The role of mountains in the South Asian monsoon/circulation*, J. Atmos. Sci. *32*, 1515–1541.

HART, J. (1976), *On the dynamics of the Somali jet*. Paper presented at a GARP workshop on MONEX, Jan. 1976 at NCAR, Boulder, Colo.

HIDE, R. (1970), *Comments in a discussion on the paper by Findlater (1969)*. Quart. J. Roy. Meteor. Soc. *96*, 551–554.

HOEKER, W. H. (1963), *Three southerly low level jet systems delineated by the weather bureau special pilot network of 1961*, Mon. Wea. Rev. *91*, 573–582.

KRISHNAMURTI, T. N., MOLINARI, J. and PAN, H. L. (1976), *Numerical simulation of the Somali Jet*, J. Atmos. Sci. *33*, 2350–2362.

MUNK, W. H. (1950), *On the wind driven ocean circulation*, J. Meteor. *7*, 79–93.

MURAKAMI, T., GODBDE, R. and KELKAR, R. R. (1970), *Numerical simulation of the monsoon along* 80°*E*, Proc. Conf. Summer Monsoon of East Asia, Navy Weather Res. Facility., Norfold, Va.

PAEGLE, J. and RASCH, G. E. (1973), *Three dimensional characteristics of diurnally varying boundary layer flows*, Mon. Wea. Rev. *101*, 746–756.

STOMMEL, H. (1948), *The westward intensification of wind-driven ocean currents*, Trans. Am. Geophys. Union *29*, 202–206.

STOMMEL, H., *The Gulf Stream* (Univ. Calif. Press, Los Angeles 1972).

WASHINGTON, W. M. (1975), *Numerical simulation of the Asian-African winter monsoon with emphasis on the reversal of the Somali Jet: A descriptive study*, National Center for Atmospheric Research Report NCAR 0903/75.

WASHINGTON, W. and DAGGUPATY, S. (1975), *Numerical simulation with the NCAR global circulation model of the mean conditions during the Asian-African summer monsoon*, Mon. Wea. Rev. *103*, 105–144.

WASHINGTON, W. (1976), *Numerical simulation of the Asian-African winter monsoon*, Monthly. Wea. Rev. *104*, 1023–1028.

WEXLER, H. (1961), *A boundary layer interpretation of the low-level jet*, Tellus *13*, 368–378.

WIPPERMANN, F. (1973), *Numerical study on the effects controlling the low-level jet*, Beit. Phys. Atmos. *46*, 137–154.

YAMADA, T. and MELLOR, G. (1975), *A simulation of the Wangara atmospheric boundary layer data*, J. Atmos. Sci. *32*, 2309–2329.

(Received 15th June 1977)

Regional Energetics Over the North Pacific, South China Sea and the Indonesian Seas During Winter[1])

by TAKIO MURAKAMI[2])

Abstract – The energy equation was applied to four limited regions to investigate the basic mechanisms through which area-averaged eddy kinetic energy is maintained during the northern winter. The regions selected for this study are as follows: extratropical North Pacific (24.2°N–44.6°N, 130°E–150°W), tropical eastern North Pacific (0°–19.6°N, 170°W–110°W), South China Sea and Bay of Bengal (0°–19.6°N, 80°E–140°E), and Timor Sea and eastern Indian Ocean (0°–19.6°S, 80°E–140°E). The zonally averaged upper flows over the first region were found to be barotropically stable. In contrast, they were barotropically unstable over the second region; namely, eddy motions over the tropical eastern North Pacific are maintained by receiving energy from zonal flows via barotropic interaction. The third and fourth regions are characterized by the importance of the conversion process between eddy available potential and eddy kinetic energy.

Key words: Eddy kinetic energy maintenance; Energy conversion.

1. Introduction

Tropical disturbances account for a major portion of the rainfall during early winter (December–early January) over the South China Sea and its vicinity. These disturbances are possible when the northeast monsoonal trades are sufficiently broad and deep, surging south–southwest from the north of the South China Sea and eventually merging with the near-equatorial trough and the low-level equatorial westerlies (BRYANT, 1958). Although they are generally weak, rainfall is substantially large, occasionally exceeding 100 mm/day. In later winter, tropical disturbances over the South China Sea are less distinct and ill organized in satellite photographs than those of early winter. No statistical information has been available concerning the frequency of the development of tropical disturbances over the South China Sea. However, an inspection of satellite photographs in December 1965–69 indicates an average period of about 4–6 days.

As yet no attempt has been made to identify the vertical structural features of South China Sea disturbances. A question of fundamental importance is the origin of these disturbances. What is the lateral coupling process between the cold air outbreaks

---

[1]) Contribution No. 77–5, Department of Meteorology, University of Hawaii, USA.

[2]) Department of Meteorology, University of Hawaii, Honolulu, Hawaii 96822, USA.

and the development of tropical disturbances over the South China Sea? What instability mechanism is responsible for their development? Are they barotropically or baroclinically unstable systems or is the main driving provided by convection? The present study is aimed at shedding some light on these problems.

Limited research on the Australian summer monsoon has revealed some similarities to the Northern Hemisphere summer monsoon. Disturbances form in the near-equatorial Southern Hemisphere trough in the vicinity of the Arafura and Timor Seas and propagate west–southwestward, with rain concentrated mainly on the low-latitude side of the tracks. Many of these disturbances become tropical storms as they move towards the Indian Ocean. Based on a global general circulation model, MANABE *et al.* (1970) investigated the generation mechanism and structural features of tropical storms that developed over the Indian Ocean. However, no detailed observational information is available concerning the mechanisms responsible for the disturbance development in the Southern Hemisphere.

MURAKAMI and UNNINAYAR (1977) showed that during the northern winter transient eddy kinetic energy at 200 mb is quite large over the tropical eastern North Pacific. Here, the position and intensity of the upper oceanic trough are subject to some variation, sometimes facilitating the development of cyclonic vortices in and around the trough without apparent connection with convective activity. Occasionally, midlatitude systems in the Northern Hemisphere westerlies penetrate far southwards resulting in anomalous variations in the intensity of equatorial upper westerlies over the central Pacific. This suggests the possibility of strong lateral coupling in the upper troposphere between the extra-tropical and tropical latitudes over the North Pacific. Murakami and Unninayar also postulated that local barotropic instability processes may, occasionally, be instrumental in initiating upper disturbances in the tropical eastern North Pacific. This possibility will be examined in the present study.

TRIPOLI and KRISHNAMURTI (1975) formulated the energy equation for barotropic nondivergent flows over a limited domain. Separating 850 mb winds into area-averaged zonal flow and the departure from it, they investigated the effect of eddy-zonal flow interactions, and energy fluxes across boundaries upon maintaining the area-averaged eddy kinetic energy. They analyzed three domains in the GATE A-scale area. In the present study, a more generalized energy equation is introduced and applied over four limited domains of specific interest. In Section 5, computations of barotropic and baroclinic energy transformations and energy fluxes across the boundaries are presented and their implications discussed.

2. *Data*

It is not the intent of this study to construct an extensive set of maps, which involves considerable effort and expense. Instead, available data as determined by

operational analyses at the National Meteorological Center (NMC) and the United States Navy (USN) will be utilized. The USN analyses of temperature are available at the pressure levels 700 mb, 500 mb, 300 mb and 200 mb during the period from December 1970 to February 1971. Unfortunately, the USN analyses of geopotential is not available in the present study. Upper wind data are obtained from the NMC analyses for the same period (December 1970–February 1971).

During this 90-day period, both commercial aircraft and ATS 1/ATS 3 data were utilized in the NMC operational analysis. We therefore felt that the NMC data might be realistic enough to resolve the characteristic features of large-scale disturbances during the northern winter. Wind analyses are available for the 72 × 23 NMC tropical grid point from 48.1°S to 48.1°N, equally spaced on a Mercator projection (approximately 5° longitude-latitude resolution). This horizontal resolution appears to be adequate to describe large-scale disturbances in the midlatitude westerlies. However, a higher degree of horizontal resolution is certainly desirable for the study of tropical disturbances developing over the South China Sea and Indonesian Seas with characteristic scales of 1000 km or less. Thus, data coverage and quality remain a problem over these regions. Furthermore, the fields of divergence as derived from the NMC wind analyses are probably somewhat smoothed, being intended for use as initial data to the NMC numerical prediction models. Thus, the divergence fields associated with smaller scale disturbances may not be too realistic. However, day-to-day changes of computed divergence agreed, at least qualitatively, with those in satellite observed cloudiness during the northern winter.

3. Disturbance activity during the northern winter

Figure 1 illustrates the differences in the character of disturbance activity at 700 mb between December 1970 and February 1971. Transient eddy kinetic energy was computed at every NMC grid point (approximately 5° latitude-longitude) as follows:

$$k^* = \tfrac{1}{2}\langle u^{*2} + v^{*2}\rangle, \tag{1}$$

where $\langle\ \rangle$ represents the monthly average, and * the departure from it. Thus, u^* is defined as the transient component of u.

In contrast to other tropical areas, 700 mb k^* in December is quite large over two regions, one equatorward of the Bay of Bengal, and another encompassing the South China Sea, northern Borneo, and the southern Philippines (Fig. 1. top). Here, low-level tropical disturbances frequently develop in and around the near-equatorial Northern Hemisphere trough during early winter (December-early January). A band of large k^* along about 130°E and from Japan to north Borneo is probably associated with the northeast monsoonal surges bursting out of the Siberian high. Perhaps, this points to the importance of midlatitude and tropical interaction in

December. In general, such low-level lateral coupling appears to be more pronounced over eastern Asia than over any other tropical area. During early winter, the NE monsoon surges are strong and deep (7000–9000 feet) over the South China Sea with low-level convergence, cyclonic shear and vigorous air-sea interaction. Although tropical disturbances developing over the South China Sea are generally weak, rainfall is substantial, occasionally causing severe and widespread flooding over the

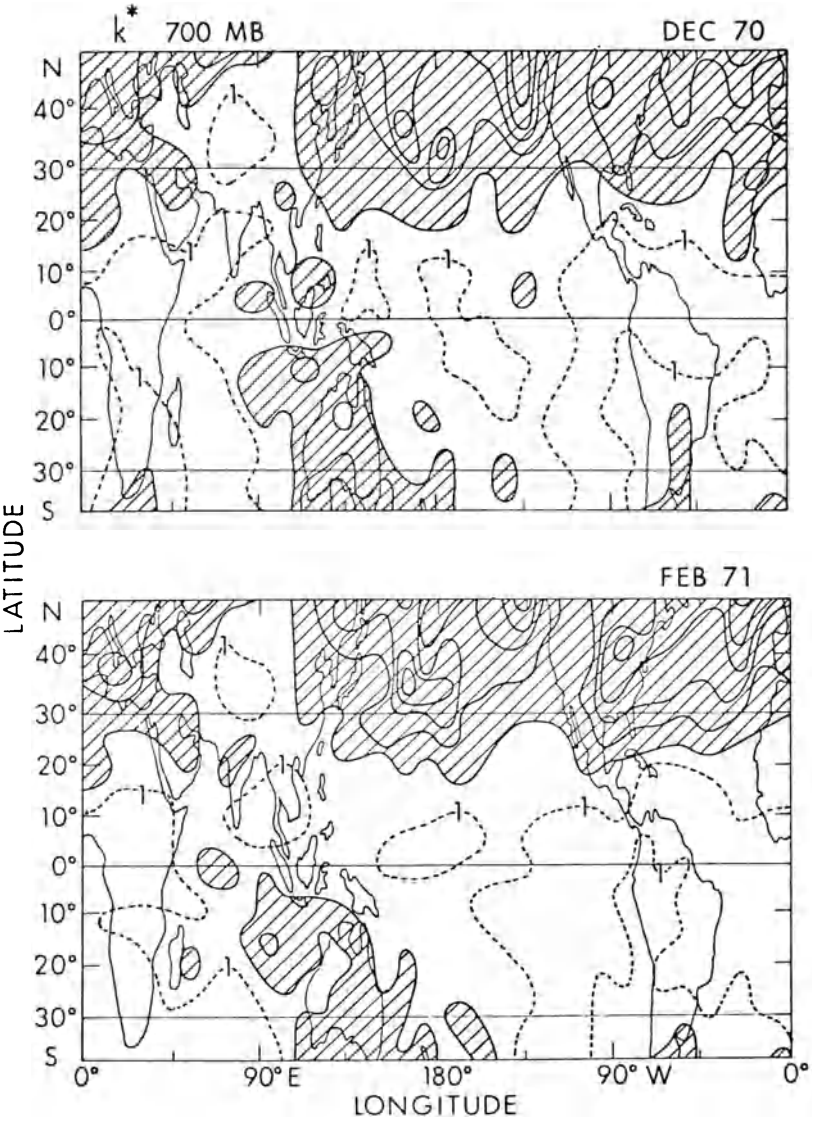

Figure 1

Top: Transient eddy kinetic energy at 700 mb computed from equation (1) during December 1970 in units of 10 m^2 sec^{-2} (every 2 unit interval). Regions of k^* greater than 2 units are shaded. Dashed lines are for 1 unit. Bottom: as in the top except for February 1971.

Malaysian region. In Fig. 1 (top), note a general smallness of 700 mb k^* over the western North Pacific and near the Malaysian peninsula, perhaps indicating that tropical disturbances develop, propagate and decay in the South China Sea. In fact, an inspection of satellite photographs in December 1965–69 reveals that they generally form in the vicinity of northern Borneo and the southern Philippine Islands and reach maximum intensity over the central South China Sea. Often, South China Sea disturbances propagate slowly west–southwestward, generally requiring 3–5 days to cross over the South China Sea, usually decaying rapidly as they approach the Malaysian peninsula.

In Fig. 1 (bottom), less frequent disturbance activity over the South China Sea in February is reflected by small k^*, concurrent with less rainfall and occasional drought conditions over that region in late winter. In contrast, disturbance activity around the Southern Hemisphere near-equatorial trough has become more pronounced in late southern summer than in early summer. Note the existence of a distinct band of large k^* extending along about 15°S from north Australia, through the Indian Ocean, to Madagascar. Here, tropical disturbances formed near the Arafura and Timor Seas generally propagate or meander west–southwestward along 10°–15°S. Some of them intensify and become tropical storms. RAMAGE (1974) showed that the frequency of hurricane development over the South Indian Ocean is largest in January through March. However, a detailed description or explanation of the disturbance development in the Southern Hemisphere is absent in the literature.

Figure 2 (top), showing 200 mb k^* in December, is to be compared with Fig. 2 (bottom) which corresponds to mean February conditions. In both, 200 mb k^* is quite large poleward of about 30°N with a maximum near 35°N–40°N, 170°E–170°W. Here the upper tropospheric jet stream periodically changes in intensity and location in association with the passage of eastward propagating waves in the westerlies. A marked k^* maximum (> 500 m^2 sec^{-2}) in February near 35°N, 170°E is perhaps due to unusual disturbance activity during that particular month. (The corresponding k^* value in that vicinity is only 260 m^2 sec^{-2} in February 1972.) In contrast, 200 mb k^* is notably small over the tropical latitudes between about 20°S and 10°N. Transient eddy kinetic energy is conspicuously small (< 50 m^2 sec^{-2}) over the Malaysia, Indonesian and South China Sea regions, a key area for the Winter Monsoon Experiment in 1979.

Yet another feature of interest in Fig. 2 is a distinct band of large 200 mb k^* extending from about (20°N, 160°W) to (20°S, 140°W), and crossing the equator around 150°W. This band nearly coincides with the axis of upper oceanic troughs embedded in equatorial westerlies over the North and South Pacific (MURAKAMI and UNNINAYAR, 1977). In Fig. 1, it is worth noting that 700 mb k^* is also somewhat large over the eastern tropical Pacific along about 130°–150°W. During the northern winter, heavy rain occasionally falls in the neighbourhood of the Hawaiian Islands in association with southward penetration of midlatitude systems.

In Figs. 1 and 2, it is evident that the character of disturbance activity differs

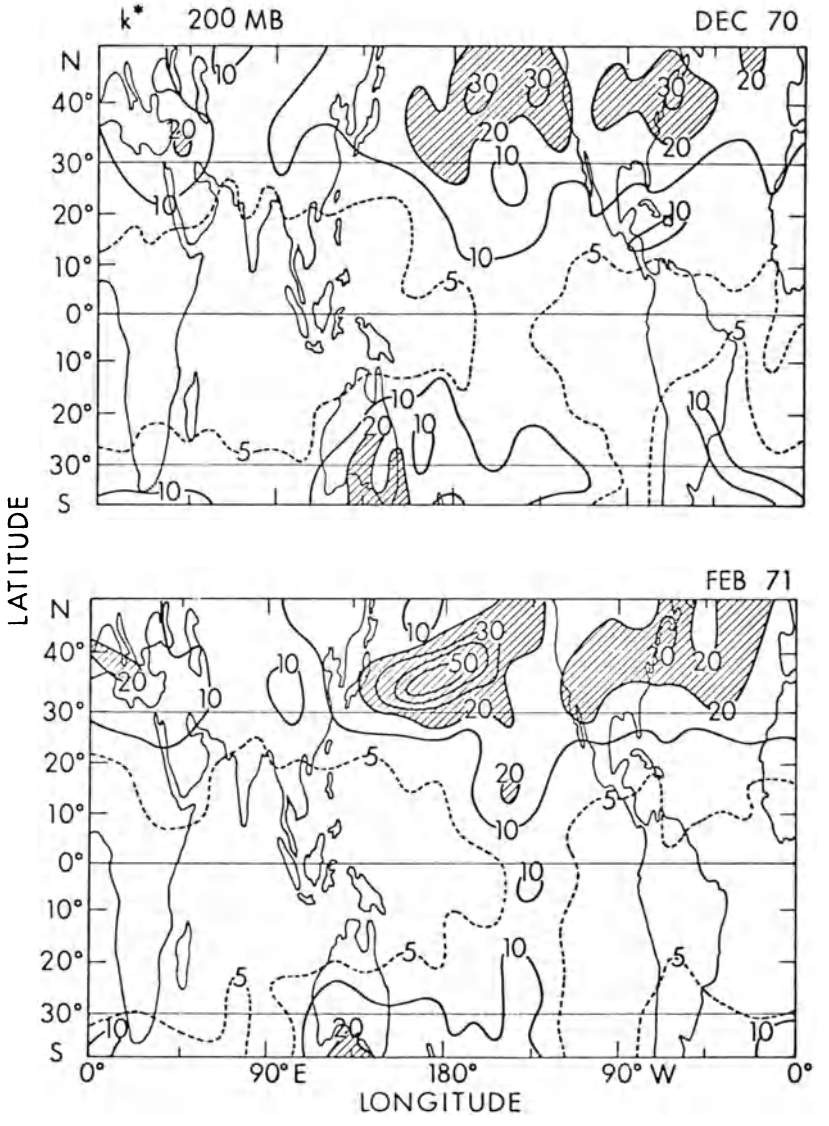

Figure 2

Top: 200 mb k^* during December 1970 in units of 10 m^2 sec^{-2} (every 10 unit interval). Regions of k^* greater than 20 units are shaded. Dashed lines are for 5 units. Bottom: as in the top except for February 1971.

significantly with different regions during the northern winter. To facilitate further study we have selected four limited regions as follows:

Region 1: 24.2°N–44.6°N, 130°E–150°W; waves in the midlatitude westerlies.

Region 2: 0°–19.6°N, 170°W–110°W; strong disturbance activity in the upper oceanic trough and less pronounced activity in low-level trough embedded in the trade winds.

Region 3: 0°–19.6°N, 80°E–140°E; frequent (less frequent) development of low-level disturbances in the near-equatorial trough over the Bay of Bengal and South China Sea during early (late) winter.

Region 4: 0°–19.6°S, 80°E–140°E; tropical disturbances forming in the near-equatorial Southern Hemisphere trough in the vicinity of the Arafura and Timor Seas and propagating west–southwestwards.

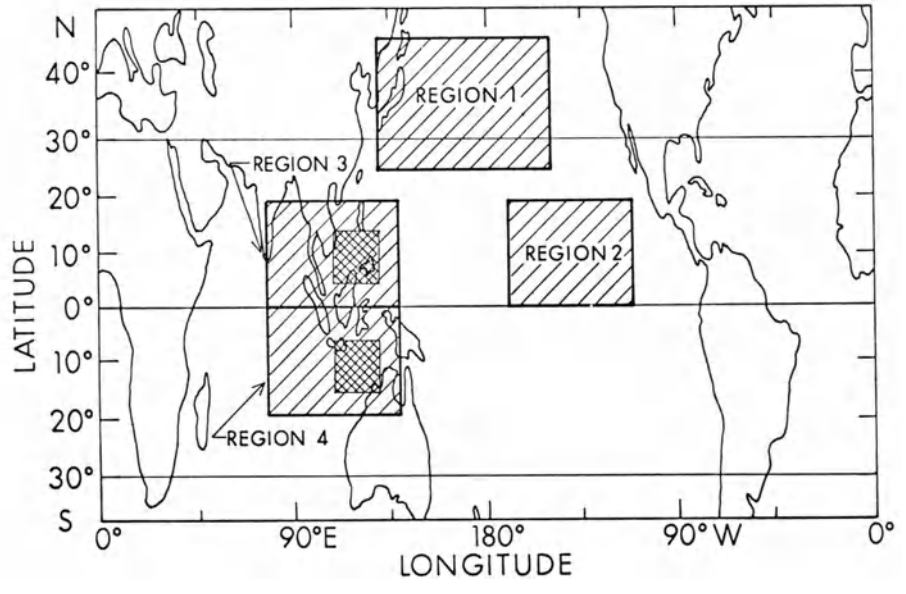

Figure 3
Regions 1 to 4, to which the energy equation (9) is applied. Subregions where the conversion terms (equation (14)) are evaluated are crosshatched.

These regions are shown in Fig. 3. Their dimensions were chosen in order to be large enough to define zonally averaged flow and its departure (eddy), and yet small enough to identify their regional aspects. In Section 5 we investigate the role of both barotropic and baroclinic processes in maintaining the area-averaged eddy kinetic energy over each of the selected regions.

4. Heat sources and sinks

Energy generation due to baroclinic processes is associated with the correlation between vertical motions and temperature perturbations. The vertical motion may be obtained from divergence, directly determined from NMC wind data. The results obtained from this method were checked against daily synoptic conditions and cloudiness changes. As a by-product of this checking, we also calculated the atmospheric heating rate by applying the thermodynamic equation to each region.

As in the NMC wind analyses, the thermodynamic energy equation was expressed on a Mercator map projection as follows:

$$\frac{\partial T}{\partial t} + \sec\theta\left(\frac{\partial uT}{\partial x} + \frac{\partial vT\cos\theta}{\cos\theta\,\partial y}\right) + \sigma\omega = \frac{H}{c_p}, \tag{2}$$

where H is the heating rate per unit mass and the horizontal coordinates are taken as

$$x = a\lambda, \qquad y = a\ln\left(\frac{1+\sin\theta}{\cos\theta}\right), \tag{3}$$

in which a denotes the radius of the earth, λ is longitude, and θ latitude. The measure of static stability σ is defined by

$$\sigma = \frac{T_s}{\theta_s}\frac{\partial\theta_s}{\partial p}, \tag{4}$$

where T_s (θ_s) represents the 90-day mean temperature (potential temperature) averaged over each region. Thus, σ is a function of p alone.

The rate of temperature change in equation (2) was evaluated everyday by

$$\left(\frac{\partial T}{\partial t}\right)_t = \frac{1}{\Delta t}\left(\frac{T_{t-2}}{12} - \frac{2}{3}T_{t-1} + \frac{2}{3}T_{t+1} - \frac{T_{t+2}}{12}\right), \tag{5}$$

where the suffix 't' refers to the quantity on the t-day. The finite difference scheme (5) is fourth-order approximation in $\Delta t = 1$ day and represents a high accuracy.

The flux divergence term in equation (2) was expressed in a finite difference form similar to that in KURIHARA and HOLLOWAY (1967). Thus, when integrated over a limited domain, net flux divergence is determined exactly by the sensible heat transports across the boundaries.

The vertical velocity at the pressure level p was obtained by

$$\omega_p = -\int_{100}^{p} \nabla\cdot V\,dp, \tag{6}$$

where we assumed that $\omega = 0$ at 100 mb. The vertical velocity was computed at 200, 300, 500 and 700 mb, respectively. Based on comprehensive wind and temperature data during AMTEX, NINOMIYA (1975) found that the magnitude and sign of vertical velocity changed significantly with height in the lower troposphere over the Kuroshio region where air mass modification is quite active and the supply of moisture and sensible heat is abundant over the underlying warm water. Since no wind data is available below 700 mb, the vertical integration in equation (6) was performed downward (increasing pressure), rather than upward.

In equation (6), the horizontal divergence was determined directly from NMC wind data as follows:

$$\nabla\cdot V = \sec\theta\left(\frac{\partial u}{\partial x} + \frac{\partial v\cos\theta}{\cos\theta\,\partial y}\right). \tag{7}$$

Table 1

Monthly and season mean heating rate (10^{-5} cal gr^{-1} sec^{-1}) at 200, 300, 500 and 700 mb, over the regions 1 to 4. Also shown is the net heating rate integrated from the 200 mb to 700 mb level over each region, in units of 100 ly day^{-1}. See text for further information.

Month	mb	Region 1	Region 2	Region 3	Region 4
Dec.	200	−0.893	−0.322	−0.039	0.026
	300	−0.257	−0.297	0.067	0.108
	500	0.204	−0.195	0.020	0.103
	700	0.096	−0.299	−0.032	0.080
	Net	−0.284	−1.119	0.077	0.399
Jan.	200	−0.757	−0.268	−0.040	0.038
	300	−0.186	−0.400	0.041	0.176
	500	0.298	−0.272	−0.033	0.246
	700	0.451	−0.394	−0.088	0.233
	Net	0.336	−1.445	−0.098	0.870
Feb.	200	−0.429	−0.117	−0.077	0.028
	300	0.382	−0.250	−0.002	0.172
	500	0.381	−0.181	0.007	0.236
	700	0.319	−0.183	−0.044	0.182
	Net	1.244	−0.846	−0.063	0.800
Season	200	−0.704	−0.240	−0.051	0.031
	300	−0.038	−0.320	0.037	0.152
	500	0.291	−0.219	−0.003	0.195
	700	0.291	−0.298	−0.056	0.166
	Net	0.464	−1.154	−0.028	0.690

Table 1 presents the monthly mean and 90-day mean heating rate, averaged over each region at 200, 300, 500 and 700 mb, respectively. Also shown is the net heating rate in the atmospheric layer between 200 mb and 700 mb (500 mb thickness). The following points are noteworthy:

(1) In the region 1, H is positive (heating) in the lower troposphere while it is negative (cooling) in the upper troposphere. The net heating is a maximum in February, amounting to 124.4 ly/day. KUBOTA (1970) showed that during the northern winter, heat sources exist in the lower troposphere below 500 mb over a region almost identical to our region 1 (the northwestern part of the North Pacific Ocean). He also showed that the maximum value of the heat sources reaches 395 ly/day off the east coast of Japan in January due to the large sensible heat flux from the warm sea surface and to the rather heavy precipitation in the vicinity.

(2) At all levels, H is negative (cooling) over region 2, characterized by dominant descending motions underneath the upper oceanic trough. In the lower troposphere below 500 mb, the diabatic (radiational) cooling approximately balances the adiabatic warming due to prevailing descending motions. In the upper troposphere, the effect due to horizontal temperature advection becomes substantial, although it is still smaller than the vertical advection term in equation (2).

(3) As mentioned earlier, disturbance activity is most pronounced in December over region 3. H is positive (warming) at 300 mb and 500 mb in December. Although H is negative at 700 mb and 200 mb, there exists net heating (7.7 1y/day) in December. In contrast, net H is negative in January and February. The monthly mean cloudiness over region 3 also decreases from December to February; 4.06 okta in December 1970, 4.02 in January 1971 and 3.91 in February 1971.

(4) Region 4 is characterized by positive H at all levels. The net H-heating is somewhat small (39.9 1y/day) in December but large (>80 ly/day) in January and February, probably reflecting the changes in disturbance activity from early to late southern summer. The monthly mean cloudiness averaged over region 4 was 4.17 okta in December and increased to 4.32 (4.35) in January (February) 1971.

We have so far shown that the H-heating rate computed over regions 1 to 4 was compared with the changes in monthly mean cloudiness with reasonable agreement. Perhaps this confirms that NMC wind data is fairly representative of the horizontal and vertical circulations over four limited regions of specific interest. In the next section in which we investigate the energetics over each region, we continue to use the vertical velocity as determined from the continuity equation (6).

5. *Energetics over the limited domains*

We investigate the physical processes responsible for maintaining the area-averaged eddy (not transient eddy) kinetic energy over the four regions of interest. The problem was approached by separating the horizontal motions over each region into zonally averaged flows and departures from them. Based on the primitive equations of motion on a Mercator map projection, the energy equation for eddy motions may be obtained to be[3])

$$\frac{\partial[\overline{K'}]}{\partial t} = I(K, K') + I(K', P') + F(K') + F(P'), \tag{8}$$

where $(\bar{})$ denotes the zonal mean, $(\,)'$ the departure from it, and $[\,]$ the meridional average over the domain. The other quantities are defined as:

[3]) The energy equation for zonally averaged flows is presented in the Appendix. A description of the mechanisms through which zonal mean flows are maintained during the winter, is not pertinent to the main purpose of this paper.

$$K' = \tfrac{1}{2}(u'^2 + v'^2),$$

$$K = \tfrac{1}{2}(\bar{u}^2 + \bar{v}^2),$$

$$I(K, K') = -\left[\overline{u'v'}\frac{\partial}{\partial y}\left(\frac{\bar{u}}{\cos\theta}\right) + \overline{u'\omega'}\frac{\partial \bar{u}}{\partial p}\right] - \left[\overline{v'^2}\frac{\partial \bar{v}}{\cos\theta\,\partial y} + \overline{v'\omega'}\frac{\partial \bar{v}}{\partial p} - \frac{\tan\theta}{a}\overline{\bar{v}u'^2}\right], \quad (9)$$

$$I(K', P') = -\frac{R}{p}[\overline{\omega' T'}], \quad (10)$$

$$F(K') = F_x(K') + F_y(K') + F_p(K') = -\left[\frac{\partial \overline{uK'}}{\cos\theta\,\partial x}\right] - \left[\frac{\partial \overline{vK'}\cos\theta}{\cos^2\theta\,\partial y}\right] - \left[\frac{\partial \overline{\omega K'}}{\partial p}\right], \quad (11)$$

$$F(P') = -\left[\frac{\partial \overline{u'\phi'}}{\cos\theta\,\partial x}\right] - \left[\frac{\partial \overline{v'\phi'}\cos\theta}{\cos^2\theta\,\partial y}\right] - \left[\frac{\partial \overline{\omega'\phi'}}{\partial p}\right] - D(K'). \quad (12)$$

For nondivergent barotropic flows, equation (8) reduces to TRIPOLI and KRISHNAMURTI's (1975) equation (7.1). The terms $I(K, K')$, $I(K', P')$ and $F(K')$ were calculated every day at 200, 300, 500 and 700 mb, respectively. The vertical velocity ω was estimated from the continuity equation. Since data for geopotential height ϕ was not available, the $F(P')$ term was estimated as a residual in equation (8). As shown in equation (12), $F(P')$ is related not only to the convergence of potential energy fluxes across the boundaries but also to frictional dissipation of eddy kinetic energy, $D(K')$. Since the $F(P')$ term is not based on direct measurement, one must be cautious in drawing inferences about the contribution of this term to the maintenance of area-averaged eddy kinetic energy.

The $I(K, K')$ term expresses the interaction between eddies and zonal mean flows over the limited regions. $I(K', P')$ represents the conversion of eddy available potential energy to eddy kinetic energy. $F(K')$ describes the convergence due to eddy kinetic energy fluxes across the boundaries. To help clarify the energetic processes, we separate $F(K')$ into the following three components: east–west flux convergence $F_x(K')$, north–south flux convergence $F_y(K')$, and vertical flux convergence, $F_p(K')$. The results of these calculations are summarized in Tables 2 to 5.

Table 2 for region 1 shows that the 90-day season mean $I(K, K')$ is negative at all levels with a minimum (-13.8×10^{-4} m^2 sec^{-3}) at 200 mb. This means that the kinetic energy of the zonally-averaged motion tends to increase at the expense of the kinetic energy of the eddy motion. Hence, the zonally-averaged flows are considered to be barotropically stable over region 1. This can be substantiated from an inspection of daily 200 mb maps. The jet stream is generally strongest around 35°N. Equatorward of that latitude, the wave axis possesses a pronounced NE–SW inclination,

Table 2

Monthly and season mean $I(K, K')$, $I(K', P')$, $F_x(K')$, $F_y(K')$, $F_p(K')$ and $F(P')$, measured from equations (9)–(12) at 200 mb, 300 mb, 500 mb and 700 mb over the region 1 (see Fig. 3), in units of 10^{-4} m^2 sec^{-3}.

Month	mb	$I(K, K')$	$I(K', P')$	$F_x(K')$	$F_y(K')$	$F_p(K')$	$F(P')$
Dec.	200	−19.298	0.906	23.727	−9.748	−0.351	4.329
	300	−14.632	3.587	16.547	−9.903	−0.297	4.749
	500	−3.326	2.559	5.049	−2.561	0.095	−1.994
	700	−1.049	−0.026	1.476	−0.735	0.368	−0.100
Jan.	200	−12.168	−0.943	4.502	−7.722	0.138	16.501
	300	−7.524	0.274	4.546	−6.822	−0.192	9.815
	500	−1.671	1.792	1.100	−1.804	−0.133	0.716
	700	−0.502	1.480	0.302	−0.715	0.003	−0.590
Feb.	200	−9.460	−1.148	2.826	−8.005	0.824	15.045
	300	−4.713	−1.731	−1.145	−7.994	−0.118	15.853
	500	1.016	0.138	0.170	−2.653	−0.357	1.658
	700	0.700	1.171	0.245	−0.724	0.135	−1.534
Season	200	−13.753	−0.382	10.478	−8.491	0.180	11.956
	300	−9.071	0.785	6.872	−8.215	−0.205	9.932
	500	−1.417	1.550	2.150	−2.244	−0.124	0.087
	700	−0.323	0.879	0.681	−0.724	0.166	−0.710

signifying northward transport of westerly momentum. Since the westerly current increases rapidly northward in the same region, the momentum flux is against the gradient and the conversion of eddy to zonal mean kinetic energy is readily apparent. Poleward of about 35°–45°N, however, the momentum flux is along the gradient, but its magnitude is much smaller since the wave axis tilts less.

A positive sign of $I(K', P')$ indicates the transfer of energy from eddy available potential to eddy kinetic energy. Its winter mean value in Table 2 is positive in the midtroposphere between 300 mb and 700 mb. Near and off the east coast of Japan during the winter, the jet stream is quite strong with large vertical shear, probably indicating active local baroclinic instability. $F_x(K')$ suggests that region 1 receives large amounts of energy due to a flux convergence of eddy kinetic energy across the east–west boundaries. The positive contribution by the term can be seen observationally by the frequent eastward (inward) passage of intensified disturbances through the western boundary near Japan. In Table 2, a negative sign of $F_y(K')$ is due to the overwhelming effect at the southern boundary. Here, transports of eddy kinetic energy are directed southwards; namely, region 1 exports eddy kinetic energy into the tropical North Pacific.

The results of similar calculations for region 2 are shown in Table 3. In this region, frequent disturbance development occurs in and around the oceanic trough

Table 3
As in Table 2 except for region 2.

Month	mb	$I(K, K')$	$I(K', P')$	$F_x(K')$	$F_y(K')$	$F_p(K')$	$F(P')$
Dec.	200	1.501	0.231	1.556	0.697	−0.323	−3.635
	300	1.660	1.170	0.807	−0.408	−0.026	−3.093
	500	0.122	0.719	−0.052	−0.010	0.148	−0.878
	700	0.133	0.723	−0.117	0.001	0.127	−0.839
Jan.	200	2.949	−0.415	1.546	3.158	−0.379	−7.155
	300	1.417	−0.465	2.163	2.397	−0.019	−5.716
	500	−0.195	0.074	0.744	0.173	0.163	−0.995
	700	−0.012	0.924	0.259	−0.037	−0.019	−1.131
Feb.	200	3.955	−0.661	−2.814	2.363	−0.320	−2.459
	300	1.772	−0.323	−1.613	1.888	0.046	−1.843
	500	−0.054	0.550	−0.497	0.116	0.194	−0.308
	700	−0.142	0.167	−0.146	0.010	0.041	0.065
Season	200	2.765	−0.272	0.231	2.088	−0.342	−4.548
	300	1.606	0.130	0.564	1.297	−0.001	−3.660
	500	−0.046	0.435	0.101	0.094	0.167	−0.748
	700	−0.002	0.627	0.010	−0.010	0.049	−0.671

in the upper troposphere. Table 3 shows this to be a region of marked barotropic instability of the upper zonal mean flows, the winter mean $I(K, K')$, at 200 mb amounting to 2.8×10^{-4} m^2 sec^{-3}. Thus, the barotropic instability processes can account, at least partly, for the development of upper disturbances over the eastern tropical North Pacific. Also illustrated in Table 3 is a large convergence of eddy kinetic energy across the north–south boundaries in the upper troposphere. This is primarily associated with the import of eddy kinetic energy across the northern boundary. The winter mean $F_y(K')$ is 2.1×10^{-4} m^2 sec^{-3} at 200 mb. It is somewhat small in December but increases sharply between December and January. In late winter, $F_y(K')$ is as large as the $I(K, K')$ term. This implies that the eddy kinetic energy in the upper troposphere is maintained almost equally by barotropic instability and lateral coupling processes over region 2. According to 200 mb streamline analyses of SADLER (1975), the jet stream tends to shift slightly southward while increasing its speed from early to late winter over an extensive region covering north India, south China, and the western and central North Pacific. Perhaps, this favors more frequent southward penetration of midlatitude waves into the tropical North Pacific and results in larger $F_y(K')$ value in late winter. In comparison, the small $F_p(K')$ term may suggest that vertical coupling is not as important as lateral coupling in maintaining eddy kinetic energy in region 2. In Table 3, of interest is a tendency for eddy kinetic energy to slightly decrease (increase) in the upper (lower) troposphere due to the $F_p(K')$ effect; namely, low-level eddy motions tend to develop at the expense of the kinetic energy of the eddy motion in the upper troposphere.

Table 4
As in Table 2 except for region 3.

Month	mb	$I(K, K')$	$I(K'P')$	$F_x(K')$	$F_y(K')$	$F_p(K')$	$F(P')$
Dec.	200	−0.713	−0.348	0.479	−0.805	−0.009	1.373
	300	−0.202	0.040	0.370	0.077	−0.007	−0.302
	500	0.157	−0.229	0.274	0.087	0.002	−0.364
	700	−0.047	−0.187	0.152	−0.052	−0.012	0.052
Jan.	200	−0.206	0.148	0.459	−0.645	0.020	0.197
	300	−0.334	−0.020	0.416	−0.255	−0.046	0.240
	500	0.573	0.003	−0.009	0.007	−0.066	−0.521
	700	0.031	0.019	−0.075	−0.026	−0.073	0.129
Feb.	200	−0.135	−0.058	−0.052	−0.409	−0.007	0.683
	300	−0.083	−0.094	0.090	−0.299	−0.049	0.453
	500	−0.366	−0.016	0.102	0.165	0.011	0.096
	700	0.065	−0.499	0.065	0.062	0.066	0.244
Season	200	−0.356	−0.082	0.312	−0.627	0.002	0.740
	300	−0.214	−0.022	0.302	−0.156	−0.034	0.122
	500	0.149	−0.081	0.120	0.082	−0.020	−0.281
	700	0.015	−0.207	0.044	−0.008	−0.010	0.138

Table 4 summarizes the energy conversion and boundary flux convergence terms computed for region 3. They are much smaller and harder to corroborate with observational evidence than the corresponding results for regions 1 and 2. The winter mean $I(K, K')$ term is positive and small below 500 mb suggesting weak barotropic instability. Season mean $I(K', P')$ is negative implying baroclinic stability. These results appear to contradict expectations of substantial barotropic and/or baroclinic instability in region 3, where tropical disturbances frequently develop over the South China Sea and Bay of Bengal.[4]) A positive $F_x(K')$ term is probably due to the frequent passage of westward moving disturbances through the eastern boundary (east of the Philippines) and less frequent eddies across the western boundary (near India). Winter mean $F_y(K')$ is small and negative, implying a net meridional export of eddy kinetic energy across the north–south boundaries. On the contrary, it is very likely that region 3 gains large amounts of eddy kinetic energy through the northern boundary where strong NE monsoonal trades dominate the lower troposphere with maximum speed near 850 mb. A detailed monitoring of low-level winds is, thus, essential to identify the dynamical and thermal structure of monsoon surges to which the development and structure of South China Sea disturbances may be related.

[4]) Interestingly, though $I(K, K')$ and $I(K', P')$ are small and seem to contribute little to the maintenance of the eddy kinetic energy of region 3, their daily fluctuations corresponded rather well with the time changes in K'. This will be reported elsewhere.

Table 5
As in Table 2 except for region 4.

Month	mb	$I(K, K')$	$I(K',P')$	$F_x(K')$	$F_y(K')$	$F_p(K')$	$F(P')$
Dec.	200	−0.301	−0.004	−1.506	0.167	0.074	1.463
	300	−0.051	0.169	−0.791	0.365	0.028	0.266
	500	0.011	−0.089	−0.174	0.237	−0.042	0.075
	700	0.092	−0.103	−0.080	0.099	−0.064	0.025
Jan.	200	−0.059	0.009	−0.270	0.114	0.044	0.202
	300	−0.099	0.012	−0.142	0.171	0.077	−0.016
	500	−0.036	0.071	0.132	−0.105	0.023	−0.063
	700	0.090	−0.016	0.207	−0.098	−0.020	−0.063
Feb.	200	−0.506	−0.120	−0.396	−0.247	0.049	1.177
	300	−0.363	−0.059	−0.125	−0.043	0.078	0.551
	500	−0.059	0.017	0.149	−0.228	0.018	0.089
	700	0.021	−0.091	0.024	−0.076	−0.050	0.189
Season	200	−0.276	−0.034	−0.725	0.023	0.056	0.922
	300	−0.163	0.044	−0.356	0.172	0.061	0.251
	500	−0.027	0.000	0.034	−0.027	−0.000	0.029
	700	0.070	−0.068	0.055	−0.025	−0.044	0.043

Tropical disturbances are also quite common over region 4 during the southern summer. Despite this, the baroclinic conversion term $I(K', P')$ is near zero or even negative over region 4 (Table 5). Perhaps this puzzling discrepancy is due, in part, to the sparsity and poor quality of the data over regions 3 and 4, and the lack of low-level data. It is also possible that the regional energetics were applied to too large an area; i.e., active and inactive subregions may have been compounded together to yield misleading results. This was ascertained by computing the conversion term $I(K', P')$ over a subsection 3 (5.0°N–14.8°N, 110°E–130°E) and subregion 4 (5.0°S–14.8°S, 110°E–130°E), crosshatched in Fig. 3. These are two of the most active subregions of disturbance development during the northern winter. The conversion term was defined by

$$-\frac{R}{p}[\overline{\omega T}], \tag{13}$$

where T and ω represent the departure from the globally averaged zonal mean temperature and vertical velocity, respectively.[5])

In Table 6, it is evident that baroclinic processes are, at least partly, responsible for maintaining eddy kinetic energy in both subregions. This conclusion is tentative

[5]) Since the subregions are too small to define regionally averaged zonal flows and eddies, no attempt was made to evaluate other energetic terms, including the barotropic interaction term.

Table 6
Monthly and season mean conversion term, measured from equation (13) at 200 mb, 300 mb, 500 mb, and 700 mb (10^{-4} m^2 sec^{-3}) over the subregions 3 and 4 (see Fig. 3).

mb	Dec.	Jan.	Feb.	Season
	Subregion 3			
200	0.108	0.359	−0.351	0.060
300	1.837	0.697	1.926	1.453
500	0.425	−0.627	0.789	0.156
700	0.468	−0.212	−0.743	−0.144
	Subregion 4			
200	0.387	0.749	0.175	0.453
300	0.563	0.763	0.203	0.526
500	0.476	0.435	−0.062	0.299
700	0.152	0.517	0.091	0.265

because of the uncertainty in obtaining accurate vertical velocity and temperature in the tropics. However, there are grounds for believing that the results may at least be qualitatively correct. Over the subregion 3 (South China Sea), the conversion term is positive with substantial magnitude in December, while small and even negative at some levels in January and February. This reflects the differences in South China Sea disturbance activity between early and late winter. In subregion 4 (Timor Sea), the conversion term is a maximum at almost all levels, congruent with pronounced activity there, in January. In short, baroclinic processes can, at least partly, account for disturbance development over the South China Sea and the Timor Sea. Unless we have data at many more levels, particularly in the lower troposphere, it is not possible to identify other important physical processes responsible for initiating these disturbances. Further study is certainly needed in order to understand the relationship between cold monsoonal surges and disturbance development over the South China Sea.

Table 7 presents the monthly mean and season mean H-heating rate, averaged over each subregion. In subregion 3, the net H-heating rate amounts to about 80 ly/day in December and decreases to 13 ly/day in January. Conspicuously, it increases sharply from January to February, reaching 106 ly/day in February. Why the net H-heating is a maximum in February (not in December) is not yet known. In subregion 4, the net H-heating is somewhat small (29 ly/day) in December but large ($>$ 200 ly/day) in January and February, probably reflecting more pronounced disturbance activity in late than early southern summer. Limited research on the Australian summer monsoon has revealed that it possessed relatively poorly developed monsoon rains. In comparison, the Indian summer monsoon is associated with strong heat sources, exceeding 400 ly/day in July and August (KUBOTA, 1970).

Table 7
Monthly and season mean H heating rate over the subregions 3 and 4. Refer to Table 1 for further information.

mb	Dec.	Jan.	Feb.	Season
	Subregion 3			
200	0.012	−0.003	0.113	0.037
300	0.179	0.045	0.250	0.152
500	0.202	0.025	0.267	0.158
700	0.116	0.014	0.098	0.074
Net	0.795	0.130	1.064	0.637
	Subregion 4			
200	0.057	0.192	0.115	0.124
300	0.124	0.473	0.356	0.320
500	0.054	0.558	0.500	0.371
700	−0.033	0.388	0.498	0.279
Net	0.290	2.309	2.091	1.562

6. *Concluding remarks*

In this study, NMC wind data and USN temperature data were used to investigate the maintenance of local area-averaged eddy kinetic energy over four limited domains of specific interest during the northern winter. The main results of this study are:

(1) The upper-level zonal flow over the extratropical North Pacific (region 1, Fig. 3) is found to be barotropically stable; namely, zonally averaged flows gain large amounts of energy from eddy motions through barotropic interaction processes. Of interest is a large export of eddy kinetic energy across the southern boundary into the tropical North Pacific.

(2) In contrast to region 1, zonally averaged flows are barotropically unstable over region 2 (tropical eastern North Pacific). This is one mechanism responsible for the development of disturbances in the upper oceanic trough. Eddy motions there are also maintained by energy fluxes through the northern boundary.

(3) An examination of the energetics over subregion 3 (South China Sea) and subregion 4 (Timor Sea) reveals that eddy motions are most probably supported by the conversion of eddy available potential to eddy kinetic energy.

The foregoing is admittedly somewhat speculative, being based on NMC and USN operational analysis data of, perhaps, questionable accuracy and coverage in certain regions. More research needs to be done to understand the basic mechanisms through which tropical disturbances are generated and maintained over the South China Sea and Indonesian Seas. Perhaps, this problem can best be investigated during

the Winter Monsoon Experiment in 1978–79. Hopefully, more definite energetic measurements will be feasible when the final validated FGGE/MONEX data set becomes available.

Acknowledgments

The author is indebted to Mrs. M. Frydrych for programming assistance. He also thanks Mrs. S. Artia for typing the manuscript.

This research has been supported by the Global Atmospheric Research Program, Climate Dynamic Research Section, National Science Foundation, Washington, D.C., under Grant No. ATM76–02502.

Appendix

The kinetic energy equation for zonal mean flows over a limited domain may be expressed as

$$\frac{\partial[K]}{\partial t} = -I(K, K') + I(K, P) + F(K) + F(P), \tag{A1}$$

where

$$I(K, P) = -\frac{R}{p}[\bar{\omega}\bar{T}],$$

$$F(K) = -\left[\frac{\partial(\overline{uK + \bar{u}u'^2 + \bar{v}u'v'})}{\cos\theta\,\partial x}\right] - \left[\frac{\partial(\bar{v}K + \bar{u}\overline{u'v'} + \bar{v}\overline{v'^2})\cos\theta}{\cos^2\theta\,\partial y}\right] - \left[\frac{\partial(\overline{\omega K + \bar{u}u'\omega'} + \bar{v}\overline{v'\omega'})}{\partial p}\right]$$

$$F(P) = -\left[\frac{\partial(\overline{u\phi + \bar{u}\phi})}{\cos\theta\,\partial x}\right] - \left[\frac{\partial v\overline{\phi}\cos\theta}{\cos^2\theta\,\partial y}\right] - \left[\frac{\partial\omega\overline{\phi}}{\partial p}\right].$$

The flux term $F(K)$ is associated with boundary fluxes not only of zonal mean kinetic energy but also of other physical quantities, not directly related to kinetic energy. In comparison, the $F(K')$ term defined in equation (8) is explicitly related to boundary fluxes of eddy kinetic energy. A question of uniqueness for equations (8) and (A1) arises because of the difficulty in discriminating between boundary fluxes and internal conversions in an open system. This was previously discussed by TRIPOLI and KRISHNAMURTI (1975).

An alternative definition of the interaction term may be

$$\{K, K'\} = \left[\bar{u}\left(\frac{\partial\overline{u'v'}\cos^2\theta}{\cos^2\theta\,\partial y} + \frac{\partial\overline{u'\omega'}}{\partial p}\right)\right] + \left[\bar{v}\left(\frac{\partial\overline{v'^2}\cos\theta}{\cos^2\theta\,\partial y} + \frac{\partial\overline{v'\omega'}}{\partial p} + \frac{\tan\theta}{a}\overline{u'^2}\right)\right]. \quad \text{(A2)}$$

In an open system associated with fluxes of energy and other physical quantities across the boundaries, $\{K, K'\}$ in equation (A2) is not equal to $I(K, K')$ in equation (9). The difference between the two turns out to be substantial over region 1 but less significant over other regions.

References

Bryant, K. (1958), *Comparison of months giving extremes of rainfall during north–east monsoon at Changi, Singapore Island,* Meteor. Mag. *87*, 307–312.

Kubota, I. (1970), *Seasonal variation of energy sources in the earth surface layer and in the atmosphere over* the northern hemisphere, J. Meteor. Soc. Japan *48*, 30–46.

Kurihara, Y. and Holloway, J. L. (1967), *Numerical integration of a nine-level global primitive equation model formulated by the box method,* Mon. Wea. Rev. *95*, 509–530.

Manabe, S., Holloway, J. L. Jr. and Stone, H. M. (1970), *Tropical circulation in a time-integration of a global model of the atmosphere*, J. Atmos. Sci. *27*, 580–613.

Murakami, T. and Unninayar, M. S. (1977), *Atmospheric circulation during December 1970 through February 1971*, Submitted to Mon. Wea. Rev.

Ninomiya, K. (1975), *Large-scale aspects of air-mass transformation over the East China Sea during AMTEX '74*, J. Meteor Soc. Japan *53*, 285–303.

Ramage, C. S. (1968), *Role of a tropical 'maritime continent' in the atmospheric circulation,* Mon. Wea. Rev. *96*, 365–370.

Sadler, J. C. (1975), *The upper tropospheric circulation over the global tropics*, Tech. Rept. Grant No. GA–36301, Department of Meteorology, University of Hawaii, 35 pp.

Tripoli, G. J. and Krishnamurti, T. N. (1975), *Low-level flows over the GATE area during summer 1972*, Mon. Wea. Rev. *103*, 197–216.

(Received 15th June 1977)

Pageoph, Vol. 115 (1977), Birkhäuser Verlag, Basel

Synoptic Features and Structures of some Equatorial Vortices Over the South China Sea in the Malaysian Region During the Winter Monsoon, December 1973

By BOON KHEAN CHEANG[1])

Abstract – In December 1973, Peninsular Malaysia and Sarawak[2]) experienced a few periods of heavy rain caused by westward moving equatorial vortices from the South China Sea. In this report, the synoptic characteristics associated with the development and intersification of these vortices are shown. Structure of one of the disturbances was examined. Disturbances in the trades associated with lateral shear were found to be important for the genesis of the equatorial vortices. However, the intensification of these disturbances depended on the interaction with the cold monsoon surge.

Key words: Monsoon: Synoptic features; Equatorial vortices.

1. Introduction

Climatologically, the near-equatorial trough in December lies just north of the equator between 60E and 160E. Cyclonic vortices are known to form in the troughs of the lower troposphere over the equatorial regions of the South China Sea and the West Pacific. These disturbances generally move slowly westwards bringing widespread heavy rain, particularly to Sarawak and the east coast of Peninsular Malaysia. Occasionally these equatorial vortices intensify into depressions when there are outbreaks of intense cold surges from the Asiatic Continent. These depressions are associated with torrential rain bringing about severe flooding and caused serious damage to the economy of the country. For an example, the total cost of damage due to torrential rain and flooding caused by the 3rd Jan. 1971 depression amounted to about U.S.$25 million. The fact that these equatorial vortices intensify into depressions only in the presence of cold surges from the Asiatic Continent indicates that there is a strong lateral interaction between the extratropical westerly circulation and these equatorial disturbances. Some causes appear to link the heat source over the Malaysian region, the equatorial easterly regime and the extratropical westerly circulation system. However the exact mechanisms of this interaction is not yet

[1]) Malaysian Meteorological Service, Jalan Sultan, Petaling Jaya, Selangor, Malaysia.

[2]) Sarawak is a state in East Malaysia. It is situated in the northwestern part of the Borneo Island.

known. This study has not been possible, primarily due to the lack of upper air data over the South China Sea. It is probably due to the same reason that several authors did not study the development of the equatorial vortices in their studies on heavy rainspells in Malaysia caused by cold monsoon surges.

The network of upper air stations in Malaysia has been improving since 1971. This has helped to improve the analyses of the weather charts. Hence an attempt is now made to study the general synoptic features associated with the development and intensification of the heavy-rain producing equatorial vortices. The month December 1973 was chosen for this study because five equatorial vortices developed and intensified in the presence of cold surges bringing along heavy rain.

The first part of this report summarises the synoptic characteristics associated with the development and intensification of the disturbances. In the second part of the report, the development and the structure of the vortex which occurred during the period, 4–9 December 1973 were examined more closely. It was selected because the density of upper air data was the best.

Composite method was used to increase the upper air data. Based on the composite data, computation of the fields of relative vorticity, divergence and kinematic vertical motion was carried out for the disturbance on 7–8 December 1973.

A brief discussion is also made on the genesis and maintenance of the disturbances.

2. *Previous studies*

Low tropospheric vortices in the tropics have been studied by many authors (SADLER, 1967; CARLSON, 1969; PEDGLEY and KRISHNAMURTI, 1976). In recent years there has been considerable controversy over the origin of these vortices. That is whether they develop from wave disturbance (FETT, 1966; YANAI, 1961) or in the wind shear zone between two opposing currents (SADLER, 1967)?

In the equatorial region, PALMER (1952) studied the equatorial easterly wave.

In the Malaysian region several authors have studied the occurrences of heavy rainspells during the winter monsoon. WATTS (1955) described the occurrence of heavy rainspells over Peninsular Malaysia as taking place on air-stream boundaries. According to him, the line separating two streams of similar properties in the equatorial region is defined as an 'Air-stream boundaries'. This definition is not widely used.

BRYANT (1958) attributed the extremes of rainfall during northeast monsoon at Singapore to near equatorial depressions. GAN (undated) noted that heavy rain occurred along the east coast of the Malayan Peninsular following the appearance of a large cold anticyclone over China during the winter monsoon with subsequent movement of a cold front into the South China Sea from China, and low level strengthening of the northeast trades. Associated with this, he also noted the presence of a zonal northeasterly flow of width about 10° latitude and a maximum strength

of 15 knots or more, stretching from Guam Island in the Pacific to the vicinity of Ceylon during days of heavy rain in Peninsular Malaysia. He concluded that equatorial westerlies were often present. Conversely, he noted that there was no heavy rain in Peninsular Malaysia when a tropical cyclone was present over the South China Sea north of 9°N. Using Hong Kong surface pressure data, he showed how they could be used to forecast the occurrence of heavy rain in Peninsular Malaysia.

RAMAGE (1971) studied the heavy rain in Sarawak during the occurrence of nonfrontal surges, and attributed the rain to the presence of active Hadley cell.

In most of these studies on heavy rain spell over Malaysia during the winter monsoon, no reference was made to the westward propagating or quasi-stationary equatorial vortices and the presence of low-level easterly jet over the northern part of Peninsular Malaysia or South Thailand. Therefore the author feels that synoptic studies such as those presented here may be relevant.

3. *Synoptic features associated with the development and intensification of the equatorial vortices during December 1973*

In December 1973, five equatorial vortices formed over the South China Sea. Only three of the vortices on the 3rd, 9th and 14th are shown clearly in Fig. 1 which is a time section of 850 mb winds along longitude 102°E (across Peninsular Malaysia) from the equator to latitude 15°N. The heavy rain periods are also indicated by arrows below the time axis in Fig. 1. Two other vortices on the 21st and 26th do not

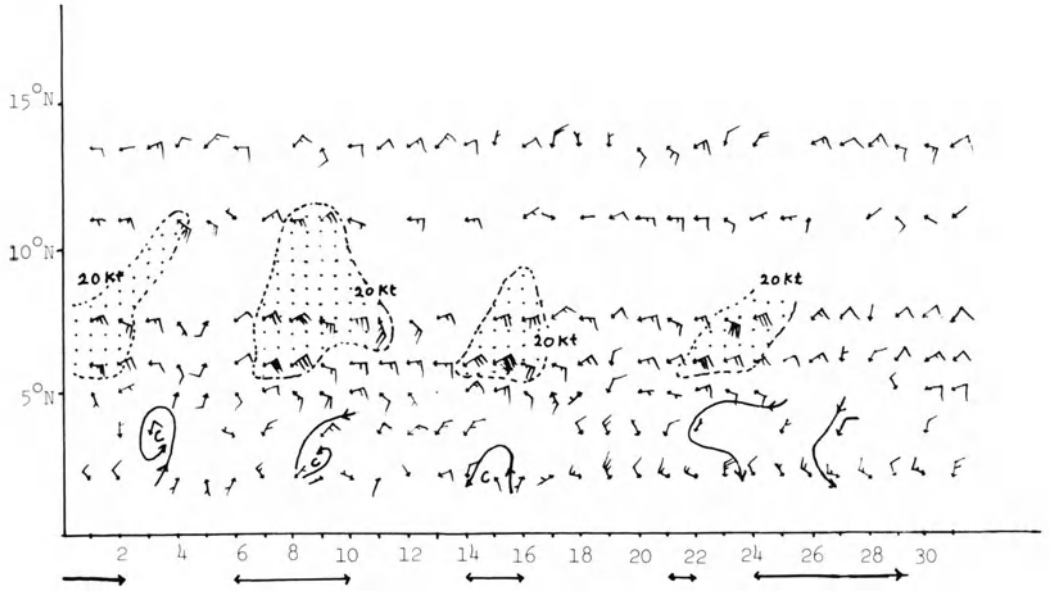

Figure 1
Time cross-section of 850 mb winds along 102°E December 1973. ↔ heavy rain period.

show out clearly in this time section because they dissipated before reaching Peninsular Malaysia. In fact, the one on the 26th brought about heavy rain only to Sarawak. This is the normal pattern as equatorial vortices which develop during late December and January usually bring heavy rain only to Sarawak.

850 mb streamline charts for December 1973 show that three of the five equatorial vortices were observed to develop in the near-equatorial trough during the presence of cold surges over the South China Sea. Conversely, the other two vortices developed before the presence of cold surge. In the following section, it will be shown that they formed from pre-existing disturbances in the easterlies of the near-equatorial trough.

3.1. Disturbance in the easterlies of the near-equatorial trough

Although the near-equatorial trough is a persistent feature over the South China Sea during the winter monsoon, its intensity varies accordingly to the variation of lateral shear which is mainly controlled by the strength of the trades. Intensity of the trades probably depends on the position and the intensity of the subtropical high over the West Pacific. Whether the trades in the low levels can penetrate the South China region during the winter monsoon depends very much on the cold monsoon surge activity. This was clearly shown by KRISHNAMURTI and PAN's film (1977).

To verify the latter statement, an analysis of the surface winds obtained from ship reports over the South China Sea was carried out. An example is shown in Fig. 2

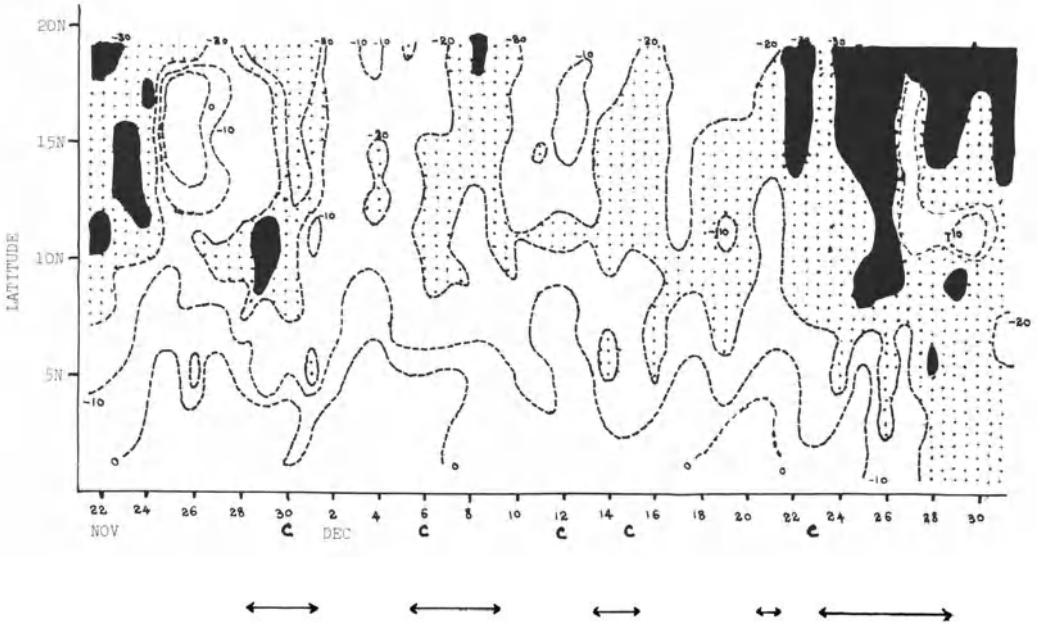

Figure 2
Northerly surge over the South China Sea November–December 1973. ↔ heavy rain period, ⊡ ≥ 20 Kt, ■ ≥ 30 Kt.

for 22 November–31 December 1973. Surface winds were resolved into N and S components, and isotachs were drawn at intervals of 10 knots. This method of analysis had been carried out by RAMAGE (1971). Five periods of cold northerly surges extending from latitude 20°N can be noted. They are 28 November–1 December, 7–10 December, 14–16 December, 21–26 December and 28–31 December. The earlier period of strong northerly winds, 22–25 November, is connected with typhoon activity. During the intervals between successive cold northerly surge periods, we can notice northerly wind maxima between latitudes 15N and 5N. They occurred during the following periods, 3–6 December, 10–13 December, 17–20 December. These must be caused by the penetration of the strengthening trades when the cold monsoon surges weakened. The period of occurrence from one to another is roughly a week. The days when the vortices were first detected were indicated by the letter *C* below the time axis in Fig. 2. Lateral shear was strong during these days due to the presence of strong northerly winds.

Comparison with the cloudiness during the same period over the South China Sea between 110° and 112.5°E (Fig. 3) shows some interesting results. This cloudiness was estimated in okta from satellite pictures. Isolines were drawn at intervals of 2 okta. Cloudiness extending southwards from latitude 20°N was connected with cold surge. There was also fairly good relation between the increase in maximum northerly

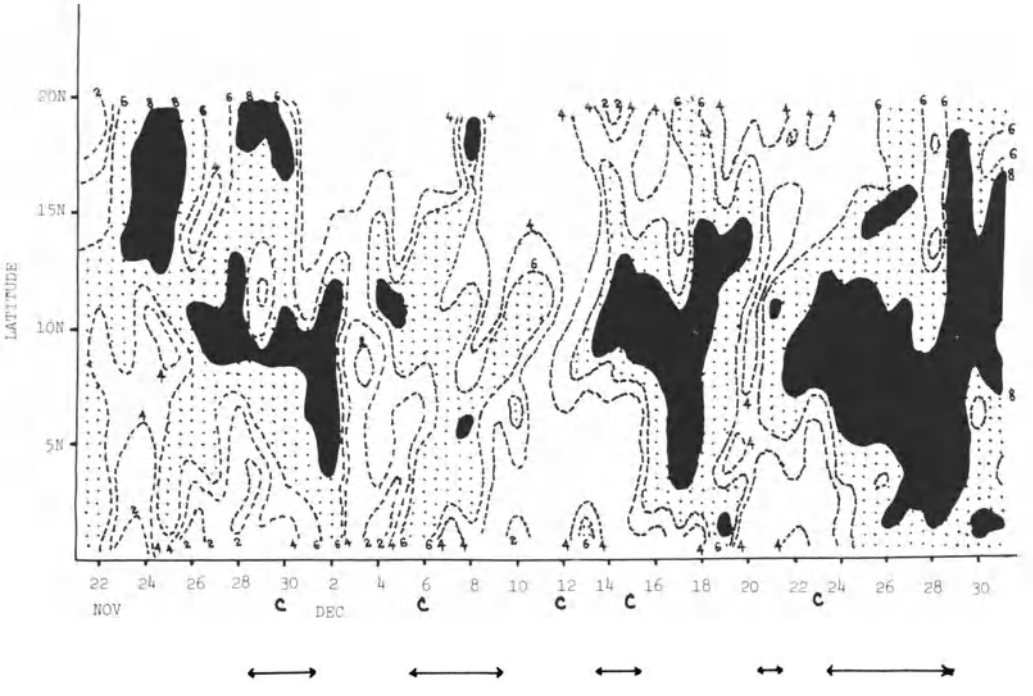

Figure 3
Cloudiness estimated from satellite pictures between longitudes 110°–112.5°E November–December 1973. ↔ Heavy rain period, ⊡ 6–7 okta, ■ 8 okta.

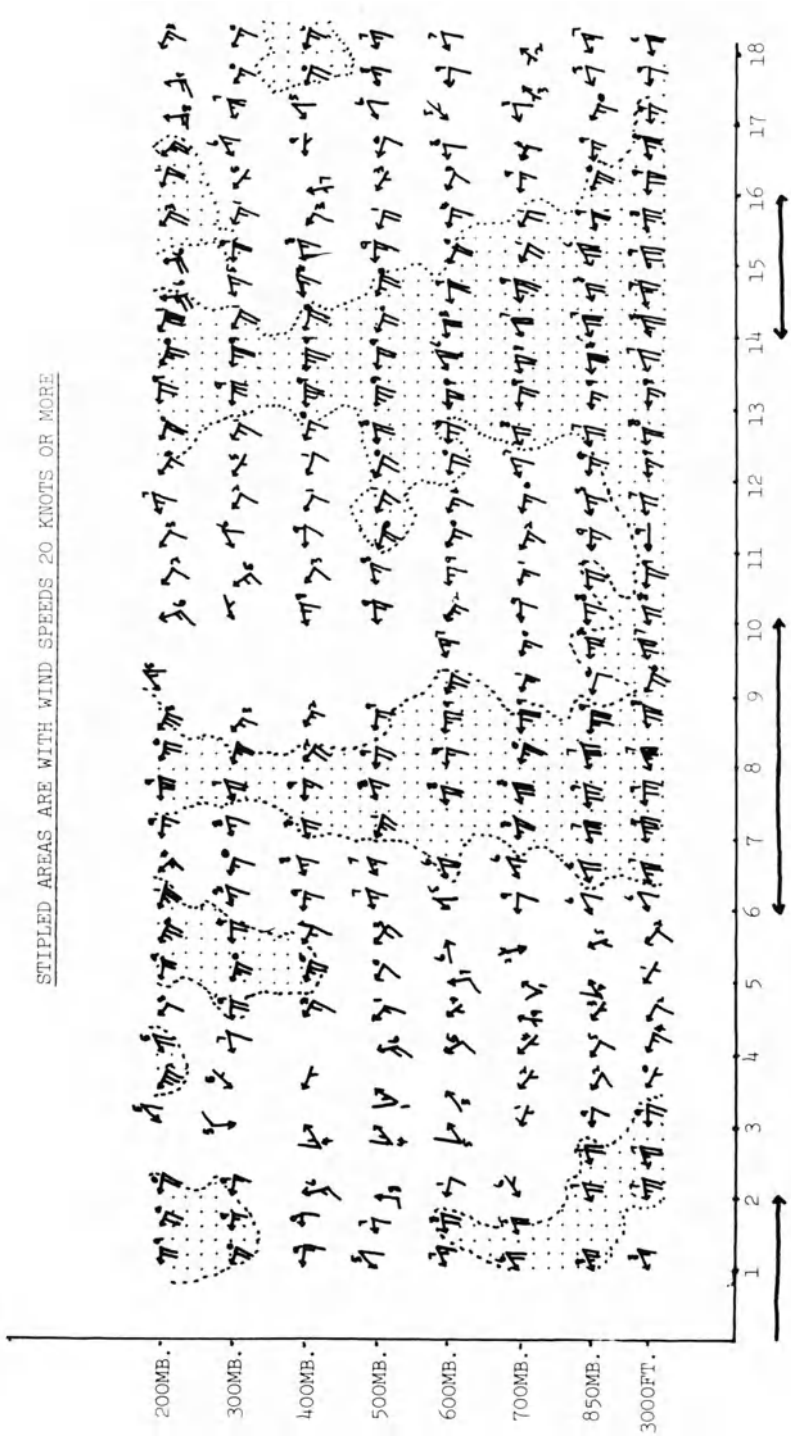

Figure 4
Vertical time series – Kota Bharu, 1–18 December 1973. ↔ Heavy rain period.

wind during the interval (nonsurge) period and the increase in cloudiness between latitudes 15N and 5N. This illustrates the importance of lateral shear in the formation of cloud clusters as has been shown by WILLIAMS (1970).

Examination of the vertical time series for the same period at Kota Bahru (situated at about latitude 6°N) reveals some interesting features (Figs 4 and 5). There were fluctuations in the easterlies in deep layer occurring at intervals of about one week. The strengthening of the easterly winds at 850 mb and below was attributed to the cold surge, while those in the middle and upper troposphere cannot be due to the same cause. If compared with the surface maximum trades over the South China Sea (Fig. 2) during the nonsurge period, the fluctuation in the easterlies in the middle and upper troposphere over Kota Bahru seems to lag about four days behind. It should be noted that Kota Bahru is located along longitudes 102°E, while South China Sea surface winds shown in Fig. 2 were taken from area between longitude 110°E and 115°E.

Examination of the surface winds over the South China Sea and vertical time series for other months also reveals the same phenomenon except that the fluctuation in the easterlies in the middle and upper troposphere did not occur at a regular period of one week or four to five days as has been noted in West Pacific (YANAI *et al.*, 1968; WALLACE, 1969; REED, 1970). From the above, it is suspected that most of the

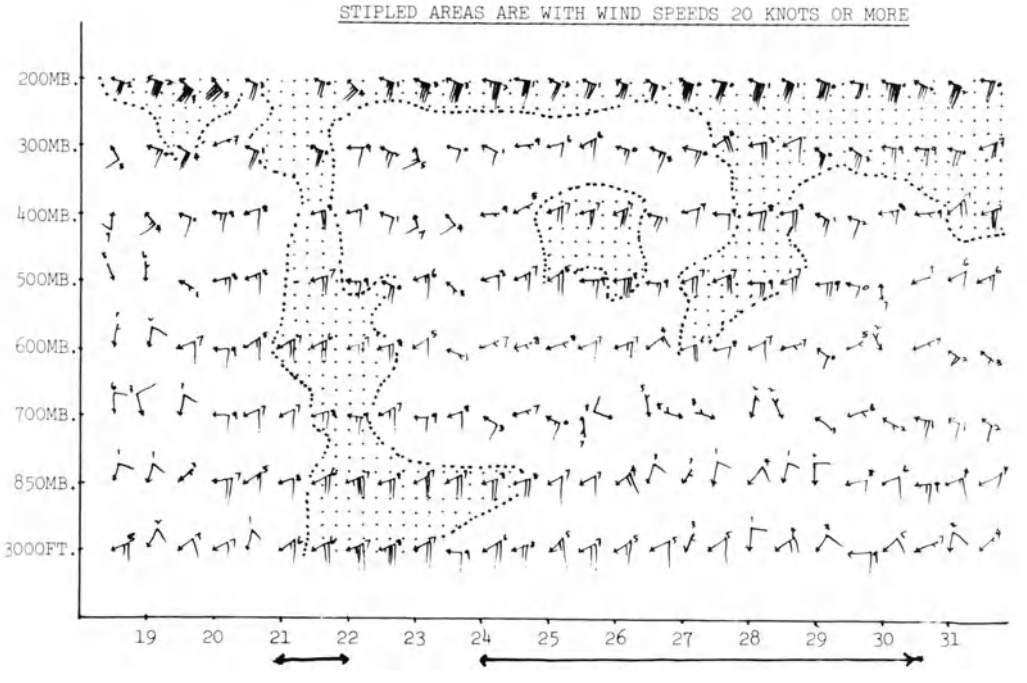

Figure 5
Vertical time series – Kota Bharu, 19–31 December 1973. ↔ Heavy rain period.

heavy rain producing equatorial vortices in this study might have initiated from disturbances in the trades which possessed significant lateral shear.

3.2. Cold monsoon surges and low-level easterly jet

RIEHL *et al.* (1969) observed that the Asiatic anticyclone which was associated with cold monsoon surges was confined only in a shallow layer in South China extending from surface to 850 mb. They also noted that at 700 mb, the passage of a short wave westerly trough across East China is usually accompanied by cold monsoon surges. Fig. 6 shows the time section of 700 mb winds along longitude 115°E over China from latitude 20°N to 35°N. Thick lines are streamlines while thin dashed lines are trough axes. Isotherms drawn at −5°C interval are depicted by thin lines. Four westerly wave troughs moved across 115°E on the 6th, 13th, 21st and 26th. The third trough was followed by persistent northwesterlies which were enhanced by another shorter trough on the 26th. The southward dip of the isotherms behind every trough indicates the cold outbreaks. There is also a general tendency of southward dip of the isotherms towards the end of the month. This shows that the cold monsoon surge became more intense. Comparing Fig. 2 and Fig. 6, it is observed that the South China Sea surface winds freshened from latitude 20°N southwards almost on the same day when the northwesterlies behind the 700 mb trough axis invaded southwards to latitude 25°N. It is during these periods of cold surges that the five vortices intensified and brought along heavy rainfall. The periods of heavy rainfall are depicted in both Figs. 2 and 6. Therefore, the development of the short

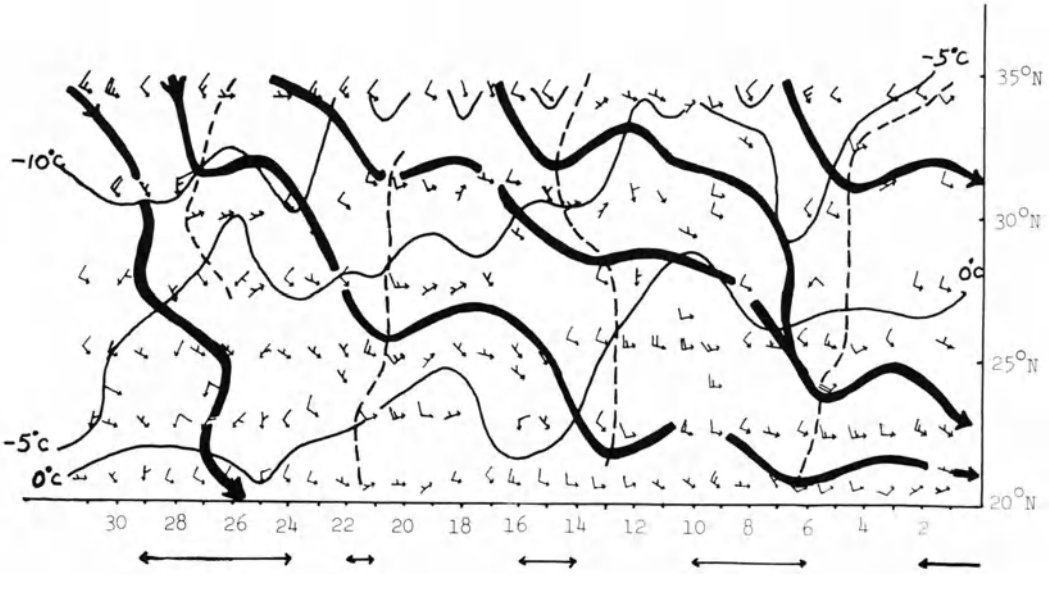

Figure 6
Time section of 700 mb winds along longitude 115°E over China, December 1973. ↔ Heavy rain period.

wave westerly trough over East China and the equatorial vortices over the South China Sea should be viewed as an integral part of the lateral interaction processes occurring over a fairly extensive region.

Another important feature connected with the cold surge is the presence of low-level easterly jet. From vertical time series, it has been found to appear most frequently at 850 mb. In extreme case, its speed can reach a maximum of 48 knots (CHEANG, 1977). In December 1973, four jets are clearly shown during the heavy rain periods in Fig. 1. They were generally of 5° width (from 5°N to 10°N). Due to lack of upper air data, it is not possible to study the horizontal and vertical structures of the jets. Nevertheless vertical time series at Kota Bahru (Figs. 4 and 5) do show some interesting features. During the heavy rain periods the easterly maximum in the middle and upper troposphere as mentioned in Section 3.1 cannot be caused by the cold surge. Due to the presence of deep and steady easterly winds vertical shear is weak between the surface and the upper troposphere. On the other hand, due to the presence of the low-level jet, the vertical shear is much stronger between the lower and middle troposphere. It can reach a value of about 20 knots between 850 mb and 600 mb (Figs. 4 and 5). Therefore the jets possessed strong lateral shear and vertically in the lower troposphere, they possessed considerable vertical shear. Hence mixed barotropic and baroclinic instability may be involved in the energy transformation process for the maintenance of the depressions (BURPES, 1972; PEDGLEY and KRISHNAMURTI, 1976).

Furthermore, it is observed that during the last cold surge when heavy rain occurred only in Sarawak caused by the depression on the 26th, the low-level easterly jet was absent over Peninsular Malaysia (Figs. 1 and 5). It is suspected that the intense cold surge could have caused the easterly (or northeasterly) jet to move southwards. At 700 mb (Fig. 5), the northwesterlies at Kota Bahru due to the intense cold surge had prevented the penetration of the trades. At higher levels, the easterly disturbance was not affected. This feature is distinctly different from that associated with depressions which brought along heavy rain to Peninsular Malaysia in the earlier part of December 1973.

4. Synoptic features and structure of a cyclonic vortex

It is not possible to show the synoptic features of all the five disturbances in this report. Hence the one which has better upper air data coverage is selected. The period chosen is 4–9 December 1973.

4.1 Synoptic features

The streamline analyses at 850 mb, 700 mb, 500 mb and 200 mb are illustrated in Figs. 7–17. The 700 mb, 500 mb, and 200 mb analyses are shown only for the 6th and 7th when the disturbance was at its intensification stage.

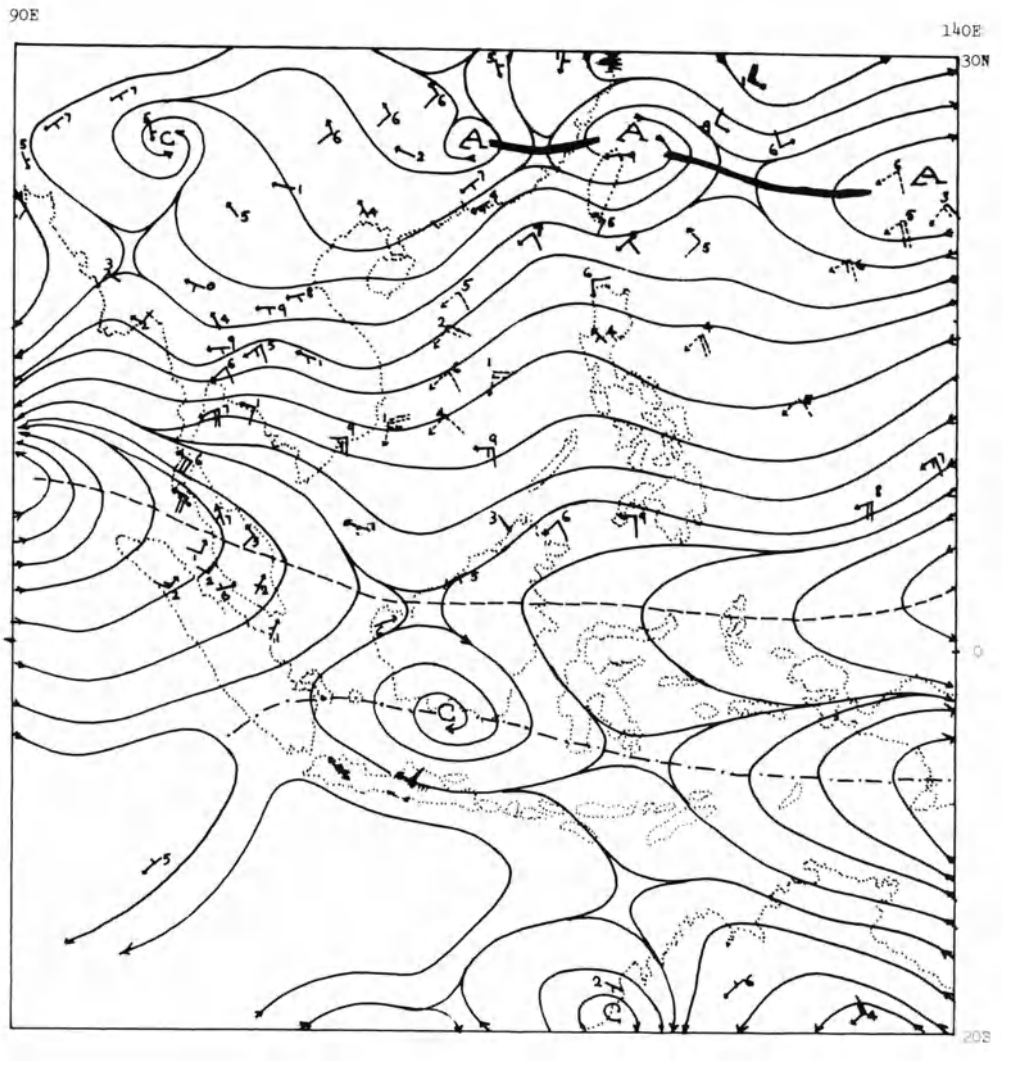

Figure 7
850 mb: 0000Z, 4-12-73. ———— Subtropical ridge, — — — northern equatorial trough line, — southern equatorial trough line. Dashed arrows over the South China Sea and the West Pacific are surface winds obtained from ship reports.

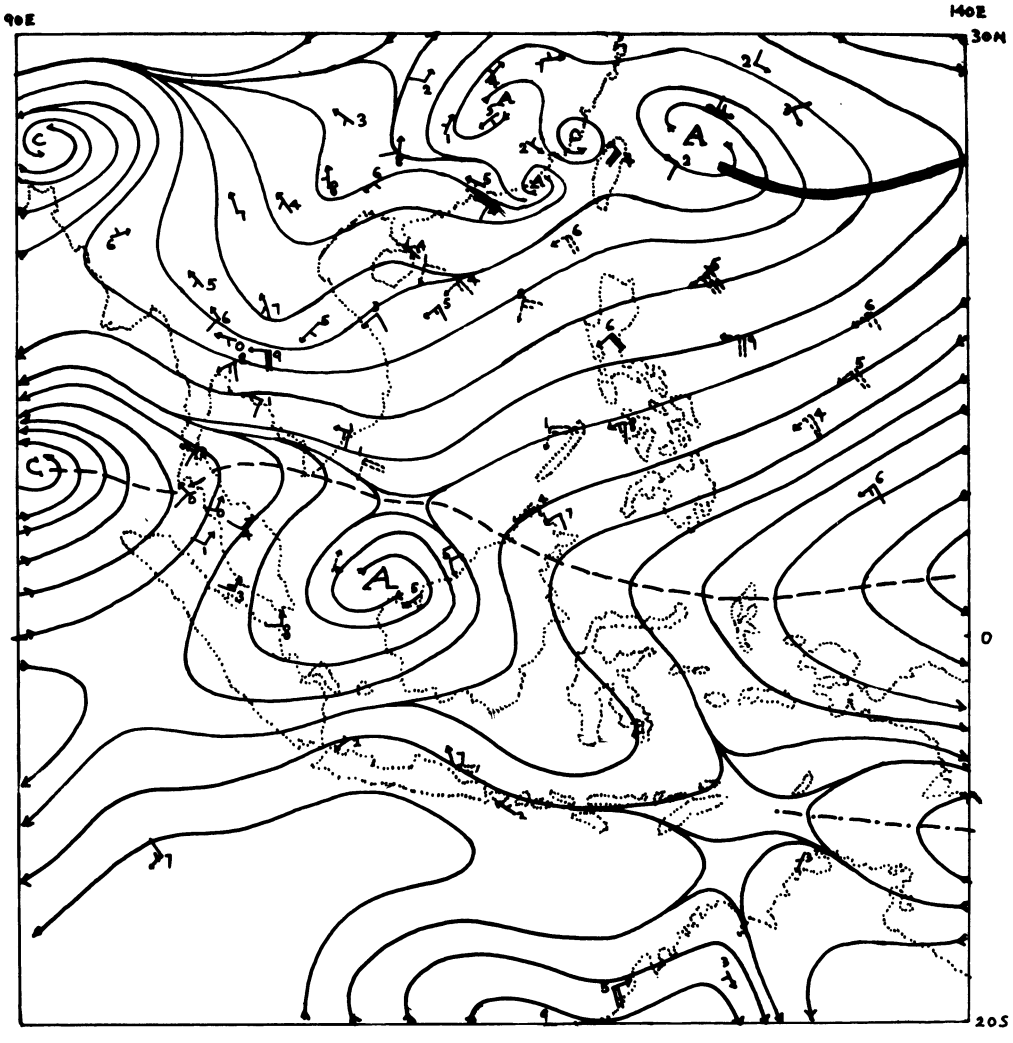

Figure 8
850 mb: 0000Z, 5-12-73.

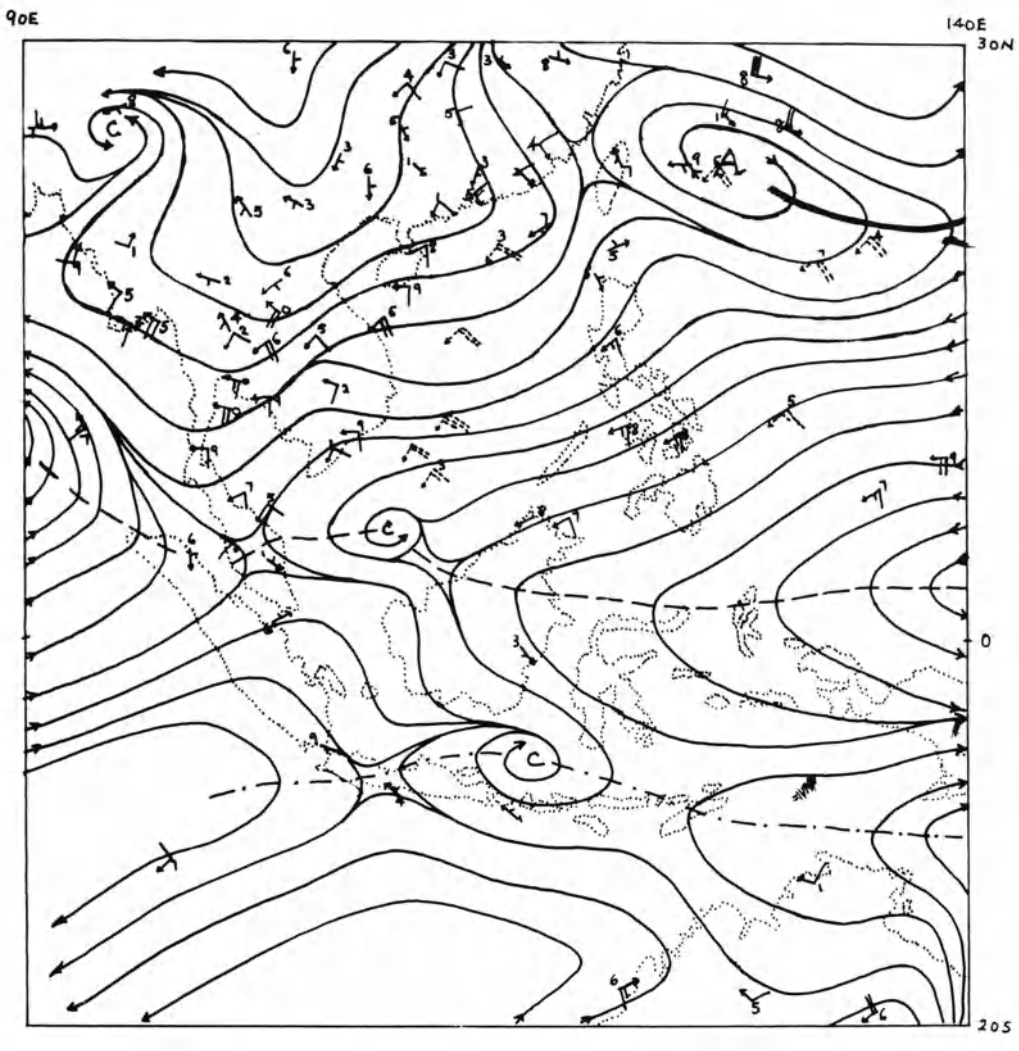

Figure 9
850 mb: 0000Z, 6-12-73.

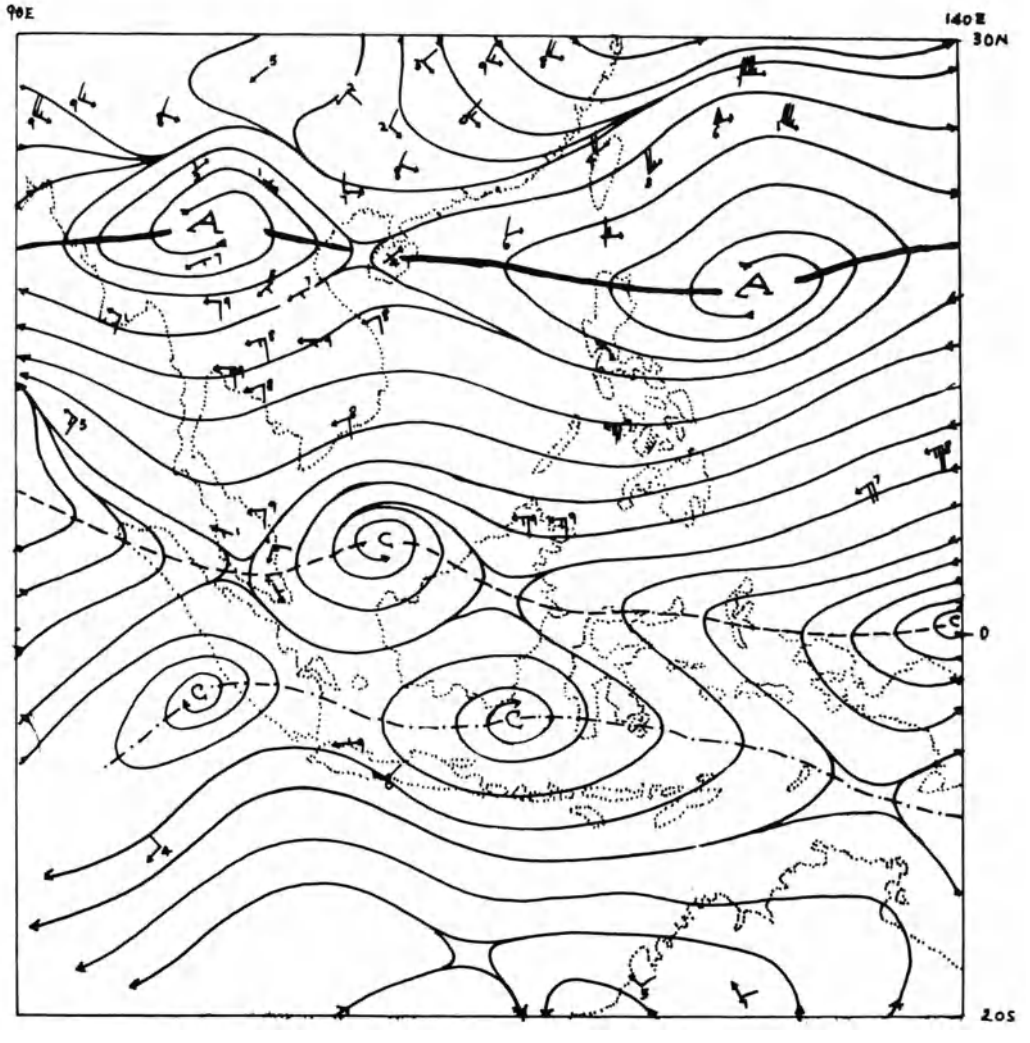

Figure 10
700 mb: 0000Z, 6-12-73.

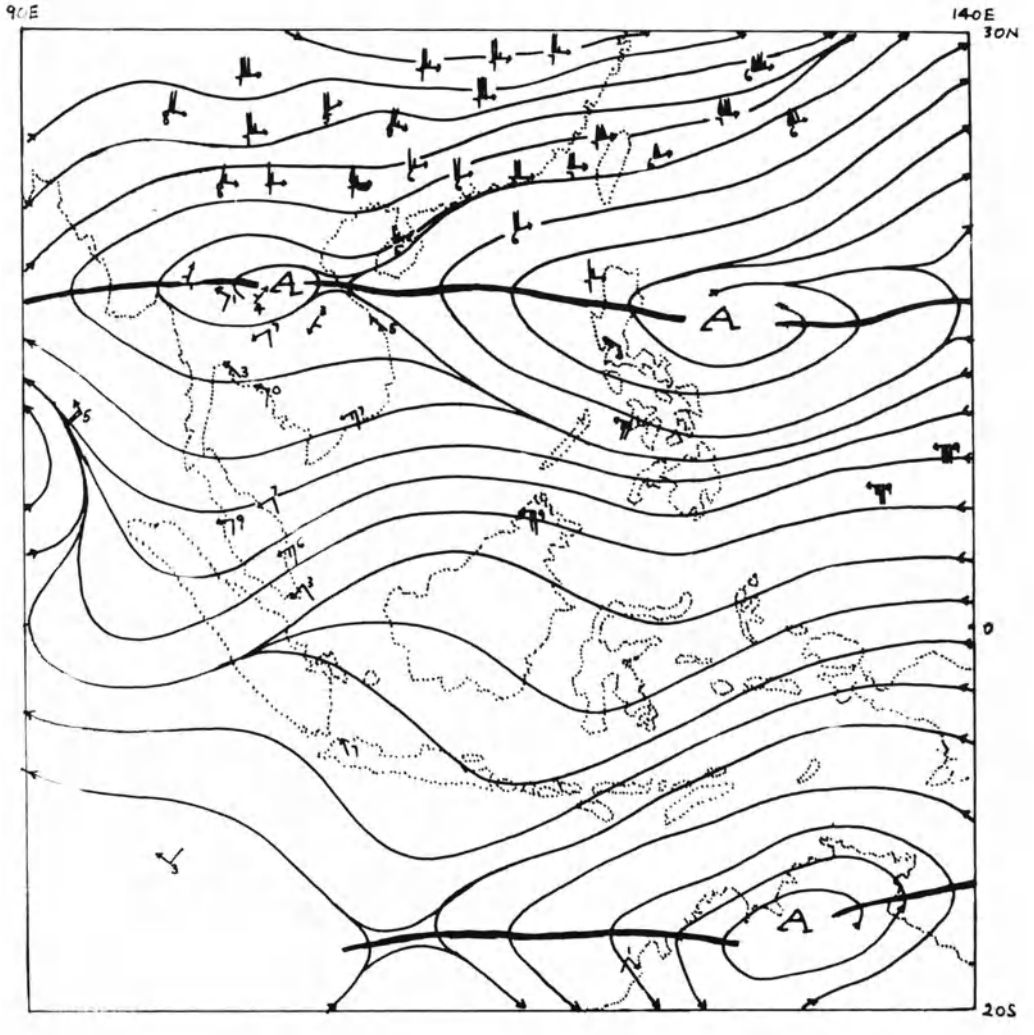

Figure 11
500 mb: 0000Z, 6-12-73.

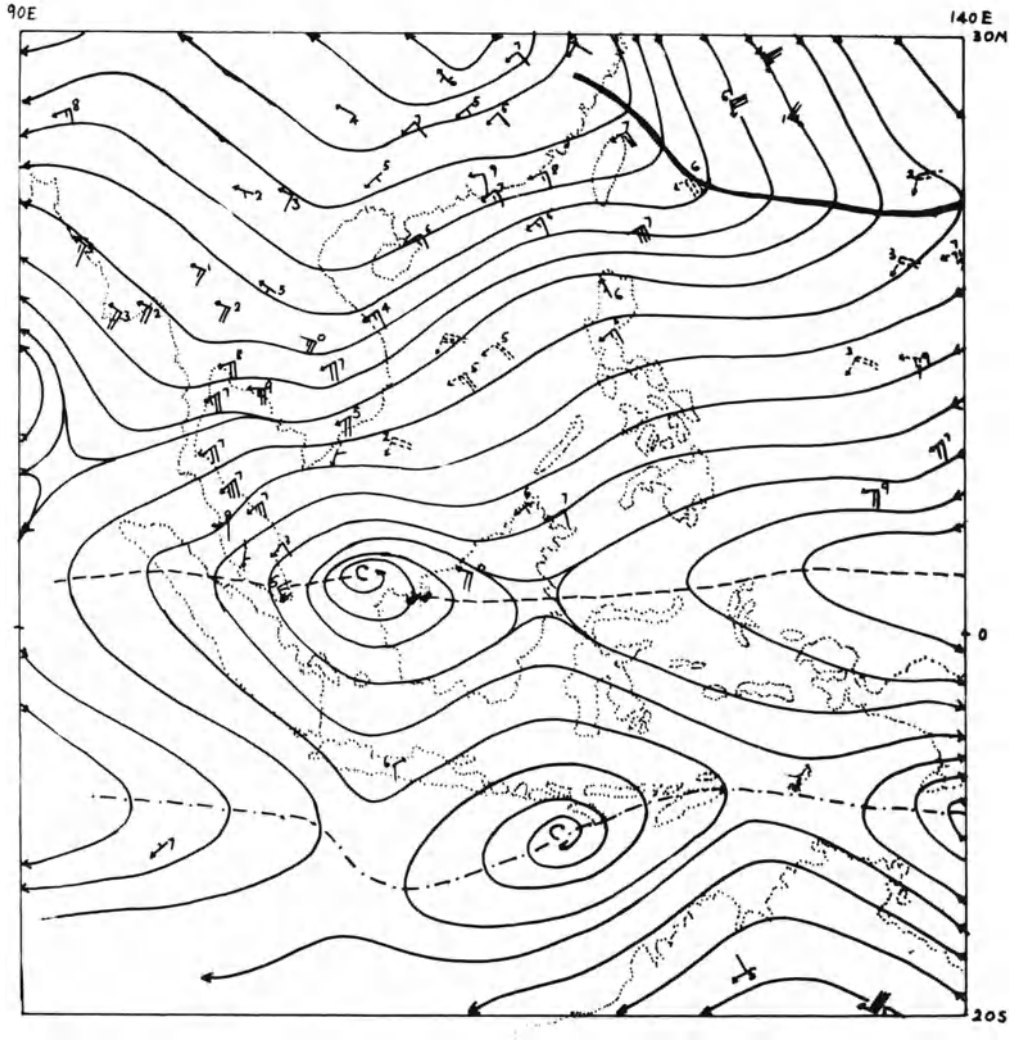

Figure 12
850 mb: 0000Z, 7-12-73.

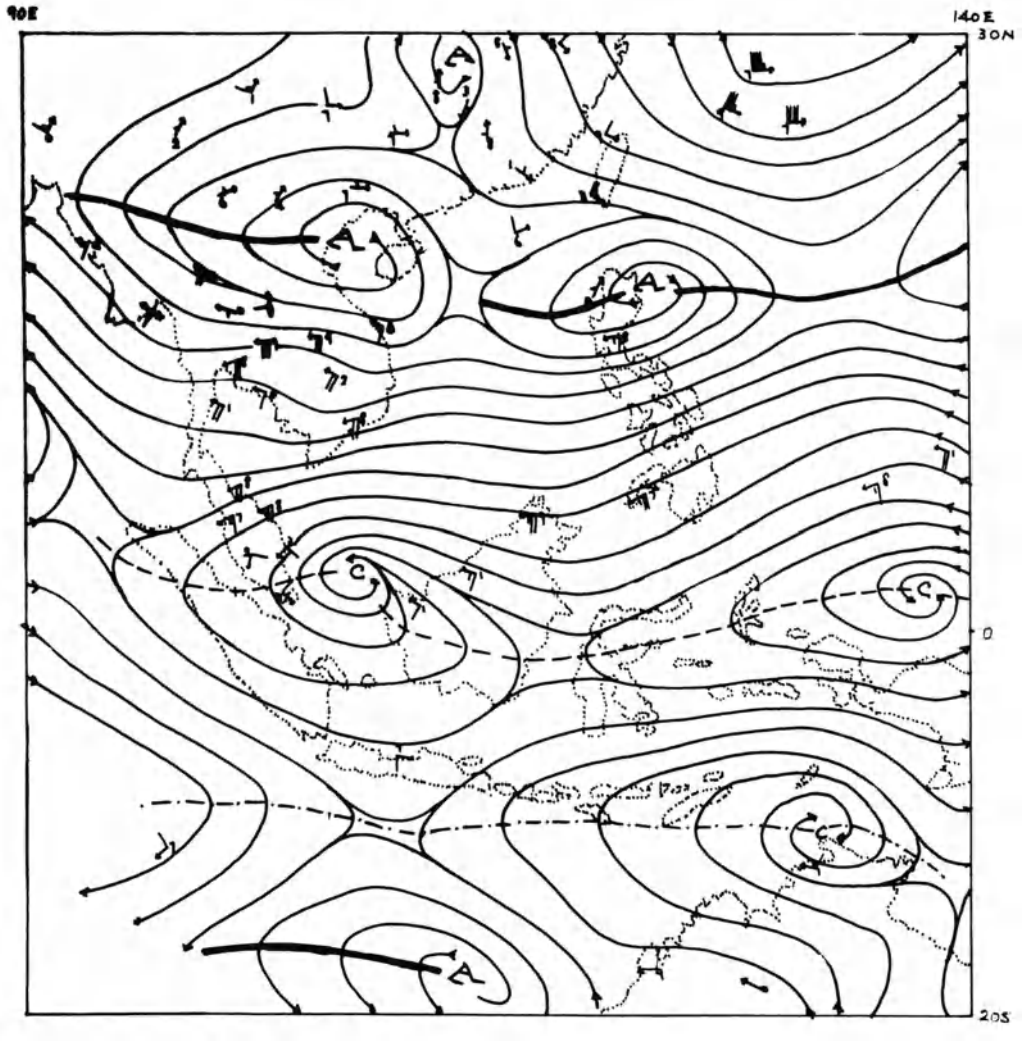

Figure 13
700 mb: 0000Z, 7-12-73.

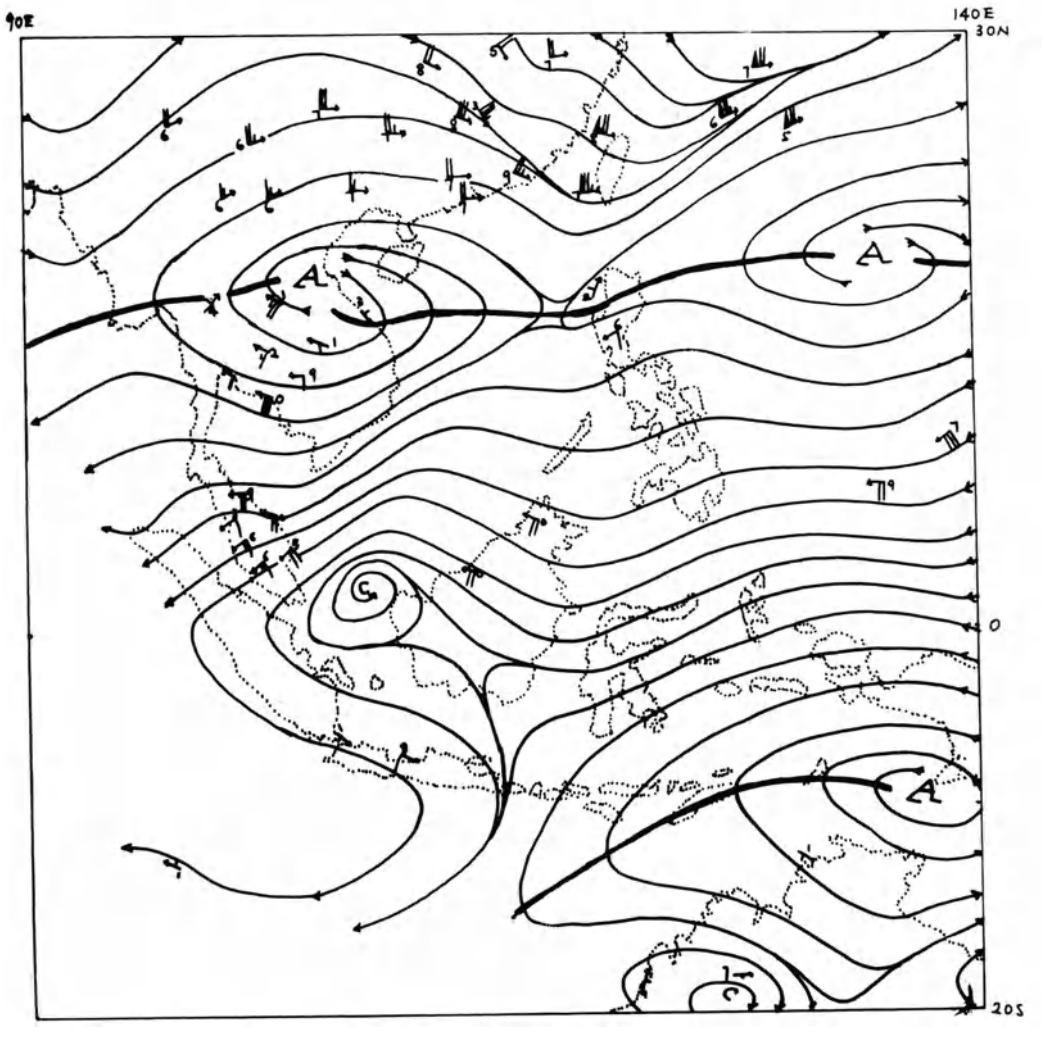

Figure 14
500 mb: 0000Z, 7-12-73.

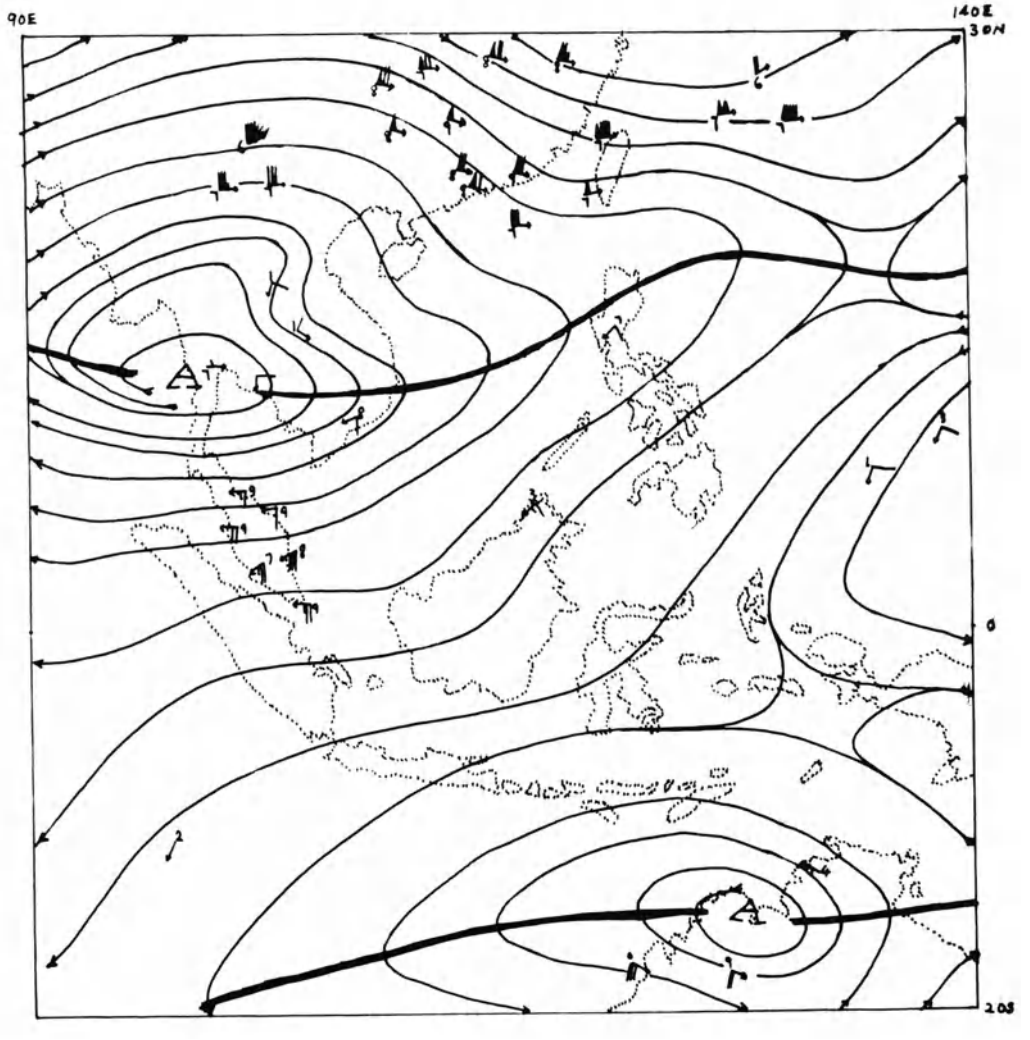

Figure 15
200 mb: 0000Z, 7-12-73.

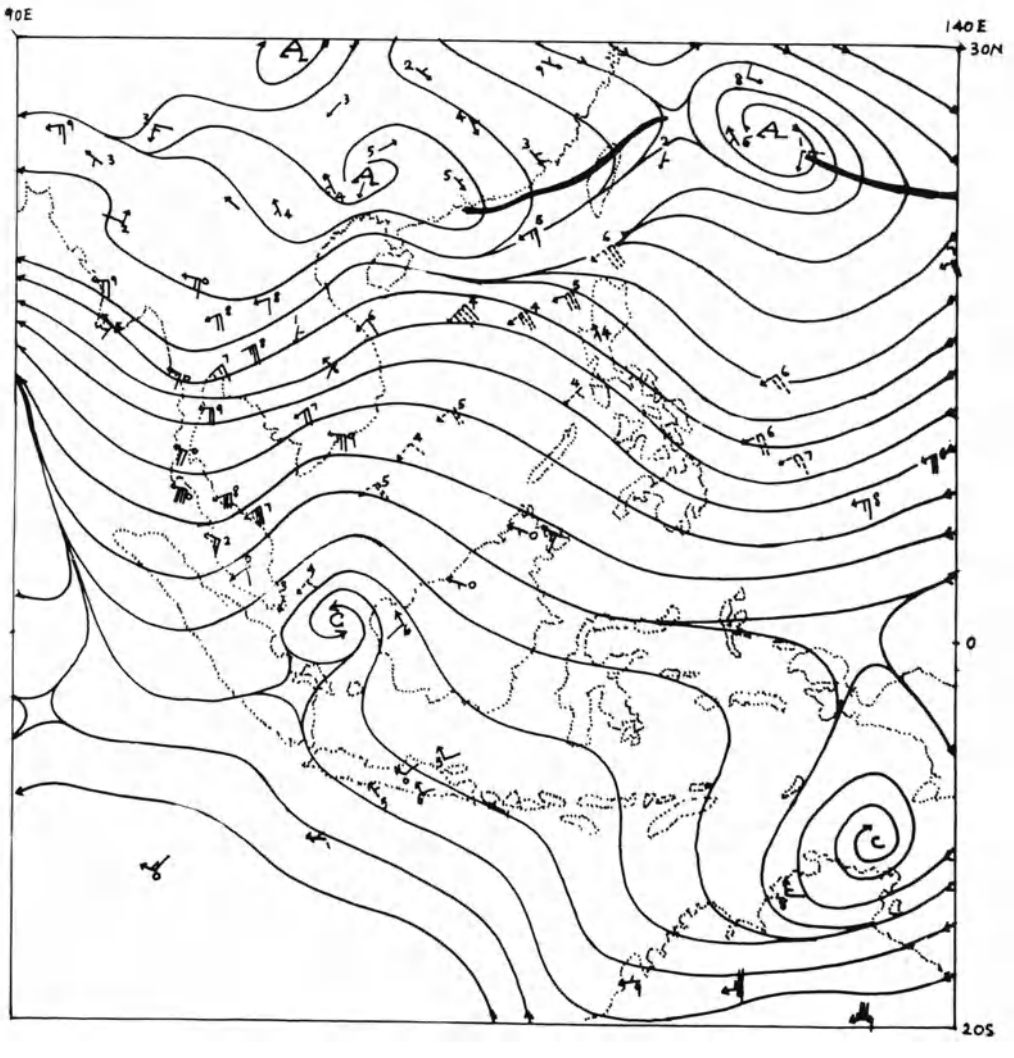

Figure 16
850 mb: 0000Z, 8-12-73.

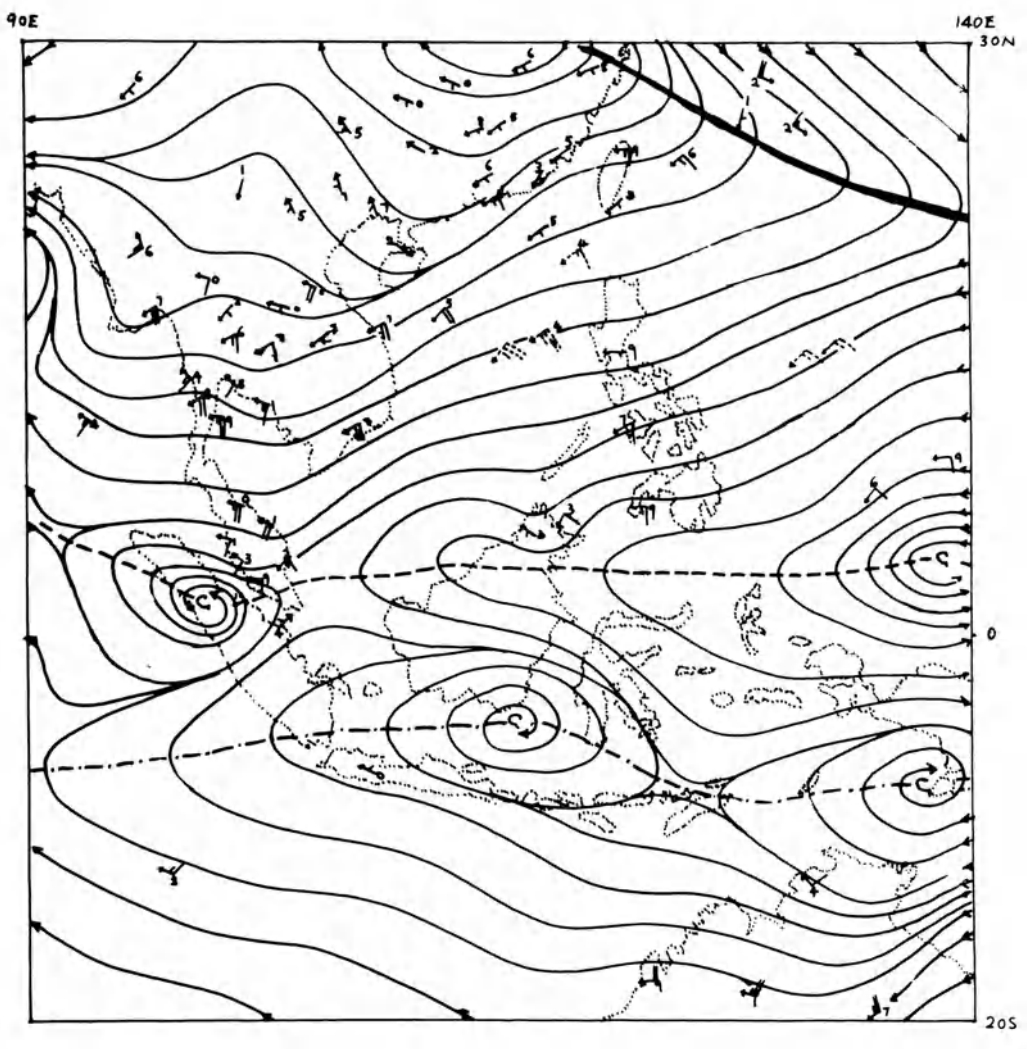

Figure 17
850 mb: 0000Z, 9-12-73.

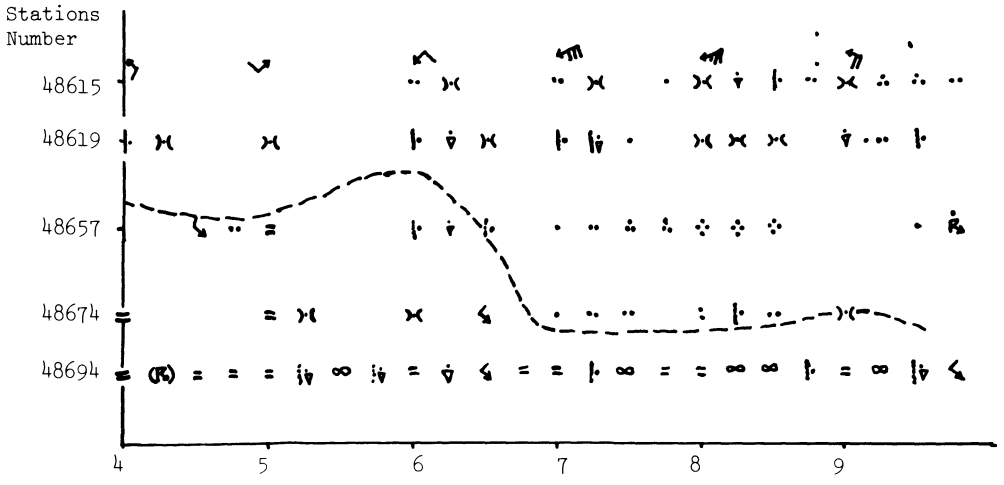

Figure 18
Horizontal time section of 6-hourly weather along the east coast of Peninsular Malaysia. — — — Near equatorial trough line.

The six-hourly weather along the east coast of Peninsular Malaysia during the same period is shown in the horizontal time section in Fig. 18. 850 mb winds at Kota Bahru are also shown in this figure. The near-equatorial trough line is indicated as dashed line.

The above figures show the following significant features.

(a) When the cold surge in the beginning of December 1973 receded (Figs. 7 and 8) on the 4th and 5th, the low-level trades freshened over the southern part of the South China Sea. A big convective cloud cluster developed over the South China Sea between 7°N and 12.5°N.

(b) On the 6th, the intensification of an anticyclone over Central China was evident at 850 mb (Fig. 9). The 700 mb short wave trough over East China was also a prominent feature (Fig. 10). At the surface, pressure over China and at Hong Kong started to increase from the 3rd (Table 1).

(c) An equatorial vortex developed over the South China Sea just above 300 km away from the east coast of Peninsular Malaysia on the 6th. It appeared up to 700 mb but just as a wave at 500 mb (Figs. 10 and 11).

(d) On the 7th the cold surge had moved out of China, shown by the sharp rise in surface pressure at Hong Kong and pressure drop over Central China (Table 1). The cyclonic disturbance had by then moved southwestwards near the equator (Fig. 12). It can be detected up to 500 mb. Heavy rain started from the 7th along the east coast of Peninsular Malaysia (Fig. 18).

(e) On the days of intense cold surge, 7th and 8th, two belts of strong easterly winds can be noted in the low levels; one over Indo China and the other over the northern part of Peninsular Malaysia (Figs. 12 and 16). Maximum easterly

Table 1

China average surface pressure between 33°N *and* 35°N *Hong Kong surface pressure and Kota Bharu (station number 48615) 850 mb wind.*

Date	China average surface pressure between 33°N and 35°N (in mb)	Hong Kong surface pressure (in mb)	Kota Bharu 850 mb wind (in deg. and knot)
3 Dec. 1973	1027.1	1019.5	090/11
4	1031.6	1021.1	150/09
5	1026.7	1021.8	110/04
6	1030.3	1020.6	060/09
7	1028.5	1023.7	070/34
8	1027.4	1023.7	070/35
9	1028.8	1021.7	100/19
10	1026.2	1018.7	080/22

wind of 35 knots was reported at Kota Bahru. As noted earlier (Figs. 4 and 5), the vertical shear was weak between 850 mb and 200 mb, but it was stronger, about 20 knots, between 850 mb and 600 mb.

(f) The short wave trough over East China at 700 mb and 500 mb moved to Japan as the high pressure weakened on the 7th (Figs. 10, 11, 13 and 14).

(g) At 200 mb (Fig. 15), speed divergence was evident in the easterlies over the Malaysian region.

(h) Figures 16 and 17 show the subsequent westward movement of the equatorial disturbance to Sumatra on the 9th when the cold surge was weakening.

(i) When the near-equatorial trough was intensifying on the 4th and 5th due to the strengthening trades over South China Sea, only isolated cases of convective weather were reported along the east coast of Peninsular Malaysia (Fig. 18). When the vortex developed on the 6th, more scattered weather was reported. Heavy continuous rain only started on the 7th. It can be noted that heavy rain was confined to area around the near equatorial trough axis and south of the low-level easterly jet. Heavy continuous rain was mainly from stratiform clouds. There were only isolated convective clouds.

4.2. Structure of the disturbance

Due to lack of upper air data over the South China Sea, composite method was applied. This method has been used by many authors (WILLIAMS, 1970; PEDGLEY and KRISHNAMURTI, 1976). In this investigation data at 0000 GMT from pibals, and rawinsondes, were supplemented by compositing data on 7 and 8 December 1973 when there was little change in the intensity of the disturbance. Upper air data were then subjectively interpolated on a 2° grid over 20° and 20° mesh.

(*a*) *Horizontal pattern of relative vorticity, divergence and vertical motions.* Figure 19 shows the field of relative vorticity at 850 mb with a cyclonic maximum of 4×10^{-5} sec^{-1} north of the cyclonic centre. Cyclonic relative vorticity decreased with height in the area of the disturbance.

Fields of divergence had a maximum value of convergence 1.5×10^{-5} sec^{-1} at 700 mb (Fig. 20) in the area of the disturbance. Divergence prevailed over the vortex at 500 mb and above.

Vertical motions were estimated by the well known kinematic method. At the lower boundary, $p = 1000$ mb, w was set to zero and the continuity equation was integrated up to 100 mb. A correction to the divergence was applied following REED and RECKER (1971), assuming zero means in the vertical.

Upcurrents occurred over extensive area around the equatorial vortex. Strongest ascent was slightly north of the 850 mb cyclone centre with maximum value of 22×10^{-3} mb sec^{-1} at 400 mb (Figure not shown here).

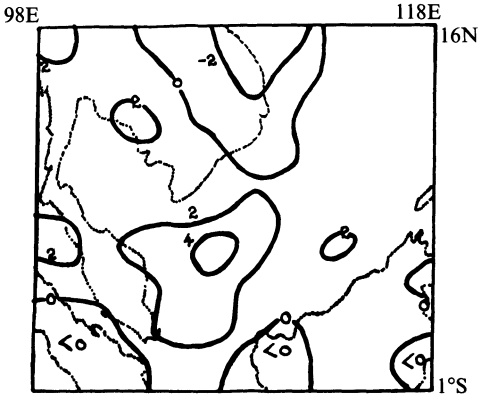

Figure 19
850 mb relative vorticity.
Unit:—10^{-5} sec^{-1}

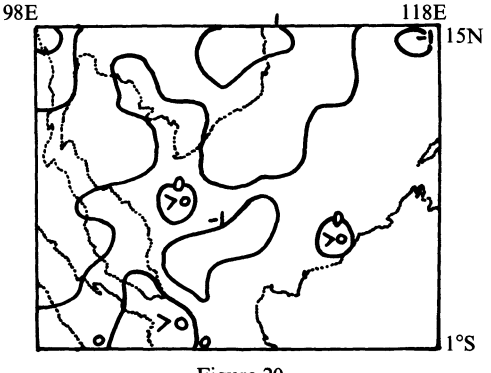

Figure 20
700 mb divergence.
Unit:—10^{-5} sec^{-1}

(*b*) *Vertical patterns of wind, relative vorticity and vertical motions.* The vertical cross sections were drawn through the vortex centre at about latitude 2°N and longitude 109°E near the vortex centre at 850 mb on the 7th.

In the north–south plane, equatorial westerlies were confined to the lower troposphere south of 2°N (Fig. 21). Two easterly maxima show out clearly; one around 7°N at 850 mb and the other around 14°N at 900 mb. Another jet in the upper troposphere near the equator can also be noted. Northerly component winds were confined mainly in the low levels while southerly component winds were mainly in the middle and upper troposphere and north of 6°N (Fig. 22).

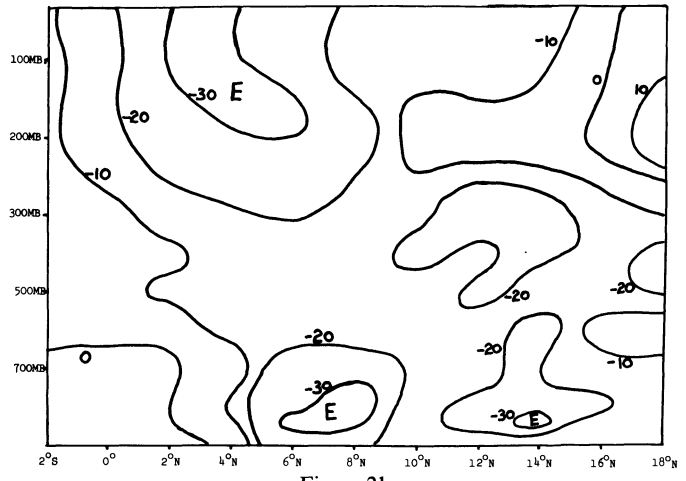

Figure 21
U-component, 8-12-73.
Unit:—in knots

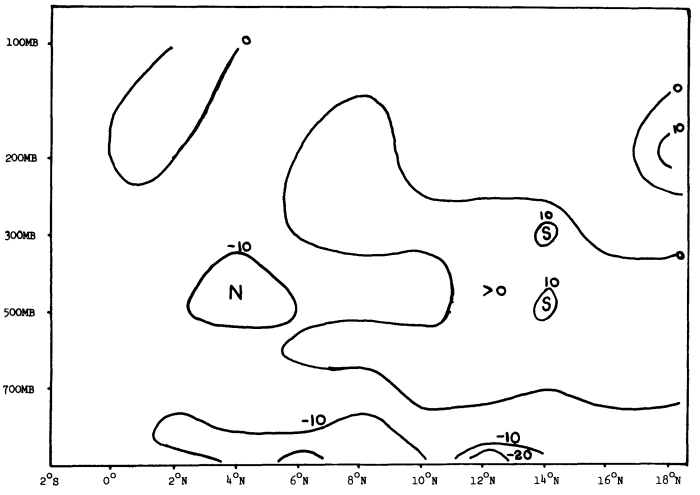

Figure 22
V-component, 8-12-73.
Unit:—in knots

Cross section of relative vorticity (Fig. 23) is complex. Cyclonic relative vorticity was observed at most levels south of 10°N. Anticyclonic relative vorticity was confined only in the lower troposphere north of 10°N.

Vertical motions (Fig. 24) have a simpler distribution. Downcurrents were observed north of 10°N and at 700 mb and above.

In the east–west plane, the westerly component winds were confined only in the lower levels generally below 850 mb (Fig. 25). Easterly winds in the upper troposphere

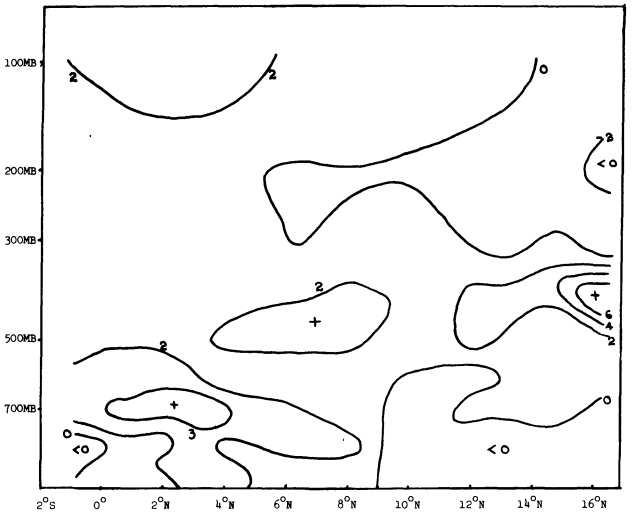

Figure 23
Relative vorticity, 8-12-73.
Unit:—10^{-5} sec^{-1}

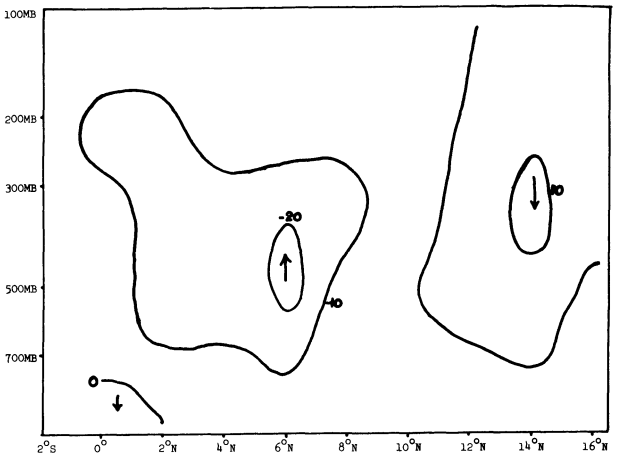

Figure 24
Vertical motion, 8-12-73.
Unit:—10^{-3} mb sec^{-1}

increased downstream from east to west with the maximum located slightly to the west of the vortex centre which was situated along 109°E. Northerly component winds (Fig. 26) were observed mainly west of 107°E in deep layer whereas southerly component winds were observed mainly east of 107°E. This separation resembles a wave trough with a slightly eastward tilt with height up to about 400 kb.

Cyclonic relative vorticity was observed over large area. Anticyclonic relative vorticity was confined mainly in low levels west of 101°E and east of 113°E (Fig. 27).

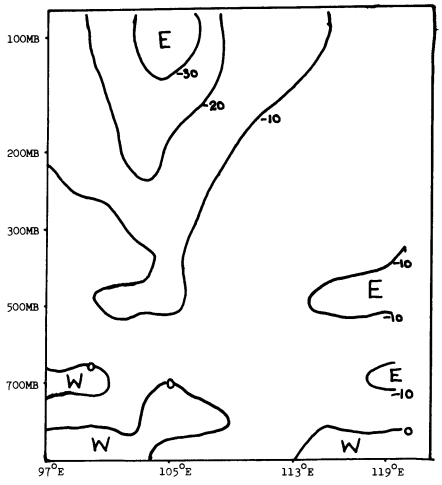

Figure 25
U-component, 8-12-73.
Unit:—in knots

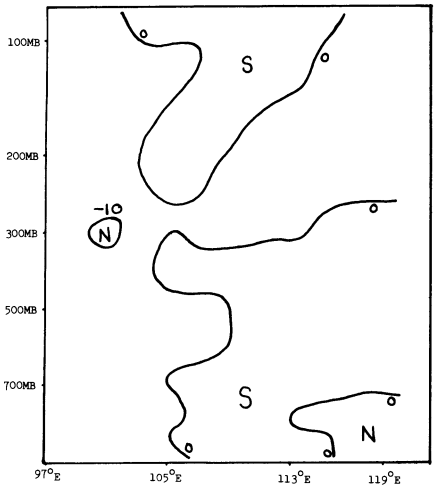

Figure 26
V-component, 8-12-73.
Unit:—in knots

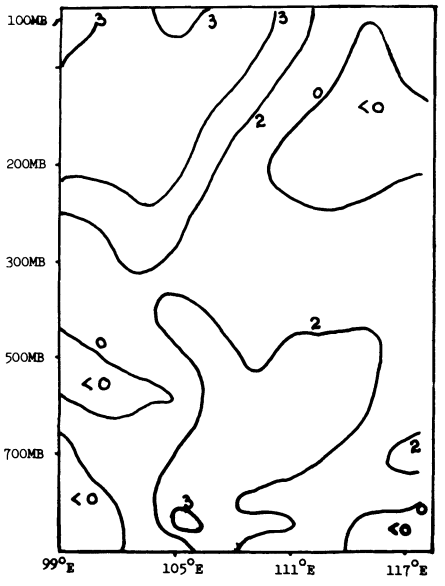

Figure 27
Relative vorticity, 8-12-73.
Unit:—10^{-5} sec^{-1}

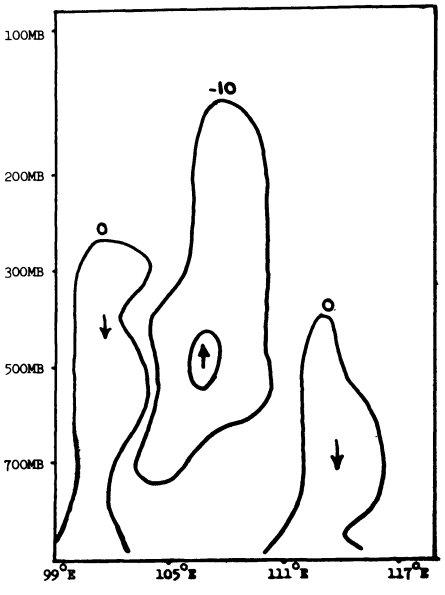

Figure 28
Vertical motion, 8-12-73.
Unit:—10^{-3} mb sec^{-1}

Up-currents were over large areas of the disturbance (Fig. 28). Down-currents occurred mainly west of 103°E and east of 113°E where there was anticyclonic relative vorticity. The area of down-currents east of 113°E occurred in the area of southerly component winds or east of the wave trough. Weather in the area east of 113°E and between 2° and 5°N (over East Malaysia) did really clear up on the 7th and 8th. This weather pattern seems to be different from that associated with the well known easterly wave.

5. *Genesis and maintenance of the vortices*

As noted earlier, some of the disturbances can originate over the South China Sea while others can originate over the West Pacific. It has also been shown that easterly disturbance in the form of fluctuation of easterly winds in the horizontal as well as the vertical existed before and during the development of equatorial vortices. This easterly disturbance was associated with lateral shear. Hence barotropic

Table 2

Meridional variation of absolute vorticity over the South China Sea

November			December		
Latitude °N	Mean wind (in knots)	$\beta - \frac{\partial^2 u}{\partial y^2} (\times 10^{-11})$	Latitude °N	Mean wind (in knots)	$\beta - \frac{\partial^2 u}{\partial y^2} (\times 10^{-11})$
2	250/04		2	220/02	
4	060/02	3.8	4	100/03	4.0
6	060/03	−2.9	6	040/05	−2.1
8	030/08	2.8	8	030/12	4.9
10	030/10	1.8	10	040/13	1.7
12	040/12	4.1	12	040/14	0.3
14	050/16	4.4	14	040/15	2.2
16	060/17	−0.3	16	040/17	2.9
18	060/18	0.5	18	040/18	1.5
20	050/16	−2.3	20	040/17	0.8
January			February		
2	010/08		2	020/07	
4	030/11	1.4	4	020/08	1.3
6	040/13	−1.3	6	030/10	4.2
8	050/15	2.8	8	030/11	0.3
10	060/17	1.4	10	040/12	4.1
12	070/18	−1.1	12	040/13	0.5
14	070/18	−2.4	14	040/13	1.5
16	070/16	−2.0	16	060/12	4.4
18	070/15	9.7	18	070/12	1.0
20	070/12	−2.0	20	080/12	1.8

instability due to horizontal shear in the zonal flow may be the cause for the formation of these disturbances in these areas (NITTA and YANAI, 1969; HOLTON, 1972). The requirement for barotropic instability is that absolute vorticity of the zonal flow must change sign. Due to lack of upper air data over the South China Sea, it is difficult to test this condition for the disturbances in this study. However the mean monthly charts for the gradient level prepared by SADLER (1970) show distinct horizontal shear in the easterlies over the West Pacific and the South China Sea during the winter monsoon months of November, December and January. Based on wind data extracted from the mean gradient level charts, computation of the meridional variation of absolute vorticity ($\beta - \partial^2 u/\partial y^2$) for the month of November, December, January and February was carried out. The results are depicted in Table 2 only for the South China Sea Area.

The condition of changing sign is satisfied over the equatorial region of the South China Sea from November till January. It is not satisfied for February which is generally a dry month for Peninsular Malaysia. For the West Pacific area, this condition is also satisfied for the four months. It must be noted that the zonal winds may vary significantly over a month, and the disturbances might have developed when the winds were more unstable than indicated by their monthly average. Hence, it could be possible that the disturbances were formed by barotropic transformation of energy associated with horizontal shear in the mean flow.

For equatorial vortices which originate over the South China Sea, topography apart from barotropic instability in the zonal flow may also play a very important role in their formation. The orientation of the Annam Range in Vietnam, the main range (which runs from north to south) in Peninsular Malaysia and the mountain range (which runs from southwest to northeast) in Borneo is suitable for the easterly flow to turn cyclonically and this may induce low-level cyclonic circulation to develop.

Once the disturbance develops, there will be large diabatic process (condensation, sensible and latent heat from ocean, etc.) in operation. Hence, barotropic transformation cannot be a probable mechanism for the intensification of the disturbances. Certain form of CISK mechanism may be a more lilely one. However due to the interaction with the cold monsoon surge for the more intense vortices during the winter monsoon, and the presence of low-level easterly jet, a more complicated transformation of energy may be needed for the maintenance of the disturbance. The easterly jet possesses strong lateral shear and also considerable vertical shear in the low and middle troposphere. Hence a combination of CISK mechanism and a mixed barotropic and baroclinic instability may be a possible one for the maintenance of equatorial vortices during the winter monsoon.

7. *Summary*

Out of the five equatorial vortices studied in this investigation, the following significant features are obtained.

1. Disturbances in the trades associated with lateral shear were found to be important for the genesis of these equatorial vortices.
2. Intensification of these disturbances depended very much on the timing of the occurrence of the cold surge and the presence of the disturbance in the trades.
3. Low-level easterly jets at 850 mb were found over the northern part of Peninsular Malaysia during the intensification stage of the four equatorial vortices that interacted with the cold monsoon surge and brought heavy rain to Peninsular Malaysia.

   Associated with the jet there was significant vertical shear about 20 knots between the lower and middle troposphere.
4. Heavy rain was confined to the cyclonic shear side of the easterly jet and around the near-equatorial trough axis.
5. For the equatorial vortex that brought along heavy rain only to Sarawak, the low-level easterly jet was absent over Peninsular Malaysia even though there was intense cold surge.
6. For those vortices that affected Peninsular Malaysia, the vertical wind fields were distinctly different from those associated with the vortex that affected only Sarawak.
7. For the maintenance and intensification of the disturbances, a complex combination of CISK mechanism and mixed barotropic and baroclinic instability is suspected.

It is hoped that with more upper air data to be collected during the coming winter MONEX in 1979, a more detailed investigation can be carried out to study the genesis, synoptic structure and energetics of the equatorial vortices.

Acknowledgement

The author wishes to thank the Director General of Malaysian Meteorological Service for his permission to publish this report and for his encouragement.

References

BRYANT, K. (1958), *Comparison of months giving extremes of rainfall during northeast monsoon at Changi, Singapore Island*, Meteor. Mag. *87*, 307–312.

BURPEE, R. W. (1972), *The origin and structure of easterly waves in the lower troposphere of North Africa*, J. Atmos. Sci. *29*, 77–90.

CARLSON, T. N. (1969a), *Synoptic histories of three African disturbances that developed into Atlantic hurricanes*, Mon. Wea. Rev. *97*, 256–276.

CHEANG, B. K. (1977), *Structure of a cyclonic disturbance over the South China Sea and the Malaysian region during the winter Monsoon* – to be published in the proceedings of International Symposium on Monsoons, New Delhi, India.

FETT, R. W. (1966), *Upper-level structure of the formative tropical cyclone*, Mon. Wea. Rev. *94*, 9–18.

GAN, T. L. (undated), *A study of some heavy rainspells on the east coast of Malaya during the northeast monsoon season*. Memoir of the Malayan Meteorological Service, No. 6.

HOLTON, J. R., *An introduction to Dynamic Meteorology* (Academic Press, New York, 1972), pp. 290–294.

KRISHNAMURTI, T. N. and PAN, H. L. (1977), *Long term variability in Monsoon flows over the lower troposphere* – to be published in the Proceedings of International Symposium on Monsoons. New Delhi, India.

NITTA, T. and YANAI, M. (1969), *A note on barotropic instability of the tropical easterly current*, J. Meteor. Soc. *47*, 183–197.

PALMER, C. E. (1952), *Tropical meteorology*, Quart. J. Roy. Met. Soc. *78* (336), 126–164.

PEDGLEY, D. E. and KRISHNAMURTI, T. N. (1976), *Structure and behaviour of a monsoon cyclone over West Africa*, Mon. Wea. Rev. *104* (2), 149–167.

RAMAGE, C. S., *Monsoon Meteorology*, (Academic Press, 1971), pp. 79–85.

REED, R. J. (1970), *Structure and characteristics of easterly waves in the equatorial Western Pacific during July–August 1967*, Proceedings of the Symposium on Tropical Meteorology 1970, University of Hawaii.

REED, R. J. and RECKER, E. E. (1971), *Structure and properties of synoptic-scale wave disturbances in the equatorial western Pacific*, J. Atmos. Sci. *28*, 1117–1133.

RIEHL, H., BELL, G. J., RAMAGE, C. S., AUGUSTIN, E., FROST, R., HASTENRATH, S., KRISHNAMURTI, T. N. and VAN DER BOOGARD, H. M. E. (1969), *The Diagnosis and prediction of SE Asia northeast monsoon weather*, NWRF 12–0669–144, Navy Weather Research Facility.

SADLER, J. C. (1967), *On the origin of tropical vortices*. Proceedings of the Working Panel on Tropical Dynamic Meteorological, August 1967, NWRF 12–1167–132, Navy Weather Research Facility, pp. 39–76.

SADLER, J. C. (1970), *Mean cloudiness and gradient-level-wind charts over the tropics, Vol. II: Charts Technical Report 215*. Air Weather Service (MAC) United States Air Force.

WALLACE, J. M. and CHANG, C. P. (1969), *Spectrum analysis of large-scale wave disturbances in the tropical lower troposphere*, J. Atmos. Sci. *26*, 1010–1025.

WATTS, I. E. M., *Equatorial weather* (University of London Press, 1955), pp. 97–98.

WILLIAMS, K. T. (1970), *A statistical analysis of satellite-observed trade wind cloud clusters in the western north Pacific*, Atmospheric Science Paper No. 161. Department of Atmospheric Science, Colorado State University.

YANAI, M., MARUYAMA, T., NITTA, T. and HAYASHI, Y. (1968), *Power spectra of large-scale disturbances over the tropical Pacific*, J. Meteor. Soc. Japan *46*, 308–323.

(Received 15th June 1977)

Pageoph, Vol. 115 (1977), Birkhäuser Verlag, Basel

Effects of a Variety of Indian Ocean Surface Temperature Anomaly Patterns on the Summer Monsoon Circulation: Experiments with the NCAR General Circulation Model

By WARREN M. WASHINGTON[1]), ROBERT M. CHERVIN[1]) and G. V. RAO[2])

Abstract – The time mean response of the summer monsoon circulation, as simulated by the 2.5° latitude–longitude resolution, July version of the National Center for Atmospheric Research (NCAR) General Circulation Model (GCM), to a variety of Indian Ocean surface temperature anomaly patterns is examined. In separate experiments, prescribed changes in surface temperature are imposed in the Western Arabian Sea, the Eastern Arabian Sea, or the Central Indian Ocean. The influence of these anomaly patterns on the simulated summer monsoon circulation is evaluated in terms of the geographical distribution of the prescribed change response for any field of interest. This response is defined as the grid point difference between a 30-day mean from a prescribed change experiment and the ensemble average of the 30-day means from the control population for which the same set of climatological ocean surface temperatures are used in each simulation. The statistical significance of such a prescribed change response is estimated by relating the normalized response (defined as the ratio of the prescribed change response to the standard deviation of 30-day means as estimated from the finite sample of control cases) to the classical Student's *t*-statistic. Using this methodology, the most prominent and statistically significant features of the model's response are increased vertical velocity and precipitation over warm anomalies and typically decreased vertical velocity and precipitation in some preferred region adjacent to the prescribed change region. In the case of cold anomalies, these changes are of opposite sign. However, none of the imposed anomaly patterns produces substantial or statistically significant precipitation changes over large areas of the Indian sub-continent. The only evidence of a major nonlocal effect is found in the experiment with a large positive anomaly (+3°C) in the Central Indian Ocean. In this instance, vertical velocity and precipitation are reduced over Malaysia and a large area of the Equatorial Western Pacific Ocean. Thus, while these anomaly experiments produce only a local response (for the most part), it is hoped, as one of the purposes of the planned Monsoon Experiment (MONEX), that the necessary data will be provided to produce detailed empirical evidence on the extent to which Indian Ocean surface temperature anomalies correlate with precipitation anomalies over the Indian subcontinent – a correlation which generally does not appear in these GCM results.

Key words: Monsoon circulation: Anomaly patterns, effect of ocean surface temperature.

1. Introduction

The extent to which Indian Ocean surface temperature (OST) anomalies influence the summer monsoon circulation has been largely conjectural until recently. Since such anomalies alter the sensible and latent heat fluxes to the atmosphere, OST

[1]) National Center for Atmospheric Research, Boulder, Colorado 80307. The National Center for Atmospheric Research is sponsored by the National Science Foundation.

[2]) Department of Earth and Atmospheric Sciences, Saint Louis University, Saint Louis, Missouri 63103, USA.

anomalies are believed to be important in effecting monsoon circulation changes. In a report on the forthcoming Monsoon Experiment (MONEX), the JOINT ORGANIZING COMMITTEE OF GARP (1976) endorsed several numerical experiments along the lines described here, to determine which heat sources and sinks drive the monsoon circulation and to indicate which factors are more sensitive than others in modifying the circulation. In this paper, we report the results of a series of experiments with a version of the National Center for Atmospheric Research (NCAR) General Circulation Model (GCM) designed to test the climatic effects of prescribed changes of ocean surface temperature on the summer monsoon.

The first numerical experiment for this purpose was performed with the Geophysical Fluid Dynamics Laboratory (GFDL) GCM by SHUKLA (1975 and 1976) who modified the OST near the Somali coast with a cold anomaly having a maximum change of $-3°C$. He observed changes in the computed rainfall patterns in the vicinity of India and found modifications to pressure, evaporation, and wind fields. Although he attempted to separate signal from noise in this analysis of the results, his conclusion probably was biased by a questionable experimental design.

We repeated the Shukla experiment with a substantially different statistical and experimental design. The anomaly was introduced at Day 60 of an existing control perpetual July experiment. The model, with altered lower boundary condition, was then integrated to Day 120. The first 30 days allowed the atmosphere to adjust to the new OST, and the last 30 days were used to examine the new quasi-equilibrium state and to test the model's response to the prescribed change. This approach differed from that of Shukla who examined the results within the immediate period of 45 days from the initial introduction of the anomaly. The methodology used in our study for estimating the statistical significance of the results in GCM climate change experiments comes from CHERVIN, GATES and SCHNEIDER (1974), CHERVIN and SCHNEIDER (1976a, b), and CHERVIN, WASHINGTON and SCHNEIDER (1976).

This method has been used with the NCAR GCM in such prescribed change experiments as mid-latitude ocean temperature anomalies (CHERVIN *et al.*, 1976; KUTZBACH, CHERVIN and HOUGHTON, 1977), testing the effects of desert aerosols (JOSEPH, 1976), and assessing temperature changes owing to thermal pollution (LLEWELLYN and WASHINGTON, 1977). It is based on a variant of the classical Student's t-test in which we run several experiments from the control. Each experiment has slightly different initial conditions which, because of the nonlinear nature of the model, cause the model's solutions to differ in time from the original control case. Since the external conditions are unaltered, it is assumed that these experiments are independent realizations from the same population (for time intervals within which the transient predictability effects are no longer dominant) and hence have the same general mean climatology, although the day-to-day fluctuations are different. The collection of such experiments from the basic control case configuration is used to estimate the climatic mean and inherent variability of the model.

Two additional prescribed change experiments were performed with different

OST anomalies. From the surface charts of temperature for June 1963 and 1964 (RAMAGE, MILLER and JEFFERIES, 1972), it is clear that a large interannual variation of OST can exist over the Eastern Arabian Sea. This portion of the sea was relatively warm in 1963 and cool in 1964. Guided by this difference, we inserted a warm anomaly of some 1°C in the Eastern Arabian Sea.

The third experiment consisted of introducing an anomaly with a maximum change of 3°C in the Equatorial Indian Ocean between the longitudes 65°E and 100°E. Some justification for such an anomaly came from RAMAN (1965) and SAHA (1970). The purpose of this experiment was to study the resulting modifications of the Southern Equatorial Trough (SET) and the overall monsoon circulation with special reference to precipitation over northern India. As described by RAO and RAGHAVENDRA (1967), this trough corresponds to the location in the Equatorial Central Indian Ocean where easterlies turn into westerlies. SRINIVASAN (1968) noted that cloudiness, precipitation, and the position of SET were well-correlated. He speculated that the mean position of SET was due to the distributions of OST and ocean and land areas.

Section 2 describes the characteristics of the NCAR model version used in this study. Sections 3 and 4 give the experimental design and method for determining statistical significance. The climatology of the ensemble of control cases is described in Section 5. Sections 6, 7, and 8 show the results of Western Arabian, Eastern Arabian, and Central Indian Ocean surface temperature anomaly experiments. Conclusions and a summary of the experiments are given in Section 9.

2. *Model description and initial boundary conditions*

The model version used in this study is global, with 2.5° latitude-longitude horizontal grid and 6 vertical layers, each with a 3 km height thickness. The continental outline over the region of interest is shown in Fig. 1. The physical processes included in the model are solar and infrared radiation, cloudiness, and the horizontal and vertical diffusion of sensible heat, moisture, and momentum. The model includes both large-scale precipitation dependent on local relative humidity and small-scale precipitation consistent with the convective latent heat release predicted by the cumulus parameterization of KRISHNAMURTI and MOXIM (1971) (see also WASHINGTON and WILLIAMSON, 1977). Ocean surface temperatures are specified from WASHINGTON and THIEL (1970) and held constant in time. The continental surface temperatures are calculated from a surface energy balance. Snow cover and soil moisture are computed from a simplified surface hydrology, and the dynamical effects of orography are included. A more complete description can be found in WASHINGTON and DAGGUPATY (1975) and WASHINGTON and WILLIAMSON (1977).

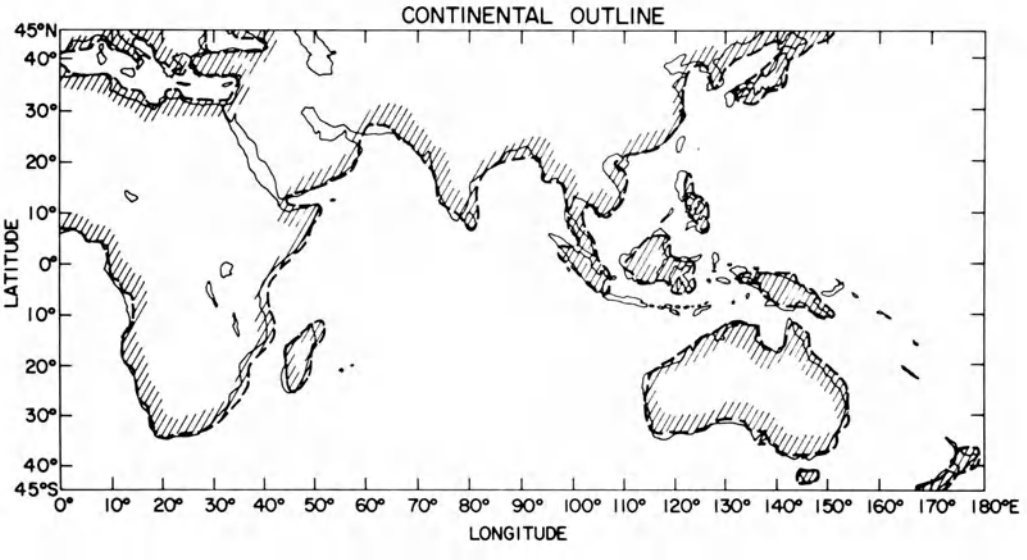

Figure 1
Continental outline. Light line is actual and heavy line is model.

3. *Design of experiments*

All experiments examined here were started in the same manner. First, a basic control case evolved from an isothermal atmosphere at rest, with the solar declination angle held fixed in time at 21.2° corresponding to mid-July. The ocean surface temperature changes were introduced at Day 60 of the basic control experiment and this altered version of the model was run to Day 120. To provide a better estimate of the control climatic mean and inherent variability for statistical significance testing purposes, two additional experiments were run. These experiments were started from the control at Day 60 or 61 with initial data slightly altered by the addition of small random perturbations (e.g., CHERVIN and SCHNEIDER, 1976a, b). This small perturbation grows nonlinearly so that after 20 days or so the instantaneous flow patterns appear quite different from the control. We refer to these experiments as random or alternate controls and assume that they are statistically independent of the first control, especially for the interval Day 91–120. The ensemble of controls is used for estimating the standard deviations (or inherent variability) of the model's mean July climate as well as the climatic mean itself.

The ocean temperature anomalies chosen for this study do not exhaust all suggested, but are representative of those recommended in the document on MONEX by the JOINT ORGANIZING COMMITTEE OF GARP (1976). Our first experiment for sensitivity testing purposes in the Western Arabian Sea followed the anomaly pattern used earlier in a numerical experiment by SHUKLA (1975) (Fig. 2a). This pattern is

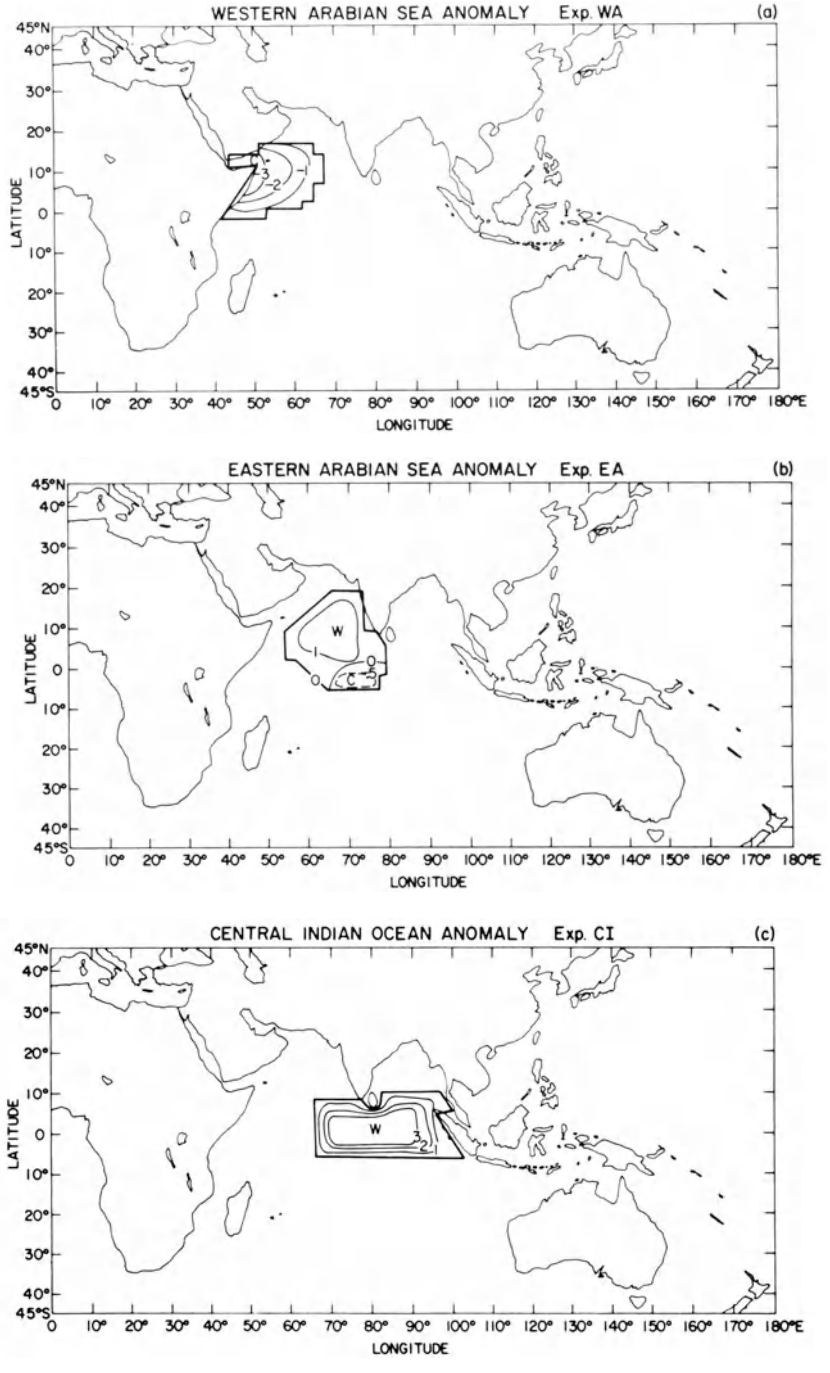

Figure 2

Ocean surface temperature anomaly distributions: (a) WA – Western Arabian Sea, (b) EA – Eastern Arabian Sea, (c) CI – Central Indian Ocean. Contours in degrees Celsius.

referred to as WA (Western Arabian) here. The anomaly has a maximum change of -3°C. Shukla was testing the hypothesis that lower ocean temperatures in this region would reduce the evaporation and, as a result, the rainfall over India. The second anomaly pattern is an Arabian Sea temperature prescription from RAMAGE and RAMAN (1972) for July 1963 of the International Indian Ocean Expedition. This year featured relatively warm surface temperatures in the Eastern Arabian Sea and a small negative anomaly of -0.5°C near the equator south of India (Fig. 2b). By contrasting the ensemble of controls with the anomaly experiment, we may have an idea of the effect on the monsoon circulation of year-to-year differences in ocean temperatures. This anomaly experiment is referred to as EA (Eastern Arabian). The third anomaly pattern was suggested by the tropical meteorology group at Saint Louis University which was especially interested in the Equatorial Indian Ocean. This anomaly (Fig. 2c) has a maximum change of 3°C centered at 2.5°N and is referred to as CI (Central Indian). The purpose of testing such an anomaly is to determine how ocean temperature changes in this region affect the SET. Moreover, if the SET were to change position, other areas of the monsoon circulation might be affected as well.

4. *Statistical significance testing procedure*

A focal point of this study is to determine if the anomalous ocean temperature causes statistically significant changes in the simulation. The method follows closely standard practices in statistics and has been applied to GCM experiments by CHERVIN and SCHNEIDER (1976a, b). It is based upon defining a normalized response r for any particular field at each model grid point as follows:

$$r = \frac{\Delta_{30}}{\sigma_{30}}, \tag{1}$$

where Δ_{30} is the prescribed change response (i.e., the difference between the 30-day mean from the prescribed change experiment and the ensemble average of the 30-day means from the control population) and σ_{30} is the standard deviation of 30-day means as estimated from the finite sample of control cases.

Following CHERVIN *et al.* (1976), we can relate r to the test variate widely used in the Student's t-test to obtain an objective measure of significance. In this way, we can obtain a significance level which serves as an estimate of the probability that a given value of r could be exceeded by chance (i.e., by random fluctuations generated in the model, sometimes referred to as noise). Since we have only three control cases to establish an estimate of standard deviation, this allows only two degrees of freedom. Table 1 summarizes the relationships of r, Student's t, and the significance level for one- and two-sided tests. The significance test is of the null hypothesis that no change in the model's climatological statistics was caused by the ocean surface temperature change in the model. Following CHERVIN *et al.* (1976), the null hypothesis can be

Table 1

Significance level for rejecting the null hypothesis for a selection of normalized responses corresponding to 2 degrees of freedom

$r = \Delta_{30}/\sigma_{30}$	Student's t $t = (\sqrt{3/2})r$	One-sided test significance level (%)	Two-sided test significance level (%)
1	0.87	23.80	47.60
2	1.73	11.29	22.58
3	2.60	6.08	12.15
4	3.46	3.72	7.43
5	4.33	2.46	4.92
6	5.20	1.75	3.51
7	6.06	1.31	2.62
8	6.93	1.01	2.02
9	7.79	0.80	1.61
10	8.66	0.65	1.31

rejected for a given value of r which implies that a significant change has occurred in the model statistics with a probable error from random fluctuations given by the significance level. The smaller the value of significance level, the more confident we are that the change resulted directly from the imposed prescribed change. The t-distribution for one- and two-sided tests for 2 degrees of freedom was obtained from SMIRNOV (1961). The use of a one- or two-sided t-test is based upon whether there is an anticipated specific signed difference (either positive or negative) in the population means. If a specific signed difference is expected, then a one-sided t-test is appropriate with its associated smaller numerical values of significance level (Table 1). Even though we expect in some cases a preferred signed change, we use the two-sided test for our discussion of the results. We accept a normalized response greater than 5 as significant, implying a significance level of approximately 2.5 or 5 percent depending on whether a one- or two-sided test is used. In subsequent figures of precipitation and vertical velocity change, we stipple those areas containing grid points with normalized response greater than 5.

5. *Climatology of ensemble of controls*

We show in Fig. 3 the time means of winds at 1.5 and 13.5 km for the ensemble of controls. Because a detailed comparison with observations has already been carried out by WASHINGTON and DAGGUPATY (1975), we do not repeat that discussion here. The low-level flow is in general agreement with the studies of FINDLATER (1969) and RAMAGE *et al.* (1972) in terms of direction and speed; however, the model tends to smooth the Somali jet. As is evident from Fig. 3 (bottom), the SET for the ensemble average of control cases is located between 5°S and 2.5°S, in agreement with the observations reported by RAO and RAGHAVENDRA (1967). The upper-level flow shows

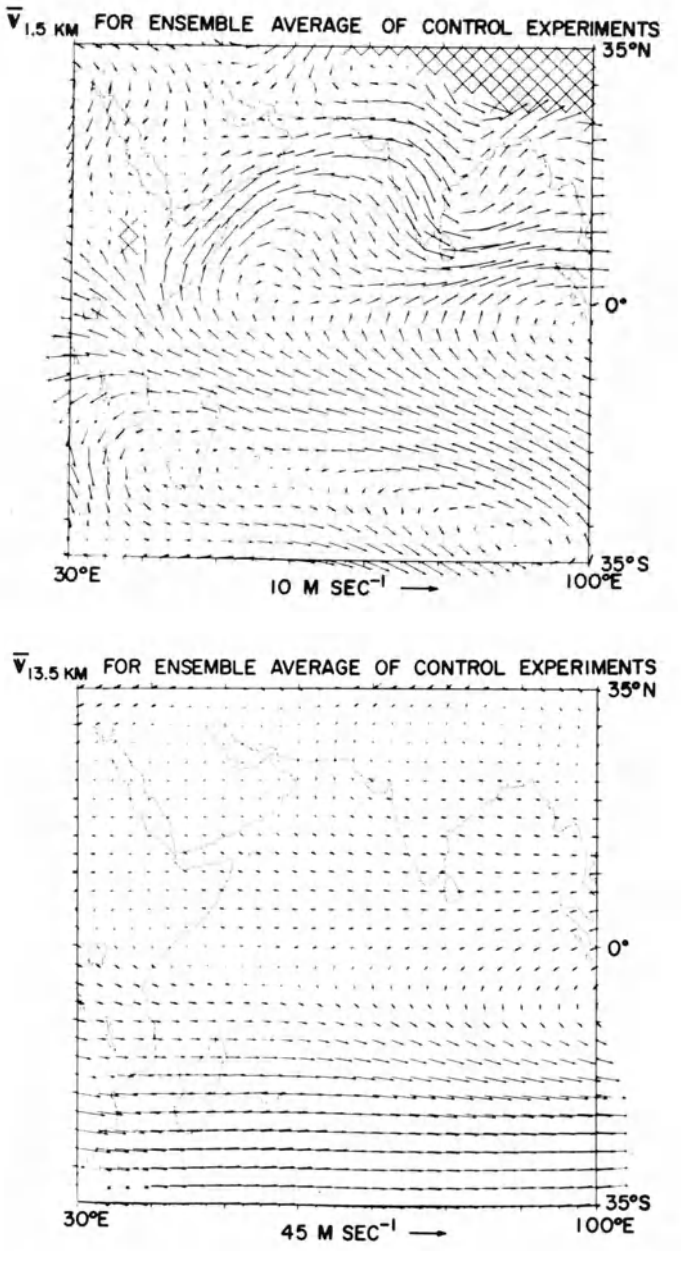

Figure 3
1.5 and 13.5 km wind vectors for the average of the ensemble of controls time-averaged over Days 91–120. Representative wind vector at bottom of each figure.

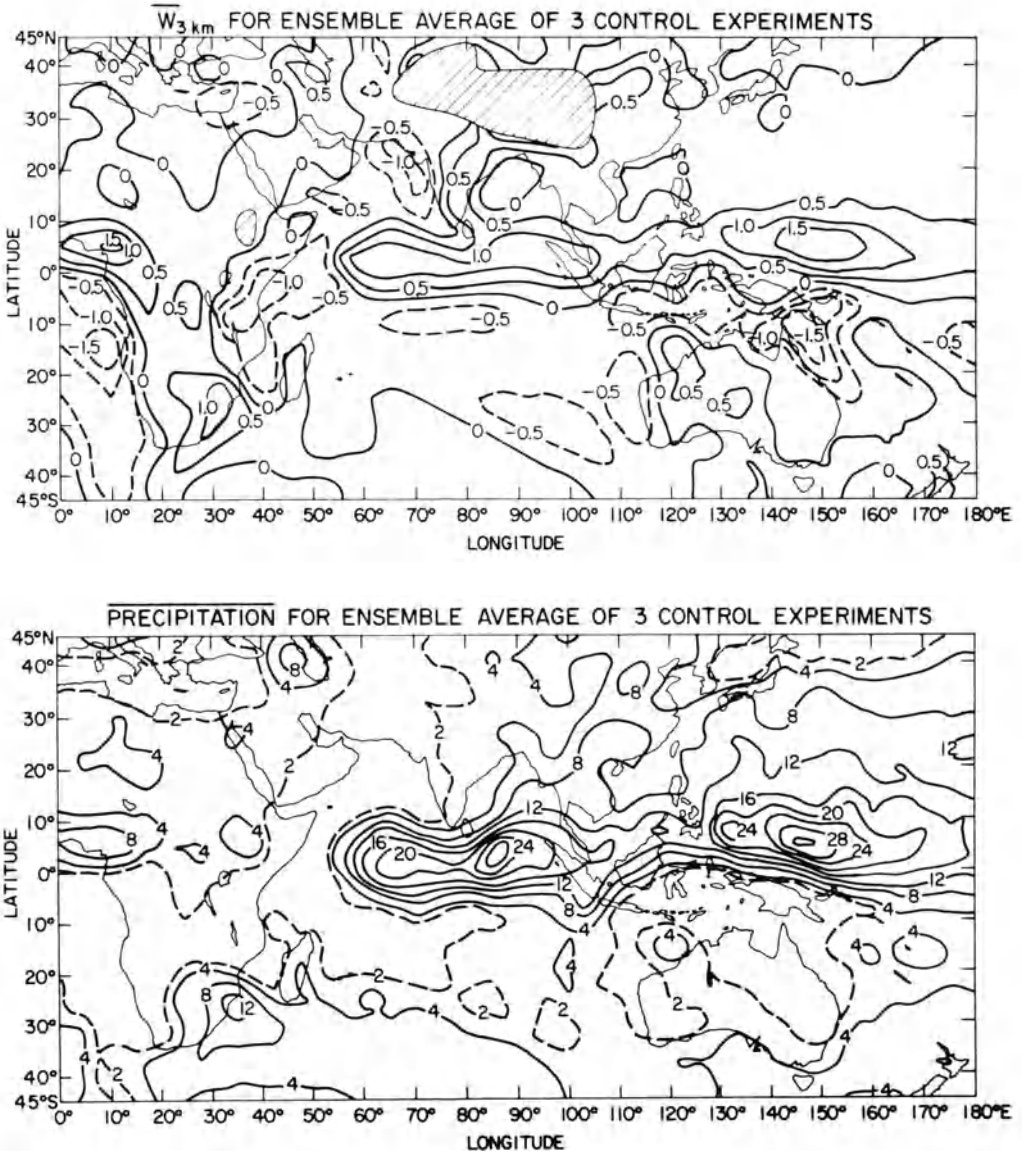

Figure 4

Vertical velocity at 3 km and precipitation for ensemble of controls time-averaged over Days 91–120. Contours are: 0.5 cm sec^{-1} for vertical velocity and 4 mm day^{-1} (solid) for precipitation, with the additional 2 mm day^{-1} contour (dashed). Slanted shading indicates mountains exceeding 3 km.

a model-generated tropical easterly jet of 8 m sec^{-1} rather than the observed 20–25 m sec^{-1} of RAMAGE and RAMAN (1972). Possible reasons for this discrepancy were discussed in WASHINGTON and DAGGUPATY (1975). Figure 4 shows mean vertical velocity w and precipitation for the ensemble of controls. Because precipitation is closely tied to vertical velocity in the model, the two are highly correlated. As discussed by WASHINGTON and DAGGUPATY, the model generates precipitation maxima in the oceanic tropics over local maxima in ocean temperature. This model behavior has also been seen in the GFDL model by MANABE *et al.* (1974) and HAHN and MANABE (1975) (see the correspondence between SIKKA, RAGHAVAN and SHUKLA, 1976.) Neither model obtains proper rainfall over the Indian subcontinent and along the western Ghats. The most likely explanation for the lack of rainfall on the western side of the Ghats is that the resolution of the mountains is crude and such features are smoothed out. Also, the models do not generally have realistic monsoon depressions which move along the Ganges valley. These storms are below or at the threshold of the resolution of the models. Without such storms, the rainfall pattern over India would be in error because a great deal of the rainfall occurring naturally results from this type of storm activity. In spite of these difficulties, GCMs are able to model the major large-scale features of the monsoon without, say, simulating the small-scale features such as the monsoon trough or the rainfall over India. Consequently, the smaller-scale features may not be important to the overall energetics of the summer monsoon. Future development of GCMs may include such features because of improved horizontal and vertical resolution, even though their inclusion will probably not greatly change the large-scale aspects now successfully simulated. Taking into account the above limitations of the model, we feel that it is still useful to conduct sensitivity tests as described in Section 3 to establish a baseline for GCM response to Indian Ocean surface temperature anomalies and to provide guidance for the upcoming MONEX.

Figure 5 shows the geographical distribution of σ_{30} for the 3 km vertical velocity and precipitation fields. Both distributions show the largest variability in the tropics near the equator. The vertical velocity σ_{30} ranges from 1–3 mm sec^{-1} except near the Central Indian Ocean where values close to 6 mm sec^{-1} are found. The σ_{30} distribution for precipitation ranges from 2–12 mm day^{-1} and thus is more variable than vertical velocity. Again, the region of largest inherent variability is in the vicinity of the equator. Therefore, because the noise level (or σ_{30} value) is so large in this region, the difference between the anomaly and control experiments has to be large in order to be statistically significant.

6. *Results of Western Arabian (WA) Sea anomaly experiment*

As mentioned in the introduction, this experiment was performed by SHUKLA (1975) with the GFDL GCM. We repeated this experiment with the NCAR GCM using the same anomaly pattern.

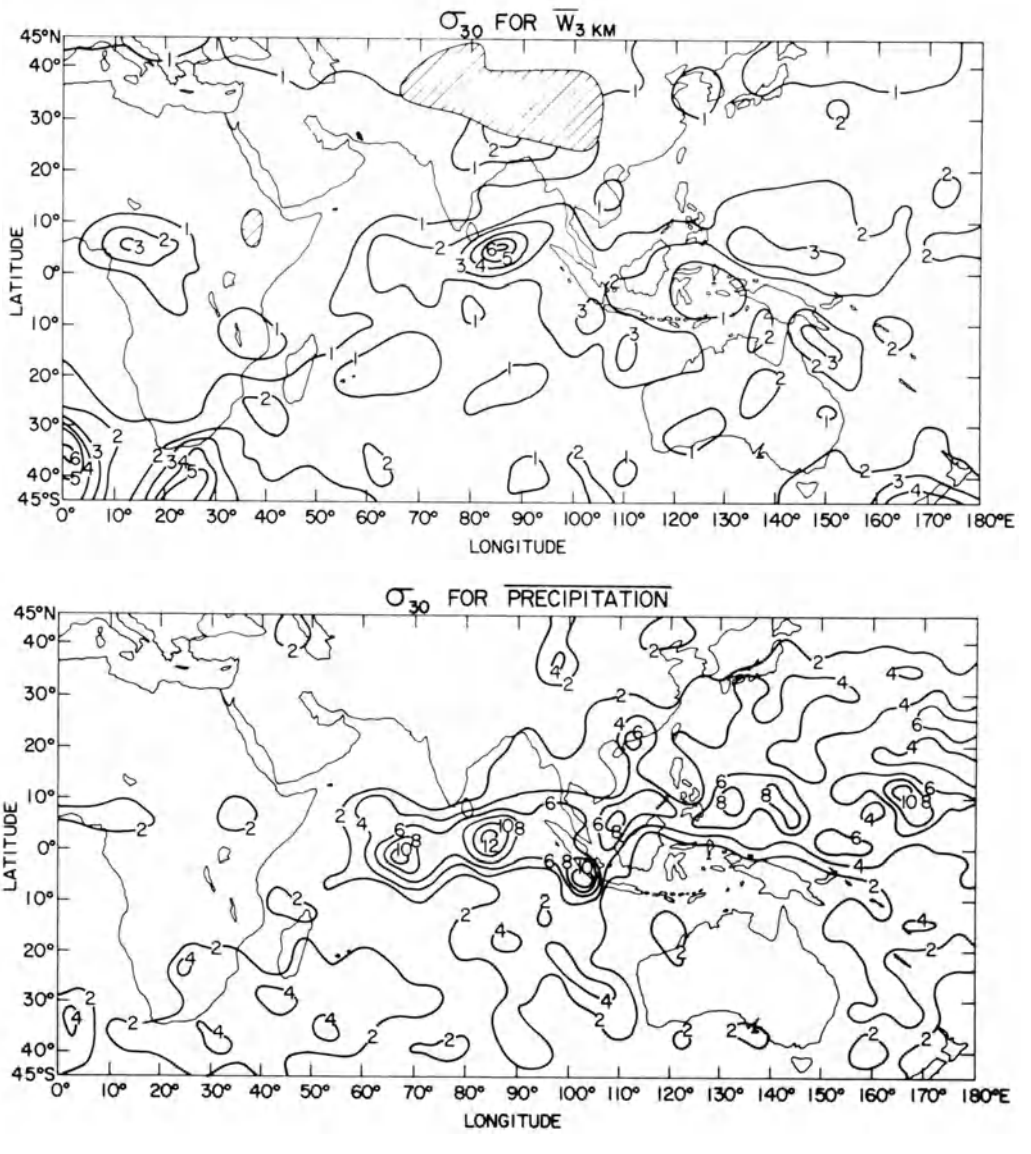

Figure 5
Geographical distribution of the estimated standard deviation σ_{30} for 3 km vertical velocity (mm sec^{-1}) and precipitation (mm day^{-1}) from the ensemble of controls.

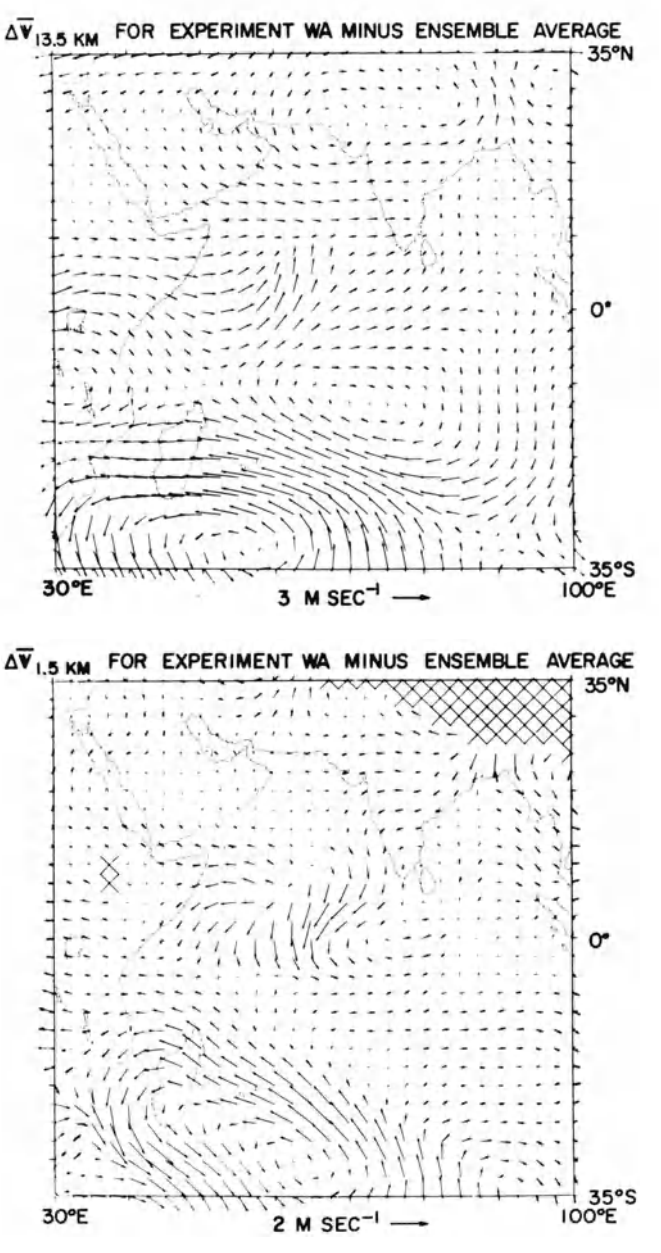

Figure 6
Difference 1.5 and 13.5 km wind fields for the WA experiment minus average of ensemble time-averaged over Days 91–120. Representative vector at bottom of each figure.

In Fig. 6, we have the difference of the winds at both levels (1.5 and 13.5 km) between the anomaly experiment and the ensemble average of controls. The difference in precipitation and vertical velocity is shown in Fig. 7. (The heavy dark line in each figure encloses the anomaly area.) Near 10°N over the Arabian Sea, we see a strong sinking region with diffluence in the lowest layer and confluence at 13.5 km. Near India, the easterly component of 1.5 km wind difference implies weaker westerlies; the same could be said for the flow near Somali. Associated with this sinking motion, precipitation has decreased. Note the stippled regions where $r \geq 5$. The area of rising motion south of the area of sinking motion extends into Somali and Kenya. Associated with rising motion is increased precipitation, some of which is $r \geq 5$ and can be highly significant. Although there may be teleconnections with other parts of the globe, it appears that the circulation caused by the cell is quite local, that is, sinking in the eastern and southern parts of the anomaly region and rising directly adjacent to it. Of course, this pattern is superimposed on the time means of the ensemble average shown in Figs. 3 and 4. The region of most significant change agrees with what Shukla found in his experiment even though the methods for computing significance are quite different. The region over India appears to have more sinking, but the normalized response does not exceed 5. The precipitation difference field agrees with Shukla's experiment by showing less rainfall over India but not at a high significance level. Over India, the r value (not shown) ranges from 1 to 3 yielding significance levels of 48 percent to 12 percent. Consequently, the precipitation decreases there cannot be attributed to the anomaly with much confidence. Differences over Malaysia and the western Pacific are not systematic. The other isolated regions with $r \geq 5$ are probably small random effects where σ_{30} is small and thus should be ignored. It must also be noted that the region of large wind change shown in Fig. 6 near Madagascar is characterized by r values in the range from 1 to 2. Consequently, these wind changes cannot be considered significant by the criterion described in Section 4.

7. *Results of Eastern Arabian (EA) Sea anomaly experiment*

As in Section 6, we show the differences of horizontal wind, vertical velocity, and precipitation from the ensemble of control experiments in Figs. 8 and 9. (The anomaly region is indicated by a heavy, dark line.) The low-level difference wind field shows confluence over the warm anomaly and diffluence aloft. Changes in the wind field extend over the Bay of Bengal and south of the equator. The low-level winds are speeded up on the southern edge of the anomaly and slowed down on the northern edge. This is expected with increased precipitation which results in increased latent heat release causing low pressure. The wind field responds to the pressure pattern but is modified because of the coriolis effect finally resulting in the difference wind field shown in Fig. 8. The region near 20°S–30°S has large wind changes, although not

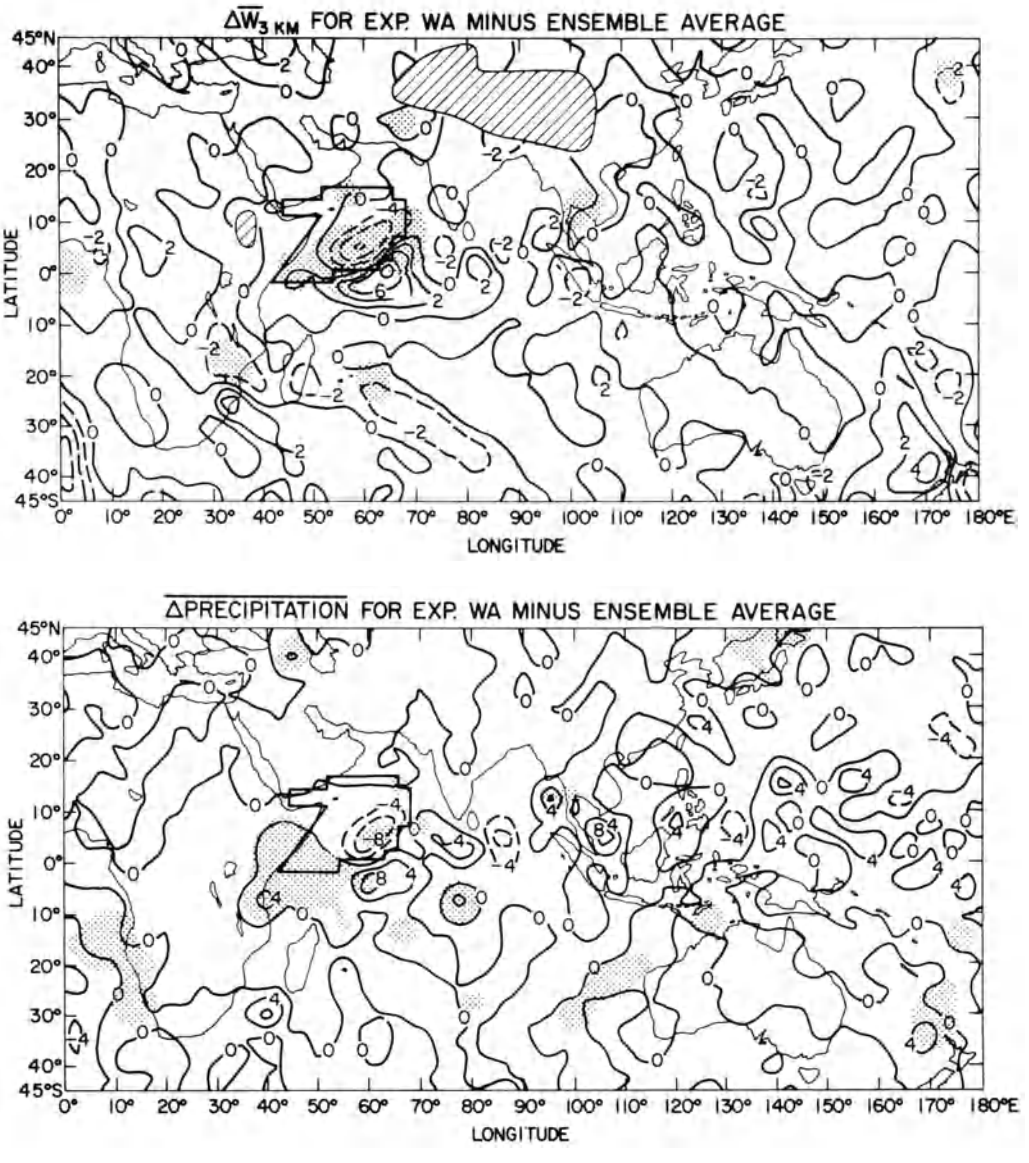

Figure 7

Difference vertical velocity at 3 km and precipitation for the WA experiment minus average of ensemble time-averaged over Days 91–120. Contours are: 2 mm sec^{-1} for vertical velocity and 4 mm day^{-1} for precipitation. The anomaly region is outlined with a heavy line. Stippled areas correspond to normalized responses $r \geq 5$.

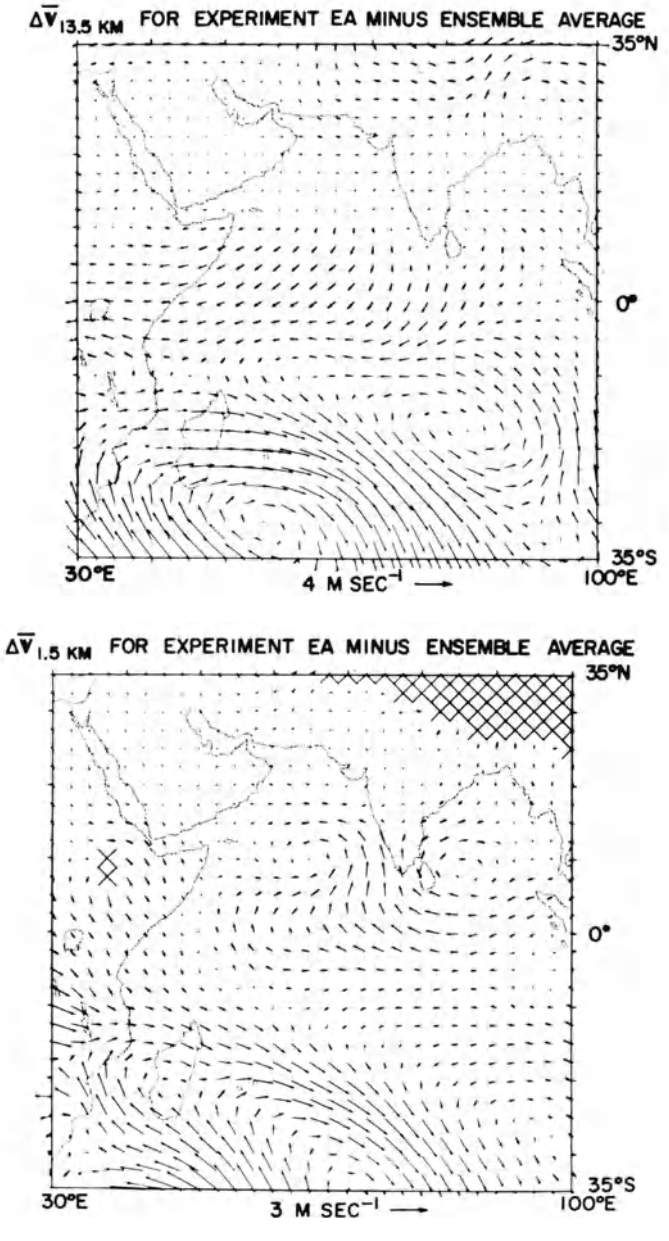

Figure 8
Difference 1.5 and 13.5 km wind fields for the EA experiment minus average of ensemble time-averaged over Days 91–120. Representative vector at bottom of each figure.

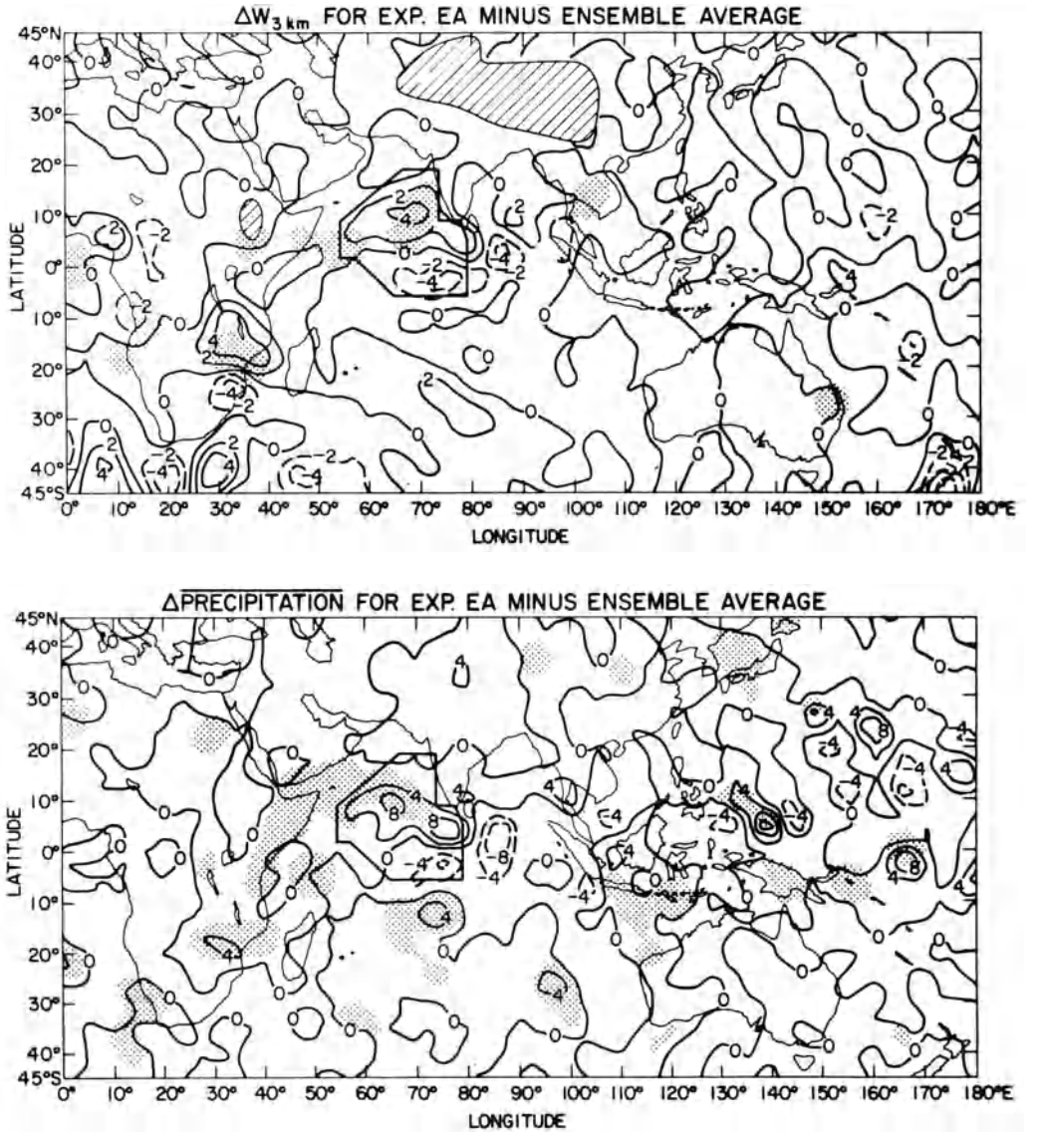

Figure 9

Difference vertical velocity at 3 km and precipitation for EA experiment minus average of ensemble time-averaged over Days 91–120. Contours are: 2 mm sec^{-1} for vertical velocity and 4 mm day^{-1} for precipitation. The anomaly region is outlined with a heavy line. Stippled areas correspond to normalized responses $r \geq 5$.

statistically significant because the r values range from 1 to 2. Vertical velocity and precipitation have greatly increased over the anomaly and have a ratio of $r \geq 5$. The precipitation has increased over Somali and Kenya but the amounts are small. Sinking motion and less precipitation appear south and east of the anomaly region. The r values over India are 1–2 (not shown), suggesting that the differences in precipitation are not highly significant. The lack of significance over India contrasts with the observed positive correlation coefficient (~ 0.3) found by SHUKLA and MISRA (1977) between Arabian Sea temperatures and monsoon rainfall from 60 years of data. However, this implies that the OST is not a perfect predictor of rainfall over the Indian subcontinent for any particular year and, in fact, accounts for less than 10 percent of the variance. Thus, the local circulation generated by this anomaly pattern is predominantly between the Western Arabian Sea and Central Indian Ocean rather than over India.

8. Results of Central Indian Ocean anomaly experiment

The Central Indian Ocean is of interest because the SET occasionally modifies its position and such a change may alter the monsoon circulation. The wind, vertical velocity, and precipitation difference fields are shown in Figs. 10 and 11. The low-level difference wind field shows inflow south of India into the region of the warm anomaly and speeding up of the Somali jet and slowing down of the westerlies over the Bay of Bengal. Also, south of the equator there is inflow into the anomaly region. From the 1.5 km wind field for the CI experiment (not shown), we find a 2.5° northward shift of the SET in the region between 82.5°E and 100°E. At the upper layer, we see diffluence over the anomaly region acting to slow down the tropical easterly jet. Consistent with the EA anomaly experiment, increased upward motion and precipitation are centred over the warm ocean anomaly. In this region, both changes have $r \geq 5$ and are highly significant. Surrounding the upward motion region is weaker downward motion, some of which appears to be significant. In addition to the local circulation cells, there is an east-west circulation cell between the CI region and Malaysia and the western Pacific, where we find significant downward motion indicating a teleconnection between the two regions. The large increase in upward motion off the southwest coast of Africa is predominantly not significant by our objective criterion. In fact, the small region in this area with normalized response greater than 5 is primarily a consequence of the non-uniform nature of the distribution of σ_{30} for $\overline{W}_{3\,\mathrm{km}}$ (see Fig. 5) and hence should be ignored. Over India, we find rising motion in the western half and sinking motion in the eastern half. The western half change is very significant ($r \geq 5$), and the eastern half change ranges between 2 and 4 – also significant, but not at our *a priori* acceptance level. The precipitation over the western and southern tip of India increased by only a small amount, but even this small amount appears to be significant. The decreases in precipitation over Malaysia and the western Pacific are not as

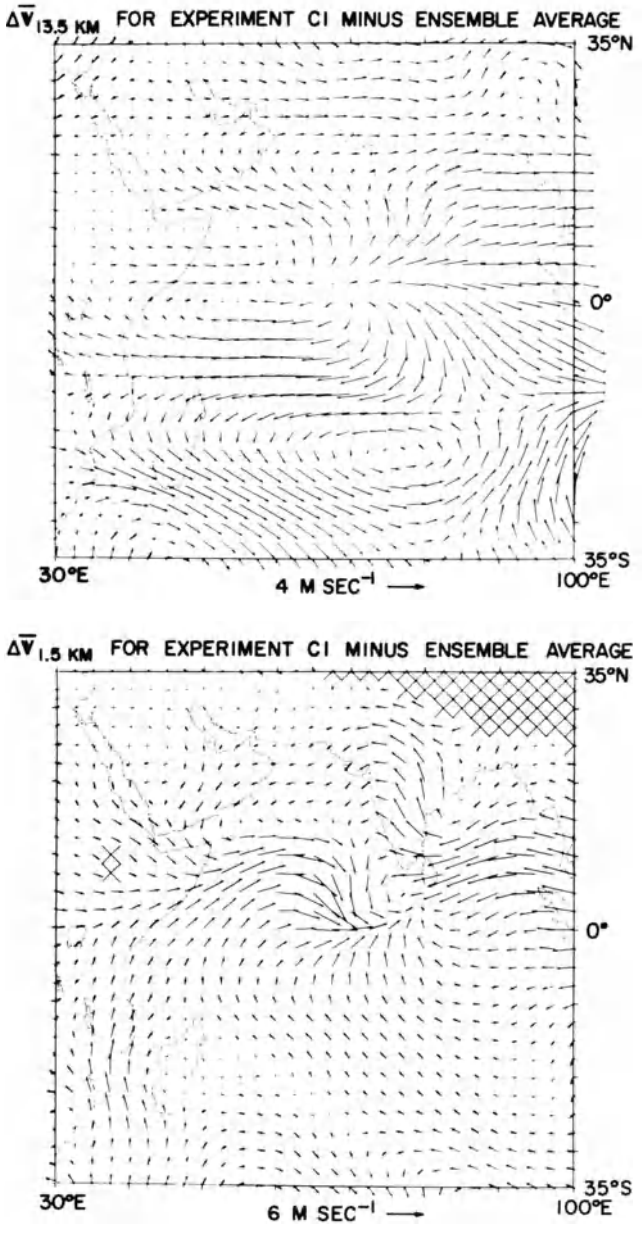

Figure 10
Difference 1.5 and 13.5 km wind fields for the CI experiment minus average of ensemble time-averaged over Days 91–120. Representative vector at bottom of each figure.

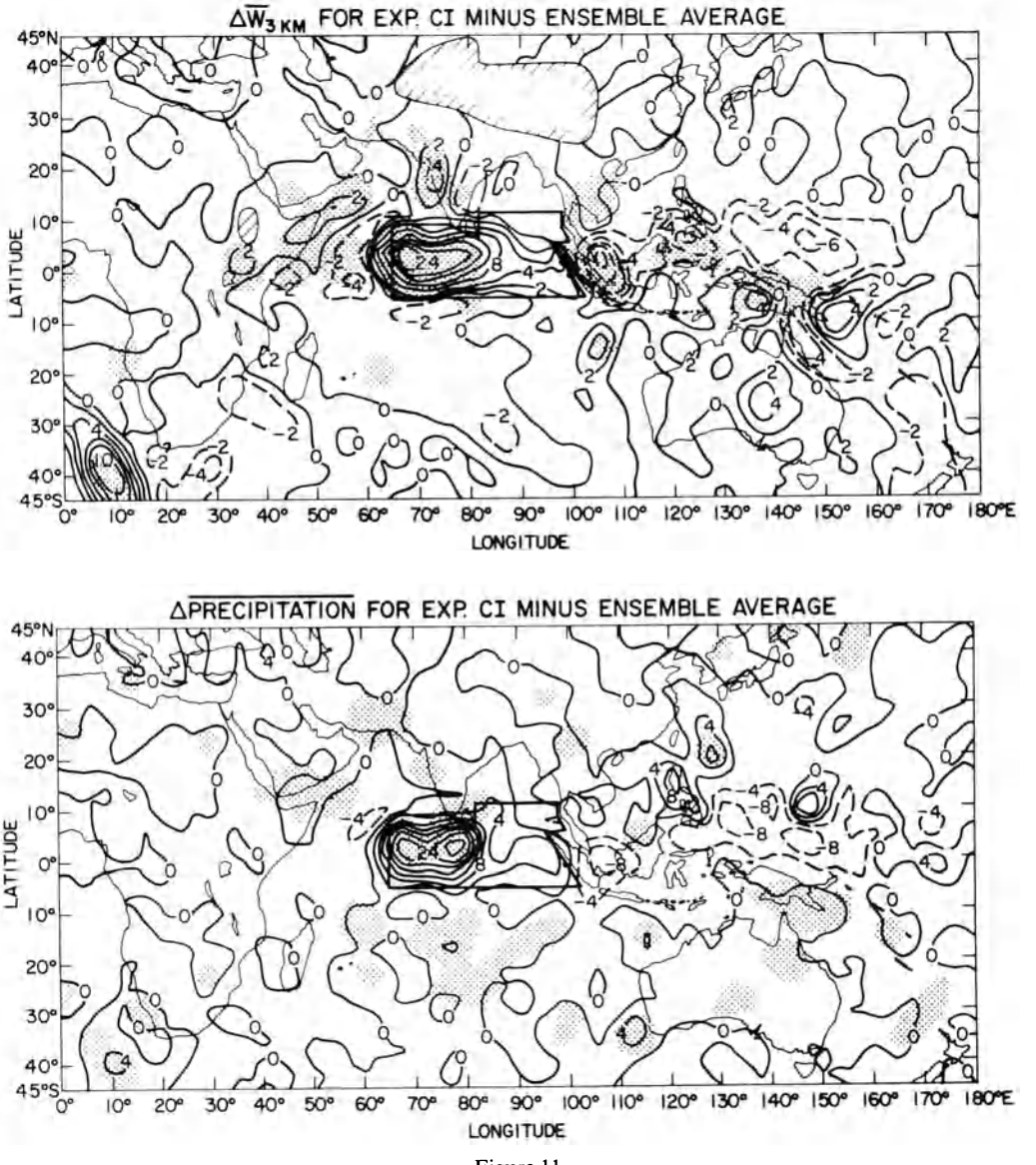

Figure 11

Difference of vertical velocity at 3 km and precipitation of the CI experiment minus average of ensemble. Contours are: 2, 4, 8, 12, 16, 20, 24 mm sec^{-1} for vertical velocity and 4 mm day^{-1} for precipitation. The anomaly region is outlined with a heavy line. Stippled areas correspond to normalized responses $r \geq 5$.

significant as the vertical velocity changes, but they are consistent with the increased downward motion there. In his observational study, SRINIVASAN (1968) found little direct evidence between the changes in the SET and the monsoon characteristics over India, and our experiment seems to support this conclusion. The major circulation change other than local appears to be in the east-west direction.

9. *Conclusions and summary*

Three different ocean temperature anomalies have been tested to determine how they modified the summer monsoon circulation in the NCAR GCM. Following the earlier work of SHUKLA (1975), the first was a cold ocean surface temperature anomaly in the Western Arabian Sea. The response of the model was similar to Shukla's in that the most significant response was immediately downstream of the cold anomaly maxima where there was decreased precipitation. Over India and adjacent regions, there was decreased precipitation, but the statistical significance of these changes was not great. For this experiment, we also found that most of the circulation change for, say, vertical velocity was local.

The Eastern Arabian Sea experiment yielded increased precipitation and upward motion over the warm region. There was less precipitation and downward motion immediately south and east of the warm anomaly near the SET, indicating again the relatively local model response in the region.

The Central Indian Ocean anomaly showed a large response in the SET. The precipitation greatly increased over the warm anomaly and decreased over Malaysia and the western Pacific. The vertical velocity pattern showed evidence of an east-west, teleconnecting circulation between the two regions. We thus find both a local and a nonlocal model response for this experiment.

In summary, the results of the model experiments suggest two major requirements for better understanding the summer monsoon. The first is to have highly accurate measurements of the ocean surface temperature, and the second is to know the year-to-year variations of ocean temperatures because they are probably a large factor in determining year-to-year differences in the monsoon circulation. The upcoming MONEX should be designed to provide such data and thereby produce detailed empirical evidence on the extent to which Indian Ocean surface temperature anomalies correlate with precipitation anomalies over the Indian subcontinent – a correlation which generally does not appear in our GCM results.

Acknowledgments

The authors greatly appreciate the painstaking efforts of Gloria Williamson in making the necessary model changes and supervising the running of the several

experiments required for this study on the NCAR Control Data Corporation 6600 computer. We also thank the members of the NCAR Graphics Group and Gerald Meehl for drafting the figures and Ann Modahl for editing and typing of the original manuscript and its many revisions.

References

CHERVIN, R. M., GATES, W. L. and SCHNEIDER, S. H. (1974), *The effect of time averaging on the noise level of climatological statistics generated by atmospheric general circulation models*, J. Atmos. Sci. *31*, 2216–2219.

CHERVIN, R. M. and SCHNEIDER, S. H. (1976a), *A study of the response of NCAR GCM climatological statistics to random perturbations: Estimating noise levels*, J. Atmos. Sci. *33*, 391–404.

CHERVIN, R. M. and SCHNEIDER, S. H. (1976b), *On determining the statistical significance of climate experiments with general circulation models*, J. Atmos. Sci. *33*, 405–412.

CHERVIN, R. M., WASHINGTON, W. M. and SCHNEIDER, S. H. (1976), *Testing the statistical significance of the response of the NCAR General Circulation Model to North Pacific Ocean surface temperature anomalies*, J. Atmos. Sci. *33*, 413–423.

FINDLATER, J. (1971), *Mean monthly airflow at low levels over the western Indian Ocean*, Meteor. Office Geophys. Mem., No. 155, 53 pp.

HAHN, D. G. and MANABE, S. (1975), *The role of mountains in the south Asian monsoon circulation*, J. Atmos. Sci. *32*, 1515–1541.

JOINT ORGANIZING COMMITTEE OF GARP (1976), *The monsoon experiment*, GARP Publication Series No. 18, GARP WMO/ICSU Joint Organizing Committee, October, 1976, 123 pp.

JOSEPH, J. H. (1976), *The effect of desert aerosol on a model of the general circulation*, Paper presented at the IUGG Symposium on Radiation of the Atmosphere, Garmisch-Partenkirchen, 19–28 Aug. 1976, Federal Republic of Germany (to be published).

KRISHNAMURTI, T. N. and MOXIM, W. J. (1971), *On parameterization of convective and nonconvective latent heat release*, J. Appl. Meteor. *10*, 3–13.

KUTZBACH, J. E., CHERVIN, R. M. and HOUGHTON, D. D. (1977), *Response of the NCAR general circulation model to prescribed changes in ocean surface temperature. Part I: Mid-latitude changes*, J. Atmos. Sci. in press.

LLEWELLYN, R. A. and WASHINGTON, W. M. (1977), Regional and global aspects. In *Energy and Climate, Studies in Geophysics*, National Academy of Sciences Report, Washington, D.C., in press.

MANABE, S., HAHN, D. G. and HOLLOWAY, J. L. JR. (1974), *The seasonal variation of the tropical circulation as simulated by a global model of the atmosphere*, J. Atmos. Sci. *33*, 43–83.

RAMAGE, C., MILLER, F. R. and JEFFERIES, C. (1972), *Meteorological Atlas of the International Indian Ocean Expedition, Vol. 1*, National Science Foundation, Washington, D.C. (Superintendent of Documents, Washington, D.C., Stock No. 3800–00123).

RAMAGE, C. and RAMAN, C. R. V. (1972), *Meteorological Atlas of the International Indian Ocean Expedition, Vol. 2*, National Science Foundation, Washington, D.C. (Superintendent of Documents, Washington, D.C., Stock No. 3800–00124).

RAMAN, C. R. V. (1965), *Cyclonic vortices on either side of the equator and their implications*, Proceedings of Symposium on Meteorology, Results of IIOE, Bombay, 11 pp.

RAO, Y. P. and RAGHAVENDRA, V. K. (1967), *Variation of pressure, wind, cloudiness and rainfall across equator in the Indian Ocean*, Proceedings of Symposium on Indian Ocean, March 1967, New Delhi, Part II, 1011–1014.

SAHA, K. R. (1970), *Zonal anomaly of the sea surface temperature in equatorial Indian Ocean and its possible effect on monsoon circulation*, Tellus *22*, 403–409.

SHUKLA, J. (1975), *Effect of Arabian sea-surface temperature anomaly on Indian summer monsoon: A numerical experiment with the GFDL model*, J. Atmos. Sci. *32*, 503–511.

SHUKLA, J. (1976), *Reply*, J. Atmos. Sci. *33*, 2253–2255.

SHUKLA, J. and MISRA, B. M. (1977), *Relationships between sea-surface temperature and wind speed over the Arabian Sea, and Monsoon Rainfall over India*, Mon. Wea. Rev., in press.

SIKKA, D. R. and RAGHAVAN, K. (1976), *Comments on 'Effects of Arabian sea-surface temperature anomaly on Indian summer monsoon: A numerical experiment with the GFDL model,'* J. Atmos. Sci. *33*, 2252–2253.

SMIRNOV, N. V. (Ed.), *Tables for the Distribution and Density Functions of 't'-distribution (English translation)* (Pergamon Press, New York 1961), 129 pp.

SRINIVASAN, V. (1968), *Some aspects of broad-scale cloud distribution over Indian Ocean during Indian southwest monsoon season*, Indian J. Meteor. Geophys. *19*, 39–53.

WASHINGTON, W. M. and THIEL, L. G. (1970), *Digitized global monthly mean ocean surface temperatures*, Technical Note No. 54, National Center for Atmospheric Research, Boulder, Colorado, 94 pp.

WASHINGTON, W. M. and DAGGUPATY, S. M. (1975), *Numerical simulation with the NCAR global circulation model of the mean conditions during the Asian–African summer monsoon*, Mon. Wea. Rev. *103*, 105–114.

WASHINGTON, W. M. and WILLIAMSON, D. L. (1977), *A description of the NCAR global circulation models*, in *Methods in Computational Physics, Vol. 17, General circulation models of the atmosphere*, in press.

(Received 15th June 1977)

Pageoph, Vol. 115 (1977), Birkhäuser Verlag, Basel

Numerical Weather Prediction Relevant to the Monsoon Problem

T. N. KRISHNAMURTI,[1]) JOHN MOLINARI,[1]) HUA-LU PAN,[1]) and VINCE WONG[1])

Abstract – In this short paper we have identified some of the modelling groups that have the capability of simulating or carrying out short range numerical weather prediction over the monsoon belt. We have next outlined some of the important and desirable ingredients for a multilevel primitive equation model over the tropics, with most of the emphasis on the present version of Florida State University's Tropical Prediction Model. Finally, we present briefly some important results based on the present version of our prediction models that relate to the NWP efforts over the monsoon belt. Here we have identified the importance of mountains, convection, the radiative heating balance of the earth's surface, and the planetary boundary layer over the Arabian Sea.

Key words: Monsoon, numerical weather prediction.

1. Introduction

The problem of short range (real data) numerical weather prediction in all latitudes has much in common; the monsoon belt is no exception in this regard. Perhaps the areas where greater care needs to be exercised in numerical modelling are in the treatment of steep mountains and in the problems of parameterization of convection, radiative heat balance of the earth's surface and in the specification of boundary layer processes.

Ideally speaking, what is desirable is a global model which uses the earth's surface with a detailed topography as a coordinate surface (see PHILLIPS, 1957). However, from considerations of economy and regional interests, only limited area models with a fine mesh of grid points are frequently used. Here it would be desirable if one could use as lateral boundary conditions the solution of a global model, the regional model being a nested fine mesh model. This provides a one way interaction between the global model and the regional model.

As stated in a number of studies in this issue of *Pure and Applied Geophysics*, the tropical quasi-stationary long waves are a major source of energy for shorter waves. The rate of energy exchange from zonal and long waves to shorter synoptic scale waves is found to be quite large on the time scale of a few days. Thus, short range numerical weather prediction of an isolated monsoonal disturbance may not be very

[1]) Department of Meteorology, Florida State University, Tallahassee, Florida 32306, USA.

accurate if its interaction with the large scale monsoonal circulations is not somewhat properly accounted for. In two recent papers some results from the Florida State University Tropical Prediction Model are addressed, KRISHNAMURTI *et al.* (1976) and (1977). The model is described in some detail in KRISHNAMURTI *et al.* (1973) and KANAMITSU (1975). Here we shall not try to review these earlier results since they are already published. In this paper we present a survey of some newer areas where emphasis is required.

2. *NWP models and important ingredients for monsoon prediction*

The following are a list of some of the well known large models that have the capability of handling the monsoon circulations.

(i) GFDL Princeton, USA, Global General Circulation Model.
(ii) NCAR, Boulder, USA, General Circulation Model.
(iii) NMC, Washington, USA, Global Prediction Model.
(iv) U.K. Meteorological Office, Global General Circulation Model.
(v) Japan Meteorological Agency, Hemispheric Model.
(vi) Canadian Meteorological Service, Hemispheric Model.
(vii) Oregon State, USA, Global General Circulation Model.
(viii) Florida State University, Global Tropical Prediction Model, and
(ix) Fleet Numerical Weather Facility, Monterey, Operational Model.
(x) Giss (Goddard Institute of Space Sciences) General Circulation Model.

The relative performance of these various models in the day to day prediction over the monsoonal belt is not known. In the case of the global and hemispheric operational models, the interest on day to day verification is still regional. Hence, in many instances it is almost impossible to determine the skill in the day to day prediction of monsoons. The general circulation models have carried out very interesting simulations of the monsoons. The message that emerges from these modelling studies is that numerical weather prediction over the monsoon belt should be done with a fairly sophisticated model.

The following is a list of some of the important ingredients for a multi-level primitive equation model.

(i) *Basic primitive equation model in the σ frame* (PHILLIPS, 1957, KASAHARA, 1974):

(a) Stable finite differencing scheme for handling linear and non-linear computational stability,
(b) Horizontal resolution of the order of 100 kms,
(c) Vertical resolution of the order of 100 mbs, at least 10 levels in the atmosphere.
(d) If an unstaggered grid is used in space for variables u, v, and z, then it is desirable that care be exercised in the handling of divergence and pressure

gradient forces to avoid a splitting of solution which has the form of a two grid distance gravity wave. KANAMITSU (1975) has shown a procedure for handling this problem.

(ii) *Air-sea interaction*: The bulk aerodynamic formulae are considered to be suitable for estimates for the sensible heat and evaporative fluxes from the ocean to the atmosphere. In this regard the sea-surface temperature field is a desirable input for short range numerical weather prediction. Modelling studies, KRISHNAMURTI *et al.* (1976) and T. MURAKAMI *et al.* (1970) show that monsoon simulations and short range predictions are not very sensitive to small changes in the sea surface temperature. It is the land temperature which produces the crucial thermal drive. The ocean is however very important for it provides the needed moisture supply.

(iii) *Momentum exchange between the atmosphere and the earth's surface*: The usual drag laws are still quite useful over the oceans with values of drag coefficient $\approx 1 \times 10^{-3}$. Over land areas the value is increased to 2×10^{-3} and over mountainous areas one uses values as high as 3×10^{-3}. (GARP PUBLICATION, No. 16, p. 49.) The surface roughness z_0 varies considerably and not much is known about the precise manner in which this should be handled.

(iv) *Dry convective adjustment*: Numerical weather prediction over land areas requires a very careful programming of the dry convective adjustment process. Due to diurnal heating superadiabatic lapse rates frequently occur over large areas in the lowest layer. Superadiabatic lapse rates can also form due to diabatic heating in the troposphere. The adjustment is necessary for the parameterization of dry convection and should be carried out subject to the invariance of $\int_{\ln p_T}^{\ln p_S} \theta d \ln p$. If a layer of instability is encountered, its adjustment can lead to dry instability in a neighbouring layer. It is thus essential to invoke a successive correction technique that eliminates the dry instability in all layers as is demonstrated in detail by KANAMITSU (1975). A tropical primitive equation model over the monsoon belt is not easy to run without this prescription. The alternative to this might be a strong diffusion in the vertical, however this has other undesirable problems such as the destabilization of very stable situations.

(v) *Parameterization of cumulus convection*: Because of the heavy rainfall in many monsoon disturbances, an effective scheme is desirable. The approaches followed at the Florida State University's primitive equation model has all been adaptations of the so-called KUO's (1965) scheme. The U.K. Meteorological Office's limited area model utilizes an adjustment scheme. An obvious shortcoming of the present schemes is that they are not able to handle intense precipitation rates of the order of 20 cm/day which is typical of many monsoon depressions. This was noted by KRISHNAMURTI *et al.* (1976) and CARR (1977). It is not clear at this stage whether or not any of the newer schemes such as that proposed by ARAKAWA and SCHUBERT (1974) would perform better in terms of yielding more realistic rainfall rates. Realistic prediction of motion, structure and weather all require a major improvement in the parameterization of cumulus convection.

(vi) *Large scale condensation*: In those grid points of the computational domain where dynamic ascent of saturated stable air occurs, large scale condensation and associated heating is invoked. Care should be exercised in defining the 'saturation state' very carefully. This is a function of the various forms of diabatic heating each of which can alter the temperature and thus saturation specific humidity. A rigorous derivation of the large scale condensation was presented by KANAMITSU (1975).

(vii) *Treatment of the boundary layer*: The treatment of the convective boundary layer in the monsoonal belt is not very clearly defined. Since detailed measurements below the cloud base are almost nonexistent, the experience from GATE would be most useful for this problem. The diurnal change being large, the diurnal modification of the PBL[2]) over land areas of the monsoonal belt is another area where presently no definitive observations exist. It would be desirable to have some detailed observations, during the GARP Monsoon Experiment, of turbulent fluxes and the height of the boundary layer during the course of several days. Such observations should be coupled with surface agrometeorological observations of parameters such as soil temperature and soil moisture.

There are at least four parameters that a PBL model should determine for a primitive equation prediction model.

(a) Surface values of the turbulent fluxes of momentum, heat and moisture,
(b) Their variation in the vertical,
(c) The height of the top of the boundary layer, and
(d) The vertical velocity at the top of the boundary layer.

In a so-called Prandtl layer whose height is of the order of 75 meters the vertical fluxes of momentum, sensible heat and moisture are given by,

Momentum

$$\tau = \rho(h) C_D(h) |\mathbb{V}(h)| \mathbb{V}(h) \tag{2.1}$$

where

$$C_D = u^*/u_0 = k_0 / \ln \frac{h + z_0}{z_0} \tag{2.2}$$

u_0 is the surface velocity,
u^* is the friction velocity described by the logarithmic profile,
h is the thickness of the Prandtl layer, and
z_0 is the roughness length.

We use z_0 = 20 cm over mountains,
= 2 cm over flat land,
= 0.02 cm over the ocean.
k_0 = Von Karman constant = 0.35.

Sensible Heat

$$H = C_p \rho(h) C_D(h) |\mathbb{V}_h| \{T^* - T(h)\} \tag{2.3}$$

where T^* is the surface temperature.

[2]) PBL refers to Planetary Boundary Layer.

Evaporative flux

$$E = \rho(h)C_D(h)|\mathbb{V}_h|\{q(T^*) - q(h)\}. \tag{2.4}$$

In the present tropical primitive equation models the height of the PBL is not explicitly calculated for reasons stated earlier. The vertical convergence of flux of u, v momentum and moisture q is given by the relations,

$$\begin{Bmatrix} F_u \\ F_v \\ F_q \end{Bmatrix} = \frac{\partial}{\partial p} l^2 \left|\frac{\partial \mathbb{V}}{\partial p}\right| \frac{\partial}{\partial p} \begin{Bmatrix} u \\ v \\ q \end{Bmatrix} \tag{2.5}$$

where l is the mixing length specified according to:

$$l = \begin{cases} k_0 z & z \leq h \\ k_0 \underline{h(H - z)} & h \leq z \leq H \\ 0 & z > H \end{cases} \tag{2.6}$$

The boundary layer thickness is taken to be the height of the 900 mb surface. This preferably should be forecasted by a separate equation as shown, for example, by DEARDORFF (1972).

(viii) *Radiative processes*: We make some reference to this in another section where we emphasize its importance for the monsoon problem.

(ix) *Inclusion of mountains*: The present version of the Florida State University's Tropical Prediction Model is capable of handling mountains of slope $\leq 5 \times 10^{-3}$. This is a limitation experienced by most numerical models. Computational instabilities compounded by resulting deep convection in moist regions renders the predictions useless if larger slopes are used in conventional numerical models. This problem is severe if the so-called (σ) sigma coordinate is used, since in this frame the pressure gradient force is a small difference of two very large terms. One usually computes the pressure gradient force on the pressure surfaces and interpolates such values on to the σ surfaces. These schemes are not able to handle steep mountains. Further research in the handling of steep mountains, for the monsoon problems, is needed.

(x) *Initialization procedure*: The monsoon problems are characterized by strong cross-equatorial flows. This makes it necessary to go to primitive equation prediction models rather than filtered type (geostrophic or balanced) models. In real data short range prediction a good initialization procedure is a necessity. Experience with the Florida State University's multilevel primitive equation model has shown that dynamic initialization is necessary for low latitude problems. The dynamic initialization is a forward-backward integration with an adiabatic frictionless model (where smoothed mountains are retained), that uses the same finite difference framework as the basic prediction model. Even the most complete balanced models that carry a rather complete omega equation are unsuitable for initialization, since the differences in the

structure of the primitive and balance equations are major. The most obvious difference is in the order of the omega equation, which is first order for the primitive system, while it is second order for the non-linearly balanced system. Because of these differences, the divergent part of the motion field is incompatible in the two systems and an adjustment ensues during the prediction causing a degree of contamination. For further details on the dynamic initialization references may be made to WINNINGHOFF (1973) and KANAMITSU (1975).

3. *On the westward propagation of a monsoon depression*

A number of possible mechanisms can be invoked to explain the westward propagation of a monsoon disturbance over northern India. This is an important problem since it is not altogether obvious why these disturbances move westward in a basic southwesterly monsoon current. The following is a summary of results from a series of numerical weather prediction experiments that address this question.

(a) *Barotropic dynamics*: A positive vorticity tendency west of the disturbance center and a negative vorticity tendency to the east is required for its westward propagation. The beta effect is well known for its contribution to the westward propagation. This is often counteracted by the advection of relative vorticity such that a forecast at around 850 mb is found to produce almost no westward motion for periods as long as 48 hours. Since the amplitude of the monsoon depressions are largest near this level, it is desirable to have a reasonable prognosis at this level.

(b) *Quasi-geostrophic convergence*: In a multilevel adiabatic quasi-geostrophic model the convergence/divergence field can create or destroy vorticity at low levels. In the westward propagating monsoon depressions over northern India one does find weak quasi-geostrophic convergence to the west of the disturbance centre (the converse being the case to the east). This small convergence arises from the quasi-geostrophic rising motions. The latter are contributed by (i) the advection of warm air in the low level northerly flows, and by (ii) the negative vorticity advection at low levels. The production of vorticity by this effect in adiabatic models is found to be negligibly small to account for the observed westward motion of the disturbance.

(c) *Influence of cumulus convection*: A multilevel primitive equation model has been shown to produce a reasonable westward motion of a monsoon disturbance (KRISHNAMURTI *et al.*, 1976). The largest precipitation (computed as well as observed) occurs west of the disturbance center. In the numerical model, the large scale convergence, surface friction and the rate of cumulus scale heating acquires a state of equilibrium in the conditionally unstable atmosphere such that the magnitude of convergence at low levels is much larger than that given by a quasi-geostrophic model. A large production of vorticity occurs to the west of the disturbance and this accounts for the rapid westward motion of the disturbance.

(d) *Effect of Mountains*: A number of monsoon disturbances move northwest-

ward over northern India. The effect of a sloping mountain is very similar to the beta effect and it can give rise to convergence west of the disturbance center and a westward propagation of the disturbance. This is best illustrated from a one level primitive equation model with bottom topography.

Momentum equations:

$$\frac{\partial u}{\partial t} = -u\frac{\partial u}{\partial x} - v\frac{\partial u}{\partial y} + fv - \frac{\partial}{\partial x}g(h + z). \tag{3.1}$$

$$\frac{\partial v}{\partial t} = -u\frac{\partial v}{\partial x} - v\frac{\partial v}{\partial y} - fu - \frac{\partial}{\partial y}g(z + h). \tag{3.2}$$

Mass continuity equation:

$$\frac{\partial z}{\partial t} = -u\frac{\partial z}{\partial x} - v\frac{\partial z}{\partial y} - z\left(\frac{\partial u}{\partial x} \quad \frac{\partial v}{\partial y}\right). \tag{3.3}$$

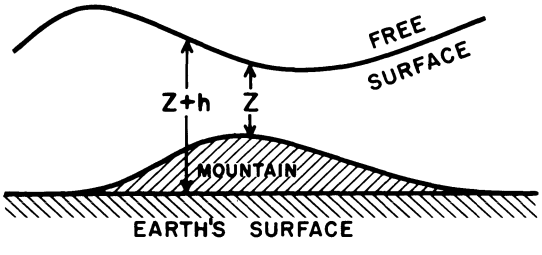

Figure 1
The geometry of the one level primitive equation model. h is the height of the mountain.

Figure 1 illustrates the relation between z and h; note that $z + h$ is the height of the free surface and the mountain height is h. The potential vorticity of this system of equations may be written in the form:

$$\frac{d}{dt}\left(\frac{\partial v/\partial x - \partial u/\partial y + f}{z}\right) = 0. \tag{3.4}$$

Figure 2 illustrates the change in z encountered by a southward moving parcel as it traverses downslope. At the point P,

$$\frac{dz}{dt} > 0, \qquad \frac{1}{z}\frac{dz}{dt} > 0$$

hence

$$-\left(\frac{\partial u}{\partial x} + \frac{\partial v}{\partial y}\right) > 0$$

from equation (3.3). Thus downslope motion is consistent with convergence and a

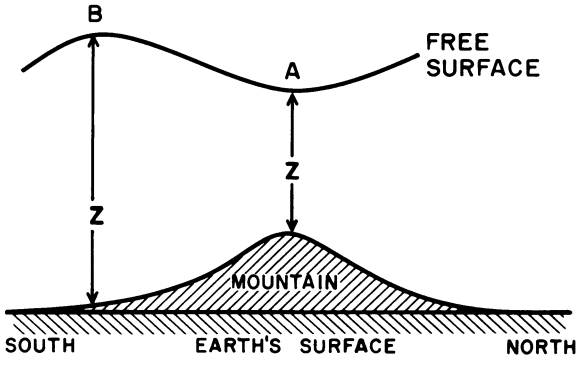

$$\left(\frac{\zeta + f}{z}\right)_B = \left(\frac{\zeta + f}{z}\right)_A$$

$$z(B) > z(A)$$

$$(\zeta + f)_B > (\zeta + f)_A$$

$$f_B < f_A$$

$$\zeta_B > \zeta_A$$

Figure 2
An illustration that demonstrates reasons for $\partial\zeta/\partial t > 0$ west of disturbance center due to the influence of mountains in downslope northerly flows.

production of vorticity and conservation of potential vorticity, i.e., equation (3.4). We illustrate this effect very effectively in real data numerical prediction experiments with a primitive equation model, see Fig. 3. Here two 48 hour forecasts with the one level primitive equation model are illustrated. The left panels do not include the bottom topography while the right panels include this effect. The experiments were carried out using the finite differencing and initialization procedures of the Florida State University's Tropical Prediction Model, KRISHNAMURTI *et al.* (1973). A two degree latitude/longitude grid mesh and smoothed topography is used as in KRISHNAMURTI *et al.* (1976). The original mountain heights come from the tabulation of GATES and NELSON (1975). The maximum height of the mountains is around 1.5 km and the mean height of the free surface is assigned a value of 3 km. Without the bottom topography the storm motion is almost negligible in the 48 hours, while the inclusion of bottom topography yields a very realistic northwestward storm motion.

(e) *Summary*: Figure 4 illustrates the observed versus the predicted storm tracks for the above mentioned series of experiments carried out at Florida State University. The combined effect of the mountains and cumulus convection seems to be most important for the westward motion of the storm. It is interesting to note that the high level easterlies are not explicitly invoked for the steering of the storm in this analysis. Since most of the storm circulation is confined to the lower troposphere, the steering by high level easterlies does not seem to be a necessary mechanism. The results

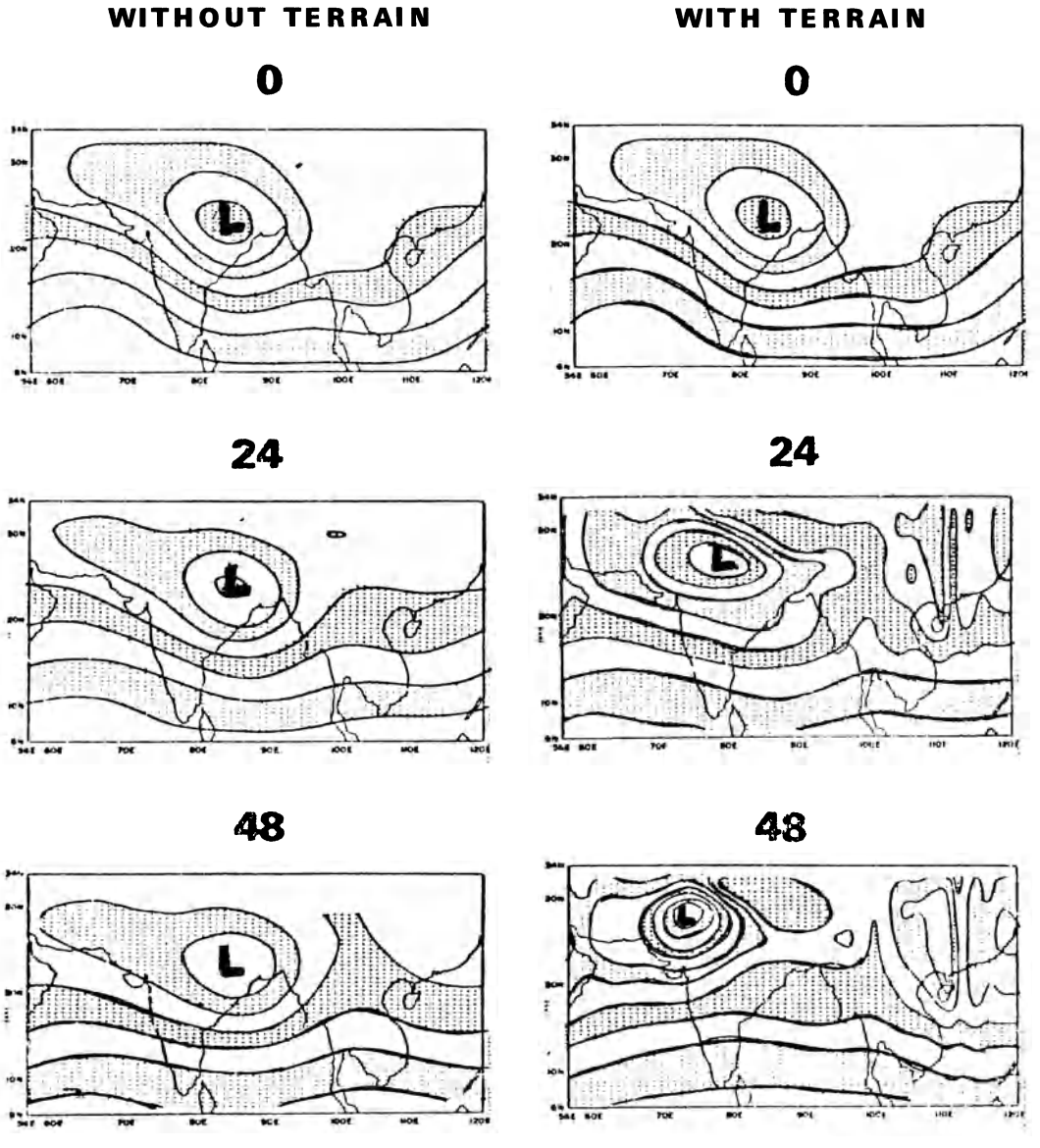

Figure 3
Predicted 850 mb height field for two experiments. The left panel is for an experiment without mountains, while the right panel includes the effect of mountains. The contours are drawn at 50 geopotential meter intervals and the maps are 24 hours apart.

presented here are still somewhat preliminary. What is, of course, needed is an operational numerical weather prediction center with a capability to forecast with a fine resolution (≈ 100 km) multi-level primitive equation model. If a large number of carefully analyzed initial states are subjected to prediction with such a model and the results diagnosed, then we can obtain further understanding on the motion of these disturbances.

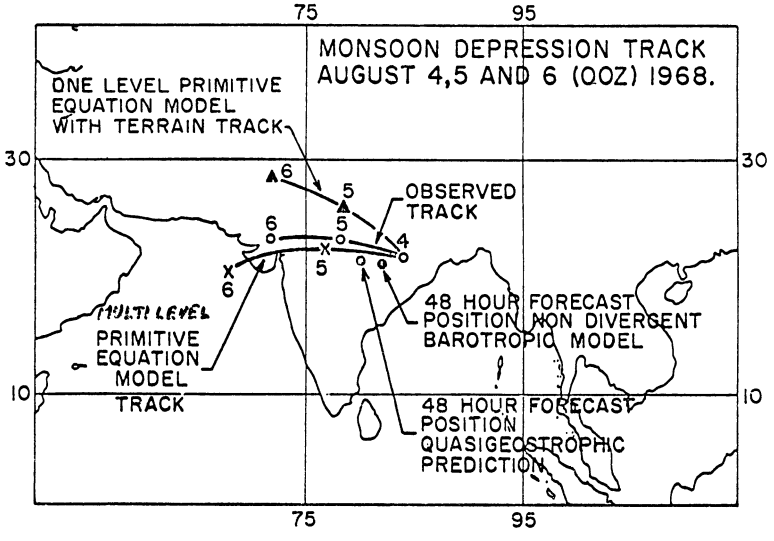

Figure 4
Observed versus predicted storm tracks for a series of numerical weather prediction experiments.

4. *On the parameterization of the vertical transport of momentum by the cumulus scale for numerical prediction models*

Budget studies of vorticity in tropical disturbances have been discussed by a number of authors recently, WILLIAMS and GRAY (1974), REED and JOHNSON (1974), CHU (1977) and GODBOLE (1977). Among these the study of Godbole appears in this issue of the *Pure and Applied Geophysics*. Although Godbole does not specifically address the question of the parameterization of vertical transport of momentum by the cumulus scale motions for numerical weather prediction models, we feel that his calculations are quite relevant for such an extension. Furthermore, since Godbole's study deals with the data obtained from a composite monsoon disturbance, the following analysis may be useful to those who are concerned with numerical weather prediction over the monsoonal belt. Our choice in taking Godbole's budget study rather than the other studies referenced above was also based on the fact that considerable regional differences exist in the various vorticity budgets. Godbole (1977) has obtained from his budget study the vertical profiles of $\overline{u'\omega'}$ and $\overline{v'\omega'}$ for the four

sectors around a composite monsoon disturbance. We can make use of these by the following equivalent expression for the vertical diffusion of momentum by the cumulus scale,

$$\frac{\partial}{\partial p}\left(k_u \frac{\partial \bar{u}}{\partial p}\right) = -\frac{\partial}{\partial p}\overline{u'\omega'}$$

and

$$\frac{\partial}{\partial p}\left(k_v \frac{\partial \bar{v}}{\partial p}\right) = -\frac{\partial}{\partial p}\overline{v'\omega'}.$$

Upon integration of these expressions from a reference cloud base level to a reference level p and noting that $\overline{u'\omega'}$ and $\overline{v'\omega'}$ are to be set to zero at the cloud base level, we may write,

$$k_u = -\frac{\overline{u'\omega'}}{\partial \bar{u}/\partial p}$$

and

$$k_v = -\frac{\overline{\omega'v'}}{\partial \bar{v}/\partial p}.$$

According to Godbole, the intense convective rainfall is concentrated in the south-west quadrant, hence the subgrid scale effects of cumulus convection would be very large there. It should be noted the bar refers to a grid scale flow in a monsoon disturbance. $\bar{u}$ and $\bar{v}$ here refer to the zonal and meridional components, which vary from quadrant to quadrant of the storm. Table 1 shows a calculation of the 'equivalent diffusion coefficients' for the cumulus-scale momentum transport. In the rainy areas of the monsoon disturbance the vertical distribution of k_u and k_v, in Table 1, is consistent with the results of the budget study of Godbole. Unlike the usual simple

Table 1

Pressure	$\bar{u}$	$\bar{v}$	$\partial\bar{u}/\partial p$	$\partial\bar{v}/\partial p$	$\overline{\omega'u'}$	$\overline{\omega'v'}$	k_u	k_v
	(mps)		(mps mb^{-1})		(10^{-2} mb m sec^{-1})		(mb^2 sec^{-1})	
1000	6.0	0.5						
900			−0.045	0.0025	0	0	0	0
800	15.0	−1.0						
700			−0.025	0.0025	−1.15	0.52	0.44	−2.00
600	10.0	−1.5						
500			−0.05	0.0025	−1.82	1.05	0.36	−4.06
400	0	−2.0						
300			−0.06	0.015	−1.45	0.75	0.24	−0.52
200	−12.0	−5.0					0	0

down-the-gradient type diffusion coefficients, here the sign of the 'equivalent diffusion coefficients' are of opposite sign. The vertical eddy flux of zonal momentum by the cumulus scale motion ($-\overline{u'\omega'} > 0$) is upwards, i.e. down the gradient of zonal momentum – from the lower tropospheric westerlies to the higher level easterlies. The vertical flux of southerly momentum is directed downwards ($-\overline{v'\omega'} < 0$), i.e. towards increasing southerlies which is an up the gradient transport.

The prescription of k_u and k_v would thus decrease the high level easterlies as well as the low level westerlies and at the same time they would strengthen the low level southerlies as well as the upper level northerlies.

In the actual practice of numerical weather prediction, this effect should be invoked only in those regions where deep cumulus convection is called for by the parameterization procedure for cumulus convection. And these values of k_u, k_v may be only valid for studies for monsoon disturbances. Furthermore, this effect should be separated from other vertical diffusion terms that may be used in numerical models more generally in all regions.

5. *The broad scale monsoons and the monsoon disturbances coexist*

In short range numerical weather prediction of small scale monsoonal disturbances, such as monsoon lows and depressions, one might wonder how important it is to have the appropriate physics to handle the broad scale monsoons as well. The scale of disturbances are around 2000 km while that of the broad scale monsoons is larger than 10 000 km. In many numerical weather prediction studies, that do not include the broadscale differential heating between land and ocean, the broadscale monsoons, in fact, collapse in a matter of a few days. Although the physics of such a model may include a parameterization of cumulus convection capable of capturing the magnitude of condensation heating for the disturbance, the forecast deteriorates rapidly because of the decay of the broadscale monsoons which provide the boundary information (or so to speak boundary conditions) for the disturbance. A recent study, based on GATE initial state, shows this very clearly. In this instance, the westward propogation of a West African monsoon disturbance imbedded in the broadscale West African monsoons was studied in considerable detail in the context of a short range numerical prediction experiment. The broadscale differential heating of the land-ocean system was defined by the following elements.

(a) *At the earth's surface*

Oceans: Sensible and latent heat fluxes at the air–sea interface.

Land: Detailed heat balance of the earth's surface: Incoming short and long wave radiation, outgoing radiation, albedo of the earth's surface and reflected short wave radiation, sensible and evaporative fluxes from land area. Diurnal variation is included via the variation of the zenith angle of the sun.

(b) *Above the earth's surface*

Over oceans and land: short and land wave radiative warming, effect of clouds, convective and nonconvective condensation heating, dry convective adjustment and adiabatic warming. Diurnal variation is also included in the radiation.

The above ingredients were evaluated in the course of integration. What became clear from the above prescription is that the broadscale monsoon is similar to a giant sea breeze where the effects of earth's rotation are important. The meridional kinetic energy was used as a measure of the intensity of the monsoons; the meridional motion between the warm land areas and the relatively colder oceans describe the Hadley type vertical overturnings. Figure 5 shows the time change of the domain integrated meridional kinetic energy in two experiments which were run with and without the differential heating, respectively. The meridional kinetic energy of the whole domain collapses to very low values if the heating is suppressed. In these experiments the domain contained within it the broadscale monsoons as well as a monsoon disturbance. The numerical prediction (2 to 4 days) of the disturbance improved considerably when this heating field was retained. In summary, these experiments show that for the short range numerical weather prediction (2 to 4 days) of a monsoon disturbance, it is essential to feed energy via the differential heating (between land and ocean) to the broadscale monsoons. It is interesting to note here that the local sea breeze phenomenon does not exist on days of complete and heavy cloud cover. It

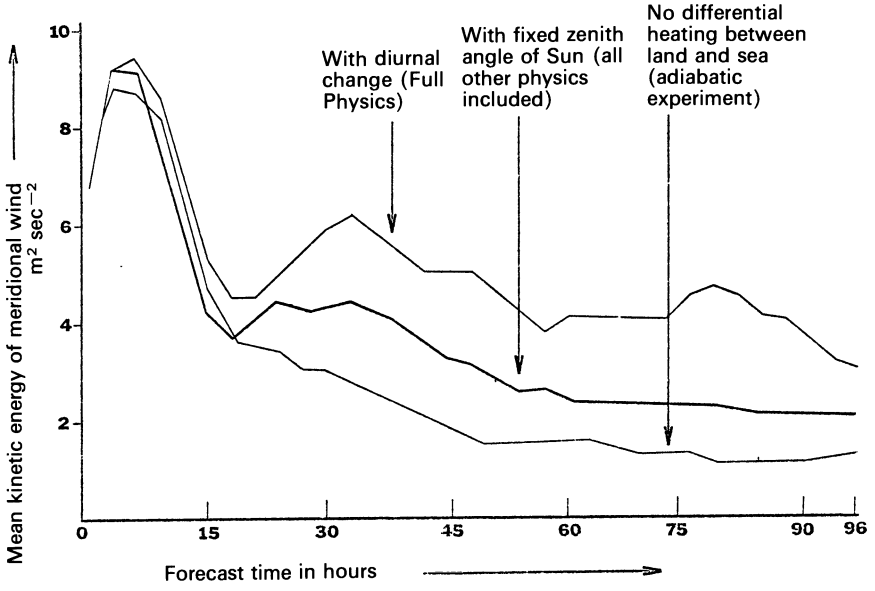

Figure 5
Time evolutions of the domain averaged kinetic energy of the meridional wind for three numerical weather prediction experiments.

seems that the broadscale monsoons can carry their identity for a couple of days if the heating required to drive it is suppressed completely.

Thus we feel that the design of a short range numerical weather prediction experiment for the monsoon belt should include the heating ingredients listed above. The following are some relevant references for this problem: JOSEPH (1966), KATAYAMA (1972), CHANG (1977), KRISHNAMURTI *et al.* (1977).

6. *Some comments on the planetary boundary layer (PBL) structure over the Arabian Sea*

The question of an adequate vertical resolution to represent the gross characteristics of the PBL is important for the numerical weather prediction over the monsoon belt. For this purpose, KRISHNAMURTI and WONG (1977) designed a detailed PBL model over the Arabian Sea during the northern summer. The main purpose of this multilevel primitive equation model was to simulate the cross-equatorial low level jet and to study the structure and dynamics of the boundary layer, essentially following the rationale presented by YOUNG (1972) and MAHRT (1972). The experimental domain extended from 30°S to 30°N with a horizontal resolution of 1 km and a vertical resolution of 300 m. The model was successful in simulating many of the observed features of the Somali jet. As a byproduct the study identified an Ekman type PBL with backing of wind with height near the southern boundary. The boundary layer changed to an advective type with dominant horizontal advection south of the Somali jet with a pronounced veering of wind with height. North of the Somali jet a weak backing and an advective type boundary layer was noted. Next as one proceeds northwards, a dry ITCZ with a dominant vertical advection was encountered. North of the ITCZ over Arabia the PBL gradually changed over to an Ekman type with a typical veering of wind with height. Although observations are presently lacking to verify these structures, it is clear that a PBL model should, at least, have a resolution of roughly 500 m below 2 km to adequately handle such features and thus have the capability of properly representing the field of vertical velocity on top of the PBL.

7. *Concluding remarks*

Numerical weather prediction over the monsoon belt is expected to improve considerably with the active participation of countries of Africa and South Asia. If the objectives of these experiments are to go beyond 48 hours, then a fairly sophisticated model that includes the following features may be necessary.

(i) A primitive equation model with the earth's surface as a coordinate surface is essential. Steep mountains (as far as possible) should be included.

(ii) Detailed prescription of radiative effects is essential, including diurnal change,

effects of clouds and the radiative heat balance of the earth's surface, surface albedo, soil temperature and moisture.

(iii) A procedure for the parameterization of cumulus convection capable of describing intense rainfall rates (≈ 20 cm/day) in monsoons is essential.

(iv) A boundary layer formulation that handles the complex structures of cross-equatorial flows and also the diurnally varying convective layers over the warm land areas should be included. The model should have adequate resolution for the parameterization of these features. Observational basis is presently lacking for many of these problems. Our preliminary studies on the PBL over the Arabian Sea suggests that below 2 km the model should have at least 4 layers.

(v) A detailed dynamic initialization scheme is essential for a real data primitive equation prediction model over the tropics. Since the geopotential height amplitude and the temperature wave amplitudes are small and are respectively of the order of 20 geopotential meters and 1°C, large contamination of the initial analysis can occur if spurious computational gravity inertia oscillations occur during the initial stages of prediction.

(vi) It is desirable to include possible interactions of the monsoon disturbances with the planetary scale monsoon components. Since this cannot be accomplished without a truly global model, efforts should be made to either increase the computational domain to cover half the tropical belt or to have a nested fine mesh within a coarse mesh global model.

(vii) The meridional extent of a regional model should, at least, cover the region from 25°S to 45°N in order to represent the large cross-equatorial flows in the lower and upper troposphere that are very characteristic of the monsoons.

Acknowledgements

The research and the computations reported here were supported by the National Science Foundation via NSF Grant No. ATM75-18945 and the Computing Facility of the National Center for Atmospheric Research. The satellite data support was provided by NOAA Grant No. 04-5-158-26.

References

Arakawa, A. and Schubert, W. (1974), *Interaction of a cumulus ensemble with the large-scale environment*, Part I, J. Atmos. Sci. *31*, 674–701.

Carr, Frederick H. (1977), *Numerical simulation of a mid-tropospheric cyclone*, Report No. 77-1, Department of Meteorology, Florida State University, Tallahassee, pp. 1–267.

Chang, C. B. (1977), *On the influence of solar radiation and diurnal variation of surface temperature on North African circulations*, Report No. 75-2, Department of Meteorology, Florida State University, Tallahassee, Fla.

Chu, Jan-Hwa (1977), *Vorticity in maritime cumulus clouds and its effects on the large scale budget of vorticity in the tropics*. To be published in J. Atmos. Sci.

DEARDORFF, J. (1972), *Parameterization of the planetary boundary layer for use in general circulation models*, Mon. Wea. Rev. *100*, 93–106.

GARP PUBLICATION No. 16 (1975), *The physical basis of climate and climate modelling*, World Meteorological Organization, Geneva, pp. 1–265.

GATES, W. L. and NELSON, A. B. (1975), *A new (revised) tabulation of the Scripps topography on a 1° global grid, Part 1 terrain heights*, Rand report No.: R-1276-1-ARPA. Rand Corporation, Santa Monica, California, pp. 1–132.

GODBOLE, R. V. (1977), *On cumulus-scale transport of horizontal momentum in monsoon depression over India.* (Appears in this issue of Pure and Applied Geophysics.)

JOSEPH, J. H. (1966), *Calculation of radiative heating in numerical general circulation models*, Tech. Rept. No. 1, Department of Meteorology, University of California, Los Angeles, pp. 1–60.

KANAMITSU, M. (1975), *On numerical prediction over a global tropical belt*, Report No. 75-1, Department of Meteorology, Florida State University, pp. 1–282.

KASAHARA, A. (1974), *Various vertical coordinate systems used for numerical weather prediction.* Mon. Wea. Rev. *102*, 509–522.

KATAYAMA, A. (1972), *A simplified scheme for computing radiative transfer in the troposphere*, Technical Report No. 6, Department of Meteorology, University of California, Los Angeles, pp. 1–77.

KRISHNAMURTI, T. N., KANAMITSU, MASAO, CESELSKI, B. and MATHUR, M. (1973), *Florida State University's tropical prediction model*, Tellus *25*, 523–535.

KRISHNAMURTI, T. N., KANAMITSU, M., GODBOLE, RAMESH, CHANG, CHIA-BO, CARR, F. and CHOW, J. H. (1976), *Study of a monsoon depression (II). Dynamical structure*, J. Meteor. Soc. Japan *54*, 208–225.

KRISHNAMURTI, T. N., PAN, H. L. and CHANG, CHIA-BO (1977), *Numerical prediction of a GATE disturbance*, Part II, FSU Report No. 77-4. Department of Meteorology, Florida State University, Tallahassee, Florida.

KRISHNAMURTI, T. N. and WONG, V. (1977), *A simple numerical model on the boundary layer of the Somali jet* (paper in preparation).

KUO, H. L. (1965), *On formation and intensification of tropical cyclones through latent heat release by cumulus convection*, J. Atmos. Sci. *22*, 40–63.

MAHRT, L. J. (1972), *A numerical study of the influence of the advective accelerations in an idealized, low latitude, planetary boundary layer*, J. Atmos. Sci. *29*, 1477–1484.

MURAKAMI, T., GODBOLE, R. V. and KELKAR, R. R., *Numerical simulation of the monsoon along 80°E*, in *Proceedings of the Conference on the Summer Monsoon of Southeast Asia* (ed. C. S. Ramage), (Navy Weather Research Facility, Norfolk, Virginia 1970), pp. 39–51.

PHILLIPS, N. A. (1957), *A coordinate system having some special advantages for numerical forecasting*, J. Meteor. *14*, 184–185.

REED, R. J. and JOHNSON, R. C. (1974), *Diagnosis of cloud population properties in tropical easterly waves*, Preprints, international tropical meteorology meeting, Nairobi, Kenya. American Meteorological Society, pp. 50–56.

WILLIAMS, K. T. and GRAY, W. M. (1974), *Statistical analysis of satellite-observed trade wind cloud clusters in the western North Pacific*, Tellus *25*, 313–337.

WINNINGHOFF, F. J. (1973), *Note on a simple restorative-iterative procedure for initialization of a global forecast model*, Mon. Wea. Rev. *79*, 79–84.

YOUNG, J. (1972), *Lecture notes on boundary layer on the dynamics of the tropical atmosphere*, National Center for Atmospheric Research, Boulder, Colorado, pp. 411–421.

(Received 15th June 1977)

On Cumulus-scale Transport of Horizontal Momentum in Monsoon Depression over India

By RAMESH V. GODBOLE[1])

Abstract – A diagnostic method of cumulus parameterization is suggested in which vertical transport of horizontal momentum by cumulus-scale is derived by making use of large-scale vorticity as well as divergence budget equations. Data for composite monsoon depression over India available from our earlier studies are used to test the method. As a first approximation, the results are obtained using only the vorticity budget equation.

The results show that in the southwest sector of the monsoon depression, which is characterized by maximum cloudiness and precipitation, there is an excess of cyclonic vorticity in the lower troposphere and anticyclonic vorticity in the upper troposphere associated with the large-scale motion. The distribution of eddy vertical transport of horizontal momentum is such that anticyclonic vorticity is generated in the lower troposphere and cyclonic vorticity aloft. Cumulus-scale eddies thus work against the large-scale system and tend to off-set the large-scale imbalance in vorticity.

Key words: Monsoon depression: Transport of momentum; Cumulus parameterization; Cumulus: Transport of momentum.

Introduction

In the Tropics, the importance of cloud clusters or cloud ensemble in the vertical redistribution of heat, moisture, momentum and vorticity has been amply brought out in numerous studies (YANAI and NITTA, 1969; GRAY, 1973; WILLIAMS and GRAY, 1973; REED and JOHNSON, 1974; FEIN, 1975 and others). YANAI *et al.* (1973), in their diagnostic study of cumulus parameterization, used large-scale heat and moisture budgets and a cloud ensemble model to estimate vertical transport of heat and moisture by cumulus clouds. Following a similar treatment but using a large-scale vorticity budget, REED and JOHNSON (1974) have concluded that the imbalance in the large-scale vorticity budget is neutralized by cloud clusters which carry an appreciable amount of large-scale vorticity excess from the lower troposphere and deposit it to the upper troposphere. Their results could be directly verified if one knew how to calculate the vertical transport of horizontal momentum by cumulus-scale eddies. However, in the tropics, since the large-scale horizontal pressure gradient is weak, it is difficult to make a diagnostic study of momentum budget using the momentum equations. AUSTIN and HOUSE (1973) suggested a technique in which precipitation

[1]) Department of Meteorology, Florida State University, Tallahassee, Florida 32306, USA.

data are utilized to obtain directly the eddy vertical transport of horizontal momentum. However, very few quantitative radar data suitable for this technique are routinely available. In the present paper, we propose a new approach for estimating the cumulus-scale transport of horizontal momentum by making use of large-scale vorticity and divergence budget equations.

Formulation of the method

Vorticity equation in the flux form may be written as

$$\frac{\partial \xi}{\partial t} + \nabla\cdot\xi\mathbb{V} + (\xi + f)\nabla\cdot\mathbb{V} + \beta v + \frac{\partial}{\partial p}\left\{\omega\frac{\partial v}{\partial x} - \omega\frac{\partial u}{\partial y}\right\} + \frac{\partial\omega}{\partial x}\frac{\partial v}{\partial p} - \frac{\partial\omega}{\partial y}\frac{\partial u}{\partial p} = 0$$

or

$$\frac{\partial \xi}{\partial t} + \nabla\cdot\xi\mathbb{V} + (\xi + f)\nabla\cdot\mathbb{V} + \beta v + \frac{\partial}{\partial p}\left\{\frac{\partial}{\partial x}(\omega v) - \frac{\partial}{\partial y}(\omega u)\right\}$$

$$+ v\frac{\partial}{\partial x}(\nabla\cdot\mathbb{V}) - u\frac{\partial}{\partial y}(\nabla\cdot\mathbb{V}) = 0 \tag{1}$$

where ξ is the relative vorticity, f the coriolis parameter, β the Rossby parameter, $\mathbb{V}$ the horizontal velocity vector having u and v as components and ω the vertical velocity. Following YANAI *et al.* (1973), equation (1) may be expressed as

$$Z \equiv \frac{\partial \bar{\xi}}{\partial t} + \nabla\cdot\overline{(\xi + f)}\,\bar{\mathbb{V}} + \overline{(\xi + f)}\,\overline{\nabla\cdot\mathbb{V}} + \frac{\partial}{\partial p}\left\{\frac{\partial}{\partial x}(\bar{\omega}\bar{v}) - \frac{\partial}{\partial y}(\bar{\omega}\bar{u})\right\}$$

$$+ \bar{v}\frac{\partial}{\partial x}\overline{(\nabla\cdot\mathbb{V})} - \bar{u}\frac{\partial}{\partial y}\overline{(\nabla\cdot\mathbb{V})} = -\overline{\frac{\partial}{\partial p}\left\{\frac{\partial}{\partial x}(\omega' v') - \frac{\partial}{\partial y}(\omega' u')\right\}} \tag{2}$$

where Z is the residual of the large-scale vorticity budget. Bar denotes the horizontal area average and prime denotes the deviation from the area average. $\omega' u'$ and $\omega' v'$, thus, represent the vertical transport of horizontal momentum by cumulus-scale eddies. The right-hand side of equation (2) is analogous to the expression for vertical component of vorticity ξ. By analogy, therefore, we write equation (2) as

$$Z = -\overline{\frac{\partial}{\partial p}[A_\xi]} \tag{3}$$

where

$$A_\xi = \frac{\partial}{\partial x}(\omega' v') - \frac{\partial}{\partial y}(\omega' u').$$

Extending the analogy further, we write

$$Z = -\overline{\frac{\partial}{\partial p}[\nabla^2 A_\psi]} = -\overline{\nabla^2\left[\frac{\partial A_\psi}{\partial p}\right]} \tag{4}$$

where A_ψ is analogous to stream function.

Following similar treatment for divergence equation, we can write

$$\begin{aligned} D \equiv\ & \overline{\nabla^2\Phi} + \overline{\frac{\partial}{\partial t}(\nabla\cdot\mathbb{V})} + \overline{\nabla\cdot(\nabla\cdot\mathbb{V})\mathbb{V}} - f\bar{\zeta} + \beta\bar{u} + \overline{(\nabla\cdot\mathbb{V})^2} \\ & + 2\left(\frac{\partial\bar{v}}{\partial x}\frac{\partial\bar{u}}{\partial y} - \frac{\partial\bar{u}}{\partial x}\frac{\partial\bar{v}}{\partial y}\right) + \bar{\mathbb{V}}\cdot\overline{\nabla(\nabla\cdot\mathbb{V})} + \frac{\partial}{\partial p}\left\{\frac{\partial}{\partial x}(\overline{\omega u}) + \frac{\partial}{\partial y}(\overline{\omega v})\right\} \\ =\ & -\frac{\partial}{\partial p}\left[\frac{\partial}{\partial x}(\omega' u') + \frac{\partial}{\partial y}(\omega' v')\right] \end{aligned} \tag{5}$$

where D is the residual of the large-scale divergence budget and Φ is the geopotential height. Again by analogy, we write

$$D = -\overline{\frac{\partial}{\partial p}[\nabla^2 A_x]} = -\nabla^2\left[\overline{\frac{\partial A_x}{\partial p}}\right] \tag{6}$$

where A_x is analogous to velocity potential.

Combining the so-called rotational part and divergent part, we can write

$$\begin{aligned} \overline{\omega' u'} &= -\frac{\partial}{\partial y}\overline{(A_\psi)} + \frac{\partial}{\partial x}\overline{(A_x)} \\ \overline{\omega' v'} &= \frac{\partial}{\partial x}\overline{(A_\psi)} + \frac{\partial}{\partial y}\overline{(A_x)} \end{aligned} \tag{7}$$

It may easily be seen from the foregoing that $\omega' u'$ and $\omega' v'$ could be obtained by relaxing equations (4) and (6). Note that the residuals Z and D are obtainable from the observed large-scale data.

Computation of A_ψ from large-scale vorticity budget is simple but that of A_x from large-scale divergence budget is rather difficult because of the $\nabla^2\Phi$ term appearing in the expression for D in equation (5). We may further simplify equation (7) by assuming that, as a first approximation only, the so-called divergent part or the contribution due to A_x is small as compared to the so-called rotational part. Equation (7) may then be written as

$$\begin{aligned} \overline{\omega' u'} &= -\frac{\partial}{\partial y}\overline{(A_\psi)} \\ \overline{\omega' v'} &= \frac{\partial}{\partial x}\overline{(A_\psi)}. \end{aligned} \tag{8}$$

The rationale used in the above assumption is the following. The large-scale system in the present study is a composite monsoon depression over India which is a strong voetex tube of diameter of about 1500 km extending up to 400 mb in the vertical (GODBOLE, 1977). For such a system, clearly the rotational part of the wind dominates over the divergent part. If we now apply the same analogy which was used to derive equations (3) and (4) to equation (7), it, in effect, tantamounts to neglecting the so-called divergent part or the contribution due to A_x in equation (7). The above assumption is, however, made only as a first approximation. The justification for the assumption is borne out by the results which are discussed in the subsequent sections.

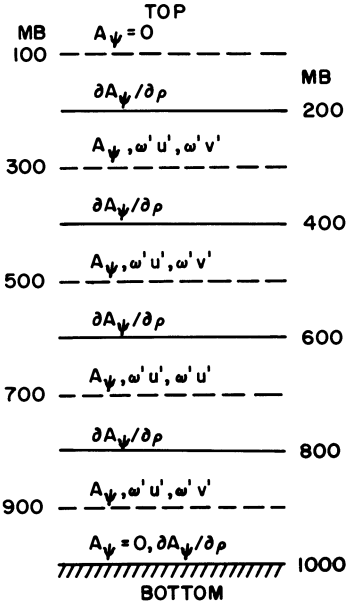

Figure 1
The vertical staggering of isobaric levels at which various quantities as indicated are computed.

In actual practice, we solve equation (4) for $(\partial A_\psi/\partial p)$ by the method of successive relaxation. To obtain A_ψ from $(\partial A_\psi/\partial p)$, we assume that A_ψ vanishes at the top of the atmosphere which is 100 mb in the present study and work downwards up to 1000 mb which is the lower limit (see Fig. 1). Further, in order to ensure that both $\omega'u'$ and $\omega'v'$ vanish at the top (100 mb) as well as at the bottom (1000 mb), $(\partial A_\psi/\partial p)$ at each level was so adjusted as to satisfy the condition

$$\int_{\text{bottom}}^{\text{top}} \frac{\partial A_\psi}{\partial p}\, dp = 0. \tag{9}$$

The method of adjustment used is similar to that used for adjusting the divergence for computing the kinematic vertical velocity (KRISHNAMURTI *et al.*, 1976).

Results

It may be of interest first to examine what kind of vorticity budget we get for the system considered in the present study which is a composite monsoon depression over India. Figure 2 shows a vertical distribution of residual Z as obtained from large-scale parameters of equation (2). The results shown are for the southwest (SW) sector of the composite monsoon depression. This sector is characterized by heavy convective activity as compared to the other sectors such as NW, NE and SE sectors (GODBOLE, 1977). It is seen that the imbalance in the vorticity budget is such that the lower troposphere has a vorticity sink whereas the upper troposphere has a vorticity source associated with the large scale motion. Similar results were obtained by REED and JOHNSON (1974) for a composite easterly wave in the tropical western Pacific. Their results for the region of a wave trough are reproduced in the figure for comparison. The changeover from negative to positive residual occurs at a higher level in the results of Reed and Johnson which appears to be mainly due to the fact that the twisting term was not considered in their equation for vorticity budget. Comparison of the magnitudes of the two profiles in the figure clearly shows that the system in the present study, i.e., monsoon depression over India is much stronger than the tropical easterly wave over the western Pacific.

The imbalance in the large-scale vorticity budget as shown in Fig. 2 suggests a mechanism which should operate such that it removes vorticity-rich air from the lower troposphere and deposits that in the upper troposphere. In other words, the mechanism should act in a way so as to generate anticyclonic vorticity in the lower layers and cyclonic vorticity aloft. The results which are to follow lead to this conclusion which means that the mechanism at work is a convective process in which the transport of momentum and vorticity is effected by cumulus-scale eddies.

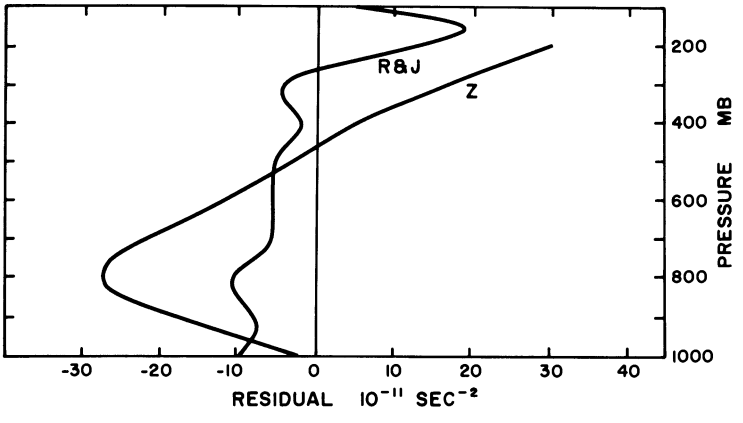

Figure 2
Vertical distribution of residual Z as obtained from large-scale vorticity budget. The curve indicating (R & J) represents the results of Reed and Johnson.

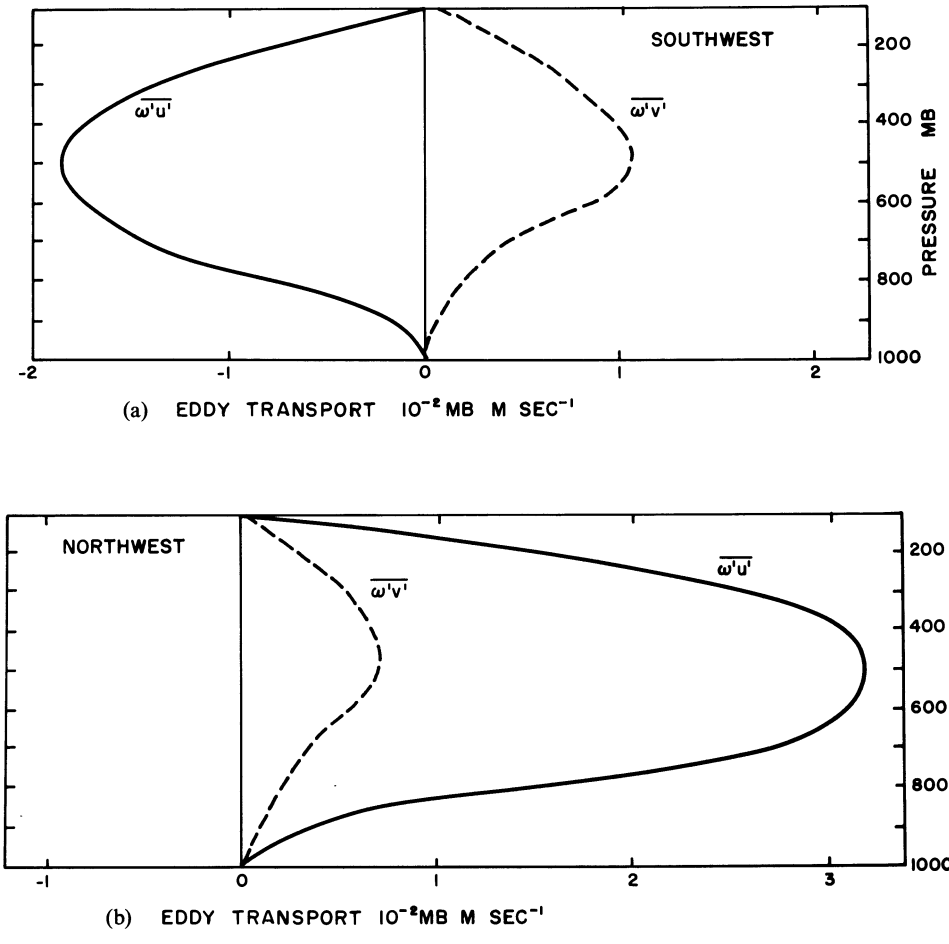

Figure 3
Vertical distribution of $\omega'u'$ (solid line) and $\omega'v'$ (broken line) for (a) southwest sector, (b) northwest sector, (c) Northeast sector, and (d) southeast sector of the monsoon depression.

In Fig. 3 are shown the vertical profiles of $\omega'u'$ and $\omega'v'$ for the four sectors, i.e., SW, NW, NE and SE sectors of the monsoon depression. Since our primary purpose is to examine only the effect of cumulus-scale transport on the large-scale circulation, we may restrict our attention only to the following two terms in the equations of motion.

$$\frac{\partial \bar{u}}{\partial t} = -\overline{\frac{\partial}{\partial p}(\omega' u')} \quad \text{and} \quad \frac{\partial \bar{v}}{\partial t} = -\overline{\frac{\partial}{\partial p}(\omega' v')}.$$

From above, we see that if $\omega'u'$ increases (decreases) upward, $\partial\bar{u}/\partial t$ becomes positive (negative). Hence the cumulus-scale eddies add westerly (easterly) momentum to the

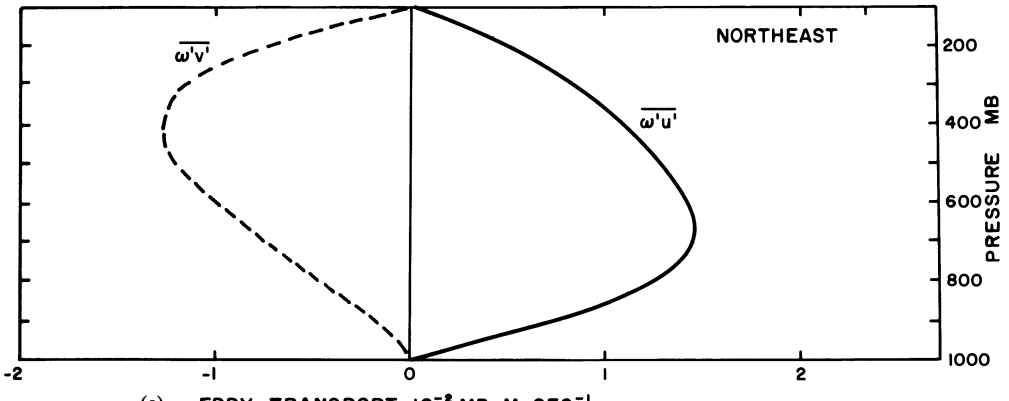

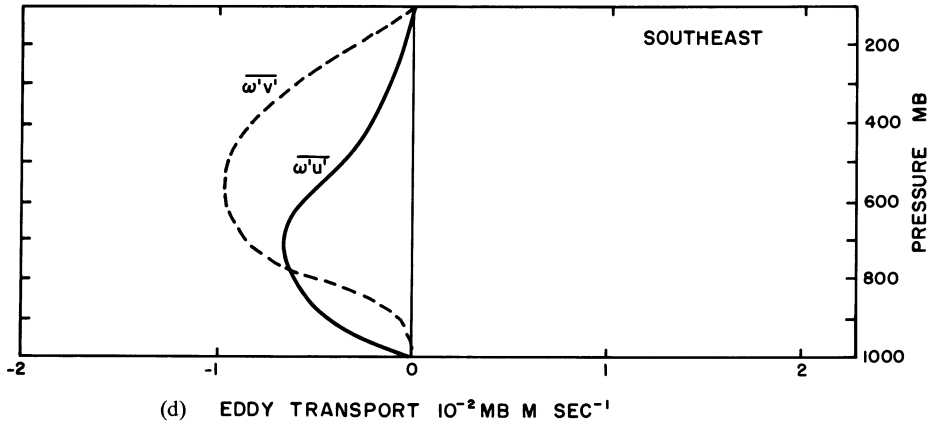

Figure 3 (*cont.*)

large-scale. Similarly for $\omega'v'$ increasing (decreasing) upward, $\partial\bar{u}/\partial t$ is positive (negative) and the eddies will add southerly (northerly) momentum to the large-scale motion. Following this line of argument, one could see that in the SW sector (Fig. 3a), eddies would generate easterly and southerly momentum in the lower layers and westerly and northerly momentum aloft. The large-scale flow in this sector (i.e., SW) has westerly and northerly components in the lower layers and easterly and northerly components aloft. This means that eddies work against the large-scale flow at least in the lower layer of 1000–700 mb. In the NW sector (Fig. 3b), eddies generate westerly and southerly momentum in the lower layers and easterly and northerly momentum aloft. The large-scale flow in this sector has easterly and northerly components in the lower layers as well as in the upper layers. Here again, the eddies work against the large-scale flow in the lower layers. Examination of Figs. 3c and 3d for NE and SE

sectors respectively leads to the similar results, namely, eddies work against the large-scale flow in the lower layer of 1000–700 mb.

The above results are summerized in Fig. 4 in which flow due to large-scale and eddies is schematically shown by arrows. The large-scale flow is also represented by streamlines. It is seen that in a layer from 1000–700 mb, the large-scale flow is cyclonic whereas the eddies generate anticyclonic flow. In the upper tropospheric layer from 300–100 mb, the large-scale flow is under the influence of Tibetan anticyclone whereas the eddies generate cyclonic flow. In the two middle layers, i.e., from 700–500 mb and 500–300 mb, the flow due to both large-scale and cumulus-scale undergoes transitions.

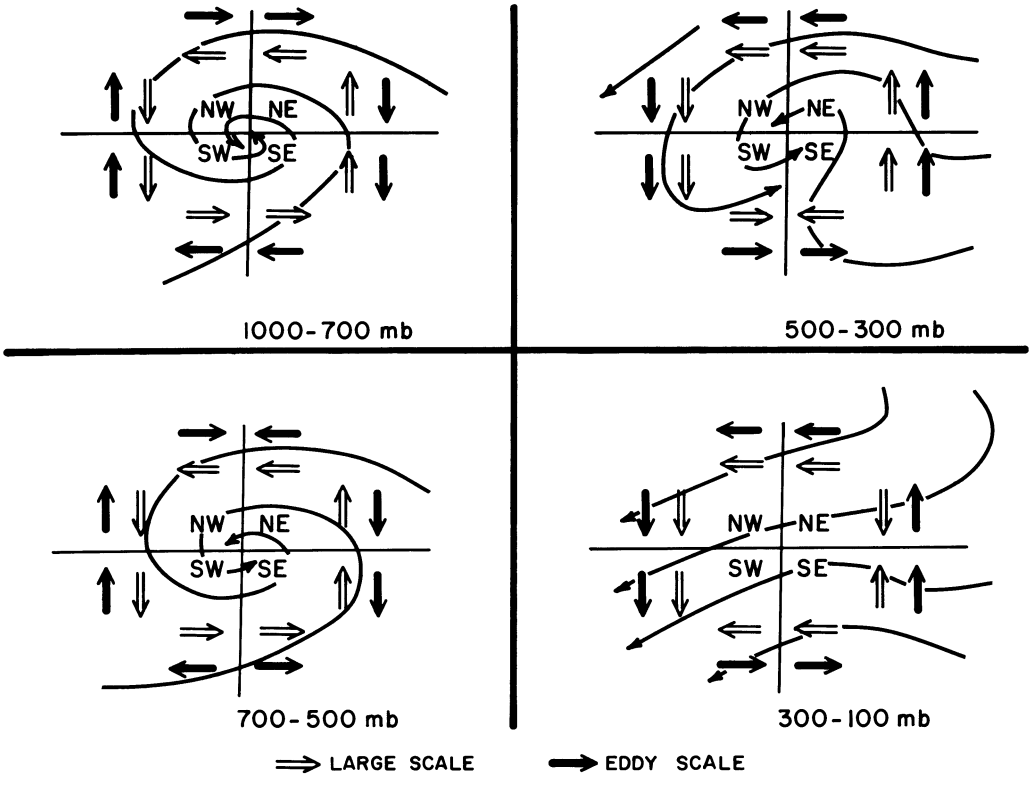

Figure 4
Schematic representation of large-scale (open arrows) and cumulus-scale (solid arrows) flow in various sectors of the monsoon depression. The large-scale flow is also represented by streamlines.

Conclusions

In the present study, we have proposed a diagnostic method to parameterize cumulus transport of horizontal momentum in terms of observable large-scale quantities. Using only the vorticity budget equation, our results confirm that in yet

another tropical disturbance like the monsoon depression, imbalance exists in the large-scale vorticity with an excess of cyclonic vorticity in the lower troposphere and anticyclonic vorticity aloft. The merit of the method is to obtain cumulus transport of horizontal momentum which, in turn, could be expressed in terms of vorticity. The eddies of cumulus-scale can generate vorticity through twisting effect and transport it through vertical advection. Our results have demonstrated that eddies generate vorticity which has an opposite sign to that generated by large-scale flow. Cumulus clouds thus work against the large-scale system in maintaining the vorticity balance of the system as a whole.

The assumption that the divergence budget equation is not so important in contributing to the cumulus transport of horizontal momentum has found a justification in the result itself. This is especially true when a large-scale system has a strong vorticity associated with it. It would be worthwhile, however, to try to solve the divergence budget equation side-by-side the vorticity budget equation as demanded by equation (7). That will at least serve to estimate the relative magnitude of the divergence induced by cumulus-scale *vis-à-vis* the vorticity. The present results, however, do tend to indicate that in a highly disturbed tropical system, cumulus-scale induced vorticity is all too important.

Acknowledgements

The author wishes to express his sincere thanks to Dr. T. N. Krishnamurti for many helpful discussions during the course of this investigation. This work was supported by Atmospheric Science Section of the NSF under grant ATM 75-18945.

References

AUSTIN, P. M. and HOUSE, R. A. Jr. (1973), *A technique for computing vertical transports of precipitating cumuli*, J. Atmos. Sci. *30*, 1100–1111.

FEIN, J. S. (1975), *Vorticity budgets during AMTEX*, Scientific report of the fourth AMTEX study conference. AMTEX report No. 8 Tokyo. 26–29 Sept 1975.

GODBOLE, R. V. (1977), *The composite structure of the monsoon depression*, Tellus *29*, 25–40.

GRAY, W. M. (1973), *Cumulus convection and large-scale circulations, Part I: Broadscale and meso-scale considerations*, Mon. Wea. Rev. *101*, 839–855.

KRISHNAMURTI, T. N., KANAMITSU, M., GODBOLE, R., CHANG, C. B., CARR, F. and CHOW, J. H. (1975), *A study of a monsoon depression. Part I: Synoptic structure*, J. Met. Soc. Japan *53*, 362–383.

REED, R. J. and JOHNSON, R. H. (1974), *The vorticity budget of synoptic-scale wave disturbances in the tropical western Pacific*, J. Atmos. Sci. *31*, 1784–1790.

WILLIAMS, K. T. and GRAY, W. M. (1973), *Statistical analysis of satellite-observed trade wind cloud clusters in the western north Pacific*, Tellus *25*, 313–336.

YANAI, M. and NITTA, T. (1969), *Computation of vertical motion and vorticity budget in a Caribbean easterly wave*, J. Met. Soc. Japan *45*, 444–446.

YANAI, M., ESBENSEN, S. and CHU, J.-H. (1973), *Determination of bulk properties of tropical cluster from large-scale heat and moisture budgets*, J. Atmos. Sci. *30*, 611–627.

(Received 15th June 1977)

Pageoph, Vol. 115 (1977), Birkhäuser Verlag, Basel

Mid-Tropospheric Cyclones of the Summer Monsoon

By FREDERICK H. CARR[1])

Abstract – Mid-tropospheric cyclones are often observed on daily and monthly mean maps over southern Asia during the summer southwest monsoon season. Although they are important activators of monsoon rains over certain regions, only a few observational studies are available, and even fewer theoretical and numerical studies have been performed. This article attempts to summarize the present observational knowledge about mid-tropospheric cyclones and reviews current ideas on the formation, maintenance and dissipation of these systems. A recent numerical simulation of a mid-tropospheric cyclone is described. In general, latent heat release plays the dominant role in the dynamics of the cyclone. Much is still to be learned about mid-tropospheric cyclones and several promising areas of future research are suggested.

Key words: Mid-Tropospheric cyclones, monsoon.

1. Introduction

The southwest monsoon season over southern Asia is a period of heavy rains over much of the region. Yet, as is now well known, these rains are not continuous in time or space but exhibit large fluctuations. As in mid-latitude climates, the main reason for this variability is that synoptic-scale weather systems embedded in the large-scale monsoon circulation exert a significant control on the temporal and spatial distribution of rainfall. The best example of this is the monsoon depression which is extensively discussed elsewhere in this volume. Another synoptic disturbance which is responsible for important rainfall events over India and Southeast Asia is the subject of this review. It will be defined as the mid-tropospheric cyclone, hereafter denoted by the initials MTC.

The name MTC is, of course, a descriptive one and is used here to refer to only those disturbances found over southern Asia during the summer months whose vorticity structure has a maximum between 700 and 500 mb with much smaller values at the surface. These systems are often present in both daily and monthly mean maps, as they may move slowly westwards or remain quasi-stationary for many days. Figure 1, taken from KRISHNAMURTI and HAWKINS (1970), depicts the mean 500 mb streamlines and isotachs for July. The large arrows denote three cyclonic vortices which they call MTC's. The heavy dashed line which connects the three

[1]) Department of Atmospheric Science, State University of New York at Albany, Albany, New York 12222, USA.

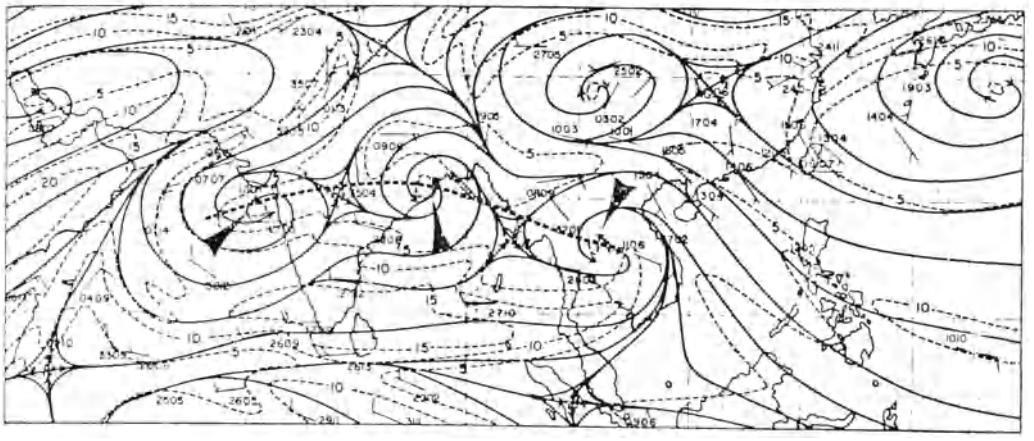

Figure 1
July mean map showing streamlines (solid lines) and isotachs every 5 kt (dashed lines) (from KRISHNAMURTI and HAWKINS, 1970).

vortices represents the mean monsoon trough at 500 mb. Since most of the observational and theoretical emphasis during the past decade has been on the MTC located over the northeastern Arabian Sea, it will receive the most attention in this review. The vortex over the Bay of Bengal is not considered as a MTC here but as the statistical result of the previously mentioned monsoon lows and depressions of that region, which have a different vertical structure than their partners to the east and west. Some of these structural differences and the question of the distinction between monsoon depressions and MTC's in the Bay of Bengal are discussed later. Cyclonic vortices over Indochina also have a slightly different structure than the Arabian Sea MTC but are similar enough to warrant the MTC designation.

RAMAGE (1966,1971) has chosen to refer to these mid-tropospheric vortices as subtropical cyclones, a term that originally applied to upper-level cut-off lows over the Pacific Ocean that are completely disassociated from the mid-latitude westerlies (RAMAGE, 1962). A careful comparison of the disturbance structure found in the above paper with that of the MTC's to be discussed here has convinced this writer that a distinction between them should remain. Also, the formation mechanisms are significantly different, especially in the case of the Arabian Sea MTC whose environmental influences are truly unique, a fact RAMAGE (1966) has pointed out.

The remainder of this review is divided into four main sections. The first one will present some of the various observational facts about the MTC that have been reported. The second section is a summary of the various ideas that have been advanced to explain the formation, maintenance and dissipation of the cyclone. Next, results from a numerical study of a MTC will be presented in an attempt to answer some of the questions raised in previous sections. In the final section, an attempt will

be made to synthesize what is now known about the MTC and suggestions for future observational and theoretical work will be made.

2. *Observational aspects*

Although a few limited studies have been published (e.g., THIRUVENGADATHAN, 1972), no comprehensive climatological survey of mid-tropospheric disturbances is known to the author. Thus their seasonal frequency and mean structure have not been determined. Most of the observational and dynamical knowledge on MTC's is based on a few case studies. In this section, the important observational aspects of these studies will be summarized. A few comments will then be made on the amount of variability that might be expected among all types of MTC's.

During the International Indian Ocean Experiment (IIOE) conducted from 1960 to 1965, a comprehensive observational study of a MTC which developed *in situ* over the northeastern Arabian Sea was performed over the period from 26 June to 14 July 1963. A detailed analysis of these unprecedented observations was presented by MILLER and KESHAVAMURTHY (1968). This particular MTC never moved more than 250 km from its original position during its lifetime. Since the large-scale features of the storm remained in quasi-steady state from 2 July to 10 July, Miller and Keshavamurthy were able to composite all the observations relative to the MTC center over this period. The following four figures are taken from their composite model of this MTC.

Figure 2 is the composite streamline-isotach analysis at 600 mb. Maximum wind speeds, which are highest at this level, are 20 m sec^{-1}, located in mesoscale bands about 300 to 400 km west and south of the center. The composite 600 mb height field is shown in Fig. 3. Note that the low center deviates less than 100 m from the surrounding high values. Comparison with Fig. 2 illustrates the cross-contour flow within 250 km of the center, indicating a possible generation of kinetic energy at this level.

At the surface (Fig. 4) no closed circulation is noted, although there is a weak trough off the coast north of Bombay. This trough is the result of the upper level intensification of the MTC; it was not present during the early stages of its lifetime (before 2 July). In general, the day to day variations in wind direction over the Arabian Sea are small but significant fluctuations in wind speed may exist. On the average, though, the speeds were weaker before and after the MTC and strongest during its lifetime, with speed convergence along the coast.

Above 300 mb (not shown), the winds are always from the east over the MTC, with maximum speeds of 20 to 40 m sec^{-1} between 150 and 100 mb. No discernible relationship between fluctuations in the easterlies and MTC's have been reported except that an increase in wind speeds is sometimes observed after an intense rainfall event (RAMAN and RAMANATHAN, 1964).

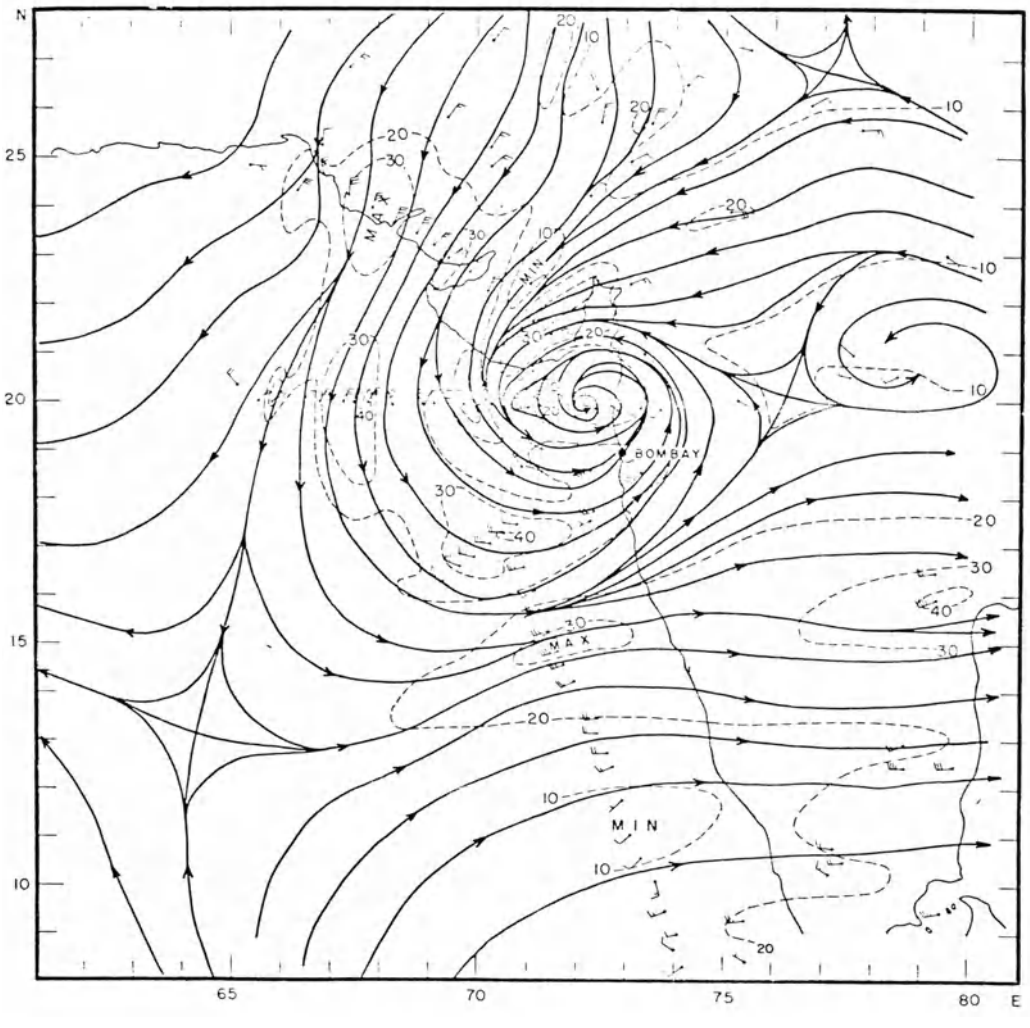

Figure 2
Composite kinematic analysis for 600 mb. Solid lines are streamlines; dashed lines are isotachs, labeled in kts (from MILLER and KESHNAVAMURTHY, 1968).

From the above figures and others not shown, it appears as if the vertical scale of the MTC is about 6 to 8 km and the horizontal scale is on the order of 1000 km. Since the Coriolis parameter is near 5×10^{-5} sec^{-1} at the latitude of the MTC center and the characteristic velocity is 10 m sec^{-1}, the Rossby number for the MTC is about 0.2.

The vertical structure along north–south and east–west cross-sections of the divergence and vorticity of the composite MTC is shown in Fig. 5. Convergence is a maximum (-6×10^{-5} sec^{-1}) between 600 and 500 mb with a weaker maximum

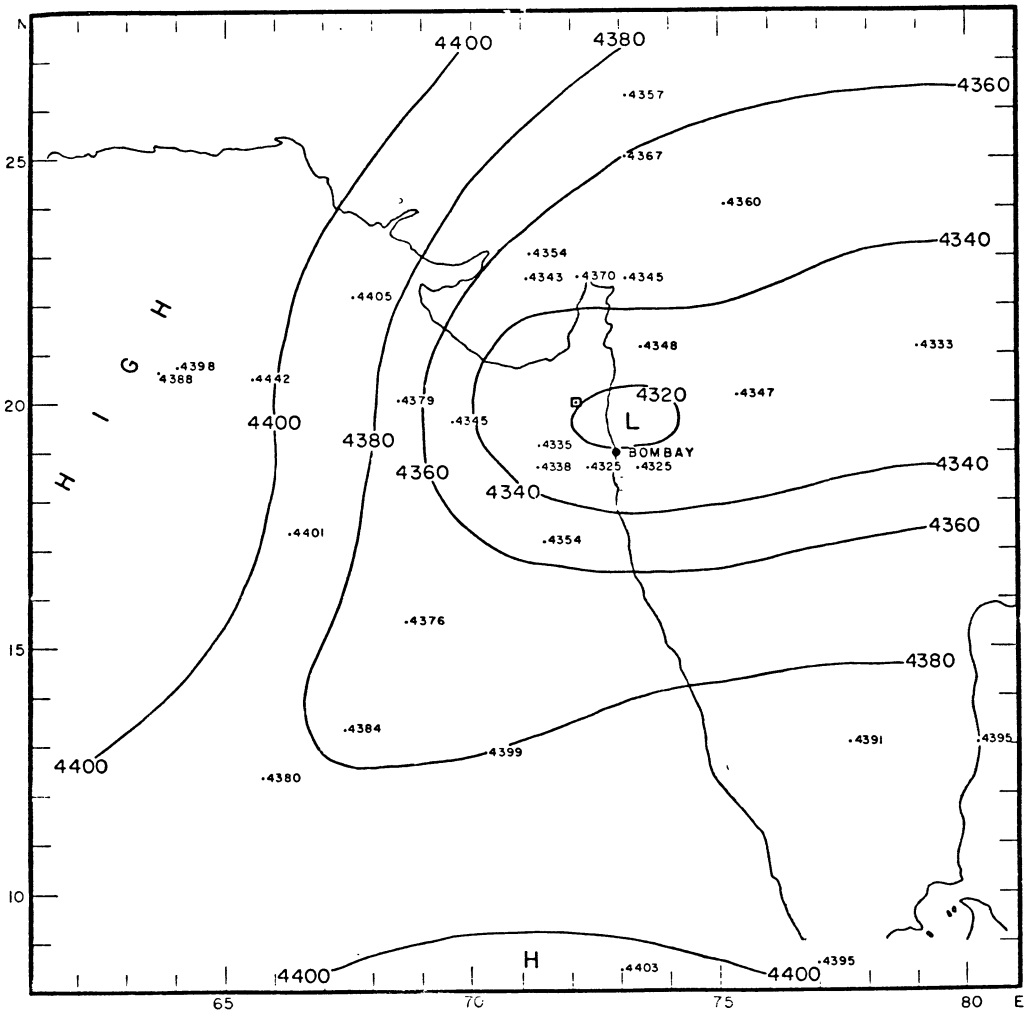

Figure 3
Composite height analysis for 600 mb. The contour interval is 20 m. The squared dot represents the composite center of the cyclone at this level (from MILLER and KESHAVAMURTHY, 1968).

near the surface. Compensating divergence of equal magnitude exists above 300 mb over the MTC. Despite the weak height gradient, the vorticity maximum is 16×10^{-5} sec^{-1} near 500 mb, reflecting the mesoscale wind shears near the center. There is weak cyclonic vorticity near the surface and anticyclonic vorticity above 300 mb. The four panels indicate that the MTC center slopes slightly to the south and west with height which is consistent with the mean thermal environment (see Fig. 7b).

CARR (1977), while preparing for the numerical experiments reported in Section 4, analyzed the data for 1 July 1963 – 12 GMT, a time just before the Miller and Keshava-

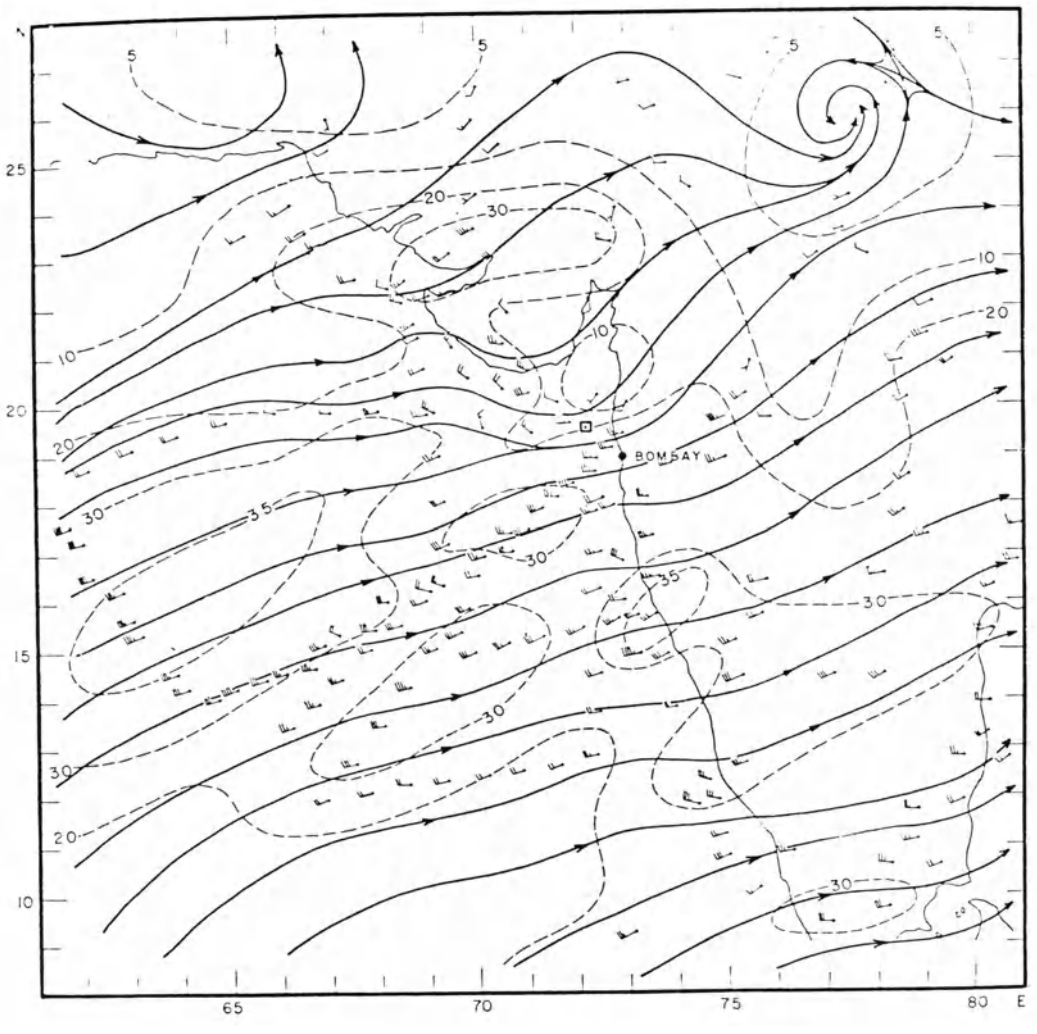

Figure 4
Composite kinematic analysis for the surface layer (500–900 m). Solid lines are streamlines; dashed lines are isotachs, labeled in kts (from MILLER and KESHAVAMURTHY, 1968).

murthy MTC became most intense. The vertical kinematic structure along 18°N of this incipient MTC is shown in Fig. 6. The amplitude of the v-component at this time is 4 m sec^{-1} at 500 mb. The vorticity maximum (Fig. 6b) is at 600 mb and has similar vertical structure (although weaker) to the composite cross-section shown in Fig. 5. Since a monsoon depression existed over eastern India at this time, Fig. 6 illustrates some of the differences between the two disturbances. The monsoon depression vorticity, for example, has a maximum near 700 mb and extends down to the surface.

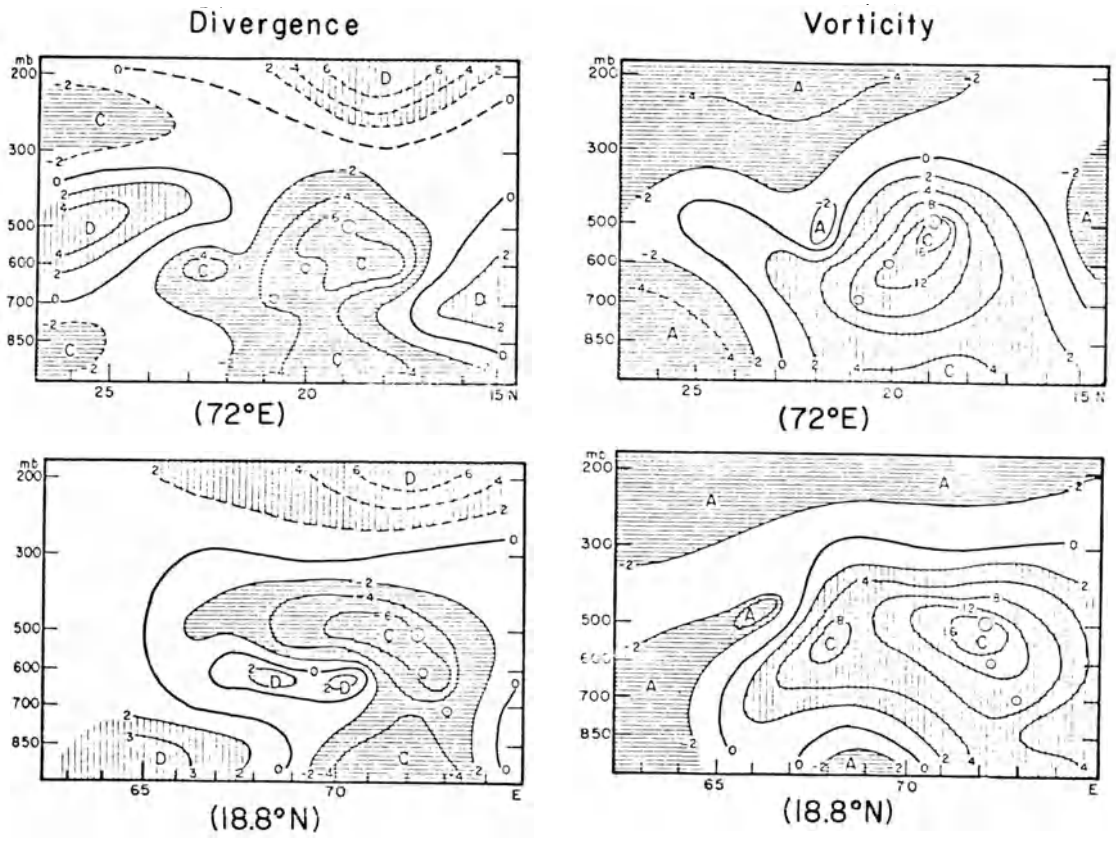

Figure 5
Meridional (top panels) and zonal (bottom panels) cross-sections of divergence and vorticity through the 500 mb composite center (18.8°N, 72°E). Both divergence and vorticity are given in units of 10^{-5} sec^{-1}. The circled dots represent the composite centers of the MTC at different levels (from MILLER and KESHAVAMURTY, 1968).

The initial vertical motion field in the east–west plane (Fig. 6c) shows two rising centers; one extends from the surface to 900 mb and reflects the influence of the Western Ghats; the second center is at 500 mb where the maximum convergence is. The magnitudes of both are just under 3×10^{-3} mb sec^{-1}. The vertical motion profiles Miller and Keshavamurthy derive (not shown) from the convergence values shown in Fig. 5 have a maximum upward value over 40 cm sec^{-1} near 300 mb. The large differences between these two estimates are due to: (i) the finite difference grid interval was 100 km for Miller and Keshavamurthy versus 220 km for Carr; (ii) Carr's values are computed after a divergence correction and 18 hours of dynamic initialization have been applied and (iii) the 1 July MTC is not fully developed. Miller and Keshavamurthy's values are consistent with the observed rainfall amounts of 5 to 8 mm hr^{-1} near the center, much of which is due to convection.

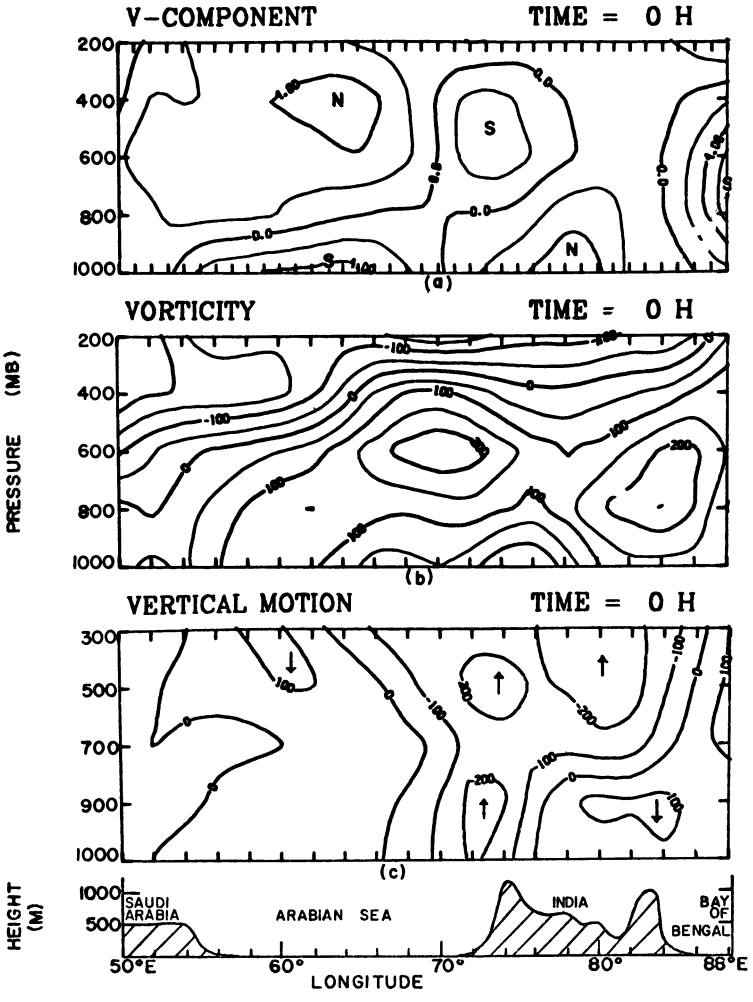

Figure 6
East-west vertical cross-section along 18°N at the initial time; (a) v-component (m sec^{-1}); (b) vorticity ($\times 10^{-7}$ sec^{-1}); (c) vertical velocity ($\times 10^{-5}$ mb sec^{-1})

The vertical thermodynamic structure along 18°N for the 1 July MTC is displayed in Fig. 7. The top panel depicts the varying dry static stability over the region. In Fig. 7b, the temperature anomaly cross-section shows that both the MTC and monsoon depression are cold core in the lower troposphere, with a larger scale warm anomaly above 500 mb. Due to the inclusion of the hot Arabian desert, the cold anomalies are exaggerated; an amplitude of 1–2°C is more realistic. Miller and Keshavamurthy also showed that the MTC was cold-cored below 500 mb and warm-cored above. Since this is consistent with the observed vorticity structure, the

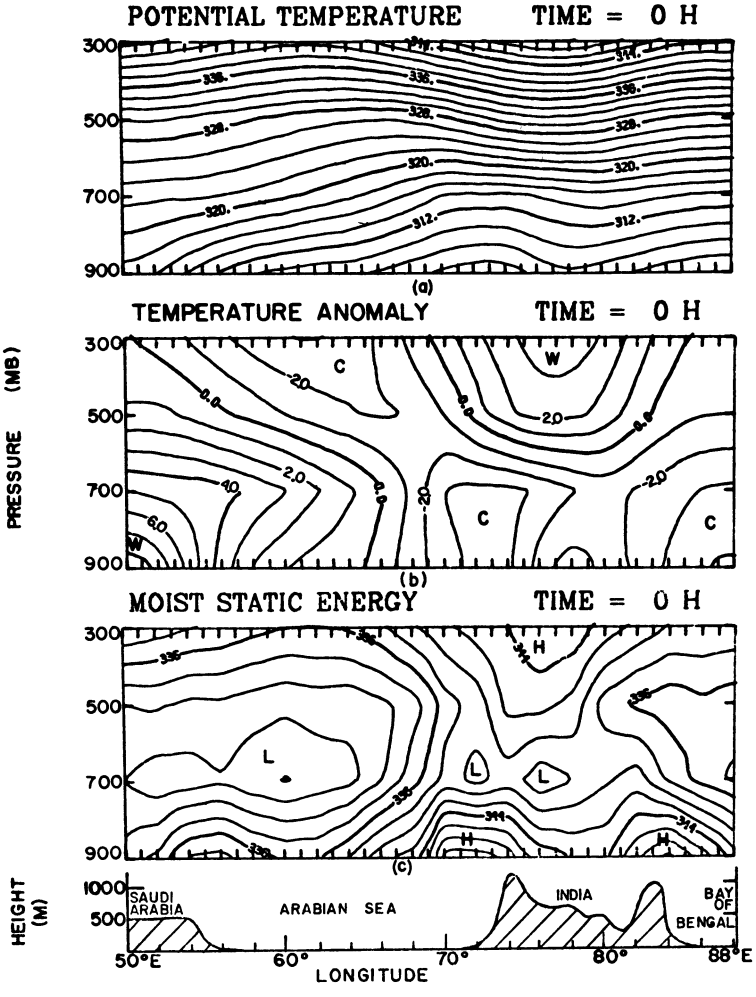

Figure 7
East–west vertical cross-section along 18°N at the initial time; (a) potential temperature (°C); (b) temperature anomaly (°C); (c) moist static energy ($\times 10^3$ m^2 sec^{-2}).

maintenance of these temperature anomalies is an important problem and will be discussed in the next section.

Figure 7c presents the vertical structure of moist static energy, E_s. Two important features should be noted: (i) that the MTC exists above a regional maximum of high energy boundary layer air, and (ii) that the convective instability (determined from the vertical gradient of E_s) is largest within the MTC domain. This combination indicates that this region is highly conducive towards the development of deep convection. Both Figs 6 and 7 demonstrate that this incipient MTC existed in a favorable dynamic and thermodynamic environment for development.

Relative humidity cross-sections (not shown) portray a column of 80 percent values extending above 500 mb in the MTC center. According to Miller and Keshavamurthy, there are two sources of this mid-tropospheric moisture; the westward flux of moisture from the pre-existing Bay of Bengal disturbance, and vertical transport from the deep, moist boundary layer over the eastern Arabian Sea. Due to the presence of an intense low-level inversion over the western Arabian Sea and the heat low which gives way to a warm, dry anticyclone north of the Arabian Sea, a strong lower and mid-tropospheric temperature and moisture gradient exists to the north and west of the MTC. These features are expected to exert a considerable influence on the development and movement of the MTC.

As the MTC intensifies and the warm and cold anomalies develop, the center of the MTC becomes less unstable than its periphery (see Fig. 9). This is consistent with Miller and Keshavamurthy's observations that showed convection to be most intense away from the center in the western and southern quadrants of the storm where the lapse rates are steepest. Although the predominant cloud type reported during monsoon rains over the west coast of India is nimbostratus, radar and aircraft reports documented that convective elements were indeed present in and around the MTC, with some tops reaching 15 km.

Rainfall totals along the west coast of India during the MTC lifetime were quite large. Many stations averaged over 5 cm day^{-1} for periods of a week or longer; some daily totals were near 30 cm. Figure 8 provides more information on the rainfall distribution. In Fig. 8a the hatched area outlines the region that averaged over 4 cm day^{-1} during the MTC existence. Also indicated are the composite MTC centers at different levels (circled dots) and the extent and type of prevailing clouds. In Fig. 8b, the rainfall averaged among 70 coastal stations over the eight-day period from 1 July to 8 July 1963 is shown. The rainfall maximum is at 17°N, just south of the MTC center. The distribution is slightly bimodal, as a secondary maximum is located at 12°N. This is consistent with the climatological rainfall distribution along the west coast.

Miller and Keshavamurthy also examined two other cases of heavy rainfall near Bombay and found both to be associated with mid-tropospheric vortices. They concluded that in the past (and even today), with the conventional observational network, it is possible for a MTC to exist over the north eastern Arabian Sea without being detected as a distinct and important kinematic feature. They showed that satellite photos proved useful in the detection of changes in cloud patterns as the MTC forms and dissipates. They also point out that in most cases of MTC development over the west coast of India, the coastal stations receive more rain initially than the inland stations on the western slope of the Western Ghats. This suggests that a synoptic-scale disturbance is controlling the rainfall distribution and only later might orographic rainfall become greater due to the enhanced onshore flow. Miller and Keshavamurthy conclude that MTC's must be the principal activators and regulators of rain over western India.

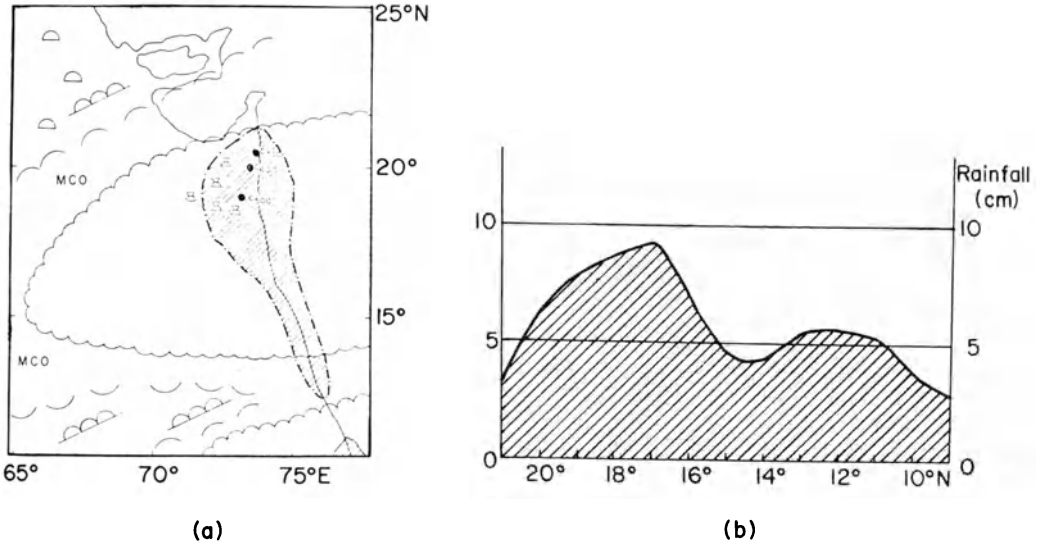

Figure 8

(a) Model of cloud and rainfall distribution associated with the composite MTC. The hatched area shows the extent of rainfall exceeding 4 cm day^{-1} associated with the mid-tropospheric cyclone; cumulonimbus symbols surrounding the cyclone centers schematically show the region of greatest vertical cloud development. Stippled areas outline broken to overcast middle and high clouds; broken arcs show extent of broken to overcast low clouds and scattered high clouds. (b) Precipitation profile along the west coast of India averaged over the period from July 1 to July 8. Daily rainfall amounts from 70 coastal stations were averaged to obtain these values (from MILLER and KESHAVAMURTHY, 1968).

In search of a partial answer to the MTC frequency question (for the Arabian Sea region only), CARR (1977) made a cursory survey of the daily satellite photographs over the 10-year period 1967 to 1976 in conjunction with the annual summaries of summer monsoon activity published by the *Indian Journal of Meteorology and Geophysics*. The following impressions were noted: (i) MTC's are not as frequent or regular a phenomenon as monsoon depressions and may exist from one to four times per year; (ii) they are more common in the first half of the summer monsoon season; (iii) the period of most MTC's is three to seven days; only rarely do they last for over a week as did the July 1963 MTC; (iv) most are more transitory than the July 1963 MTC and (v) many MTC's do not develop *in situ* over the northeastern Arabian Sea. A few MTC's originated as monsoon depressions over the Bay of Bengal, moved eastwards and took on MTC characteristics as they completed their life cycle over western India. Others have formed in the southeastern Arabian Sea and moved northwards along the coast; these occasionally initiate the southwest monsoon season over western India if they occur in late May or early June. Rarely, a disturbance intensifies enough to have a significant surface vortex, in which case it is not a MTC as defined here. This event is more common in spring or fall during which intense cyclones can form in the Arabian Sea.

Finally, THIRUVENGADATHAN (1972) has made an attempt to classify disturbances associated with heavy rain along the Konkan coast. The four categories he found and their percent frequency over a seven-year period are: (i) cyclonic circulations extending from the surface to 6 km or more – 19 percent; (ii) cyclonic circulations restricted to below 2 km – 29 percent; (iii) cyclonic circulation above 2 km – 26 percent and (iv) no cyclonic circulation; possibility of a trough – 26 percent. More studies like the above are needed but with an increased observational network over the Arabian Sea.

RAMAGE (1964) discussed evidence of a mid-tropospheric cyclone located in the Bay of Bengal during June 1963. The system was most intense at 500 mb with no detectable circulation at the surface or above 300 mb. The air below 500 mb near the center was cooler than its surroundings while a warm anomaly existed above

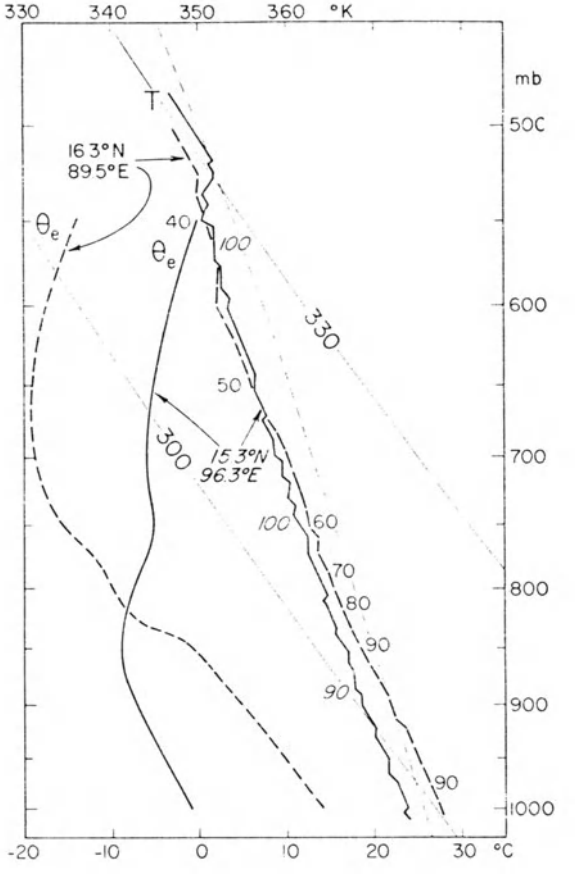

Figure 9

Distribution of temperature (T), relative humidity, and equivalent potential temperature (θ_e) determined from RFF drop soundings on 1 June 1963, made west of a monsoon rain area (dashed lines) and within the rain area (full lines) (from RAMAGE, 1971).

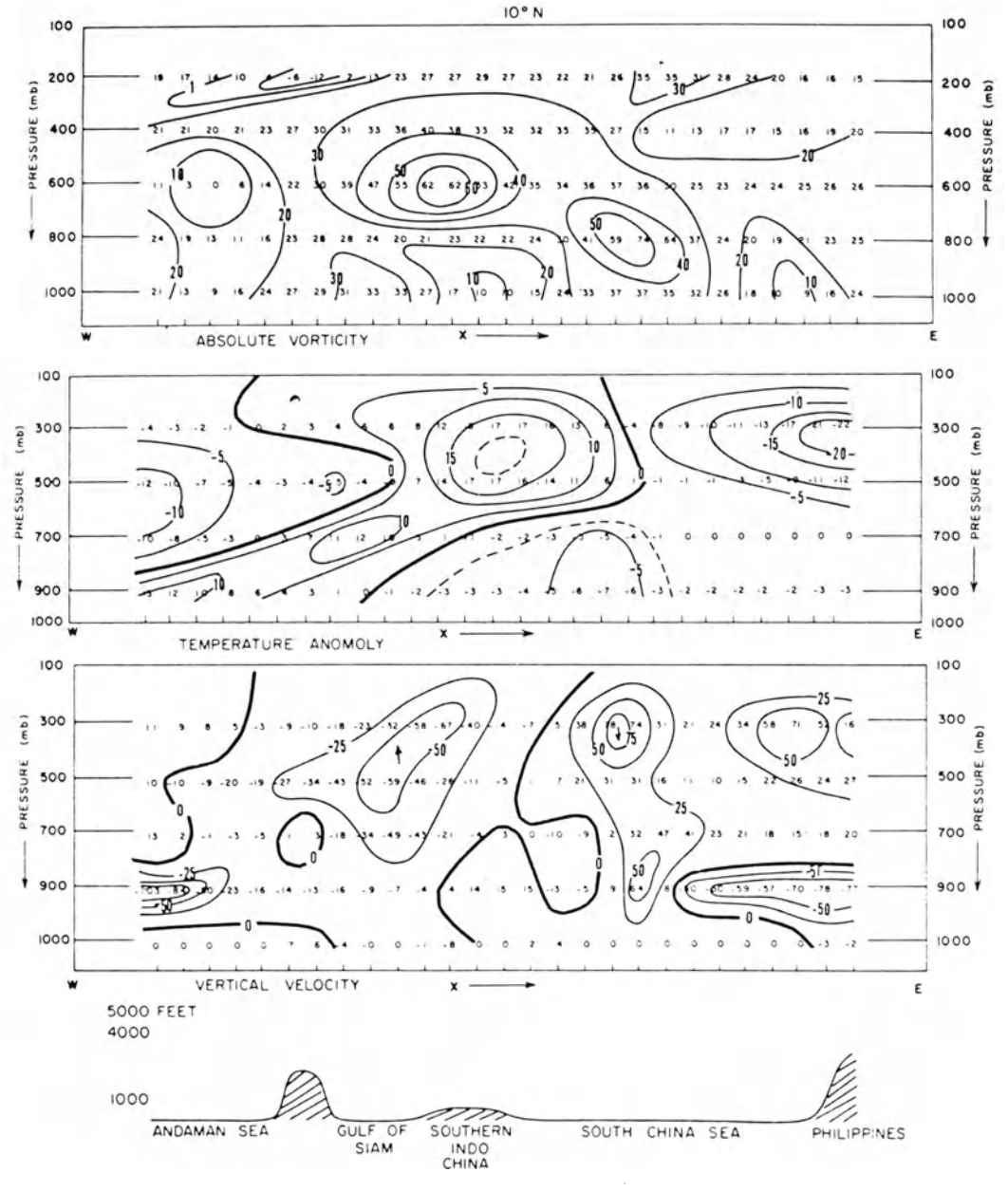

Figure 10

Vertical cross-section from west to east at 10°N for 0000 GMT 17 June 1966 through the mid-level cyclone over southern Indochina. Top: isopleths of absolute vorticity (10^{-6} sec^{-1}); middle: isopleths of temperature anomaly (10^{-1} C); bottom: isopleths of vertical velocity (10^{-5} mb sec^{-1}). A profile of the smoothed terrain is indicated at the bottom of the cross-sections (from KRISHNAMURTI and HAWKINS, 1970).

500 mb. Figure 9 portrays profiles of temperature, relative humidity and equivalent potential temperature from two soundings; one near the center of the MTC and one from its periphery. It illustrates that the heavy rains observed near the center are associated with much weaker convective instability than exists at the periphery where scattered cumulonimbus were observed. The questions of how many of these Bay of Bengal MTC's exist during the summer, and whether they remain independent of or become associated with monsoon depressions have yet to be answered.

Mid-tropospheric vortices are also observed over Indochina during the summer. KRISHNAMURTI and HAWKINS (1970) performed a diagnostic study of one such disturbance that occurred during July 1966. This MTC was characterized by a weak surface low, a vigorous 500 mb vortex and east-northeasterly flow above 300 mb. The system sloped quite sharply to the west and moved slowly westward during its lifetime. The vertical structure of this MTC in the east–west plane along 10°N is portrayed in Fig. 10. Maximum absolute vorticity ($f \approx 2.5 \times 10^{-5}$ sec^{-1}) exists at 600 mb and slopes eastward to the surface. The cyclone is warm-cored above 600 mb with a weak cold anomaly at the surface. Upward motion is found west of the disturbance and subsidence to the east. They also found a marked diurnal oscillation in the wind field which modulated the vertical motion and rainfall distributions. A discussion of the quantitative aspects of this MTC will be included in the next section.

3. *Dynamical aspects*

As the observational facts about the MTC become known, many questions regarding the dynamics of MTC genesis, morphology and evolution arise. For example, what is the instability mechanism that initiates the MTC? What maintains the mid-tropospheric vorticity maximum? How are the warm and cold anomalies created? Why is the MTC over the northeast Arabian Sea quasi-stationary? A first attempt to supply answers to these questions has been made by several authors and a summary of their results is given in the next two sections. This section will concentrate on dynamical aspects deduced by diagnostic or analytical studies while the next section will discuss results obtained from a numerical simulation of a MTC.

(*a*) *MTC formation*

One of the both contributory and complicating factors in the formation of a MTC off the west coast of India is the climatological presence of the mean monsoon trough in the lower and mid-troposphere across northern India during the southwest monsoon (see Fig. 1). Since weak positive vorticity may already be present before MTC formation, several authors have speculated on the mechanism for the intensification of the existing vorticity gradient that would lead to MTC genesis. MILLER and KESHAVAMURTHY (1968) found that a Bay of Bengal disturbance usually preceded the

formation of a MTC. As this disturbance moves west and northwestwards towards northern India, it may increase the vorticity in the mean trough over western India. The mid-tropospheric westward moisture flux provided by the circulation around the system also contributes to the subsequent increase in rainfall. The precise location and movement of the resulting MTC depends on the regional kinematic and thermodynamic conditions at that time. For example, Figs. 6 and 7 indicated that a position just west of Bombay was the most favorable location for development of the July 1963 MTC.

RAMAGE (1966) proposed an alternative source for the needed vorticity. He applied a form of the vorticity equation in x–y–θ coordinates first used by PETTERSSEN (1953) to explain the large-scale steady-state features of the monsoon

$$\nabla\cdot(Q\mathbf{V}) = F - \frac{\partial Q}{\partial\theta}\frac{d\theta}{dt} \tag{1}$$

where θ is potential temperature, Q is vorticity normal to a θ-surface, $\mathbf{V}$ is the horizontal wind vector and F is the vorticity of the frictional force. The term on the left represents the rate of export of potential vorticity across the boundaries of some unit area; i.e., the intensity of the vorticity source or sink. The sign of the vorticity flux depends on the balance between the intensity of the heat source, $d\theta/dt$ ($\equiv \dot{H}\theta/(c_pT)$, where $\dot{H}$ is the diabatic heating rate), the sign of $\partial Q/\partial\theta$ and the value of F, which is negative (positive) where cyclonic (anticyclonic) vorticity exists.

Equation (1) is applied to the region northwest of India where an intense heat low is present during the summer months. Ramage notes that the development of the heat low always precedes the onset of heavy rains over western India. Clear skies, intense radiative heating and subsequent upward heat flux from the surface keep $d\theta/dt$ positive during the spring and early summer months. Since the heat low gives way to an anticyclone above 700 mb, $\partial Q/\partial\theta$ is negative while F is positive in the middle troposphere. Hence both terms on the right side are positive and the atmosphere above the heat low exports cyclonic vorticity to its surroundings. As the moisture builds up over western India as summer progresses, Ramage states that the continual supply of vorticity towards the northeastern Arabian Sea ultimately triggers the MTC and causes the monsoon rains along the west coast of India. Bay of Bengal disturbances also play a role in Ramage's scenario, since their existence may increase subsidence northwest of India and intensify the heat low and, therefore, the vorticity export. As the MTC intensifies, a positive feedback may occur, as the intense latent heating and upward motion in the MTC may induce middle and upper tropospheric subsidence on its periphery, again leading to the intensification of the vorticity export toward the MTC. This is also equivalent to a statement that the role of differential radiative heating between West Pakistan and western India is very important in the formation and maintenance of the MTC.

Ramage also shows that the rains over central India are largest when the Pakistan heat low is deepest. It is not stated that the anticyclonic vorticity in the mid-tropo-

sphere, which makes the left side of (1) positive, is also largest at this time. More measurements are needed to examine the above question and to show that the magnitude of $\nabla \cdot Q\mathbf{V}$ is highly correlated with MTC formation. Certainly all the factors that Ramage mentions are operating favorably for MTC formation but the search must go on to further define the necessary and sufficient conditions for cyclogenesis.

The first attempt (and only one to date) to identify the actual instability mechanism of the MTC was by MAK (1975). He notes that barotropic and frontal instabilities are unlikely due to the absence of significant mid-level horizontal shear and concentrated baroclinic zones respectively. Despite the baroclinic basic state (as evidenced by the strong easterly shear from near the surface to 150 mb), the classical baroclinic instability theory (CHARNEY, 1947; EADY, 1949) is not expected to apply due to the large differences in the horizontal and vertical structure of the MTC from extratropical cyclones. Mak, noting the east–west temperature gradient between the Arabian Sea and India to the east, hypothesized that the change in meridional flow with height could constitute an additional source of potential energy in the basic state. Thus he attributes cyclogenesis to the baroclinic instability of a basic state with meridional as well as zonal shear.

Performing a linear, quasi-geostrophic instability analysis on a modified Eady problem, Mak obtains solutions for the wave length, growth rate, phase speed and structure of the most unstable mode that are in encouraging agreement with observations. The validity of the results remains unclear, though, due to some of the assumptions made about the basic state. While the July mean zonal shear is near 4×10^{-2} m sec^{-1} mb^{-1}, the mean meridional shear is only on the order of 1×10^{-2} m sec^{-1} mb^{-1} (RAO, 1962). The meridional shear that Mak assumes in his model for the lower troposphere, though, is four times that of the zonal shear, an assumption that is off by an order of magnitude. In reality, the meridional shear is only present after the formation of an MTC. The resulting length scale, growth rate, phase speed and structure of the most unstable mode when realistic shear is incorporated ($\varepsilon = -0.1$ in Mak's analysis) are quite different from observations. Although modifications to the theory are necessary, the solutions from this unique class of baroclinic flow are intriguing and further research is needed.

SHUKLA (1976), in his work on the dynamics of the monsoon depression, suggested that its growth is due to the CISK (conditional instability of the second kind; CHARNEY and ELIASSEN, 1964) mechanism in conjunction with the combined barotropic-baroclinic instability. A similar analysis for the MTC may also be relevant. One of the reasons CISK has been discounted as important for the MTC is the lack of a pre-existing cyclonic circulation in the Ekman layer. But subsequent work on the original CISK theory has generalized it to include other physical situations such as the growth of disturbances without surface moisture convergence (BATES, 1973), or in a translating boundary layer (CHARNEY, 1973). Further modification of the theory to analyze the case where pre-existing weak vorticity in the middle troposphere overlays a deep, moist, eastward moving boundary layer could be a rewarding exercise. Despite the

lack of a cyclonic Ekman layer at the surface, speed convergence along the coast and orographic uplift due to the Western Ghats provide a significant upward motion at the top of the boundary layer (see Fig. 6c). Once initiated, the strong mid-tropospheric moisture convergence (Fig. 5) supplies additional fuel for convection (and stable heating) and the feedback process continues. CARR (1977) proposed that the CISK process is the primary mechanism which intensified and maintained the MTC. A numerical test of that hypothesis is described in the next section.

(*b*) *Diagnostic studies*

The only quantitative diagnostic study of a MTC was performed by KRISHNAMURTI and HAWKINS (1970) on the Indochina cyclone discussed in Section 2. The vertical motions shown in Fig. 10 were computed via a complete non-linear balance model designed by KRISHNAMURTI (1968). This allows partitioning of the physical contributions to the total ω field. Krishnamurti and Hawkins found that thermal advection was the largest contributor to the total vertical velocity of the system. This is in agreement with the observed rising maximum west of the MTC, which is a region of warm advection from the land area to the north. To the east of this MTC, advection of cool, oceanic air from the south is consistent with the subsidence found there. Thus the slow, westward movement of this MTC is seemingly explained by simple quasi-geostrophic concepts, although other significant but compensating influences may be operating.

The mechanisms for the maintenance of the warm anomaly were investigated by Krishnamurti and Hawkins by constructing three-dimensional backward trajectories passing through the MTC and evaluating terms in the first law of thermodynamics. They found that subsidence warming at 500 mb and above could not completely account for the warm temperatures observed over the MTC. A cumulus-scale diabatic heating term after KUO (1965) supplied the additional warming necessary to maintain the anomaly. They attribute the subsidence to the convergent easterlies in the upper troposphere. Since in many cases rising motion in the MTC center extends to 300 mb or above, two other suggestions could be made to account for the warm anomaly. Recent work on cloud populations and cumulus parameterization has stressed that the warming by deep convection is actually accomplished by the associated compensating subsidence between the convective elements. Thus synoptic scale subsidence can also be forced by the cumulus scale. In addition, where the soundings are moist but stable (e.g., in the middle and upper troposphere near the center of an MTC) and rising motion is present, the stable latent heat release maintains a near moist adiabatic lapse rate which keeps the MTC core warmer in the upper troposphere than its surrounding environment, which has a lapse rate closer to the dry adiabatic rate. Since all the processes mentioned above are physically related, it is difficult to partition the exact contributions of each one; it should be enough to say that latent heat release plays the major role in creating and maintaining the warm anomaly.

No corresponding quantitative study has been made to explain the cold anomaly below 600 mb. MILLER and KESHAVAMURTHY (1968) attribute the cool air to the combined effects of adaibatic cooling and evaporative cooling. MAK (1975) showed that in the early stages of development, advection of cool air from the oceans is the most important effect.

Krishnamurti and Hawkins also examined the energetics of the Indochina MTC. Due to the limited domain, a kinetic energy budget study was carried out. A method for estimating the kinetic energy generation due to the cumulus scale motions is a unique feature of their analysis. The results averaged over four map times are:

(i) convergence of flux of potential and kinetic energy into region: -13×10^{18} erg sec^{-1}
(ii) dissipation of kinetic energy by surface friction: -4×10^{18} erg sec^{-1}
(iii) generation of kinetic energy by $[\omega' T']$ on the synoptic scale: -25×10^{18} erg sec^{-1}
(iv) generation of kinetic energy by $[\omega' T']$ on the cumulus scale: $+39 \times 10^{18}$ erg sec^{-1}

leaving an imbalance of -3 units. Thus they found that the synoptic scale $[\omega' T']$ contribution converts kinetic energy into potential energy because the centers of maximum rising (sinking) motion were closer to the cold (warm) temperature anomalies (see Fig. 10). The important role of the convective scale is illustrated here, as it maintains the MTC against synoptic scale conversion and frictional dissipation and accounts for the energy exported to its surroundings. Thus while both scales of motion act to maintain the warm anomaly, they oppose each other in the energetics of the system. This dual role in the coupling of different scales of motion is an interesting aspect of their study and may be worthwhile studying in other tropical systems.

Comparing the vertical motion and temperature anomaly cross-sections in Figs. 6c and 7b, it is clear that the energetics of the July 1963 MTC is somewhat different than that just described. Although no budget study has been carried out for this storm (see Fig. 16 for the complete energy cycle of this MTC), the figures show that the cold and warm anomalies and the maximum upward motion co-exist at the center of the MTC. This structure would indicate a generation of kinetic energy above 600 mb by the synoptic scale motions and a destruction below 600 mb. This could help explain the lack of a cyclonic circulation at the surface. The kinetic energy created above 300 mb probably goes immediately into the kinetic energy of the zonal easterly flow and thus does not extend the mid-level circulation upwards.

(c) *MTC dissipation*

As MILLER and KESHAVAMURTHY (1968) point out, the seeds for the destruction of the MTC are sown when the storm intensifies to its mature stage. Since the level of non-divergence is above 500 mb (Fig. 5), dry air from the north and west is entrained into the central region of the cyclone. As time goes on, the air near the center becomes

drier and cooler and the buoyancy of the system is reduced. Once a decrease in convection occurs, convergence and vertical motion decrease and latent heating is further suppressed. Eventually subsidence prevails over most of the region and a break occurs in the monsoon rains.

Other factors which may or may not be important in some instances are: (i) the northward movement of a Bay of Bengal disturbance and the subsequent cutting off of the moisture supply from the east; (ii) the warming and stabilization of the upper troposphere due to the copious latent heat release; also the increased subsidence after a particularly heavy rainfall event; (iii) intrusion of a large-amplitude trough from the polar westerlies into the Indian peninsular and its attendant advection of cooler, drier air (RAMASWAMY, 1962); and (iv) the decrease of surface wind speeds (especially in the onshore flow from the Arabian Sea) and/or more convergent easterlies aloft. All of these may be related to the more general concept that dissipation of the MTC may be associated with the changes in the larger scale flow patterns which are connected with the 14–16-day oscillation in monsoon behavior studied by MURAKAMI and FRYDRYCH (1974), M. MURAKAMI (1976), KRISHNAMURTI and BHALME (1976) and others. Subtle changes in flow trajectories around a MTC caused by larger scale adjustments could lead to increased injection of drier air and rapid dissipation of the system.

4. Numerical simulation of a MTC

From the previous discussion, it is clear that many physical factors may have to be taken into account to explain the structure and dynamics of the MTC. Some of these that pertain to the MTC over the northeastern Arabian Sea are the heat lows to the north and northwest, the orography to the east and north, the strong, moist southwesterly surface flow, the upper tropospheric easterly jet, the mean monsoon trough and the influences on it by Bay of Bengal disturbances and the large-scale flow, the varying moist static stability over the region, differential radiative heating and the presence of simultaneous stable and convective heating. Since only a three-dimensional primitive equation model with fairly complete physics can hope to include all these factors, CARR (1977) applied such a model in a real data case study in an attempt to increase our quantitative understanding of the MTC.

(*a*) *The model*

The model utilized was the limited-area, x–y–p primitive equation model that has been developed and applied by Dr. Krishnamurti and his colleagues at Florida State University over the past decade (e.g., see KRISHNAMURTI *et al.*, 1976). The horizontal resolution varied between a 2° latitude–longitude grid (coarse mesh) and a 1° grid (fine mesh). The model has five layers in the vertical with $\omega = 0$ at 100 mb as the top

boundary condition. The lower boundary condition of $w = 0$ except in the presence of terrain gives rise to a tendency equation for z_0, the 1000 mb height surface. The east–west lateral boundary conditions are cyclic while rigid, slippery walls are imposed to the north and south. A semi-Lagrangian scheme is used for the non-linear advective terms in the equations while the Euler-backward method is used for time-differencing.

The main physical processes included in the model are surface friction, orography, horizontal and vertical diffusion, and the diabatic heating effects of large-scale condensation (stable heating), convective heating (via a modified version of the KUO, 1965, scheme), short- and long-wave radiative heating and sensible and latent heat flux from the surface. Care was taken to ensure physical consistency during the simultaneous occurrence of stable and convective precipitation.

(*b*) *Data and initialization*

All experiments were real data forecasts. The initial state was chosen to be 1 July 1963, at 1200 GMT, an early stage in the July 1963 MTC documented by Miller and Keshavamurthy. Some of the initial structure of this MTC was displayed in Figs 6 and 7. The data was obtained from subjective analyses of wind, temperature and relative humidity fields at the standard levels and of surface pressure. From these fields, the five prognostic variables u, v, θ, q, and z_0 were obtained at the model levels, where u and v are the zonal and meridional components of velocity respectively and q is specific humidity. The divergence correction procedure as described by WASHINGTON and BAUMHEFNER (1975) was applied. Finally, a dynamic or iterative initialization

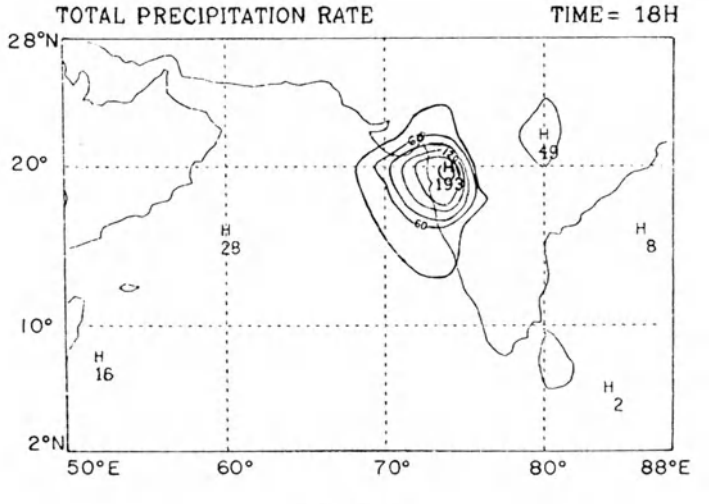

Figure 11
Total precipitation rate at 18 hours ($\times 10^{-7}$ gm sec^{-1} cm^{-2}).

period of 18 hours preceded each prediction in order to allow small-scale gravity waves and the external gravity-inertial wave to disperse or dissipate.

(c) *Forecast results*

Only a few of the many experiments will be summarized here. Since the wind, temperature, moisture and other large-scale fields were generally forecast well out to 36–48 hours, the discussion will first concentrate on rainfall prediction. Figure 11 is a coarse mesh prediction of the rainfall rate after 18 hours. The forecast rainfall distribution is encouraging (see Fig. 8) but the maximum value corresponds to just

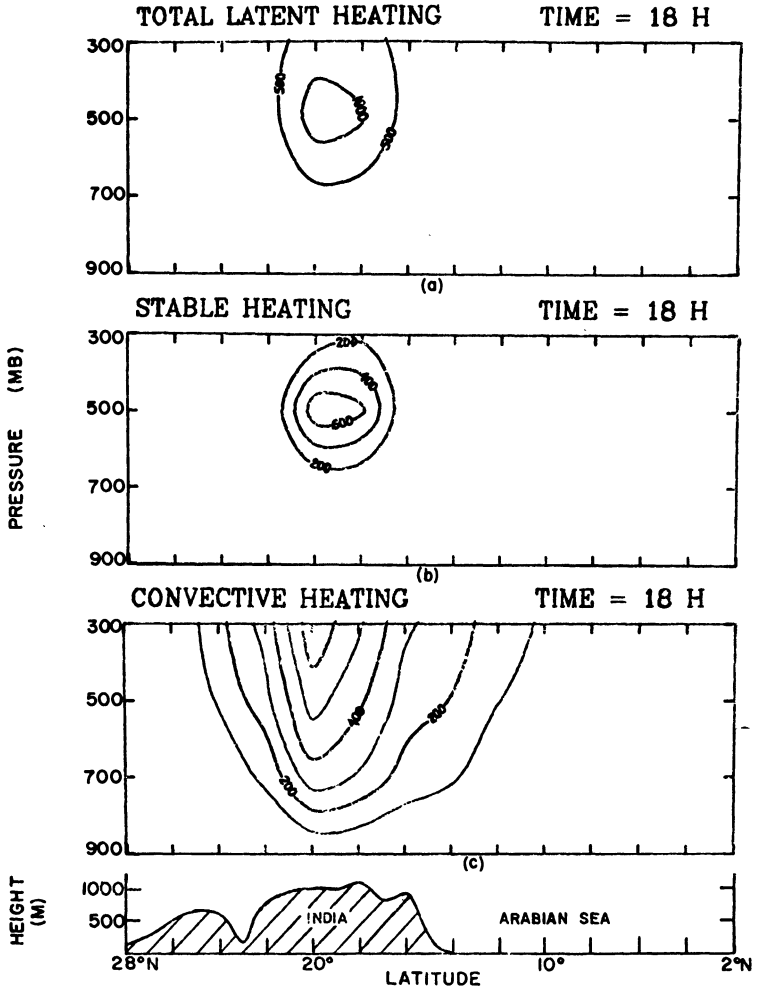

Figure 12
North–south vertical cross-section along 74°E of the predicted latent heating rates at 18 hours ($\times 10^{-7}$ °C sec^{-1}); (a) total latent heating rate; (b) stable heating rate; (c) convective heating rate.

2 cm day^{-1}, well under the observed amounts. Figure 12 depicts the vertical distribution of latent heating in the north–south plane along 74°E. Convective heating (Fig. 12c) is spread along the coast as observed and is a maximum at 300 mb near 19°N, near where deep cumulonimbus clouds were observed. This contrasts with the stable heating profile (Fig. 12b), which has its maximum at 500 mb in the center of the MTC where the maximum rising motion is. The presence of stable heating is important since the total latent heating profile (which theoretical work on tropical disturbances has shown to have a strong influence on the structure and dynamics of the system) also has its maximum of 12°C day^{-1} at 500 mb (Fig. 12a).

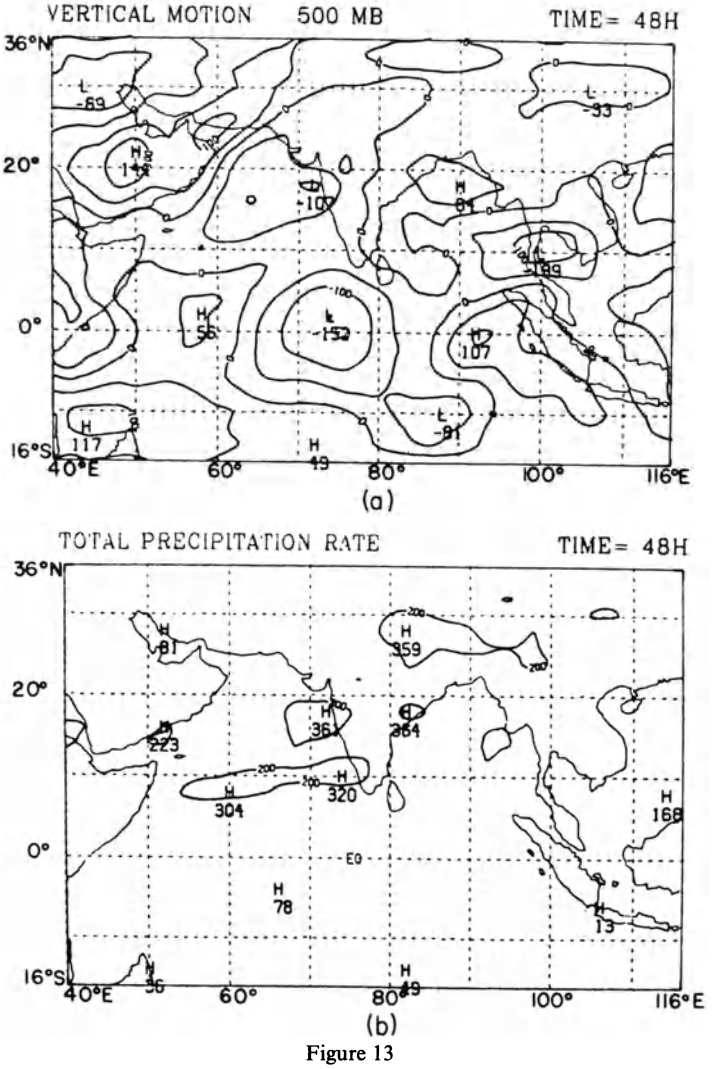

Figure 13
Large domain forecast at 48 hours; (a) vertical velocity at 500 mb ($\times 10^{-5}$ mb sec^{-1}); (b) total precipitation rate ($\times 10^{-8}$ gm sec^{-1} cm^{-2}).

The result of a 48 hour coarse mesh forecast over the entire southwest monsoon regime is shown in Fig. 13. Since the data quantity and quality was poor over 75 percent of this region, it was interesting to see if any useful predictability existed over this area after 48 hours. In Fig. 13a, the forecast 500 mb vertical motion field looks qualitatively reasonable, with rising motion over the northeastern Arabian Sea and subsidence over the Arabian desert. The precipitation patterns (but not amounts) are quite realistic; the horizontal scale of the MTC rainfall is reasonable, the last remnants of the monsoon depression rainfall appear on the east coast of India, orographic

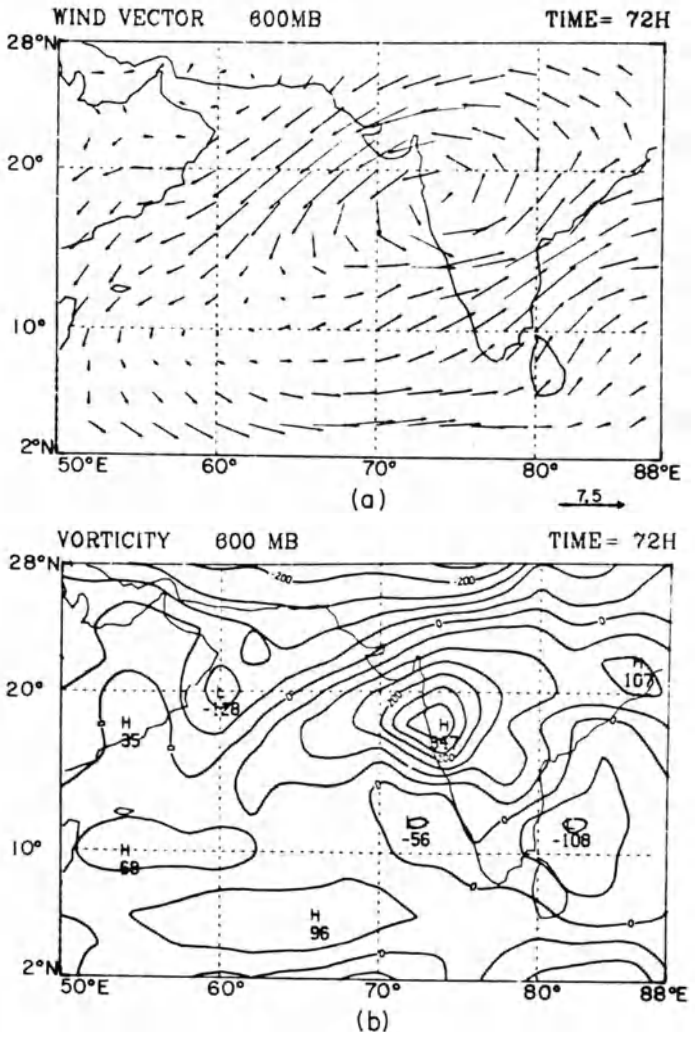

Figure 14
600 mb wind field at 72 hours; (a) wind vectors (m sec^{-1}); (b) vorticity ($\times 10^{-7}$ sec^{-1}).

precipitation is predicted along the southern escarpment of the Himalayas and the east–west band of convection near 10°N can also be verified observationally. The general east–west alignment of the rainfall in this figure indicates (and is borne out by calculations) that latent heating can generate available potential energy for the long waves and zonal flows as well as for the eddy motions.

Despite the qualitative success of the forecasts, if the rainfall rates are not correct then a quantitative analysis of the forecasts would not represent the observed MTC. Here, the predicted rates were too low, primarily because the convective parameterization scheme used could not account for all the mesoscale and cloud-scale moisture convergence that must occur in active convective systems. In order to develop motion and thermal fields which are internally consistent with the true precipitation rates, the observed rainfall amounts were used to derive an analytical expression for the latent heating term at each grid point in the heavy rain area (see Fig. 8a). Based on earlier results shown in Fig. 12, a parabolic vertical heating profile was assumed. For more complete details of this procedure, see CARR (1977). Except for the specified latent heating, the model remains the same, with real data initial conditions.

In Fig. 14, the results of a 72-hour coarse-mesh integration are shown for 600 mb. The circulation intensifies as observed over the west coast of India, with the vorticity maximum (Fig. 14b) nearly twice as large as that predicted by earlier experiments. Although the vorticity center has the correct horizontal scale, the circulation as shown by the wind vectors (Fig. 14a) is too large, a common problem with coarse-mesh limited-area models. Note that the predicted southwestward extension of the MTC seen in both panels is observed in the composite MTC shown in Fig. 2.

Figure 15 is a north–south cross-section along 74°E of the same 72-hour forecast. The top panel shows that cyclonic vorticity has nearly extended to the surface (compare with Fig. 5) but remains below 300 mb. The vorticity maximum is maintained at 600 mb and slopes southward from the surface. This distribution can be partially explained using the lower two panels. The divergence pattern in Fig. 15b indicates that vorticity-generating convergence has a maximum in the lower troposphere beneath the MTC center, while divergence exists above 400 mb. The resulting vertical motion field (Fig. 15c) has a rising maximum at 600 mb, hence advecting lower level vorticity into the mid-troposphere.

Fine-mesh forecasts (not shown) were made and yielded quantitative improvements over the forecasts just shown. The MTC intensified more realistically and the rising motion maximum became -5×10^{-3} mb sec^{-1}. A fine-mesh experiment in which no latent heating was allowed resulted in an MTC which rapidly weakened and moved westward.

(*d*) *Dynamical analysis of the forecasts*

To examine the question concerning the maintenance of the mid-tropospheric vorticity maximum, a vorticity budget was performed at 600 mb for the two fine-

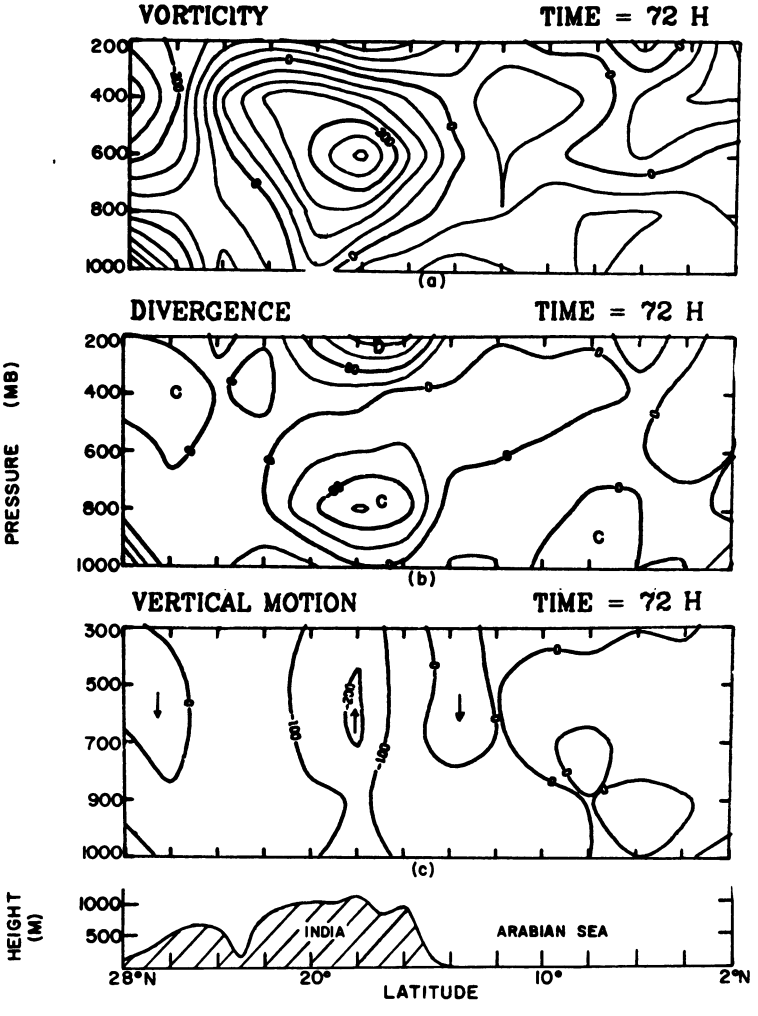

Figure 15
North–south vertical cross-section along 74°E at 72 hours; (a) vorticity ($\times 10^{-7}$ sec^{-1}); (b) divergence ($\times 10^{-7}$ sec^{-1}); (c) vertical velocity ($\times 10^{-5}$ mb sec^{-1}).

mesh experiments. The results, averaged over a 5° × 5° box centered over the MTC and averaged over the 24–48-hour forecast period, are presented in Table 1. In the specified heating forecast, the horizontal vorticity advection and frictional dissipation are the largest sinks of vorticity while horizontal convergence and vertical advection of vorticity are the main sources of vorticity at 600 mb. A net gain in relative vorticity is predicted over the period in contrast to the no-heating experiment in which the negative tendency is the largest term. The results suggest that the effects of latent heat are essential in creating and maintaining the vorticity maximum.

Table 1

Vorticity budget results at 600 mb for two fine mesh experiments. The values represent 24 hour averages over a 5° × 5° box centered on the MTC. All numbers have units of 10^{-12} sec^{-2}.

Term	$-\mathbf{V}\cdot\nabla\zeta$	$-f\cdot\mathrm{Div}$	$-\zeta\cdot\mathrm{Div}$	$-\omega\frac{\partial\zeta}{\partial p}$	$-\frac{\partial\omega}{\partial x}\frac{\partial v}{\partial p}+\frac{\partial\omega}{\partial y}\frac{\partial u}{\partial p}$	$-\beta v$	$K_H\nabla^2\zeta$	$K_v\frac{\partial^2\zeta}{\partial p^2}$	$\frac{\partial\zeta}{\partial t}$
Experiment									
Specified latent heating	−59	47	34	32	2	−8	−19	−5	24
No latent heating	−14	−10	−4	4	−7	−8	−9	−5	−53

In order to examine the mechanisms responsible for the quasi-stationary character of this particular MTC, the vorticity budget was evaluated separately over the eastern and western domains of the storm. Table 2 indicates that horizontal vorticity advection as well as the beta term predict a westward movement of the MTC. Also, as in the Indochina MTC, warm and cold advection exist on the west and east sides respectively, again indicating a westward movement. Despite this combination of barotropic and quasi-geostrophic westward forcing, and unlike nearly all other tropical disturbances, the MTC remains quasi-stationary over the west coast. Table 2 shows that the stationarity is due mostly to the large convergence production of vorticity in the western half of the domain (western India). Since part of this convergence is because of the coastal mountains, the MTC may be said to be quasi-stationary due partly to topographic anchoring and partly due to the dry, subsiding air over the western Arabian Sea. Hence the MTC position may be the net result of continuous cyclogenesis due to CISK near the Indian coast and continuous cyclolysis over the central Arabian Sea as the dynamical tendency for the storm to move westwards is negated by the quenching of convection in the dry air.

The energetics of the MTC as determined by a domain average over 48 hours of the fine-mesh specified heating experiment are shown in Fig. 16. It is seen that latent heating (H_L) and differential radiative heating (H_R) create available potential energy for the eddies (A') and the zonal flow ($\bar{A}$) (here, the domain average over 5000 km). A large energy conversion from $\bar{A}$ to the kinetic energy of the zonally averaged flows, $\bar{K}$, represents the large-scale reverse Hadley cell characteristic of the monsoon regime. Eddy heat flux also transforms $\bar{A}$ into A'. The largest energy transformation is from A' to eddy kinetic energy, K', indicating that latent heat release enables this MTC to be an energy-producing system on the synoptic as well as smaller scales. The small conversion of $\bar{K}$ to K' illustrates the minor role of barotropic energetics in MTC dynamics.

Table 2

Vorticity budgets at 600 mb for east and west sides of the MTC in the specified latent heating experiment. Values represent 6 hour averages over a 3° longitude by 5° latitude box. All numbers have units of 10^{-12} sec^{-2}

West of Center		East of Center
−34	$-\mathbf{V}\cdot\nabla\zeta$	−80
18	$-f\cdot\text{Div}$	66
24	$-\zeta\cdot\text{Div}$	53
40	$-\omega\dfrac{\partial\zeta}{\partial p}$	−10
−16	$-\dfrac{\partial\omega}{\partial x}\dfrac{\partial v}{\partial p}+\dfrac{\partial\omega}{\partial y}\dfrac{\partial u}{\partial p}$	39
25	$-\beta v$	−42
−27	$K_H\nabla^2\zeta$	−11
−6	$K_v\dfrac{\partial^2\zeta}{\partial p^2}$	−2
24	$\dfrac{\partial\zeta}{\partial t}$	13

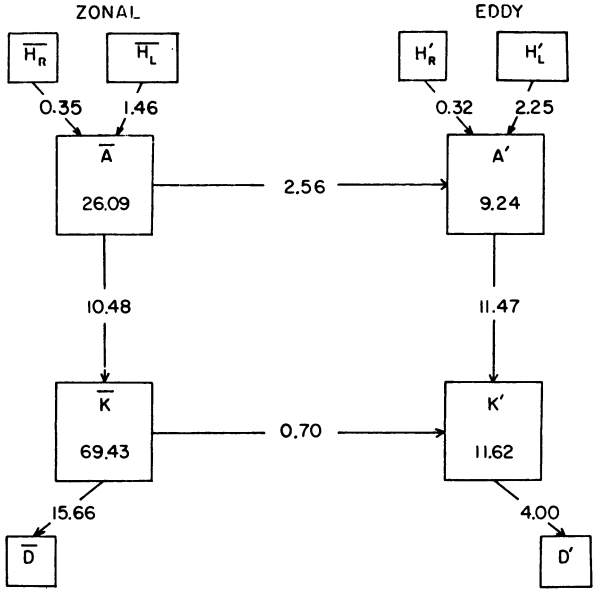

Figure 16

Baroclinic energetics computed from the fine mesh, specified latent heating forecast. The energy values inside the boxes have units of 1×10^{17} J. The energy exchange rates indicated by the arrows are in units of 1×10^{12} W.

5. *Concluding remarks*

Since the numerical studies by CARR (1977) on a pre-existing MTC are not capable of ascertaining what the original instability mechanism is for the cyclone, this process is still an important scientific problem. The different physical processes involved in all the hypotheses about MTC formation discussed in Section 3 are not necessarily mutually exclusive and probably act together in a cooperative manner. The fact that most MTC's differ somewhat in structure and evolution indicates that no one instability sequence operates all of the time but that the relative role of the various dynamical and thermodynamical influences will vary depending on the local environment and geographical conditions.

Before the first MTC event of the southwest monsoon season occurs, the heat low over Pakistan develops, the moist, southwesterly boundary layer flow streams over the coast, deep convective instability builds up and monsoon rains begin in the northeastern Bay of Bengal area. After these events, a weak monsoon trough may develop across northern India, and the entire region becomes highly cyclogenetic. At this stage, many possibilities exist for the triggering of MTC formation. Any of the various mechanisms discussed earlier for increasing the local vorticity gradient could apply. The hypotheses advanced by RAMAGE (1966) and MAK (1975) would be most important at a very early stage, before extensive rains begin. The pre-existence of a Bay of Bengal disturbance appears to be an important but not necessary indication for MTC development. Another potential source for an increase of the vorticity gradient could be the long planetary waves so important in the general circulation of the tropics. ABBOTT (1973) showed that wave–wave interaction among these planetary waves could generate kinetic energy on the synoptic scale in the vicinity of the mean monsoon trough.

If weak vorticity is already present in a region of imminent MTC formation, an increase in moisture flux or cumulus activity alone could initiate the development sequence. This could be accomplished by the moisture flux from the east mentioned earlier, or from increased onshore flow from the Arabian Sea. The existence of squall lines in the Arabian Sea is not uncommon and the possibility of boundary layer instabilities arising from mesoscale velocity streaks in the conditionally unstable southwesterly flow should not be ignored. Again, it appears that a proper modification of one of the generalized CISK theories could be the key to developing a theory for MTC intensification.

Once the MTC is initiated, the work of KRISHNAMURTI and HAWKINS (1970) and CARR (1977) indicates that latent heat release plays the dominant role in creating and maintaining the temperature and vorticity structure and in driving the energy cycle. In Southeast Asia, where the environmental conditions needed for the Ramage and Mak hypotheses to apply are not so prevalent, a modified CISK theory could still be valid, as moist, low-level flow, deep convective instability and pre-existing weak mid-tropospheric vorticity may all be present.

A unique feature of the MTC is the weak or non-existent surface vortex. Several reasons for this can be suggested: (i) a surface circulation requires too large of a perturbation easterly component due to the strong, prevailing westerlies; (ii) eddy kinetic energy is decreased near the surface due to the large, positive $[\omega' T']$ correlation there; (iii) vorticity-producing convergence is strongest from the top of the boundary layer to the mid-troposphere and (iv) over coastal India, the conservation of potential vorticity concept applied to the flow over the Western Ghats yields anticyclonic curvature over the coastal region and cyclonic curvature returning as the air flows out over the Bay of Bengal.

Equally interesting is the lack of circulation above 400–300 mb. Planetary wave theory (CHARNEY and DRAZIN, 1961) indicates that vertical propagation of energy is inhibited by the existence of easterly flow aloft and that the energy of the waves would be absorbed at the level where the phase speed becomes equal to the speed of the zonal flow. KRISHNAMURTI and HAWKINS (1970) suggest that the role of critical level absorption may be important in confining the vorticity to the mid-troposphere.

It has already been pointed out several times that more observational studies are needed to obtain more climatological and structural information about the MTC. The author wishes to further point out, however, the unique opportunity that the MTC over northeastern Arabian Sea provides for the study of the scale interaction between an ensemble of convective clouds and its large-scale environment. The MTC can be thought of as a vigorous, quasi-stationary cloud cluster, whose convective population exists in quasi-equilibrium with the large-scale disturbance for periods of a week or more. It appears as if the MTC satisfies some of the crucial assumptions made in the recent parameterization theory of ARAKAWA and SCHUBERT (1974) and that this theory could be verified using MTC data. It is hoped that future observational programs will further study the MTC so that our knowledge of the symbiotic role between a synoptic scale system and its convective elements will be enhanced.

Acknowledgements

The author's work reported in this review was supported by the National Science Foundation Grant ATM75-18945 during his studies at Florida State University. Appreciation is expressed to Dr. T. N. Krishnamurti for his support and guidance during that time. Computational support was provided by the National Center for Atmospheric Research which is sponsored by the National Science Foundation. The author is grateful to his wife Meg who drafted the figures and typed the manuscript.

REFERENCES

ABBOTT, D. A. (1973), *Scale interactions of forced quasi-stationary planetary waves at low latitudes*, Rept. 73-2, Dept. of Meteorology, Florida State University, Tallahassee, 190 pp.

ARAKAWA, A. and SCHUBERT, W. H. (1974), *Interaction of a cumulus cloud ensemble with the large-scale environment. Part I.*, J. Atmos. Sci. *31*, 674–701.

CARR, F. H. (1977), *Numerical simulation of a mid-tropospheric cyclone,* Rept. 77-1, Dept. of Meteorology, Florida State University, Tallahassee, 267 pp.

CHARNEY, J. G. (1947), *The dynamics of long waves in a baroclinic westerly current,* J. Meteor. *4*, 135–162.

CHARNEY, J. G. and DRAZIN, P. G. (1961), *Propagation of planetary disturbances from the lower into the upper atmosphere,* J. Geophys. Res. *66*, 83–109.

CHARNEY, J. G. and ELIASSEN, A. (1964), *On the growth of the hurricane depression,* J. Atmos. Sci. *21*, 68–75.

EADY, E. T. (1949), *Long waves and cyclone waves,* Tellus, *1*, 33–52.

KRISHNAMURTI, T. N. (1968), *A diagnostic balance model for studies of weather systems of low and high latidues, Rossby number less than 1,* Mon. Wea. Rev. *96*, 197–207.

KRISHNAMURTI, T. N. and BHALME, H. N. (1976), *Oscillations of a monsoon system. Part I: Observational aspects.* J. Atmos. Sci. *33*, 1937–1954.

KRISHNAMURTI, T. N. and HAWKINS, R. S. (1970), *Mid-tropospheric cyclones of the southwest monsoon,* J. Appl. Meteor. *9*, 442–458.

KRISHNAMURTI, T. N., KANAMITSU, M., GODBOLE, R., CHANG, C.-B., CARR, F. and CHOW, J. (1976), *Study of a monsoon depression (II)—Dynamical structure,* J. Meteor. Soc. Japan *54*, 208–225.

KUO, H. L. (1965), *On formation and intensification of tropical cyclones through latent heat release by cumulus convection,* J. Atmos. Sci. *22*, 40–63.

MAK, M.-K. (1975), *The monsoonal mid-tropospheric cyclogenesis,* J. Atmos. Sci. *32*, 2246–2253.

MILLER, F. R. and KESHAVAMURTHY, R. N. (1968), *Structure of an Arabian Sea summer monsoon system,* I.I.O.E. Meteorological Monograph *1*, (East–West Center Press, Honolulu), 94 pp.

MURAKAMI, M. (1976), *Analysis of summer monsoon fluctuations over India,* J. Meteor. Soc. Japan *54*, 15–31.

MURAKAMI, T. and FRYDRYCH, M. (1974), *On the preferred period of upper wind fluctuations during the summer monsoon,* J. Atmos. Sci. *31*, 1549–1555.

PETTERSSEN, S. (1953), *On the dynamics of the Indian monsoon,* Proc. Indian Acad. Sci. Ser. A *37*, 229–233.

RAMAGE, C. S. (1962), *The subtropical cyclone,* J. Geophys. Res., *67*, 1401–1411.

RAMAGE, C. S. (1964), *Some preliminary results from the International Meteorological Center,* In Proc. Symp. Tropical Meteor., New Zealand Meteorological Service. Wellington, 403–408.

RAMAGE, C. S. (1966), *The summer atmospheric circulation over the Arabian Sea,* J. Atmos. Sci. *23*, 144–150.

RAMAGE, C. S., *Monsoon meteorology* (Academic Press, New York 1971), 296 pp.

RAMAN, C. R. V. and RAMANATHAN, Y. (1964), *Interaction between lower and upper tropical tropospheres,* Nature *204*, 31–35.

RAMASWAMY, C. (1962), *Breaks in the Indian summer monsoon as a phenomenon of interaction between the easterly and the sub-tropical westerly jet streams,* Tellus *14*, 337–349.

RAO, Y. P. (1962), *Meridional circulation associated with the monsoons of India,* Ind. J. Meteor. Geophys. *13*, 157–166.

SHUKLA, J. (1976), *On the dynamics of monsoon disturbances,* Ph.D. Dissertation, Dept. of Meteorology, Massachusetts Institute of Technology, Cambridge.

THIRUVENGADATHAN, A. (1972), *Synoptic situations associated with spells of strong and weak monsoon over Konkan,* Ind. J. Meteor. Geophys. *23*, 207–210.

WASHINGTON, W. M. and BAUMHEFNER, D. P. (1975), *A method of removing Lamb waves from initial data for primitive equation models,* J. Appl. Meteor. *14*, 114–119.

(Received 15th June 1977)

Pageoph, Vol. 115 (1977), Birkhäuser Verlag, Basel

Orographic Effects on the Southwest Monsoon: A Review

By SULOCHANA GADGIL

Abstract – An overview of the problem of orographic effects on the southwest monsoon using the contributions of all the available analytical and numerical models is attempted. A quasi-geostrophic model is applied to deduce the effect of the topographic complex on the Indian peninsula. This model suggests that the southward bending of the low-level isobars on the peninsula can be ascribed to the topographically-induced southward velocity. This southward velocity triggers a Rossby wave to the east of the peninsula which is manifested as a trough on the southern Bay of Bengal.

Key words: Monsoon, quasi-geostrophic model, orographic effects on flow.

1. Introduction

More than half a century ago, SIMPSON [1] investigated the role played by the topography of the Indian subcontinent in determining the summer monsoon rainfall and emphasized its importance in a lecture before the Royal Society with the remark: 'The monsoon . . . is produced by a combination of circumstances involving consideration of temperature, pressure, humidity, geographical relationship between land and sea, the rotation of the earth and lastly but probably the most important the distribution of the mountain ranges.'

Following Simpson, the influence of topography on the monsoon has been investigated with the help of simple models treating the interaction between circulation and topography as an isolatable phenomenon (BANERJEE [2], SARKAR [3], GADGIL and SIKKA [4]) and numerical models of the monsoon incorporating many of the important factors mentioned by Simpson (MURAKAMI *et al.* [5], GODBOLE [6], HAHN and MANABE [7]). When numerical models are used, the effect of the topography on the circulation or rainfall patterns is obtained directly by comparison of the model runs with and without the mountain barriers. In deducing the effect on rainfall from simple dynamical models, an additional assumption relating rainfall to some feature of the circulation has to be made. Since the monsoon air is conditionally unstable in the summer (NORMAND and RAO [8]), forced ascent up to the level of lifting condensation results in rainfall. Hence the rainfall is generally assumed to be proportional to the upward vertical velocity.

[1]) Centre for Theoretical Studies, Indian Institute of Science, Bangalore 560012, India.

In the last two decades, two major developments have led to considerable insight into the nature of the influence of large-scale topographic features on circulation patterns in rotating systems as well as the relation of organized convection to circulation. CHARNEY and ELIASSEN's [9] formulation of the concept of the conditional instability of the second kind (CISK) relates organized convection over synoptic or larger scales to the vorticity above the planetary boundary layer, which determines the vertical velocity out of the layer. This concept has been shown to be valid for the large-scale rainfall associated with the summer monsoon by KESHAVAMURTHY [10] and SIKKA and GADGIL [11]. The variation of the rainfall in the Gangetic plain is known to be correlated with that of the vorticity around the monsoon trough, active spells being associated with high cyclonic vorticity and weak spells or breaks with anticyclonic vorticity in this region. In fact, it has now been established that the major difference between regions and seasons with varying amounts of rainfall is in the dynamics of the circulation which determines the extent to which the moist air near the surface is pumped upwards; the moisture content of the lower layer of the atmosphere being high during the summer monsoon irrespective of these variations. (SRINIVASAN and SADASIVAN [12], RAMAMURTHY *et al.* [13], SIKKA and ANANTHAKRISHNAN [14]). Thus it seems reasonable to assume the variations of the large-scale rainfall to be proportional to the vorticity above the frictional boundary layer.

The other important development has been the demonstration that the topography directly influences the vorticity via the stretching or shrinking of vortex tubes in rotating systems. This problem has been investigated by several authors since TAYLOR's [15] original experiment on the Taylor column, stimulated particularly by HIDE's [16] suggestion of the relevance of this phenomenon for the red spot of Jupiter and WARREN's [17] application of ROSSBY's [18] potential vorticity equation to relate the meanders of the Gulf stream to the underlying topography (e.g., INGERSOLL [19], ROBINSON and NIILER [20], ROBINSON and GADGIL [21], VAZIRI and BOYER [22], HOGG [23], JACOBS [24], etc.). These studies suggest that many of the features arising from the influence of large-scale topographic features in rotating fluids can be deduced qualitatively from appropriate quasi-geostrophic vorticity conservation equations. Such a model has been applied by GADGIL and SIKKA [4] to investigate the interaction between the topography on the Indian peninsula and the low-level circulation of the monsoon.

In this paper we shall attempt an overview of the problem of orographic effects on the southwest monsoon using the results of all the available investigations. We begin with a description of the observational background in Section 2. The contributions of the previous investigations are summarized in Section 3. We discuss GADGIL and SIKKA's [4] application of a quasi-geostrophic model to deduce the effect of the topography on the Indian peninsula on the southwest monsoon in Sections 4 and 5 and on the basis of this, speculate about the effects of other topographic features in Section 6.

2. *Observational background*

The topography of the region of interest is shown in Fig. 1. The mean rainfall for the summer (June–September) computed from 50 years of data (1901–50) at 2700 rain-gauge stations distributed throughout India (from INDIA METEOROLOGICAL

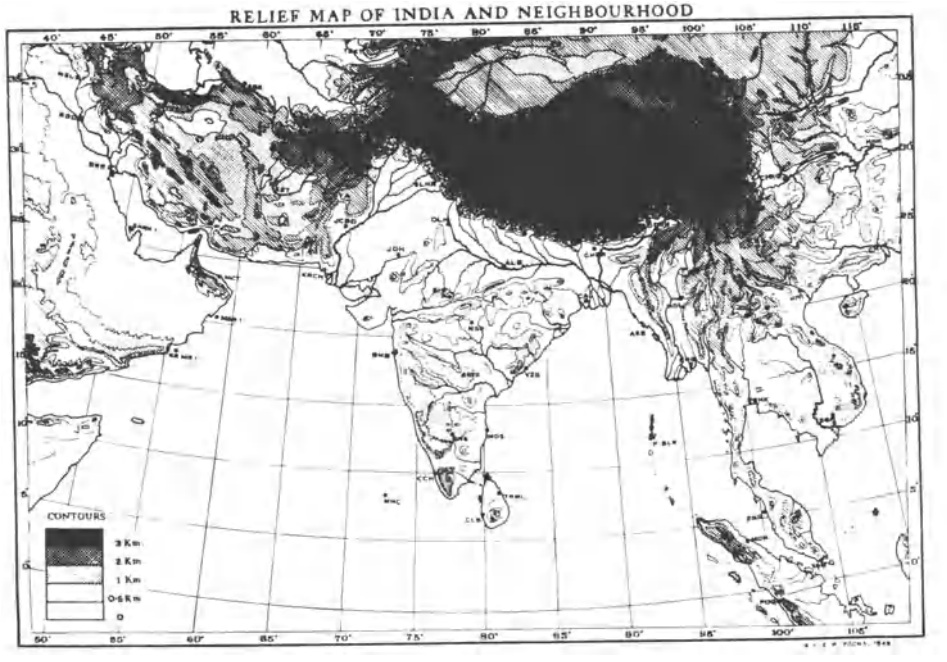

Figure 1
Relief map of India and neighbourhood.

DEPARTMENT [25]) is shown in Fig. 2. The rainfall contours over Burma are shown in Fig. 2 and have been taken from RAO and RAMAMURTHY [26]. The mean monthly surface pressure distributions for the summer (after ANANTHAKRISHNAN *et al.* [27]), the mean July wind field at 900 mb (after RAO and RAMAMURTHY [26]) and Simpson's idealization of the mountain ranges and the monsoon streamlines are shown in Fig. 3 (a–d, e, f), respectively. Figures 1 and 3f show the major topographic features to be (i) a topographic complex formed by the Western Ghats (KL) and the Deccan Plateau to their east, (ii) the mountain ranges along the west coast of Burma (GF), (iii) the Khasi Hills in Assam (HJ), and a continuous range extending from the high hills north of the Mekran coast (AB) in the northwest to the Himalayas in the north (CD) and the chain of mountains in Burma (DE) to the northeast.

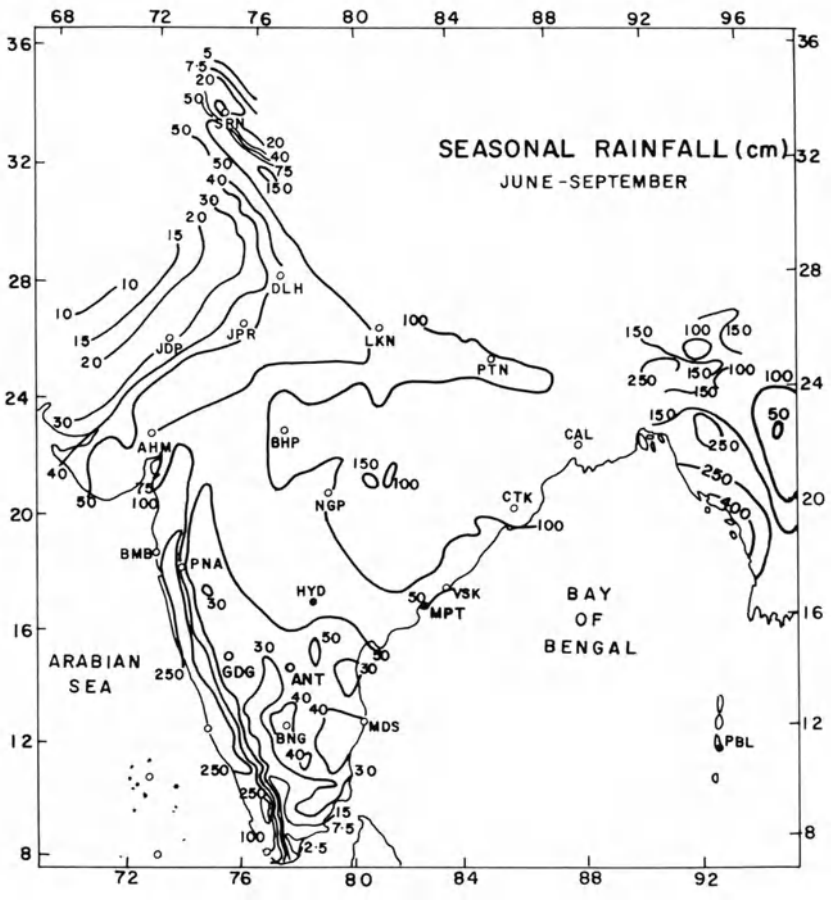

Figure 2
Normal rainfall during the summer (June–September) (after INDIA METEOROLOGICAL DEPARTMENT [25]) over the Indian region and (after RAO and RAMAMURTHY [26]) over Burma.

Important features of the surface pressure distribution associated with the summer monsoon are (i) southward bending of the isobars on the peninsula, (ii) the trough in the southern Bay of Bengal (e.g., the trough around 87°E, 7°N in the 1008 isobar for July in Fig. 3), (iii) the ridge over Burma and (iv) the prominent trough on the Gangetic plain extending from the low pressure area over Pakistan (70°E, 32°N) to the head of the Bay of Bengal. All these features are also present in the pressure distribution at higher levels, above the frictional boundary layer (INDIA METEOROLOGICAL DEPARTMENT [28]). The winds at the lower levels have a predominant westerly component on the Arabian sea and the peninsula, a significant southerly component together with the westerly component upstream of the Burmese coast, a southerly direction near the Head Bay and easterly direction north of the monsoon trough in the plains of north India. The westerlies on the Arabian sea and peninsula

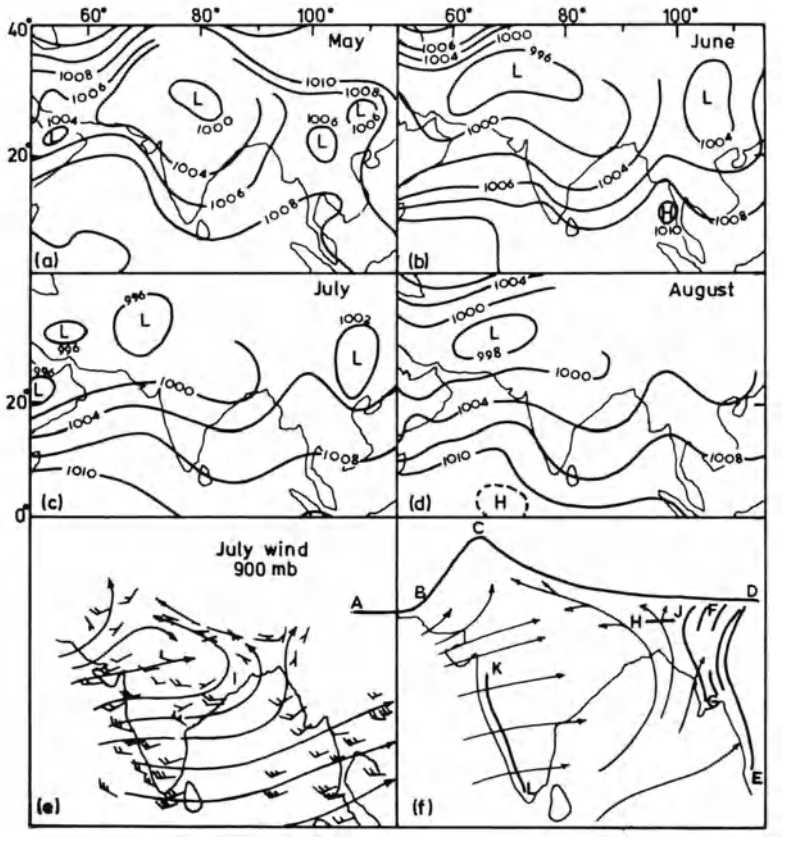

Figure 3
The mean monthly surface pressure distribution for May to August (a–d) after ANANTHAKIRHSNAN *et al.* [27]; the mean July wind field at 900 mb (e) (after RAO and RAMAMURTHY [26]) and idealized mountain barriers and monsoon streamlines (f), from SIMPSON [1].

are strongest in July, the major monsoon month. The meridional shear between the westerlies to the south of the trough and the easterlies to the north implies a large vorticity around the trough.

The rainfall is high on the west coast, upstream of the Western Ghats, and decreases, eastward of the ghats. A remarkable feature of the low rainfall on the peninsula is the occurrence of a minimum around 77°E at least 100 km inland from the east coast. The northeastern region receives copious rainfall, and the Gangetic plains around the mean seasonal position of the trough receive significant rainfall.

3. *Previous studies*

In his pioneering investigation, Simpson determined the vertical component of the wind over the monsoon region by considering the interaction of the *observed* horizontal wind field with idealized mountain ranges (Fig. 3f). In his view, the con-

tinuous mountain ranges from the northwest to the northeast of India are equivalent to two sides of a box into which air streams through the other two sides. He suggested that the ascent resulting from this convergence into the northern parts and particularly the Gangetic plain, was responsible for the significant rainfall in this region. An important cause of the sparse rainfall in the northwest was identified as the peculiar geographical position of the region with respect to the mountain ranges which delimit the convergence of moist air. The heavy rainfall upstream of the Western Ghats, the mountain ranges near the west coast of Burma and the Khasi hills was rightly attributed to the topographically forced ascent of the monsoon air impinging on them practically at right angles. The descending motion downstream of these ranges and the loss of water-content of the air due to the heavy rainfall upstream were suggested as the reasons for the occurrence of the dry area on the peninsula. On the basis of such reasoning, i.e., the rainshadow theory, one would expect the rainfall to decrease monotonically downstream of the mountains. Note from Fig. 2 that this is not consistent with the observed longitudinal variation of the rainfall on the peninsula which has a pronounced minimum around 77°E near the centre of the peninsula, downstream of which the rainfall increases.

Simpson's remarkable paper inspired a more formal treatment of the problem of orographic influence on the summer monsoon by BANERJEE [2]. Banerjee considered the effect of the idealized mountain ranges (Fig. 3f) on a basic current whose direction (westerly or southwesterly) was specified only on the Arabian sea, i.e., upstream of the first topographic feature encountered. The streamlines in the other regions were obtained by using the then popular theory of irrotational flow in the presence of obstacles. Except for the Himalayas, which were considered insurmountable, the air was assumed to flow around the mountain ranges below the level of the top of the range and above this level, the horizontal component of the wind was assumed to be unaffected by the topography. The high rainfall upstream of a range was attributed to the ascent resulting from frictional decceleration of the basic current just upstream of the mountain range, at all levels below the level of the top of the mountain. Although Banerjee's investigation is a significant contribution to this problem, some of the results are incorrect primarily because all the important effects of the rotation of the earth could not be taken into account. For example, in order to get the observed southward bending of the isobars on the peninsula, he had to assume a northwesterly direction for the basic current (see Fig. 4 in [2]). In addition, some of his assumptions such as the existence of a discontinuity in the nature of streamlines at the level of the top of the obstacle appear to be unjustified.

A quasi-geostrophic model for a homogeneous fluid on a β-plane has been applied by GADGIL and SIKKA [4] to deduce the effect of the topography of the peninsula on the low-level summer monsoon circulation and the associated rainfall. This simple model can explain the occurrence of the minimum rainfall in the centre of the peninsula. Further, two features of the circulation, viz. the southward bending of the isobars on the peninsula and the prominent trough in the southern Bay of Bengal

(Fig. 3) are identified as manifestations of the influence of this topography. Some aspects of this model will be discussed in Sections 4 and 5.

In addition to these models in which the dynamical effect of a particular feature of the topography is studied as an isolatable phenomenon, more complex numerical models of the monsoon have also been studied with and without mountain barriers to discern the role of these in determining the nature of the circulation. Whereas the models of the former category consider only the dynamical effect of the mountains, these numerical models consider the thermal effect as well, which is particularly important in the case of the Tibetan plateau which acts as an elevated heat source (FLOHN [29]). GODBOLE [6] has considered a zonally-symmetric model for the motion in the vertical plane along 80°E with and without the Himalayas (which is the only topographic feature at this longitude). The results show that the mountains are very important and the zonal flow is significantly different in the two cases. In the case with mountains, in the entire latitude belt shown (0–40°N) westerlies with speeds up to 10 m sec^{-1} prevail in the lower troposphere up to 5 km from the surface, and easterlies with speeds up to 30 m sec^{-1} prevail aloft. When the mountains are excluded, weaker westerlies with speeds less than 4 m sec^{-1} prevail south of about 25°N up to a maximum height of 3 km from the surface, and easterlies aloft are also weaker with maximum speeds of 8 m sec^{-1}.

HAHN and MANABE [7] have used the global general circulation model developed at the Geophysical Fluid Dynamics Laboratory (GFDL model) and compared the results for the cases with and without the mountain barriers. Of the topographic features shown in Fig. 1, only the Himalayas are considered in their investigation since the other features are smoothed out (Fig. 2.1 of their paper). In the model with mountains, the pressure distribution is characterized by a well-marked low in the lower troposphere over the highest point in Tibet near 30°N, capped by an anticyclone in the upper troposphere. The positions of both these is shown to be sensitive to the presence of the mountains, that of the low shifting by 20° to the north and 30° to the east and that of the high shifting by several degrees to the south in their absence. Thus the south to north pressure gradients over India and the Arabian sea are much weaker in the absence of the mountains. However the upper troposphere winds are stronger in the absence of mountains in contrast to the results obtained by GODBOLE [6] and MURAKAMI *et al.* [5]. The effect of the mountains on temporal variations of the monsoon is also shown to be significant.

Thus, while all the investigations of numerical models are in agreement in the recognition of the importance of the Tibetan plateau, the manifestations of its influence on the circulation and rainfall patterns are as yet not clear. This may be because there are major differences between the results of these models, even when the mountains are included, and the observations with respect to the latitudinal position and intensity of the monsoon trough, the presence of lower tropospheric easterlies on the plains of India and the rainfall distribution over the Indian region (SIKKA and RAGHAVAN [30], SADLER and RAMAGE [31]).

4. Some results from a quasi-geostrophic model of topographic influence

In this section we consider a quasi-geostrophic model of topographic influence. The derivation of the governing equations follows GADGIL [32] and the results are from GADGIL and SIKKA [4] unless otherwise indicated. Consider, quasi-geostrophic motion of a homogeneous fluid on a β-plane, with the x, y, z axes chosen to point eastward, northward and vertically upward respectively, in the presence of topography given in nondimensional coordinates as

$$z = \delta h(x, y). \tag{1}$$

The fluid is assumed to be bounded above by a rigid lid and no-slip conditions are imposed at the top and bottom.

$$u = v = w = 0 \quad \text{at} \quad z = 1, \quad \delta h. \tag{2}$$

Expansion of the equations of motion in the largest of the small parameters multiplying the ageostrophic contributions (say γ), e.g.,

$$u = u_0 + \gamma u_1 + \gamma^2 u_2 + \cdots$$

as in GADGIL [32], yields the equations in the interior region between the Ekman layers near the top and bottom, for the zeroth order components as

$$u_0 = -p_{0y} \tag{3}$$

$$v_0 = p_{0x} \tag{4}$$

$$0 = p_{0z} \tag{5}$$

$$\varphi_0 = v_{0x} - u_{0y} \tag{6}$$

$$\frac{\varepsilon}{\gamma}(u_0\varphi_{0x} + v_0\varphi_{0y}) + \frac{\beta}{\gamma}v_0 + w_{1z} = \frac{\sigma}{\gamma}(\varphi_{0xx} + \varphi_{0yy}) \tag{7}$$

$$w_1 = \frac{\delta}{\gamma}(u_0 h_x + v_0 h_y) + \frac{\sqrt{E}}{2\gamma}(v_{0x} - u_{0y}) \quad \text{at } z = 0$$

$$= -\frac{\sqrt{E}}{2\gamma}(v_{0x} - u_{0y}) \quad \text{at } z = 1 \tag{8}$$

This determines the vortex stretching produced by the flow over topography and suction in the Ekman layers, represented by the last term on the left side of (7) and yields the equation governing the zeroth order (after dropping the suffix) as

$$\varepsilon(u\varphi_x + v\varphi_y) + \beta v + \delta(uh_x + vh_y) = -\sqrt{E}\,\varphi + \sigma(\varphi_{xx} + \varphi_{yy}). \tag{9}$$

Note that all the parameters occurring in (9) have to be less than unity for the validity of the quasi-geostrophic model considered. These parameters are given in terms of L,

the horizontal scale; U_0 the scale of the velocity; D, the height of the topography, the total height H, the mean latitude θ_0, the Coriolis parameter f_0, the radius of the earth R and viscosity ν as

$$\varepsilon = \frac{U_0}{f_0 L}, \quad \delta = \frac{D}{H}, \quad \beta = \frac{L \cot \theta_0}{R}, \quad \sqrt{E} = \sqrt{\frac{\nu}{f_0 H^2}}, \quad \sigma = \frac{\nu}{f_0 L^2}.$$

The terms in the vorticity equation (9) represent advection, change of the planetary vorticity due to meridional motion, topographically induced vortex stretching, the dissipation in Ekman layers and lateral diffusion of vorticity respectively.

If friction is unimportant (i.e., $\sqrt{E}, \sigma \ll \varepsilon, \delta, \beta$) the vorticity equation (9) can be integrated with the use of (3) and (4) to yield a potential vorticity integal of the form

$$\varepsilon\varphi + \delta h + \beta y = F(p).$$

The potential vorticity, which is the sum of the relative vorticity, the height of the underlying topography and the Coriolis parameter is conserved along streamlines for inviscid flows. The function $F(p)$ is evaluated by use of upstream conditions. Thus if the current is uniform upstream of the obstacle and in the westerly direction,

$$p = -y \quad \text{as} \quad x \to -\infty.$$

Hence

$$F(p) = -\beta p$$

and the equation (9) governing the inviscid flow becomes

$$\varepsilon\varphi + \delta h + \beta(p + y) = 0.$$

In terms of the perturbation pressure, P,

$$P = p + y$$

the equation becomes

$$\varepsilon\varphi + \delta h + \beta P = 0 \tag{10}$$

with

$$\varphi = P_{xx} + P_{yy}.$$

In what follows, we shall discuss mainly the inviscid flow results although some effects of including friction will also be briefly mentioned.

(a) *Obstacles on f-plane*

On the f-plane, the conservation of potential vorticity along streamlines (10), implies that a negative vorticity is induced over the obstacle due to the shrinking of

vortex tubes, the flow being irrotational everywhere else. In general both the terms v_x and u_y in (6) contribute to the induced vorticity. In most applications it is necessary to understand whether the major manifestation of the topographic influence will be as a curvature in the streamlines (as in Gulf-stream meanders) or as a shear in the velocity component parallel to the basic current. In the problem in which the basic current is uniform and the fluid homogeneous, the ratio of scales of the two components of the induced vorticity is related to the scales of the obstacle. This relationship can be investigated by considering the flow past a rectangular plateau with scales $\bar{x}$ and $\bar{y}$ in the zonal and meridional direction,

$$\begin{aligned} h(x, y) &= 1 \quad -\bar{x} < x < \bar{x}; \quad -\bar{y} < y < \bar{y} \\ &= 0 \quad \text{otherwise.} \end{aligned} \tag{11}$$

The governing equation (10) (with $\beta = 0$) can be solved by taking Fourier transforms to yield the meridional component of the velocity in terms of

$$\begin{aligned} x_1 &= x + \bar{x}, \qquad x_2 = x - \bar{x} \\ y_1 &= y + \bar{y}, \qquad y_2 = y - \bar{y} \end{aligned}$$

as

$$\begin{aligned} v = \frac{1}{2\pi\varepsilon}\frac{\delta}{}\Bigg[& \frac{y_2}{2}\log\left(\frac{x_1^2 + y_2^2}{x_2^2 + y_2^2}\right) - \frac{y_1}{2}\log\left(\frac{x_1^2 + y_1^2}{x_2^2 + y_2^2}\right) \\ & - |x_1| \tan^{-1}\left(\frac{2\bar{y}|x_1|}{x_1^2 + y_1 y_2}\right) + |x_2| \tan^{-1}\left(\frac{2\bar{y}|x_2|}{x_2^2 + y_1 y_2}\right)\Bigg] \end{aligned} \tag{12}$$

(GADGIL and SIKKA [4]). The induced zonal component has a similar expression and is omitted here for brevity. The variation of the scales of the induced velocity components v_{max} and u_{max} deduced from the above solution and of one of the components of the vorticity, v_x at the centre, with the ratio $\bar{y}/\bar{x}$ is shown in Fig. 4. It can be seen

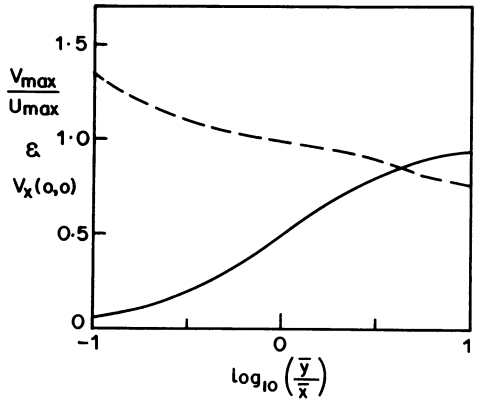

Figure 4
The variation of the ratio of v_{max}/u_{max} (— — —) and $v_x(0, 0)$ (———) with y/x from the solution (12).

that the scales of the two velocity components are comparable over a wide range of variation of $\bar{y}/\bar{x}$. The dominant component of the induced vorticity comes from the variation of the velocity in the direction of the smaller scale, i.e., v_x for small values of $\bar{x}/\bar{y}$, this term comprising about 95 percent of the vorticity over the centre of the obstacle when the meridional extent $\bar{y}$ is an order of magnitude larger than the zonal extent $\bar{x}$. For the specific obstacle chosen, however, at the edges $\pm\bar{y}$, the other term u_y becomes equally important. For large $\bar{y}/\bar{x}$, and away from the edges, $\pm\bar{y}$, the solution for the finite obstacle can be approximated by the one dimensional solution for flow past a ridge of the form

$$\begin{aligned} h(x) &= 1 \quad -\bar{x} < x < \bar{x} \\ &= 0 \quad |x| > \bar{x}. \end{aligned} \tag{13}$$

Thus we have shown that the solution for flow over a finite obstacle with large meridional extent can be well approximated by that for flow over an infinite ridge away from the meridional edges of the obstacle. Hence solutions for flow over an infinite meridional ridge for various cases become relevant.

For an infinite ridge, the induced vorticity is independent of y. If the pressure and velocity perturbation are also assumed to be independent of y, the solution of (10) for the induced meridional component is

$$\begin{aligned} v &= 0 \qquad x < -\bar{x} \\ v &= -\frac{\delta}{\varepsilon}\int_{-\bar{x}}^{x} h(x')\,dx' \qquad -\bar{x} < x < \bar{x} \\ v &= -\frac{\delta}{\varepsilon}\int_{-\bar{x}}^{\bar{x}} h(x')\,dx \equiv \Delta h \qquad x > \bar{x}. \end{aligned} \tag{14}$$

Here the arbitrary constants have been chosen so that the induced velocity vanishes at sufficiently large distances upstream (as $x \to -\infty$) and is continuous at the edges $\pm\bar{x}$. The net effect of the ridge is a southward component on and downstream of the ridge whose magnitude increases with downstream distance on the ridge and remains constant and proportional to the integrated height change, Δh, downstream of the ridge.

In an investigation of a general model of rotating stratified flow over large-scale topographic features in which quasi-geostrophy was not assumed, JACOBS [24] has shown that the flow of a barotropic westerly current over an infinite meridional ridge also leads to a southward velocity downstream of the ridge, which becomes barotropic and persists far from the ridge, without any decay in magnitude, producing a permanent deflection in the streamlines.

In the case when the bottom friction is also important in the interaction between a westerly current and an infinite ridge, the result is again a southward component on and downstream of the ridge given by

$$v = 0 \qquad x < -\bar{x}$$

$$v = -\frac{\delta}{\sqrt{E}}[1 - \exp[-(\sqrt{E}/\varepsilon)(x + \bar{x})]] \qquad -\bar{x} < x < \bar{x}$$

$$v = -\frac{2\delta}{\sqrt{E}} \sinh\left(\frac{\bar{x}\sqrt{E}}{\varepsilon}\right) \exp[-(\sqrt{E}/\varepsilon)x] \qquad x > \bar{x}. \tag{15}$$

The topographically induced velocity decreases with distance downstream of the ridge over a horizontal scale of the order of $\varepsilon/\sqrt{E}$.

VAZIRI and BOYER's [22] investigation of a quasi-geostrophic model for the flow past axi-symmetric obstacles has shown that even when the depth of the Ekman layer is comparable to that of the obstacle, the flow over the obstacle has a southward component. Thus the production of a northerly velocity due to the clockwise turning of streamlines over the obstacle is a result which is valid over a wider range of parameters than the quasi-geostrophic inviscid model discussed in what follows.

(b) *Obstacles on a β-plane*

On the β-plane, any displacement in the meridional direction triggers Rossby waves. The solution for the effect of an axisymmetric obstacle on a β-plane has been obtained by MCCARTNEY [33, 34] for homogeneous as well as a two-layer model by imposing a radiation condition that there be no waves upstream of the obstacle, i.e., at large distances in the direction opposite to the group velocity of the Rossby waves. In the homogeneous case, the incoming westerly current acquires northerly component over the obstacle resulting in a meandering wake. The streamlines for a tall obstacle ($\delta/\varepsilon = 4$) when ε and β are comparable given by MCCARTNEY [34] are shown in Fig. 5(a). The two-layer model with westerly flow in the lower layer and easterly flow aloft, also has at least one wavy mode.

For the perturbation generated by an infinite meridional ridge of the form (13), the appropriate radiation condition implies that there would be no waves to the west of, i.e., upstream of the ridge. Using this, the solution of the induced meridional component is (GADGIL and SIKKA [4])

$$v = 0 \qquad x < -\bar{x}$$

$$v = -\frac{\delta}{\sqrt{\beta\varepsilon}} \sin\left(\sqrt{\frac{\beta}{\varepsilon}}(x + \bar{x})\right) \qquad -\bar{x} < x < \bar{x}$$

$$v = \frac{\delta}{\sqrt{\beta\varepsilon}}\left[\sin\left(\sqrt{\frac{\beta}{\varepsilon}}(x - \bar{x})\right) - \sin\left(\sqrt{\frac{\beta}{\varepsilon}}(x + \bar{x})\right)\right] \qquad x > \bar{x}$$

This solution is illustrated in Fig. 5b. It is seen that the topographically induced southward component gives rise to Rossby waves downstream of the ridge with a wavenumber $\sqrt{\beta/\varepsilon}$ and amplitude proportional to the topographical forcing δ. (If the

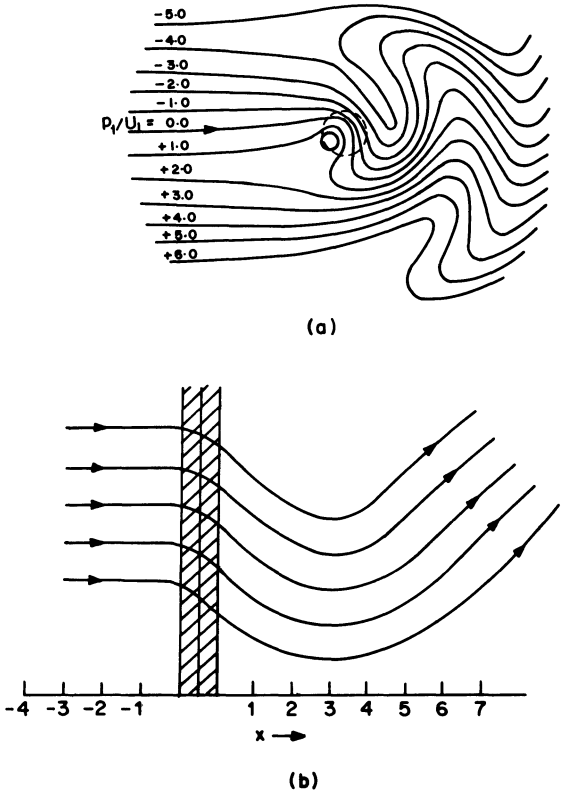

Figure 5
(a) McCartney's [34] solution for homogeneous flow past an axisymmetric obstacle. $\varepsilon = \beta = \delta/4$. (b) Streamlines for flow past an infinite meridional ridge from (16); $\delta = \varepsilon = 5\beta$.

zonal extent of the obstacle, $\bar{x}$, is smaller than the Rossby wavelength, the solution on the β-plane can be well approximated by the f-plane solution, over the obstacle, provided it satisfies the appropriate upstream conditions.)

5. *Effect of the topography of the Indian peninsula*

(*a*) *Topography, vorticity and rainfall*

Consider the variation of the rainfall on the peninsula in the direction of the low-level current from the Arabian sea, i.e., in the westerly direction. The copious rainfall upstream of the Western Ghats is clearly due to the ascent induced in the air in climbing over this range. Westward and within about 50 km of their peak, the Western

Ghats are very steep (with slopes $\sim 3 \times 10^{-2}$) implying a vertical velocity of about 30 cm sec^{-1} via the first term in the boundary condition (8). For these scales of horizontal variation and vertical velocity, it is necessary to consider the variation of the vorticity about the horizontal axes as well as the effects of stratification (LONG [35]). SARKAR [3] has applied a model incorporating these features to deduce the high rainfall on the west coast and its rapid decrease to the east of the Western Ghats. We shall consider the implications of the potential vorticity equation for the zonal variation of the vorticity on the region to the east of the narrow Western Ghats.

In this region, the topography is characterized by a longitudinal extent of about 500 km and a height of about 600 m above the sea level. This height decreases to the east and vanishes at a distance of about 100 km or more inland of the Bay of Bengal. The conservation of the potential vorticity implies that as the monsoon current descends from the highest levels of the plateau, the vorticity increases due to vortex stretching. Thus, relative to the vorticity at the maximum level of the plateau, the cyclonic vorticity should increase as the height of the underlying topography decreases. This variation of the vorticity in the inviscid model (which would correspond

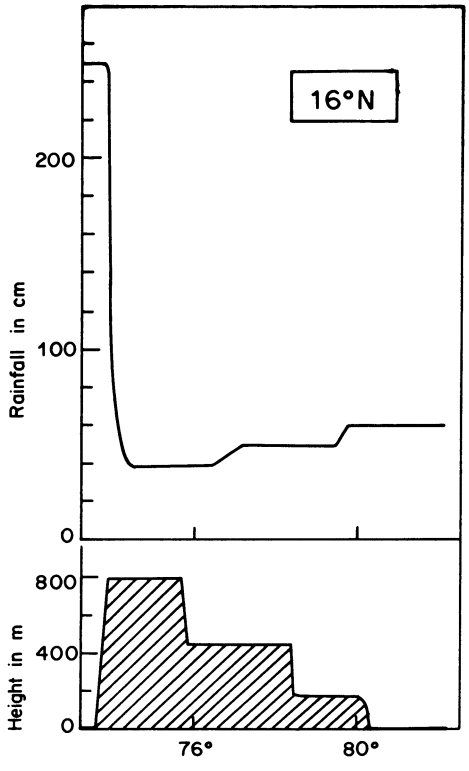

Figure 6
Zonal variation of June–September rainfall and underlying topography at 16°N.

to that of the vorticity above the frictional boundary layer in a viscous model) in turn implies a similar variation in the seasonal rainfall if CISK is valid. The observed zonal variation of the summer monsoon rainfall and the underlying topography at 16°N deduced from the positions of the rainfall contours for the June–September rainfall and the height contours is depicted as a histogram in Fig. 6. The height of the topography between two contours is assumed to be their arithmetic mean and is therefore taken to be discontinuous at the contours for illustration in this figure. Note that the rainfall does increase eastward as the height of the underlying topography decreases, as predicted. This suggests that the simple quasi-geostrophic model does incorporate some of the essential physics for determining the large-scale variation of the circulation and could be exploited for deducing some of the effects of the topographic features.

(*b*) *Effect on the low-level circulation*

The parameters for the interaction between the low-level monsoon and the peninsular topography are given in Table 1. It can be seen that ε, β, δ are smaller than unity and qualitative predictions from the quasi-geostrophic model can be tested. From Section 4, the predicted effects of the topographic complex on the peninsula are,

(i) a southward velocity on and downstream of the topography of magnitude δ/ε, i.e., 2 m sec^{-1} from Table 1.

(ii) a Rossby wave with wavelength $2\pi\sqrt{\varepsilon/\beta}$, i.e., 3900 km from Table 1.

Note that these results are valid in the region above the frictional boundary layer and are to be compared with observations above this layer.

Table 1

U_0	L	D	H*
10 m sec^{-1}	5×10^5 m	600 m	6000 m
f	β	ε	δ
4×10^{-5}	0.3	0.5	0.1

*) H refers to the depth of the lower troposphere.

The first prediction was tested by using pilot balloon observations for the mean monthly meridional wind at 900 mb for the monsoon months. It was found that the mean meridional wind is northerly for all the stations south of 17°N indicated in Fig. 2. (SIKKA, personal communication.) The northerly velocity is generally of the order of 2 m sec^{-1} throughout the monsoon season and is minimum in July when the velocity of the impinging westerly current and hence ε, is maximum. Thus the observed direction, magnitude as well as the variation of the meridional component with ε are consistent with the predictions. Since the pressure is the streamfunction

in the quasi-geostrophic model, a southward flow implies a southward bending of isobars. Since the southward bending of the isobars is observed at levels higher than the frictional layer, it can be considered as a manifestation of the orographic effect. Further, the deflection of the isobars is also minimum in July as expected.

The observed trough in the southern Bay and the ridge on Burma to its east are suggested as features of the Rossby wave generated downstream of the topography. The observed distance of the trough from the topography ($\sim$900 km), of the ridge from the trough ($\sim$900 km) are consistent with the solution (16) for the parameters of Table 1. McCARTNEY's [34] two-layer model predicts two modes of wavelength 4200 and 6300 km for the parameters of the summer monsoon (GADGIL and SIKKA [4]). We therefore conclude that the trough in the southern Bay of Bengal is a manifestation of a Rossby wave triggered by topographically induced southward velocity on the peninsula. Assuming this, we speculate in the next section about the dynamical effects of the other topographic barriers that the monsoon current encounters.

6. *Effect of the other topographic features*

Following the monsoon current beyond the southern Bay, we speculate about the effect of the other orographic features, and suggest a modern version of Simpson's theory.

The location of the mountain ranges on the Burmese coast with respect to the Rossby wave is such that the current impinging on them has a significant southerly component, i.e., a significant component parallel to this range. In general the proportion of the current that flows over the obstacle to that which avoids the obstacle by flowing parallel to it, depends upon the ratio of the inertia of the current (measured by the Rossby number, R_0, based on the component normal to the height contours) and the height and/or slope of the obstacle δ. In the limit of vanishing, R_0/δ, the current avoids the obstacle completely resulting in a Taylor column. Since the height of the Burmese Hills is more than that of the Western Ghats, and the velocity of the normal (westerly) component of the impinging current smaller (because of the southwesterly direction), the ratio R_0/δ is somewhat smaller than for the interaction of the current from the Arabian sea, with the peninsular topography. We, therefore, expect a larger portion of the current to avoid flowing over the range and flow in a southerly direction onto the northeastern region. Of this, a part crosses the Khasi hills in Assam, and a part flows eastward and parallel to the insurmountable Himalayas in the north. The vorticity of the meridional shear between the easterlies in the north and the westerlies in the south results in significant rainfall in this region through CISK. Thus the role of the mountain ranges in determining this rainfall is likely to be more subtle than that suggested by Simpson. Perhaps, the absence of easterlies over north India, in the model discussed by HAHN and MANABE [7], in which other factors such as latent and sensible heat sources are included, could be attributed to the omission of the

detailed effects of the orographic features of the type discussed here. We have considered here the role of mountains in the mean summer circulation. To understand orographic effects in various phases of the monsoon such as the break when the low-level winds are westerly in the entire region south of the Himalayan foothills, a more complex model which incorporates latent and sensible heat sources will have to be investigated.

Acknowledgements

It is a pleasure to acknowledge the fruitful collaboration in working on various aspects of the monsoon with D. R. Sikka and the many stimulating discussions with R. Narasimha.

References

[1] Simpson, G. C. (1921), *The southwest monsoon*, Quart. Jl. Roy. Met. Soc. *47*, 151–172.
[2] Banerjee, S. K. (1929), *The effect of Indian mountain ranges on the configuration of isobars*, Ind. J. Phys. *4*, 477–502.
[3] Sarkar, R. P. (1966), *A dynamical model of orographic rainfall*, Mon. Wea. Rev. *94*, 555–572.
[4] Gadgil, Sulochana and Sikka, D. R. (1976), *The influence of the topography of the Indian peninsula on the low level circulation of the summer monsoon*, Fluid Mechanics Report 76 FM 16, I.I.Sc., Bangalore, India.
[5] Murakami, T., Godbole, R. V. and Kelkar, R. R. (1970), *Numerical simulation of the monsoon along 80°E*, Proc. Conf. Summer Monsoon Southeast Asia.
[6] Godbole, R. V. (1973), *Numerical simulation of the Indian summer monsoon*, Ind. J. Met. Geophys. *24*, 1–14.
[7] Hahn, D. G. and Manabe, S. (1975), *The role of mountains in the South Asian monsoon circulation*, J. Atmos. Sci. *32*, 1515–1541.
[8] Normand, C. W. B. and Rao, K. N. (1946), *Distribution of wet bulb potential temperature in latitude and altitude*, Nature *158*, 128.
[9] Charney, J. G. and Eliassen, A. (1964), *On the growth of a hurricane depression*, J. Atmos. Sci. *21*, 68–75.
[10] Keshavamurthy, R. N. (1971), *On the maintenance of the mean Indian southwest monsoon circulation and the structure and energetics of monsoon disturbances*, Ph.D. thesis, University of Mysore, India.
[11] Sikka, D. R. and Gadgil, Sulochana, (1976), *Large-scale rainfall over India during the summer monsoon and its relation to the lower and upper tropospheric vorticity*, Fluid Mechanics Report 76 FM 19, I.I.Sc., Bangalore, India.
[12] Srinivasan, V. and Sadasivan, V. (1975), *Thermodynamic structure of the atmosphere over India during the southwest monsoon*, Ind. J. Met. Geophysics Hydro. *26*, 169–180.
[13] Ramamurthy, K., Jambunathan, R. and Sikka, D. R. (1976), *Moisture distribution and water vapour flux over the Arabian sea during active and weak spells of southwest monsoon*, Ind. J. Met. Geophysics and Hydro *27*, 127–139.
[14] Sikka, D. R. and Ananthakrishnan, R. (1974), *On the influence of synoptic scale system in controlling convective activity during the southwest monsoon*, Proc. Int. Trop. Met. Meeting, Am. Met. Soc. Nairobi, Jan–Feb 1974, 115–120.
[15] Taylor, G. I. (1923), *Experiments on the motion of solid bodies in rotating fluids*, Proc. Roy. Soc. *A 104*, 213–218.
[16] Hide, R. (1961), *Origin of Jupiter's red spot*, Nature *190*, 895–896.

[17] WARREN, B. A. (1963), *Topographical influences on the path of the Gulf stream*, Tellus *15*, 168–183.
[18] ROSSBY, C. G. (1945), *On the propagation of frequencies and energy in certain types of oceanic and atmospheric waves*, J. Met. *12*, 187–204.
[19] INGERSOLL, A. P. (1969), *Inertial Taylor columns and Jupiter's great red spot*, J. Atmos. Sci. *26*, 744–752.
[20] ROBINSON, A. R. and NIILER, P. P. (1967), *The theory of free inertial currents, I: Path and structure*, Tellus *19*, 269–291.
[21] ROBINSON, A. R. and GADGIL, SULOCHANA (1970), *Time-dependent topographic meandering*, Geophysical Fluid Dynamics *1*, 411–438.
[22] VAZIRI, A. and BOYER, D. L. (1971), *Rotating flow over shallow topographies*, J. Fluid Mech. *50*, 79–95.
[23] HOGG, N. G. (1973), *On the stratified Taylor column*, J. Fluid Mech. *58*, 517–537.
[24] JACOBS, S. J. (1964), *On stratified flow over bottom topography*, J. Mar. Res. *22*, 223–235.
[25] INDIA METEOROLOGICAL DEPARTMENT, *Rainfall Atlas of India* (1972).
[26] RAO, Y. P. and RAMAMURTHY, K. S. (1968), *Climate of India, Forecasting Manual*, India, Met. Dept., FMU, Rep. 1–2.
[27] ANANTHAKRISHNAN, R., SRINIVASAN, V. and RAMAKRISHNAN, A. R. (1968), *Monthly mean sea level isobaric charts, Forecasting Manual*, India Met. Dept., FMU Rep. I-1.
[28] INDIA METEOROLOGICAL DEPARTMENT, *Upper Air Atlas of India and neighbourhood* (1972).
[29] FLOHN, H. (1968), *Contributions to the meteorology of the Tibetan highlands*, Atmos. Sci. Paper No. 130, Colorado State Univ. 120 pp.
[30] SIKKA, D. R. and RAGHAVAN, K. (1976), *Comments on effects of Arabian sea-surface temperature anomaly on India summer monsoons, A numerical experiment with the GFDL model*, J. Atmos. Sci. *33*, 2252–2253.
[31] SADLER, J. C. and RAMAGE, C. S. (1976), *Comments on the role of mountains in the south Asian monsoon circulation*, J. Atmos. Sci. *33*, 2255–2258.
[32] GADGIL, SULOCHANA (1976), *On Inertial Taylor columns*, Fluid Mechanics Report 76 FM 18, I.I.Sc., Bangalore, India.
[33] MCCARTNEY, M. S. (1972), *Taylor columns and Rossby wakes generated by isolated topographic features on a β-plane*, Notes of the 1972 summer study program in Geophysical Fluid Dynamics at the Woods Hole Oceanographic Institution.
[34] MCCARTNEY, M. S. (1975), *Inertial Taylor columns on a beta plane*, J. Fluid Mech. *68*, 71–95.
[35] LONG, R. R. (1972), *Finite amplitude disturbances in the flow of inviscid rotating and stratified fluids over obstacles*, Ann. Rev. Fluid Mech. *4*, 69–93.

(Received 15th June 1977)

Pageoph, Vol. 115 (1977), Birkhäuser Verlag, Basel

The Simulation of the Asian Summer Monsoon by General Circulation Models

By A. GILCHRIST[1])

Summary – The monsoon simulations of four general circulation models are illustrated. Additional results from the Meteorological Office model showing factors that are important in determining its simulation are presented. The large-scale flow patterns of all the models reproduce the large-scale flow fairly realistically, but more detailed characteristics and, in particular, the rainfall, are poorly represented.

Key words: Monsoon, general circulation models.

Introduction

Global integrations for July which therefore include a simulation of the Asian summer monsoon, have been produced by a number of general circulation models. The results from an integration of the GFDL model through the year have been reported by MANABE *et al.* (1974), and the simulation of the Asian summer monsoon in it has been discussed by HAHN and MANABE (1975). Further discussion of these results is contained in correspondence between SADLER and RAMAGE (1976) and HAHN and MANABE (1976). The NCAR model simulation of the monsoon has been described by WASHINGTON and DAGGUPATY (1975). Results of the July global simulation of the Rand model are included in the paper by GATES and SCHLESINGER (1977), while those of the Meteorological Office model are described by GILCHRIST (1974, 1976).

The results of these four models have been considered in preparing this paper. It was not possible to include results from two other global models that have been integrated to provide July simulations; namely, the UCLA model (MINTZ *et al.*, 1972) and the GISS model (STONE *et al.*, 1977). An attempt is made here to compare the monsoon simulations of the four models, usually by relating the other simulations to that of the Meteorological Office model with which the author is most familiar. Some additional results from the latter, which are of relevance in understanding its simulation of the monsoon, are illustrated and discussed in the expectation that similar considerations may also be of importance in the other simulations.

[1]) Meteorological Office, London Road, Bracknell, Berkshire, England.

The models

In this section the main features of the models are very briefly summarized. The objective is to present them in a convenient form for comparison and no attempt has been made to make the descriptions complete or fully self-explanatory. For further details the reader must refer to the original articles cited.

In Table 1 characteristics of the grids and of aspects of the physical parameterizations of the models are listed.

Table 1
Characteristics of general circulation models whose results are illustrated

	GFDL	NCAR	RAND	Meteorological Office
Horizontal Grid	250 km irreg. quasi-constant on sphere.	$2\frac{1}{2}°$ lat.-long. 275 km at equator.	4° lat. 5° long. 440 550 km at equator.	330 km irreg. quasi-constant on sphere.
Vertical Grid	σ coord. 11 level at 0.99, 0.94, 0.83, 0.69, 0.50, 0.31, 0.19, 0.11, 0.07, 0.04, 0.01.	z coord. 6 level at 1.5, 4.5, 7.5, 10.5, 13.5, 16.5 km.	σ coord. 2 level at 0.8, 0.4.	σ coord. 5 level at 0.9, 0.7, 0.5, 0.3, 0.1.
Convection	Convective adjustment. MANABE *et al.* (1965)	Kuo-type depending on moisture convergence. KRISHNAMURTI and MOXIM (1971)	Heating dependent on lapse-rate. MINTZ (1968)	Partial mixing dependent on boundary layer height. CORBY *et al.* (1977)
Radiation	Annual/zonal mean climatological cloud. No diurnal variation. MANABE and WETHERALD (1967)	Two layers of interactive cloud. Diurnal variation. OLIGER *et al.* (1970)	Interactive; one layer plus deep/shallow convective cloud. No diurnal variation. GATES *et al.* (1971)	Parameterized. Cloud implicit. Simple diurnal variation.
Surface Exchanges	Log profile to lowest level, C_d assuming $z_0 = 1$ cm. HOLLOWAY and MANABE (1971)	Bulk transfer. Wind extrapolated to near-surface, $C_d = 0.003$. (C_d)water $= 0.7\ C_d$.	Bulk transfer. Wind extrapolation to surface, C_d dependent on wind (ocean) and topographic height (land).	Geostrophic drag coeff. Values for land/sea stable/unstable.
Surface Conditions	Climatological sea-surface temperatures (all models)			
	Albedo fixed. POSEY and CLAPP (1964)	Albedo $= 0.3 - 0.1 \times \frac{\text{Soil Moisture}}{\text{Field Capacity}}$.	Albedo = 0.14 land 0.07 sea.	Land Albedo – zonal mean value.
	Interactive ground hydrology. Surface Temp. – Radiation balance.	Interactive ground hydrology. Surface Temp. – Radiation balance.	Interactive ground hydrology. Surface Temp. – Radiation balance.	(R.H.) sea = 80% (R.H.) land = 50% Surface Temp. – Prognostic with heat capacity 12.5 J cm^{-2} K^{-1}.

The form of the physical parameterizations have a large effect on the models' simulations in the tropics. For example, the transient energy distribution in July in the GFDL model shown by MANABE *et al.* (1974) and the standard deviations of wind in the Meteorological Office model shown by GILCHRIST (1976) can be compared and they indicate that the energy in the transient systems is much greater in the former model. This is believed to be due primarily to the different methods of parameterizing the effects of subgrid-scale convection. A moist convective adjustment removes vertical instabilities instantaneously, exciting wind and temperature variations at neighbouring grid-points. The partial mixing approach allows stabilization and the process of mass and wind field adjustment to occur more gradually. Nevertheless the models appear to agree in many aspects of their time-average tropical simulations, and both find maximum values of transient kinetic energy in the upper troposphere associated with areas of marked convective activity. It may also be noted that the tropical simulations of the Meteorological Office model with the original convection parameterization described by CORBY *et al.* (1972) and with the scheme developed later, show rather large differences. The former gave rise to areas of excessive convective activity, which after some time could be associated with features in the surface pressure field.

Two of the models use cloud parameterizations and allow the model-generated clouds to affect the radiation calculations, while the other two determine the effects of cloud from the observed climatology. The latter method constrains certain estimates within the model to approximately realistic values, but it may lead to unrealistic features which an interactive scheme could remove; for example see next section.

The surface albedo is also an important factor in tropical simulations since it to a large extent determines the temperatures of land surfaces, the contrast between these and the sea-surface temperature being a primary cause of the monsoon circulation. Further, it has a strong influence on the amount of heat available for exchange with the atmosphere in latent or sensible form. The models use a variety of specifications of the albedo. The NCAR model for example has values dependent on the soil moisture content, and the GDFL model uses values specified from climatology. The other two models do not attempt a variation with longitude. All of the models assume sea-surface temperatures that are fixed in time, the values almost certainly differing somewhat from one to another. Where the lower atmosphere is stable and subsiding, small differences in sea-surface temperatures, with consequent minor changes in land/sea contrasts are unlikely to have any major impact on the simulations. Where the atmosphere is close to vertical instability differences of sea-surface temperature may be more significant; it has been noted however that the Meteorological Office model is not sensitive (except in the sense of local rainfall amount) to changes in sea-surface temperatures in the Bay of Bengal ($\sim$1–2°C), even though they are high relative to those in other parts of the Indian Ocean.

It may be noted that there is a difference in the approach to the inclusion of a diurnal variation. This is included in the NCAR model. In the Meteorological Office

model where the interaction of the boundary layer and the free atmosphere is controlled by the height of the boundary layer carried as an explicit variable, it seemed important to allow a diurnal variation, and this was done in a particularly simple way – by assuming the time of day everywhere the same and making the solar energy input through the hours of daylight vary sinusoidally ($0 - \pi$).

The simulations

The Asian monsoon exists by virtue of the differential heating (sensible and latent) experienced by the atmosphere over the oceans and over the land. MURAKAMI *et al.* (1970) have shown that significant features of the circulation along 80°E can be reproduced by a simple model in which the vertical circulation is driven in effect by differing temperatures at the earth's surface. Figure 1(b) illustrates the importance of differential heating in the Meteorological Office general circulation model. It shows the sensible heat input into the lowest layer, the combined effect of sensible heating at the surface and the net radiational cooling. A small contribution due to the exchange of infrared radiation with the surface and also the effect of condensation within the layer have been ignored because they could not be readily estimated from the available data. It will be noted that there is cooling over the oceans and for the most part, heating over the land. While the quantity shown is not entirely independent of the motion, it is evident that the land/sea distinction is largely imposed, since the sea-surface temperature is fixed and the temperature attained by the land is governed by the assumptions about radiation, which imply surface albedos and cloud amounts dependent on latitude only. The direct effect of the heat input is to tend to cause descent over the oceans and ascent over the land. This vertical motion reinforces the tendency for the land to provide a positive and the oceans a negative heat input.

Over land, the heat input shows a strong dependence on the air motion. There are maxima on the mountain upslopes (see Figs. 1(a) and 3(d)), notably over the eastern and southern slopes of the Himalayas and on the western Ghats of India. They arise partly because there is more heat available at the surface since the solar radiation passes through a lesser depth of air, but more because a larger proportion of the available heat enters the atmosphere as sensible rather than as latent heat. This implies that the humidity of the low level air is relatively high due to ascent and possibly also because of evaporation from rain. The extent to which this dependence of heating on surface elevation is realistic is not clear; certainly the heating associated with the Himalayas seems excessive. The model does not take account of the effect of rising motion and humidity on cloudiness and the surface relative humidity is fixed at 50 percent; further, the surface albedo may be too low since there is no allowance for permanent snow at these latitudes. To represent the variation of physical effects in the vicinity of mountains well clearly requires more elaborate parameterization schemes than the model uses at present.

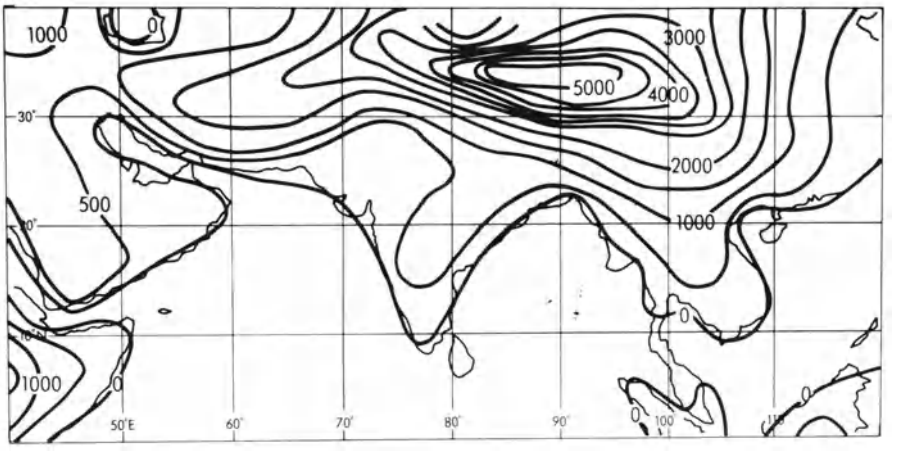

(a)

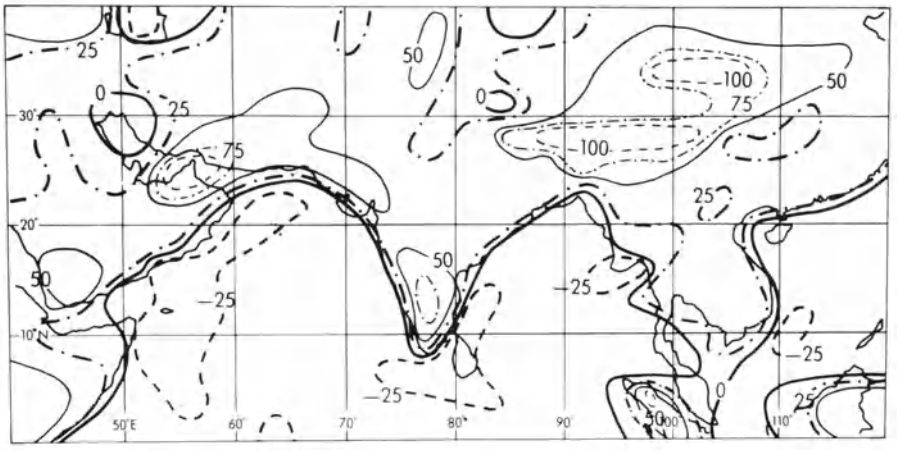

(b)

Figure 1

(a) The horizontal distribution of height of the earth's surface above mean sea-level used for the monsoon area in integrations of the Meteorological Office general circulation model. (Units gpm). (b) Sensible heating of the lowest layer of the Meteorological Office model for a 30-day mean state derived from days 71–100 of a July integration (GILCHRIST 1976). The layer is between $0.8p_*$ and p_* where p_* is the pressure at the surface of the earth. (Units Wm^{-2}).

Over parts of the Persian Gulf, there is a very large sensible (and latent) heating of the atmosphere, the effect of the motion being particularly evident since there is transfer of heat from the atmosphere to the sea in the northern part of the Gulf where the vertical motion is downwards. The difference in sea surface temperature between the areas of rising and descending motion is less than 2°K.

The mean sea-level pressure distribution in the model, though not a direct response to the surface heating, is strongly influenced by it. The surface pressure field

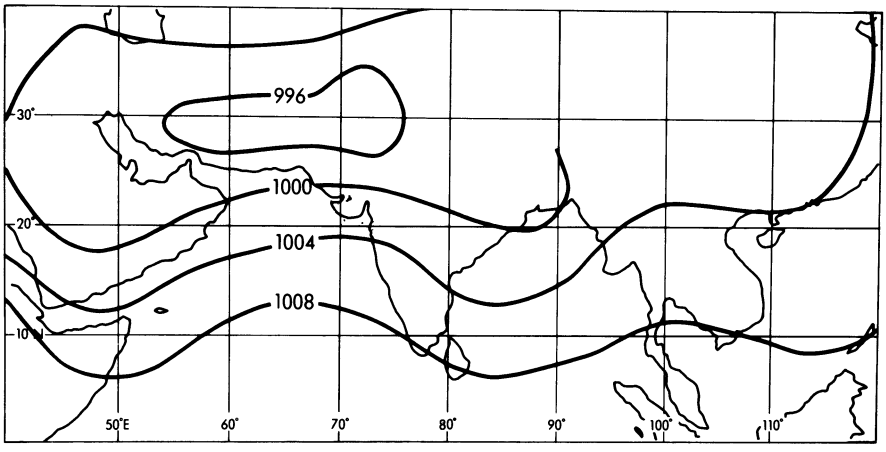
996
1000
1004
1008
30°
20°
10°N
50°E
60°
70°
80°
90°
100°
110°

(a)

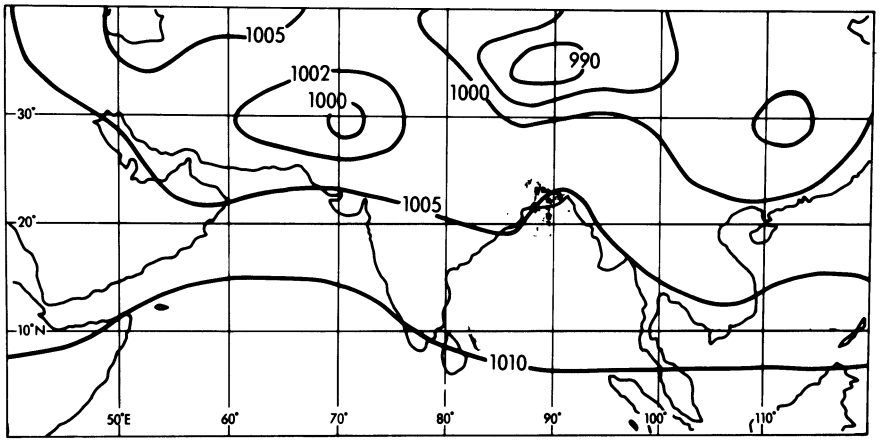
1005
1002
1000
990
1000
1005
1010
30°
20°
10°N
50°E
60°
70°
80°
90°
100°
110°

(b)

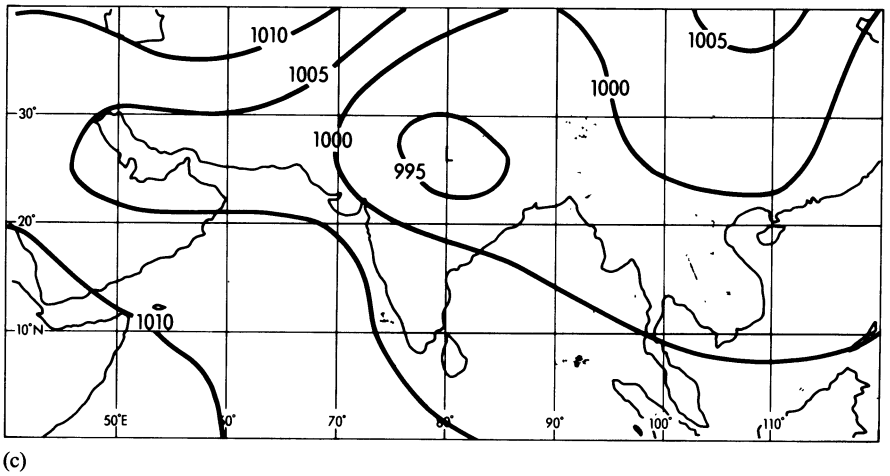
1010
1005
1000
1005
1000
995
1010
30°
20°
10°N
50°E
70°
90°
100°
110°

(c)

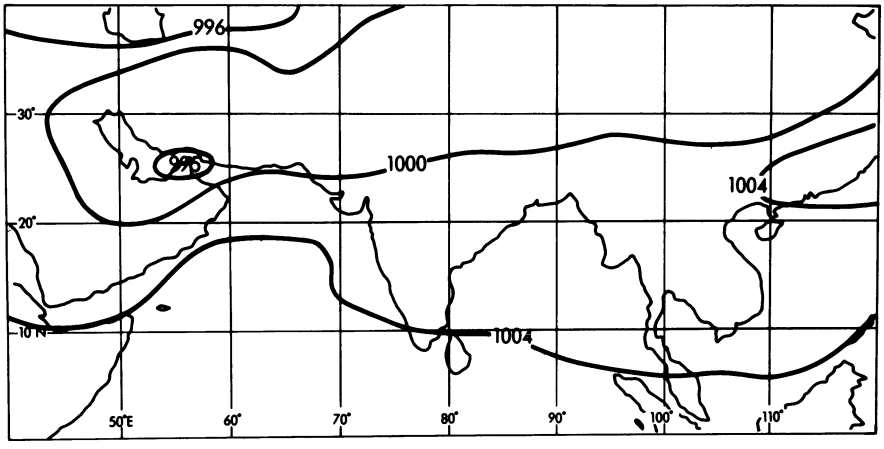

(d)

Figure 2

Mean sea-level pressure distribution over the monsoon area. (Units mb).

(a) Observed climatological values for July.

(b) The July simulation from an annual integration of the GFDL general circulation model (HAHN and MANABE, 1975).

(c) Average values for the last 31 days of a July integration of the RAND model (GATES and SCHLESINGER, 1977).

(d) Average values for the Meteorological Office model; details as Fig. 1(b).

in the Meteorological Office model (see Fig. 2(d)) has a trough at about the latitude of maximum heating. The general level of pressure is low (partly because the total mass of air in the model is somewhat deficient) and south of the trough, the pressure gradient is weaker than in the July climatology (Fig. 2(a)). It is also relatively weak in comparison with other models (Fig. 2(b), (c)). The overall pressure pattern with a trough over Arabia, a ridge over the Arabian Sea and a further downstream trough is reproduced, though the detail over India and the Bay of Bengal is not realistic. A notable error is the extension of the monsoon trough northeastwards into China, possibly due to the excessive heating on the Himalayan upslopes to which attention has already been drawn. The pressure fields in the GFDL and RAND models (Fig. 2(b) and (c)) also show a trough at about the same latitude, though there are variations in the position of the lowest pressure, and none of the models illustrated reproduces the shape of the monsoon trough well. Over the Himalayas it is not possible to make meaningful comparisons because of the different methods of reducing pressure to sea-level values.

Air emerging at low levels from the divergent pressure systems south of the equator is accelerated northwards by the pressure gradient between the southern hemisphere highs and the monsoon trough over the entire length of the Indian Ocean. As it flows northward in the northern hemisphere, it turns eastward under the influence of the Coriolis effect. The winds in Figs. 3(c) and (d) should be comparable with the gradient level climatological fields of ATKINSON and SADLER (Fig. 3(a)). The

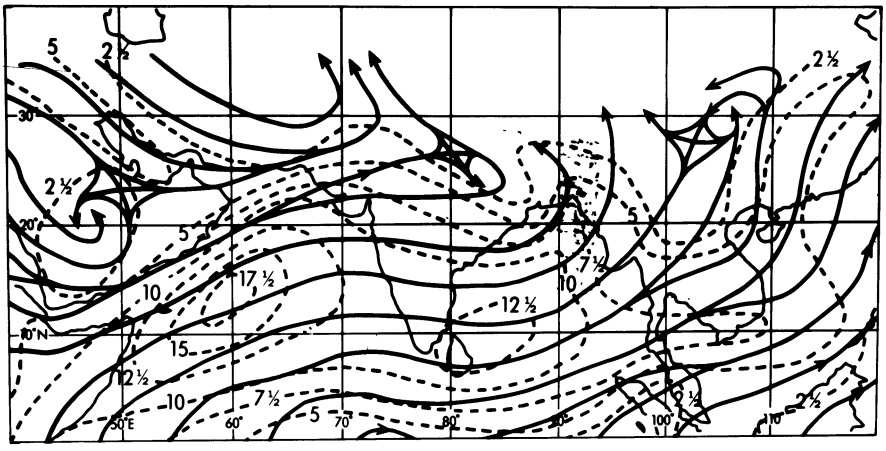
5
2½
30°
2½
20°
5
17½
10
10°N
15
12½
10
50°E
60°
7½
5
70°
80°
12½
7½
10
2½
100°
2½

(a)

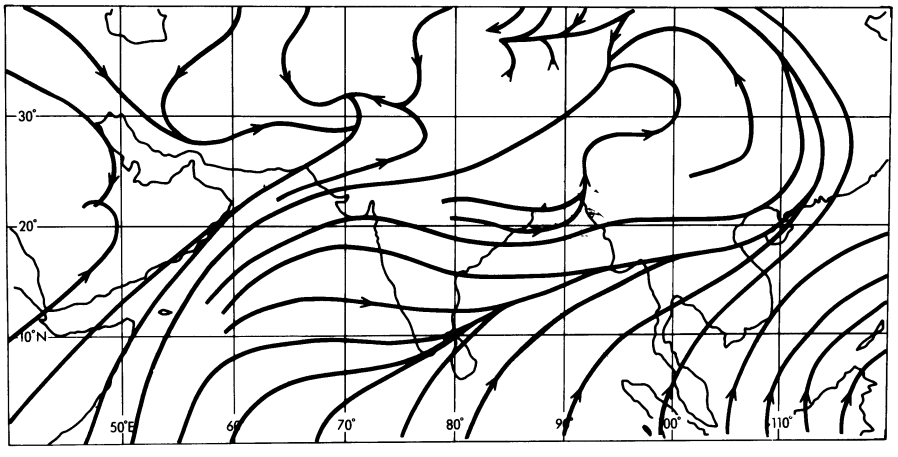
30°
20°
10°N
50°E
60°
70°
80°
90°
100°
110°

(b)

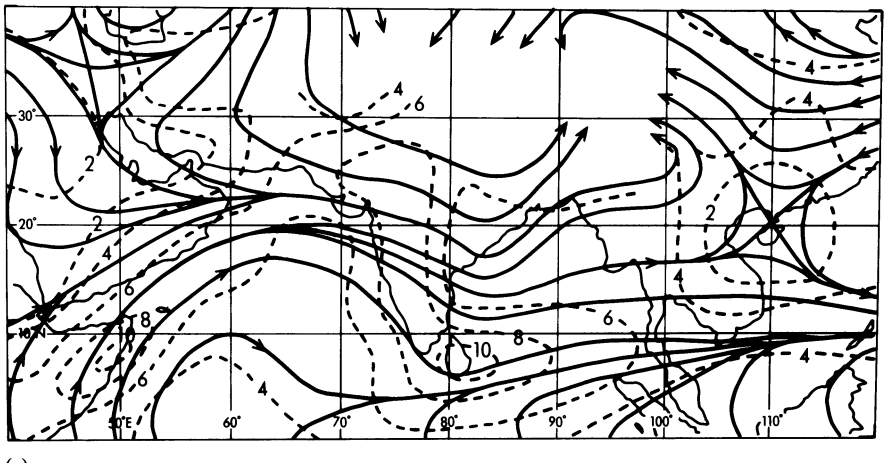
4
6
30°
2
0
2
20°
2
4
6
8
10°N
6
4
50°E
60°
70°
80°
8
10
90°
100°
110°
2
4
6
4
4
4

(c)

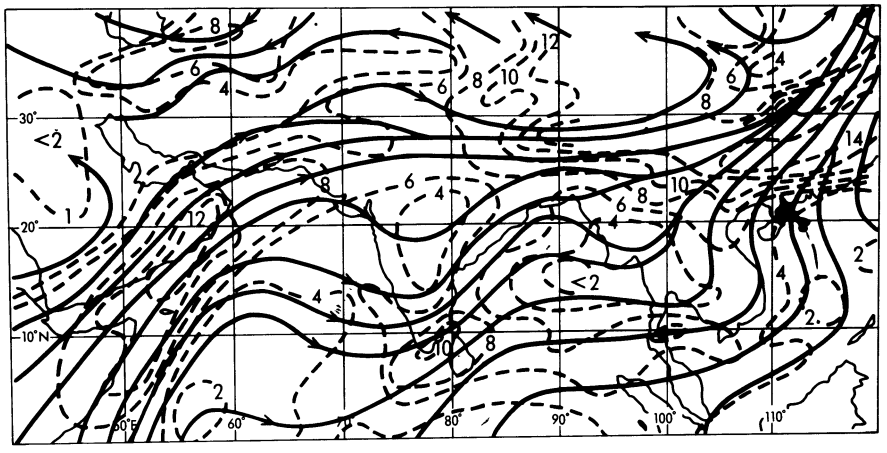

(d)

Figure 3

Low-level wind distribution (stream lines and isotachs) over the monsoon area. (Isotach units ms^{-1}).

(a) Observed climatological gradient level winds (ATKINSON and SADLER, 1970).

(b) Near-surface ($\sigma = p/p_* = 0.99$, p_* = surface pressure) winds from the GFDL model; details as in Fig. 2(b). Isotachs omitted. Stream lines estimated from published streak-diagrams.

(c) Average winds at 1.5 km from days 91–120 of a July integration of the NCAR model (WASHINGTON and DAGGUPATY, 1975).

(d) Average winds at the lowest level ($\sigma = 0.9$) for the Meteorological Office model; details as Fig. 1(b).

GFDL winds (Fig. 3(b)) are for a lower level and should therefore be generally backed with respect to the gradient level winds and less strong; only the stream lines are shown. A strong flow off the coast of Africa and Arabia is a feature of all the simulations, though the direction is nearer to southerly, and its position closer to the coast, than observed. Downstream, the ridge over the Arabian Sea tends to be too pronounced and the simulated flows near the Indian coast are veered with respect to the relevant climatological normals. Over the Bay of Bengal there is again a systematic bias in the simulations towards a too anticyclonic flow. None of them obtain a strong enough flow onto the south-facing slopes of the Himalayas (crucial presumably for reproducing rainfall in this area realistically), and this mirrors their failure to simulate the shape of the monsoon trough in this region adequately. The possibility that this is because they do not create monsoon depressions realistically has been discussed by HAHN and MANABE (1975).

The model simulations of flow in the upper troposphere (Fig. 4(b), (c), (d)) may be compared with the observed climatology at 200 mb (Fig. 4(a)). The effects of vertical truncation can be expected to be fairly severe for all the models, and it would probably be preferable to compare mass fluxes between specified depths of the atmosphere than winds at a particular level, but the former are not readily available. For the Meteorological Office model, which has no level near 200 mb the effect of vertical truncation is evident in the substantial wind changes between the upper two levels $\sigma = 0.3$ and $\sigma = 0.1$. At the lower level there is flow (5–10 ms^{-1}) a little north

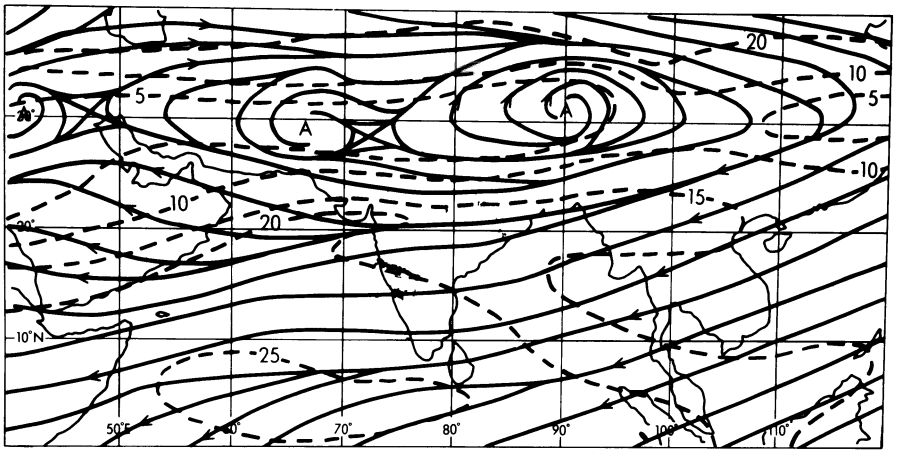
20
10
5
5
A
A
10
10
20
15
10°N
25
50°E
60
70
80
90
100
110

(a)

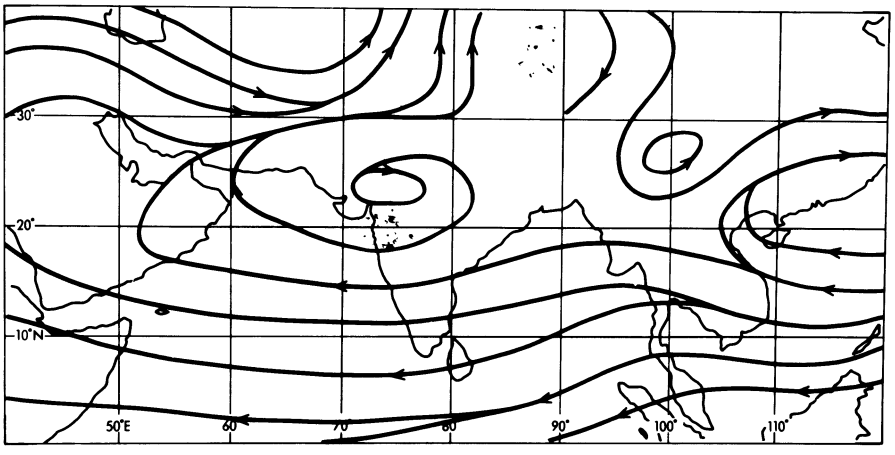
30°
20°
10°N
50°E
60
70
80
90
100
110

(b)

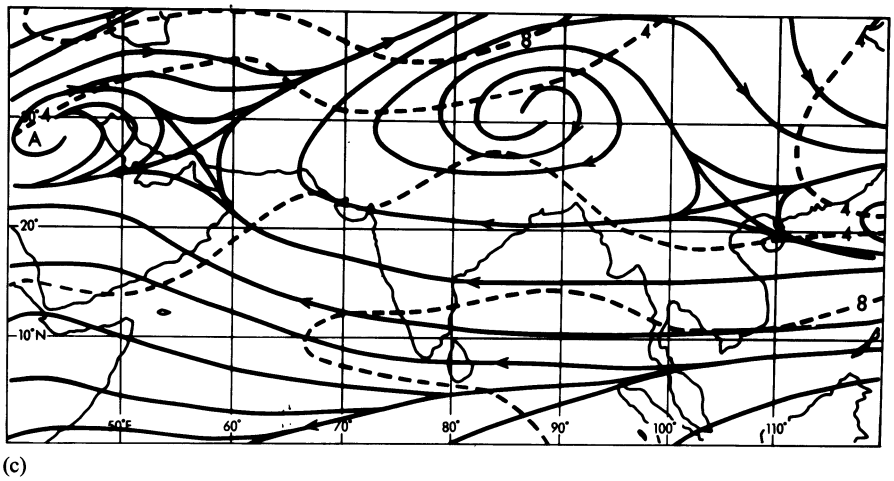
8
A
20°
8
10°N
50°E
60
70
80
90
100
110

(c)

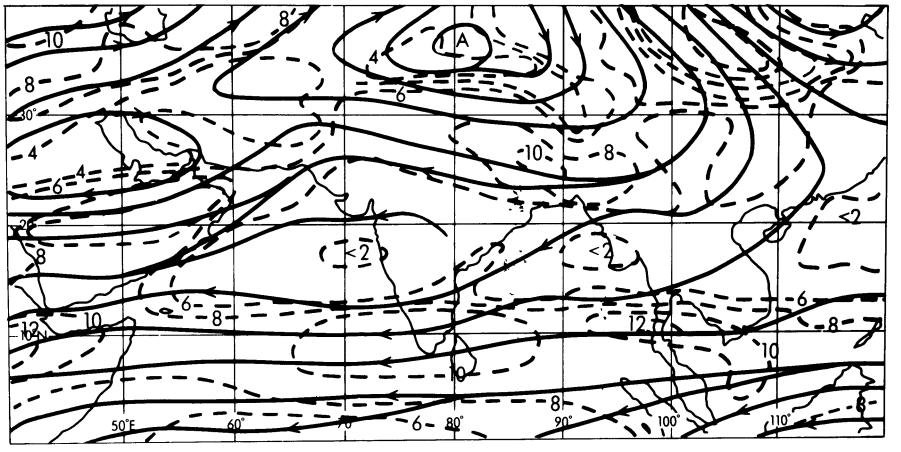

(d)

Figure 4

High tropospheric wind distributions (stream lines and isotachs) over the monsoon area. (Isotach units ms^{-1}).

(a) Observed climatological 200 mb winds (RAMAGE and RAMAN, 1972).

(b) Winds at 190 mb from the GFDL models; details as in Fig. 2(b). Stream lines are estimated from published streak diagrams.

(c) Winds at 13.5 km from the NCAR model; details as in Fig. 3(c).

(d) Winds from the Meteorological Office model. They are the average of the $\sigma = 0.1$ and the $\sigma = 0.3$ values to give an estimate at approximately the same level as the observed winds; details as in Fig. 1(b).

of east over southern India and Ceylon, a region of light winds (interpretable as a weak anticyclonic centre) immediately to the north, and a strong anticyclonic centre at about 37°N, 90°E with southeasterly winds over northern India. At the upper level, there are easterlies between the equator and approximately 35°N with maximum speeds 15–20 ms^{-1} over southern India, around an anticyclonic region, less well-defined than at the lower level, between 35 and 40°N. The winds shown in Fig. 4(d) are the average of the values at the two upper levels; in view of the uncertainty concerning the best way to interpret them, no attempt was made to interpolate consistently to 200 mb. Had this been done, the main effect would have been to move the anticyclonic centre in Fig. 4(d) a little to the south, since the $\sigma = 0.5$ winds over the highest parts of the Himalayas are from a westerly point.

All of the models illustrated obtain an extensive easterly stream covering the greater part of India, but its strength is weak and its direction lacks the consistently northerly component of the observed flow. The GFDL model's anticyclonic centre is too far south; however, HAHN and MANABE (1976) show that this feature is more realistic in the GFDL August simulation and, allowing for the lag in developments in the integration following the annual cycle, the latter may be the more appropriate comparison with the other simulations. The strength of the easterly flow in this model (not shown in the diagrams) appears from the mean vectors of HAHN and MANABE (1975, 1976) closer to reality than in the other two.

We now consider the rainfall simulations. No attempt has been made to illustrate

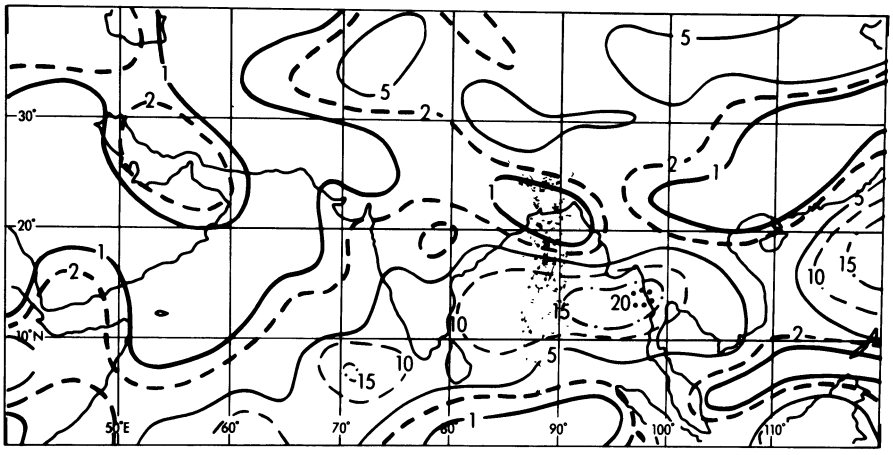
30°
20°
10°N
50°E
60°
70°
80°
90°
100°
110°
1
2
5
10
15
20

(a)

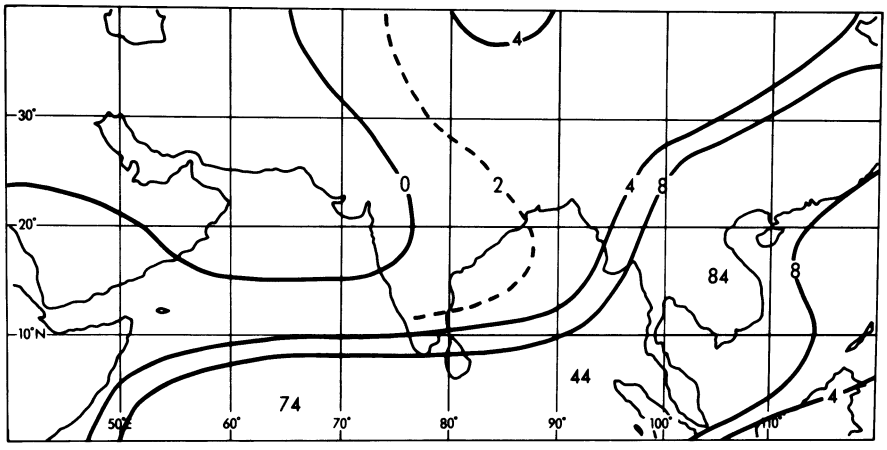
30°
20°
10°N
50°E
60°
70°
80°
90°
100°
110°
0
2
4
8
84
74
44

(b)

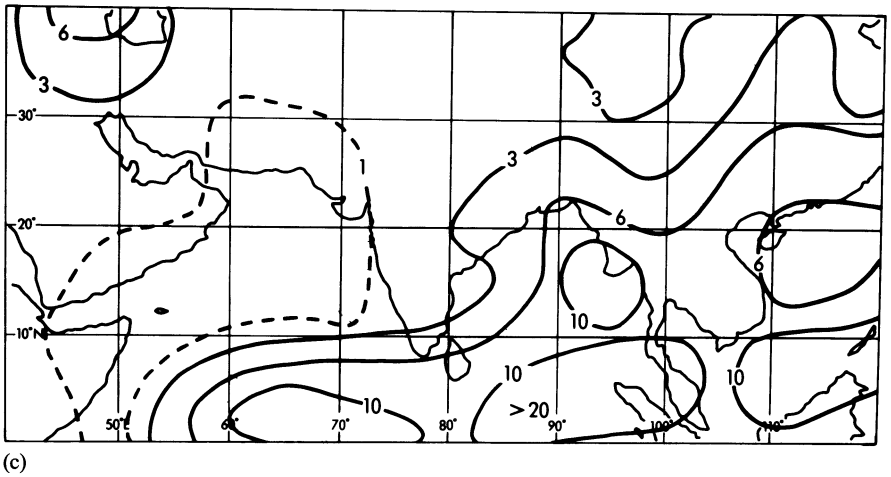
30°
20°
10°N
50°E
60°
70°
80°
90°
100°
110°
1
3
6
10
>20

(c)

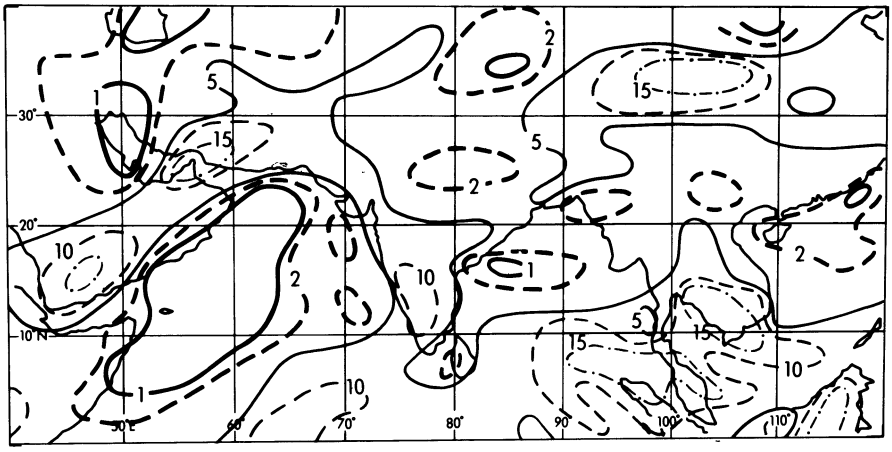

(d)

Figure 5

Mean July rainfall distributions over the monsoon area (units mm day^{-1}).

(a) From the GFDL model; details as in Fig. 2(b).
(b) From the RAND model; details as in Fig. 2(c).
(c) From the NCAR model; details as in Fig. 3(c).
(d) From the Meteorological Office model; details as in Fig. 1(b).

the actual rainfall distribution for July. There are dependable estimates for India (e.g., see RAO, 1976) and surrounding land areas, but values over the oceans are not known with confidence. In any case the model simulations at this stage are comparatively crude and close comparison with climatological values is hardly justified. The main features of the distribution with which it should be possible to make meaningful comparisons are (i) high values on the slopes of the western Ghats and low values east of this over the Plateau and eastern India, (ii) a secondary maximum over parts of northern central India and the Ganges valley and (iii) maxima associated with the southern slopes of the Himalayas north of the Bay of Bengal and with the western slopes of the Burmese mountains.

For the Meteorological Office model (Fig. 5(d)), the rainfall maxima over land correlate fairly closely with the heat input into the lowest layer (Fig. 1(b)). Thus there are maxima over the Indian peninsula, simulating in some measure the heavy rain over the western Ghats, and over the eastern Himalayas where the air at low levels is tending to rise over the mountains and where as already noted there is excessive low level sensible heating. The Himalayan maximum is considerably to the north of that observed. There are minima over the Ganges valley and over the Burmese coast, which are at variance with observation. There is also a spurious maximum over Arabia and the desert region of Pakistan. This model has no ground hydrology to reduce the availability of moisture when evaporation exceeds rainfall, and this is probably partly responsible for this notable shortcoming. WASHINGTON and DAGGUPATY (1975) have noted that the introduction of an interactive ground hydrology in the

NCAR model improved the rainfall simulation in desert regions. The grid point representation also tends to increase the extent of the Red Sea and the Persian Gulf thus allowing a greater amount of evaporation from very warm seas than is realistic.

Over the oceans there are large areas of little rainfall, particularly in the cold current off Arabia. However, there is also an extensive rainfall maximum in equatorial regions between 60 and 85°E and then running northeastwards to Malaya and southeast Asia. Over the latter land areas, rainfall amounts are high, reaching about 20 mm per day at two locations. This belt of rain does not appear to be associated with a maximum of sea temperature. There is in general an increase eastwards across the Indian Ocean but the gradient is small and there is no close association of high sea temperatures with rainfall. Over the Bay of Bengal, points with the same temperature are near the high and low extremes of rainfall amounts. This belt of rain appears to be associated directly with low-level convergence in the air stream originating in the southern hemisphere. As the stream turns eastwards under the influence of the Coriolis force, there must be confluence, and this is accompanied by convergence.

In the GFDL, RAND and NCAR simulations (Fig. 5(a), (b), (c)) a greater proportion of the rain occurs over the oceans. Also, to a greater extent than for the Meteorological Office model, the rain occurs in a continuous belt, centred near the equator at 60–70°E but broader and mainly further north in the longitude of southeast Asia. As previously noted this rainbelt appears to be a dynamical consequence of the low level wind field response to imposed large-scale differential land/sea heating rather than a direct response to local forcing at the surface. Since the observed rainfall distribution is dominated by maxima and minima that are clearly related to tropographical features, it is clear that the simulations generally lack realism.

Figure 1(b) showed the diabatic heating of the lowest layer of the Meteorological Office model, omitting the latent heating due to condensation, and it is fairly evident that some aspects of the model's simulation of surface pressure, low-level winds and rainfall can be related to features in it. It seems reasonable to question whether a more valid 'forcing' for the monsoon is not the total diabatic heating through the atmospheric column, including the release of latent heat in rain. For comparison with Fig. 1(b), Fig. 6 shows this quantity. There are areas of negative heating for which the time-mean temperature structure must be maintained by convergence of heat, probably with subsidence and a relatively high lapse-rate through the atmosphere. Conversely areas of positive heating are generally associated with low level convergence, upper level divergence and a lapse-rate closer to the moist adiabatic. Overall, there is net heating over the area, and heat is exported to other regions. In Fig. 1(b) there is a fairly clear distinction between the northern land where the air is being heated, and the oceans to the south where the air is being cooled, a pattern that favours the direct circulation primarily responsible for creating the monsoon. The pattern of total diabatic heating in Fig. 6 is notably different, with, on the whole, two maxima, one just north of the equator, the other at about 35°N, and a minimum mainly over the Arabian Sea and the Bay of Bengal, between. The relation of this

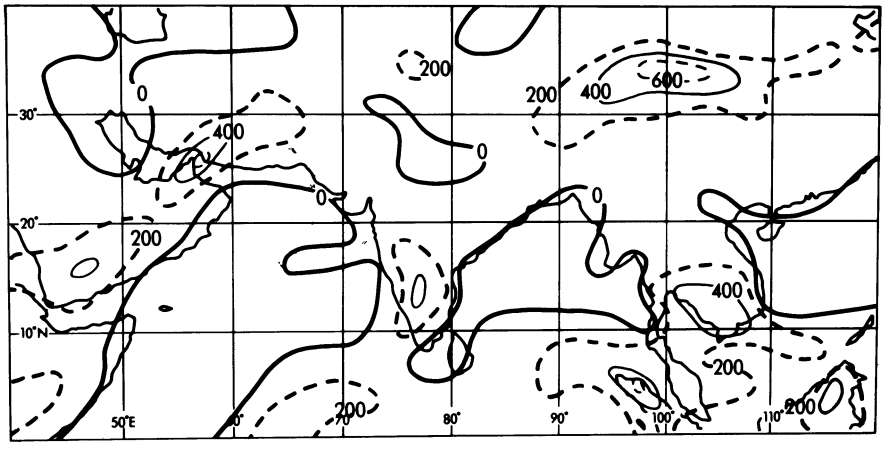

Figure 6
Integrated diabatic heating of the atmosphere in the Meteorological Office model; details as in Fig. 1(b).

pattern to the overall gross features of the atmospheric monsoon simulation is less clear than in the low-level heating of Fig. 1(b).

An illustration of the effect of changing the topography

In order to investigate the sensitivity of the monsoon simulation to the effects of topography, the Meteorological Office model was run with topography deliberately set high enough to represent the 'blocking' height of mountains rather than, as originally, the average height over a grid square. The results are presented briefly here since they help to illustrate significant features.

The topography used for the experiment is shown in Fig. 7(a). The model's finite difference representation was able to handle this new topography unaltered without giving rise to numerical instabilities. The low-level wind field and rainfall for a thirty-day period of integration are shown in Figs. 7(b) and 7(c). The low-level wind flow in the vicinity of the Himalayas is markedly different from the original integration, and elsewhere though the changes are less, they are significant. Thus, it is apparent that the airflow has adjusted so that more of the flow goes round the heightened mountains in India and in Burma. One of the objectives was to see whether the mountains would increase the tendency of air over the Bay of Bengal to curve northwards so that it would impinge on the southern Himalayan slopes. It is however not evident that this effect was produced.

The changes in the topography did tend to improve the simulation of the rainfall. There are for example significant increases in the rain over the upslopes to the Indian plateau and the Burmese mountains, which are accompanied by reductions

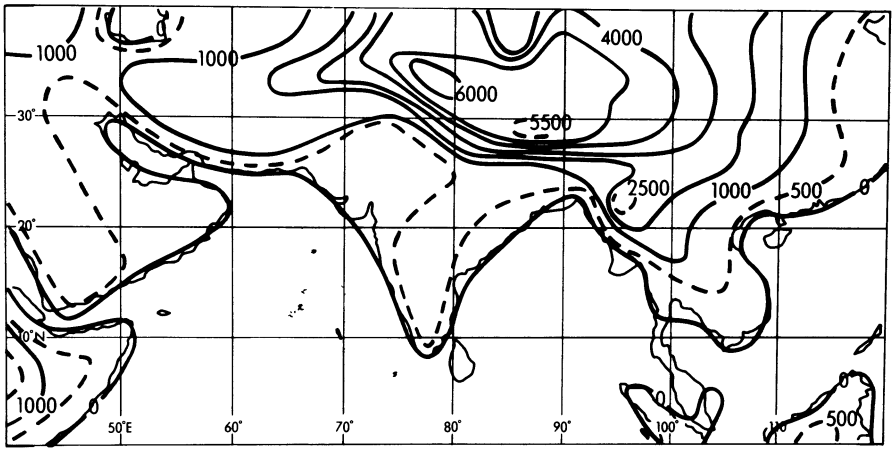

(a)

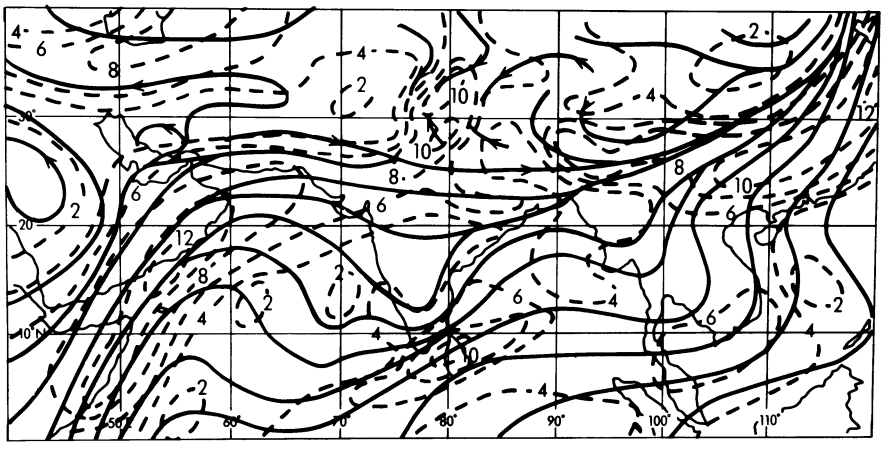

(b)

over the eastern half of the Arabian Sea and the Bay of Bengal. There is also an increase in rain over central India at about $22\frac{1}{2}$°N and immediately to the north of the Bay of Bengal where totals are 6–8 mm per day. Significantly also the excessive rainfall over the eastern slopes of the Himalayas have been eliminated and the only region of heavy rain at these latitudes is near 30°N 75–80°E and is associated with strong convergence and upslope motion.

Conclusions

Some features of the south west Asian monsoon simulations of several general circulation models have been illustrated. In general the models obtain the gross

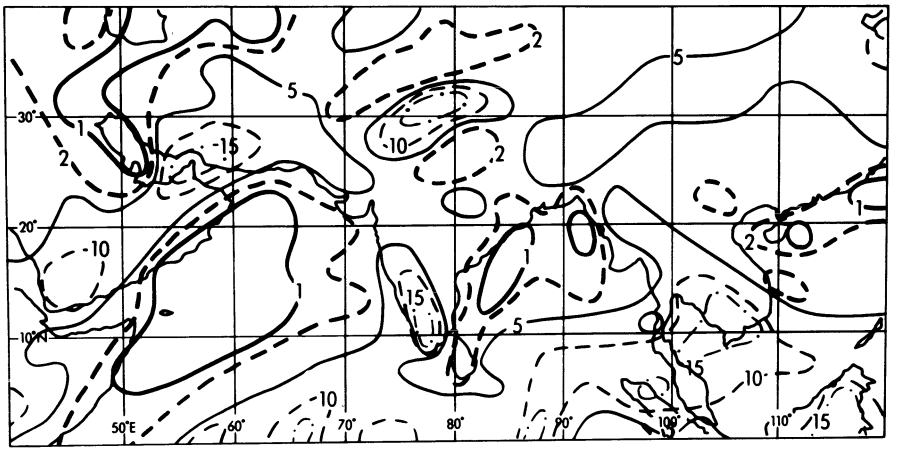

(c)

Figure 7

Results from an additional integration of the Meteorological Office model, started from day 50 of the original integration. Values shown are averages over days 71–100 of the experiment.

(a) The horizontal distribution of height of the earth's surface above mean sea-level for the monsoon area used in the integration (unit gpm).

(b) The low-level wind flow at $\sigma = 0.9$. Stream lines and isotachs unit ms^{-1}).

(c) The rainfall distribution (unit mm day^{-1}).

features of the air flow with reasonable fidelity, but on other more detailed characteristics, particularly the rainfall distributions, the simulations leave a great deal to be desired. An attempt has been made to consider the sensitivity of the simulations to particular features of the parameterizations. Many of the shortcomings seem to be most evident near mountains. This may be due to their direct dynamical influence; however, less is known about the details of the atmospheric heat balance over mountains and errors in its representation may be as, or even more, important.

Note

Details of simulations from models other than the Meteorological Office model have been copied manually from published material. Any inaccuracies that may have arisen because of this are regretted.

References

Atkinson, G. D. and Sadler, J. C. (1970), *Mean cloudiness and gradient-level wind charts over the tropics*, U.S. Air Weather Service, Technical Report No. 215.

Corby, G. A., Gilchrist, A. and Newson, R. L. (1972), *A general circulation model of the atmosphere suitable for long period integrations*, Quart. J. Roy. Met. Soc. *98*, 809–833.

Corby, G. A., Gilchrist, A. and Rowntree, P. R., *The U.K. Meteorological Office 5-level general circulation model, Methods in Computational Physics, Vol. 17* (Academic Press Inc., New York 1977), pp. 67–110.

GATES, W. L., BATTEN, E. S., KAHLE, A. B. and NELSON, A. B. (1971), *A documentation of the Mintz-Arakawa two-level atmospheric general circulation model*, R-877-ARPA, The RAND Corporation, Santa Monica, pp. 408.

GATES, W. L. and SCHLESINGER, M. E. (1977), *Numerical simulation of the January and July global climate with a two-level general circulation model*, J. Atmos. Sci., In press.

GILCHRIST, A. (1974), *A general circulation model of the atmosphere incorporating an explicit boundary layer top*, Tech. Note II/29, Meteorological Office, Bracknell.

GILCHRIST, A. (1976), *Tropical results from a July integration of a general circulation model incorporating an explicit boundary layer top*, Tech. Note II/46, Meteorological Office, Bracknell.

HAHN, D. G. and MANABE, S. (1975), *The role of mountains in the South Asian monsoon circulation*, J. Atmos. Sci. *32*, 1515–1541.

HAHN, D. G. and MANABE, S. (1976), *Reply to* SADLER and RAMAGE (1976), J. Atmos. Sci. *33*, 2258–2262.

HOLLOWAY, J. L. Jr. and MANABE, S. (1971), *Simulation of climate by a global general circulation model*, Mon. Wea. Rev. *99*, 335–370.

KRISHNAMURTI, T. N. and MOXIM, W. J. (1971), *On parameterization of convective and non-convective latent heat release*, J. Appl. Met. *10*, 3–13.

MANABE, S., SMAGORINSKY, J. and STRICKLER, R. F. (1965), *Simulated climatology of a general circulation model with a hydrologic cycle*, Mon. Wea. Rev. *93*, 769–798.

MANABE, S. and WETHERALD, R. T. (1967), *Thermal equilibrium of the atmosphere with a given distribution of relative humidity*, J. Atmos. Sci. *24*, 241–259.

MANABE, S., HAHN, D. G. and HOLLOWAY, J. L. Jr. (1974), *The seasonal variation of the tropical circulation as simulated by a global model of the atmosphere*, J. Atmos. Sci. *31*, 43–83.

MINTZ, Y., *Very long-term Global Integration of the Primitive Equations of Atmospheric Motion: An experiment in climatic simulation*, *Met. Monographs*, *Vol. 8*, *No. 30*, (A.M.S. Boston 1968), pp. 20–36.

MINTZ, Y., KATAYAMA, A. and ARAKAWA, A. (1972), *Numerical simulation of the seasonally and inter-annually varying tropospheric circulation*, Climatic Impact Assessment Program, Proc. of Survey Conference, Feb. 1972, (ed. A. E. Barrington), U.S. Dept. of Transportation, pp. 194–216.

MURAKAMI, T., GODBOLE, R. V. and KELKAR, R. R. (1970), *Numerical simulation of the monsoon along 80°E*, Proceedings of the Conference on the Summer Monsoon of South-east Asia (ed. C. S. Ramage), Navy Weather Research Facility, Norfolk, Va., pp. 39–51.

OLIGER, J. E., WELLCK, R. E., KASAHARA, A. and WASHINGTON, W. M. (1970), *Description of the NCAR global circulation model*, NCAR Tech. Note No. 56, Boulder, Colo., pp. 94.

POSEY, J. W. and CLAPP, P. F. (1964), *Global distribution of Normal Surface Albedo*, Geofiscia International *4*, 33–48.

RAMAGE, C. and RAMAN, C. V. R. (1972), *Meteorological Atlas of the International Indian Ocean Expedition*, *Vol. 2*, National Science Foundation, Washington, D.C.

RAO, Y. P. (1976), *Indian Southwest Monsoon*, Met. Monograph Synop. Met. No. 1/1976, India Met. Dept., Poona, pp. viii + 367.

SADLER, J. C. and RAMAGE, C. S. (1976), *Comments on 'The role of mountains in the South Asian Monsoon Circulation'*, J. Atmos. Sci. *33*, 2255–2258.

STONE, P. H., CHOW, S. and QUIRK, W. J. (1977), *The July climate and a comparison of January and July climates simulated by the GISS general circulation model*, Mon. Wea. Rev. *105*, 170–194.

WASHINGTON, W. M. and DAGGUPATY, S. M. (1975), *Numerical simulation with the NCAR global circulation model of the mean conditions during the Asian–African summer monsoon*, Mon. Wea. Rev. *103*, 105–114.

(Received 15th June 1977)

Pageoph, Vol. 115 (1977), Birkhäuser Verlag, Basel

Barotropic-Baroclinic Instability of Mean Zonal Wind During Summer Monsoon

By J. SHUKLA[1])

Abstract – Barotropic-Baroclinic instability of horizontally and vertically shearing mean monsoon flow during July is investigated numerically by using a 10-layer quasi-geostrophic model. The most unstable mode has a wavelength of about 3000 km and westward phase speed of about 15 m sec^{-1}. The most dominant energy conversion is from zonal kinetic energy to eddy kinetic energy. The structure of the most unstable mode is such that the maximum amplitude is concentrated at about 150 mb and the amplitude at the lowest layers is negligibly small. Barotropic instability of the zonal flow at 150 mb seems to be the primary excitation mechanism for the most unstable mode which is also similar to the observed westward propagating waves in the upper troposphere during the monsoon season. The results further suggest that Barotropic-Baroclinic instability of the mean monsoon flow cannot explain the occurrence of monsoon depressions which have their maximum amplitude at the lower levels and are rarely detected at 200 mb.

Key words: Monsoon; Mean zonal wind; Barotropic-baroclinic instability.

1. Introduction

It is observed that during the northern summer an extensive low-pressure area persists between north Africa and east China, and its central area lies over west Pakistan, where the lowest mean surface pressure observed anywhere on the globe exists during June–September. The southeasterly trade winds of the southern hemisphere, which cross the equator under the influence of this thermal forcing due to asymmetric continentality, and turn into southwesterly currents, are referred to as the southwest monsoon. Although the monsoonal flow pattern over the Indian region persists for about four months, June through September, the mean conditions during July are considered to represent the most typical structure of the mean monsoon circulation. The vertical structure of the mean circulation is characterized by lower tropospheric westerlies and upper tropospheric easterlies, the transition occurs at about 500 mb. The mean circulation is also characterized by appreciable horizontal shear.

The purpose of this paper is to carry out the barotropic-baroclinic instability analysis of the horizontally and vertically shearing mean monsoon flow during July

[1]) Massachusetts Institute of Technology, Cambridge, Mass. 02139, USA.

along 85°E. The purpose of such linear stability analyses is to see if the dynamical structure of the observed mean flow is such that it permits growth of infinitesimal linear perturbations, and if it does, the flow is considered to be 'unstable'. If the necessary and sufficient conditions for instability are satisfied, it may provide an explanation for the occurrence of disturbances which are observed during the monsoon season. The plausibility of such explanation would, of course, depend upon the agreements between the most unstable mode and the observed disturbances, with respect to the wavelength, phase speed, structure and energetics.

Figure 1 shows the cross-section of mean monthly zonal wind speed for the month of July along 85°E from 20°S to 40°N. One of the noteworthy features of this cross-section is the presence of easterly winds between the two westerly maxima. Such a structure of the zonal flow is favorable for satisfying the necessary conditions for the internal jet instability (CHARNEY and STERN, 1962). KRISHNAMURTI *et al.* (1975) have shown that for the synoptic situation studied by them, the necessary condition for the joint barotropic-baroclinic instability was satisfied. However, the instability analysis of the horizontally and vertically shearing monsoon flow has not been carried out before. This paper gives the results of the instability analysis of the zonal flow along 85°E.

One of the necessary conditions for the joint barotropic-baroclinic instability is that the gradient of potential vorticity on an isentropic surface should vanish in the region. Figure 2 shows the cross section of potential vorticity along 85°E. It is seen that the necessary condition for instability is satisfied. Figure 3 shows similar

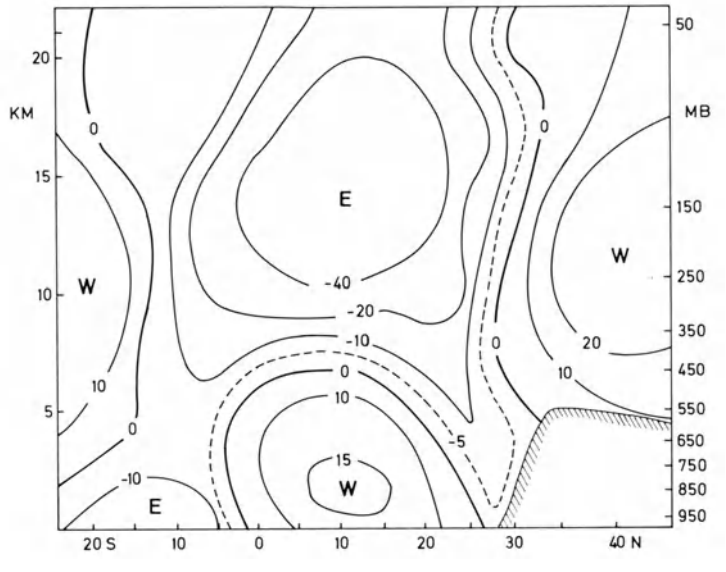

Figure 1
Cross-section along 85E for the observed mean July values of zonal wind (knots).

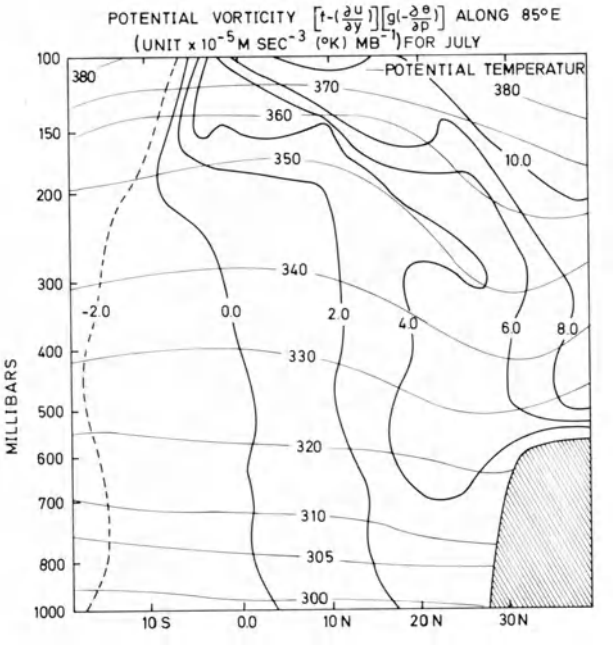

Figure 2
Cross-section of potential vorticity (10^{-5} ms^{-3} mb^{-1} (°K)) along 85E.

cross-sections along 73°E and 100°E. The necessary condition is satisfied in these cross sections also. Homogeneity of the potential vorticity field for a longitudinal span of about 30° (longitude) justifies a linear perturbation analysis in which large scale flow is assumed to be homogeneous along x (and perturbations are sinusoidal along x).

2. *The mathematical model*

The combined barotropic-baroclinic instability of mean monsoon zonal flow, $\overline{U}(y, p)$ is examined using a ten-layer quasi-geostrophic model. Because $\overline{U}$ is a function of y and p, the problem becomes non-separable, and this is a manifestation of the fact that there are two sources of energy (available kinetic energy and available potential energy).

Therefore, the initial value approach to instability analysis is used in which the linearized perturbation equations for a given wavelength are numerically integrated in time for an arbitrary initial condition. The integration is continued until the phase speeds and the growth rates converge to their constant values over the whole computational domain. These are the values of phase speed and growth rate for the most unstable mode. Integrations are performed for a range of wavelengths. The linearized

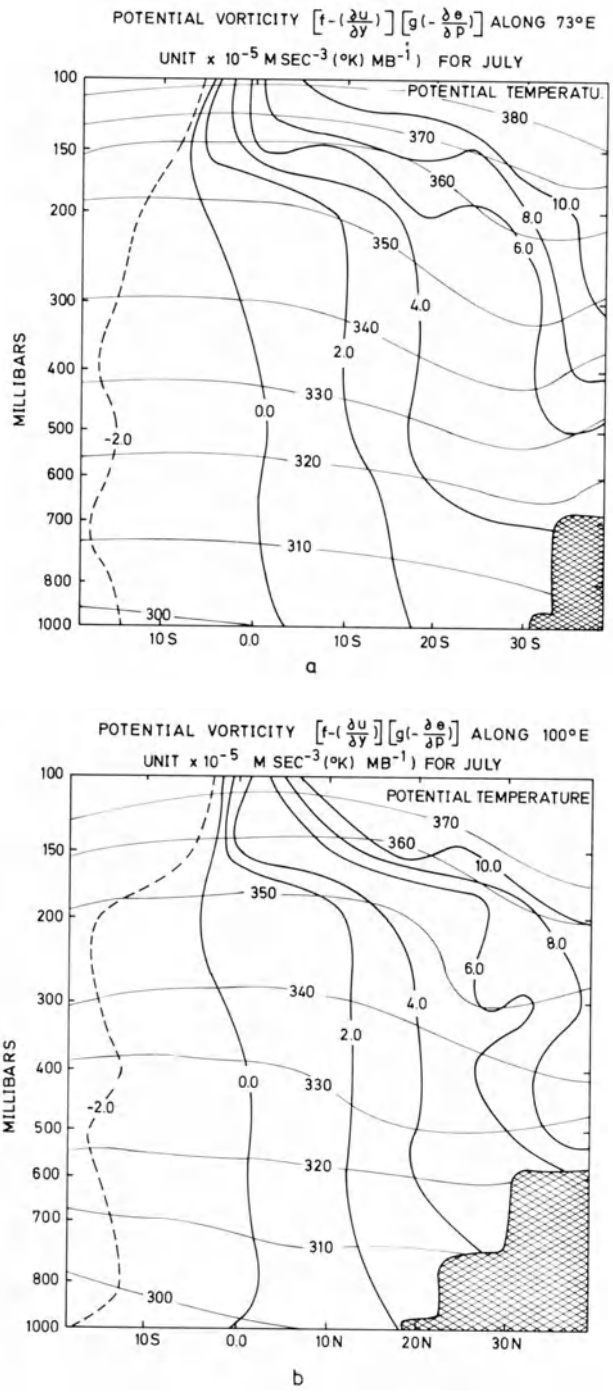

Figure 3
Cross-section of potential vorticity (10^{-5}ms^{-3} mb^{-1} (K°)) along (a) 73E, (b) 100E.

form of the vorticity and thermal equation may be written as:

$$\left(\frac{\partial}{\partial t} + \bar{U}\frac{\partial}{\partial x}\right)\nabla^2\psi' + \left(\beta - \frac{\partial^2\bar{U}}{\partial y^2}\right)\frac{\partial\psi'}{\partial x} - f_0\frac{\partial\omega'}{\partial p} = 0 \tag{2.1}$$

$$\left(\frac{\partial}{\partial t} + \bar{U}\frac{\partial}{\partial x}\right)\frac{\partial\psi'}{\partial p} - \frac{\partial\bar{U}}{\partial p}\frac{\partial\psi'}{\partial x} + \frac{\sigma\omega'}{f_0} = 0 \tag{2.2}$$

where ψ' and ω' are the perturbation stream function and vertical velocity (dp'/dt), respectively. σ is the stability parameter, which is a function of p only, and is given as:

$$\sigma(\bar{p}) = -\frac{R\bar{T}}{p\bar{\theta}}\frac{\partial\bar{\theta}}{\partial p} \tag{2.3}$$

where the bar ($\bar{}$) denotes the mean over an isobaric surface. f_0 is the constant value of the coriolis parameter and $\beta = \partial f/\partial y$. Assuming geostrophic balance between the mass field and the motion fields, we may derive the omega equation for ω' from (2.1) and (2.2), viz:

$$f_0\frac{\partial^2\omega'}{\partial p^2} + \frac{\sigma}{f_0}\nabla^2\omega' = \frac{\partial}{\partial p}\left\{(\bar{U}\nabla^2 + \beta - U_{yy})\frac{\partial\psi'}{\partial x}\right\} - \nabla^2\left\{\bar{U}\frac{\partial}{\partial p}\left(\frac{\partial\psi'}{\partial x}\right) - \frac{\partial\bar{U}}{\partial p}\frac{\partial\psi'}{\partial x}\right\}. \tag{2.4}$$

The first and second terms on the right-hand side of (2.4) are respectively the differential vorticity advection and the Laplacian of thickness advection. (A diagnostic ω equation yields that value of vertical velocity that is needed to maintain geostrophic and hydrostatic balance.)

The perturbation ψ' is taken to be of the form

$$\psi'(x, y, p, t) = \mathrm{Re}\{\Psi(y, p, t)\, e^{ikx}\}$$

where Ψ is complex. k is the wavenumber along x.

$$\Psi = \Psi_r + i\Psi_i$$

$$\Psi = \{F_r(y, p) + iF_i(y, p)\}\, e^{(\nu - ikc)t}.$$

Then,

$$\Psi_r = \{F_r\cos(kct) + F_i\sin(kct)\, e^{\nu t}$$

and

$$\Psi_i = \{F_i\cos(kct) - F_r\sin(kct)\}\, e^{\nu t}.$$

Solving for ν and c, we obtain the growth rate

$$\nu = \frac{\Psi_r(\partial\Psi_r/\partial t) + \Psi_i(\partial\Psi_i/\partial t)}{\Psi_r^2 + \Psi_i^2} \tag{2.5}$$

and the phase speed

$$c = \frac{\Psi_i(\partial\Psi_r/\partial t) - \Psi_r(\partial\Psi_i/\partial t)}{k(\Psi_r^2 + \Psi_i^2)}. \tag{2.6}$$

We may also write

$$w' = \mathrm{Re}\,\{W e^{ikx}\}$$

where

$$W = W_r + iW_i.$$

We may decompose (2.1) and (2.3) for the real and imaginary parts of the complex amplitudes Ψ and W.

Since

$$\nabla^2 = \left(-k^2 + \frac{\partial^2}{\partial y^2}\right)$$

we have

$$\frac{\partial}{\partial t}\left(-k^2 + \frac{\partial^2}{\partial y^2}\right)\Psi_r = \bar{U}k\left(-k^2 + \frac{\partial^2}{\partial y^2}\right)\Psi_i + (\beta - \bar{U}_{yy})k\Psi_i + f_0\frac{\partial W_r}{\partial p} \tag{2.7}$$

$$\frac{\partial}{\partial t}\left(-k^2 + \frac{\partial^2}{\partial y^2}\right)\Psi_i = -\bar{U}k\left(-k^2 + \frac{\partial^2}{\partial y^2}\right)\Psi_r - (\beta - \bar{U}_{yy})k\Psi_r + f_0\frac{\partial W_i}{\partial p} \tag{2.8}$$

$$\frac{\sigma}{f_0}\left(-k^2 + \frac{\partial^2}{\partial y^2}\right)W_r + f_0\frac{\partial^2 W_r}{\partial p^2} = \left[k\left(-k^2 + \frac{\partial^2}{\partial y^2}\right)\left\{\bar{U}\frac{\partial\Psi_i}{\partial p} - \Psi_i\frac{\partial\bar{U}}{\partial p}\right\}\right.$$
$$\left. -k\frac{\partial}{\partial p}\left\{\bar{U}\left(-k^2 + \frac{\partial^2}{\partial y^2}\right) + \beta - \bar{U}_{yy}\right\}\Psi_i\right] \tag{2.9}$$

$$\frac{\sigma}{f_0}\left(-k^2 + \frac{\partial^2}{\partial y^2}\right)W_i + f_0\frac{\partial^2 W_i}{\partial p^2} = \left[-k\left(-k^2 + \frac{\partial^2}{\partial y^2}\right)\left\{\bar{U}\frac{\partial\Psi_r}{\partial p} - \Psi_r\frac{\partial\bar{U}}{\partial p}\right\}\right.$$
$$\left. +k\frac{\partial}{\partial p}\left\{\bar{U}\left(-k^2 + \frac{\partial^2}{\partial y^2}\right) + \beta - \bar{U}_{yy}\right\}\Psi_r\right]. \tag{2.10}$$

3. Numerical integration of the 10-layer quasi-geostrophic model

A finite difference representation of (2.7) through (2.10) for the model shown schematically in Fig. 4, was integrated using centered differences in space and time. A forward difference in time was used for the first time step and also at every 50th time step, to suppress the separation of the solutions at even and odd numbered time steps. The upper and lower boundary conditions were $\omega' = 0$ at $p = 0$ and $p =$

1000 mb. The lateral boundary conditions were $v' = 0$, i.e., $\psi' = 0$ at the lateral boundaries.

Integrations were performed for two geometrical configurations (Fig. 4). In the first case (domain I), a vertical wall was placed at 28.75N. In the second case (domain II), steeply-sloping Himalayan topography was simulated by a vertical wall extending

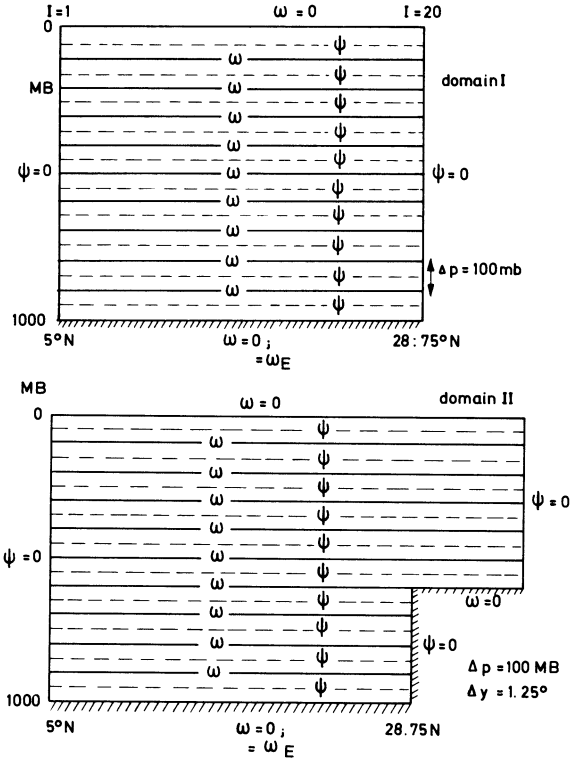

Figure 4
Schematic representation of the ten-layer model for domain I and domain II.

up to 600 mb; the Tibetan plateau extended polewards to 40N, which is the northernmost limit of the domain of integration in the model. A horizontal grid length (Δy) of 138.89 km (1.25 degrees of latitude) and a vertical grid length (Δp) of 100 mb, were used for numerical integrations. The time increments (Δt) used depended upon the wave number $k(=2\pi/L$, where L is the wavelength); the actual values of Δt were given by

$$\Delta t = (k\overline{U}_{\max})^{-1} \quad \text{with} \quad \overline{U}_{\max} = 40 \text{ m/s}.$$

The tendency terms $\partial\Psi_r/\partial t$ and $\partial\Psi_i/\partial t$, were found from (2.7) and (2.8) by use of a one-dimensional relaxation technique. The Liebman relaxation technique with overrelaxation coefficient of 0.3 was used to solve (2.9) and (2.10) at each time step. At the end of every 50 time steps, the phase speed c and growth rate ν were calculated

from (2.5) and (2.6). If they had converged to constant values, the integration was terminated. All the integrations began with a constant value of Ψ specified over the whole domain.

It may be pointed out that KLEIN (1974) used $\Delta y = 300$ km for similar numerical calculations and found that for a middle latitude winter profile of $\bar{U}(y, p)$, the most unstable wavelength was 4000 km. In order to assess the effect of the horizontal grid resolution (Δy), three experiments with $\Delta y = 69.45$ km, 138.9 km and 277.8 km were carried out. For the given $\bar{U}(y, p)$, the wavelength of maximum growth rate remained nearly the same for the cases $\Delta y = 69.45$ km and $\Delta y = 138.9$ km, but for the case $\Delta y = 277.8$ km, the wavelength of maximum growth rate increased by nearly 1000 km. These integrations indicated that coarse resolution may introduce a numerical viscosity which may change the shape of the growth rate curve.

4. Structure of the most unstable mode

Figure 5 shows the growth rate and phase speed versus wavelength curves obtained for domains I and II. In both these cases, the wavelength of the most rapidly growing

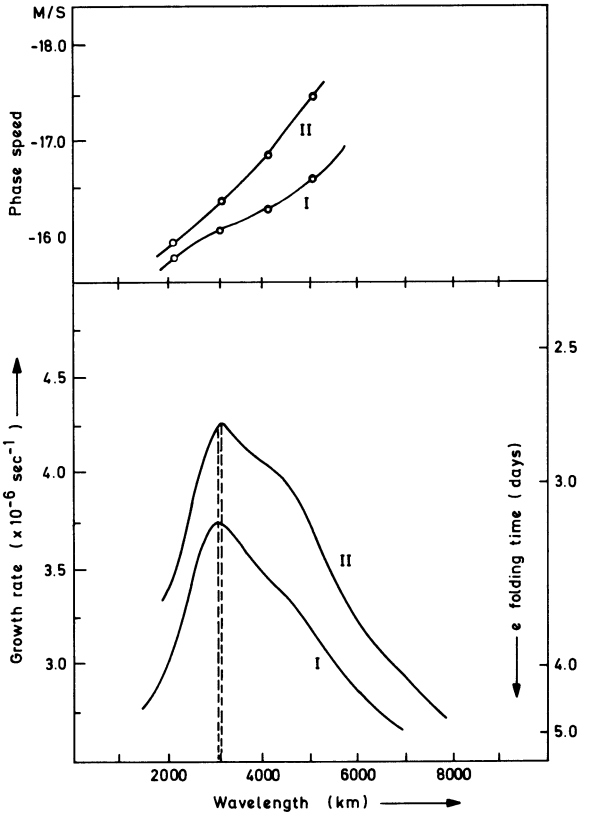

Figure 5
Growth rate and phase speed versus wavelength for domain I and domain II.

perturbation is 3000 km. The e-folding times for cases I and II were 3.2 days and 2.6 days, respectively. This difference in the growth rates is due to the differences in available kinetic energy density. These, in turn, are due to the relative locations of the subtropical westerly jet and the tropical easterly jet at 150 mb. Figure 6 shows the structures of the amplitude and phase of Ψ for both cases. The amplitudes are found to be concentrated at 150 mb and fall off very rapidly at the lower layers.

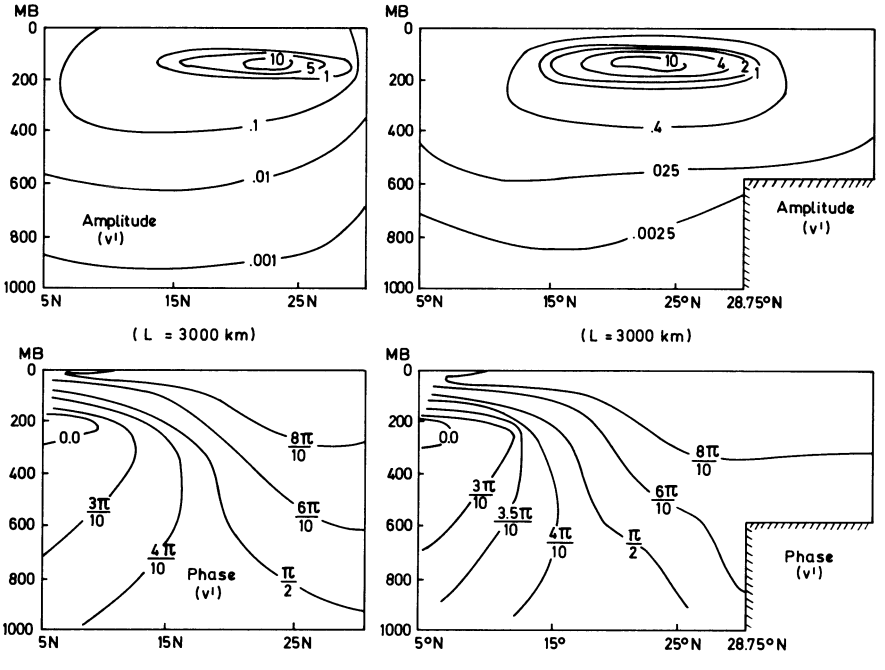

Figure 6
Amplitude and phase structure of the most unstable mode (wavelength = 3000 km) for domain I and domain II.

Since the amplitudes vary over orders of magnitude in the vertical, the phase lines are not very meaningful. The presence of an elevated plateau in domain II has no appreciable effect on the structure of the perturbation above 600 mb. It only affects the kinematics near the plateau boundary.

These results suggest that it is the barotropic instability of the flow at 150 mb which is responsible for the structure and the growth of the most unstable mode; since the model is vertically coupled through the $f_0(\partial\omega/\partial p)$ term, the fastest growing mode of the barotropically unstable 150 mb flow dominates the whole domain. This suggestion will be examined further in the next section.

Since the horizontal scale of the most unstable mode is about 3000 km, the horizontal uniformity of the mean zonal flow over a longitudinal belt of 3000 km was examined by computing the cross-section of potential vorticity along 73E and 100E.

It was found that the mean zonal flow is homogeneous between the longitudes 73E and 100E, and therefore, such a perturbation analysis is justified.

5. *Energetics of the most unstable mode*

In order to gain some further insight into the characteristics of the unstable modes, energy transformations were calculated for the most unstable mode (L = 3000 km) for domains I and II. Results for both domains were nearly identical (the northern boundary did not affect the results), because the amplitudes of the fastest growing perturbations were concentrated at 150 mb.

Expressions for the conversion of eddy kinetic energy to zonal kinetic energy, C(KE, KZ); for zonal available potential energy to eddy available potential energy, C(AZ, AE); and for eddy available potential energy to eddy kinetic energy, C(AE, KE),

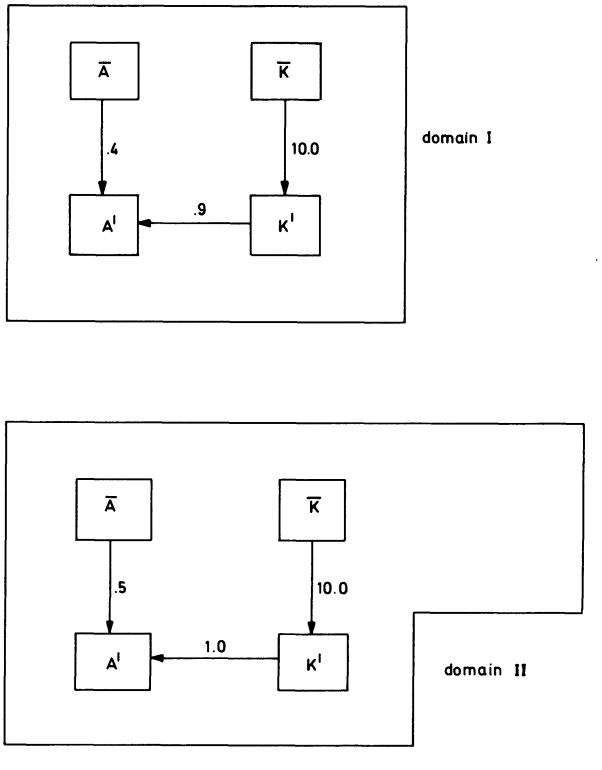

Figure 7
Energy transformations (in arbitrary units) for the most unstable mode (wavelength = 3000 km) for domain I and domain II.

are given as follows:

$$C(KE, KZ) = \int_0^{p_0}\int_0^{D} \bar{\Psi}\frac{\partial^2(\overline{u'v'})}{\partial y^2}\,dy\,dp = \frac{k}{2Dg}\int_0^{p_0}\int_0^{D}\frac{\partial \bar{U}}{\partial p}\left(\Psi_i\frac{\partial \Psi_r}{\partial y} - \Psi_r\frac{\partial \Psi_i}{\partial y}\right)dy\,dp$$

$$C(AZ, AE) = \int_0^{p_0}\int_0^{D}\frac{f_0^2}{\sigma}\frac{\partial \bar{\Psi}}{\partial y}\frac{\partial}{\partial y}\left\langle\frac{\partial \psi'}{\partial x}\frac{\partial \psi'}{\partial p}\right\rangle dy\,dp$$

$$= \frac{kf_0^2}{2Dg}\int_0^{p_0}\int_0^{D}\frac{1}{\sigma}\frac{\partial \bar{U}}{\partial p}\left(\Psi_r\frac{\partial \Psi_i}{\partial p} - \Psi_i\frac{\partial \Psi_r}{\partial p}\right)dy\,dp$$

$$C(AE, KE) = \int_0^{p_0}\int_0^{D} f_0\,\omega'\frac{\partial \psi'}{\partial p}\,dy\,dp = \frac{f_0}{2Dg}\int_0^{p_0}\int_0^{D}\left(W_r\frac{\partial \Psi_r}{\partial p} + W_i\frac{\partial \Psi_i}{\partial p}\right)dy\,dp$$

where D = lateral width of the domain = $19\Delta y$ and p_0 = surface pressure = 1000 mb, $\langle\ \rangle$ denotes domain average.

Figure 7 shows the numerical values of these conversions in arbitrary units.

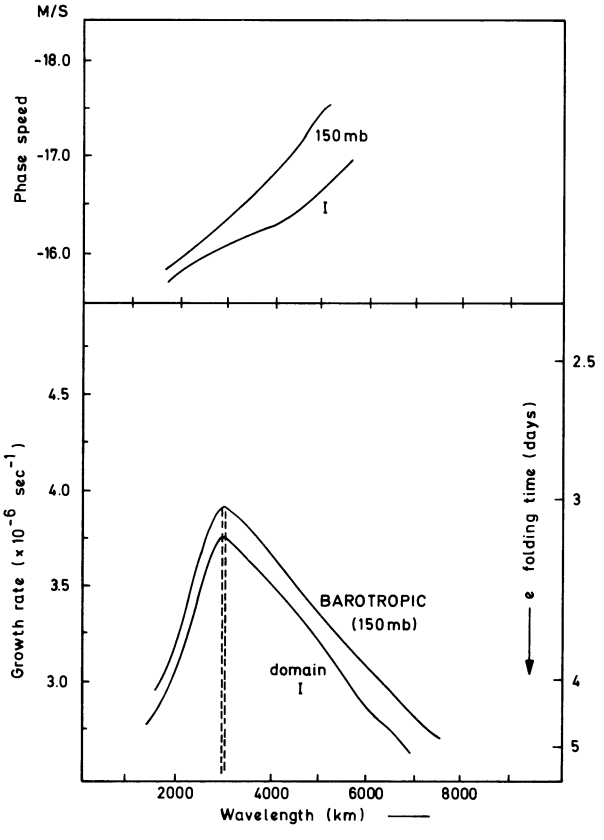

Figure 8
Growth rate and phase speed versus wavelength for domain I and for barotropic instability at 150 mb.

We see that the most dominant conversion is from KZ to KE, which demonstrates the importance of barotropic instability.

This also suggests that the barotropic instability of the zonal flow at 150 mb may be the primary excitation mechanism for these modes. In order to verify this result, a barotropic instability analysis was performed for the zonal flow at the 150 mb level.

Figure 8 displays the results of the barotropic-baroclimic instability analysis for the entire domain I, and the barotropic instability analysis of the zonal flow at 150 mb. It may be seen that both curves are almost identical, confirming the earlier suggestion that most of the contribution to the instability shown in Fig. 5 comes from the barotropic instability at 150 mb. In fact, the growth rate is slightly higher for the barotropic (150 mb) case, because the lower levels have weaker horizontal and vertical shears, and therefore, smaller available kinetic energy and available potential energy. The same conclusion could have been reached by examining the time evolution of the patterns of convergence for phase speed and growth rate during the integration. For example, it was observed that the convergence of c and v occurred first at 150 mb and then proceeded downwards. This reflects the influence of the instability at 150 mb level on the lower levels, through the vertical coupling. However, the time scale over which all the levels become 'contaminated' by the instability of 150 mb is very large (50 days), compared to the period of the most unstable wave at 150 mb (3 days).

The growth rates and the phase speeds for a range of wavelengths were also calculated for the case where $\partial U/\partial p = 0$ and $U(y)$ at each level was the same as $U(y)$ at 150 mb. The results were very similar to the one shown in Fig. 8 for the 150 mb barotropic case.

6. *Concluding remarks*

It is found that the meridional profile of the zonal wind at 150 mb is barotropically unstable and that the fastest growing mode has the wavelength of 3000 km. The structure of the most unstable mode is such that most of the amplitude is concentrated at 150 mb. The conversion C(AZ, AE) is small and, therefore, the baroclinic instability mechanism is not important.

In an earlier paper COLTON (1973) has suggested that 'nonlinear barotropic interaction between the quasi-stationary forced planetary waves and transient synoptic scale waves is important in producing several features of the tropical upper tropospheric general circulation. In particular, the development of the small-scale waves and vortices often present in the mid-oceanic troughs and the disturbances observed by Krishnamurti which form along the easterly jet over the Indian Ocean is shown to be due to scale interactions involving short-term nonlinear barotropic instability.'

In the present paper we have used the linear barotropic instability analysis to

show that the mechanism for the generation of transient synoptic scale waves is the barotropic instability of the mean zonal flow. The phase speed of the computed most unstable perturbation agrees reasonable well with the observed phase speed of 10–12° longitude/day at 200 mb (KRISHNAMURTI, 1971). Since barotropically unstable perturbations draw energy from the mean motion, these results are also in agreement with the hypothesis of COLTON (1973) that small-scale waves at 200 mb are continuously draining the energy of the mean motion and quasi-stationary large-scale waves.

Finally it may be remarked that it is rather unlikely that the barotropically unstable disturbances at 150 mb could account for the observed monsoon depressions which have their amplitude maxima at the lower tropospheric levels and are rarely detected at 200 mb. Therefore, proper inclusion of moist-convective heating seems to be not only desirable, but essential to explain the growth of the monsoon depressions. The author (SHUKLA, 1976) has investigated the instability of a basic state in which the zonal wind has horizontal and vertical shear, the vertical thermal structure is conditionally unstable, and the moist convective heating is parameterized in terms of the large-scale variables. These results have been reported in another paper (SHUKLA, 1977).

Acknowledgements

The author expresses his gratitude to Professors Jule G. Charney and Norman A. Phillips, who were the thesis advisers at MIT, for their valuable suggestions and guidance. Computer facility at the Goddard Institute of Space Studies was used for performing the numerical integrations.

REFERENCES

CHARNEY, J. G. and STERN, M. E. (1962), *On the stability of internal baroclinic jets in a rotating atmosphere*, J. Atmos. Sci. *19*, 159–172.

COLTON, D. E. (1973), *Barotropic scale interactions in the tropical upper troposphere during the northern summer*, J. Atmos. Sci. *30*, 1287–1302.

KLEIN, W. D. (1974), *Ozone kinematics and transports in unstable waves*, PhD Thesis, Dept. of Meteorology, MIT, Cambridge, Mass.

KRISHNAMURTI, T. N. (1971), *Observational study of the tropical upper tropospheric motion field during the northern hemisphere summer*, J. Appl. Meteor. *10*, 1066–1096.

KRISHNAMURTI, T. N., KANAMITSU, M., GODBOLE, R. CHANG, C. B., CARR, F. and CHOW, J. H. (1976), *Study of a monsoon depression (II), Dynamical structure*, J. Meteor. Soc. Japan *54*, 208–255.

SHUKLA, J. (1976), *On the dynamics of Monsoon depressions*, ScD Thesis, Dept. of Meteorology, MIT, Cambridge, Mass.

SHUKLA, J. (1977), *CISK-barotropic-baroclinic instability and the growth of monsoon depressions*, Submitted to J. Atmos. Sci. for publication.

(Received 15th June 1977)

Pageoph, Vol. 115 (1977), Birkhäuser Verlag, Basel

Mechanisms Effecting the State, Evolution and Transition of the Planetary Scale Monsoon[1])

By PETER J. WEBSTER[2]) [3]), LANG CHOU[2]) and KA MING LAU[2])

Summary – An attempt is made to identify the basic structure of the planetary scale monsoon and to define and describe the various mechanisms effecting or producing that structure and its variation on a variety of time scales. Both observational and theoretical descriptions are used to define the monsoon system or to point towards problems that require clarification.

The basic mean summer and winter monsoon regimes are described and a discussion presented on their degree of dependence on the distributions of orography, the form and distribution of land and ocean and the state of the interactive oceans adjacent to the major land masses. It is suggested that orography plays a critical role in determining the state of the mean summer and winter circulations behaving principally as an elevated heat source in summer and a mechanical perturber of the mean flow in winter. The spatial variation of sea-surface temperature and the distribution of land are shown to be the *primum mobile* of the mean seasonal monsoon.

Various modes and time scales of the variable monsoon are defined. It is shown that the principal time scale variation or phasing of the *interseasonal* transition is determined by the different response times of the oceans and land areas to variable solar heating. The reaction of the ocean is a strong function of latitude because of its ability to be heated by solar radiation and mixed mechanically by the atmosphere. The return heating distribution imposed on the atmosphere by the ocean strongly effects the circulation. The inclusion of a hydrology cycle adds a further time scale to the monsoon system allowing much more rapid variations to be superimposed on the modulations caused by radiative and sensible heating effects. The inclusion of clouds introduces a further *intra-seasonal* time-scale into the monsoon circulation causing 'break-like' variations of the precipitation pattern and circulation fields during the late summer.

Finally, a brief discussion is given on the various forms of interhemispheric interaction. It is suggested that contrary to earlier theoretical speculation, the equatorial latitudes may be considerably more 'porous' to mid-latitude disturbances than hitherto anticipated.

Key words: Monsoon evolution, monsoon structure.

1. Introduction

Occupying an extremely large part of the variance of the total energy in the global annual cycle, the planetary scale monsoon circulation is a phenomenon with influences and effects which dominate the meteorology of large sections of the globe. For example, the southwest summer monsoon of India and Southeast Asia cannot be thought of as a regional phenomena, but as one part of a system extending from the

---

[1]) Contribution number 432, Department of Atmospheric Sciences, University of Washington, USA.

[2]) Department of Atmospheric Sciences, University of Washington, Seattle, Washington 98195, USA.

[3]) Present affiliation, Division of Atmospheric Physics, CSIRO, Aspendale, Victoria, Australia.

southern oceans of the southern hemisphere to the northern reaches of Eurasia. Furthermore, influences of the system extend in longitude across Africa to the west and probably assert some measure of control to circulations across the Pacific Ocean. The extent of the winter monsoon circulation possesses a scale of influence at least as large as its summer counterpart. Both monsoon regimes exercise enormous economic and social control over large segments of global society. Indeed, the very existence and life of more than 50 percent of the total population of earth is almost completely dependent upon the monsoon circulation.

The objectives of this paper are extremely modest and by no means exhaustive either in the delineation of a problem nor in its explanation. Basically, we will attempt to review observational studies which define the structure of the planetary monsoon circulation or point towards problems that require clarification. We then follow with a discussion of models, both observational or theorectical, which suggest a dominating process or phenomena.

In the next section we will consider the seasonal mean structure of the monsoon system and attempt to break down into a phenomenological substructure the components which constitute its identity. In the third section we consider the transient behavior of the monsoon system on time scales ranging from the variation of the system between its mean solstitial states to shorter period interactions between phenomena of different hemispheres.

To define spatial and temporal bounds for the study, we will consider only planetary scale motions possessing time scales from longer than synoptic to seasonal and annual. This means that disturbances with somewhat shorter time scales, for example, Bay of Bengal disturbances, will not be discussed, even though it is conceded that they form an integral part of the overall monsoon circulation. Rather, we will concentrate on describing the seasonal modulation of the monsoon circulation and planetary scale interaction with other circulation regimes.

2. *Seasonal mean circulation*

(*a*) *Description*

In the simplest sense the monsoon circulation may be thought of as possessing two major regimes. These may be termed the northern hemisphere summer monsoon and the northern hemisphere winter monsoon (hereafter referred to simply as the summer and winter monsoons). The gross features of these regimes may be discerned from Fig. 1 which shows seasonal mean streamline patterns for 850 mb and 200 mb for the periods June, July and August (JJA) and December, January and February (DJF). Such analyses are typical of a number of observational studies of the large-scale tropospheric circulation. Of particular interest are the studies of NEWELL *et al.* (1972), RAMAGE and RAMAN (1972), KRISHNAMURTI (1971 and SADLER (1975). The latter two works utilize commercial aircraft flight path observations which fill in

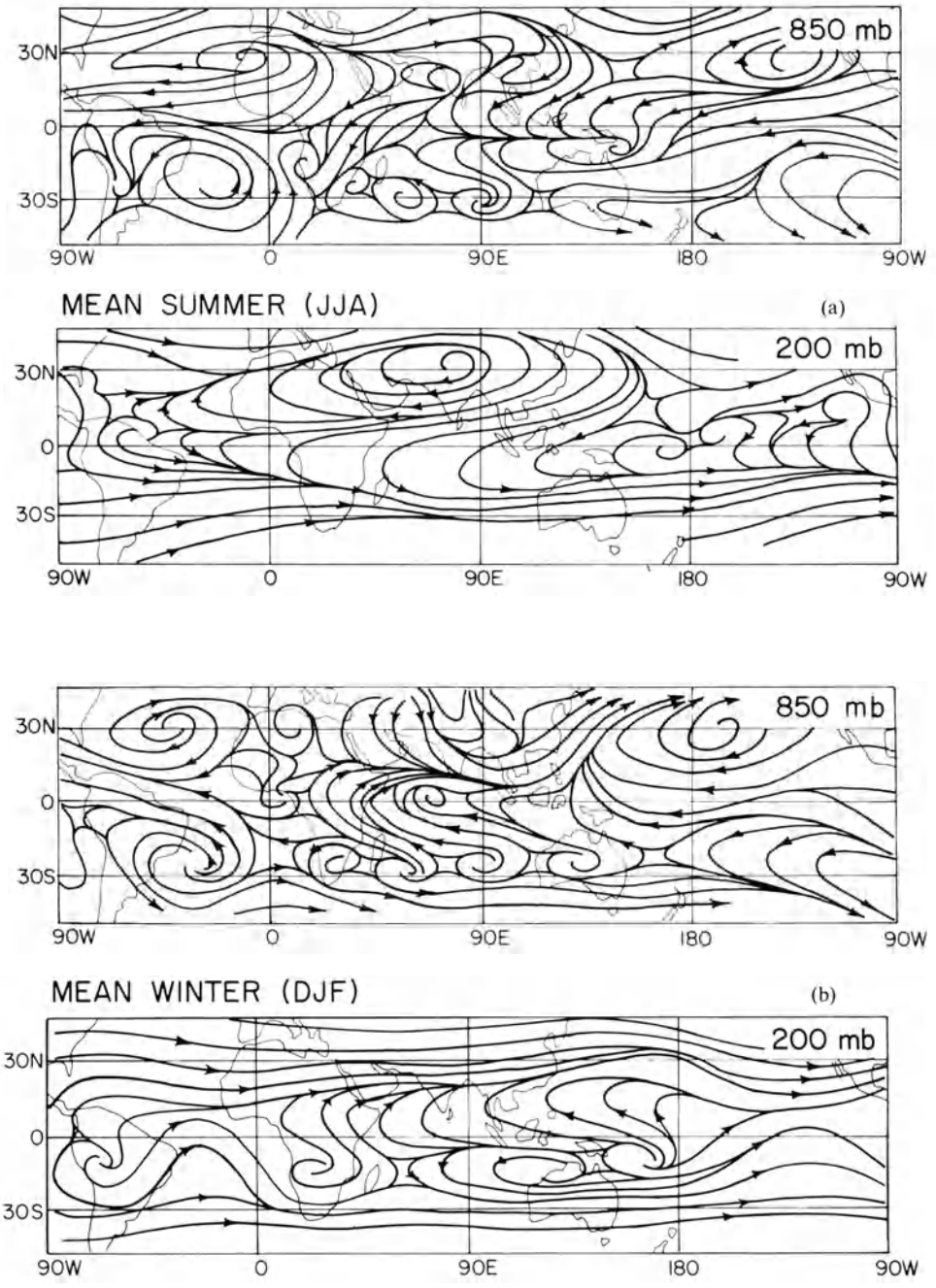

Figure 1

Mean seasonal streamline pattern at 850 mb (upper panel) and 200 mb (lower panel) for (a) the northern hemisphere summer and (b) the northern hemisphere winter. Adapted from NEWELL *et al* (1972) and SADLER (1975).

many of the dataless regions of the ocean areas. Ramage and Raman's analyses refer specifically to data collected in the International Indian Ocean Expedition. In all analyses, the data in the southern hemisphere is relatively sparse compared to its northern counterpart.

The most significant features of the monsoon circulation may be summarized as follows. In the lower troposphere in summer a strong cross-equatorial flow emerges from the southern hemisphere subtropics and forms a generally west to southwest flow across the Indian Ocean and Southeast Asia. This is joined by a relatively dry low-level flow from the northwest which merges, in a climatological sense, over the northern Indian Ocean. At 200 mb an intense anticyclone centered over the Tibetan plateau dominates the upper troposphere and provides intense easterly winds along and to the north of the equator from the South China Sea to eastern Atlantic Ocean. This region also corresponds to the return cross-equatorial flow to the subtropical westerlies of the southern hemisphere. In winter the basic circu-

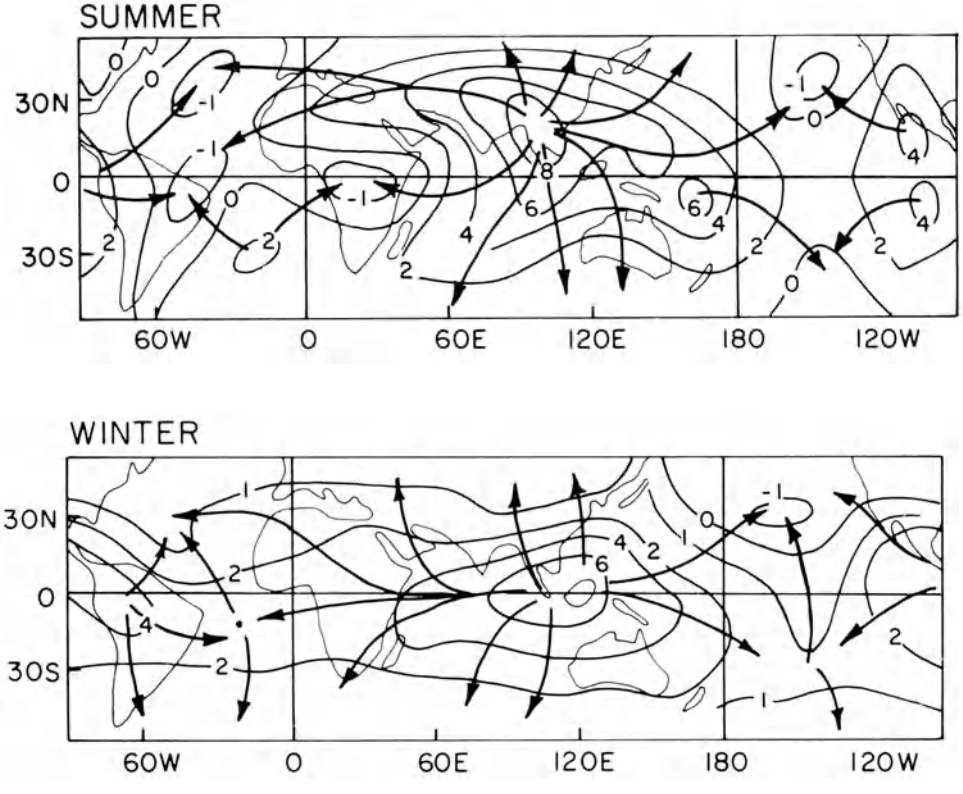

Figure 2
Mean seasonal distributions of velocity potential (solid lines) and vectors of the divergent part of the mean wind field (arrows) for the northern hemisphere summer (upper panel) and winter (lower panel). Adapted from KRISHNAMURTI (1971a) and KRISHNAMURTI *et al.* (1973).

lation reverses. At low levels the flow is off the Asian continent and forms the northeast monsoons of the China Sea and Indian Ocean regions. On crossing the equator the flow converges in the Indonesian–Australian region to provide the somewhat weaker southern hemisphere summer monsoon. A return flow at 200 mb emerges from the southern hemisphere tropics, but the intensity of the anticyclone, or the resultant equatorial easterlies, do not match that of the summer monsoon of the northern hemisphere. After crossing the equator the upper tropospheric mean flow merges with the strong northern hemisphere westerlies which are, in an average sense, to the south of the Himalayas.

Although much of the structure of the mean monsoon flow may be obtained from mean streamline analyses such as those shown in Fig. 1, a breakdown of the fields into divergent and non-divergent parts is instructive. Such analyses were performed by KRISHNAMURTI (1971a) and KRISHNAMURTI, *et al.* (1973). Figure 2 shows the mean velocity potential distribution (i.e., divergent part of the wind) at 200 mb for both July and January. The solid lines, which are orthogonal to the contours, denote the direction of the divergent part of the wind. The details of the distributions are not important and perhaps even the data does not permit us to note but the grossest features. However, from the analyses emerges a rather significant point. During each season there exists one major maximum in the monsoon region and a weaker maximum in Central America. In the summer the major maximum is located over the northern Bay of Bengal–Burma region with elongated maxima extending eastward across the Phillipines and the South China Sea. In winter the maximum velocity potential lies over the South China Sea–Indonesian region. So extensive are the summer and winter maxima that the mean divergent motions emerging from them are of planetary scale. This allows one to construe that the convective regions associated with both the summer and winter monsoons must be dominant over most phenomena in the tropics and perhaps even at higher latitudes.

(*b*) *Mechanisms*

The traditional explanation for the circulation distributions of both the winter and summer monsoons is based upon the interaction of the seasonally varying insolation and the distribution of the continents and oceans. Originating with HALLEY (1686), the concept of the monsoons as a planetary scale land–sea breeze circulation has dominated meteorology for nearly three centuries. Indeed, despite the accumulation of considerable new data and the rapid advancement of theoretical meteorology, the planetary scale rotational sea-breeze model has persisted. The improvements and modifications deal mostly with the nuances of the circulation and its seasonal phasing (WALKER, 1972).

Possibly four major factors render the winter and summer monsoons completely different phenomena each possessing its own distribution of parameters and character; neither being the mere mirror image of the other, as may be seen in Fig. 1. Three of the

factors depend directly upon the physical form of the earth. They are the distribution of mountains in the monsoon region, the relative sizes of the continental land masses of Australia and Asia and the distribution of the large mountainous islands which contribute the 'maritime' continent (RAMAGE, 1968) made up of Sumatra, Borneo, New Guinea plus numerous other smaller islands characterized by equally high terrain, all of which are surrounded by extremely warm ocean water. The fourth factor is the distribution of sea surface temperature and, in particular, its temperature during the established summer and winter monsoon (July and January, respectively). Ultimately, of course, the sea-surface temperature depends considerably upon the distribution of land and sea.

The large orographic structures of the monsoon regions appear to possess dif-

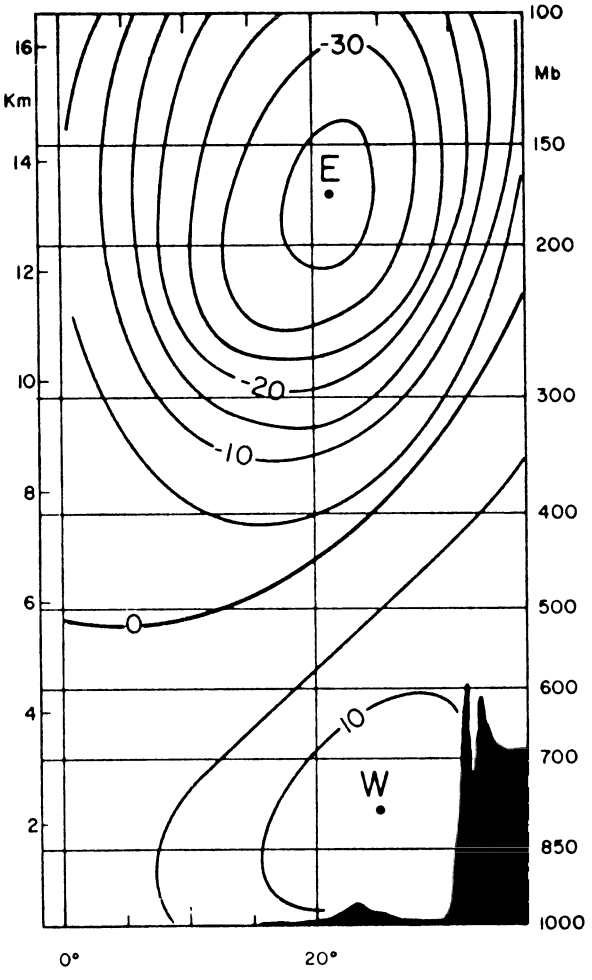

Figure 3
Latitude-height section of the computed zonal wind component distribution of MURAKAMI *et al.* (1970). Shaded region denotes the Himlayas.

ferent roles in the summer and winter monsoon regimes. For the summer monsoon, FLOHN (1950, 1960) was first to suggest that the role of the Himalayan region may be different from that of a mechanical deviator of the mean summer flow. It was suggested, in fact, that the Tibetan Plateau acted as an elevated source of sensible heat which was responsible for the generation of the warm upper tropospheric anticyclone which dominates this region in Fig. 1. Later RIEHL (1959) suggested that the latent heating was the dominant process. Using satellite data which showed the central and southeastern parts of Tibet to be snow free through most parts of the year, FLOHN (1968) was able to confirm earlier work (STAFF MEMBERS, ACADEMIA SINICA, 1958) that the Plateau was indeed a candidate for rapid heating with the advancing sun in spring but conceded that in the southeastern regions, where precipitation occurs many weeks before the onset of widespread precipitation over most of India, latent heating was probably the dominant process.

The role of the Himalayas in the maintenance of the mean summer circulation has stimulated a number of numerical studies. MURAKAMI *et al.* (1970) studied the role of orography by considering a number of numerical experimenta in which cases with mountains were contrasted with cases without mountains. The model was an 8-level two-dimensional hemispheric model extending from the equator to the pole. Cross-equatorial flow and deviations from the mean zonal state (disturbances) were precluded from the analysis. Without mountain effects only relatively weak easterlies in the upper hemisphere were produced. Only with a condensation cycle and the inclusion of the Tibetan Plateau was the mean field similar to the observed structure. The computed field of the zonal velocity component is shown in Fig. 3. It would seem that the model results of MURAKAMI *et al.* confirm the thermal role of the Tibetan Plateau.

More recently, WASHINGTON and DAGGUPATY (1975) and HAHN and MANABE (1975) have used global general circulation models to concentrate on the dynamics of the summer monsoon. In both studies many of the gross features of the monsoon are reproduced although computational problems arising from the inclusion of the abrupt Himalayan Plateau itself, affects some parameters such as the mean precipitation distribution, which, to varying degrees, often is too far southward of the observed maximum. A discussion of some of these points is given by SADLER and RAMAGE (1976) and HAHN and MANABE (1976).

The study of HAHN and MANABE (1975) is especially geared towards studying the effects of mountains on the summer monsoon which is achieved by comparing mountain and no-mountain cases. It was found that the mountains were responsible for the formation and maintenance of the warm upper-tropospheric anticyclone via latent heating. Without orography, the summer monsoon was found to slowly extend into Asia and arrive at a poleward limit some 10° short of the case with mountains. Whereas the conclusions cannot be considered definitive until the climatology of the control case matches more closely the observed climatology, the results are suggestive of an extremely important control exerted by the large-scale orography.

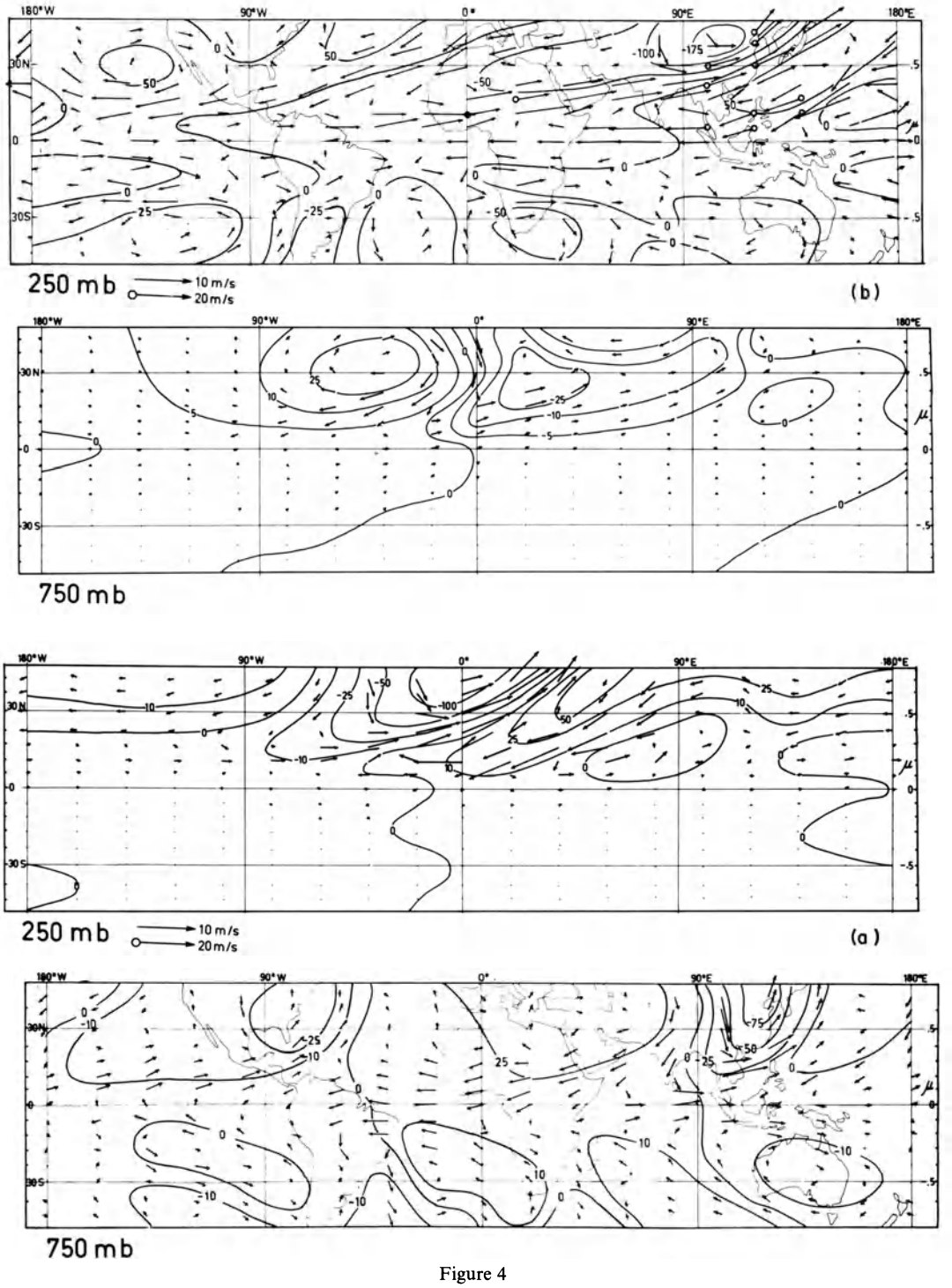

Figure 4

Perturbation velocity distributions at 250 mb and 750 mb for (a) imposed orographic barrier located at 25°N and (b) imposed realistic distributions of heating and orography. Both (a) and (b) refer to the northern hemisphere winter. From WEBSTER (1972).

During the northern hemisphere winter the role of the Himalayas changes substantially. With the maximum insolation occurring in the summer hemisphere, the elevated regions of Asia lose their ability to anomalously heat the middle and upper troposphere through winter. With the mean westerlies considerably poleward of their summer position, the Himalayas act as a strong mechanical perturber of the mean zonal flow. Such an effect is evident in Fig. 4 from WEBSTER (1972). Using a simple linear primitive equation model, Webster attempted to assess the relative roles of orography and heating at low latitudes. Figure 4a shows the 250 and 750 mb perturbation (i.e., with the zonally averaged flow subtracted out) circulation fields resulting from the interaction of a mean flow and an orographic structure situated at 25°N and the prime meridian. For our purposes it is sufficient to note the extremely high amplitude trough-ridge system which dominates flow downstream and in the vicinity of structure. In Fig. 4b, a realistic orographic distribution has been included together with the seasonal heating field. Comparing Figs. 4a and 4b, WEBSTER (1972) concluded that the orographic forcing from the Himalayas was a dominant process during the winter, at least north of the equator in the South-east Asian region.[4])

An understanding of the degree of control imparted by the distribution of ocean and continents on the earth's climate emanates from HALLEY (1686). The importance of the longitudinal differences produced by the ocean–land contrast and the effect on the lower boundary heating caused by the different character of the lower boundary was initially emphasized by ROSSBY *et al.* (1939) and SMAGORINSKY (1953), at least for the mid-latitudes. Considering principally the very low-latitude flow, WEBSTER (1972) suggested that the variations in the latent heating distribution arises, in part, from the land–sea contrasts and the variations in sea-surface temperature were responsible for much of the character of the large-scale flow. The basic character of the circulation was explained in terms of the equatorially-trapped Kelvin wave which matched both the selective response and the horizontal scales of the motion. However the vertical scale of the Kelvin wave did not match observations and it was not until the work of CHANG (1977), who illustrated the effect of dissipation on the vertical structure of equatorial modes, that the great east–west overturnings shown in Fig. 2 which dominate much of the mean low-latitude, could be seen to be atmospheric manifestations of viscous controlled Kelvin waves.

In an attempt to investigate further the role of land and ocean and the dynamic interaction of the oceans and the atmosphere, WEBSTER and LAU (1977a, b) and LAU and WEBSTER (1977) developed a simple coupled model. Much more complicated coupled ocean–atmosphere models have been developed (e.g. MANABE *et al.*, 1975) but most of these are sufficiently complicated to deny extended integration or too

[4]) Professor T. Murakami (private communication) contends that the different mean circulation features of early and late winter are a result of orographic forcing in the region to the east of Southeast Asia. In later winter, the mean zonal westerlies are over and to the south of the Himalaya such that the position and strength of the trough constrain disturbances in the South China Sea. In early winter the westerlies are further north and the South China Sea is disturbed.

simple (e.g., PIKE, 1971) to include ocean–land contrasts. The domain-averaged model fits between these two extremes. The physical structure of the model is shown in Fig. 5. Basically, the simplest prototype of the model, shown here, consists of two atmospheres of finite longitudinal extent surmounting, respectively, a land mass which is truncated in latitude at 18°N and a dynamic and interactive ocean. A similar ocean lies to the south of the truncated continent. The equations of motion which represent the atmosphere are averaged over the longitudinal extent of each domain. The domains 'communicate' via interaction terms at each domain. The ocean domains are also dynamic and are represented by an advective mixed layer model which allows transport of heat by the ocean. The primitive equation atmospheric model and ocean model are presented in detail by WEBSTER and LAU (1977). A later version of the ocean model allows for wind-driven circulations and longitudinal temperature variations (LAU, 1977).

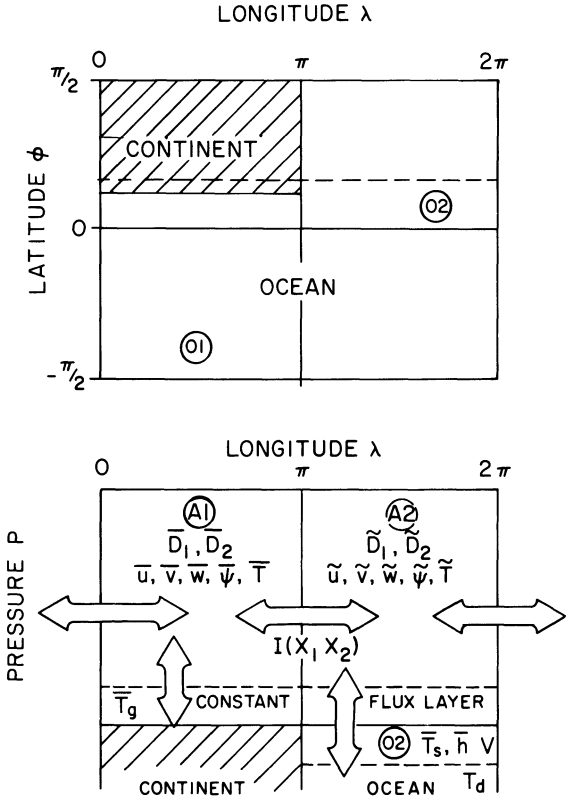

Figure 5
Latitude-longitude (upper diagram) and latitude-pressure (lower diagram) of a two-atmosphere and two-ocean domain-averaged model. One atmosphere A1 surmounts a truncated continental region with an ocean to the south (O1), whereas A2 lies over O2. Variables are defined and interdomain fluxes and interaction terms are denoted by arrows. From WEBSTER and LAU (1977).

Figures 6 and 7 show the temperature and zonal velocity component response of the domain averaged model described in Fig. 5 to summer solstice and winter solstice insolation. The vertical dashed line in all cases denotes the land–sea boundary. Solid lines signify the fields over the ocean–continent domains (A1 in the lower section of Fig. 5) and dashed lines for the atmosphere which lies over the uninterrupted ocean (A2). The surface temperature field emphasizes the importance of ocean–atmosphere contrast. At the land–sea boundary an abrupt change in surface temperature is apparent during the summer and the land temperature remains significantly warmer than that of the ocean further to the north. At the winter solstice the land region is considerably cooler than either the adjacent ocean or the ocean equatorward. To

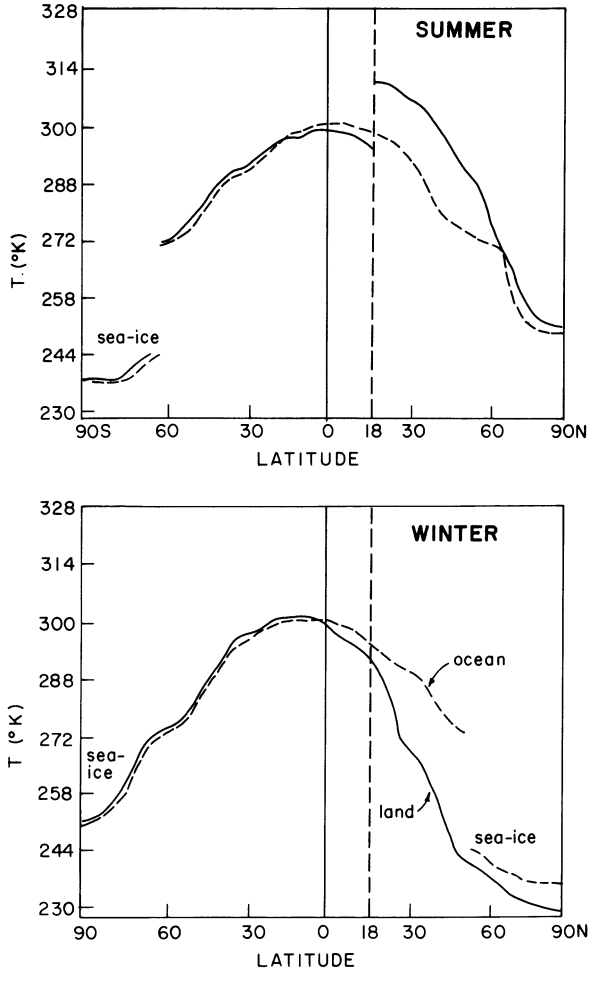

Figure 6
Surface temperature for the two atmospheric domains A1 and A2 defined in Fig. 5, for the winter and summer solstices. Dashed lines refer to A2 and solid lines to A1. WEBSTER and LAU (1977b).

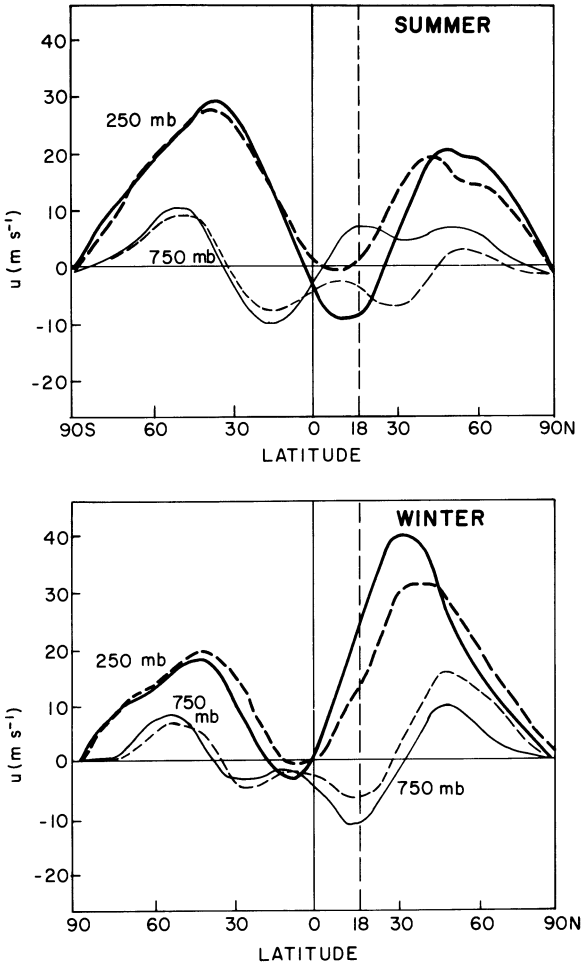

Figure 7
Same as Fig. 6 but for the zonal velocity component. WEBSTER and LAU (1977b).

the north the land has cooled at a much more rapid rate than the ocean although the sea–ice margin has advanced considerably equatorward. Between the solstices, the equator to land-margin temperature gradient has reversed and the dramatic effect this has had upon the upper tropospheric mean flow is apparent from Fig. 7. During the summer a relatively strong easterly maximum[5]) exists at the land margin whereas during winter it has been replaced by a substantial westerly wind. Similarly at 750 mb the strong summer westerlies have been replaced by winter easterlies. Over the ocean

[5]) The results shown in Figs. 6 and 7 refer to a case where moisture has been omitted. Inclusion of a hydrology cycle, including ground water immediately reduces the surface temperature over land between 18°N and 30°N by 5°C but simultaneously increases the magnitude of the upper troposphere easterly maximum by nearly a factor of three.

(A2) less dramatic but similar variations have occurred but mainly through zonal interaction than by variations in the surface temperature, which in the equatorial regions (see dashed line in Fig. 6) remains effectively constant throughout the year.

3. *Transient circulations*

a. Description

Consideration of only the mean seasonal structure of the monsoon circulation, as displayed in Figs. 1 and 2, belies the importance of the transient stage through which the atmosphere must transgress during the equinoctial (or transitional) seasons and also the variations which occur at time scales less than seasonal. SADLER's (1975) careful analyses of the mean *monthly* upper tropospheric circulation are important and helpful in understanding the transition. The picture which emerges from Sadler's analyses is not simple, however, and does not display mere linear variation between the summer and winter seasons. Instead the transitions are characterized by rapid variations from one state to another with timing that varies spatially. Such variability in other atmospheric parameters through the annual cycle has been well documented by RAMAGE (1971) and RAMAGE and RAMAN (1972).

Figure 8 shows time-latitude sections of the zonal wind component adapted from Sadler's analyses. Six latitude-time sections of the zonal velocity component (ms^{-1}) are shown for the meridians 80°E, 100°E, 150°E, 180° and 150°W. Heavy lines denote ridge positions and the dashed lines represent troughs. All six sections show extreme seasonal variation with distinctive winter and summer distributions and rapid transitions between them. The sections may be divided up into two groups which roughly categorize their annual variation.

The first group (80°E, 100°E, and 115°E) are characterized by a rapid development of easterly winds between the equator and 25°N to north of 40°N. In the southern hemisphere a rapid increase in the westerlies appears to match, or perhaps lead, the development of the easterly maximum in the northern hemisphere. The suggestion that the development of the westerlies in the 80°E–180° sector leads the easterly maximum in the northern hemisphere was originally made by RADOK and GRANT (1957). They further suggested that the diminuation of the northern hemisphere summer easterlies, and therefore the return of the northern hemisphere westerlies, leads the decay of the southern hemisphere westerlies.

The second group of sections (150°E, 180° and 150W) does not show the development of strong equatorial easterlies during the summer. On the contrary, the 150°W section exhibits westerlies during the entire year along the equator and only weak easterlies are evident in the other sections. North of the equator convoluted structures rapidly evolve in late spring and summer. At 180° and 150°W a double trough-ridge system develops with an attendant double easterly maxima and intervening strong westerlies (~ 20 ms^{-}1) near 20°N. Such complicated structures quickly replace the

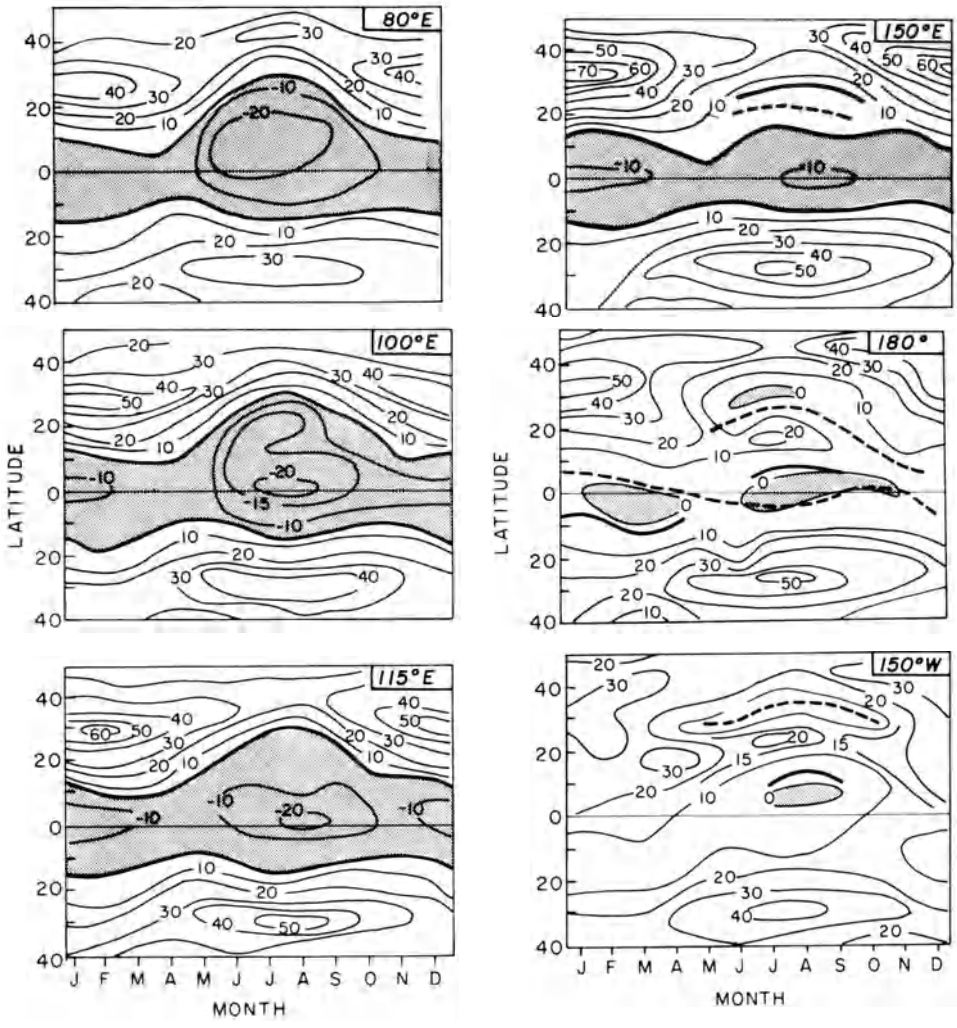

Figure 8

Latitude-time sections of the zonal velocity at 200 mb component for selected meridians. Dashed lines denote mean troughs and heavy solid lines show mean ridges. Units are m s^{-1}. Adapted from SADLER (1975).

intense westerly maxima in the most western sections, which reappear equally rapidly in the northern hemisphere fall. In the southern hemisphere the structure appears somewhat simpler although, in the same manner as the first group of sections, the westerly maximum assumes its southern winter position and magnitude with some rapidity.

The variations in the mean flow in the southern hemisphere cannot be well represented by the few latitude-time sections shown in Fig. 8. This is because during the southern hemisphere summer the westerly maximum is further to the south and west than can be seen in Fig. 8. Figure 9 shows a compilation of the hemispheric

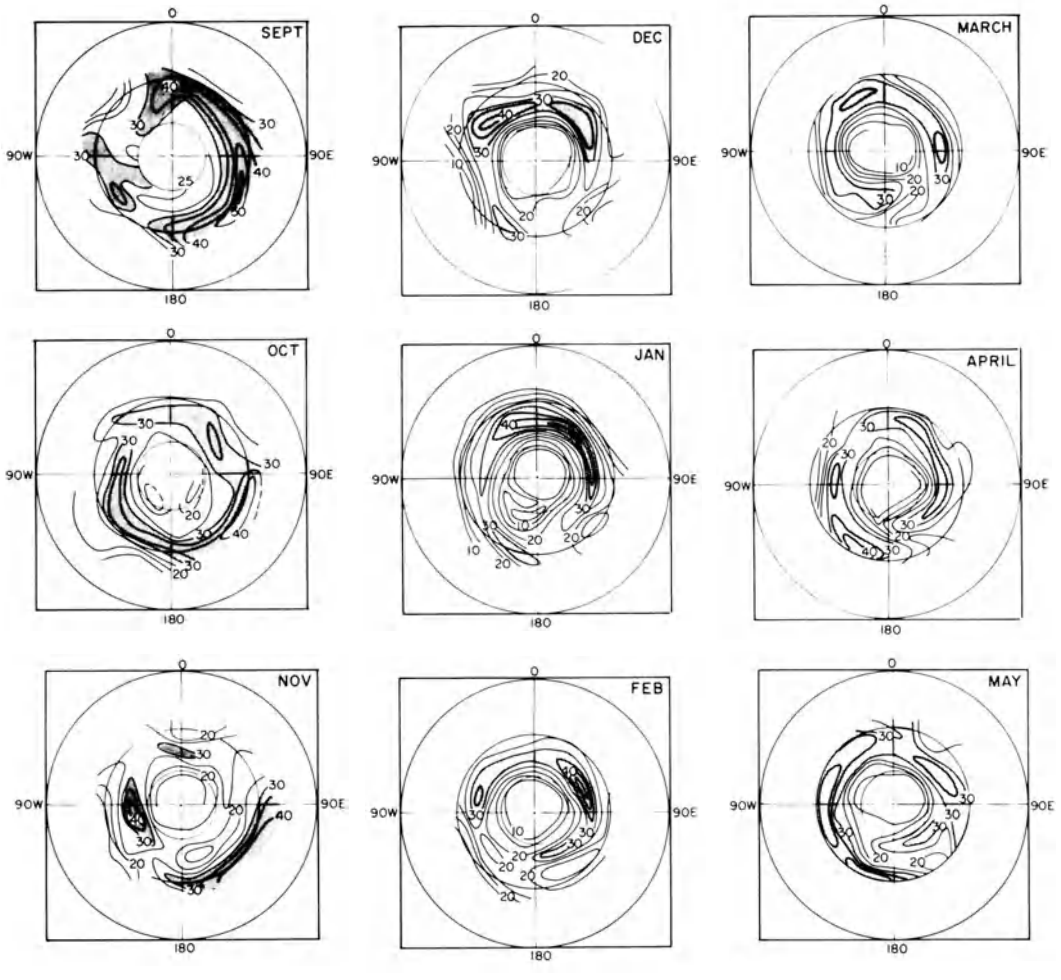

Figure 9
Mean monthly distribution of the zonal velocity at 200 mb as determined by WEBSTER and CURTIN (1975) from the EOLE epxeriment, September 1971 to July 1972.

distribution of the 200 mb zonal velocity component compiled from data obtained during the EOLE experiment (WEBSTER and CURTIN, 1975). Of particular interest is the rapid change of amplitude and phase of the monthly mean zonal flow. In the southern hemisphere summer, the westerly maximum is located in the sector between 90°W–0°–90°E and near 40°S. In the southern spring (and also in the southern winter) the maximum changes phase by nearly 180° and moves equatorward by 10° of latitude. In the northern hemisphere large-scale seasonal variations also occur in the strength and position of the westerly maximum. However, these changes are perhaps more associated with latitudinal shifts and variations in intensity that can be more easily attributed to variable seasonal forcing.

Besides the considerable change in the monsoon structure which occurs on a seasonal or even a monthly time scale, large variations occur interannually. This may be seen, for example, from SADLER *et al.* (1976) who has compiled and analyzed eight separate years of satellite data over the Pacific Ocean region. Whereas certain features are often discernable from year to year, large variations in cloud cover are also obvious. It is assumed that mean cloud cover and mean circulation are related, then the existence of the anomalies is indicative of variations in circulation. Similar variability appears to occur during the 'onset' and 'withdrawal' phases of the southwest monsoon. This has been emphasized by RAMAGE (1971) who finds, from observational studies of many years of data, including the International Indian Ocean Expedition, little evidence of a single or reproducible sequence of events but rather many phenomenological variations placed upon the background of a somewhat irregular annual variation. Whether this viewpoint is true or whether a unifying theory lurks amidst the data waiting elucidation is difficult to foretell.

A further factor which may play a strong role in determining the transient state of monsoon is the interaction between the two hemispheres. Unfortunately, interhemispheric relationships have received little observational and theoretical consideration, even though the interhemispheric nature of the monsoons, at least in its mean solsticial state, is readily apparent from Fig. 1.

The mean interhemispheric flow in summer in the Indian Ocean region is confined to a narrow low-level jet off East Africa whereas a much broader return flow exists in the upper troposphere (FINDLATER, 1969, 1971). In winter a southward flow in the western Indian Ocean is still characterized by a maximum stream off the African coast. However, in the winter FINDLATER (1969) estimates that the flow in this region accounts only for 10 percent of the total cross-equatorial flow in the Indian Ocean whereas its stronger counterpart in summer accounts for some 50 percent.

An intra-seasonal variability in the low-level cross-equatorial flow in the Indian Ocean region has been suggested by KRISHNAMURTI and BHALME (1976) who infer a phenomenological linkage from the southern Indian Ocean to the Indian subcontinent during the summer monsoon. The meridional teleconnection was apparent from variations in the Mascarene High which were transmitted northward via the cross-equatorial Somali jet stream and then across the Indian Ocean to the monsoon trough where it was speculated that imposed variations in stability effected the development of monsoon depressions. At this stage the cross-equatorial teleconnection should be treated as tentative and speculative until considerably more data becomes available in order to enhance the statistical significance of the chain of events. However, even with the small data set that is available, the relative phase relationships of the various quantities do establish a sequence which probably allow one to conclude that teleconnections did exist, at least during the data period. Furthermore, long-period variations have been noted in the southern hemisphere troposphere by WEBSTER and KELLER (1975) which could effect the structure of the Mascarene High.

Less observational definition exists for the cross-equatorial aspects of the winter

monsoon mainly because of the data scarcity in the central Indian Ocean and over Indonesia. Outflow from the cold Asian landmass towards the warm equatorial regions and the southern hemisphere occurs at low levels along its southern and eastern flanks. Rather than being a continuous stream flowing equatorward to form the northeast monsoon, the outflow occurs as irregular spurts or surges with intervening lulls which appear to be tied to the dynamics of the entire monsoon system. Such cold surges are reflected in the variations of atmospheric parameters at least as far south as Indonesia and occasionally into the summer hemisphere. Their longitudinal extent appears limited in the west due to the barrier of the Himalaya which shields India from the influence of the low-level surges. The development or modification of near-equatorial disturbances in the South China Sea appears to be connected to the occurrences of cold surges although the details of the connection are obscure. In turn, the development of disturbances in the northern hemisphere often corresponds to a temporary cessation of activity in the North-Australian monsoon region.[6])

The variations of the monsoon cycle and the cross-equatorial flow described above could be thought of as local manifestations of meridional circulations. With a meridional circulation model in mind, a number of observational studies have emerged to account for the position of the mean trough(s), precipitation distributions and cloudiness structures, especially for the summer monsoon. Basically each model pattern shows strong ascending motion over the land areas with descent occurring equatorward and in the winter hemisphere. This simple picture, established for the summer circulation by KOTESWARAM (1958) and many others, has been subject to a number of complicating adaptations, for example by ASNANI (1967), in order to account for nuances of the gross circulation which have emerged via an ever improving data set. Asnani replaces Koteswaram's single equatorial cell for the summer monsoon with a combination double cell which enhances descent near the equator and ascent near 5°N. Further, to account for disturbed conditions to the south of the equator, Asnani adds a second and distinct southern hemisphere circulation. Whereas some insight may be gained by continuing to add mean circulations to account for all new variations of differences introduced by new data, it must be considered a dubious practice which does not even allow for the consideration of rectification of shorter period phenomena which may play an important role in producing the discerned mean state.

An appreciation of the complication involved in even the structure of mean meridional circulations in the winter monsoon may be gained from BLACKMAN *et al.* (1977) who have compiled schematic representations of the *winter* mean meridional circulations along meridians through central Asia and through the central Pacific Ocean, or, upstream and downstream of the upper tropospheric jet stream located over Japan. Such a representation is reproduced in Fig. 10. For our purposes it is

[6]) Personal communication: Professor T. Murakami, University of Hawaii.

sufficient to concentrate upon the zonal variation of the structure. Basically, the upstream (or continental) section is dominated by a strong thermally *direct* meridional circulation whereas the downstream (or oceanic) section is dominated by an equally strong but thermally *indirect* meridional circulation. Both circulations are consistent with the eddy momentum and heat fluxes and the distribution of the disturbed weather in the winter monsoon circulation. The complexity in the zonal direction has the immediate implication that the monsoon circulation is a strong function of longitude as well as latitude. Unfortunately, BLACKMON *et al.*, have not as yet extended their analyses to include the northern hemisphere summer circulation.

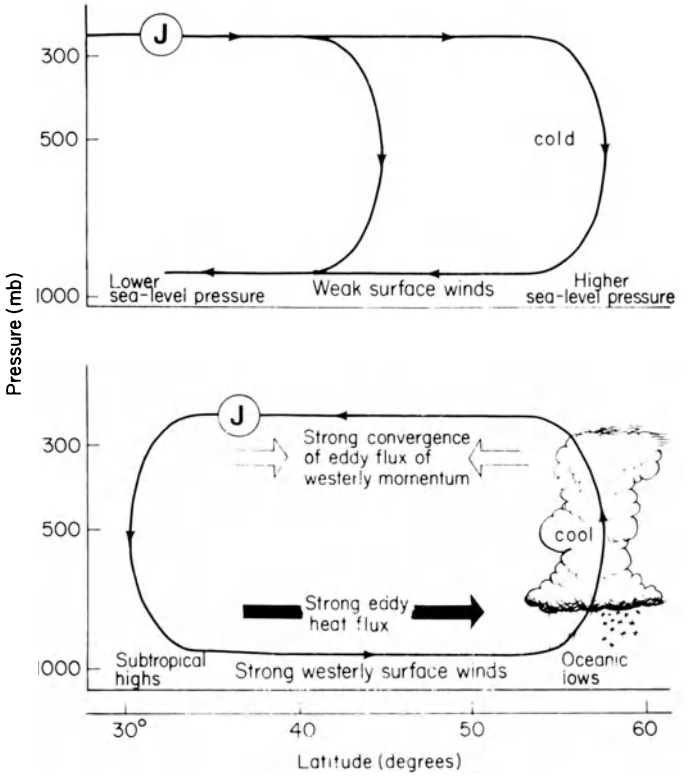

Figure 10
Schematic description of the wintertime mean meridional circulation through Central Asia (upper panel) and the Western Pacific Ocean (lower panel). From BLACKMON *et al.* (1977).

Cross-equatorial interactions of a much shorter time scale which may influence the monsoon circulation is apparent from Fig. 11 where the 200 mb perturbation kinetic energy distribution calculated by MURAKAMI and UNNINAYAR (1977) is displayed. In the equatorial regions, the most notable feature is the relative maximum to the east of the date line which bridges the gap between the mid-latitude maxima of

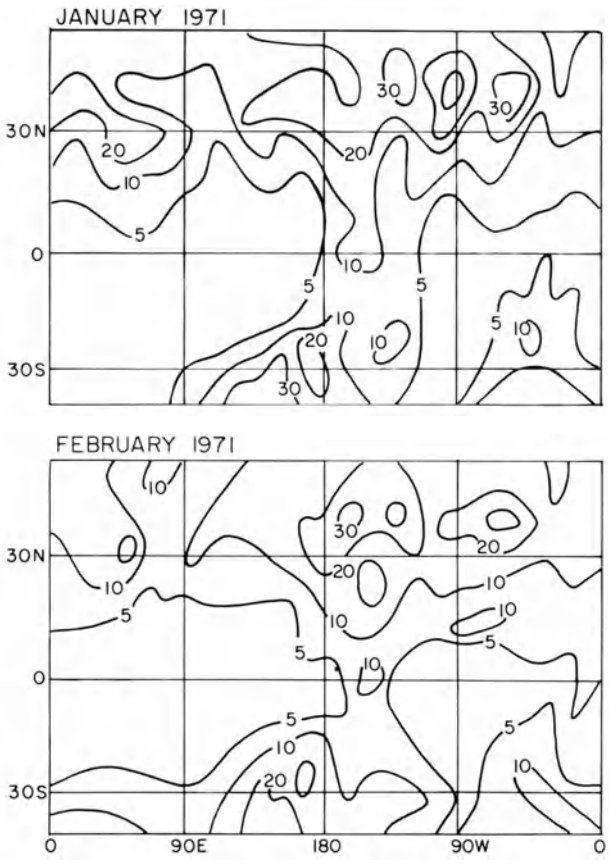

Figure 11

Perturbation kinetic energy distribution at 200 mb for January and February 1971. From MURAKAMI and UNNINAYAR (1977).

each hemisphere. A second maximum, which is somewhat smaller, exists near 45°W. Both regions correspond to locations of slowly varying and strongly tilted upper-tropospheric disturbances (WEBSTER and KELLER, 1975) and centers of anomalously large poleward momentum maxima (WEBSTER and CURTIN, 1975) especially in the Pacific Ocean. Both correspond to regions of mean seasonal westerly winds in the upper troposphere (see Figs. 8 and 12). The Pacific Ocean zone of maximum kinetic energy lies to the south of the upper tropospheric mid-Pacific trough of the northern hemisphere which has been linked to transients of the northern hemisphere summer monsoon (COLTON, 1973). The possible nature of an interhemispheric interaction in these particular locations will be discussed in the next section.

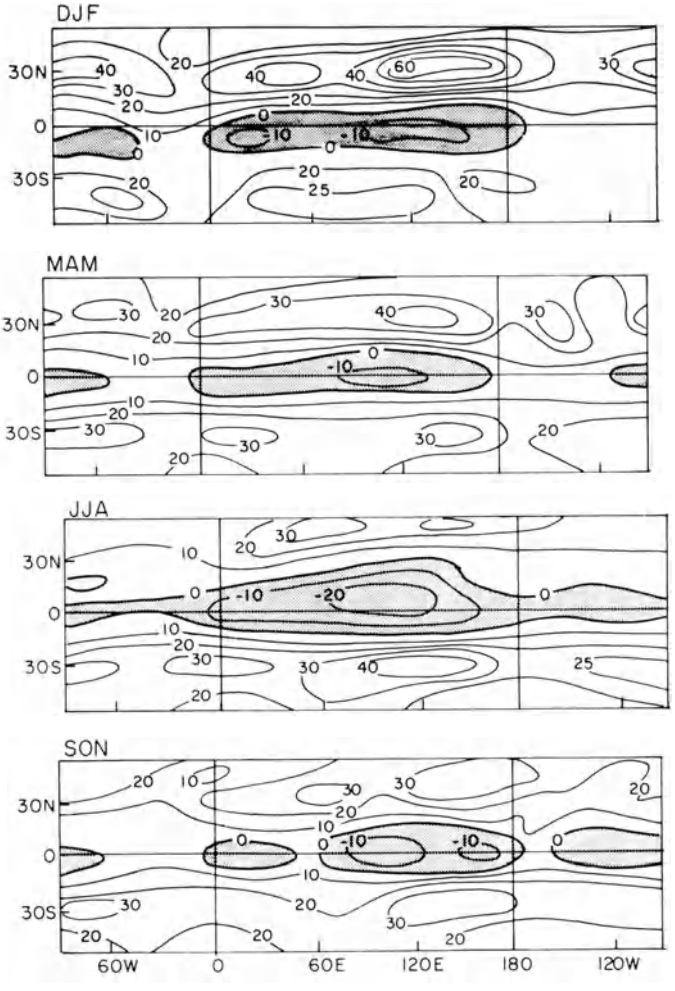

Figure 12
Mean seasonal distributions of the zonal velocity component at 200 mb as a function of longitude and latitude. Shaded areas denote easterly winds. Adapted from NEWELL *et al* (1972), and SADLER (1975).

b. Mechanisms

Few theoretical or numerical studies have considered the transient behavior of the monsoon system on annual time scales. This is because the models are either too simple to allow the inclusion of a land–ocean contrast, in which the ocean is capable of a dynamic feedback, or too complex to allow the required extended integration. As the domain averaged model described in WEBSTER and LAU (1977) was designed to specifically study large-scale phenomena on an annual time scale, we will use it to illustrate physical processes which may be important in determining the manner the large-scale monsoon flow may vary.

To accomplish the investigation we will consider three versions of the domain averaged model all of which contain similar domain configurations shown in Fig. 5. In the first case we will omit a hydrology cycle in order to isolate the annual cycle produced by purely land and ocean contrasts and transient variation in the state of the ocean. Similar experiments are discussed by WEBSTER and LAU (1977b) and LAU and WEBSTER (1977). Here we show results for a three-domain model which is the same as that shown in Fig. 5 except for a second ocean which is added to the east of O2 (LAU, 1977). This allows for a better ocean model in which wind-driven circulations and transportations are included. The improved ocean model is described in detail by LAU (1977). In the second experiment we include a hydrology cycle and in the third experiment allow clouds to interact with both the incoming and outgoing radiation fields. The inclusion of a hydrology cycle and its effects are discussed by WEBSTER and CHOU (1977). The domain configuration used in the latter two experiments is not precisely compatible to that of the first experiment as are the land–ocean domain of Fig. 5 which is considered. However, experiments with a dry version of the one-domain model roughly approximate the condition in the like domain in the three-domain version so that a meaningful comparison may be made.

Figures 13 and 14 show the upper tropospheric zonal velocity component and the surface temperature variation as a function of latitude and time for the three domains. A1 refers to the atmosphere over the eastern ocean, A2 to the atmosphere over the western ocean and A3 to the atmosphere over the truncated land domain. The dashed line in A3 denotes the 18°N coastline and the heavy isopleth in Fig. 14 represents zero zonal wind. Comparing Fig. 13 with Fig. 8, the observed latitude-time sections at specific longitudes, we find considerable similarity. Most importantly, variation in magnitude is a maximum over land where the equatorial easterlies and mid-latitude westerlies are maximum. A similar variation in latitude occurs although perhaps less abrupt in the simulated case. In A1 and A2 the variations are less severe and out of phase with the changes over land. Maxima tend to occur slightly later than over land, which is also apparent in the surface temperature structure shown in Fig. 14 and may be attributed to the phase lag of the ocean surface temperature. Interestingly, the upper atmospheric fields over the ocean tend to *lead* the ocean surface parameters slightly in phase but still lag their counterparts over land. This may be interpreted as an indication of the lateral effect of the continents on the oceans (and vice versa). An interesting similarity between observed and simulated may be seen between the zonal flow in A1 (the upper troposphere over the eastern ocean) and the observed section along 150°W in Fig. 8. Although the model cannot simulate the nuances of the mid-Pacific trough structure due to its extremely coarse longitudinal resolution, it is interesting to note that westerlies are maintained at the equator throughout the year.

Much of the surface temperature structure shown in Fig. 14 was alluded to in the discussion of the zonal velocity component. Most striking is the variation of the temperature over the land and the degree to which the temperature only slightly lags

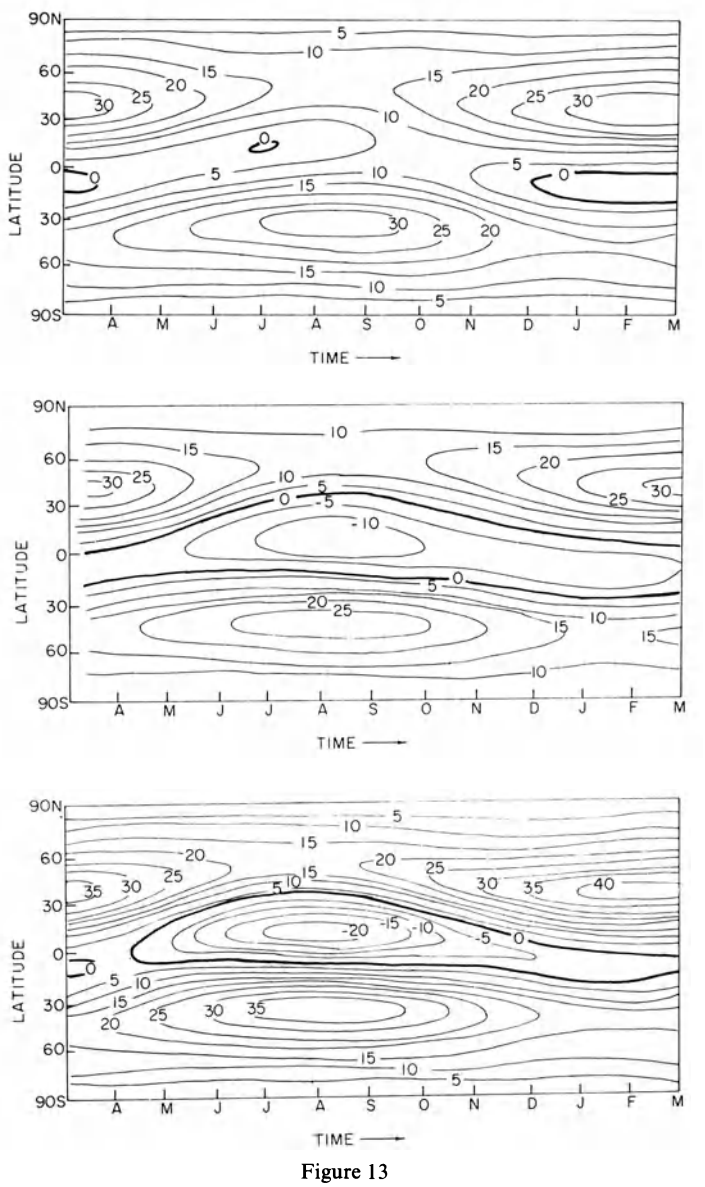

Figure 13
Time-latitude variation of the 250 mb zonal velocity component distribution computed by LAU (1977) for a three domain version of the domain averaged model. See text for details.

the solar variation. Of similar interest is the large lag of the ocean temperature. To the south of the land area a warm water pool develops both to the thermal lag of the ocean and to the adjacent warm land. The anomalously warm ocean has the effect of extending somewhat the warm conditions over the land area into the fall (WEBSTER and LAU, 1977b) and therefore increasing slightly the lag of the surface temperature over land behind the solar variation.

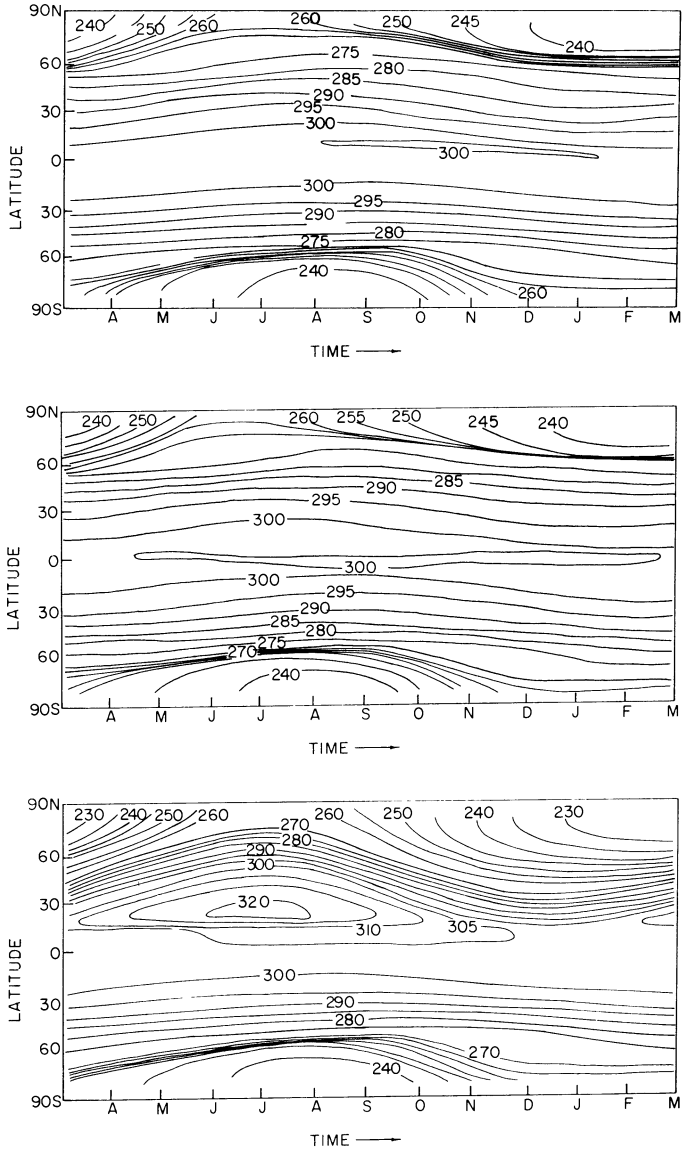

Figure 14
Same as for Fig. 13 except for the surface temperature.

The most important feature noted above is that the inclusion of land into a mobile interactive ocean produces a considerable spatial variation in the annual atmosphere flow, although the transitions between the solstices are somewhat smoother than those noted in Fig. 8. The addition of a hydrology cycle, which allows evaporation, precipitation, the transport of water vapor both in the vertical and the horizontal and

the possibility of moisture build up in the land areas, alters the relatively smooth transition by imposing a significant intra-seasonal time scale on the monsoon flow.

The effect of the hydrology cycle may be best seen by viewing the precipitation rate distribution (10^2 cm yr^{-1}) in the land–ocean domain of Fig. 6. This is reproduced from WEBSTER and CHOU (1977) in Fig. 15. The precipitation rate is also indicative of the vertical velocity field.

The most significant feature of Fig. 15 is the rapid change of the position of maximum precipitation (and therefore maximum upward motion) from south of the equator in middle April to north over the coastal boundary (18°N). Little change in the location of the maximum occurs throughout summer with the precipitation pattern gradually returning to its winter position south of the equator. The rapid transition in late spring may be thought of as a competition between two processes although it should be remembered that this experiment is cloud-free. In the winter the land is cool and the sea surface temperature maximum lies just to the south of the equator. Strong subsidence dominates the northern hemisphere and the ascending leg of the Hadley circulation is highly convective. After the equinox, the northern land mass starts to become warmer (see Fig. 14) which starts to counteract the low-level southward flow of the Hadley circulation. The weak onshore flow is moist and the weak rising motion results in the release of latent heat which counteracts the existing circulation. During the fall as the maximum insolation moves southward the onshore flow gradually weakens but at this stage ground moisture accumulated during the summer provides a local moisture source which may tend to make the autumnal transition somewhat weaker. At this time of year the latitudinal temperature contrast is very weak and the effect of that is further diminished by the local latent heat source.

The results of an identical experiment to that described above, but with a cloud model included, is also shown in Fig. 15. The long-term variation is principally the same. Rapid jumps occur in both cases after the spring equinox but the effect of the clouds is to install a long-period modulation on the precipitation and dynamic fields. Such an effect can be best seen in late June and July which corresponds to the time of maximum heating. From this time on the precipitation pattern occasionally makes abrupt jumps for intervals of roughly five to ten days when the region to the north of the coast becomes dry and precipitation shifts southward to near the equator and also further inland.

The effect of cloud is two-fold. First, in regions of high precipitation, and therefore high cloudiness, the incoming solar radiation is reduced therefore depleting the insolation at the earth's surface. However, this is nearly compensated by the increased opacity of the atmosphere to terrestrial radiation. The overall effect is a slow decreasing surface temperature which instills a long-period reduction on the local heating rate. This continues until the heating of the atmosphere by the adjacent cloud-free regions dominates, shifts the regions of upward vertical velocity both equatorward and poleward and so changes the precipitation distribution. It is interesting to note that during these 'break' periods the precipitation in the equatorial regions is much

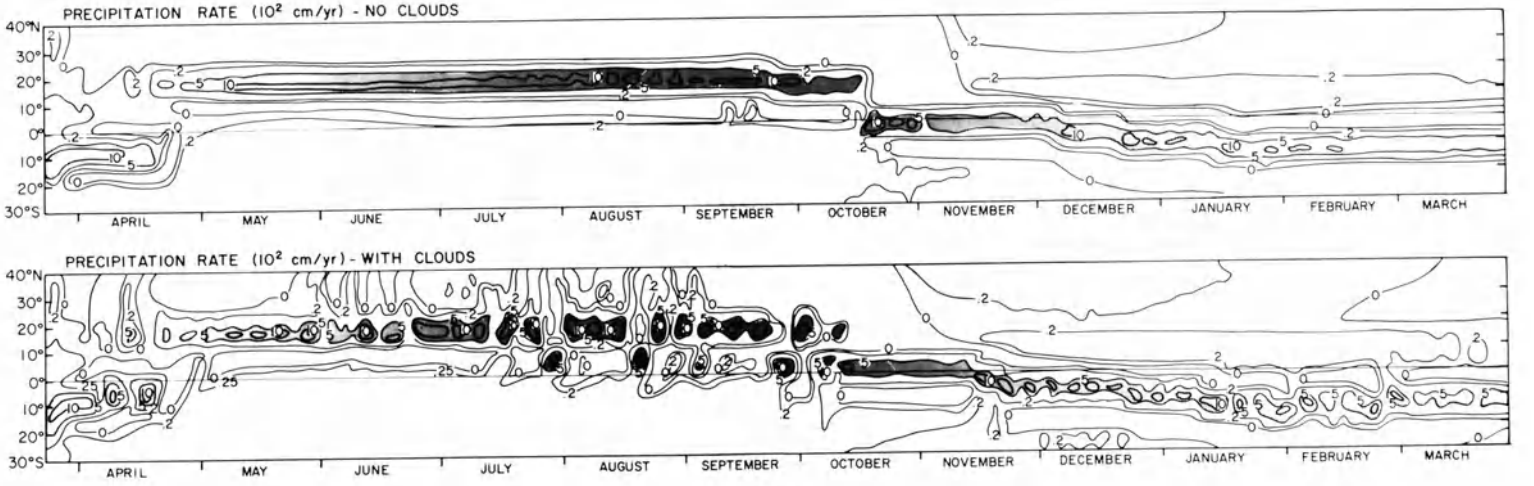

Figure 15
Time-latitude distribution of precipitation rate (10^2 cm yr $^{-1}$) for cloud-free case (upper panel) and for cloud-feedback case (lower panel). From WEBSTER and CHOU (1977).

stronger than that farther inland. Perhaps this is because the model contains no orographic variation. Because of that the general distribution of precipitation is similar to the 'no-mountain' case of HAHN and MANABE (1975).

The results shown in Figs. 13–16 were shown to indicate that a number of factors are of importance in determining the transient behavior of the monsoon system. They were not meant to illustrate attempts to simulate the precise structure of the monsoon but rather to indicate dominant processes.

In Section 3a we indicated that one of the most interesting features of the transient monsoon was the rapid change in the location and strength of the westerly maximum in the southern hemisphere. Some of that character can be noted in the model from Fig. 14 which shows the zonal velocity structure. The strongest westerly winds in the southern hemisphere occur in the lowest panel which corresponds to the land–ocean domain and over the ocean domain to the west. This distribution is consistent with the momentum advection across the equator from the summer monsoon and its convergence into the southern hemisphere. However, the rapid transition noted in Fig. 10 is absent from the model results. VAN LOON (1972) attributes the rapid change of the southern hemisphere circulation in May, not to the effect of the northern hemisphere summer monsoons, but to the rapid cooling of the Australian continent which is emphasized as a cold area by the extremely warm tropical oceans to the north. He concludes that the initial rapid changes in the circulation are instigated in this manner although the momentum flux from the northern hemisphere is of much greater importance later in the southern winter.

The interaction between the hemispheres on shorter time scales is not well understood. Earlier theoretical studies by CHARNEY (1969) and BENNETT and YOUNG (1971) indicate the difficulty of a wave disturbance passing through the equatorial regions which are characterized by basic zonal winds which move westward relative to the phase speed of the wave. The effect of this restriction was to suggest that equatorial regions should be impervious to incident waves. A corollary may be that the hemispheres could be considered independent on time scales less than seasonal. However, MURAKAMI and UNNAINAYEAR'S (1977) data seems to suggest zones or corridors of perturbation kinetic energy bridging the gap between the mid-latitudes, credence to which is added by the observations of WEBSTER and CURTIN (1975). We are thus faced with a paradox. Theory, on one hand, suggests the impossibility of major interhemispheric interactions occurring on relatively short-time scales whereas data implies strong regional interactions. The link between observation and theory perhaps lies in Fig. 13 from which we noted earlier that the regions of high perturbation kinetic energy at the equator corresponded with mean *westerly* winds whereas regions of near-zero energy correspond to mean *easterlies*. If we assume that the basic zonal flow shown in Fig. 12 is maintained by forcing on a much longer time scale than that of the incident disturbances, it is conceivable to speculate that the waves are transmitted horizontally through corridors of weak easterlies or westerlies in much the same way as vertically propagating waves are ducted by distribution of zonal flow

in the vertical (e.g., MATSUNO, 1970). Preliminary investigations are reported by WEBSTER (1977).

4. Some concluding remarks

We have attempted to document and place in perspective the current knowledge of some aspects of the planetary scale monsoon which has been developed from a number of observational and theoretical studies. We have placed particular emphasis on four features of the monsoon circulation: the mean seasonal structure, the seasonal variation, the intra-seasonal variation and interhemisphere interaction. Obvious from the discussion of the results of the various studies is the large degree of uncertainty remaining in a physical interpretation of the monsoon system, even though certain factors, for example the effect of variable oceans, emerge from various studies as critical processes. The following stand out as particular and pertinent problems:

(i) The precise role of the large-scale orography of southern Asia. It remains yet to decide if its influence emanates from its control on mid-tropospheric latent and sensible heat release or from some other, perhaps more obscure, dynamic effect. During winter we can but say that the orographic mechanical effect appears to be important but as yet we have difficulty in appreciating the nuances of atmosphere–orography interaction which may, for example, produce the vast differences between early and late winter in Southeast Asia.

(ii) The interseasonal variation of the southern hemisphere circulation and its relationship to the seasonal variations within the northern hemisphere. Whereas both observational and theoretical studies indicate that the planetary scale monsoons are of interhemispheric scale, the distinct seasonal structure of the southern hemisphere circulation is puzzling.

(iii) The interactive role of the ocean and atmosphere on the seasonal time scale. It appears that the monsoon circulation over land may be affected by oceans both adjacent in longitude and latitude but what are their precise influences on the phasing and variation of the monsoon?

(iv) The intra-seasonal variation of the monsoon circulation both in summer and winter. Variations in the evolving monsoon, such as breaks, are of extreme importance in the forecasting aspects of monsoon meteorology. However, their nature remains basically unknown. Lying in a similar state of uncertainty is the degree to which adjacent hemispheres influence each other on time scales less than seasonal.

Continuation of the progress made towards understanding some of the problems mentioned above may be achieved by further observational and theoretical studies, especially if the two approaches are carried out in concert. Some problems, however, defy extension merely because necessary data does not exist. For problems such as the influence of orography during various phases of the summer and winter monsoons,

for example, there is a special need for detailed and precise measurements. It is hoped that during the winter and summer parts of the Monsoon Experiment to be held during the First-GARP Global Experiment in 1978–79, such data sets will evolve.

Acknowledgment

This work was supported by the Atmospheric Science Section, National Science Foundation, under Grant DES–74–01762.

References

ASNANI, G. C. (1967), *Meridional circulation in summer monsoon of South-east Asia*, Nature *214*, 73–74.

BLACKMON, M., WALLACE, J. M., LAU, N. G. and MULLEN, S. (1977), *An observational study of the northern hemisphere wintertime circulation*, to appear in J. Atmos. Sci. *34*, July.

BENNETT, J. R. and YOUNG, J. A. (1971), *The influence of latitudinal wind shear upon large-scale propagation into the tropics*, Mon. Wea. Rev. *99*, 202–214.

CHANG, C. P. (1977), *Viscous internal gravity waves and low-frequency oscillations in the tropics*, J. Atmos. Sci. *34*, 901–910.

CHARNEY, J. G. (1969), *A further note on large-scale motions in the tropics*, J. Atmos. Sci. *26*, 182–185.

COLTON, D. E. (1973), *Barotropic scale interactions in the tropical troposphere during the northern summer*, J. Atmos. Sci. *30*, 1287–1302.

FINDLATER, J. (1969), *Interhemispheric transport of air in the lower troposphere over the western Indian Ocean*, Quart. J. Roy. Met. Soc. *95*, 400–403.

FLOHN, H. (1950), *Studien zur allgemeinen Zirkolation der Atmosphäre III*, Ber. Dent. Wetterd. *18*, 34–50.

FLOHN, H. (1960), *Recent investigations on the mechanism of the 'Summer Monsoon' of Southern and Eastern Asia*, Proc. Symp. Monsoons of the World.

FLOHN, H. (1968), *Contributions to a meteorology of the Tibetan Highlands*, Atmospheric Sci. Paper No. 130, Colorado State University, 120 pp. (Available from National Technical Information Service, Springfield, VA, 22161, No. PB-182255.)

HAHN, D. G. and MANABE, S. (1975), *The role of mountains in the South Asian monsoon circulation*, J. Atmos. Sci. *32*, 1515–1541.

HAHN, D. G. and MANABE, S. (1976), *Reply to 'Comments on "The Role of Mountains in the South Asian Monsoon Circulation"'*, J. Atmos. Sci. *33*, 2255–2258.

HALLEY, E. (1686), *An historical account of the trade winds and monsoons observable in the seas between and near the tropics with an attempt to assign a physical cause of the said winds*, Phil. Trans. Roy. Soc. London *16*, 153–168.

KOTESWARAIN, P., *Monsoons of the World* (Indian Meteorological Department 1958), p. 105.

KRISHNAMURTI, T. N. (1971a), *Tropical east–west circulations during the northern summer*, J. Atmos. Sci. *28*, 1342–1347.

KRISHNAMURTI, T. N. (1971b), *Observational study of the tropical upper troposphere motion field during the northern hemisphere summer*, J. Appl. Meteor. *10*, 1066–1096.

KRISHNAMURTI, T. N., KANAMITSU, N., KOSS, W. J. and LEE, J. D. (1973), *Tropical east–west circulations during the northern winter*, J. Atmos. Sci. *30*, 780–787.

KRISHNAMURTI, T. N. and BHALME, H. N. (1976), *Oscillations of a monsoon system, Part 1. Observational Aspects*, J. Atmos. Sci. *33*, 1937–1954.

LAU, K. M. W. (1977), *A large-scale ocean-atmosphere interaction model*, Ph.D. Thesis, Department of Atmospheric Sciences, University of Washington, Seattle, July.

LAU, K. M. W. and WEBSTER, P. J. (1977), *Simulation of the annual cycle with a simple interactive ocean-atmosphere model*, to be submitted to *J. Atmos. Sci.*

MATSUNO, T. (1970), *Vertical propagation of stationary planetary waves in the winter northern hemisphere*, J. Atmos. Sci. *27*, 871–883.

MANABE, S., BRYAN, K. and SPELMAN, M. J. (1975), *A global ocean-atmosphere climate model. Part 1. The atmospheric circulation,* J. Phys. Oceanogr. *5*, 3–29.

MURAKAMI, T., GODBOLE, R. V. and KELKAR, R. R., *Numerical simulation of the monsoon along 80°E*, in Proceedings Conf. Summer Monsoon Southeast Asia (ed. C. S. Ramage) (Navy Weather Res. Facility, Norfolk, Virginia 1970), pp. 39–51.

MURAKAMI, T. and UNNINAYAR, M. S. (1977), *Changes in atmospheric circulations during the northern hemisphere winter,* submitted to Mon. Wea. Rev.

NEWELL, R. E., KIDSON, J. W., VINCENT, D. G. and BOER, G. J., *The General Circulation of the Tropical Atmosphere and Interaction with Extratropical Latitudes,* Vol. 1 (MIT Press, Cambridge, Mass. 1972), 258 pp.

PIKE, A. C. (1971), *Intertropical convergence zone studied with an interacting atmosphere and ocean model,* Mon. Wea. Rev. *99*, 469–477.

RADOK, U. and GRANT, A. M. (1957), *Variation in the high tropospheric mean flow over Australia and New Zealand,* J. Meteor. *14*, 141–149.

RAMAGE, C. (1968), *Role of a tropical 'Maritime Continent' in the atmospheric circulation,* Mon. Wea. Rev. *96*, 385–390.

RAMAGE, C., *Monsoon Meteorology* (Academic Press, New York and London 1971), 296 pp.

RAMAGE, C. and RAMAN, C. V. R., *Meteorological Atlas of the International Indian Ocean Expedition*, Vol. 2 (National Science Foundation, Washington, D.C. 1972). (Superintendent of Documents, Washington, D.C., Stock No. 3800–00124.)

RIEHL, H., *On production of kinetic energy from condensational heating* in *The Atmosphere and Sea in Motion,* The Rossby Memorial Volume (The Rockefeller Institute Press, New York 1959), pp. 381–399.

ROSSBY, C. G. *et al.* (1939), *Relation between the intensity of the zonal circulation of the atmosphere and the displacements of the semipermanent centers of action,* J. Mar. Res. *2*, 38–55.

SADLER, J. C. (1975), *The upper tropospheric circulation over the global tropics,* Rept. UHMET 75-05, Dept. of Meteorology, University of Hawaii, Honolulu, 35 pp.

SADLER, J. C., ODA, L. and KILONSKY, B. J. (1976), *The Pacific Ocean cloudiness from satellite observations,* UHMET 76–01, Department of Meteorology, University of Hawaii.

SADLER, J. C. and RAMAGE, C. (1976), *Comments on 'The role of mountains in the South Asian Monsoon Circulation'*, J. Atmos. Sci. *33*, 2255–2258.

SMAGORINSKY, J. (1953), *The dynamic influence of the large-scale heat sources and sinks on the quasi-stationary mean motions of the atmosphere*, Quart. J. Roy. Met. Soc. *75*, 417–428.

STAFF MEMBERS ACADEMIC SINICA, INST. GEOPHYS. METEOR. PEKING (1957–58), *On the general circulation over Eastern Asia I–III*, Tellus *9*, 432–446; Tellus *10*, 58–75 and 299–312.

VAN LOON, H. (1972), *Wind in the southern hemisphere, meteorology of the southern hemisphere, Meteorological Monographs 13* (ed. Chester W. Newton), 283 pp.

WALKER, J. M. (1972), *The monsoon of southern Asia: A review*, Weather *27*, 178–189.

WASHINGTON, W. M. and DAGGUPATY, S. M. (1975), *Numerical simulation with the NCAR global circulation model of the mean conditions during the Asian–African summer monsoon*, Mon. Wea. Rev. *103*, 105–114.

WEBSTER, P. J. (1972), *Response of the tropical atmosphere to local steady forcing,* Mon. Wea. Rev. *100*, 518–541.

WEBSTER, P. J. (1977), *Lateral effects on monsoon systems,* Proceedings of the International Symposium on Monsoons, New Delhi, March 1977, (in press).

WEBSTER, P. J. and CURTIN, D. G. (1975), *Interpretations of the EOLE experiment II, Spatial variation of transient and stationary modes,* J. Atmos. Sci. *32*, 1848–1863.

WEBSTER, P. J. and LAU, K. M. W. (1977a), *A simple ocean-atmosphere climate model: Basic model and a simple experiment*, J. Atmos. Sci. *34*, 1063–1084.

WEBSTER, P. J. and LAU, K. M. W. (1977b), *Simulation of the global monsoon sequence by a simple ocean-atmospheric interaction model*, Proceedings of the International Symposium on Monsoons, New Delhi, March 1977 (in press).

WEBSTER, P. J. and CHOU, L. (1977), *A simple model of monsoon transitions,* to be submitted to J. Atmos. Sci.

(Received 15th June 1977)

Pageoph, Vol. 115 (1977), Birkhäuser Verlag, Basel

Global Vorticity Budget Over the Tropics and Subtropics at 200-mb During Northern Hemisphere Summer

By JAY S. FEIN[1])

Abstract – The large-scale terms in the vorticity equation are evaluated using KRISHNAMURTI's (1971a, b) summer mean winds at 200 mb for a global belt from 25°S to 45°N. The production of vorticity by the divergent wind field is found to be imbalanced over all of the tropical and subtropical belt. As a result there is a requirement for a sub-grid scale (space or time) mechanism which removes negative vorticity from the regions of strong divergence (Tibetan and Mexican highlands) and removes positive vorticity from the regions of strong convergence (mid-oceanic troughs) at 200 mb during northern summer at a rate of approximately 4×10^{-10} sec^{-2}. As suggested by HOLTON and COLTON (1972), in regions of strong and persistent convection, such as the Tibetan Plateau, deep cumulus clouds can account for this transport. However, the mechanism for removing positive vorticity in the vicinity of the upper tropospheric mid-oceanic troughs is still an intriguing and open question.

Key words: Vorticity budget; Upper level tropical and subtropical flow.

Introduction

Over the past several years, studies investigating synoptic and planetary scale vorticity budgets over the tropics and subtropics have shown that sizable imbalances exist when the budgets are evaluated using only the large-scale variables. The balancing mechanism is thought to be vertical advection by subgrid scale convective processes. (See, for example, RIEHL and PEARCE, 1968; WILLIAMS, 1970; REED and JOHNSON, 1974.)

HOLTON and COLTON (1972) diagnosed the 200 mb, northern summer mean vorticity field using KRISHNAMURTI's (1971a, b) observed winds and horizontal divergences. They noted that the summer mean vorticity and divergence fields were nearly exactly out of phase, with centers of maximum divergence at 200 mb coincident with the southeast Asian and Mexican anti-cyclones, and centers of maximum convergence at 200 mb coincident with the mid-Atlantic and mid-Pacific troughs (see Figs. 1 and 2). Therefore, they went on, the generation of vorticity by the field of horizontal divergence could not be balanced by the horizontal advection of vorticity. Such a balance would require a quarter wave phase shift between these two fields. They were, however, able to balance the production of vorticity in their diagnostic

[1]) Department of Meteorology, University of Oklahoma. On leave-of-absence at the National Science Foundation, Climate Dynamics Research Section.

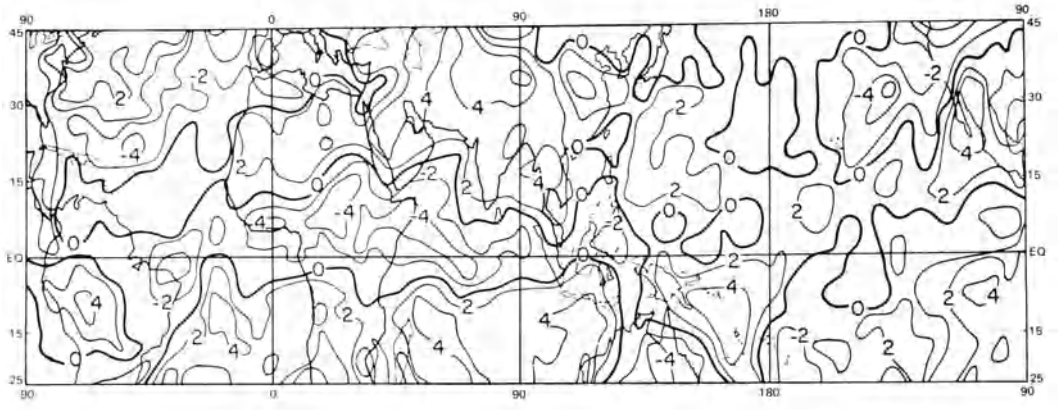

Figure 1
Isopleths of seasonal mean relative vorticity (10^{-5} sec^{-1}). (After KRISHNAMURTI, 1971a.)

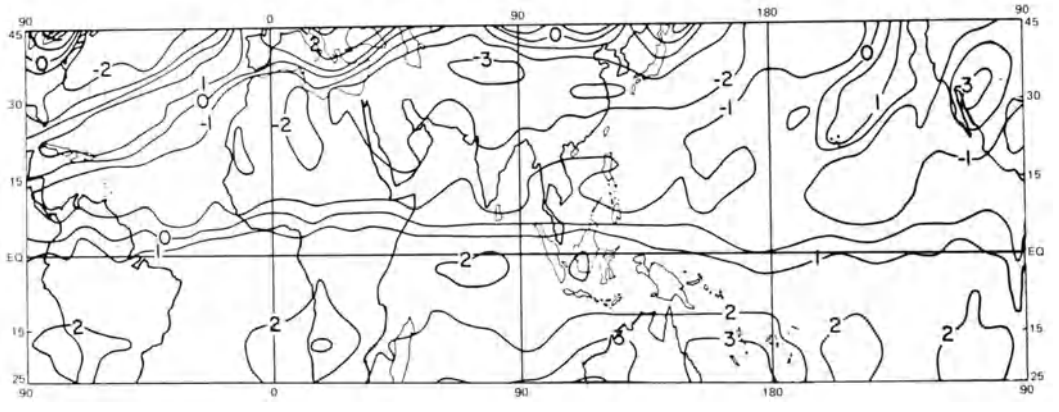

Figure 2
Isopleths of seasonal mean divergence (10^{-6} sec^{-1}). (After KRISHNAMURTI, 1971a.)

model by introducing a viscous drag coefficient which everywhere had the constant value 1.5×10^{-5} sec^{-1}, corresponding to a dissipation time scale of about 19 hours. That balance yielded a solution, in terms of a streamfunction, which resembled closely Krishnamurti's observed streamfunction (see Fig. 3) and they concluded that the observed seasonal mean vorticity and divergence fields at 200 mb were mutually consistent only if the vorticity produced by the divergence field was dissipated on a time scale of less than one day. However, using Krishnamurti's values for the seasonal mean divergence over south Asia, Holton and Colton estimated that deep cumulus towers would convect to the 200 mb level on a time scale of about two days. They further reasoned that because their model failed to account for transient contributions to the production of vorticity, the magnitude of that term could have been overestimated by a factor of three. If that were the case, the time scales for vorticity

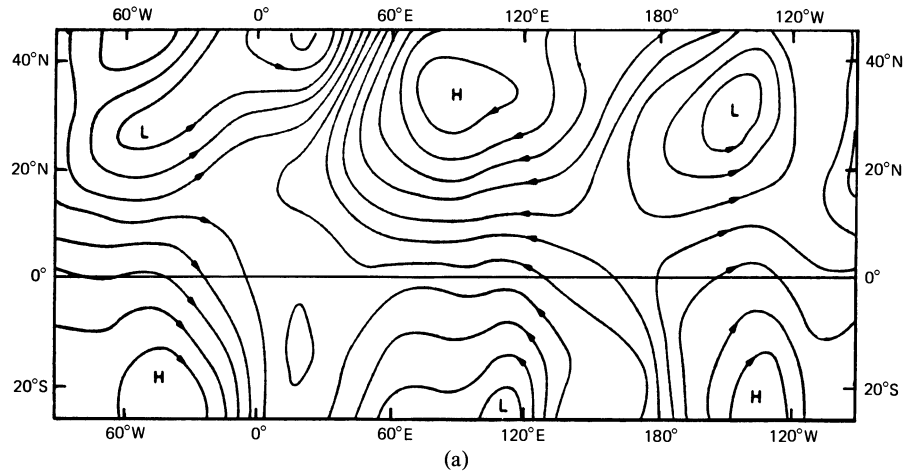

Figure 3

(a) Observed 200-mb perturbation streamfunction (zonal mean removed) based upon Krishnamurti's mean data for June–August 1967. Contour interval is 5×10^6 m^2 sec^{-1}. (After HOLTON and COLTON, 1972.) (b) Perturbation streamfunction computed with Holton and Colton's diagnostic model for a damping rate of $D = 1.5 \times 10^{-5}$ sec^{-1}. Contour interval is 5×10^6 m^2 sec^{-1}. (After HOLTON and COLTON, 1972.)

production by the divergence field and vorticity depletion by sub-grid scale tall cumulus convection, transporting cyclonic boundary layer vorticity to the upper troposphere, would be comparable. Hence, they concluded that the viscous drag term parameterized the vertical transport of vorticity by deep cumulus convection.

Holton and Colton's conclusions concerning the influence of sub-grid scale convection on the large-scale vorticity field at 200 mb are similar to those expressed by the authors of the papers cited above, all of whom computed vorticity budgets for large-scale tropical motions.

A perplexing question arises from Holton and Colton's study. The viscous drag term was used uniformly over the whole of the tropical and subtropical global belt. What then is the physical mechanism acting on a time scale of less than one day (or, given Holton and Colton's argument about their overestimate of the production term, at most two days) which balances the production of cyclonic vorticity over the mid-oceanic troughs? There seems to be no physical basis for invoking convective scale processes as a balancing mechanism in these regions where convective activity is minimal in summer (TAYLOR and WINSTON, 1968).

Is the balance accomplished by nonlinear horizontal advection which Holton and Colton neglected? Both ABBOTT (1973) and COLTON (1973) concluded that nonlinear advection can serve as an important vorticity sink for the forced, quasi-stationary, planetary scales. However, in order to satisfy other requirements of their models they produced vorticity and divergence fields which, unlike those observed, were approximately one-quarter wave length out of phase. Therefore, they, *a priori*, made nonlinear advection of vorticity an important part of the vorticity balance.

This paper reports on an attempt to examine some of these problems by means of a computed vorticity budget using KRISHNAMURTI's (1971a, b) data. Consistent with Holton and Colton's findings, the results indicate that the production of vorticity by divergence is imbalanced in the large-scale vorticity equation over *all* of the tropical and subtropical belt at 200 mb during northern summer, and that these imbalances require a physical mechanism depleting vorticity on a time scale of the order of a day or two.

The budget equation

The vorticity equation used for the budget calculation is

$$\underset{\substack{\text{Time}\\\text{Tendency}\\\text{Term}}}{\frac{\partial}{\partial t}\bar{\zeta}} + \underset{\substack{\text{Horizontal}\\\text{Advection}\\\text{Term}}}{[\bar{\mathbb{V}}\cdot\nabla\bar{\zeta} + \overline{\mathbb{V}'\cdot\nabla\zeta'}]} + \underset{\substack{\text{Beta-}v\\\text{Term}}}{\beta\bar{v}} + \underset{\substack{\text{Generation}\\\text{Term}}}{[(\bar{\nabla}\cdot\bar{\mathbb{V}})(\bar{\zeta}+f) + (\overline{\nabla\cdot\mathbb{V}'})\bar{\zeta}']} = \underset{\text{Residual}}{\bar{R}} \qquad (1)$$

where, $\mathbb{V} = u\hat{\imath} + v\hat{\jmath}$

u = eastward or zonal velocity

v = northward or meridional velocity

$$\zeta = \frac{\partial u}{\partial x} + \frac{\partial v}{\partial y} + \frac{u\tan\varphi}{a}$$

$dx = a\cos\varphi\, d\lambda$

$dy = a\, d\lambda$

λ = longitude

φ = latitude

a = earth's radius

$$f = 2\Omega \sin \varphi$$
$$\Omega = 7.29 \times 10^{-5} \text{ sec}^{-1}$$
$$\beta = \partial f / \partial y$$
$$( ) = \bar{( )} + ( )'$$
$$\bar{( )} = \frac{1}{T} \int_1^T ( ) \, dt$$
$$T = 92 \text{ days (1 June through 31 August, 1967).}$$

The terms omitted in equation (1) are the twisting term, the vertical advection term, and the viscous diffusion term – all of which have been shown to be of relatively small magnitude for large-scale circulations in the upper troposphere by the classical scale analyses of CHARNEY (1947, 1948, 1963) and BURGER (1958) as well as by the earlier budget studies cited above.

Discounting errors of measurement and assuming the omitted terms are indeed small, the seasonal mean residual $\bar{R}$ can be interpreted as a measure of the sum of the sub-grid scale contributions not accounted for by the synoptic scale variables on the left-hand side of equation (1).

Each term on the left-hand side of equation (1) was tabulated directly from Krishnamurti's observed winds and computed horizontal divergences and vorticities at 200 mb on a 2.5 degree square grid around the global belt from 25°S to 45°N. At each of the 4205 grid points the sum of these terms produced a residual $\bar{R}$. Each term, including $\bar{R}$, was Fourier analyzed into zonal harmonics.

Results

Krishnamurti's spectra for the horizontal winds u and v, and the field of stream-function, ψ, showed that most of the variance in the u and ψ fields were contained in the first two or three zonal harmonics. On the other hand, the v spectra was fairly broad with most of the variance in the first 10 zonal harmonics.

Correspondingly, a large proportion of the total variance of the individual terms in the vorticity budget is contained in the first 10 zonal harmonics. For example, the generation term and the residual have, on the average over all latitudes, approximately 75 per cent of their variance in those modes. Moreover, a large part of that variance is contained in the first three zonal harmonics. This is especially true for the generation term, beta-v term, and residual north of 20°N where they account for about 60 per cent of the first ten harmonics. This is, no doubt, a result of the strong forced planetary circulations at these latitudes.

Figures 4 a, b, c, and d show the amplitude of the sum of the first ten zonal harmonics of the horizontal advection term, the beta-v term, the generation term, and the residual, respectively, as a function of latitude and longitude over the tropical and subtropical global strip. At all grid points the time tendency term is at least an order of magnitude smaller than any of the other terms in equation (1) and is not shown.

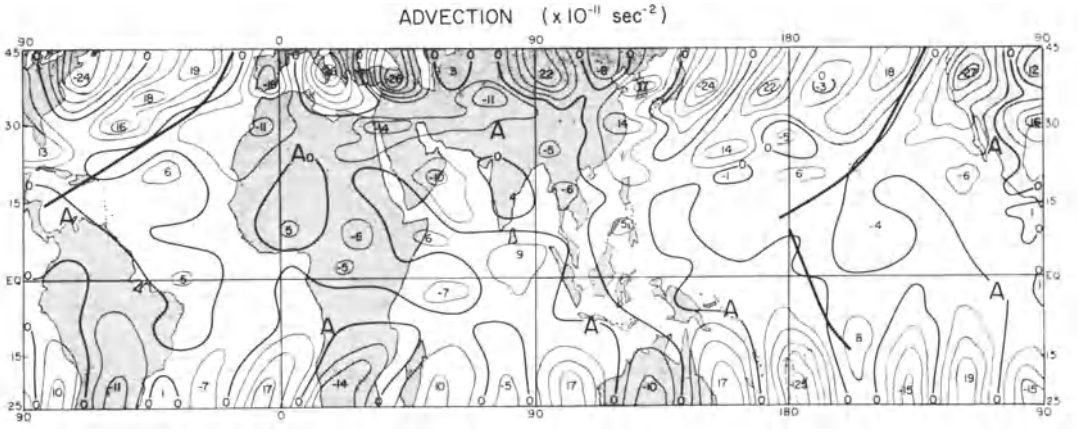

(a)

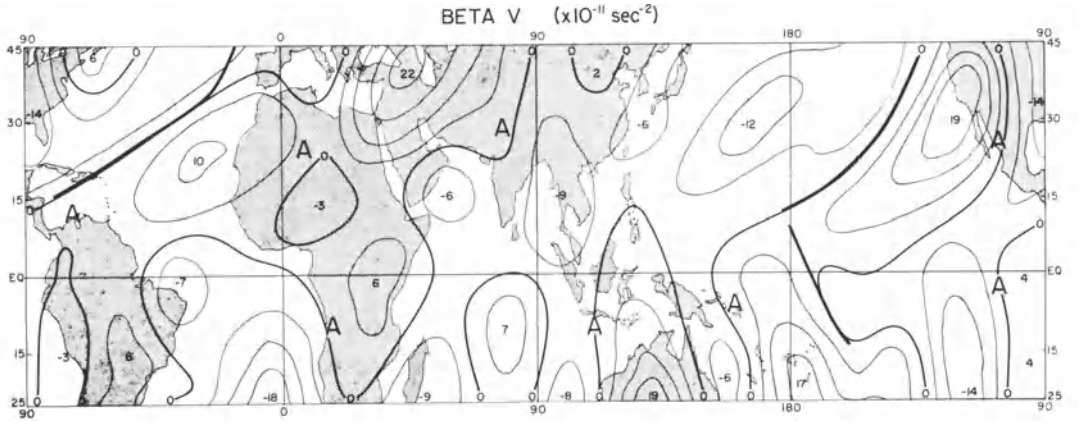

(b)

The anticyclones, designated by '*A*'s', and troughs, designated by heavy solid lines, are the seasonal mean positions.

The salient features of these plots may be summarized as follows:

(1) There are large vorticity imbalances (residuals) over all latitudes.

(2) All terms of the vorticity equation have minimum amplitudes near the equator which increase irregularly with increasing latitude. Leading order terms are about 10^{-10} sec^{-2} in low latitudes and from two to four times larger in subtropical latitudes.

(3) In subtropical latitudes the beta-v term tends to oppose the horizontal advection term, especially in the large scales, but is somewhat weaker. The generation term in these latitudes is largely imbalanced and, thus, strongly

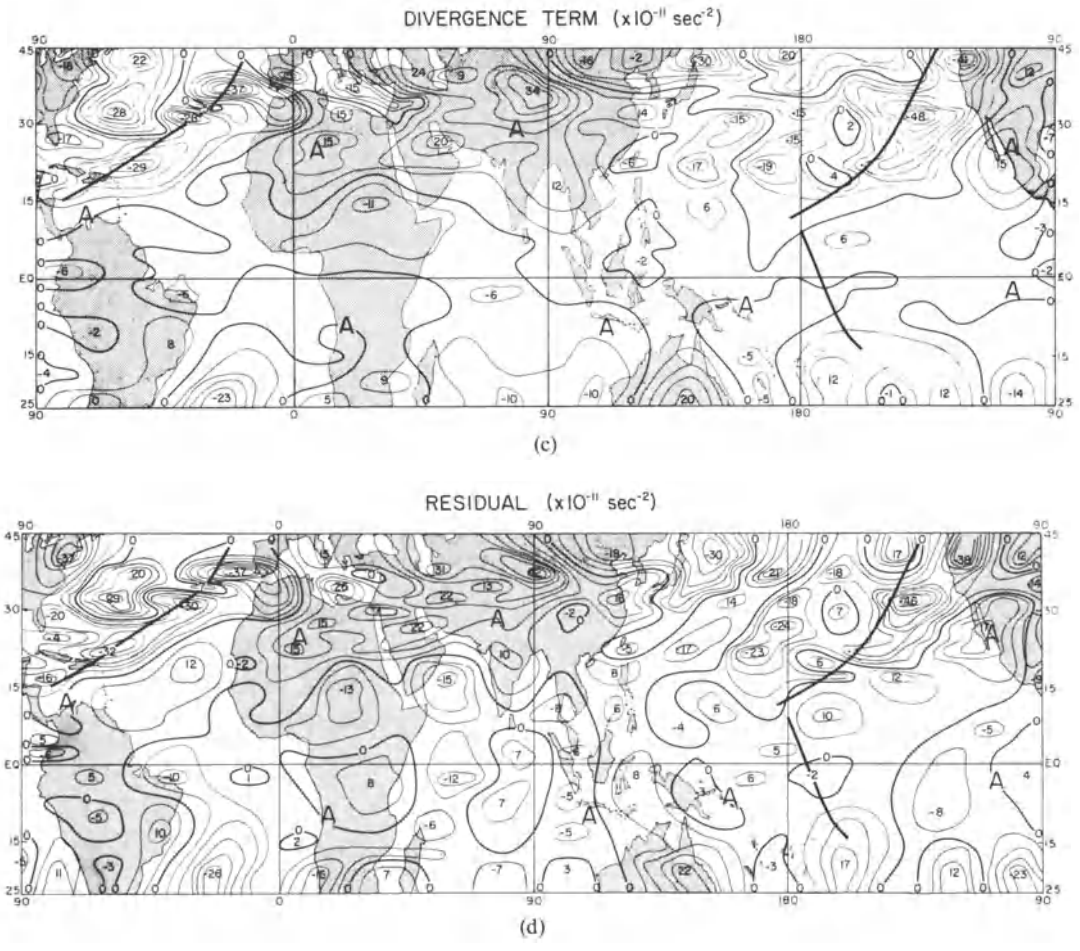

Figure 4

Isopleths of the 200-mb summer-mean terms of the vorticity equation (1). The seasonal mean anticyclones and troughs are designated by 'A's' and heavy solid lines, respectively. (a) Advection, (b) Beta V, (c) Divergence term, (d) Residual.

correlated to the residual. Most striking in the northern hemisphere is the imbalanced cyclonic vorticity generated in the vicinity of the mid-oceanic troughs, and the imbalanced anticyclonic vorticity generated near the Mexican high and along the belt of highs across the South Asian highlands into North Africa. In the southern hemisphere most striking is the strong, largely imbalanced generation of cyclonic (negative) vorticity over the Australian continent and anticyclonic vorticity in the western South Atlantic.

(4) In equatorial regions, where all terms are relatively small, there are no strong correlations evident from the data.

(5) When the stationary and transient parts of each term in equation (1) were evaluated separately it was found that the stationary contribution was approximately equal to the total contribution. This was not unexpected since in the tropics and subtropics the large-scale day-to-day summer fields resemble closely the summer climatology.

These results show that there is a requirement for a sub-grid scale (space or time) mechanism which removes negative vorticity from the regions of strong divergence (Tibetan and Mexican Highlands) and removes positive vorticity from the regions of strong convergence (mid-oceanic troughs) at 200 mb during northern summer at a rate of approximately 4×10^{-10} sec^{-2}. As shown by HOLTON and COLTON (1972), in regions of strong and persistent convection, such as the Tibetan Plateau, deep cumulus clouds can account for this transport. However, the mechanism for removing positive vorticity in the vicinity of the upper tropospheric mid-oceanic troughs is an intriguing and open question.

Acknowledgements

This research was begun at the Florida State University under a 6 month Post Doctoral appointment supported by the National Science Foundation under Grant NSF–GA–17822. The research was continued at the University of Oklahoma, supported by a Junior Faculty Summer Research Fellowship administered by the Office of the Vice Provost for Research Administration. The author offers his sincere thanks for this support.

REFERENCES

ABBOTT, D. A. (1973), *Scale interactions of forced quasi-stationary planetary waves at low latitudes.* Rept. 73–2, Dept. of Meteorology, Florida State University, Tallahassee, 190 pp.

BURGER, A. P. (1958), *Scale considerations of planetary motions of the atmosphere*, Tellus *10*, 195–205.

CHARNEY, J. G. (1947), *The dynamics of long waves in a baroclinic westerly current*, J. Meteor. *4*, 135–162.

CHARNEY, J. G. (1948), *On the scale of atmospheric motions*, Geophys. Publ. *17*, 17 pp.

CHARNEY, J. G. (1963), *A note on large-scale motions in the tropics*, J. Atmos. Sci. *20*, 607–609.

COLTON, D. E. (1973), *Barotropic scale interactions in the tropical upper troposphere during the Northern summer*, Unpublished manuscript, Dept. of Atmos. Sci., University of Washington, Seattle, Wash., 43 pp.

HOLTON, J. R. and COLTON, D. E. (1972), *A diagnostic study of the vorticity balance at 200 mb in the tropics during the northern summer*, J. Atmos. Sci. *29*, 1124–1128.

KRISHNAMURTI, T. N. (1971a), *Observational study of tropical upper tropospheric motion field during northern hemisphere summer*, J. Appl. Meteor. *10*, 1066–1096.

KRISHNAMURTI, T. N. (1971b), *Tropical east–west circulations during the northern summer*, J. Atmos. Sci. *28*, 1342–1347.

REED, R. J. and JOHNSON, R. H. (1974), *The vorticity budget of synoptic-scale wave disturbances in the tropical Western Pacific*, J. Atmos. Sci. *31*, 1784–1790.

RIEHL, H. and PEARCE, R. P. (1968), *Studies on the interaction between synoptic and mesoscale weather elements in the tropics, Part II: Vorticity budgets derived from Caribbean data*, Atmos. Sci. Paper No. 126, Colorado State University, 33 pp.

WILLIAMS, K. T. (1970), *A statistical analysis of satellite-observed trade wind cloud clusters in the western North Pacific.* Rept. No. 161, Dept. of Atmospheric Science, Colorado State University, Fort Collins, 1–80.

(Received 15th June 1977)

Pageoph, Vol. 115 (1977), Birkhäuser Verlag, Basel

Some Aspects of the Life History, Structure and Movement of Monsoon Depressions

By D. R. SIKKA[1])

Summary – Monsoon depression is one of the most important synoptic scale disturbances on the quasi-stationary planetary scale monsoon trough over the Indian region during the summer monsoon season (June to September). Salient features of the climatology of the depressions with regard to frequency of cyclogenesis, life expectancy, horizontal scale and tracks are discussed. Rainfall aspects of the depressions are discussed in some detail and the role of local, dynamical and sub-synoptic scale factors are brought out. Work done on the life history such as formation, intensification and maintenance of depressions has been reviewed based on synoptical and theoretical approaches. Structure of the depression based on composited, synoptical and dynamical studies is discussed. Wind circulation, thermal and moisture patterns, vertical motion field, vorticity budget etc., of a recent case study are brought out in some detail. The problem of movement of the depression against the low level basic westerly wind is briefly discussed and the results of several numerical and climatological prediction models are presented.

Key words: Monsoon depression.

1. Introduction

Monsoon depression is one of the important synoptic scale tropical disturbances which forms periodically on the quasi-stationary monsoon circulation prevailing over the Indian region during the southwest monsoon season of June to September. Its existence and pre-eminent position as a rain producing system was recognised by ELIOT [18] in the very early years of synoptic meteorology in India. In the words of Eliot, 'Cyclonic storms or disturbances are a regular and frequent feature of the whole southwest monsoon period. Atmospheric whirls of all degrees of intensity and magnitude pass up from the Bay of Bengal to the coastal districts and interior of India.' He named a class of these whirls as 'The smaller or the Minor storm' which subsequently came to be known as the monsoon depression. As per the current definition followed in the India Meteorological Department, low pressure systems are referred to as depressions when surface winds in cyclonic circulation are between 17 to 33 nautical miles and pressure gradient between the centre and at a distance 250 km from it ranges between 5 to 13 mb. Depressions in which the wind speed exceeds 33 nautical miles are termed as cyclonic storms.

[1]) Indian Institute of Tropical Meteorology, Poona 411 005, India.

Since the first work of Eliot on this subject, several research workers have contributed to the study of monsoon depressions. It would be our endeavour in this article to review the massive work on this subject and bring to the fore the pertinent questions on which our knowledge is still rather sketchy. As further intensive study of monsoon depression is one of the important objectives of the forthcoming MONEX 1979, it may be expected that the additional intensive data proposed to be collected during this international experiment would fill vital gaps in our knowledge.

2. *Climatological aspects of monsoon depression*

2.1. *Monsoon environment*

Monsoon depression has to be considered in the overall setting of the large scale southwest monsoon circulation over the Indian Ocean region. The monsoon system owes its existence primarily to complex interactions of the annual cycle of solar heating and differential heating of land and sea surfaces and the peculiar geographical position of India. Exhaustive discussion of the large scale monsoon environment over the Indian region is given by RAMAGE [46] and RAO [48]. KRISHNAMURTI and BHALME [31] have brought out the important oscillations in various parameters of the broad scale monsoon system. Broad scale monsoon circulation features which are relevant to the formation and life history of monsoon depressions are: (i) lower tropospheric heat low over Pakistan and the monsoon trough stretching from it across the Gangetic valley towards the Bay of Bengal and southeast Asia, the lower tropospheric air converging in the vicinity of the trough region; (ii) upper tropospheric warm anticyclonic circulation centred over Tibet with its ridge extending up to very large distances in the east–west direction; (iii) markedly high temperature in the lower troposphere (up to 700 mb) over Arabia and rather lower temperature over India and southeast Asia in the monsoon trough region; (iv) temperature gradient in the meridional direction in the troposphere with the higher temperature centred near about 30°N; (v) comparatively warmer sea surface temperature than the surface air temperature over the Bay of Bengal and the northeast Arabian sea; (vi) higher moisture content of the air particularly in the layers 700–500 mb between 70°–100°E and 15° to 25°N; and (vii) horizontal and vertical shears dominating the zonal wind flow in the lower and upper troposphere. Monsoon depressions form over the warm surface of the Bay of Bengal within the moist environment of monsoon air and move in the west or northwest direction along the monsoon trough towards the warmer and drier environment of the heat low system over western India and Pakistan.

2.2 *Frequency of formations and mean track*

Systematic records about the monsoon depressions are available from the year 1891 onwards. The data published by the India Meteorological Department shows

that the depressions form over the Bay of Bengal, east Arabian sea and even over land but the contribution of the Bay of Bengal systems is by far the largest (over 80 percent of the total) and the Arabian sea being the smallest (less than 10 percent). Although the average number of depressions which form in each of the four months of the season (June to September) varies roughly between 2 to 2.5, yet the scatter in individual years can be large. There is a very high probability (over 80 percent) for the formation of at least one system in each month of the season but the probability of formation of four or more systems in a month is very small.

An examination of the number of depressions based on decadal averages shows that the number of depressions which formed in the decades 1951–60 and 1961–70 have decreased by about 25 percent over the average. RAO and JAYARAMAN [47] had examined the data based on the period 1891–1950 and concluded that there was neither trend nor periodicity in the series of monsoon depressions in the Bay of Bengal. However, BHALME [4] fitted orthogonal polynomial to the 80 years series (1891–1970) and found a significant decreasing trend in the number of monsoon depressions.

PAUL and SIKKA [40] have studied various climatological aspects of the low pressure systems during the monsoon season. Table 1, which is based on their study, shows that there is a wide scatter in the time interval between the successive formation of two depressions. This interval may be as small as 3 days and may even exceed one month.

Table 1

Frequency distribution of the time interval between two successive monsoon depressions during July and August

	Time interval between two successive depressions (days)								
Total No. of depressions in the period 1891–1970	1–2	3–5	6–8	9–11	12–15	16–20	21–25	26–30	More than 30
	7	46	74	32	30	28	23	13	46

However, a very large number of depressions have formed in the interval ranging between 3 to 15 days in comparison to the interval ranging between 16 to 30 days. Climatological life expectancy of monsoon depressions ranges between 2 to 5 days in the majority of cases and hardly 10 percent of the systems have existed beyond 6 to 7 days. Paul and Sikka have also examined the frequency distribution of horizontal distances which separate two co-existing low pressure systems within the monsoon trough. The most frequent separation is between 1100 to 2000 km, which gives an estimate of the scale of monsoon depressions.

Individual depressions during July and August follow a track which is quite close to the mean track which runs in a west to northwest direction. Based on the

latitudinal positions of the depressions crossing each degree longitude of the tracks and the standard deviation of the positions corresponding to each longitude, a mean track and an envelope of the track with twice the standard deviation on either side of the mean track are shown in Fig. 1. The scatter of the tracks during the months of June and September is larger and the depressions in these two months recurve in a northerly to northeasterly direction in a good number of cases.

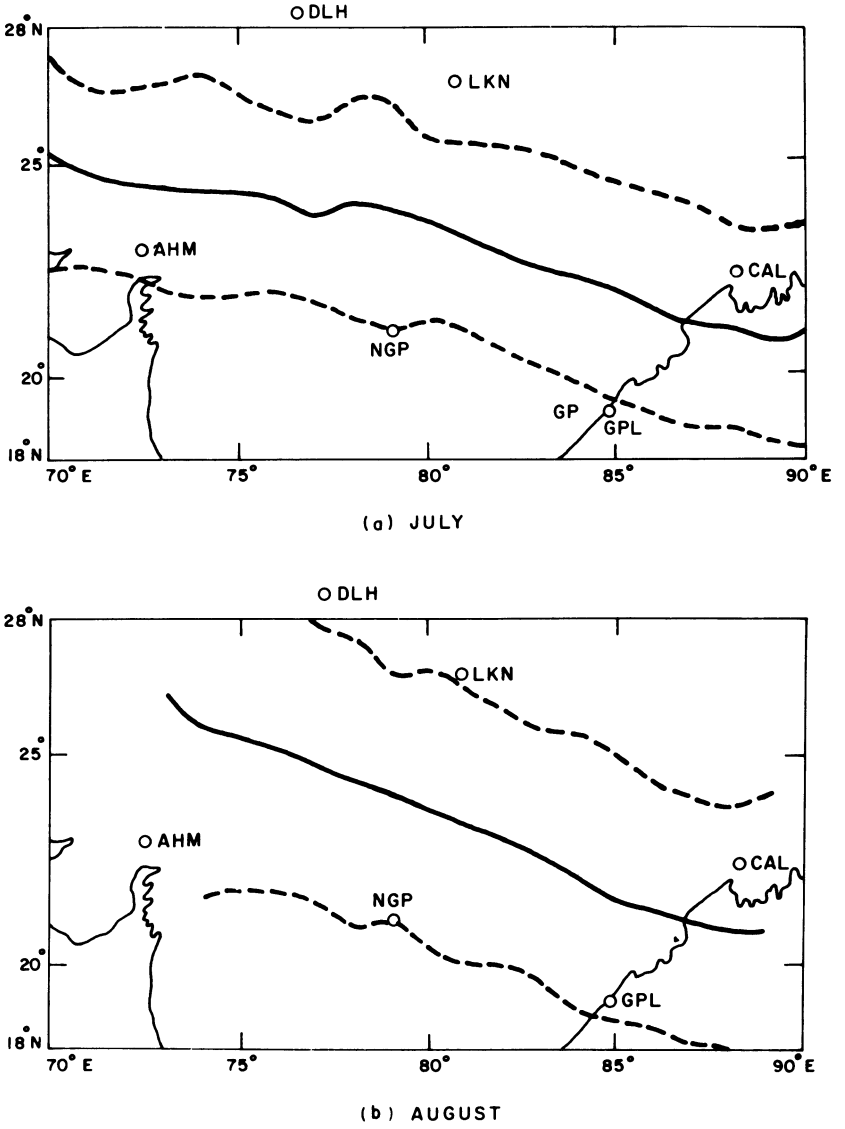

Figure 1
Mean track (full line) of monsoon depressions and envelope of twice the standard deviation (broken lines) on either side of the mean track – (a) July and (b) August.

2.3. Studies on rainfall associated with monsoon depressions

Rainfall over various parts of India during the southwest monsoon season is known to occur in spells. These spells are associated with different synoptic scale and mesoscale systems. As already mentioned, the most important large scale feature in the lower troposphere over India is the monsoon trough. The region of the monsoon trough is characterised by large-scale cyclonic vorticity, moisture convergence and upward motion. The trough oscillates in position and intensity and distributes rainfall over different parts of India, particularly in the region covered by the latitudes 20–30°N. Monsoon depression, which is the most important synoptic scale disturbance on the monsoon trough, is known to play a vital role in the space and time distribution of rainfall. Generally 24-hourly accumulated rainfall in association with a depression is 10–20 cm and isolated falls exceeding 30 cm in 24 hours are also not uncommon. Various aspects of the rainfall associated with monsoon depressions have been studied by several workers.

The earliest studies by Eliot showed that the rainfall around the depression was usually heavy and continuous over a well defined area and beyond this area it was almost negligible in amount. According to his studies, the heaviest rainfall occurred in the southern and eastern quadrants when the depression lay over Bengal and adjacent region and in the southwestern quadrant when it lay farther west over central and western India – the northern half of the depression getting only light rainfall. This general picture of the rainfall in association with monsoon depression has been hardly altered by subsequent studies. PISHAROTY and ASNANI [39] found that in west to northwest moving cases on any particular morning, heavy rainfall ($\geq$ 7.5 cm in preceding 24 hours) extends to about 500 km ahead and 500 km in the rear of the depression centre and this area has a width of about 400 km lying almost entirely to south of the track. Thus, the heavy rainfall over the subsequent 24 hours on a particular day is distributed up to a distance of about 1000 km ahead of the depression centre on that day. This indicates that the strongly ascending branch of the depression circulation extends about 1000 km ahead of the centre and about 400 km to the south of the centre. LAL [33] and BEDDEKAR and BANERJEE [3] have found general confirmation of the above aspects of depressional rainfall for slow as well as fast moving depressions. The zone of maximum rainfall is found to shift to northwest and then to northeast with the depressions changing path from northwest to north and then to northeast. MOOLEY [35] has made an exhaustive study of the depressional rainfall based on 70 year data. His study shows the following important features:

(1) Depression days constitute about 7 percent of total number of days during July and August up to 80°E and decrease to about 2 percent along 75°E.
(2) The contribution of the depression-associated rain to the total rain is about 11 to 16 percent in the left sector all along the track. However, the efficiency of the depression as a rain-giver increases rapidly to the west of 80°E.

(3) In the left sector mean rainfall per depression day increases westwards, the increase being more marked west of 80°E.
(4) Gamma probability model is a good fit to the depression rainfall in each of the four quadrants.

DHAR and BHATTACHARYA [15, 16] have shown that the distribution of depression rainfall to the total rainfall of the season in the basins of the rivers Ganges and Godavari is only about 8 to 12 percent. RAGHAVAN [43] showed that the monsoon depression is capable of redistributing the rainfall over India in such a way that in some areas (about a third of the country) the rainfall is increased (by about 10 percent) while in some other areas (about a third of the country) it is decreased (by about 10 percent). The increase of rainfall is noticeable not only within the field of depression circulation but also over regions far away from the depression such as the Punjab, West coast of India and Western India. The decrease in the rainfall occurs over the regions which lie to the north of the track. SIKKA and ANANTHAKRISHNAN [55] found that the depression organises the large-scale vertical motion in a well defined manner with upward motion in the depression field and slow sinking motion in the region surrounding the depression which accounts for the characteristic distribution of rainfall in the depression field.

From the various studies discussed above, it would appear that the contribution of the depressional rainfall to the total rainfall is rather small. This impression is further strengthened by the fact that there is not much relationship between the number of monsoon depressions and the monsoon rainfall in a year. However, we cannot underestimate the importance of the depression to the monsoon rainfall if we consider the following:

(1) In several years the advance of the monsoon over different parts of the country follows the formation of a depression and its movement.
(2) Formation of a depression is accompanied by the activation of the monsoon trough and in general the rainfall begins to increase 2–3 days prior to the actual intensification of a low pressure system into a depression and the increased rainfall activity is maintained for 2–3 days after the depression weakens into a low pressure area.
(3) A prolonged spell of dry weather during the season is usually broken by the formation of a monsoon depression.
(4) A monsoon depression in the Bay of Bengal is observed to trigger another low pressure area or mid-troposphere cyclone (MILLER and KESHAVAMURTY [34] along the west coast of India.
(5) Movement of two depressions along about the same track within a few days of one another causes heavy floods in the river basins along the tracks.
(6) Considerable amount of rainfall during the season occurs in association with low pressure areas which marginally differ from the characteristics of depressions.

Short duration rainfall based on self-recording raingauge data in association with the monsoon depression have also been studied. RAGHAVAN [44] observed that the depressional rainfall was (i) mainly convectional; (ii) there were alternate bands of wet and dry zones, the western most limit of the wet zone being at a distance of 300 km, and (iii) each wet zone was about 30–35 km wide and dry zone being 50–80 km wide. This study, however, related to the low intensity rainfall regions of the depression field and not to the southwest sector where the rain is observed to be continuous with occasional heavy convective showers. VENKATARAMAN *et al.* [62] have found diurnal variation in the intensity of depression rainfall with maximum rain occurring in the early morning hours over Central India.

Several suggestions have been put forward to explain the characteristic distribution of depressional rainfall. ELIOT [18] was of the view that the rainfall was brought about by the strong moisture bearing winds which condensed their water due to ascending motion taking place in the vicinity of the depression. Some other workers (RAMANATHAN and RAMAKRISHNAN [45]; DESAI and KOTESWARAM [14]) thought that the preferential rainfall in the southwest sector of the depression was due to upglide motion of the easterly warmer air rising over the westerly cooler air at or near the partition of the two air currents. Convergence within the isobaric channels and consequent upward motion was yet another mechanism suggested by MULL and RAO [38]. KOTESWARAM and BHASKARA RAO [27] observed that the heavy rainfall occurred over the area of warm air advection in the lower and middle troposphere. The heaviest rainfall occurs in the intense convergence zone between the north to northwesterly winds and the westerly monsoon current. However, the rainfall potential of monsoon depressions shows large variability from case to case which may depend upon local, dynamical and sub-synoptic scale factors.

Recent computations of vertical motion field by several workers suggest that different factors contribute towards enhancing the vertical motion in the southwest sector of the depression and sinking motion in the rear of the depression track. The main moisture source of the monsoon depressional rainfall is the southwesterly to southerly monsoon air which enters the depression field from the left sector. Boundary layer convergence of moisture flux contributes nearly 60–70 percent of the total moisture convergence. Although regions of rainfall and dynamically computed large-scale vertical motion fields are generally coincident, the heavy rainfall of 10 cm or even more in the vicinity of the depression emphasises the role played by convection, mesoscale circulations and other local features.

3. Life history of monsoon depressions

Monsoon depression passes through a well defined life cycle which covers about a week from the formation stage to the decay. We now discuss the general features associated with the formation, development and maintenance of these depressions which have been known as a result of several case studies by different investigators.

3.1. Formation stage

Climatology shows that monsoon depressions generally form in the northern portion of the Bay of Bengal. The zone of formation is in the head of the Bay during July and August and over the central Bay during June and September. This zone during the season is a favourable region for cyclogenesis. Several of the conditions mentioned below which prevail over the region may contribute to the formation of a depression. They also point out that the mechanism of the conditional instability of the second kind (CISK) may be important in the formation of monsoon depressions.

(i) The sea surface temperature is quite high ($>29°C$).
(ii) The lower tropospheric semi-permanent monsoon trough dips into the north Bay of Bengal and thus the low level cyclonic vorticity is usually present. The monsoon trough always shifts into the Bay before a depression forms.
(iii) This cyclonic vorticity is more in the curvature of the flow as the southerly component of the wind increases from the eastcoast of India to the coasts of Burma and Bangladesh and as such a small perturbation in the pressure field is seen in the form of a closed cyclonic circulation.
(iv) Monsoon southwesterlies are converging current downstream from peninsular India towards the Bay of Bengal.
(v) Upper tropospheric circulation in the region is anticyclonic as well as divergent in the mean and this geometry of the flow has a favourable influence on the lower tropospheric flow from the point of cyclogenesis.
(vi) Above mentioned quasi-permanent features result in more frequent organised cloud cluster formations over the northern Bay of Bengal.
(vii) Favourable locations of the hills of Burma and northeast India.

Synoptic factors which generally precede the formation of the depression and are considered favourable for cyclogenesis are the following:

(i) Fall of pressure in the north Bay of Bengal without any significant fall or rise in other parts of the monsoon trough.
(ii) This fall of pressure occurs either *in situ* or in association with the movement of a low pressure area from the east which was considered by DORAISWAMY [17] as the remnant of a typhoon. Low pressure areas moving from the east account for only about 20 percent of the total number of formations in the season. On most of the occasions these westward propagating 'lows' can only be seen in the 24-hour pressure change field.
(iii) Strengthening of the monsoon current over the Peninsular India and central Bay of Bengal to over 20 mps which is thought to be associated with fresh surge of cross-equatorial air. This increases the cyclonic wind shear in the north Bay.
(iv) Formation of the initial centre of cyclonic circulation in the lower and

middle troposphere (800 to 600 mb), its intensification and gradual descent to the sea level (DESAI [13]).

(v) Increase in the moisture content of the air within the middle troposphere (700–500 mb) over north Bay of Bengal.

(vi) Increase in rainfall activity over the Bay Islands and the coastal regions of Burma, Bangladesh, Orissa and West Bengal.

(vii) Increased divergence in the upper troposphere over north Bay of Bengal as evidenced by (a) diffluence of the flow at 200 mb (b) downstream increase of easterlies/north-easterlies from Bangladesh to west Bengal, (c) westward migration of perturbations in the upper tropospheric easterlies over west Bengal, (d) favourable shift in the position of seasonal anticyclonic circulation over the Tibetan region [25, 26, 27]. However, on several occasions a mere visual examination of the routinely analysed upper tropospheric charts may prove rather disappointing to suggest the presence of these features.

(viii) Persistence of a quasi-circular bright cloud mass (diameter 4–5 degrees) which is usually to the south of the surface centre of the low pressure area in the initial stage of formation.

(ix) Eastward movement of a north–south trough in the lower troposphere lying over Orissa and Bihar towards the north Bay resulting in the formation of a depression.

3.2. Mechanisms for the development of monsoon depressions

The problem of offering a satisfactory explanation to the intensification of low pressure systems into monsoon depressions has been investigated by several research workers. Several possible mechanisms have been suggested based on synoptic and theoretical considerations.

3.2.1. Synoptic-dynamical views. ELIOT [18] thought that as the monsoon rains over upper India are oscillatory in character, the intervening spell of light rain (break monsoon) after a spell of good rain is associated with slack pressure gradient over upper India and consequent light wind conditions prevailing during the lulls in the rains. As the monsoon winds are still strong farther south in the Bay, favourable conditions are present in the intervening region of maximum cyclonic shear. Eliot inferred that cyclonic vorticity in the north Bay, horizontal convergence in the lower levels and upward motion within moist monsoon current lead to cloud build up, heavy precipitation and release of latent heat which are responsible for the development and maintenance of the monsoon depressions.

Under the impact of the development of air mass school in the tropics several Indian meteorologists applied frontal models in order to explain the formation and intensification of monsoon depression (ROY and ROY [50]; RAMANATHAN and RAMAKRISHNAN [45]; DESAI [13] and DESAI and KOTESWARAM [14]). Much of this work was done with the surface and pilot balloon data. These workers were

chiefly guided by the colder temperature of the onrushing fresh monsoon airmass in comparison to the airstreams prevailing over the Indian region. The prevailing airmass over the region is usually somewhat warmer being particularly so if the depression is forming after a considerable lull in the rainfall activity. With the introduction of upper air soundings in India doubts were raised about the existence of airmass contrasts in the temperature field by MULL and RAO [38] as well as by other workers and the concept of airmass in the formation of monsoon depression was subsequently dropped.

DESAI [13] suggested that in some cases the centre of the cyclonic circulation first appears in the middle levels at 2 to 4 km which subsequently extends towards the surface level with the intensification of the 'low.' He also laid stress on the importance of the Arakan hills and Himalayas in the formation of the depressions. The exact mechanism through which the mountains play their envisaged role is however not clear. The formation of the depression is clearly related to the strengthening of the easterly flow in the lower troposphere to the north of the centre, i.e., along the foot hill regions of Burmese mountains and Himalayas. Such a situation occurs when the monsoon trough shifts southward into the head Bay of Bengal. The strengthening of the easterly winds may be associated with the accumulation of potential vorticity in these easterlies which may enhance the trough in the north Bay of Bengal.

KOTESWARAM and GEORGE [25, 26] and KOTESWARAM and BHASKARA RAO [27] drew analogy of the development of the monsoon depression to the mid-latitude cyclone and applied the dynamical concepts of PETTERSSEN [41]. They suggested that the intensification of the monsoon depression occurs under the favourable association of the upper tropospheric divergence and the lower tropospheric convergence. According to them favourable mechanism in the upper troposphere was provided periodically by westward propagating disturbances or by the divergence in upper tropospheric strong easterly flow. These features are associated with upper level positive vorticity advection which favour upward motion and low level convergence in the north Bay of Bengal. A schematic model after them is given in Fig. 2. These concepts are based essentially on quasi-geostrophic development and may be valid in individual cases. However, synoptic experience shows that there are several

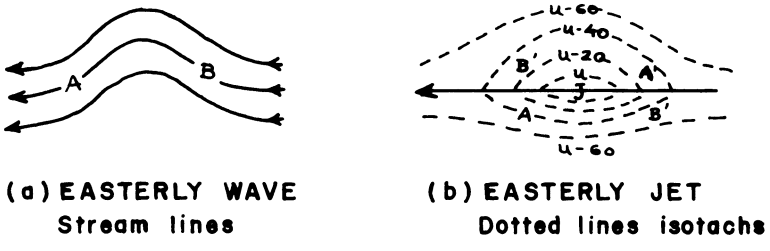

Figure 2
Models of upper tropospheric perturbations leading to cyclogenesis in the north Bay during the monsoon season (KOTESWARAM and GEORGE [26]).

cases when the development of the depressions takes place without any significant changes in the upper tropospheric circulation occurring prior to the time of intensification. Many a time the upper tropospheric easterly wave is seen after the depression has intensified. Besides, the observation that these waves do not show any systematic progression leads to the impression that the easterly wave at 200 mb may itself be an indication of the vertical extension of the depression in its most intense stage. However, no systematic and detailed investigation of the problem has been carried out and lack of upper air data in the region makes it difficult to examine all these factors in a conclusive manner.

A few other associations of the upper level features with the development of monsoon depressions are the formation of the warm pools at 200 mb in the north Bay of Bengal (MOWLA [36]) and the appearance of 'cutoff lows' in the mid-latitude westerly troughs which may induce a perturbation in the easterlies over the head Bay of Bengal (PRASAD and KRISNA RAO [42]).

Satellite photographic and radiation data have also been used to study the formation of monsoon depressions. SRINIVASAN, RAMAN and RAMAKRISHNAN [60] related the cloud organisations with different stages of the development. They found that the evolution of a depression from a low pressure area is characteristically seen in the organisation of cumulonimbus bands to the north of the depression centre as the heavy bright overcast to the south of the depression field obscures the structure. At the stage of a 'low' (easterly winds to the north being weak) the cumuliform bands are usually absent. These bands appear and get more organised with the intensification from a depression to a deep depression stage (lower tropospheric easterlies to the north being 10 to 20 mps strong). SIKKA [53] found that the cloud tops reach a height of about 14 km at the intensification stage of the depression: SIKKA and MOORTHI [56] have shown that the non-adiabatic effects due to differential infra-red cooling within the deep convective regions and the surrounding cloud-free regions contribute to the generation of positive vorticity in the depression field.

3.2.2. Theoretical approaches. The development of monsoon depressions has been studied within the framework of instability theory by a few workers. DAGGUPATTY [8] applied the linear instability analysis to quasi-geostrophic and primitive equation models and concluded that the waves are not baroclinically unstable under the prevailing vertical wind shears and the value of the coriolis parameter over the Indian region unless the static stability parameter is considerably reduced. BRAHMANANDA RAO [6] found that during the 'break' monsoon period, barotropic instability in the upper tropospheric flow prevails between the region of strong easterlies over India and strong westerlies to the north of India which may be an important factor for the development of monsoon depressions. In an observational study based on day to day examination of upper tropospheric winds over India for two monsoon seasons, SIKKA and GADGIL [57] found that the horizontal shears in

the upper tropospheric easterlies are such that barotropic instability criterion ($\beta - \partial^2 u/\partial y^2$ changing the sign somewhere within the domain) is frequently satisfied in the periods of break monsoon as well as active monsoon. However, the above barotropic instability criterion gives only a necessary but not a sufficient condition for instability of the atmospheric flow. SHUKLA [51] analysed the profile of isentropic potential vorticity and also applied the internal jet instability mechanism of CHARNEY and STERN [7] to the monsoon depression problem. He also included the idea of CISK with the cumulus scale heating based on the theory of ARAKAWA and SHUBERT [2]. His linear instability analysis suggested that the growth of a monsoon depression scale disturbance is possible in the Bay of Bengal region through such a combined barotropic–baroclinic–CISK instability and the structure of the most unstable mode had a reasonable resemblance to the observed structure of monsoon depressions.

KRISHNAMURTI *et al.* [30] calculated the meridional gradients of potential vorticity at 700 mb based on the observed data during the intensification stage of a monsoon depression over India. They showed that the meridional gradient of potential vorticity vanished near the central region of the actual position of the monsoon depression. They were, however, of the view that the mere fact a data set satisfied the necessary condition for the existence of combined barotropic–baroclinic instability did not necessarily imply that the energetics or the growth of the disturbance should follow accordingly. They also examined the problem from the study of the energetics based on the results of a numerical experiment performed with the data set of a monsoon depression. Their results suggested that the disturbance kinetic energy is maintained by the combined barotropic–baroclinic instability in which the cumulus convection plays a vital role in the energy conversions.

Although the dynamics of the formation of monsoon depression is still not completely understood, the observational, theoretical and numerical studies mentioned in the above paragraphs point out that in the early stages the barotropic dynamics may play a significant role but the later stage of development as well as maintenance of the depression is intimately related to baroclinic and CISK dynamics in which the energy supplied by the release of latent heat of condensation becomes the major energy source for the depression. It is a fact of observation that very rarely a monsoon depression intensifies to the stage of a mature tropical cyclone. This break on further intensification may be operated by several factors such as short sea travel before land fall and very large vertical wind shears between 850 and 200 mb restricting proper organisation of deep cumulus convection (GREY [22]). After the land fall there is a remarkable persistence of the depression stage over land for 3–5 days. It is observed that in some cases depressions continue to slowly intensify over land and their weakening begins only when they reach the western-most parts of India along their tracks where incursion of drier air takes place. Relatively longer life history over land of a monsoon depression is due to its existence within the deep moist monsoon environment which keeps up the supply of moisture required for organised cumulus convection.

4. *Structure of the monsoon depression*

4.1. *Composited mean structure*

MULKI and BANERJEE [37] studied the mean structure of the depressions in the wind field by compositing upper air data within 400 miles from the depression centres. Their study showed that cyclonic circulation extends in the horizontal within a radius of 400 miles from the centre (i.e., over the entire area under their consideration) and in the vertical the circulation extends from sea level to about 7 km. In the upper tropospheric levels anticyclonic vorticity and outflow dominates the circulation.

SIKKA and PAUL [58] composited the data of all depressions after their land fall which had formed during July and August for the years 1966–70. Figure 3a and Fig. 3b based on this study depict the distribution of tangential and radial winds. The data suggests the following aspects of depression circulation:

(i) Circulation is cyclonic up to 1000 km in the horizontal and up to 9 km in the vertical. Maximum cyclonic components are at a height of about 0.9 to 1.5 km (speed 15 mps) and at a distance of 300–400 km from the centre. Horizontal size of the cyclonic circulation shrinks in the vertical between 5 to 9 km.

(ii) Anticyclonic flow commences at about 10 km and its maximum (8 mps) occurs at a height of 12 km and at a radial distance of 500 to 600 km from the surface centre – a little farther away from the lower tropospheric maximum.

(iii) Inflow occurs from surface to a height of about 5 km up to radial distance of 900 km from the centre. The maximum of the inflow (about 5 mps) occurs

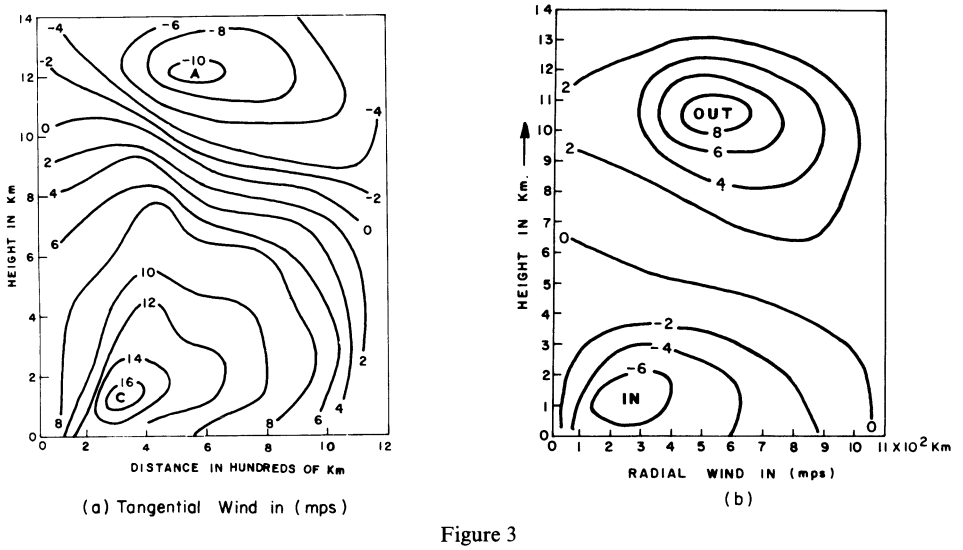

(a) Tangential Wind in (mps) (b)

Figure 3
Horizontal and vertical variations of tangential wind and radial wind components (mps) for composite monsoon depression.

at about 1.0 to 1.5 km at a radial distance of 200 to 300 km from the centre. Area of inflow is found to become smaller with height.

(iv) Outflow dominates above 6.0 km and attains its maximum at a height of about 10 to 11 km and at a radial distance of about 400 to 600 km from the surface centre. Decrease of the outflow is rather rapid between 12 to 13 km altitude.

GODBOLE [20] composited the wind, temperature and moisture data based on the grid point analyses of the monsoon depressions that had formed during the monsoon season of 1973. His results also show similar features of the cyclonic and anticyclonic circulation in the lower and upper troposphere respectively.

4.2. Structure from synoptic and dynamical studies

As already mentioned, studies undertaken during 1930–51 emphasised the role of different airmasses. KOTESWARAM and GEORGE [26] based on a case study argued that although no evidence was available for the existence of frontal characteristics, the thermal patterns were deformed into warm and cold sectors. Upward vertical motion ahead of the centre and downward vertical motion in the rear prevailed due to the convergence/divergence patterns in the lower troposphere. KOTESWARAM and BHASKARA RAO [27] emphasised that unlike tropical depressions of the oceanic regions, monsoon depressions form in the vicinity of landmass of India and as such the contrast between land and sea is a significant feature to be considered for analysing the structure and the study of their dynamics.

Depression centre is found to tilt in the vertical to the southwest or west of the sea-level centre. This is suggested from the study of (i) composite depression, (ii) the results of spectrum analysis of 15–20 days mode in the meridional components in the lower tropospheric winds which is believed to be associated with the monsoon depressions (KESHAVAMURTY [23]) and (iii) the results of the analysis of satellite photographs centres with respect to the sea level pressure centres (SHARMA and SRINIVASAN [61] and KESHAVAMURTY [24]). Individual cases of deep monsoon depressions show little tilt in the vertical at least up to 500 mb. Radar pictures show the spiral structure only when a depression intensifies into a cyclonic storm or severe tropical cyclone [5].

4.3. Detailed structure of a case study

4.3.1. Recently KRISHNAMURTI *et al.* [29] and DAGGUPATY and SIKKA [9] have examined in great detail the horizontal and vertical structure of a case of monsoon depression during 3 to 6 August 1968. This depression continuously intensified during its life history from the east coast of India to the west coast as it moved along the latitude of about 22°N. Some of the noteworthy features about the structure of the depression which have emerged from these two studies are:

(i) The wavelength of the depression was about 2000–2500 km.

(ii) The intensification of the depression was accompanied with strengthening of lower tropospheric westerlies over the Peninsular India and the easterlies over the Gangetic valley to the north of the centre. At the most intense stage, the westerlies and the easterlies reached maximum speeds of about 25 to 30 mps at 900–850 mb.

(iii) Maximum meridional winds were about 7–8 mps between 800–500 mb.

(iv) The depression extended in the vertical up to 300 mb and had very little tilt in the vertical up to 500 mb but tilted markedly to the southeast between 500 and 300 mb. At 200 mb the depression appeared to be a wave in the easterlies.

(v) Rainfall was chiefly concentrated in the western and southwestern sectors of the depression and maximum 24-hourly rainfall generally ranged between 10–15 cm with isolated falls of 30–40 cm. Convective and non-convective clouding was reported during the entire life history of the depression. Rainfall was found to increase with the intensification of the depression.

(vi) A strong core of absolute vorticity ($12–15 \times 10^{-5}$ sec^{-1}) coincided with the centre of the depression near the surface. Relative vorticity over the central region remained cyclonic up to about 250 mb and significant anticyclonic relative vorticity appeared at 200 mb. It may be mentioned that the normal absolute vorticity field at the lower troposphere associated with the monsoon trough is about 7×10^{-5}. Thus, the value of cyclonic vorticity associated with the monsoon depression lies in between those of cloud clusters and easterly waves in the lower scale and the severe tropical cyclone/hurricane on the higher scale.

(vii) Zonal gradients of moisture across the monsoon depressions were large particularly to the west and northwest of the centre where dry air of desert origin prevailed (Fig. 4). The main variations appeared in the middle tropospheric levels. A deep moist layer was seen up to 400 mb only in the vicinity of the depression. Thus the depression circulation was able to pump up large quantity of moisture into the middle troposphere from the moisture rich boundary layer of the monsoonal flow. The moisture distribution in the vertical was thus dependent upon the organisation of convection and hence under the influence of dynamical processes. Figure 5 shows the moisture convergence into a unit column for two typical days. Large moisture convergence was seen in the region of monsoon trough during the life history.

(viii) Compared to the surrounding environment, monsoon depression had a cold core in the lower troposphere (up to 600 mb) and warm core in the upper troposphere. In the lower troposphere significantly warmer temperatures were only seen to the west of the depression centre over the Arabian sea region. The thermal amplitude in the lower troposphere was

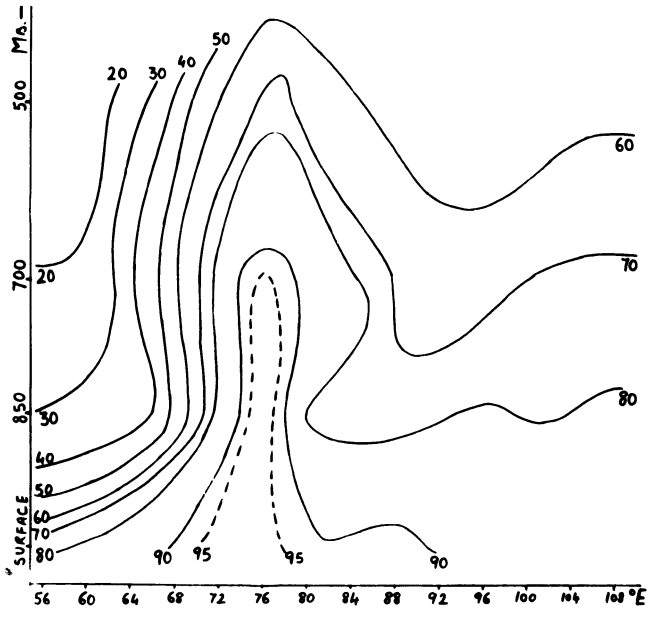

Figure 4
Vertical variation of relative humidity in the east–west direction through the centre of monsoon depression lying over western India at 00Z on 6 August, 1968 (centre of the depression 22.5°N 74.5°E).

large (about 6°C) if the west Arabian sea and the Arabia region was included in the depression environment but if this region was excluded the cold core was reduced to about 1–2°C only. Thermal amplitude in the upper troposphere was small (1–2°C).

4.3.2. Vertical motion computed at 900, 700, 500 and 300 mb for this case study following the fully balanced diagnostic model of KRISHNAMURTI [28] showed the following characteristics:

(a) Balanced vertical velocity field is chiefly accounted by five terms viz.

(i) differential vorticity advection,
(ii) Laplacian of thermal advection,
(iii) effects of frictional stresses,
(iv) differential deformation effects, and
(v) diabatic heating effects due to sub-grid scale cumulus convection parameterised after KUO's [32] scheme.

(b) Whereas the effect of frictional stress term was dominant at 900 mb, the effect of diabatic heating due to cumulus convection was found to be the most important one at 500 and 300 mb levels.

(c) The centre of the maximum upward motion existed at about 900–800 mb which was primarily due to the effects of frictional terms which contributed to the rising

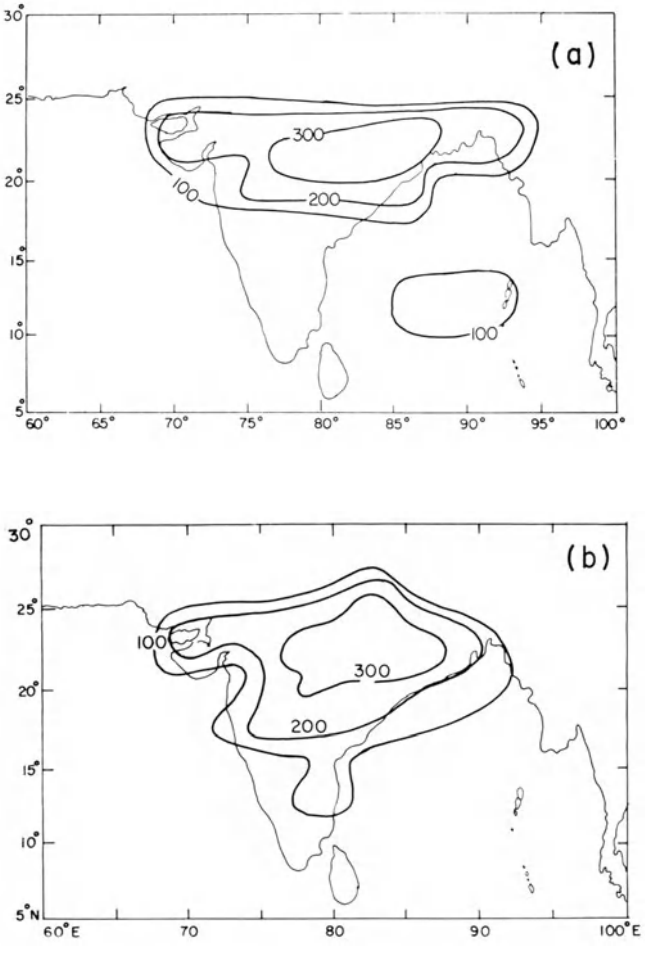

Figure 5
Moisture convergence at 900 mb in the case of monsoon depression. (a) 00Z 4 August 1968 (b) 00Z 5 August 1968 (units = 10^{-8} sec^{-1}).

motion in the areas of cyclonic vorticity. The maximum also was positioned somewhat to the west of the centre of the depression.

(d) Warm air advection to the west of the centre contributed to upward vertical motion ahead of the centre. Cold air advection to the east of the centre contributed to descending motion.

(e) Vorticity advection contributed to upward motion in the forward sector and descending motion in the rear sector.

(f) Non-geostrophic effects due to differential deformation term were well marked due to the confluence zone in northwest to west of the depression centre.

(g) Due to the characteristic structure of the depression in the lower troposphere, several factors contributed substantially to the vertical motion in these layers and

as such the computed level of non-divergence in the case was found to be around 800 mb. Thus a deeper layer of weak divergence existed over the shallow layer of strong convergence between surface to 800 mb. Although the non-linear balanced vertical motion field depended upon the various physical processes incorporated and were thus model dependent, the resulting level of non-divergence near 800 mb was found to be in general agreement with the studies by RAO and RAJAMANI [49] and DAS *et al.* [12] for other case studies based on the computations by quasi-geostrophic model.

(h) The computed vertical motion field agreed very well with the rainfall and cloud distribution.

4.4. Vorticity budget computations

DAGGUPATY and SIKKA [9] have reported the results of vorticity budget computations based on the results of non-linear balanced model for 3 August to 6 August 1968 case study. The following features of the vorticity budget are noteworthy in their study.

(a) For the lower tropospheric budget the dominant terms are the vorticity advection, divergence and frictional effects. In the lower troposphere total vorticity tendency due to all the five major forcing terms of the model was positive in the western sector and negative in the eastern sector, which meant that the positive relative vorticity was being created in the forward sector and it was being destroyed in the rear sector.

(b) In the lower troposphere the divergence term contributed to the generation of cyclonic vorticity below the level of non-divergence (i.e., in the convergence layer) and its contribution increased with the intensification of the depression. The contribution of this term was substantial in the western sector.

(c) In the lower troposphere, frictional stresses contributed to the destruction of cyclonic vorticity near the surface and this tendency was maximum at the peak intensity stage of the depression (as the vorticity tendency happens to be proportional to vorticity itself in the particular parameterisation of frictional stress terms). The frictional term was found to play a dual role. Although it was found to destroy the lower tropospheric positive vorticity, through its dominant role in the production of frictional convergence, it also indirectly contributed to the production of cyclonic vorticity through the divergence term.

(d) In the middle and upper troposphere the computed total vorticity tendency was such that there was destruction of cyclonic vorticity.

(e) In the upper troposphere, divergence term contributed to the production of anticyclonic relative vorticity and its contribution was higher in the western sector than in the eastern sector.

(f) Although the destruction of cyclonic vorticity in the eastern sector by the large-scale terms was self explanatory, and was in agreement with observation, the

destruction of cyclonic vorticity in the western sector posed a problem, as the observational data showed increase of cyclonic vorticity in this sector. To explain this discrepancy the authors have hypothesised the role of sub-grid scale vertical transports by convective clouds. As convective clouds dominate in the western sector, sub-grid scale processes presumably effect vertical transport of vorticity from the lower troposphere to the middle/upper troposphere. GODBOLE [21] following a different approach has also emphasised the role of convective processes in the vorticity budget of the composited monsoon depression.

5. *Co-existing monsoon depressions in the Bay of Bengal and the Arabian Sea*

Cases of simultaneous formation and intensification of monsoon depressions in the Arabian Sea and the Bay of Bengal are rather rare. Such a case, however, occurred recently during 3–10 July 1973. During this period research ships of the USSR were also taking observations over the Arabian Sea under the Indo-Soviet monsoon experiment, 1973. Synoptic charts for the first 10 days of July 1973 have been carefully analysed with all conventional radiosonde, radiowind, pilot balloon and research ships data. Satellite photographs were also used for the analyses. Figure 6(a to d) show the flow features at 850, 700, 500 and 200 mb associated with this case study on 8 July 1973. Three-dimensional structure of the depressions during the formative, intensification and decay stages was obtained based on the grid point data (2 degree latitude–longitude interval). The structure of the depressions was similar in all respects to what has been discussed under section 4.3 for the case study of August 1968. Figure 7 shows the distribution of daily rainfall over India between 7 and 10 July 1973. This shows that convective phenomena were associated throughout the life history of these depressions.

The formation of the depressions appeared to be very complex. The mid-tropospheric trough system over India was very active and lay along about 15–17°N between 1 and 3 July 1973. This system shifted northward and closed cyclonic circulations were observed in the Bay of Bengal and northeast Arabian Sea. Surface pressure departures from the normal were negative in the zone of mid-tropospheric trough on 4 July 1973 and pressure fell over the entire Indian region. Pressure departures became negative over the whole of India (Fig. 8) and maximum fall got concentrated in the Bay of Bengal and northeast Arabian Sea. Surface pressure continued to fall and low pressure areas intensified into depressions in the Bay of Bengal and the Arabian Sea on 5 July and 6 July respectively. At the most intense stage of these depressions on 8 July, the pressure departure from normal was highly negative (-12 mb). Figure 9(a, b) shows the time-longitude section of the pressure change and pressure departure from normal along 20°N. This clearly suggests that the pressure changes and departures associated with the formation of both depressions did not move from the east and the formation of depressions took place *in situ*. The flow

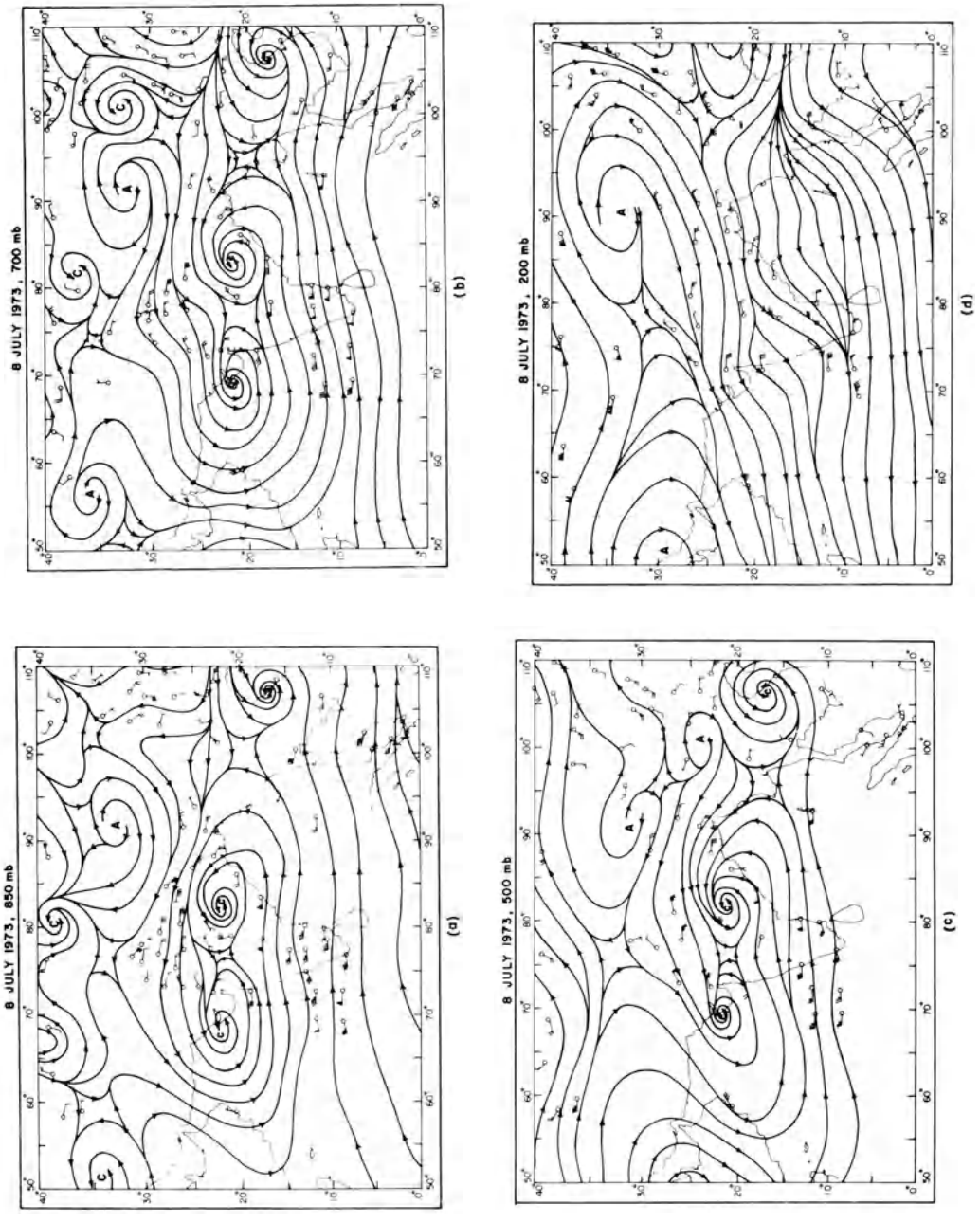

Figure 6
Streamlines of wind flow at 850, 700, 500 and 200 mb at 00Z on 8 July 1973.

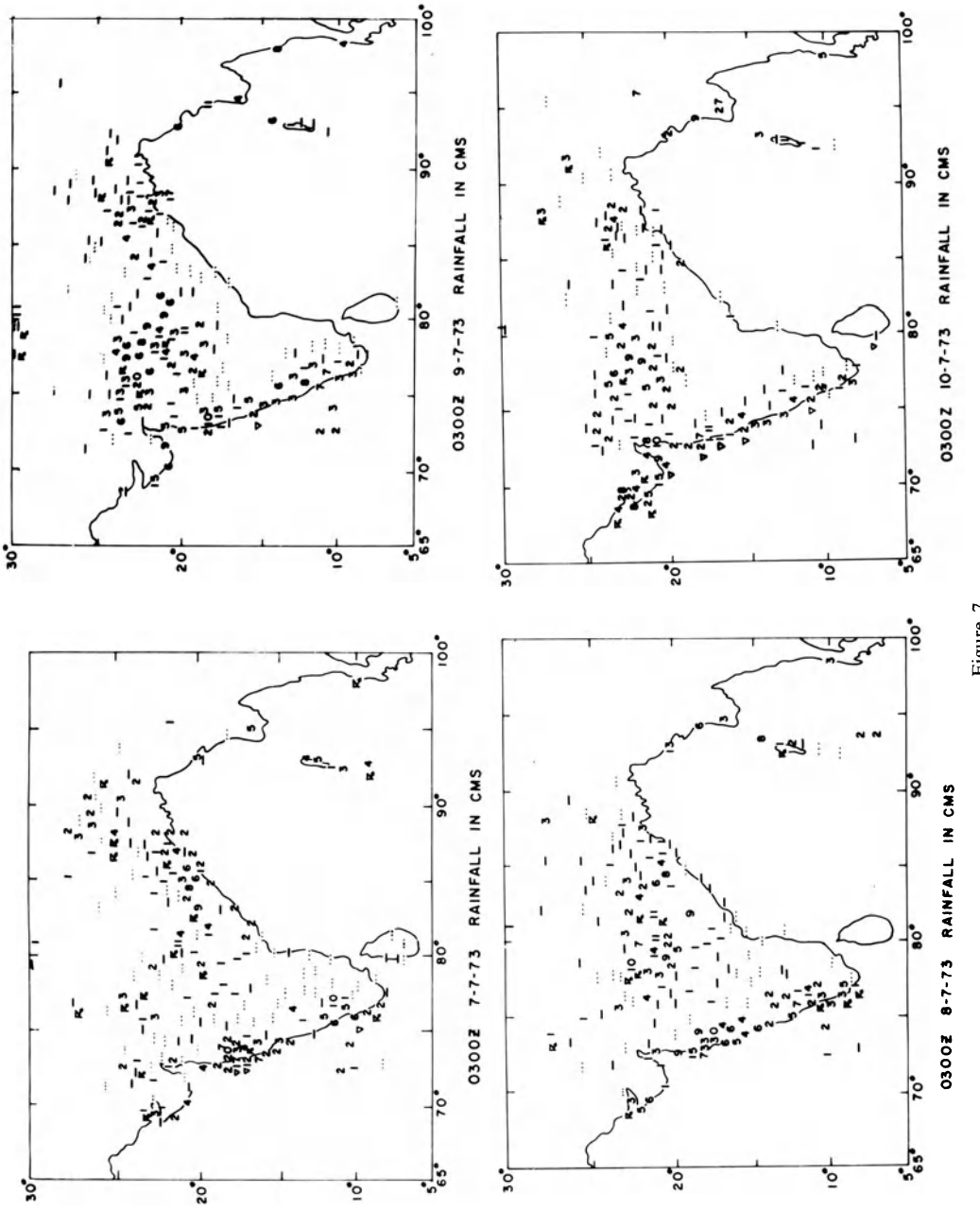

Figure 7
Rainfall for 24-hourly periods ending at 0300Z of 7, 8, 9 and 10 July 1973, depicting the westward progression of the rainfall with the movement of the Bay of Bengal depression. Convective phenomena are shown in symbols

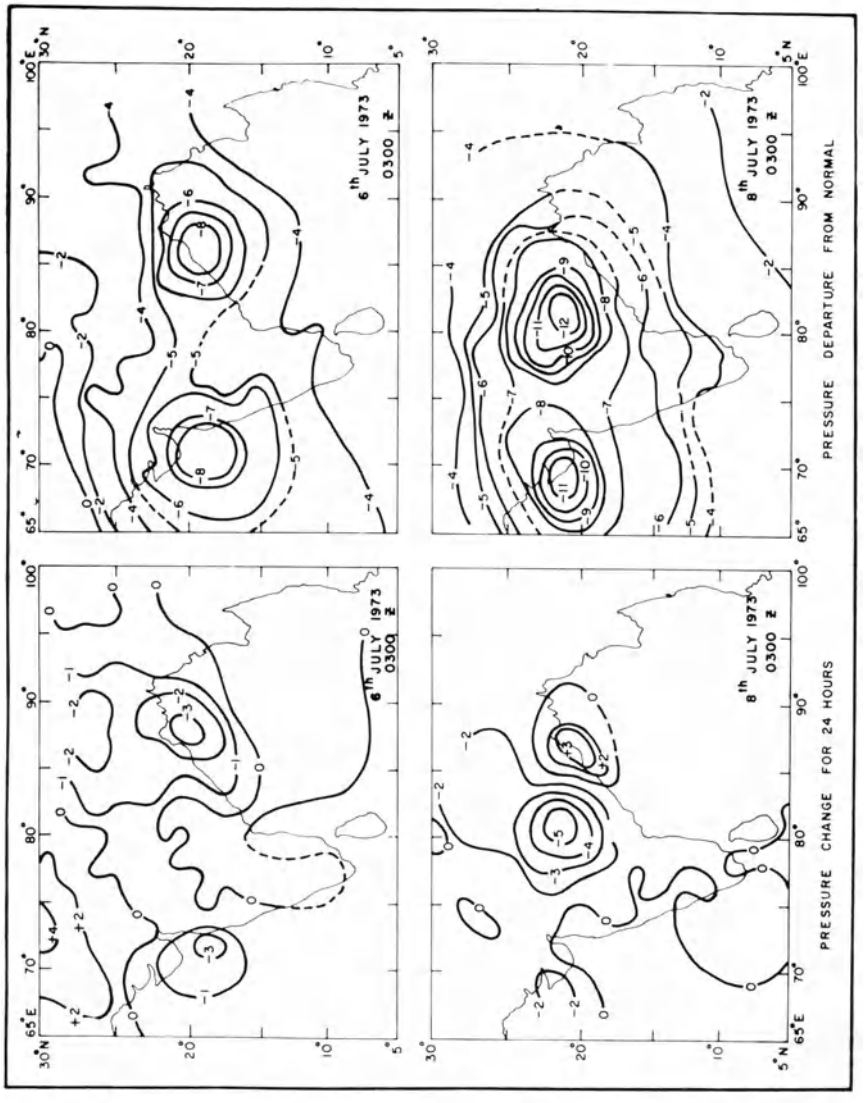

Figure 8
Pressure changes for 24 hours and pressure departures from normal at 0300Z over India on two typical days (6 July and 8 July 1973) associated with co-existence of two monsoon depressions over the Indian region.

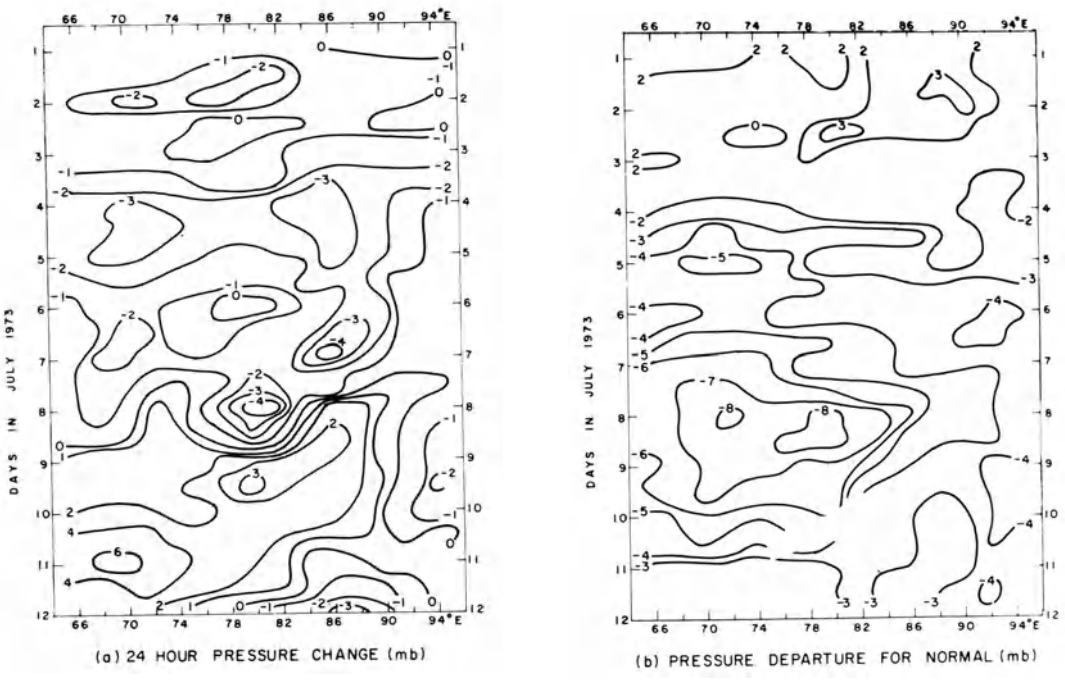

Figure 9
Time-longitude sections along 20°N for 24-hour pressure change and pressure departure from normal during 1 to 12 July 1973 between 66° and 94°E.

features at upper tropospheric levels did not show any spectacular changes and intensification process was not apparently linked with the movement of any perturbations in easterlies at those levels. The lower tropospheric westerly winds over peninsula (12–17°N) and the easterlies over India between 22 and 28°N also strengthened simultaneously with the fall of pressure over the entire belt of Central and Northern India. The lower tropospheric westerlies reached a strength of about 25 mps and the easterlies to the north a strength of about 20 mps in the most intense phase of the depressions. Details of the intensification process are not being discussed to limit space but a critical evaluation of the synoptic conditions showed that the formation and intensification were linked with the assemblage of abnormal concurrent conditions of pressure and wind in the lower tropospheric levels with the strengthening of cyclonic shears followed by heavy rainfall over north Bay of Bengal and northeast Arabian Sea regions. Depressions originated during the period when pressure departures were below normal over an extensive area. The possibility whether large scale pressure falls over extensive parts of India and the simultaneous occurrence of locally intense falls over the cyclogenetically active region of the Bay of Bengal are linked with the intensification of depressions needs further investigation.

6. *Movement of the monsoon depressions*

Monsoon depressions move along a well defined track from north Bay of Bengal to western/northwestern India. Their movement along a general westerly direction against the prevailing monsoonal westerlies of the lower troposphere has been a puzzling problem. ANANTHAKRISHNAN and BHATIA [1] found intimate connection between the path of depressions and upper tropospheric easterly flow at 10–12 km levels. KOTESWARAM and coworkers [26], [27] found that the depression moved where warm advection was taking place. This view found support in a case study by GEORGE and DATTA [19]. RAO and RAJAMANI [49] linked the westward movement to the generation of cyclonic vorticity by the convergence term. DAGGUPATY and SIKKA [9] have also stressed the role of convergence for the westward movement of the depression.

DAS [10] and DAS and BOSE [11] applied the non-divergent barotropic model to predict the movement of monsoon depressions. They used either very large time steps or graphical methods for integrations and therefore their results were not satisfactory. With the introduction of computers in India, SHUKLA and SAHA [52] applied the non-divergent model with stream function derived from observed winds at 500 mb as the basic input to predict the movement of a monsoon depression. The average vector error for the prediction of the centre in their case study was found to be 133 km for 24 hours forecast and 205 km for 48 hours forecast. SIKKA [54] used a 4 level quasi-geostrophic model with contour data as input at 900, 700, 500 and 300 mb to the August 1968 case of monsoon depression and concluded that although the model predicted the track rather satisfactorily (average 24 hours vector/error about 160 km), it did not predict the changes in the intensity of the depression. SINGH and SAHA [59] used primitive equation barotropic model to a single case and got satisfactory results.

The westward movement of the depression is an interesting dynamical problem and has been examined in some detail by KRISHNAMURTI *et al.* [30] by performing numerical experiments with non-divergent barotropic model (at 850 mb), 2 level quasi-geostrophic model and multi-level primitive equation model on the case study of 3–6 August 1968. According to their results the centre in the non-divergent barotropic experiment hardly showed any movement. This is due to the opposing tendency of the beta effect which yields a positive vorticity tendency west of the disturbance and the effect of negative relative vorticity advection. The centre of the depression showed a westward movement in their quasi-geostrophic model which was, however, much slower than the actual movement. Thus, they noticed that although quasi-geostrophic dynamics through the associated quasi-geostrophic vertical motion, could predict the movement in the right direction but the phase speed was underestimated. A major improvement for the phase speed was, however, realised by these workers when they applied the complete multi-level primitive

equation model. The improvement in the forecast was ascribed to the favourable coupling of the role of bottom topography and cumulus parameterization.

The author has extensively tested the performance of the non-divergent barotropic model for prediction of the tracks of monsoon depressions (input level 700 mb) during July and August for a five-year period, 1966–70, and compared these results against the forecasts based on persistence and climatology ($\frac{1}{2}(P + C)$).

Table 2 shows the results of these comparative forecasts. It is seen that statistically speaking methods based on persistence and climatology have the same success as the non-divergent barotropic model (input level 700 mb).

Table 2

Performance of non-divergent barotropic model against persistence and climatology for predicting the movement of monsoon depressions (July and August 1966–70)

Barotropic model				1/2(P + C)		
Average 24 hour vector error in km	Max. error (km)	Average 48 hour vector error in km	Max. error (km)	Average 24 hour vector error in km	Average 48 hour vector error in km	Max. error (km)
150	300	270	410	145	260	415
(22)		(11)		(14)	(10)	

Figures in brackets are no. of cases.

Table 3

Comparison of actual and forecast positions of the depression 4–8 August 1968 by Primitive Equation barotropic model

Date	Initial data 700 mb winds		Initial data 500 mb winds	
	24 hour vector error on date (km)	48 hours vector error on date (km)	24 hour vector error on date (km)	48 hour vector error on date (km)
4 Aug 68	125	—	220	—
5 Aug 68	55	165	270	350
6 Aug 68	125	220	170	280
7 Aug 68	165	175	70	120
8 Aug 68	—	210	—	150
Average	117	193	183	225

Table 3 shows the comparison of the results of the primitive equation model as applied to the depression of 4–8 August 1968 with input at 700 and 500 mb and a grid distance of 2 degrees. It is noticed that the vector error for this case is lower if the model is applied at 700 mb instead of 500 mb. The success of the numerical methods is expected to increase if the grid length is reduced to 1° or less as the scale of the depressions is about 2000 km and strong gradients exist near the centre.

7. *Conclusion*

Monsoon depression is an intense tropical disturbance in which the perturbation in the pressure and wind field is very large compared to easterly waves and cloud cluster systems of the Atlantic and the Pacific Oceans. It has a horizontal wave length of about 2000 km and belongs to the category of large to intermediate scale disturbances. In its most intense stage, it extends in the vertical up to about 10–12 km. The disturbance is cold in the lower troposphere and at the present state of knowledge it seems that the kinetic energy of the disturbance is maintained by combined barotropic-baroclinic-CISK instability in which the contributions from the non-adiabatic effects such as cumulus convection and differential radiative effects etc. are substantial. As the depression originates near the land mass of India and moves towards the heated region of western India and Pakistan, effects due to land-air-ocean interactions seem to play a vital role in its life history. Although a large amount of work has been done in understanding the structure and dynamics of the depression, yet for more definitive conclusions intensive empirical and dynamical studies with better data sets are still needed. It is hoped that this would become possible during the forthcoming MONEX period in the year 1979.

Acknowledgements

Part of the work was done when the author was visiting Florida State University during November 1976 to March 1977. For this the author is thankful to Prof. T. N. Krishnamurti of Florida State University for supporting the visit and for many fruitful discussions and the Director, Indian Institute of Tropical Meteorology, Poona, for permission to proceed on leave from the Institute. The author also expresses his thanks to Mr. K. V. S. Madhavan for typing the manuscript.

References

[1] Ananthakrishnan, R. and Bhatia, K. L. (1960), *Tracks of monsoon depressions and their recurvature towards Kashmir*, Symp. Monsoons of the World, 157–172.

[2] Arakawa, A. and Schubert, W. H. (1974), *Interaction of a cumulus cloud ensemble with the large scale environment* (1969). Pt. I, J. Atmos. Sci. *31*, 674–701.

[3] BEDDEKAR, V. C. and BANERJEE, A. K. (1969). *A study of climatological and other rainfall patterns over central India*, Ind. J. Met. Geophys. *20*, 23–29.

[4] BHALME, H. N. (1972), *Trends and quasi-biennial oscillations in the series of cyclonic disturbances over the Indian region,* Ind. J. Met. Geophys. *23*, 355–358.

[5] BHATTACHARJEE, P. and DE, A. C. (1965), *Radar study of the cyclonic storm of 21 September 1962 in the Bay of Bengal*, Ind. J. Met. Geophys. *16*, 81–84.

[6] BRAHMANANDA RAO, V. (1971), *Dynamic instability of the zonal current during a break monsoon*, Tellus *23*, 111–112.

[7] CHARNEY, J. G. and STERN, M. E. (1963), *On the stability of internal baroclinic jets in a rotating atmosphere*, J. Atmos. Sci. *19*, 159–172.

[8] DAGGUPATY, S. M. (1967), *On the instability of tropical zonal currents*, Ph.D. thesis submitted to Poona University.

[9] DAGGUPATY, S. M. and SIKKA, D. R. (1977), *On the vorticity budget and vertical velocity distribution associated with a life cycle of monsoon depression*, J. Atmos. Sci. *33*, 773–792.

[10] DAS, P. K. (1957), *Experiments with numerical forecasting in India*, 75 Anniv. Vol., J. Met. Soc. Japan, *35*, 275–279.

[11] DAS, P. K. and BOSE, B. L. (1958), *Numerical prediction of the movement of Bay depressions*, Ind. J. Met. Geophys. *9*, 225–232.

[12] DAS, P. K., DATA, R. K. and CHABBRA, B. M. (1971), *Diagnostic study of vertical motion vis-à-vis large scale cloud systems*, Ind. J. Met. Geophys. *22*, 331–336.

[13] DESAI, B. N. (1950), *On the development and structure of monsoon depressions in India*, Ind. J. Met. Geophys. *22*, 330–336.

[14] DESAI, B. N. and KOTESWARAM, P. (1951), *Air masses and fronts in the monsoon depressions in India*, Ind. J. Met. Geophys. *2*, 250–265.

[15] DHAR, O. N. and BHATTACHARYA, B. K. (1973), *Contribution of tropical disturbances to the water resources of Ganga basin*, Vayu Mandal *3*, 76–79.

[16] DHAR, O. N. and BHATTACHARYA, B. K. (1974), *Contribution of tropical disturbances to the water potential of Godavari basin*, Proc. Int. Trop. Met. Meeting, Nairobi, A. Met. Soc., pp. 298–301.

[17] DORAISWAMY IYER, V. (1939), *Typhoons and Indian Weather*, Mem. Ind. Met. Deptt. *26*, Pt. 6.

[18] ELIOT, J. (1884), *Account of southerwest monsoon storms generated in the Bay of Bèngal during 1877–1881*, Mem. Ind. Met. Deptt. *2*, 217–448.

[19] GEORGE, C. J. and DATA, R. K. (1965), *A synoptic study of monsoon depression in the month of September 1963*, Ind. J. Met. Geophys. *16*, 213–220.

[20] GODBOLE, R. V. (1977), *The composite structure of the monsoon depression*, Tellus *29*, 25–40.

[21] GODBOLE, R. V. (1977), *Large scale vorticity budget for a composited monsoon depression over India*, Paper presented at Int. Symp. on Monsoons, New Delhi.

[22] GRAY, W. M. (1968), *Global view of the origin of tropical disturbances and storms*, Mon. Wea. Rev. *96*, 665–700.

[23] KESHAVAMURTY, R. N. (1972), *On the vertical tilt of monsoon disturbances*, J. Atmos. Sci. *29*, 993–995.

[24] KESHAVAMURTY, R. N. (1972), *Certain aspects of monsoon depressions as revealed by satellite pictures*, Ind. J. Met. Geophys. *23*, 161–164.

[25] KOTESWARAM, P. and GEORGE, C. A. (1958), *On the formation of monsoon depressions in the Bay of Bengal*, Ind. J. Met. Geophys. *9*, 9–22.

[26] KOTESWARAM, P. and GEORGE, C. A. (1960), *A case study of a monsoon depression in the Bay of Bengal* in *Monsoons of the World* (1960), pp. 145–156.

[27] KOTESWARAM, P. and BHASKARA RAO, N. S. (1963), *Formation and structure of Indian summer monsoon depressions*, Aust. Met. Mag. *41*, 62–75.

[28] KRISHNAMURTI, T. N. (1968), *A diagnostic balance model for studies of weather systems of low and high latitudes*, Mon. Wea. Rev. *96*, 197–207.

[29] KRISHNAMURTI, T. N., KANAMITSU, M., GODBOLE, R., CHANG, C. B., CARR, F. and CHOW, J. H. (1975), *Study of a monsoon depression, (I), Synoptic structure*, J. Met. Soc. Japan, *53*, 227–240.

[30] KRISHNAMURTI, T. N., KANAMITSU, M., GODBOLE, R., CHANG, C. B., CARR, F. and CHOW, J. H. (1976), *Study of a monsoon depression, (II), Dynamical structure*, J. Met. Soc. Japan, *54*, 208–224.

[31] KRISHNAMURTI, T. N. and BHALME, H. N. (1976), *Oscillations of a monsoon system. Pt. I. Observational aspects*, J. Atmos. Sci. *33*, 1937–1954.

[32] KUO, H. L. (1965), *On the formation and intensification of tropical cyclones through latent heat release by cumulus convection*, J. Atmos. Sci. *22*, 40–63.

[33] LAL, S. S. (1958), *Rainfall around slow moving monsoon depressions over India*, Proc. Sym. Met. Hydro. aspects of floods and droughts in India, India Met. Dept.

[34] MILLER, F. and KESHAVAMURTY, R. N. (1968), *Structure of an Arabian Sea summer monsoon system*, IIOE Met. Monograph No. 1, University of Hawaii, Honolulu.

[35] MOOLEY, D. A. (1973), *Some aspects of Indian monsoon depressions and the associated rainfall*, Mon. Wea. Rev. *101*, 271–280.

[36] MOWLA, K. G. (1968), *Cyclogensis in the Bay of Bengal and Arabian Sea*, Tellus *21*, 151–162.

[37] MULKI, G. and BANERJEE, A. K. (1960), *The mean upper wind circulation around monsoon depressions in India*, J. Met. *17*, 8–14.

[38] MULL, S. and RAO, Y. P. (1949), *Indian tropical storms and zones of heavy rainfall*, Ind. J. Phys. *23*, 371–377.

[39] PISHAROTY, P. R. and ASNANI, G. C. (1957), *Rainfall around monsoon depressions over India*, Ind. J. Met. Geophys. *8*, 15–20.

[40] PAUL, D. K. and SIKKA, D. R. (1975), *Monsoon sea level pressure field*, Sci Rep. Ind. Instit. Trop. Met. Poona.

[41] PETTERSSEN, S., *Weather Analysis and Forecasting* (McGraw-Hill, New York, 1956).

[42] PRASAD, K. and KRISHNA RAO, D. (1974), *Case studies of westerly waves in the development of monsoon depressions*, Ind. J. Met. Geophys. *25*, 265–268.

[43] RAGHAVAN, K. (1967), *Influence of tropical storms on monsoon rainfall in India*, Weather *22*, 250.

[44] RAGHAVAN, K. (1965), *Zones of rainfall ahead of a tropical depression*, Ind. J. Met. Geophys. *16*, 631–634.

[45] RAMANATHAN, K. R. and RAMAKRISHNAN, K. P. (1933), *The Indian southwest monsoon and structure of depressions associated with it*, Mem. Ind. Met. Deptt. *26*, Pt. II, 1–35.

[46] RAMAGE, C. S., *Monsoon Meteorology* (Academic Press, New York 1971).

[47] RAO, K. N. and JAYARAMAN, S. (1958), *A statistical study of frequency of depressions and cyclones in the Bay of Bengal*, Ind. J. Met. Geophys. *9*, 235–250.

[48] RAO, Y. P. (1976), *Southwest monsoon*, Met. Monograph, No. 1, Ind. Met. Deptt.

[49] RAO, K. V. and RAJAMANI, S. (1970), *Diagnostic study of a monsoon depression by geostrophic baroclinic model*, Ind. J. Met. Geophys. *21*, 187–194.

[50] ROY, S. K. and ROY, A. K. (1930), *Structure and movement of cyclones in Indian southwest monsoon season*, Beit. Phys. Frei. Atmos. *16*, 224–234.

[51] SHUKLA, J. (1976), *On the dynamics of monsoon disturbances*, D.Sc. Dissertation, Dept. of Meteorology, Massachusetts Institute of Technology, Cambridge.

[52] SHUKLA, J. and SAHA, K. R. (1970), *Application of non-divergent barotropic model to predict flow patterns in the Indian region*, J. Met. Soc. Japan, *48*, 405–410.

[53] SIKKA, D. R. (1971), *Development of tropical cyclones in the Indian seas as revealed by satellite radiation and television data*, Ind. J. Met. Geophys. *22*, 317–324.

[54] SIKKA, D. R. (1973), *Experimental forecasting over the Indian region with 4 level quasi-geostrophic model*, paper presented at N.W.P. Symp. New Delhi.

[55] SIKKA, D. R. and ANANTHAKRISHNAN, R. (1974), *On the influence of synoptic scale systems in controlling convective activity during the southwest monsoon*, Proc. Int. Trop. Met. Meeting, Nairobi, A. Met. Soc. pp. 115–120.

[56] SIKKA, D. R. and MOORTHY, S. (1976), *A diagnostic study on the effects of infra-red water vapour cooling on synoptic scale disturbances during the southwest monsoon season*, Proc. Symp. Tropical Monsoons, Poona, pp. 133–141.

[57] SIKKA, D. R. and GADGIL, S. (1975), *Large scale rainfall over India during the summer monsoon and its relations to lower and upper tropospheric vorticity*, Geophysical Fluid Dynamics Workshop, Monsoon Meteorology, I.I.Sc., pp. 1–31.

[58] SIKKA, D. R. and PAUL, D. K. (1975), *A diagnostic study on the structure of monsoon depressions*, Geophys. Fluid Dynamics Workshop, Monsoon Meteorology, I.I.Sc., pp. 136–182.

[59] SINGH, S. S. and SAHA, K. R. (1976), *Numerical experiment with a primitive equation barotropic model for the prediction of movement of monsoon depressions and tropical cyclones*, J. Appl. Meteor. *15*, 805–810.

[60] SRINIVASAN, V., RAMAN, S. and RAMAKRISHNAN, A. R. (1971), *Monsoon depressions as seen in satellite pictures*, Ind. J. Met. Geophys. *22*, 337–346.

[61] SHARMA, M. C. and SRINIVASAN, V. (1971), *Centres of monsoon depressions as seen in satellite pictures*, Ind. J. Met. Geophys. *22*, 357–358.

[62] VENKATARAMAN, K. S., CHOUDHURY, A. and BANERJEE, A. K. (1974), *A study of hourly rainfall distribution around monsoon depression centre in Central India*, Ind. J. Met. Geophys. *25*, 239–244.

(Received 15th July 1977)